Biocatalytic Oxidative Dearomatization and Applications in Chemoenzymatic Total Synthesis

by

Summer A. Baker Dockrey

A dissertation submitted in partial fulfillment
of the requirements for the degree of
Doctor of Philosophy
(Chemistry)
in the University of Michigan
2020

Doctoral Committee:

Professor Alison R. H. Narayan, Chair
Professor Melanie S. Sanford
Professor Janet L. Smith
Professor John P. Wolfe

Summer A. Baker Dockrey

sbakerdo@umich.edu

ORCID iD: 0000-0002-6204-9833

© Summer A. Baker Dockrey 2020

To my family, friends and coworkers.

Acknowledgements

This work would not have been possible without the support, guidance and contributions of my mentors, coworkers and collaborators. I thank Professor Alison Narayan for her tireless support and mentorship for the duration of my studies. My growth as a scientist and student over the past few years I owe to her guidance and mentorship. Alison has opened every door to me in my career and I am immensely grateful for her commitment as a mentor. I thank also my undergraduate mentors Dr. Jason Schmink, Dr. Maryellen Nerz-Stormes, and Dr. Krynn Lukacs who each offered me opportunities to learn and apply my skills as a chemist. My time in Dr. Schmink's group was foundational to the career I pursue now, and my gratitude for that time is inexpressible.

Thank you, Professor Janet Smith, Professor John Wolfe and Professor Melanie Sanford, for serving on my dissertation committee. The advice, guidance and feedback provided over the past four years has been instrumental to my progress as a scientist.

I am also grateful to my rotator mentors Professor Melanie Sanford and Professor John Montogmery for giving me the opportunity to rotate in their labs. The skills I learned during those rotations have been invaluable.

During my time in the Narayan lab I have had the privilege to work with a phenomenal group of colleagues and collaborators. Attabey Rodrìguez Benìtez and Joshua Pyser have made remarkable progress and discoveries in the flavin world and have been a source of expertise and creativity in driving these projects forward. Working with Carolyn Suh has been the highlight of my graduate career and I cannot thank her enough for dedicating her time, remarkable intelligence and enthusiasm to the lab and the projects we’ve worked on together. I look forward to watching what will be a stellar career continue to develop. I’ll always be cheering!

To my cohort of fifth years, April Lukowski, Tyler Doyon and Stephanie Chun, have each taught me so much. Thank you for your patience and generosity in teaching me and for making grad school worthwhile with your colleagueship.

I’m grateful to our collaborators Dr. Troy Wymore and Sarah Tweedy in the Brooks group whose work has been critical to developing an understanding of our flavoproteins and greatly enriched our studies. I’d also like to thank our collaborator Dr. Leo Joyce, whose key contributions allowed us to untangle quite the snare of data. Thank you also Dr. Ren Wiscons for your expertise in crystallography and solving our crystal structures!

Thank you to Marc Becker, Jianxin Liu and Runlai Wang for their work during their time in the lab, and all past and previous members for their friendship, insights and support.

I would also like to thank my family and my partner, Andrew. Thanks for putting up with me through it all.

Table of Contents

Dedication **ii**
Acknowledgements **iii**
List of Tables **viii**
List of Figures **ix**
List of Abbreviations **xxvii**
Abstract **xxix**
CHAPTER 1: Introduction **1**
- Chapter 1.1: Flavin biocatalysts in complex molecule synthesis 1
- Chapter 1.2: References 15

CHAPTER 2: Substrate Scope of Biocatalytic Oxidative Dearomatization **17**
- Chapter 2.1: Introduction 17
- Chapter 2.2: Substrate Synthesis 21
- Chapter 2.3: Reactivity Profile 22
- Chapter 2.4: Preparative-scale Reactions 28
- Chapter 2.5: Conclusions 31
- Chapter 2.6: Experimental 32
  - Chapter 2.6.1: Substrate Synthesis 32
  - Chapter 2.6.2: Plasmids and Proteins 74
  - Chapter 2.6.3: Biocatalytic Reactions 80
  - Chapter 2.6.4: Substrate Calibration Curves 93
  - Chapter 2.6.5: UPLC Traces of Biocatalytic Reactions 99
  - Chapter 2.6.6: HPLC and SFC Traces 153
  - Chapter 2.6.7: NMR Spectra of Synthetic Compounds 168
- Chapter 2.7: References 230

CHAPTER 3: Positioning-group Enabled Biocatalytic Oxidative Dearomatization **232**
- Chapter 3.1: Introduction 232
- Chapter 3.2: Substrate Synthesis 236
- Chapter 3.3: Reactivity Profile 238
- Chapter 3.4: Preparative-scale Reactions 243

Chapter 3.5: Conclusions 245
Chapter 3.6 Experimental 246
Chapter 3.6.1: Substrate Synthesis 246
Chapter 3.6.2: Biocatalytic Reactions 266
Chapter 3.6.3: Substrate Calibration Curves 276
Chapter 3.6.4: UPLC Traces of Biocatalytic Reactions 278
Chapter 3.6.5: Determination of Enantiomeric Excess 294
Chapter 3.6.6: NMR Spectra of Compounds 299
Chapter 3.7: References 324
CHAPTER 4: Large-scale Reaction and One-pot Platform Development 326
Chapter 4.1: Introduction 326
Chapter 4.2: Whole-cell Platform 326
Chapter 4.3: Complex Molecule Synthesis 329
Chapter 4.4 Conclusions 332
Chapter 4.5: Experimental 333
Chapter 4.5.1: Whole Cell Reactions 333
Chapter 4.5.2: Synthesis of Compounds 334
Chapter 4.5.3: SFC Traces of Chiral Compounds 338
Chapter 4.5.4: NMR Spectra of Synthetic Compounds 339
Chapter 4.6: References 343
CHAPTER 5: Chemoenzymatic, Stereodivergent Synthesis of Azaphilone Natural Products 344
Chapter 5.1: Introduction 344
Chapter 5.2: Characterization of AzaH Homologs 346
Chapter 5.3: Design and Synthesis of a Common Intermediate 349
Chapter 5.4: Total Synthesis of Trichoflectin and Lunatoic Acid A 354
Chapter 5.5: Conclusion 359
Chapter 5.6: Experimental 360
Chapter 5.6.1: Synthesis of Compounds 360
Chapter 5.6.2: Plasmids and Proteins 372
Chapter 5.6.3: Biocatalytic Reactions 376
Chapter 5.6.4: Substrate Calibration Curves 379
Chapter 5.6.5: UPLC Traces of Biotransformations 381
Chapter 5.6.6: Determination of Enantiomeric Excess 393
Chapter 5.6.7: NMR Spectra of Compounds 395
Chapter 5.6: References 407

CHAPTER 6: Photocatalytic Oxidative Dearomatization of Resorcinol Compounds 409
- Chapter 6.1 Introduction 409
- Chapter 6.2 Reaction Development 411
- Chapter 6.3 Mechanistic Studies 412
- Chapter 6.4: Substrate Scope 415
- Chapter 6.5 Conclusions 416
- Chapter 6.6: Experimental 417
  - Chapter 6.6.1: Protocol for PCOD 417
  - Chapter 6.6.2: Stern-Volmer Plots 420
  - Chapter 6.6.3: NMR Spectra of Synthetic Compounds 428
- Chapter 6.7: References 434

List of Tables

Table 2.1: Turnover numbers (TN) at 1 h, based on consumption of starting material as measured by absorbance at 270 nm. Conditions: 2.5 mM substrate, 2.5 μM flavin-dependent monooxygenase, 5 mM G6P, 1 mM $NADP^+$, 1 unit/mL G6PDH, 50 mM KP_i buffer, 30 °C, 1 h. 26

Table 6.1: Optimization of photocatalytic oxidative dearomatization...................................... 411

List of Figures

Figure 1.1: Catalytically active species of flavin (flavin-adenine dinucleotide and flavin mononucleotide) referenced in this review. (A) Fl_{ox} can act as a one or two electron acceptor to afford the semiquinone or reduced flavin (Fl_{red}). (B) Fl_{red}, in the context of ene-reductases, can perform the two-electron reduction of activated olefins. Fl_{red} may also react with molecular oxygen to form the C4a-peroxy (D) or hydroperoxy flavin (E) which can be the source of an oxygen atom for incorporation into organic substrates. Elimination of peroxide affords Fl_{ox}. 2

Figure 1.2: Monoamine oxidases (MAOs) in the synthesis of enantio-enriched amines. (A) Dynamic resolution of amines using MAO-N variants and a reducing agent. (B) Monoamine oxidase initiated Pictet-Spengler cascade for the synthesis of (R)-harmicine (27).[9] 3

Figure 1.3: Reactions with ene-reductases. (A) Chemoenzymatic synthesis of amino acid derivatives via an ene-reductase-catalyzed hydrogenation.[21] (B) One-pot three-step cascade to enantioenriched γ-butyrolactones.[22] (C) One-pot, two-step cascade to generate actinol (**1.50**).[23] . 6

Figure 1.4: Reactions with BVMOs. (A) General mechanism for BVMOs. (B) *Aerangis* lactone synthesis featuring a stereoselective BV oxidation by cyclododecanone monooxygenase (CDMO) or cycopentanone monooxygenase (CPMO). (C) Chemoenzymatic synthesis of tetrahydrofuran-based natural products via a chiral intermediate generated by CPMO-mediated Baeyer-Villager oxidation a) OsO_4, NMO, DCM, rt, then acetone–$AlCl_3$, 0 °C to 40 °C, 47%; b) *m*CPBA, DCM, reflux, 98%; c) MeCN, H_2O, KOH, rt, then I_2–KI, 40 °C, dark, 75%. 11

Figure 1.5: Reactions of group A flavin-dependent monooxygenases. Access to bisorbicillin natural products via oxidative dearomatization. 12

Figure 1.6: Reactions of halogenases. (A) General reaction mechanism for halogenase-mediated halogenation (EAS = Electrophilic aromatic substitution). (B) Halogenation, Pd-catalyzed Suzuki coupling cascade for late-stage functionalization of indole natural product scaffolds.[45] (C) Evolution of RebH variants using substrate walking from simple indole derivatives to pentacyclic alkaloids.[46] 14

Figure 2.1: Small-molecule methods for asymmetric oxidative dearomatization. 18

Figure 2.2: The native reaction and biosynthetic pathway of the three flavin-dependent monooxygenases TropB,[9] SorbC[10] and AzaH.[11] 20

Figure 2.3: Retrosynthetic analysis of substrate classes for biocatalytic oxidative dearomatization. 21

Genes encoding *tropB* and *sorbC* were cloned into a pET151 vector. The plasmids were then transformed into BL21 (DE3) E. coli cells. The gene encoding *azaH* in a modified pET28 vector was a generous gift from the Tang lab at UCLA. Expression and purification conditions were slightly modified from those reported by Cox[9] and Tang[11] respectively (see Chapter 2.6.2). **Figure 2.4:** Synthetic routes to resorcinol substrates for biocatalytic oxidative dearomatization. 22

Figure 2.5: Workflow for analytical-scale oxidative dearomatization. Synthetic genes are cloned into the desired vector, transformed into a competent *E. coli* strain which is then grown in 0.5 or 1 L cultures. Overexpression is induced and cells are harvested and lysed. After Ni-affinity purification of the crude lysate the protein solution is used in small scale reactions. 24

Figure 2.6: Trends in reactivity of the three enzymes TropB, SorbC and AzaH with five substrate classes. Red arrow indicates high conversion, grey arrow indicates decreasing conversion with increasing steric bulk and yellow equal sign indicates comparable conversion of substrates...... 27

Figure 2.7: Yields and enantiomeric excesses of products obtained from preparative scale enzymatic reactions. Conditions: 2.5 mM substrate (10 mg, in DMSO), 2.5 mM flavin-dependent monooxygenase, 5 mM G6P, 1 mM NADP$^+$, 1 unit/mL G6PDH, 50 mM Kp$_i$ buffer, 30 °C, 1 h. 31

Figure 2.8: Purified AzaH, TropB, and SorbC. Approximately 5 µL of 1.25 µM each protein was loaded onto an MiniPROTEAN TGX Precast 4-15% SDS-PAGE gel (Bio-Rad). The gel was stained with Quick Coomassie stain (Anatrace) and visualized with the Azure Gel Imaging System. The relative apparent masses are consistent with the predicted estimates........ 78

Figure 2.9: Native enzyme absorbance spectra compared to denatured enzyme absorbance spectra exposing free FAD to solution........ 79

Figure 2.10: ^{1}H NMR spectra of **2.82** in A) $CDCl_3$, B) CD_3CN and C) CD_3CN with 10% D_2O showing the solvent dependence of the population of keto-enol tautomers. 87

Figure 2.11: Calibration curves of substrates. 98

Figure 2.12: Oxidative dearomatization of **2.12** by TropB. PDA traces of enzymatic reaction and control reaction. 99

Figure 2.13: Oxidative dearomatization of **Table 1, Entry 2** by TropB. PDA traces of enzymatic reaction and control reaction........ 100

Figure 2.14: Oxidative dearomatization of **2.54** by TropB. PDA traces of enzymatic reaction and control reaction. 101

Figure 2.15: Oxidative dearomatization of **2.55** by TropB. PDA traces of enzymatic reaction and control reaction 102

Figure 2.16: Oxidative dearomatization of **2.50** by TropB. PDA traces of enzymatic reaction and control reaction. 103

Figure 2.17: Oxidative dearomatization of **2.43** by TropB. PDA traces of enzymatic reaction and control reaction. 104

Figure 2.18: Oxidative dearomatization of **2.49** by TropB. PDA traces of enzymatic reaction and control reaction. 105

Figure 2.19: Oxidative dearomatization of **2.22d** by TropB. PDA traces of enzymatic reaction and control reaction. 106

Figure 2.20: Oxidative dearomatization of **2.22c** by TropB. PDA traces of enzymatic reaction and control reaction. 107

Figure 2.21: Oxidative dearomatization of **2.22e** by TropB. PDA traces of enzymatic reaction and control reaction. 108

Figure 2.22: Oxidative dearomatization of **2.53** by TropB. PDA traces of enzymatic reaction and control reaction. 109

Figure 2.23: Oxidative dearomatization of **2.58** by TropB. PDA traces of enzymatic reaction and control reaction. 110

Figure 2.24: Oxidative dearomatization of **2.59** by TropB. PDA traces of enzymatic reaction and control reaction. 111

Figure 2.25: Oxidative dearomatization of **2.47** by TropB. PDA traces of enzymatic reaction and control reaction. 112

Figure 2.26: Oxidative dearomatization of **2.50** by TropB. PDA traces of enzymatic reaction and control reaction. 113

Figure 2.27: Oxidative dearomatization of **2.61** by TropB. PDA traces of enzymatic reaction and control reaction. 114

Figure 2.28: Oxidative dearomatization of **2.22a** by TropB. PDA traces of enzymatic reaction and control reaction. 115

Figure 2.29: Oxidative dearomatization of **2.55** by TropB. PDA traces of enzymatic reaction and control reaction. 116

Figure 2.30: Oxidative dearomatization of **2.50** by TropB. PDA traces of enzymatic reaction and control reaction. 117

Figure 2.31: Oxidative dearomatization of **2.43** by TropB. PDA traces of enzymatic reaction and control reaction. 118

Figure 2.32: Oxidative dearomatization of **2.53** by TropB. PDA traces of enzymatic reaction and control reaction. 119

Figure 2.33: Oxidative dearomatization of **2.58** by AzaH. PDA traces of enzymatic reaction and control reaction. 120

Figure 2.34: Oxidative dearomatization of **2.59** by AzaH. PDA traces of enzymatic reaction and control reaction. 121

Figure 2.35: Oxidative dearomatization of **17** (**2.18**) by AzaH. PDA traces of enzymatic reaction and control reaction. 122

Figure 2.36: Oxidative dearomatization of **17** (**2.52**) by AzaH. PDA traces of enzymatic reaction and control reaction. 123

Figure 2.37: Oxidative dearomatization of **17** (**2.63**) by AzaH. PDA traces of enzymatic reaction and control reaction. 124

Figure 2.38: Oxidative dearomatization of **2.64** by AzaH. PDA traces of enzymatic reaction and control reaction. 125

Figure 2.39: Oxidative dearomatization of **2.57** by AzaH. PDA traces of enzymatic reaction and control reaction. 126

Figure 2.40: Oxidative dearomatization of **2.64** by AzaH. PDA traces of enzymatic reaction and control reaction. 127

Figure 2.41: Oxidative dearomatization of **2.72** by AzaH. PDA traces of enzymatic reaction and control reaction analyzed using UPLC Method B. 128

Figure 2.42: Oxidative dearomatization of **2.73** by AzaH. PDA traces of enzymatic reaction and control reaction analyzed using UPLC Method B. 129

Figure 2.43: Oxidative dearomatization of **2.74** by AzaH. PDA traces of enzymatic reaction and control reaction analyzed using UPLC Method B. Note that 25 μM enzyme was used to visualize product formation........ 130

Figure 2.44: Oxidative dearomatization of **2.75** by AzaH. PDA traces of enzymatic reaction and control reaction. 131

Figure 2.45: Oxidative dearomatization of **2.25a** by AzaH. PDA traces of enzymatic reaction and control reaction. 132

Figure 2.46: Oxidative dearomatization of **2.25b** by AzaH. PDA traces of enzymatic reaction and control reaction. 133

Figure 2.47: Oxidative dearomatization of sorbicillin (**2.15**) by AzaH. PDA traces of enzymatic reaction and control reaction........ 134

Figure 2.48: Oxidative dearomatization of **2.25d** by AzaH. PDA traces of enzymatic reaction and control reaction. 135

Figure 2.49: Oxidative dearomatization of **2.76** by AzaH. PDA traces of enzymatic reaction and control reaction. 136

Figure 2.50: Oxidative dearomatization of **2.25b** by AzaH. PDA traces of enzymatic reaction and control reaction. 137

Figure 2.51: Oxidative dearomatization of **2.77** by AzaH. PDA traces of enzymatic reaction and control reaction 138

Figure 2.52: Oxidative Dearomatization of **2.22d** by SorbC. PDA traces of enzymatic reaction and control reaction........ 139

Figure 2.53: Oxidative Dearomatization of **2.22e** by SorbC. PDA traces of enzymatic reaction and control reaction. 140

Figure 2.54: Oxidative dearomatization of **2.58** by SorbC. PDA traces of enzymatic reaction and control reaction. 141

Figure 2.55: Oxidative dearomatization of **2.75** by SorbC. PDA traces of enzymatic reaction and control reaction. 142

Figure 2.56: Oxidative dearomatization of **2.25a** by SorbC. PDA traces of enzymatic reaction and control reaction. 143

Figure 2.57: Oxidative dearomatization of **2.25b** by SorbC. PDA traces of enzymatic reaction and control reaction. 145

Figure 2.58: Oxidative dearomatization of **2.15** by SorbC. PDA traces of enzymatic reaction and control reaction. 146

Figure 2.59: Oxidative dearomatization of **2.25d** by SorbC. PDA traces of enzymatic reaction and control reaction. 148

Figure 2.60: Oxidative dearomatization of **2.76** by SorbC. PDA traces of enzymatic reaction and control reaction. 149

Figure 2.61: Oxidative dearomatization of **2.25c** by SorbC. PDA traces of enzymatic reaction and control reaction. 151

Figure 2.62: Oxidative dearomatization of **2.77** by SorbC. PDA traces of enzymatic reaction and control reaction. 152

Figure 2.63: PDA traces of racemic **2.13** obtained from IBX oxidative dearomatization, and **2.13** obtained from TropB-mediated oxidative dearomatization (Phenomenex Lux Cellulose-4; 90:10:0.1 water/MeCN/TFA, 1 mL/min)........ 153

Figure 2.64: PDA traces of racemic **2.81** obtained from IBX oxidative dearomatization, and **2.81** obtained from TropB-mediated oxidative dearomatization (Phenomenex Lux Cellulose-4; 90:10:0.1 water/MeCN/TFA, 1 mL/min)........ 154

Figure 2.65: PDA traces of racemic **2.97** obtained from IBX oxidative dearomatization, and **2.97** obtained from TropB-mediated oxidative dearomatization (Phenomenex Lux Cellulose-4; 90:10:0.1 water/MeCN/TFA, 1 mL/min)........ 155

Figure 2.66: PDA traces of racemic **2.80** obtained from IBX oxidative dearomatization, and **2.80** obtained from TropB-mediated oxidative dearomatization (CHIRALPAK® AD-H, 8% iPrOH, CO2, 3.5 mL/min)........ 156

Figure 2.67: PDA traces of racemic **2.84** obtained from IBX oxidative dearomatization, and **2.84** obtained from TropB-mediated oxidative dearomatization (CHIRALPAK® AD-H, 30% iPrOH, CO2, 3.5 mL/min)........ 157

Figure 2.68: PDA traces of racemic **2.13** obtained from IBX oxidative dearomatization, and **2.13** obtained from AzaH-mediated oxidative dearomatization (CHIRALPAK® AD-H, 4.5% iPrOH, CO2, 3.5 mL/min)........ 158

Figure 2.69: PDA traces of racemic **2.80** obtained from IBX oxidative dearomatization, and **2.80** obtained from AzaH-mediated oxidative dearomatization (CHIRALPAK® AD-H, 8% iPrOH, CO2, 3.5 mL/min). 159

Figure 2.70: PDA traces of racemic **2.20** obtained from IBX oxidative dearomatization, and **2.20** obtained from AzaH-mediated oxidative dearomatization (CHIRALPAK® AD-H, 30% iPrOH, CO2, 3.5 mL/min). Note two pairs of diastereomers were formed from the IBX dearomatization of ±**2.18**. 160

Figure 2.71: PDA traces of racemic **2.85** obtained from IBX oxidative dearomatization, and **2.85** obtained from AzaH-mediated oxidative dearomatization (CHIRALPAK® AD-H, 30% iPrOH, CO2, 3.5 mL/min). 161

Figure 2.72: PDA traces of racemic **2.99** obtained from LTA oxidative dearomatization, and **2.99** obtained from SorbC-mediated oxidative dearomatization (CHIRALPAK® AD-H, 10% *i*PrOH, CO_2, 3.5 mL/min). 163

Figure 2.73: PDA traces of racemic **2.88** obtained from LTA oxidative dearomatization, and **2.88** obtained from SorbC-mediated oxidative dearomatization (CHIRALPAK® AD-H, 10% *i*PrOH, CO_2, 3.5 mL/min). 164

Figure 2.74: PDA traces of racemic **2.98** obtained from LTA oxidative dearomatization, and **2.98** obtained from SorbC-mediated oxidative dearomatization (CHIRALPAK® AD-H, 10% *i*PrOH, CO_2, 3.5 mL/min). 165

Figure 2.75: PDA traces of racemic **2.89** obtained from LTA oxidative dearomatization, and **2.89** (>99% ee) obtained from SorbC-mediated oxidative dearomatization (CHIRALPAK® AD-H, 10% *i*PrOH, CO_2, 3.5 mL/min). 166

Figure 2.76: PDA traces of racemic **2.91** obtained from LTA oxidative dearomatization, and **2.91** (95% ee) obtained from SorbC-mediated oxidative dearomatization (CHIRALPAK$^{®}$ AD-H, 9.5% *i*PrOH, CO$_2$, 3.5 mL/min). 167

Figure 2.77: NMR spectra of synthetic compounds. 228

Figure 3.1: (A) Classical and biocatalytic methods enabled by directing groups. S = substrate, R = chemical reagent, DG = directing group. (B) Roles of directing groups in biocatalytic transformations including enhanced substrate binding, impact on conformation and substrate positioning within active site. 232

Figure 3.2: (A) Chemo- and biocatalytic methods for asymmetric oxidative dearomatization. (B) Sorbicillin derived natural products accessible by previous methodology and examples of *p*-quinol natural products that can be accessed via a directing-group strategy. 233

Figure 3.3: Synthetic route to ester and amide sorbicillin derivatives. 236

Several substrates were designed to probe the promiscuity of the FDMO SorbC towards substrates with varying C1 functional groups, including amides and esters of different chain length and saturation. Carolyn Suh completed the synthesis of the key carboxylic acid intermediate 3.23 through a Kolbe-Schmitt carboxylation of dimethyl resorcinol 3.22.26 Alternate routes to carboxylic acid 3.23 were attempted but were unsuccessful. For example, Pinnick oxidation of the unprotected aldehyde resulted in low conversion or oxidation of the aromatic ring. Although the

Figure 3.4: Routes to crotyl ester resorcinol compounds with varying functional groups at C2, C4 and C5. 236

Figure 3.5: Impact of C1 substituent on SorbC activity. 238

Figure 3.6: (A) The homology model of SorbC based on the TropB crystal structure. (B) Native substrate, methyl ester and crotyl ester and the corresponding K_M and K_d values. K_d values obtained by Attabey Rodríguez Benítez, homology model constructed by Troy Wymore...................... 239

Figure 3.7: Top row: homology model of SorbC (gray surface) with (A) sorbicillin (**3.13**), cyan sticks, (B) methyl ester **3.28** and (C) crotyl ester **3.26** in the major reactive pose observed in docking studies. Bottom row: Plots of the change in energy of poses relative to the lowest energy structure with (D) sorbicillin (**3.13**), (E) methyl ester **3.28** or (F) crotyl ester **3.26.**.................. 240

Figure 3.8: Values given are total turnover numbers (TTNs) of each enzyme/substrate pair. Reaction conditions: 2.5 mM substrate, 2.5 μM SorbC, 1 mM $NADP^+$, 5 mM glucose-6-phosphate (G6P), 1 U ml^{-1} glucose-6-phosphate dehydrogenase (G6PDH), 50 mM potassium phosphate buffer, pH 8.0, 30 °C, 15% v/v DMSO 1 h.. 243

Figure 3.9: Application of directing group strategy for preparative-scale oxidative dearomatization. (A) Evaluation of substrate scope and reaction enantioselectivities. Yields for racemic standard synthesis in grey. LTA = lead tetraacetate. (B) Removal of directing group through palladium-catalyzed decrotylation. (C) Elaboration of dearomatized product through [4+2] cycloaddition.. 245

Figure 3.10: A) Michaelis-Menten plot of SorbC reactions with native substrate sorbicillin (**3.13**). B) Standard curve of sorbicillin (**3.13**). 269

Figure 3.11: A) Michaelis-Menten plots of SorbC reactions with substrate **3.26**. B) Standard curve substrate **3.26**. 270

Figure 3.12: Substrate calibration curves. 277

Figure 3.13: UPLC-PDA trace of SorbC reactions with **Entry 3** and NEC............................. 278

Figure 3.14: UPLC-PDA trace of SorbC reactions with **3.25** and NEC.................................. 279

Figure 3.15: UPLC-PDA trace of SorbC reactions with **Entry 3** and NEC. 280

Figure 3.16: UPLC-PDA trace of SorbC reactions with **3.27** and NEC. 281

Figure 3.17: UPLC-PDA trace of SorbC reactions with **3.29** and NEC. Byproduct annotated with an asterisk. 282

Figure 3.18: UPLC-PDA trace of SorbC reactions with **3.30** and NEC. Byproduct annotated by an asterisk. 283

Figure 3.19: UPLC-PDA trace of SorbC reactions with **3.47** and NEC. Byproduct annotated with an asterisk. 284

Figure 3.20: UPLC-PDA trace of SorbC reactions with **3.72** and NEC. Byproduct annotated with an asterisk. 285

Figure 3.21: UPLC-PDA trace of SorbC reactions with **3.73** and NEC. 286

Figure 3.22: UPLC-PDA trace of SorbC reactions with **31** and NEC. Byproduct annotated with an asterisk. 287

Figure 3.23: UPLC-PDA trace of SorbC reactions with **3.84** and NEC. 288

Figure 3.24: UPLC-PDA trace of SorbC reactions with **3.36** and NEC. Impurity from SM denoted with #. 289

Figure 3.25: UPLC-PDA trace of SorbC reactions with **3.37** and NEC. 290

Figure 3.26: UPLC-PDA trace of SorbC reactions with **3.69** and NEC. Impurity from starting material denoted with a #. 291

Figure 3.27. With a subset of substrates, in addition to the expected product a second peak with the same *m/z* was observed (See Figure 3.29). This byproduct, formed in SorbC reactions, was not found in reactions with IBX or LTA. Attempts to isolate and characterize the material corresponding to the peak marked with an asterisk either directly from enzymatic reactions or following acylation did not produce meaningful quantities of material. Preparative HPLC of the crude reaction mixture did allow for isolation of the material, as judged by UPLC-PDA analysis of the resulting fractions; however, this material accounted for little of the mass balance of the reaction mixture (<0.1 mg isolated from 10 mg-scale reactions) insufficient material was obtained for NMR analysis. 292

Figure 3.28: (A) LC-MS trace comparing reaction of **3.26** with SorbC and IBX. (B) MS/MS spectra comparing the products of the SorbC reaction and the IBX reaction. Note the second IBX product does not correspond to the more nonpolar SorbC product. 293

Figure 3.29: SFC-UV-Vis trace of Pd(OAc)$_4$-generated ±**3.79** and SorbC-generated **3.79**. 294

Figure 3.30: SFC-UV-Vis trace of Pb(OAc)$_4$-generated ±**3.80** and SorbC-generated **3.80**. 295

Figure 3.31: SFC-UV-Vis traces of Pb(OAc)$_{4-}$ and SorbC-generated **3.81**........ 296

Figure 3.32: SFC-UV-Vis trace of Pb(OAc)$_4$ and SorbC generated **3.82**. 297

Figure 3.33: SFC-UV-Vis trace of Pb(OAc)$_4$ and SorbC generated **3.83.** 298

Figure 3.34: NMR spectra of synthetic compounds. 323

Figure 4.1: Optimization tables for whole-cell oxidative dearomatization. Left: with flash-frozen *E. coli* cells; right: with lyophilized *E. coli* cells. 327

Figure 4.2: Set-up for gram-scale whole-cell oxidative dearomatization. After the reaction is complete, the mixture is filtered and the filtrate is extracted with (3:1) EtOAc and *i*PrOH. 328

Figure 4.3: One-pot syntheses of secondary metabolites featuring biocatalytic oxidative dearomatization as a key synthetic step stipitaldehyde, urea sorbicillinoid and azaphilone from *Nigrospora* sp. YE3003. 331

Figure 4.4: PDA traces of racemic **4.13** obtained from IBX oxidative dearomatization, and **4.13** obtained from AzaH-mediated oxidative dearomatization (CHIRALPAK® AD-H, 30% iPrOH, CO_2, 3.5 mL/min). 338

Figure 4.5: NMR spectra of synthetic compounds. 342

Figure 5.1: (A) Biologically active azaphilone natural products feature both the *R*- and *S*-configuration at the C7 stereocenter.[1,4,6] Biocatalytic oxidative dearomatization gives access to either enantiomer via AzaH or AfoD mediated oxidation. (A) Approaches to enabling biocatalytic stereodiversity. 344

Figure 5.2: A) Sequence similarity network (SSN) of FAD-dependent monooxygenases (Pfam01494) using a sequence alignment score of 110. B) Results of expression, activity with model substrate **5.14** or **5.16****, site- and stereoselectivity of enzymes chosen from the SSN in panel A. *FDMO4 demonstrated <10% conversion by UPLC with substrate **5.16**. C) Selected clusters from a more stringent SSN generated with an alignment score of 150 and corresponding analysis of the multisequence alignment of each cluster. Figure by Attabey Rodrìguez Benìtez. 348

Figure 5.3: % conversion by AzaH and AfoD of potential common intermediates. 350

Figure 5.4: First-generation synthetic route[25] to common intermediate **5.22** through bromination and iterative Shonogashira couplings. 351

Figure 5.5: Second-generation synthetic route to common intermediate **5.22** through 1,2-addition and reduction. 352

Figure 5.6. Reaction conditions surveyed to improve yield and chemoselectivity of 1,2-addtion. 352

Figure 5.7: Conditions assayed for MOM-deprotection of **5.40**.......... 353

Figure 5.8: 3-step one-pot synthetic of aryl iodide **5.44**. 354

Figure 5.9: Retrosynthetic analysis for trichofectin. 354

Figure 5.10: Total synthesis of (*S*)- and (*R*)-trichoflectin. Inset: Calculated and measured CD data for (*S*)- and (*R*)-trichoflectin. *NADPH recycling system: G6P (2 equiv), NADP$^+$ (0.4 equiv), G6PDH (1 U/mL). 355

Figure 5.11: Total synthesis of deflectin and calculated (red) and measured (black) CD-spectra. 357

Figure 5.12: Retrosynthetic analysis for lunatoic acid. 358

Figure 5.13: Total synthesis of lunatoic acid A. Inset: calculated (red) and measured CD spectra of lunatoic acid A methyl ester (**5.55**). 359

Figure 5.14: Purified AzaH and AfoD. Approximately 5 µL of 1.25 µM each protein was loaded onto an MiniPROTEAN TGX Precast 4-15% SDS-PAGE gel (Bio-Rad). The gel was stained with Quick Coomassie stain (Anatrace) and visualized with the Azure Gel Imaging System. The relative apparent masses are consistent with the predicted estimates. 374

Figure 5.15: UV-vis spectra of native and denatured FDMOs AzaH and AfoD 375

Figure 5.16: Calibration curves for substrates. 380

Figure 5.17: Oxidative dearomatization of **5.18** by AfoD and AzaH. PDA traces of enzymatic reaction and control reaction. (Table 1, entry 2). SM = starting material, INT = intermediate, PRD = product, IS = internal standard. The anionic form of the intermediate elutes near the solvent front. 382

Figure 5.18: Oxidative dearomatization of **5.17** by AfoD and AzaH. PDA traces of enzymatic reaction and control reaction. 383

Figure 5.19: Oxidative dearomatization of **5.19** by AfoD and AzaH. PDA traces of enzymatic reaction and control reaction. 385

Figure 5.20: Oxidative dearomatization of **5.20** by AfoD and AzaH. PDA traces of enzymatic reaction and control reaction. 386

Figure 5.21: Oxidative dearomatization of **5.57** by AfoD and AzaH. PDA traces of enzymatic reaction and control reaction. 388

Figure 5.22: Oxidative dearomatization of **5.21** by AfoD and AzaH. PDA traces of enzymatic reaction and control reaction. 390

Figure 5.23: Oxidative dearomatization of **5.22** by AfoD and AzaH. PDA traces of enzymatic reaction and control reaction. Two wavelengths are shown to visualize product. 392

Figure 5.24: PDA traces of racemic **5.46** obtained from a 1:1 mixture of the compound generated using AzaH and AfoD, (*S*)-**25** obtained from AfoD-mediated oxidative dearomatization, (*R*)-**5.46** obtained from AzaH-mediated oxidative dearomatization (CHIRALPAK® AD-H, 30%, CO_2, 3.5 mL/min). 393

Figure 5.25: PDA traces of racemic **5.48** obtained IBX-mediated oxidative dearomatization, (*S*)-**5.48** obtained from AfoD-mediated oxidative dearomatization, (*R*)-**5.48** obtained from AzaH-mediated oxidative dearomatization (CHIRALPAK® AD-H, 30%, CO_2, 3.5 mL/min). 394

Figure 5.26: NMR spectra of synthetic compounds. 406

Figure 6.1. (A) General scheme for oxidative dearomatization (OD). (B) Mechanism for I(III)-mediated OD. (C) Abbreviated mechanism for FMDO-mediated OD. (D) Proposed single-electron OD. 410

Figure 6.2: A) Proposed catalytic cycle for PCOD. B) Mechanistic studies. Inset: Stern-Vollmer plots. Standard conditions: 0.4 mol% FMN, 50 mM tris pH 8.0 buffer, rt, blue LEDs 2h. 413

Figure 6.3: Substrate table for photocatalytic oxidative dearomatization. 416

Figure 6.4: Absorbance and emission spectra of FMN. 420

Figure 6.5: Emission quenching of FMN in water in the presence of 0 to 2.5 mM substrate **6.13** under N_2 421

Figure 6.6: Stern-Volmer quenching experiments of FMN with **6.13** under N_2. 421

Figure 6.7: Emission quenching of FMN in water in the presence of 0 to 2.5 mM substrate **6.13** under air. 421

Figure 6.8: Stern-Volmer quenching experiments of FMN with **6.13** under air 422

Figure 6.9: Emission quenching of FMN in water in the presence of 0 to 25 mM tris buffer, pH 8.0 under N_2. 422

Figure 6.10: Stern-Volmer quenching experiments of FMN with tris under N_2 422

Figure 6.11: Emission quenching of FMN in water in the presence of 0 to 25 mM tris buffer, pH 8.0 under air. 423

Figure 6.12: Stern-Volmer quenching experiments of FMN with **t**ris under air. 423

Figure 6.13: Co-plot of Stern-Volmer quenching experiments of FMN with quenchers **6.13** and Tris buffer under aerobic or anaerobic conditions. 423

Figure 6.14: Summary of the luminescence quenching data for the evaluated quenchers. Rates were calculated according to Equation 1, where I_0/I is the emission intensity ratio, τ_0 is the lifetime of the photosensitizer excited state, k_q is the rate of quenching by quencher Q, The lifetime of the emissive excited state of the FMN in the absence of a quencher (τ_0) was estimated to be 4.4 ns.[24] 424

Figure 6.15: LC-MS trace of photocatalytic reaction in unlabeled water. 425

Figure 6.16: LC-MS trace of photocatalytic reaction in H_2O^{18}. 426

Figure 6.17: LC-MS trace of photocatalytic reaction with 1 equiv H_2O^{18}. 427

Figure 6.18: NMR spectra of synthetic compounds. 433

List of Abbreviations

ADH – alcohol dehydrogenase

AIBN – azobisisobutyronitrile

BVMO – Baeyer-Villiger monooxygenase

CAM – cerium ammonium molybdate

CDMO – cyclododecanone monooxygenase

CHAO – cyclohexamine oxygenase

DMSO – dimthylsuloxide

DNP – 2,4-dinitrophenol

EAS – electrophilic aromatic substitution

ER – ene-reductases

ESI – electrospray ionization

EWG – electron withdrawing group

FAD – flavin adenine dinucleotide

FDMO – flavin-dependent monooxygenase

FMN- flavin mononucleotide

G6P – glucose-6-phosphate

IBX – 2-iodoxybenzoic acid

LTA – lead tetraacetate

MAO – monoamine oxidases

MS – mass spectrometer

NADH – Nicotinamide adenine dinucleotide

NADPH - Nicotinamide adenine dinucleotide phosphate

OD – oxidative dearomatization

OYW – Old Yellow Enzyme

PDA – photodiode array

PEG – polyethylene glycol

PHBH – *p*-hydroxybenzoate 3-hydroxylase

PIDA – (diacetoxyiodo)benzene

PIFA – (Bis(trifluoroacetoxy)iodo)benzene

PSET – photo-initiated single-electron transfer

SSN – sequence similarity network

TEMPO – (2,2,6,6-tetramethylpiperidin-1-yl)oxidanyl

TTN – total turnover number

UPLC – ultra performance liquid chromatography

WC – whole cell

λ – wavelength

Abstract

Natural products, compounds synthesized by all kingdoms of life, offer a wealth of structural diversity, giving rise to an array of biological activities. For centuries chemists looked to nature for the discovery of new medicines. More recently, chemists have begun to employ Nature's tools for complex molecule synthesis in the generation of novel compounds. My thesis describes the development of new oxidative biocatalytic methods and application of these methods in the synthesis of biologically active molecules.

Chapter 2 describes the substrate scope and selectivity of three wild type flavin-dependent monooxygenases enzymes. Together this enzyme suite provides complementary catalysts for asymmetric oxidative dearomatization.

We have developed a positioning group strategy to overcome substrate scope limitations with one of our catalysts, described in Chapter 3. We have engineered substrates to allow for improved turnover, thus, enabling access to a wide array of *o*-quinol containing natural products. Pairing experimental data with computational and biophysical characterization of the substrate-protein interactions further informed our understanding of the role of the positioning group.

A scalable platform for biocatalytic oxidative dearomatization has been developed allowing for gram-scale reactions, described in Chapter 4. We have applied this method in the synthesis of a number of natural products in one-pot cascades from simple arene starting materials, using oxidative dearomatization as the key synthetic step.

Chapter 5 describes our work to identify stereocomplementary homologs of these monooxygenases which have allowed access to enantiomeric intermediates that can be elaborated to various azaphilone natural products. Specifically, the total syntheses of two members, trichoflectin and lunatoic acid A, are described.

CHAPTER 1: Introduction

Portions adapted with permission from "Flavin-dependent biocatalysts in synthesis" *Tetrahedron* **2019,** *75*, 1115–1121.

Chapter 1.1: Flavin Biocatalysts in Complex Molecule Synthesis

Flavin-dependent enzymes are essential in primary metabolism in all kingdoms of life, performing a plethora of chemical reactions.[1] The versatile flavin cofactor that defines this enzyme family is capable of mediating both oxidative and reductive processes depending on the form of the cofactor employed.[1] Further diversifying the chemistry possible with flavoproteins, Nature has evolved flavin-dependent enzymes to carry out specialized chemistry within secondary metabolic pathways.[2] Chemists have begun to tap into this incredible set of catalysts, exploring the chemistry possible with various classes of flavin-dependent enzymes. These endeavors capture the advantages and challenges in biocatalytic synthesis.

Selectivity, tunability, safety and sustainability can motivate chemists to choose biocatalytic methods over traditional chemical catalysts and reagents.[3] For flavin-dependent enzymes, chemo-, site- and stereoselectivity can often be achieved at a higher level or with orthogonal selectivity to that attainable with small molecule reagents.[4] Mediating oxidation reactions with flavin-dependent enzymes presents the opportunity to use molecular oxygen as the stoichiometric oxidant, and similarly economical and abundant stoichiometric reductants in reductive transformations.[1] Additionally, the ability to carry out reactions in water without the need for extreme temperatures or a controlled atmosphere adds to the procedural simplicity of

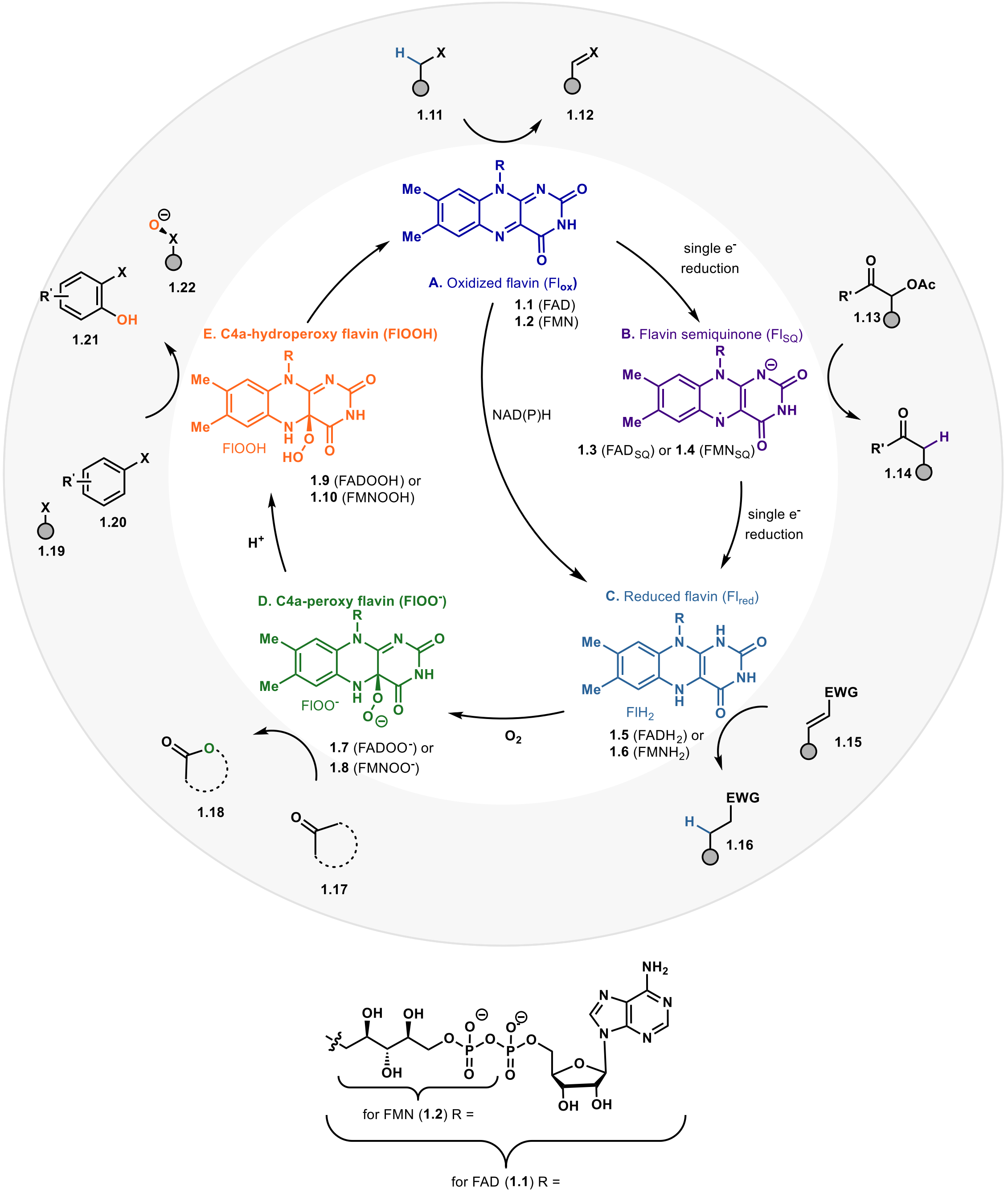
1.11
1.12
A. Oxidized flavin (Fl_{ox})
1.1 (FAD)
1.2 (FMN)
single e⁻ reduction
B. Flavin semiquinone (Fl_{SQ})
1.3 (FAD_{SQ}) or 1.4 (FMN_{SQ})
1.13
1.14
NAD(P)H
single e⁻ reduction
C. Reduced flavin (Fl_{red})
FlH_2
1.5 ($FADH_2$) or
1.6 ($FMNH_2$)
EWG
1.15
1.16
O_2
D. C4a-peroxy flavin ($FlOO^-$)
$FlOO^-$
1.7 ($FADOO^-$) or
1.8 ($FMNOO^-$)
1.17
1.18
H^+
E. C4a-hydroperoxy flavin (FlOOH)
FlOOH
1.9 (FADOOH) or
1.10 (FMNOOH)
1.19
1.20
1.21
1.22
for FMN (1.2) R =
for FAD (1.1) R =

Figure 1.1: Catalytically active species of flavin (flavin-adenine dinucleotide and flavin mononucleotide) referenced in this review. (A) Fl_{ox} can act as a one or two electron acceptor to afford the semiquinone or reduced flavin (Fl_{red}). (B) Fl_{red}, in the context of ene-reductases, can perform the two-electron reduction of activated olefins. Fl_{red} may also react with molecular oxygen to form the C4a-peroxy (D) or hydroperoxy flavin (E) which can be the source of an oxygen atom for incorporation into organic substrates. Elimination of peroxide affords Fl_{ox}.

biocatalytic chemistry. Despite these advantages, synthetic chemists have been slow to fully embrace biocatalysis in preparative-scale synthesis. The barriers to incorporating flavin-dependent biocatalysts in a synthetic route can include access to the biocatalyst, limited or unknown substrate scope of an enzyme, or catalyst stability. As the biocatalysis community expands, these obstacles are disappearing. More enzymes are commercially available than ever, and the technology for evolving proteins to access variants with an altered substrate scope and increased stability has been established.[5]

Decades of experimental and computational investigation of flavin-dependent enzyme mechanisms have provided a framework for understanding the reactions possible from each flavin state. Figure 1 illustrates a portion of the flavin states relevant to flavoprotein chemistry.[6] Starting from the oxidized form of the cofactor flavin-adenine dinucleotide (FAD, **1.1**) or flavin mononucleotide (FMN, **1.2**) addition of a single electron affords the anionic flavin semiquinone

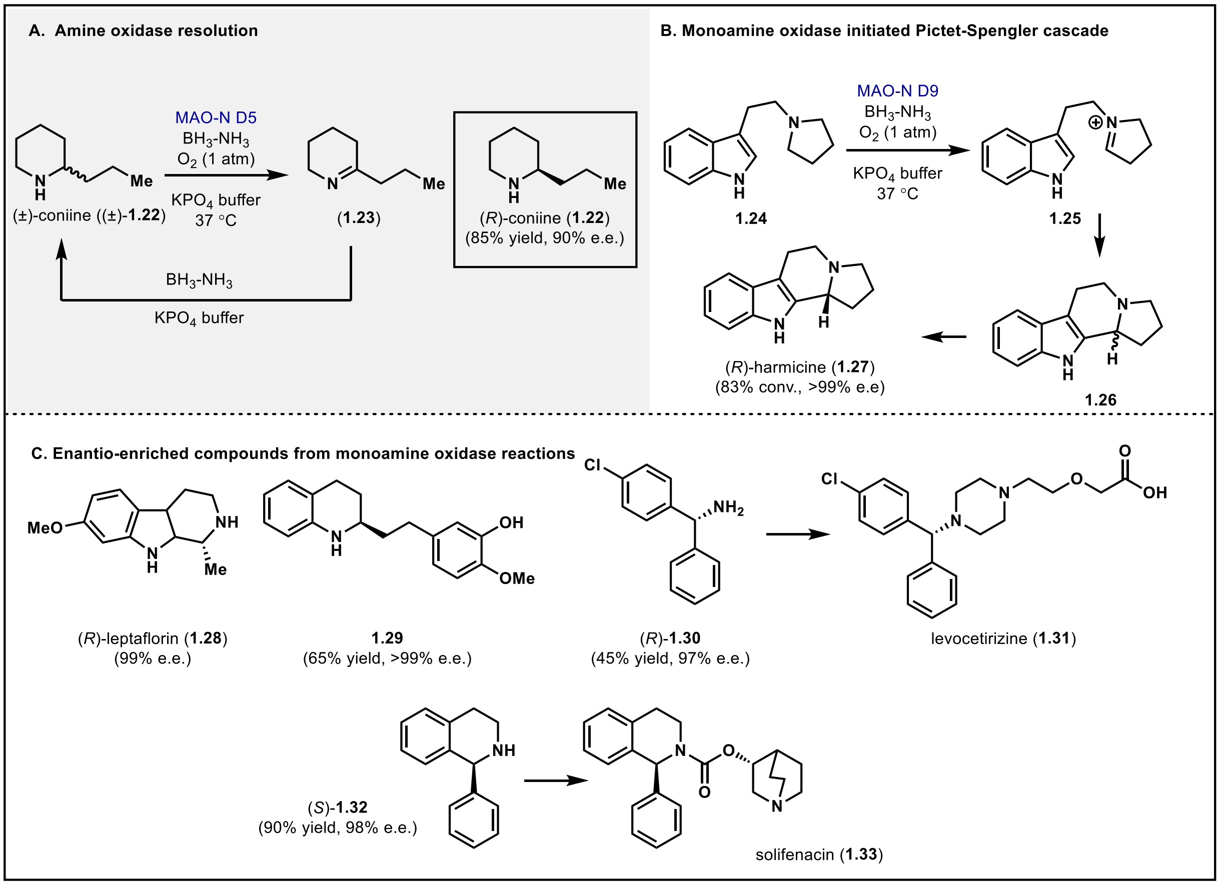
A. Amine oxidase resolution
MAO-N D5
BH3-NH3
O2 (1 atm)
KPO4 buffer
37 °C
(±)-coniine ((±)-1.22)
(1.23)
(R)-coniine (1.22)
(85% yield, 90% e.e.)
BH3-NH3
KPO4 buffer
B. Monoamine oxidase initiated Pictet-Spengler cascade
MAO-N D9
BH3-NH3
O2 (1 atm)
KPO4 buffer
37 °C
1.24
1.25
1.26
(R)-harmicine (1.27)
(83% conv., >99% e.e)
C. Enantio-enriched compounds from monoamine oxidase reactions
(R)-leptaflorin (1.28)
(99% e.e.)
1.29
(65% yield, >99% e.e.)
(R)-1.30
(45% yield, 97% e.e.)
levocetirizine (1.31)
(S)-1.32
(90% yield, 98% e.e.)
solifenacin (1.33)

Figure 1.2: Monoamine oxidases (MAOs) in the synthesis of enantio-enriched amines. (A) Dynamic resolution of amines using MAO-N variants and a reducing agent. (B) Monoamine oxidase initiated Pictet-Spengler cascade for the synthesis of (R)-harmicine (27).[9]

(**1.3**). Further one electron reduction of the semiquinone form (**1.3**) or two electron reduction of **1.1** or **1.2** provides access to $FADH_2$ (**1.5**) or $FMNH_2$ (**1.6**), respectively. NAD(P)H is the most common native cofactor used for the reduction of FAD, however this substrate is costly and unstable. As such, a number of NAD(P)H recycling systems have been developed for reactions which generate FAD from $FADH_2$. This reduced form of the cofactor can engage molecular oxygen to form peroxyflavin **1.7**, which upon protonation yields hydroperoxyflavin **1.9**. The protein scaffold and reaction conditions dictate the forms of the cofactor accessible and the chemistry that can be carried out in a given system. Presented herein are examples of flavin-dependent enzymes in organic synthesis. Examples are organized according to the form of the flavin cofactor involved in each reaction.

Oxidized flavin (Fl_{ox}). The oxidized form of the flavin cofactor, FAD or FMN (Fl_{ox} see **1** and **2**), can participate in reduction of substrates (Figure 1.1A). In the context of complex molecule synthesis, the chemistry of Fl_{ox} has been most widely exploited in the synthesis of imines from amine substrates by monoamine oxidases (MAOs).[7] MAOs have been applied to the dynamic resolution of racemic amines as outlined in Figure 1.2A.[8,9] MAOs are often selective for a single enantiomer of the amine substrate, enriching for the enantiomer not oxidized by the biocatalysts. Coupling the oxidase with a reducing reagent leads to a dynamic resolution. For example, Turner and coworkers have engineered a MAO from *Aspergillus niger* to create a panel of MAO variants with complementary substrate scope.[9] By applying both directed evolution and rational design strategies, useful catalysts for the resolution of alkyl, cyclic and benzylic amines have been generated.[9-11]

The utility of these biocatalysts has been demonstrated through the synthesis of natural products as well as enantioenriched precursors to active pharmaceutical ingredients (APIs). Notably, a number of enantioenriched alkaloid natural products were obtained through this deracemization approach including the neurotoxin (*R*)-coniine (**1.22**), plant alkaloid (*R*)-leptaflorin (**1.28**) and anti-Leishmania compound (*R*)-harmicine (**1.27**) (Figure 1.2).[9] This panel of products demonstrate the stereochemical preference of MAO-N variants for the (*S*)-enantiomer of these amine substrates, thus enriching for the (*R*)-enantiomer of each amine. Further studies have demonstrated the potential for MAO-N variants to enrich for the (*S*)-enantiomer with specific substrate classes[8] or through protein engineering.[9] MAO-mediated deracemization of complex amines provides a valuable alternative to traditional approaches, which require asymmetric installation of the amine moiety at an earlier stage in the synthesis. In addition to the resolution of alkaloid natural products, MAO deracemization has been used to access enantioenriched intermediates in the synthesis of amine-containing drugs. Specifically, the MAO-D11 variant can discriminate between two similar aryl groups to afford 4-chlorobenzhydrylamine (**1.30**) in 97% ee, which can subsequently be elaborated to the antihistamine drug, levocetirizine (**1.31**).[8] Similarly, solifenacin precursor (*S*)-tetrahydroisoquinoline **1.32** can be accessed in 98% ee. by the same MAO-N variant.[8] Amine oxidases beyond MAO-N have also been explored for synthetic applications. For example, enantio-enriched tetrahyroquinolines such as **1.29** can be obtained through deracemization with cyclohexylamine oxidase (CHAO).[12] MAOs can also be applied beyond simple deracemization reactions. For example, MAO-generated iminium ions such as **1.25** can be intercepted in a Pictet-Spengler type bond forming event (Figure 1.2B),[9] and cyclic amines can be aromatized using MAOs.[13] These are just select examples of the synthetic potential of these enzymes, in an area ripe for innovation.

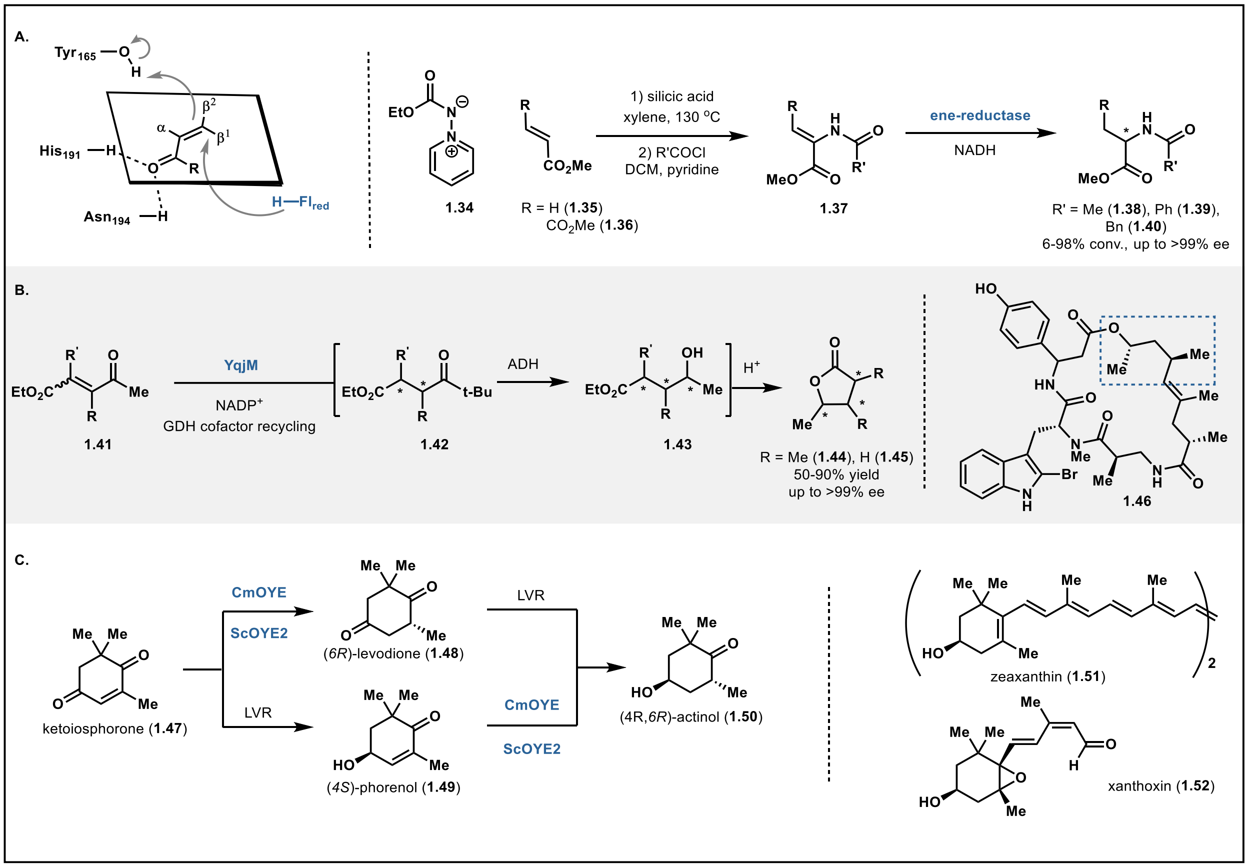
A.
Tyr165
His191
Asn194
H—Flred
1.34
R = H (1.35)
CO2Me (1.36)
1) silicic acid
xylene, 130 °C
2) R'COCl
DCM, pyridine
1.37
ene-reductase
NADH
R' = Me (1.38), Ph (1.39),
Bn (1.40)
6-98% conv., up to >99% ee
B.
1.41
YqjM
NADP+
GDH cofactor recycling
1.42
ADH
1.43
H+
R = Me (1.44), H (1.45)
50-90% yield
up to >99% ee
1.46
C.
ketoiosphorone (1.47)
CmOYE
ScOYE2
LVR
(6R)-levodione (1.48)
(4S)-phorenol (1.49)
(4R,6R)-actinol (1.50)
zeaxanthin (1.51)
xanthoxin (1.52)

Figure 1.3: Reactions with ene-reductases. (A) Chemoenzymatic synthesis of amino acid derivatives via an ene-reductase-catalyzed hydrogenation.[21] (B) One-pot three-step cascade to enantioenriched γ-butyrolactones.[22] (C) One-pot, two-step cascade to generate actinol (**1.50**).[23]

Fl$_{SQ}$. Single electron reduction of Fl$_{ox}$ provides the flavin semiquinone (Fl$_{SQ}$, **1.3**, Figure 1.1). Fl$_{SQ}$ has been extensively studied in a number of flavin-dependent enzymes, including glucose oxidase[14] and methanol oxidase.[15] Despite the accessibility of the flavin radical, there have been few reports of synthetic methods that proceed via a single electron mechanism. Recently, Sandoval and coworkers reported the ene-reductase mediated radical dehalogenation of α-bromo esters.[16a] They propose a mechanism in which reduced flavin (FMNH$_2$, **1.6**) performs a single electron transfer to the substrate; the resulting flavin semiquinone serves as a hydrogen atom donor to afford the dehalogenated products. Following this work, Biegasiewicz and coworkers applied this approach to access enantioenriched lactams from unsaturated α-halo amides.[16b] With the groundwork laid by these reports, we anticipate future biocatalytic methods will take advantage of radical flavin species.

Fl$_{\mathbf{red}}$. Ene-reductases (ERs) are a large class of enzymes characterized by their capacity to reduce activated olefins including enones, enals, unsaturated carboxylic acids, esters and cyclic imides.[17] Enantioenriched amino acid derivatives, important polymer precursors, and chiral building blocks have been synthesized using ERs as a key synthetic step.[17] The Old Yellow Enzyme (OYE) family of flavoproteins belong to this class and have been employed in a large number of reaction cascades and industrially-relevant processes due to their substrate promiscuity and excellent stereoselectivity.[18,19] The mechanism of OYEs in the asymmetric reduction of olefins has been well-studied,[20] and is understood to involve the delivery of a hydride from flavin mononucleotide ($FMNH_2$, **1.6**) to the β-position of the substrate which is coordinated by a strictly conserved histidine/asparagine or histidine/histidine pair (Figure 1.3A). To arrive at the product, tyrosine protonates the alpha position on the face opposite to the flavin cofactor.[20]

Stueckler and coworkers devised an approach that highlights the utility of this class of flavoproteins in the synthesis of stereochemically dense small moleucles.[21] They reported a chemoenzymatic route to *N*-acyl amino acid derivatives in which *N*-acetylamino acrylic esters were reduced in modest yields by OYE1-3, YqjM and OPR1 to afford products in 85-95% ee (Figure 1.3A, see **1.38-1.40**).[21] Only terminal olefins (such as **1.35**) were productive substrates, as compounds with additional substitution of the double bond gave no conversion to the corresponding saturated product with any of the enzymes tested. However, one exception to this rule was identified; diester **1.36** was converted quantitatively and with perfect stereoselectivity to afford the (*S*)-isomer of **1.38** by OYE1 and OYE3. Sterically bulky amides were also converted to products in good yields and enantioselectivities.

In 2014, Classen and coworkers reported a chemoenzymatic cascade which afforded access to γ-butyrolactones.[22] Employing YqjM, a homolog of OYE involved in *E. coli* response to oxidative stress, substrates such as **1.41** were reduced to generate a substrate which could be intercepted by a second enzyme (Figure 1.3B). For example, in a first step, α,β-unsaturated 4-oxo-esters (**1.41**), which can be accessed through a Wittig olefination of commercially available starting materials, undergo a formal anti-addition of hydrogen by enolate reductase to afford *anti*- or *syn*-γ-ketoester products (see **1.42**). Whereas the (*E*)-isomer typically gives rise to the *anti*-product and the (*Z*)-isomer gives rise to *syn*-product, this trend did not extend to all cases. Although a predictive model for YqjM stereoselectivity has not been reported to date, the authors employed deuterium-labeling and docking studies to understand the irregularities in stereoselectivity. Substrate activation occurs though hydrogen bonding to the most electron-withdrawing substituent. Umpolung selectivity was observed for substrates with particularly sterically demanding substituents proximal to the most electron-withdrawing substituent. Following YqjM reduction, intermediate **1.42** can be intercepted by an alcohol dehydrogenase (ADH) in a chemo- and stereoselective reduction of the ketone group and subsequent acid-catalyzed cyclization afford the lactone product **1.44** with high ee (>98%) and moderate to good yields. This method provides access to trisubstituted lactones with three contiguous stereocenters. Classic synthetic routes to this motif require multiple steps, and a general method for accessing various substitution patterns and stereoisomers has yet to be reported, as most methods require chiral pool reagents as a starting point.

A similar strategy was employed by Horita in the chemoenzymatic synthesis of enantioenriched actinol (**1.50**) from ketoisophorone (**1.47**).[23] (4*R*,6*R*)-actinol (**1.50**) is a valuable chiral building block that serves as an intermediate in the synthesis of carotenoids such as xanthoxin, zeaxathin. The biocatalytic cascade begins with the *Candida macedoniensis* OYE (CmOYE) reduction of ketoisophorone (**1.47**) to (6*R*)-levodione (**1.48**) followed by the reduction to actinol (**1.50**) by (6*R*)-levodione reductase. However, when these enzymes were implemented in a one-pot system, the authors noted 67% conversion to the final product with the balance of the material accumulating as an intermediate, (4*S*)-phorenol (**1.49**). This was attributed to the low activity of CmOYE on this reduced species. By obtaining crystal structures with and without substrate mimic *p*-hydroxybenzaldehyde bound, the authors identified a flexible loop that appeared to act as a lid on the active site when substrate was present. Modeling of (4*S*)-phorenol in the active site showed potential steric clashes with the gem-dimethyl group at C6 and Phe250, Pro295, and Phe296. These residues were individually mutated to Gly and each of these variants exhibited higher catalytic activity with phorenol, although substitution of these Phe residues also led to lower activity with ketoisophorone (**1.47**). The CmOYE(P295G) variant was used in the one-pot, two-step biocatalytic reaction to afford actinol (**1.50**) in 90% yield.

Innovations in the application of ERs continue to be reported. For example, Hartwig recently disclosed a ‘cooperative’ chemoenzymatic reaction in which a mixture of E/Z olefins are isomerized photocatalytically to the (*E*)-isomer preceding a stereoselective ER-mediated reduction.[24]

C4a-peroxy flavin (FlOO$^-$): Flavin-dependent monooxygenases are a large family of enzymes that can be grouped into classes A-H based on structure and activity.[25] Monooxygenases access the reactive flavin intermediate from reactions of $FADH_2$ with molecular oxygen. The reaction between $FADH_2$ and O_2 can form peroxyflavin (**1.7**, Figure 1.1), providing a nucleophilic source of oxygen (Figure 1.4A). In these reactions, one atom of oxygen is incorporated into the organic substrate, and the second atom of oxygen from O_2 is lost as water. Within this family, Baeyer-Villiger monooxygenases (BVMOs)[26] have received the most attention from the synthetic community. In addition to their canonical capacity to perform stereoselective oxidation of carbonyl containing compounds, BVMOs are also able to perform epoxidations[27], sulfoxidations[28,29] and amine oxidations[30] with excellent stereocontrol. BVMOs have been employed in the chemoenzymatic synthesis of important pharmaceutical agents, such as modafinil[31] and esomeprazole,[32] and in the dynamic kinetic resolution of chiral building blocks employed in the synthesis of epothilones[33] and isocoumarins.[34] The process relevance of these transformations was highlighted in a 200 L-scale whole-cell biotransformation.[35]

BVMOs have been employed in chemoenzymatic cascades to generate enantioenriched products. Fink reported the chemoenzymatic synthesis of the aroma compound *Aerangis* lactone.[36] Rh/C hydrogenation in continuous flow of cyclopentenone **1.54** afforded selectively the *cis*-cyclopentanone **1.55** (Figure 1.4B). Acid-mediated isomerization gave rise to the theromodynamically favored *trans*-isomer. Crude cell extract of cyclododecanone monooxygenase (CDMO) catalyzed the kinetic resolution of **1.55** with >99% ee. Cyclopentanone monooxygenases (CPMO) afforded the *trans*-lactone **1.58** in >99% ee. Using 2% w/v biocatalyst at 20 mM or 15 mM substrate concentration afforded lactone product **1.58** in 27% or 28% yield, respectively.

The utility of BVMOs to generate chiral building blocks for multistep synthesis of valuable complex molecules has been explored by a number of groups. Mihovilovic et al. reported the formal chemoenzymatic synthesis of tetrahydrofuran-based natural products using BVMOs as a key synthetic step (Figure 4C).[37] [4+3] cycloaddition of furan and tetrabromoacetone followed by reductive dehalogenation afforded prochiral oxabicycloketone **1.59**. This bicycle was subjected to fermentation with cyclopentanone monooxygenase (CPMO)-expressing *E. coli.* Using substrate feeding and product removal (SFPR) allowed for a 70% isolated yield of ester **1.60** in 95% ee. Subsequent chemical steps allowed the authors to intercept pivotal intermediates in the total syntheses of showdomycin (**1.62**), *trans*-kumausyne (**1.66**), and goniofufurone (**1.64**) analogs. Upjohn dihydroxylation of intermediate **1.60** and subsequent protection afforded acetal **1.61**. In a separate synthesis, the chiral intermediate also underwent epoxidation to afford the goniofufurone precursor **1.63**. The hydrolysis of the lactone followed by halolactonization gave access to the *trans*-kumausyne precursor **1.65**. This work demonstrated complexity-generating potential of the biooxidative desymmetrization of the simple ketone **1.59**.

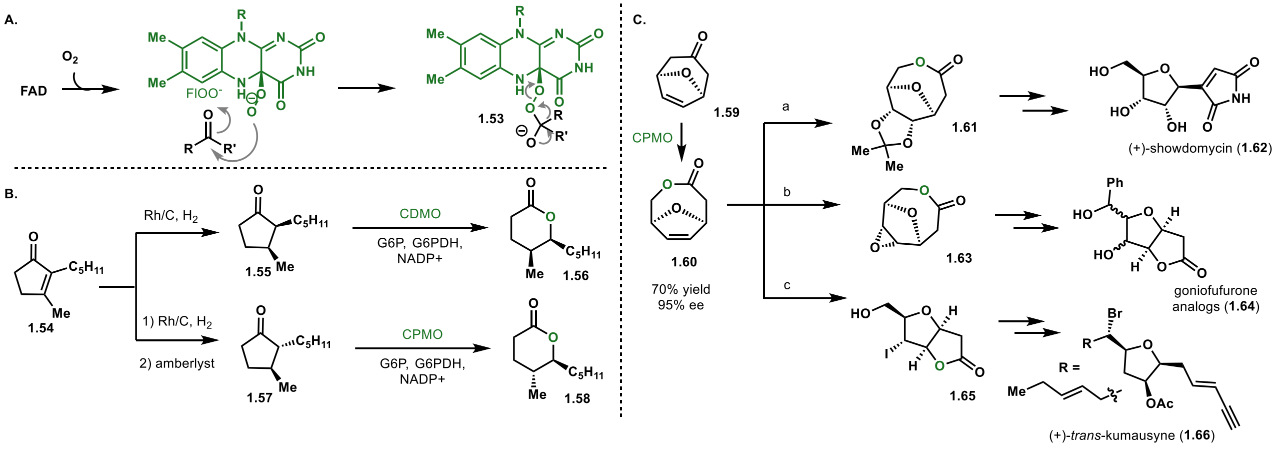

Figure 1.4: Reactions with BVMOs. (A) General mechanism for BVMOs. (B) *Aerangis* lactone synthesis featuring a stereoselective BV oxidation by cyclododecanone monooxygenase (CDMO) or cycopentanone monooxygenase (CPMO). (C) Chemoenzymatic synthesis of tetrahydrofuran-based natural products via a chiral intermediate generated by CPMO-mediated Baeyer-Villager oxidation a) OsO_4, NMO, DCM, rt, then acetone–$AlCl_3$, 0 °C to 40 °C, 47%; b) *m*CPBA, DCM, reflux, 98%; c) MeCN, H_2O, KOH, rt, then I_2–KI, 40 °C, dark, 75%.

BVMOs have also been employed for *in vivo* enzymatic cascades. Engineered *E. coli* harboring three biocatalytic enzymes allowed for the *in vivo* cascade starting from 2-cyclohexenol to caprolactone, featuring CHMO catalyzed Baeyer-Villager oxidation as the final step.[38] In addition to this canonical reactivity, CHMO has been reported to perform hydroxylation of boronic acids, and the stereoselective epoxidation of dimethyl and diethyl vinyl phosphonate.[27] Interestingly, CHMO has also been demonstrated to perform heteroatom oxidation, presumably from the hydroperoxy flavin.[27]

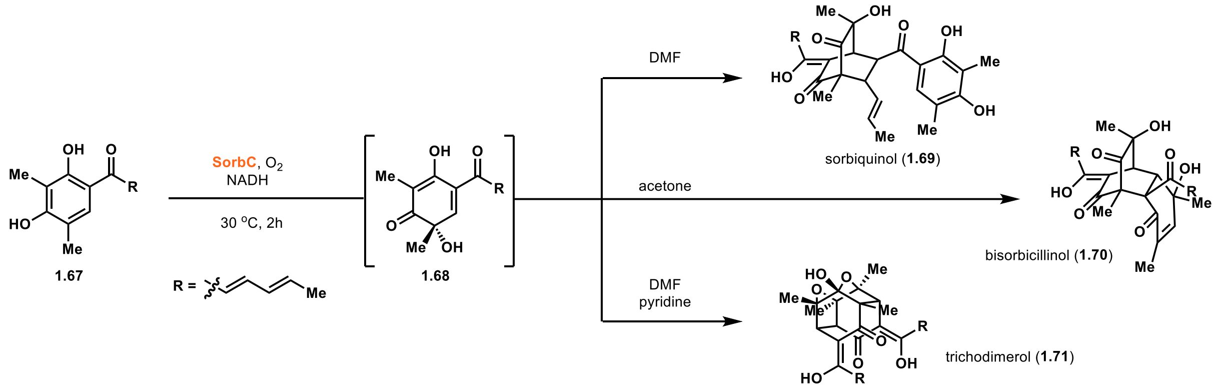

Figure 1.5: Reactions of group A flavin-dependent monooxygenases. Access to bisorbicillin natural products via oxidative dearomatization.

C4a-Hydroperoxy flavin (FlOOH): While BVMOs use peroxyflavin (**1.7**) to oxidize organic substrates, group A flavin-dependent monooxygenases perform hydroxylation on electron-rich substrates using the hydroperoxyflavin form of the cofactor (**1.8**). The prototypical group A member, *p*-hydroxybenzoate 3-hydroxylase (PHBH), has been well-studied.[39] This work has led to an understanding of the mechanism of substrate recognition, cofactor binding and flavin reduction. Recently, group A members from biosynthetic pathways have received attention for their synthetic potential.[40,41]

Sorbicillin natural products have been of interest to the synthetic community for nearly two decades due to their dense structural complexity and biological activity.[42] The shortest linear sequences to these natural products have employed an oxidative dearomatization as a key synthetic step; however, due to the lack of a general asymmetric method for this transformation, only racemic syntheses have been achieved via this route.[42] Recently, Sib and coworkers employed SorbC, a flavin-dependent monooxygenase from the sorbicillactone biosynthetic pathway,[43] as key a synthetic step in the chemoenzymatic synthesis of sorbiquinol (**1.69**), bisorbicillinol (**1.70**) and trichodimerol (**1.71**).[40] Sorbicillin (**1.67**) was transformed in a SorbC-mediated oxidative dearomatization to afford sorbicillinol (**1.68**) in >99.5% ee. In the presence of different organic cosolvents, sorbicillinol (**1.68**) could be selectively dimerized to afford the natural products **1.69**, **1.70**, or **1.71** (Figure 1.5A).

Halogenases: Group F flavin-dependent monooxygenases are structurally related to class A monooxygenases and follow the same catalytic sequence up to the formation of the C4a-hydroperoxide (FlOOH, **1.8**). Halogenases bind halide ions which are oxidized by the C4a-hydroperoxide to form hypochlorous or hypobromous acid (Figure 1.6A, **1.72**).[44] As the substrate binding site is distant from the flavin binding site, researchers hypothesize that the acid traverses a tunnel to the substrate binding site where it reacts with a lysine residue to form a covalent chloramine adduct (**1.73**), in the case of chlorination.[44] This electrophilic chlorine species is thought to undergo nucleophilic attack by an aromatic substrate (**1.75**). The Wheland intermediate is then deprotonated by a conserved Glu residue to form the chlorinated product (**1.76**).

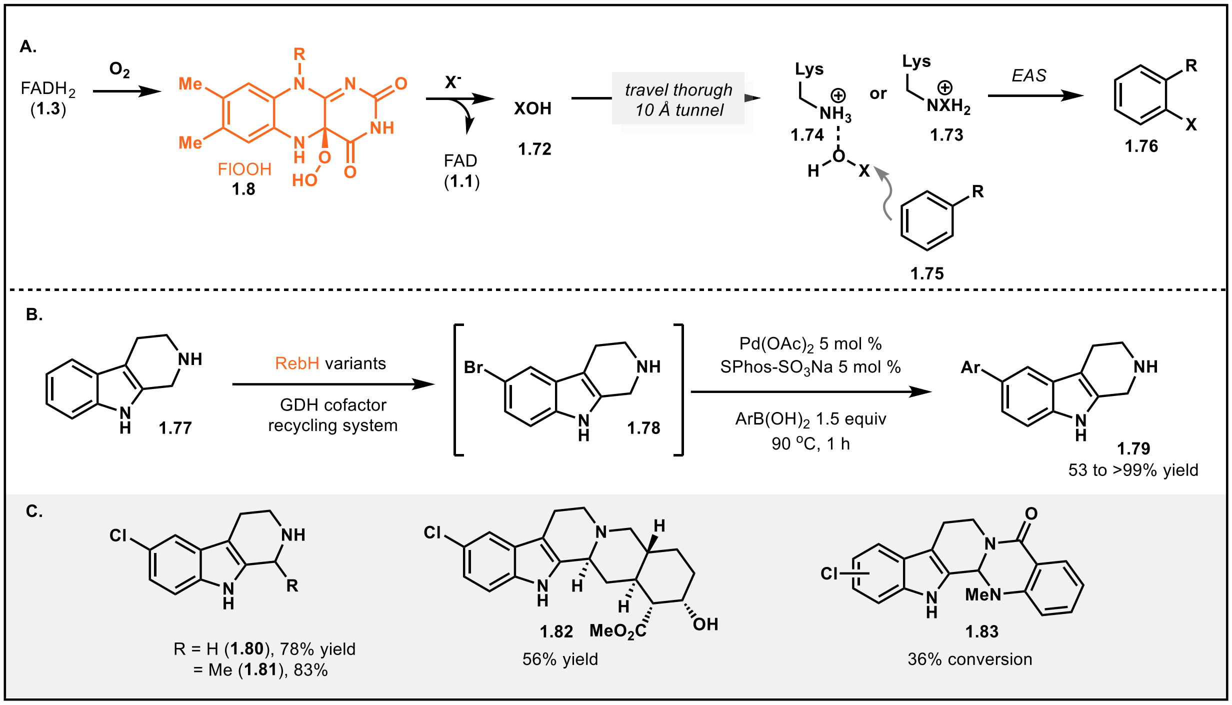
A.
FADH2
(1.3)
O2
R
Me
Me
N
N
O
NH
N
H
O
HO
O
FlOOH
1.8
X-
FAD
(1.1)
XOH
1.72
travel thorugh
10 Å tunnel
Lys
NH3
1.74
or
Lys
NXH2
1.73
H
O
X
R
1.75
EAS
R
X
1.76
B.
NH
N
H
1.77
RebH variants
GDH cofactor
recycling system
Br
NH
N
H
1.78
Pd(OAc)2 5 mol %
SPhos-SO3Na 5 mol %
ArB(OH)2 1.5 equiv
90 °C, 1 h
Ar
NH
N
H
1.79
53 to >99% yield
C.
Cl
NH
N
H
R
R = H (1.80), 78% yield
= Me (1.81), 83%
Cl
N
H
N
H
H
H
1.82
MeO2C
OH
56% yield
O
Cl
N
N
H
MeN
1.83
36% conversion

Figure 1.6: Reactions of halogenases. (A) General reaction mechanism for halogenase-mediated halogenation (EAS = Electrophilic aromatic substitution). (B) Halogenation, Pd-catalyzed Suzuki coupling cascade for late-stage functionalization of indole natural product scaffolds.[45] (C) Evolution of RebH variants using substrate walking from simple indole derivatives to pentacyclic alkaloids.[46]

Select flavin-dependent halogenases have received significant attention from the synthetic community for their ability to halogenate aromatic systems under mild reaction conditions with excellent site selectivity. For example, Durak and coworkers demonstrated the application of enzymatic halogenation of indole derivatives in conjunction with Pd-catalyzed cross coupling reactions on crude extracts of reaction mixtures to afford further functionalized products (Figure 1.6B, see **1.78** to **1.79**).[45] The parent enzyme, RebH, was evolved using a substrate-walking directed evolution strategy to obtain variants capable of halogenating a broad range of large indole and carbazole substrates (Figure 1.6C, **1.80-1.83**).[46] Recently, Fraley and coworkers characterized halogenase MalA from the malbrancheamide biosynthetic pathway, which performs iterative halogenation of the bicyclo[2.2.2]diazaoctane core.[47] These enzymes hold promise for future use in the selective halogenation of indoles and other electron-rich arenes.

The breadth of chemistry accessible with flavin-dependent biocatalysts coupled with the demonstrated scalability of these reactions positions this enzyme class to make major contributions to synthetic organic chemistry. Current applications have largely been constrained to native reaction mechanisms; however, with an ever-increasing understanding of the structural and function of these enzymes, synthetic chemists have the opportunity to employ these catalysts in novel reactions and integrate them into complexity-generating cascade sequences.

Chapter 1.2: References

1) MacHeroux, P.; Kappes, B.; Ealick, S. E. *FEBS J.* **2011**, *278* (15), 2625–2634.
2) A) Mansoorabadi, S. O.; Thibodeaux, C. J.; Liu, H. W. *J. Org. Chem.* **2007**, *72* (17), 6329–6342. B) Fagan, R. L. and Palfey, B. A. In *Comprehensive Natural Products II*; Begley, T. P., Ed.; Elsevier, **2010**; Vol 7, pp. 37-114.
3) Sheldon, R. A.; Woodley, J. M. *Chem. Rev.* **2018**, *118* (2), 801–838.
4) Ceccoli, R. D.; Bianchi, D. A.; Rial, D. V. *Front. Microbiol.* **2014**, *5*, 1–014.
5) Arnold, F. H. *Angew. Chem., Int. Ed.* **2018**, *57* (16), 4143–4148.
6) Palfey, B. A.; and Massey, V. In *Comprehensive Biological Catalysis*; Sinnott, M., ed.; Academic Press, 1998; Vol. 3, pp. 83–154
7) Scrutton, N.S. *Nat. Prod. Rep.* **2004**, *21* (17), 722–730.
8) Ghislieri, D.; Houghton, D.; Green, A. P.; Willies, S. C.; Turner, N. J. *ACS Catal.* **2013**, *3* (12), 2869–2872.
9) Ghislieri, D.; Green, A. P.; Pontini, M.; Willies, S. C.; Rowles, I.; Frank, A.; Grogan, G.; Turner, N. J. *J. Am. Chem. Soc.* **2013**, *135* (29), 10863–10869.
10) Heath, R. S.; Pontini, M.; Bechi, B.; Turner, N. J. *ChemCatChem* **2014**, *6* (4), 996–1002.
11) Li, G. Y.; Yao, P. Y.; Gong, R.; Li, J. L.; Liu, P.; Lonsdale, R.; Wu, Q. Q.; Lin, J. P.; Zhu, D. M.; Reetz, M. T. *Chem. Sci.* **2017**, *8* (5), 4093–4099.
12) Cosgrove, S. C.; Hussain, S.; Turner, N. J.; Marsden, S. P. *ACS Catal.* **2018**, *8* (6), 5570–5573.
13) Scalacci, N.; Black, G. W.; Mattedi, G.; Brown, N. L.; Turner, N. J.; Castagnolo, D. *ACS Catal*. **2017**, *7* (2), 1295–1300.
14) Stankovich, M. T.; Schopfer, L. M.; Massay, V. *J. Biol. Chem.* **1978**, *253* (14), 4971–4979.
15) Mincey, T.; Tayrien, G.; Mildvan, a S.; Abeles, R. H. *Proc. Natl. Acad. Sci. U. S. A.* **1980**, *77* (12), 7099–7101.
16) a) Sandoval, B. A.; Meichan, A. J.; Hyster, T. K. *J. Am. Chem. Soc.* **2017**, *139* (33), 11313–11316. b) Biegasiewicz, K F; Cooper, S. J.; Gau, Xin.; Oblinsky, D. G.; Kime, J. H.; Garfinkle, S. E.; Joyce, L. A.; Sandoval, B. A.; Scholes, G. D.; Hyster, T. K. *Science* **2019**, *364*, 1166–1169.
17) Knaus, T.; Toogood, H. S.; Scrutton, N. S. In *Green Biocatalysis*; Patel, R. N., Ed.; John Wiley & Sons: Hoboken, NJ, 2016; pp 473−488.
18) Winkler, C. K.; Faber, K.; Hall, M. *Curr. Opin. Chem. Biol.* **2018**, *43*, 97–105.
19) Durchschein, K.; Hall, M.; Faber, K. *Green Chem.* **2013**, *15* (7), 1764–1772.
20) Kohli, R. M.; Massey, V. *J. Biol. Chem.* **1998**, *273* (49), 32763–32770.

21) Stueckler, C.; Winkler, C. K.; Hall, M.; Hauer, B.; Bonnekessel, M.; Zangger, K.; Faber, K. *Adv. Synth. Catal.* **2011**, *353* (7), 1169–1173.
22) Classen, T.; Korpak, M.; Schölzel, M.; Pietruszka, J. *ACS Catal.* **2014**, *4* (5), 1321–1331.
23) Horita, S.; Kataoka, M.; Kitamura, N.; Nakagawa, T. *ChemBioChem* **2015**, *8502*, 440–445.
24) Litman, Z. C.; Wang, Y.; Zhao, H.; Hartwig, J. F. *Nature* **2018**, *560* (7718), 355–359.
25) Huijbers, M. M. E.; Montersino, S.; Westphal, A. H.; Tischler, D.; Van Berkel, W. J. H. *Arch. Biochem. Biophys.* **2014**, *544*, 2–17.
26) Leisch, H.; Morley, K.; Lau, P. C. K. *Chem. Rev.* **2011**, *111* (7), 4165–4222.
27) Colonna, S.; Gaggero, N.; Carrea, G.; Ottolina, G. **2002**, *43*, 1797–1799.
28) De Gonzalo, G.; Torres Pazmiño, D. E.; Ottolina, G.; Fraaije, M. W.; Carrea, G. *Tetrahedron Asymmetry* **2005**, *16* (18), 3077–3083.
29) Sheldon, R. A.; Woodley, J. M. *Chem. Rev.* **2018**, *118* (2), 801–838.
30) Branchaud, B. P.; Walsh, C. T. *J. Am. Chem. Soc.* **1985**, *107* (7), 2153–2161.
31) Riva, S., Fassi, P., Allegrini, P. & Razzetti, G. European Patent Application, EP 1777295 (2007).
32) Bong, Y. K.; Song, S.; Nazor, J.; Vogel, M.; Widegren, M.; Smith, D.; Collier, S. J.; Wilson, R.; Palanivel, S. M.; Narayanaswamy, K.; Mijts, B.; Clay, M. D.; Fong, R.; Colbeck, J.; Appaswami, A.; Muley, S.; Zhu, J.; Zhang, X.; Liang, J.; Entwistle, D. *J. Org. Chem.* **2018**, *83* (14), 7453–7458.
33) Ödman, P.; Wessjohann, L. A.; Bornscheuer, U. T. *J. Org. Chem.* **2005**, *70* (23), 9551–9555.
34) Rioz-Martínez, A.; De Gonzalo; Torres Pazmiño, D. E.; Fraaije, M. W.; Gotor, V. *J. Org. Chem.* **2010**, *75* (6), 2073–2076.
35) Baldwin, C. V. F.; Wohlgemuth, R.; Woodley, J. M. *Org. Process Res. Dev.* **2008**, *8* (7), 660–665.
36) Fink, M. J.; Schön, M.; Rudroff, F.; Schnürch, M.; Mihovilovic, M. D. *ChemCatChem* **2013**, *5* (3), 724–727.
37) Mihovilovic, M. D.; Bianchi, D. A.; Rudroff, F. *Chem. Commun.* **2006**, *8* (30), 3214–3216.
38) Oberleitner, N.; Peters, C.; Muschiol, J.; Kadow, M.; Saß, S.; Bayer, T.; Schaaf, P.; Iqbal, N.; Rudroff, F.; Mihovilovic, M. D.; Bornscheuer, U. T. *ChemCatChem* **2013**, *5* (12), 3524–3528.
39) Entsch, B.; Palfey, B. A.; Ballou, D. P.; Massey, V. *J. Biol. Chem.* **1991**, *266*, 17341.
40) Sib, A.; Gulder, T. A. M. *Angew. Chem. Int. Ed.* **2017**, 56 (42), 12888–12891.
41) Baker Dockrey, S. A.; Lukowski, A. L.; Becker, M. R.; Narayan, A. R. H. *Nat. Chem.* **2018**, *10* (2), 119–125.
42) Nicolaou, K. C.; Vassilikogiannakis, G.; Simonsen, K. B.; Baran, P. S.; Zhong, Y. L.; Vidali, V. P.; Pitsinos, E. N.; Couladouros, E. A. *J. Am. Chem. Soc.* **2000**, *122* (13), 3071–3079.
43) Al Fahad, A.; Abood, A.; Fisch, K. M.; Osipow, A.; Davison, J.; Avramović, M.; Butts, C. P.; Piel, J.; Simpson, T. J.; Cox, R. J. *Chem. Sci.* **2014**, *5* (2), 523–527.
44) Dong, C., Flecks, S., Unversucht, S., Haupt, C., Van Pee, K. H., & Naismith, J. H. **2012**, *309* (5744), 2216–2219.
45) Durak, L. J.; Payne, J. T.; Lewis, J. C. *ACS Catal.* **2016**, *6* (3), 1451–1454.
46) Payne, J. T.; Poor, C. B.; Lewis, J. C. *Angew. Chem., Int. Ed.* **2015**, *54* (14), 4226–4230.
47) Fraley, A. E.; Garcia-Borràs, M.; Tripathi, A.; Khare, D.; Mercado-Marin, E. V.; Tran, H.; Dan, Q.; Webb, G. P.; Watts, K. R.; Crews, P.; Sarpong, R.; Williams, R. M.; Smith, J. L.; Houk, K. N.; Sherman, D. H. *J. Am. Chem. Soc.* **2017**, *139* (34), 12060–1206.

CHAPTER 2: Substrate Scope of Biocatalytic Oxidative Dearomatization

Portions adapted with permission from "Biocatalytic site- and enantioselective oxidative dearomatization of phenols" *Nat. Chem.* **2018,** *10*, 119–125.

Chapter 2.1: Introduction

Oxidative dearomatization, a method which has served as a key step in the synthesis of natural products and biologically relevant molecules, is a prime example of a challenging, yet valuable chemical transformation.[1] Oxidative dearomatization of substituted arenes (see **2.7**), planar molecules that can be assembled using well-established chemistry, affords chiral *o*-quinols (**2.8,** Figure 2.1B), which readily undergo carbon-carbon and carbon-heteroatom bond-forming reactions and can be exploited to rapidly increase structural complexity. Lead tetraacetate was reported in 1950 to afford [2.2.2] bicycles from phenol starting materials, the [4+2] cycloadducts of the dearomatized intermediates.[2] In the ensuing decades, hypervalent iodide species, most notably PIDA and IBX, gained popularity as an attractive oxidant for this challenging transformation.[3] During the past two decades, a number of asymmetric methods have been reported to afford enantioenriched *o*-quinols. In 2004, Porco and coworkers described the development of a copper-oxo sparteine oxidant which was capable of delivering the azaphilone core from phenolic precursors in high yields and enantioselectivities.[4] A number of hypervalent oxidants based on the Phox and BINOL scaffolds have been developed and reported to give high enantiomeric excesses.[5]

In all of these cases, stoichiometric quantities of the chiral oxidant are required, limiting the synthetic utility of the method.

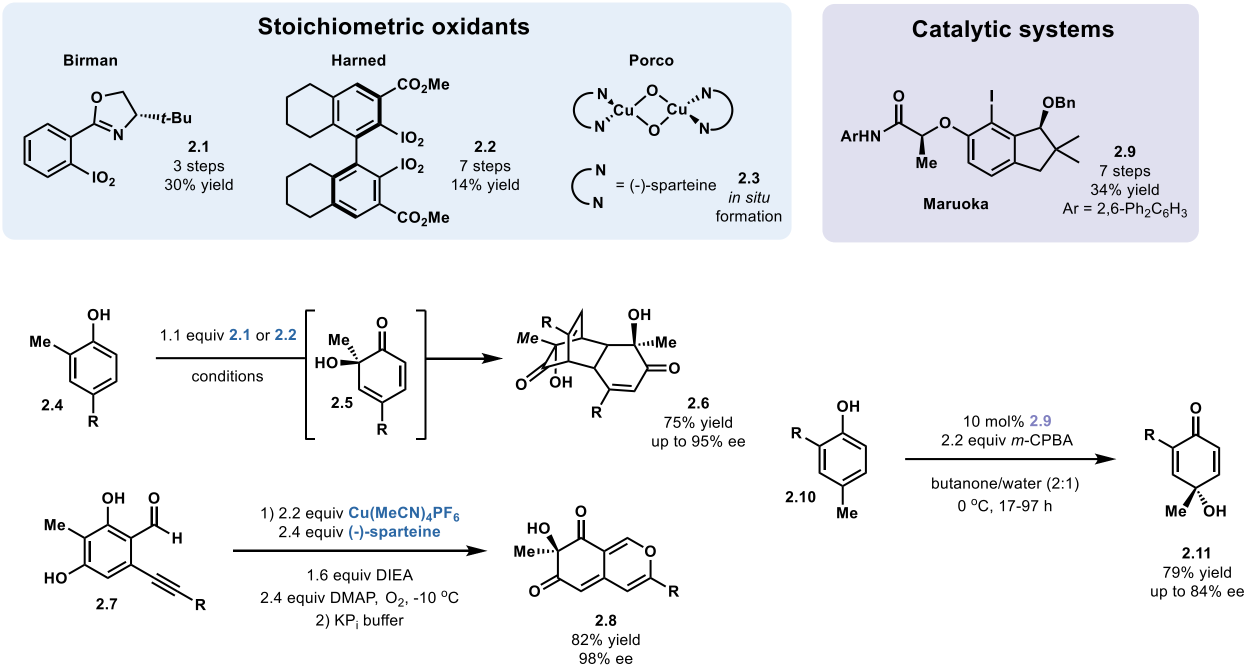

Stoichiometric oxidants
Birman
t-Bu
IO_2
2.1
3 steps
30% yield
Harned
CO_2Me
IO_2
IO_2
CO_2Me
2.2
7 steps
14% yield
Porco
Cu
Cu
= (-)-sparteine
2.3
in situ
formation
Catalytic systems
ArHN
Me
OBn
Maruoka
2.9
7 steps
34% yield
Ar = 2,6-$Ph_2C_6H_3$
2.4
1.1 equiv 2.1 or 2.2
conditions
2.5
2.6
75% yield
up to 95% ee
2.10
10 mol% 2.9
2.2 equiv m-CPBA
butanone/water (2:1)
0 °C, 17-97 h
2.11
79% yield
up to 84% ee
2.7
1) 2.2 equiv $Cu(MeCN)_4PF_6$
2.4 equiv (-)-sparteine
1.6 equiv DIEA
2.4 equiv DMAP, O_2, -10 °C
2) KP_i buffer
2.8
82% yield
98% ee

Figure 2.1: Small-molecule methods for asymmetric oxidative dearomatization.

To address this limitation, catalytic, enantioselective variants of this transformation have been developed; the benchmark selectivity of 84% ee was recently obtained by Maruoka and coworkers (Figure 2.1).[6] This remarkable achievement in chiral oxidant design highlights the challenges inherent in achieving high site- and stereoselectivity in this transformation. As the chiral environment is distal from the approach of the nucleophile, highly engineered oxidants are required to enable selectivity. Nature has overcome this challenge by controlling the positioning of the substrate within the active site of enzymes through specific substrate-protein interactions.[7]

Flavin-dependent monooxygenases perform this challenging oxidation with perfect site- and stereoselectivity.[7] These enzymes employ the noncovalent cofactor $FADH_2$ (see **1.1**, Figure 1.1) which reacts with molecular oxygen to form hydroperoxyflavin, an electrophilic source of oxygen that can be incorporated into organic substrates bound in the active site. To harness the advantages of these biocatalysts, it is important to address potential challenges, including typically narrow substrate scopes of wild-type enzymes, solubility conflicts between the substrate and the protein catalyst, and enzyme stability.[8]

Our initial investigations into enzymatic oxidative dearomatization began with three flavin-dependent monooxygenases from natural product pathways: TropB, SorbC and AzaH (Figure 2.2). The biochemical function of TropB was characterized by Cox and coworkers in 2012.[9] The first oxygenase enzyme in the biosynthesis of stipitatic acid (**2.14**), TropB, natively converts 3-methylorcinaldehyde (**2.12**) to *o*-quinol **2.13** (Figure 2.2). This intermediate undergoes further tailoring to ultimately afford the tropolone natural product stipitatic acid (**2.14**). SorbC, a homolog of TropB, was also first identified and studied by the Cox group. This enzyme mediates the oxidative dearomatization of sorbicillin (**2.15**) to sorbicillinol (**2.16**).[10] Sorbicillinol has been implicated as a key intermediate in the biosynthesis of a large number of sorbicillin natural products, including sorbicillactone A and the bisorbicillinoids.[10] Interestingly, the native substrates of these two enzymes feature a 3-methylresorcinol core, yet SorbC and TropB demonstrate orthogonal site- and stereoselectivities, offering two complementary catalysts for site-selective oxidation.

A third flavin-monooxygenase capable of oxidative dearomatization, AzaH, was discovered by Tang and coworkers in 2012.[11] AzaH mediates the oxidative dearomatization and was proposed to catalyze the subsequent cyclization of orcinaldehyde-derivative **2.18** in the biosynthesis of azanigerone A (**2.21**, Figure 2.2).[11] The stereochemical configuration at C11 and C13 of **2.21** and the absolute configuration of natural product were not disclosed in this initial report. Like TropB, AzaH also selectively oxidizes the C3 position of its native substrate.

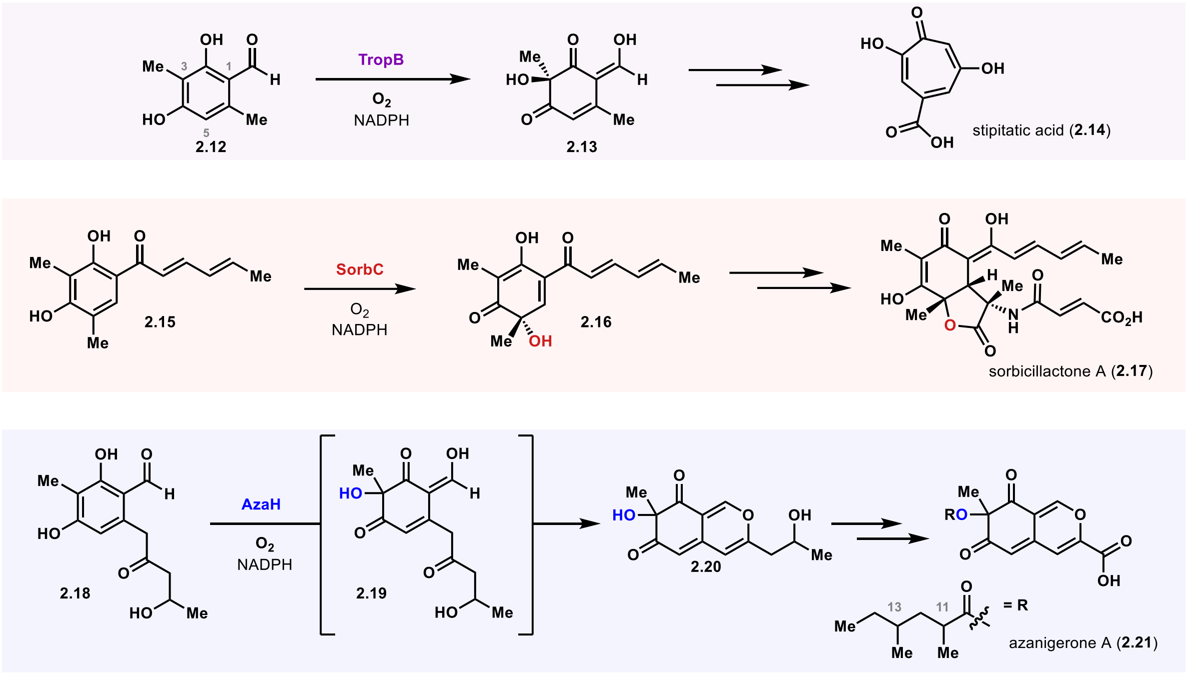
TropB
O2
NADPH
2.12
2.13
stipitatic acid (2.14)
SorbC
O2
NADPH
2.15
2.16
sorbicillactone A (2.17)
AzaH
O2
NADPH
2.18
2.19
2.20
= R
azanigerone A (2.21)

Figure 2.2: The native reaction and biosynthetic pathway of the three flavin-dependent monooxygenases TropB,[9] SorbC[10] and AzaH.[11]

In order to explore the substrate promiscuity of these flavoproteins we chose to develop routes to phenolic and resorcinol substrate analogs varying the steric and electronic properties of each substituent. These compounds were then tested for reactivity with the flavin-dependent monooxygenases TropB, SorbC and AzaH by assessing conversion to dearomatized products. The site- and facial fidelity of C–O bond formation with these catalysts with non-native substrates was determined in preparative-scale reactions with purified proteins (*in vitro* reactions) and the enantio-enrichment of each product was assessed by comparison to racemic standards.

Chapter 2.2: Substrate Synthesis

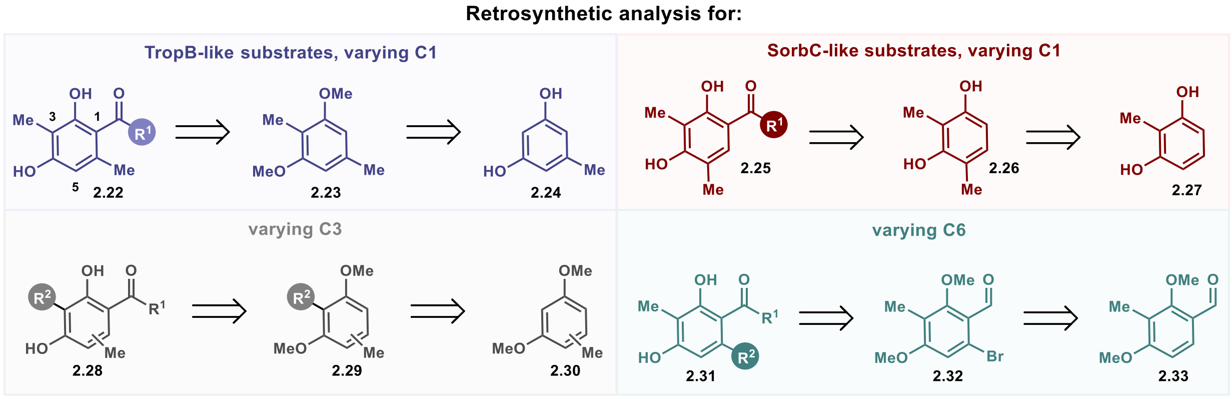
Retrosynthetic analysis for:
TropB-like substrates, varying C1
SorbC-like substrates, varying C1
varying C3
varying C6
OH
O
OMe
Me
HO
MeO
R1
R2
Br
3
1
5
2.22
2.23
2.24
2.25
2.26
2.27
2.28
2.29
2.30
2.31
2.32
2.33

Figure 2.3: Retrosynthetic analysis of substrate classes for biocatalytic oxidative dearomatization.

A small library of phenolic substrates was designed to explore the steric and electronic requirements for substrate turnover (Figure 2.3). SorbC and TropB native substrate analogs such as **2.22** and **2.25** could be accessed by acylation of the isomeric dimethylresorcinol cores. As dimethyl resorcinols **2.23** and **2.26** were prohibitively expensive, we chose to trace these intermediates back to inexpensive, singly methylated 1,3-diphenols (**2.24** and **2.27**). We envisioned generating substrates with varying alkyl groups at the C3 position through acylation of the dialkylated resorcinols (**2.29**). The variable C3 group could be incorporated through lithiation of **2.30** followed by alkylation with the desired alkyl halide. C6-substituted compounds (see **2.31**) could be generated through a Pd-catalyzed cross-coupling of aryl bromide **2.32** with either boronic acids or alkynes. A four-step route to aryl bromide **2.32** from benzaldehyde **2.33** had been previously reported by Porco.[3b]

The native substrates of TropB (**2.12**) and SorbC (**2.15**) were chosen as our first synthetic targets. This would allow us to establish conditions for our proposed divergent routes, generate significant quantities of the key intermediates **2.23** and **2.26** and enable positive controls for our enzymatic reactions. Vilsmeier-Haack formylation of **2.23** proceeded in high yield.[3b] Methyl ether deprotection of the resulting benzaldehyde was initially low yielding, potentially due to loss of material as the boron complex, but a work up procedure that included basifying the reaction mixture with 1 M NaOH to a pH of 10 followed by acidification was found to afford nearly quantitative yields reproducibly. This two-step sequence from **2.23** gave access to the TropB native substrate.

Resorcinol **2.26** underwent Friedel-Crafts acylation to afford substrate class **2.25**.[12] McOmie acylation conditions[13] afforded the corresponding benzyl ketones with unprotected phenolic groups; unfortunately, the same transformation was low yielding with more sterically hindered substrates such as **2.23**. A protecting group strategy was used to access compounds **2.25a-d** (see Figure 2.4). 6,7-bicycle **2.43** was accessed via Wittig olefination, reduction and acid-promoted Friedel-Crafts cyclization. This route was also employed to access the corresponding tetralone. Acylation of resorcinol **2.27** followed by thermal Fries-rearrangement,[14] reduction and Vilsmeier-Haack formylation afforded benzaldehyde **2.49**. Suzuki cross-coupling of aryl bromides **2.32** and **2.50** afforded the biphenyls **2.51** and **2.53** in good yield. This aryl bromide was also leveraged as a key intermediate in the synthesis of azaphilone precursors. Sonogashira cross-coupling with the appropriate alkyne, followed by an $AuCl_3$ catalyzed cyclization to the pyrillium and subsequent hydration to the ketone afforded a number of dicarbonyl substrates (see Figure 5.4).[3b]

Chapter 2.3: Reactivity Profile

Genes encoding *tropB* and *sorbC* were cloned into a pET151 vector. The plasmids were then transformed into BL21 (DE3) E. coli cells. The gene encoding *azaH* in a modified pET28 vector was a generous gift from the Tang lab at UCLA. Expression and purification conditions were slightly modified from those reported by Cox[9] and Tang[11] respectively (see Chapter 2.6.2).

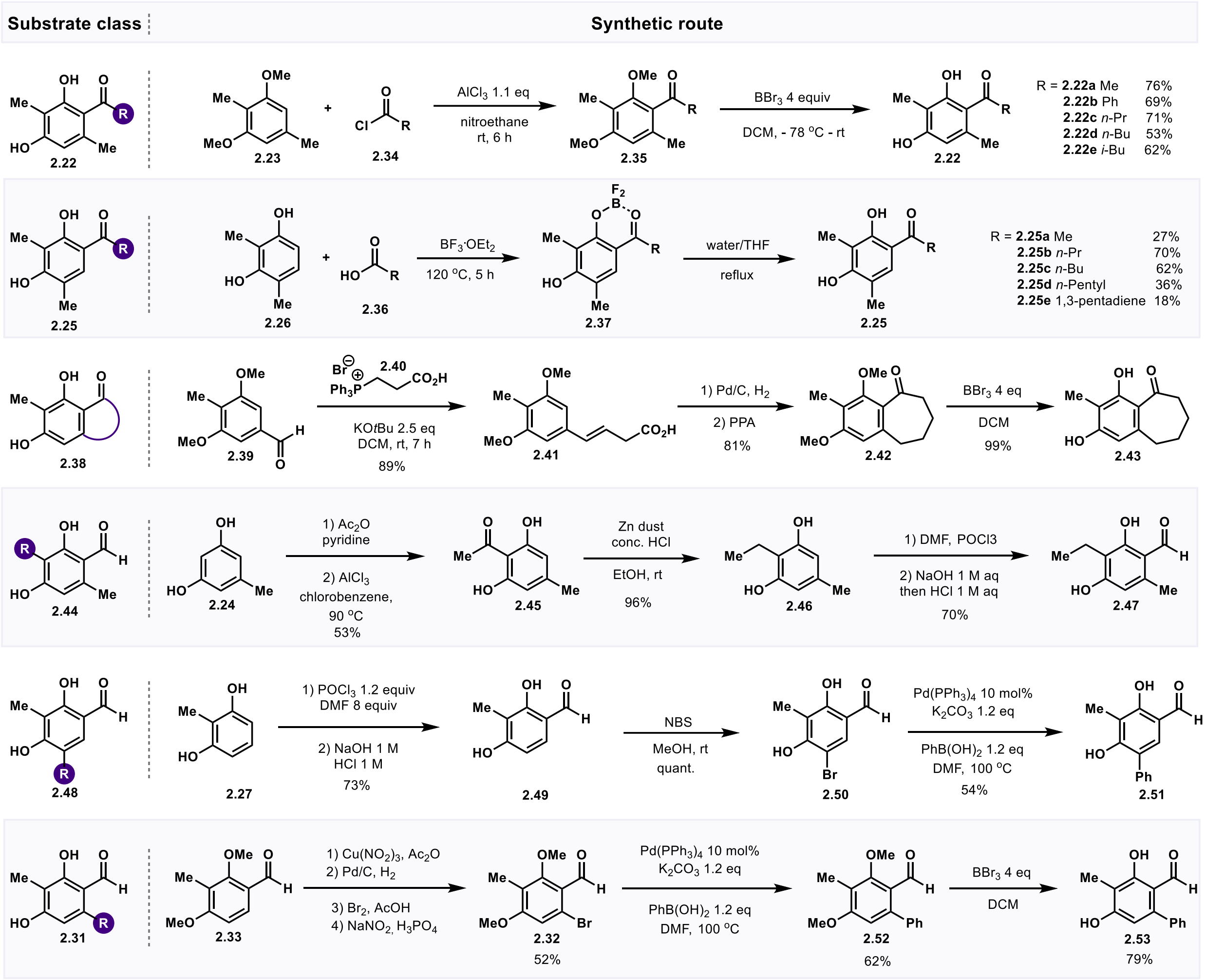
Substrate class
Synthetic route
2.22
2.23
2.34
AlCl3 1.1 eq
nitroethane rt, 6 h
2.35
BBr3 4 equiv
DCM, - 78 °C - rt
2.22
R = 2.22a Me 76%
2.22b Ph 69%
2.22c n-Pr 71%
2.22d n-Bu 53%
2.22e i-Bu 62%
2.25
2.26
2.36
BF3·OEt2
120 °C, 5 h
2.37
water/THF
reflux
2.25
R = 2.25a Me 27%
2.25b n-Pr 70%
2.25c n-Bu 62%
2.25d n-Pentyl 36%
2.25e 1,3-pentadiene 18%
2.38
2.39
2.40
KOtBu 2.5 eq
DCM, rt, 7 h
89%
2.41
1) Pd/C, H2
2) PPA
81%
2.42
BBr3 4 eq
DCM
99%
2.43
2.44
2.24
1) Ac2O pyridine
2) AlCl3 chlorobenzene, 90 °C
53%
2.45
Zn dust conc. HCl
EtOH, rt
96%
2.46
1) DMF, POCl3
2) NaOH 1 M aq then HCl 1 M aq
70%
2.47
2.48
2.27
1) POCl3 1.2 equiv DMF 8 equiv
2) NaOH 1 M HCl 1 M
73%
2.49
NBS
MeOH, rt
quant.
2.50
Pd(PPh3)4 10 mol% K2CO3 1.2 eq
PhB(OH)2 1.2 eq DMF, 100 °C
54%
2.51
2.31
2.33
1) Cu(NO2)3, Ac2O
2) Pd/C, H2
3) Br2, AcOH
4) NaNO2, H3PO4
2.32
52%
Pd(PPh3)4 10 mol% K2CO3 1.2 eq
PhB(OH)2 1.2 eq DMF, 100 °C
2.52
62%
BBr3 4 eq
DCM
2.53
79%

Figure 2.4: Synthetic routes to resorcinol substrates for biocatalytic oxidative dearomatization.

With our desired proteins in hand, we next optimized reaction conditions using TropB with the native substrate **2.12**. Initial conditions for the flavin-dependent monooxygenase-mediated oxidative dearomatization were modeled on Cox's report.[15] KP_i buffer at pH 8.0 was found to be optimal for conversion to product at one hour. A temperature screen showed that 30 °C provided highest turnover within one hour with no side product formation as observed by UPLC-PDA. The use of super-stoichiometric amounts of NAPDH employed in Cox's report,[15] however, was undesirable, due to the high cost and instability of this cofactor. To address this limitation, a well-established NADPH recycling system was used in our studies.[16]

Under these optimized conditions, fifty substrates were incubated with each of the three FAD-dependent monooxygenases (Figure 2.5). Reactions were analyzed by UPLC-PDA. Standard curves of the starting material were obtained and used to determine total turnover numbers (TTN) for each substrate-enzyme pair. Thirty-five of these substrates showed partial or full conversion by at least one enzyme at 0.1 mol% catalyst loading.

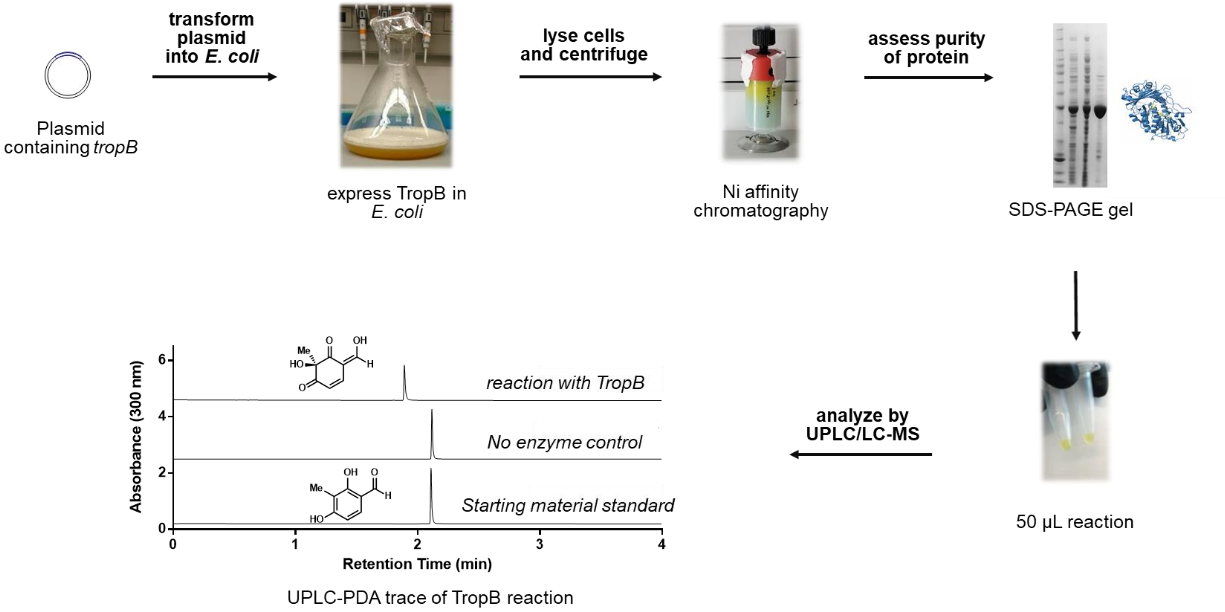
transform plasmid into *E. coli*
Plasmid containing *tropB*
express TropB in *E. coli*
lyse cells and centrifuge
Ni affinity chromatography
assess purity of protein
SDS-PAGE gel
50 µL reaction
analyze by UPLC/LC-MS
Absorbance (300 nm)
6
4
2
0
Me
HO
O
O
OH
H
reaction with TropB
No enzyme control
OH
O
Me
H
HO
Starting material standard
0
1
2
3
4
Retention Time (min)
UPLC-PDA trace of TropB reaction

Figure 2.5: Workflow for analytical-scale oxidative dearomatization. Synthetic genes are cloned into the desired vector, transformed into a competent *E. coli* strain which is then grown in 0.5 or 1 L cultures. Overexpression is induced and cells are harvested and lysed. After Ni-affinity purification of the crude lysate the protein solution is used in small scale reactions.

TropB catalyzed the oxidation of several substrates to singly hydroxylated products, with TTNs ranging from 84 to ≥ 1000 (Table 2.1).[18] Among these substrates were aryl bromides (**2.50**, **2.55**) and resorcinols with electron donating (see **2.59**) and withdrawing groups (**2.53**). Branched or straight chain ketones (see **22a-e**) were cleanly oxidized as well as a biphenyl substrate (**2.53**). We have found the C1-carbonyl motif, and C2- and C4-hydroxyl groups were critical for substrate conversion. As one might predict from examining the structure of the native substrate, increasing steric bulk at the C1 position resulted in a decrease in TTN; the largest substituent that was accepted at this position was an *iso*butyl ketone. The substitution of an alternative electron-withdrawing group such as a nitrone or nitro group was tolerated, however, esters and acids were not converted. Two attributes have been proposed to be at play for the role of the requisite electron-withdrawing group. First, we proposed this group is needed to lower the pKa of the substrate. Attabey Rodrìguez Benìtez has found that the pKa of the native substrate **2.12** is 7.2.[17] It is therefore likely that the anionic form of the substrate binds in the enzyme active site. The second feature of this functional group could be the role of the extended π system affording a lower energetic barrier to dearomatization. Current computational and experimental work is ongoing in an attempt to decouple these two features; however, we propose that it is likely the two characteristics are both critical for the design of a productive substrate.

A surprisingly large number of substrates featuring alternative substitution at the C5- and C6-position were also tolerated. Good conversion was observed with the C6-phenyl **2.53**, whereas, the C5-phenyl substrate **2.51** was not accepted, indicating the hydrophobic pocket occupied presumably by the C6-methyl group of the native substrate can accommodate significant steric bulk. However, the rotation from the active conformation required to put the C5-substituent in this C6-pocket is either too unfavored to allow for binding or alternatively places the carbon to be oxidized, C3, too far from the hydroperoxy group. Interestingly, although the substitution of the methyl group from the C6- to C5-position is tolerated with an aldehyde at C1 (see **2.58**), and the butyl ketone **2.22d** was also efficiently converted, both alterations are not tolerated when present in a single substrate (see **2.25b**).

AzaH was also able to efficiently hydroxylate phenols with significant structural differences from the native substrate **2.18** (Table 2.1). The α-hydroxy carbonyl is not critical to

Table 2.1: Turnover numbers (TN) at 1 h, based on consumption of starting material as measured by absorbance at 270 nm. Conditions: 2.5 mM substrate, 2.5 μM flavin-dependent monooxygenase, 5 mM G6P, 1 mM NADP$^+$, 1 unit/mL G6PDH, 50 mM KP$_i$ buffer, 30 °C, 1 h.

Entry	Substrate	TropB	AzaH	SorbC	Entry	Substrate	TropB	AzaH	SorbC	Entry	Substrate	TropB	AzaH	SorbC
		Total Turnover Number					Total Turnover Number					otal Turnover Numbe		
1	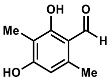 2.12	1000	296	0	*15*	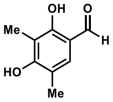 2.58	377	385	371	*29*	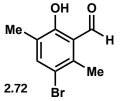 2.72	0	49	0
2	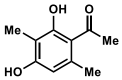 2.22a	1000	0	0	*16*	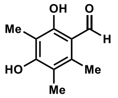 2.59	432	261	0	*30*	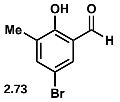 2.73	0	13	0
3	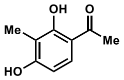 2.54	1000	0	0	*17*	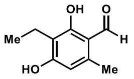 2.47	793	0	0	*31*	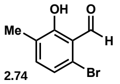 2.74	0	28	0
4	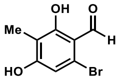 2.55	1000	1000	0	*18*	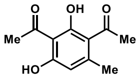 2.60	100	0	0	*32*	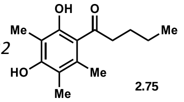 2.75	0	16	68
5	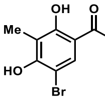 2.50	1000	534	0	*19*	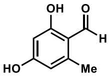 2.61	402	0	0	*33*	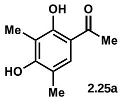 2.25a	0	329	383
6	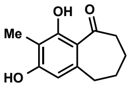 2.43	976	78	0	*20*	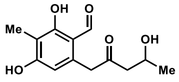 2.18	0	725	0	*34*	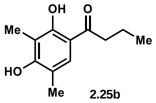 2.25b	0	277	646
7	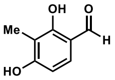 2.49	934	0	0	*21*	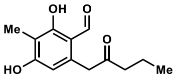 2.62	0	639	0	*35*	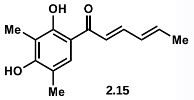 2.15	0	93	816
8	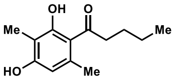 2.22d	787	0	479	*22*	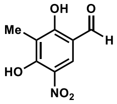 2.63	0	678	0	*36*	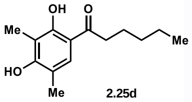 2.25d	0	308	656
9	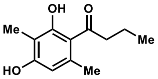 2.22c	829	0	0	*23*	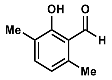 2.64	0	632	0	*37*	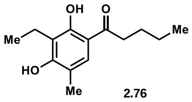 2.76	0	841	858
10	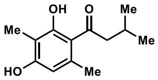 2.22e	669	0	331	*24*	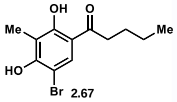 2.67	0	284	0	*38*	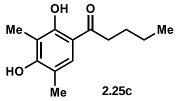 2.25c	0	418	889
11	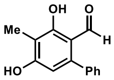 2.53	646	524	0	*25*	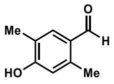 2.68	0	16	0	*39*	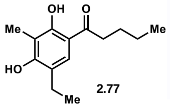 2.77	0	639	919
12	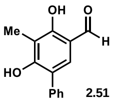 2.51	0	0	0	*26*	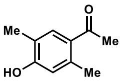 2.69	0	0	0	*40*	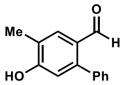 2.78	0	0	0
13	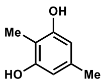 2.56	0	0	0	*27*	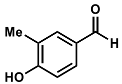 2.70	0	0	0	*41*	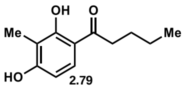 2.79	0	0	0
14	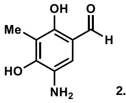 2.57	0	0	0	*28*	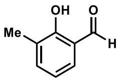 2.71	0	0	0	*42*	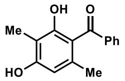 2.22b	0	0	0

substrate recognition as derivatives featuring a methyl group (**2.12**) or hydrogen atom (**2.50**, **2.63, 2.25d**) at this position undergo oxidation by AzaH. Lipophilic-substituted carbonyls at the C1-position were also tolerated (**2.25a-d**). Interestingly, C5-bromides gave much higher conversions then their C5-methyl group or hydrogen atom analogs (see **2.50** vs. **2.53** and **2.67** vs. **2.79**). Clearly the bromide is playing an important role in electrostatic interactions in the active site, but rationalization of this result will most likely require docking studies of these unnatural substrates with a homology model or crystal structure of the protein.

Only substrates with a straight-chain group extending from the carbonyl of at least 4 carbons showed significant turnover with SorbC (Table 2.1). This result could be evidence that this hydrophobic substituent is critical for substrate binding. Interestingly, when a hydrogen atom

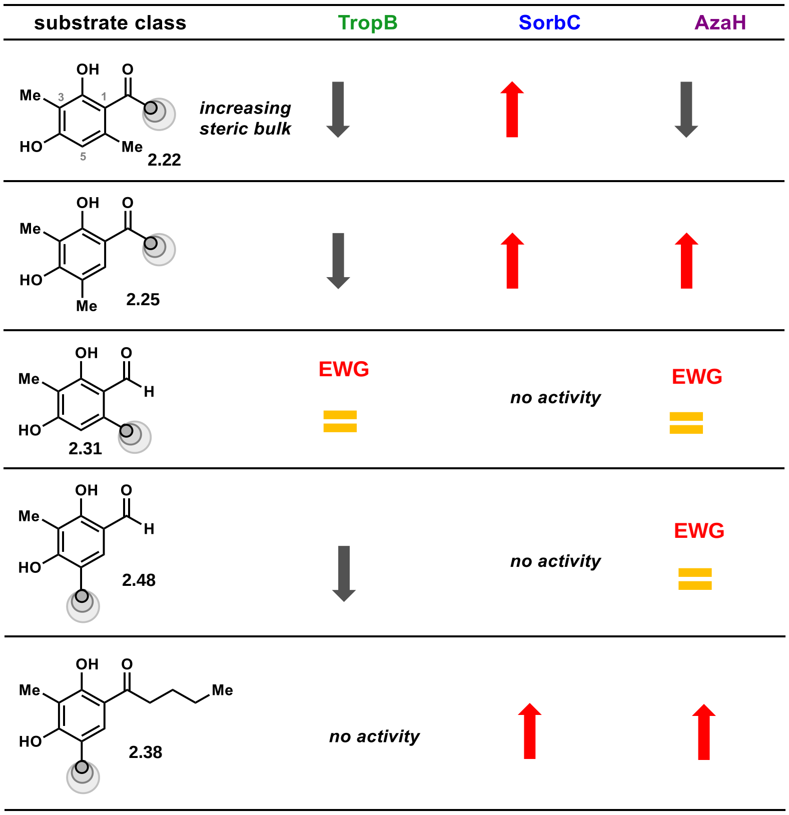
substrate class
TropB
SorbC
AzaH
OH
O
Me
3
1
HO
5
Me
2.22
increasing steric bulk
2.25
EWG
no activity
EWG
H
2.31
2.48
no activity
EWG
Me
2.38
no activity

Figure 2.6: Trends in reactivity of the three enzymes TropB, SorbC and AzaH with five substrate classes. Red arrow indicates high conversion, grey arrow indicates decreasing conversion with increasing steric bulk and yellow equal sign indicates comparable conversion of substrates.

rather than methyl group is present at C6 (see **2.22c-e**), the site of hydroxylation in the native substrate, a product with an absorption spectrum of a triphenol is formed. Hydroxylation at C6 followed by deprotonation and rearomatization would account for this result. Similar results are seen in TropB reactions with C3-proto substrates (see **2.61**). The high fidelity for C6-hydroxylation by SorbC and C4-hydroxylation by TropB with unnatural substrates has encouraged our interest in developing these enzymes as synthetically relevant catalysts.

Chapter 2.4: Preparative-scale Reactions

Several substrates were chosen for scale-up reactions to determine the enantioselectivity of the transformation mediated by the three enzymes (Figure 2.7). Gratifyingly, comparable conversions were observed on 10 mg-scale as in our analytical scale assays without alteration of the reaction conditions. Choice of reaction vessel, however, did prove to be critical to obtaining high conversion. Crystallizing dishes were employed in our initial reactions to maximize surface area of the air-buffer interface, as oxygen is required as the stoichiometric oxidant. We later found that an Erlenmeyer flask could also be employed, if shaken at a low rate (typically 100 rpm) to allow for efficient gas exchange.

The *o*-quinol products were found to rapidly dimerize through a Diels-Alder cycloaddition and other decomposition pathways upon concentration of the reaction mixture in organic solvent. To mitigate this byproduct formation, crude reaction mixtures were diluted with two volumes of acetone and centrifuged to precipitate large biomolecules. The filtrate was then concentrated and directly purified by reverse-phase preparative HPLC to afford analytically pure *o*-quinol products which could be characterized by NMR and mass spectrometry. Racemic standards of the C3-hydroxylated products could be accessed through an IBX-mediated oxidative dearomatization. Porco's conditions afforded the desired product in almost all cases (Figure 2.7).[3b] After purification by preparative HPLC sufficient material was obtained for the substrates shown in Figure 2.7 to allow for analysis by chiral HPLC or SFC. A notable exception was the 5-nitro substituted substrate **2.86** which returned only starting material or, under more forcing thermal conditions, nonspecific decomposition.

Although the stereocenter forged by TropB is later ablated in the subsequent enzymatic step, we found that the *o*-quinol native product is formed in >99% ee. A number of non-native substrates were also obtained in high enantiopurity including the 6,7-bicycle **2.84** and C6-phenyl **2.80** (Figure 2.7). Unexpectedly, we found that ketone substrates such as methyl ketone **2.82** and *iso*butyl ketone **2.83** afforded dearomatized products which favored the ketone tautomer over the exocyclic enol form which was observed for all aldehyde and aldehyde-derived compounds. This was attributed to increased allylic strain between the C1 carbonyl substituent and the C6 methyl group that was relieved in the ketone tautomer. Keto-enol tautomerization was found to be confounding in all attempts to resolve the enantiomers of these class of products. Attempts were made to form the Mosher ester[19] to determine the enantiopurity of the methyl ketone product, however, as was seen in later studies (see Chapter 5), acylation of the tertiary alcohol was challenging, and none of the conditions screened afforded high conversion to the desired ester product. However, we anticipate the ketone products are afforded in high enantiopurity based upon the high %ee observed with the bicyclic substrate, which would presumably bind within the active site in a similar manner to the ketone substrate.

Marc Becker completed the synthesis of **±2.18**, enabling us to benchmark the activity of AzaH with the enzyme's native substrate. AzaH oxidized both enantiomers with apparently equal efficiency affording a 1:1 ratio of diasteromers, both obtained in >99% ee. Fortunately, AzaH turned over several substrates that were also converted by TropB, allowing for assignment of the absolute configuration of the AzaH products. We found that, like TropB, AzaH afforded the *R* enantiomer of **2.13** (Figure 2.7). Based on the high %ee of the *o*-quinols isolated, we hypothesize that the binding mode of these nonnative substrates affords the same facial selectivity as the native substrate. This has been supported by docking studies and QM/MM calculations performed by Sarah Tweedy in the Brooks Lab.[17]

C5-hydroxylated products (see **2.87**) are constitutively locked as the cyclohexadiene tautomer and thus prone to undergo Diels-Alder cycloaddition with dienophiles at or below room temperature. SorbC products were therefore acylated *in situ* to mitigate undesired dimerization. The acylation products were stable on silica and isolable. Fortunately, Corey's $Pb(OAc)_4$ conditions[20] for the racemic synthesis of acylated **2.87** afforded the acylated dienones reproducibly. SorbC was found to afford the C5-hydroxylated products in 96 to >99% ee. Sorbicillinol, the native product, was obtained in excellent enantiopurity. Substrates with shorter akyl substituents on the C1 ketone (see **2.91**) and longer aliphatic groups at C3 gave the lowest enantiomeric excesses seen to date in the enzymatic oxidative dearomatization. Based on these data we hypothesized that the C1 hydrophobic group was critical in substrate recognition and binding. We leveraged this insight to enable a substrate engineering approach to overcome the substrate limitations encountered with SorbC.

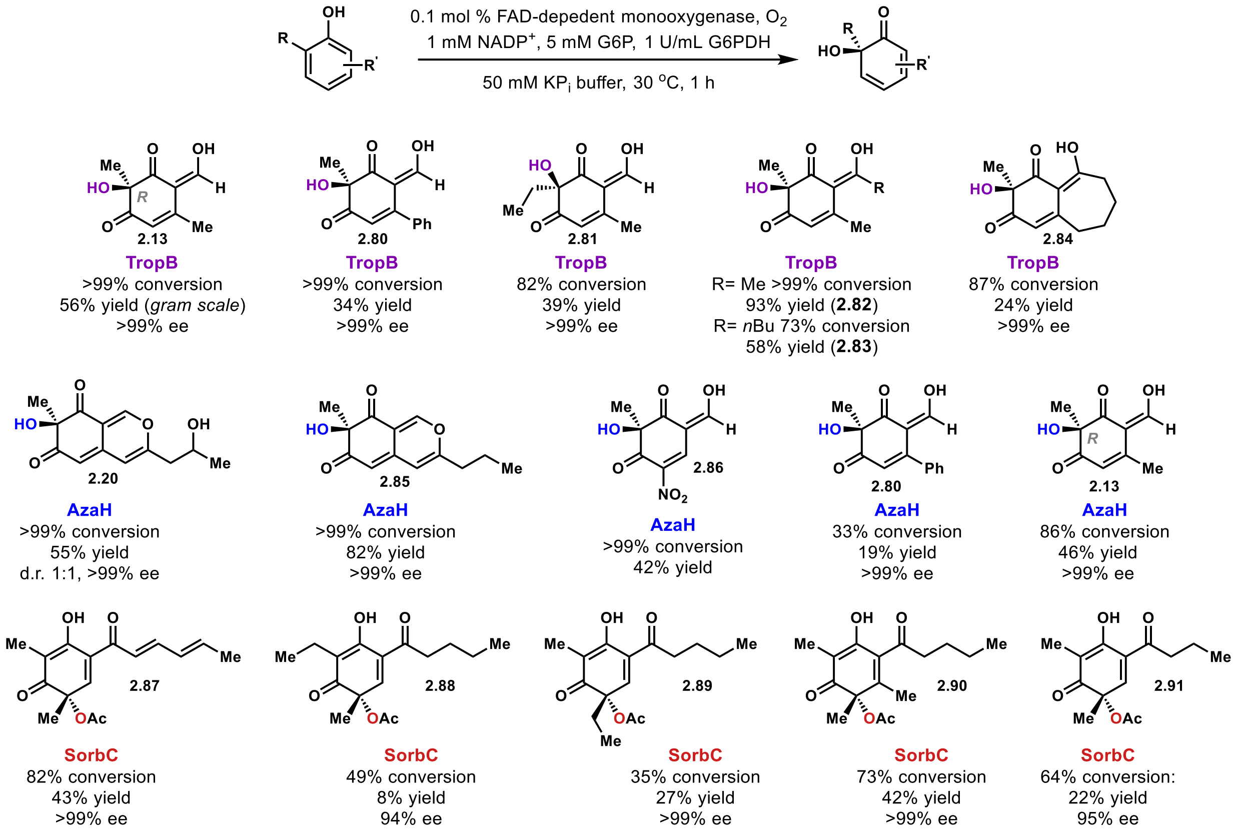
0.1 mol % FAD-depedent monooxygenase, O2
1 mM NADP+, 5 mM G6P, 1 U/mL G6PDH
50 mM KPi buffer, 30 °C, 1 h
2.13
TropB
>99% conversion
56% yield (gram scale)
>99% ee
2.80
TropB
>99% conversion
34% yield
>99% ee
2.81
TropB
82% conversion
39% yield
>99% ee
TropB
R= Me >99% conversion
93% yield (2.82)
R= nBu 73% conversion
58% yield (2.83)
2.84
TropB
87% conversion
24% yield
>99% ee
2.20
AzaH
>99% conversion
55% yield
d.r. 1:1, >99% ee
2.85
AzaH
>99% conversion
82% yield
>99% ee
2.86
AzaH
>99% conversion
42% yield
2.80
AzaH
33% conversion
19% yield
>99% ee
2.13
AzaH
86% conversion
46% yield
>99% ee
2.87
SorbC
82% conversion
43% yield
>99% ee
2.88
SorbC
49% conversion
8% yield
94% ee
2.89
SorbC
35% conversion
27% yield
>99% ee
2.90
SorbC
73% conversion
42% yield
>99% ee
2.91
SorbC
64% conversion:
22% yield
95% ee

Figure 2.7: Yields and enantiomeric excesses of products obtained from preparative scale enzymatic reactions. Conditions: 2.5 mM substrate (10 mg, in DMSO), 2.5 mM flavin-dependent monooxygenase, 5 mM G6P, 1 mM NADP$^+$, 1 unit/mL G6PDH, 50 mM KP$_i$ buffer, 30 °C, 1 h.

Chapter 2.5: Conclusions

The substrate scope, site- and stereoselectivity of three wild-type flavin-dependent monooxygenases was explored. First, a library of phenolic compounds was designed based on the native substrates of the three enzymes, TropB, SorbC and AzaH. TTNs were determined for each enzyme-substrate pair. In all productive reactions a single hydroxylated product was detected by UPLC and LC-MS. Preparative in vitro reactions were performed, allowing for structural characterization of the enzymatic products and determination of % ee. High enantioselectivities were observed in all reactions. Attabey Rodrìguez Benìtez and Sarah Tweedy have performed structural, biochemical and computational studies to elucidate the mechanisms controlling substrate specificity and reactivity of TropB.[17] Work is on-going to understand the stereoelectronic effects which govern substrate selectivity of AzaH, a homolog which is capable of turning over more electron poor substrates than either TropB or SorbC. Substrate selection and binding by SorbC is further discussed in Chapter 3.

One challenging limitation we have encountered in our exploration of the synthetic utility of the FDMOs TropB, SorbC, and AzaH, is the requirement for an electron-withdrawing group at C1. As the biosynthetic routes to the substrates for dearomatization employ non-reducing polyketide synthases, there seems to be evolutionary pressure for these enzymes and their homologs to only recognize substrates featuring this specific oxidation pattern. To access enantioenriched *o*-quinols, which do not feature this NRPKS motif, new enzyme classes should be explored for the desired reactivity.

Chapter 2.6: Experimental

Chapter 2.6.1: Substrate Synthesis

All reagents were used as received unless otherwise noted. Reactions were carried out under a nitrogen atmosphere using standard Schlenck techniques unless otherwise noted. Solvents were degassed and dried over aluminum columns on an MBraun solvent system (Innovative Technology, inc., Model PS-00-3). Reactions were monitored by thin layer chromatography using Millipore 60 F_{254} pre-coated silica TLC plates (0.25 mm) which were visualized using UV, *p*-anisaldehyde, CAM, DNP, or bromocresol green stains. Flash column chromatography was performed using Machery-Nagel 60 μm (230-400 mesh) silica gel. All compounds purified by column chromatography were sufficiently pure for use in further experiments unless otherwise indicated. ^{1}H and ^{13}C NMR spectra were obtained in $CDCl_3$ at rt (25 °C), unless otherwise noted, on Varian 400 MHz or Varian 600 MHz spectrometers. Chemical shifts of ^{1}H NMR spectra were recorded in parts per million (ppm) on the δ scale. High resolution electrospray mass spectra were obtained on an Agilent UPLC-QTOF at the University of Michigan Life Sciences Institute. IR spectra were recorded on a Perkin-Elmer Spectrum BX FT-IR spectrometer. Melting points were obtained on a MEL-TEMP capillary melting point apparatus.

List of reagents prepared or purified:

2-Iodoxybenzoic Acid (IBX) was synthesized according to the procedure described by Sputore et al.[21] **Trifluoroacetic acid** and **acetic anhydride** were distilled prior to use.

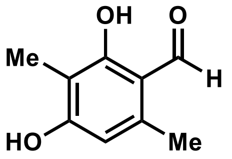

2,4-Dihydroxy-3,6-dimethylbenzaldehyde (2.12)

2.50 mL DMF was added to a flame-dried round-bottom flask equipped with a stir bar. The vessel was cooled to 0 °C and $POCl_3$ (0.50 mL, 4.4 mmol, 1.1 equiv) was slowly added over the course of 10 min. The mixture was stirred for 30 min before 2,5-dimethylbenzene-1,3-diol (0.55 g, 4.0 mmol in 2.50 mL DMF) was added dropwise. The mixture was warmed to rt. After 2 h, the reaction was quenched by the addition of ice (1.0 g) followed by 10% $NaOH_{(aq)}$ until a pH of 13 was achieved. The mixture was refluxed for 10 min before cooling to rt. Acidification to pH 3 induced the precipitation of a white crystalline solid which was isolated by vacuum filtration to yield 0.44 g (66%) of the title compound. **^{1}H NMR** (400 MHz, $CDCl_3$) δ 12.65 (s, 1H), 10.07 (s, 1H), 6.21 (s, 1H), 5.67 (s, 1H), 2.50 (s, 3H), 2.08 (s, 3H). All spectra obtained were consistent with literature values.[9]

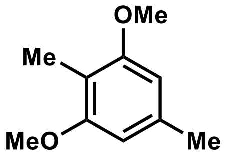

1,3-Dimethoxy-2,5-dimethylbenzene (2.23)

2,5-Dimethylbenzene-1,3-diol (1.00 g, 7.24 mmol), K_2CO_3 (5.14 g, 36.2 mmol, 5.0 equiv) and acetonitrile (14 mL) were added to a flame-dried round-bottom flask equipped with a stir bar. The vessel was cooled to 0 °C and MeI (2.25 mL, 36.2 mmol, 5.0 equiv) was slowly added. The mixture was heated to 40 °C and stirred for 16 h at this temperature. The mixture was then cooled to rt and filtered over celite. The celite was rinsed with EtOAc (5 mL). Water (20 mL) was added to the filtrate which was then extracted with EtOAc (3 x 15 mL). The combined organic layers were washed with water (15 mL) and brine (15 mL), dried over magnesium sulfate and filtered. The solvent was removed under reduced pressure to afford a colorless oil. Purification on silica gel (100% hexanes to 10% EtOAc in hexanes) afforded 0.52 g (43% yield) of resorcinol **2.23** as a colorless solid. **^{1}H NMR** (400 MHz, $CDCl_3$) δ 6.35 (s, 2H), 3.79 (s, 6H), 2.32 (s, 3H), 2.04 (s, 3H). All spectra obtained were consistent with literature values.[22]

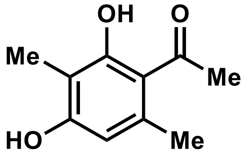

1-(2,4-Dihydroxy-3,6-dimethylphenyl)ethan-1-one (2.22a)

$AlCl_3$ (53 mg, 0.33 mmol, 1.1 equiv) and 0.5 mL of nitroethane were added to a flame-dried vial equipped with a stir bar. A solution of 1,3-dimethoxy-2,5-dimethylbenzene (50 mg, 0.30 mmol, 1.0 equiv in 0.2 mL nitroethane) was added followed by acetyl chloride (32 μL, 0.45 mmol, 1.5 equiv). The mixture was stirred for 4 h, and then, it was quenched by the addition of water (3 mL).

The mixture was extracted with DCM (3 x 10 mL). The combined organic layers were washed with brine, dried over magnesium sulfate and filtered. The solvent was removed under reduced pressure to afford a dark brown oil, which was taken up in hexanes and EtOAc (1:1) and filtered through a silica gel plug. The crude material was transferred to a flame-dried vial, dissolved in DCM (3.75 mL) and cooled to -78 °C. BBr_3 (0.625 mL, 1 M in DCM, 4.0 equiv, 0.625 mmol) was added dropwise. The mixture was then warmed to rt and stirred for 16 h at which time the reaction mixture was quenched by the slow addition of water. The resulting solution was extracted with EtOAc (3 x 10 mL). The combined organic layers were washed with brine, dried over magnesium sulfate and concentrated under reduced pressure to afford a dark brown solid. Purification on silica gel (100% hexanes to 15% EtOAc in hexanes) afforded 40.5 mg (76% yield over two steps) of the methyl ketone as a tan crystalline solid. **^{1}H NMR** (400 MHz, $CDCl_3$) δ 13.80 (s, 1H), 6.22 (s, 1H), 5.17 (s, 1H), 2.62 (s, 3H), 2.53 (s, 3H), 2.09 (s, 3H); **^{13}C NMR** (100 MHz, $CDCl_3$) δ 204.3, 164.7, 158.5, 139.1, 115.2, 111.0, 108.9, 33.1, 25.0, 7.4. All spectra obtained were consistent with literature values.[9]

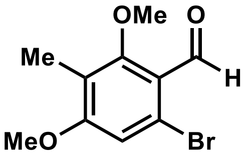

6-Bromo-2,4-dimethoxy-3-methylbenzaldehyde (2.32)

Concentrated HCl (1.96 mL) was added to a solution of (3-amino-2-bromo-4,6-dimethoxy-5-methylphenyl)methylene diacetate (1.07 g, 2.86 mmol, 1.0 equiv) in 10.0 mL of THF and 0.30 mL of distilled water. The mixture was cooled to -5 °C. Sodium nitrite (0.394 g, 5.71 mmol, 2.0 equiv) in 6.0 mL of distilled water was added, and the reaction was stirred at -5 °C for 1 h. Urea (0.172 g, 2.86 mmol, 1.0 equiv) was added to the resulting mixture followed by dropwise addition hypophosphorous acid (3.29 mL, 50% w/w aqueous solution). The solution was stirred at 4 °C for 12 h and was then warmed to 40 °C for 4 h. The reaction mixture was then cooled to rt and extracted with EtOAc (3 x 10 mL). The combined EtOAc extracts were washed with water, dried over magnesium sulfate, filtered and concentrated under reduced pressure. Purification on silica gel (100% hexanes to 30% EtOAc in hexanes) afforded 0.610 g (92% yield) of **2.32** as a white crystalline solid. ^{1}**H NMR** (400 MHz, $CDCl_3$) δ 10.28 (s, 1H), 6.93 (s, 1H), 3.90 (s, 3H), 3.81 (s, 3H), 2.10 (s, 3H). All spectra obtained were consistent with literature values.[3c]

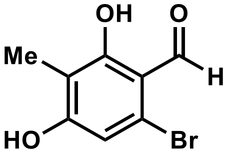

6-Bromo-2,4-dihydroxy-3-methylbenzaldehyde (2.55)

To a flame-dried vial was added 6-bromo-2,4-dimethoxy-3-methylbenzaldehyde (28.5 mg, 0.110 mmol, 1.0 equiv) in 0.5 mL DCM. The solution was cooled to -78 °C, and BBr_3 (0.44 mL, 1 M in DCM, 4.0 equiv) was added dropwise. The mixture was then warmed to rt and stirred for 24 h. The reaction mixture was quenched by the slow addition of water (2 mL). The solution was extracted with EtOAc (3 x 10 mL). The combined organic layers were washed with brine, dried over sodium sulfate and concentrated under reduced pressure to afford a tan oil. Purification on silica gel (10% to 20% EtOAc in hexanes) afforded 21.0 mg (83% yield) of the title compound as a colorless solid. ^{1}**H NMR** (400 MHz, $CDCl_3$) δ 12.67 (s, 1H), 10.11 (s, 1H), 6.68 (s, 1H), 5.50 (s, 1H), 2.08 (s, 3H). All spectra obtained were consistent with literature values.[3c]

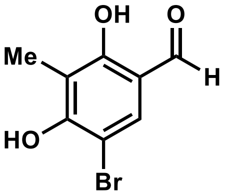

5-Bromo-2,4-dihydroxy-3-methylbenzaldehyde (2.50)

2,4-Dihydroxy-3-methylbenzaldehyde (1.00 g, 6.57 mmol, 1.0 equiv) and 17 mL of MeOH were added to a flame-dried round-bottom flask equipped with a stir bar. 1.52 g NBS (1.3 equiv) was added, and the mixture was allowed to stir at rt for 4 h. The solution was concentrated and extracted with EtOAc (3 x 15 mL). The combined organic layers were washed with brine, dried over sodium sulfate, filtered and concentrated under reduced pressure to afford an orange oil. Purification on silica gel (100% hexanes to 10% EtOAc in hexanes) afforded 1.45 g (96% yield) of the title compound as a colorless yellow solid. **^{1}H NMR** (600 MHz, $(CD_3)_2SO$) δ 11.37 (s, 1H), 9.74 (s, 1H), 7.80 (s, 1H), 2.70 (s, 3H); **^{13}C NMR** (150 MHz, $(CD_3)_2SO$) δ 195.1, 160.3, 159.4, 135.1, 116.1, 113.5, 102.1, 9.2; **HR-ESI-MS**: *m/z* calculated for $C_8H_7BrO_3$ $[M-H]^-$. 228.9506, found: 228.9507; **IR** (thin film)**:** 3504, 3220, 1610, 1233, 1062, 1159 cm^{-1}; **MP**: 141.1-141.9 °C.

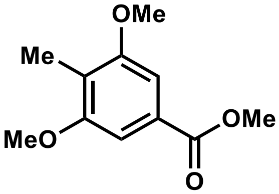

Mehtyl-3,5-dimethoxy-4-methylbenzoate (2.92)

3,5-Dihydroxy-4-methylbenzoic acid (2.00 g, 11.9 mmol, 1.0 equiv), K_2CO_3 (9.90 g, 71.4 mmol, 6.0 equiv) and 30 mL acetone were added to a flame-dried round-bottomed flask equipped with a stir bar. The vessel was cooled to 0 °C and MeI (4.4 mL, 71 mmol, 6.0 equiv) was slowly added. The mixture was then heated to 40 °C and stirred until complete consumption of the starting material was observed by TLC. The mixture was then filtered, and the residue rinsed with EtOAc. The mixture was extracted with EtOAc (3 x 100 mL) and washed with 50 mL water followed by 50 mL brine. The combined organic layers were dried over magnesium sulfate and filtered. The solvent was removed under reduced pressure to afford a colorless crystalline solid, which was recrystallized from EtOH to afford 1.90 g (76% yield) of ester **2.39**. **^{1}H NMR** (400 MHz, $CDCl_3$) δ 7.22 (s, 2H), 3.91 (s, 3H), 3.87 (s, 6H), 2.13 (s, 3H). All spectra obtained were consistent with literature values.[23]

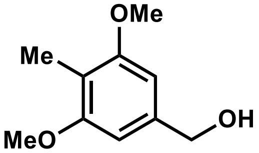

(3,5-Dimethoxy-4-methylphenyl)methanol (2.93)

3,5-Dimethoxy-4-methylbenzoate (1.50 g, 7.13 mmol, 1.0 equiv) and 8 mL of DCM were added to a flame-dried round-bottom flask equipped with a stir bar. The reaction vessel was cooled to 0 °C and DIBAL-H (15.7 mL,1 M in hexanes, 2.2 equiv) was added dropwise. The mixture was allowed to stir for 1 h and was then quenched with 1 M $HCl_{(aq)}$ (20 mL). The mixture was extracted with EtOAc. The combined EtOAc extracts were washed with water, dried over magnesium sulfate, filtered and concentrated under reduced pressure. Purification on silica gel (100% DCM to 10% MeOH in DCM) afforded 1.32 g (99%) of the benzyl alcohol **2.93** as a colorless oil. **^{1}H NMR** (400 MHz, $CDCl_3$) δ 6.54 (s, 2H), 4.64 (s, 2H), 3.81 (s, 6H), 2.06 (s, 3H). All spectra obtained were consistent with literature values.[24]

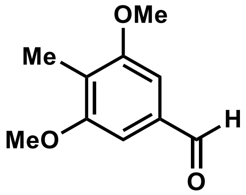

3,5-Dimethoxy-4-methylbenzaldehyde (2.39)

A solution of (3,5-dimethoxy-4-methylphenyl)methanol (1.00 g, 5.50 mmols, 1.0 equiv) in 40 mL of EtOAc was added to a flame-dried round-bottom flask equipped with a stir bar. To this mixture was added IBX (4.62 g, 16.5 mmol, 3.0 equiv). The mixture was heated to 80 °C and stirred for 5 h at this temperature. The mixture was then cooled to rt, washed with water, dried over magnesium sulfate, filtered and concentrated under reduced pressure. Purification on silica gel (100% hexanes to 15% EtOAc in hexanes) afforded 1.0 g (99% yield) of **2.39** as a crystalline white solid. **^{1}H NMR** (400 MHz, $CDCl_3$) δ 9.89 (s, 1H), 7.04 (s, 2H), 3.88 (s, 6H), 2.14 (s, 3H). All spectra obtained were consistent with literature values.[25]

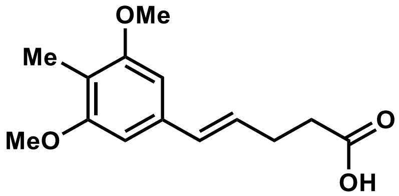

(*E*)-4-(3,5-dimethoxy-4-methylphenyl)but-3-enoic acid (2.41)

(2-Carboxypropyl)triphenylphosphonium bromide (0.852 g, 4.73 mmols, 1.2 equiv) in 3.0 mL of DCM was added to a flame-dried round-bottom flask equipped with a stir bar. The solution was cooled to 0 °C and KO*t*Bu (1.32 g, 11.8 mmol, 2.5 equiv) was added in a single portion. The mixture was allowed to stir for 1 h before the addition of (3,5-dimethoxy-4-methylphenyl)methanol (2.36 g, 1.83 mmol, 1.0 equiv). The resulting mixture was allowed to stir at rt for 8 h. The reaction was quenched by the addition of water (3 mL) and acidified to a pH of 1 with 1 M HCl. The mixture was extracted with DCM (3 x 10 mL). The combined organic layers were washed with brine, dried over magnesium sulfate, filtered, and concentrated under reduced pressure. Purification on silica gel (100% DCM to 10% MeOH in DCM) afforded 1.10 g (93% yield) of the acid **2.41** as a crystalline yellow solid. **^{1}H NMR** (600 MHz, $CDCl_3$) δ 6.55 (s, 1H), 6.43 (d, J = 15.7 Hz, 1H), 6.19 (m, 1H), 3.84 (s, 6H), 2.57 (m, 4H), 2.10 (s, 3H); **^{13}C NMR** (150 MHz, $CDCl_3$) δ 179.4, 158.3, 135.7, 131.6, 127.2, 113.9, 101.6, 55.7, 33.8, 27.9, 8.2; **HR-ESI-MS**: *m/z* calculated for $C_{14}H_{17}O_4$ $[M-H]^-$: 249.1132, found: 249.1130; **IR** (thin film)**:** 2997, 2937, 1706, 1529 cm^{-1}; **MP**: 117.0-119.3 °C.

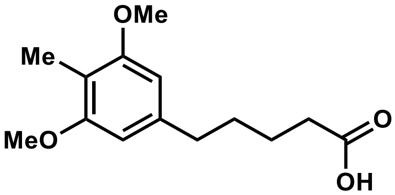

5-(3,5-dimethoxy-4-methylphenyl)pentanoic acid (2.94)

(*E*)-4-(3,5-dimethoxy-4-methylphenyl)but-3-enoic acid (1.10 g, 4.39 mmol, 1.0 equiv), Pd/C 10 wt% (0.467 g, 0.439 mmol, 0.1 equiv) and MeOH (20 mL) were added to a round-bottom flask. The flask was sparged with N_2 for 30 min then equipped with a H_2 filled balloon and sparged again for 30 min. The reaction was stirred under a H_2 atmosphere for 24 h. The mixture was then filtered through celite and concentrated under reduced pressure. Purification on silica gel (100% DCM to 10% MeOH in DCM) afforded 1.02 g (92% yield) of acid **2.94** as a white solid. **^{1}H NMR** (400 MHz, $CDCl_3$) δ 1H NMR δ 6.37 (s, 2H), 3.82 (s, 6H), 2.62 (t, J = 7.2 Hz, 2H), 2.41 (t, J = 6.6 Hz, 2H), 2.06 (s, 3H), 1.71 (m, 4H); **^{13}C NMR** (150 MHz, $CDCl_3$) δ 179.9, 158.2, 140.5, 105.1, 103.8, 55.7, 36.1, 33.9, 30.9, 24.3, 7.9; **HR-ESI-MS**: *m/z* calculated for $C_{14}H_{19}O_4$ $[M-H]^-$; 251.1289, found: 251.1291; **IR** (thin film)**:** 2995, 2958, 2459, 1529 cm^{-1}; **MP**: 83.7-85.8 °C.

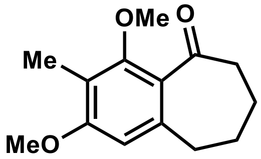

2,4-dimethoxy-3-methyl-6,7,8,9-tetrahydro-5H-benzo[7]annulen-5-one (2.42)

5-(3,5-dimethoxy-4-methylphenyl)pentanoic acid (1.02 g, 4.04 mmol, 1.0 equiv) and polyphosphoric acid (10.0 mL) were added to a flame-dried round-bottom flask equipped with a stir bar. The mixture was heated to 60 ˚C and stirred for 2 h. The reaction was then quenched by the addition of water (10 mL) and extracted with EtOAc (3 x 15 mL). The combined organic layers were dried over magnesium sulfate, filtered and concentrated under reduced pressure. Purification on silica gel (100% hexanes to 15% EtOAc in hexanes) afforded 0.745 g (81% yield) of **4.42** as a colorless solid. **^{1}H NMR** (600 MHz, $CDCl_3$) δ 6.40 (s, 2H), 3.84 (s, 3H), 3.75 (s, 3H), 2.73 (m, 2H), 2.60 (m, 2H), 2.10 (s, 3H), 1.77 (m, 4H); **^{13}C NMR** (150 MHz, $CDCl_3$) δ 196.1, 161.9, 160.2, 145.7, 119.7, 119.4, 105.6, 60.9, 55.7, 55.6, 40.7, 31.3, 23.0, 8.2; **HR-ESI-MS**: *m/z* calculated for $C_{14}H_{17}O_3$ $[M-H]^-$: 233.1183, found: 233.1186; **IR** (thin film)**:** 2935, 1682, 1593, 1573 cm^{-1}; **MP**: 62.3-63.9 °C.

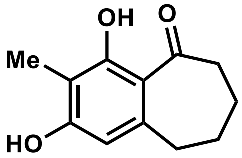

2,4-dihydroxy-3-methyl-6,7,8,9-tetrahydro-5H-benzo[7]annulen-5-one (2.43)

2,4-dimethoxy-3-methyl-6,7,8,9-tetrahydro-5H-benzo[7]annulen-5-one (50.0 mg, 0.213 mmol, 1.0 equiv) was dissolved in 1.10 mL DCM. The solution was cooled to -78 °C and BBr_3 (0.853 mL, 1 M in DCM, 4.0 equiv) was added dropwise. The mixture was then warmed to rt and stirred for 24 h. The reaction mixture was quenched by the slow addition of water (5 mL). The solution was extracted with EtOAc (3 x 10 mL). The combined organic layers were washed with brine, dried over sodium sulfate and concentrated under reduced pressure to afford a brown oil. Purification on silica gel (10% to 20% EtOAc in hexanes) afforded 44.0 mg (99% yield) of the title compound as a colorless solid. **^{1}H NMR** (600 MHz, $CDCl_3$) δ 13.49 (s, 1H), 6.22 (s, 1H), 5.22 (s, 1H), 2.86 (m, 4H), 2.10 (s, 3H), 1.83 (m, 4H); **^{13}C NMR** (151 MHz, $CDCl_3$) δ 208.2, 164.2, 158.8, 144.6, 114.3, 108.9, 108.8, 41.4, 33.5, 24.6, 20.7, 7.3; **HR-ESI-MS**: *m/z* calculated for $C_{12}H_{14}O_3$ $[M-H]^-$: 205.0870, found: 205.0872; **IR** (thin film)**:** 2927, 1574, 1439, 1296, 1127 cm^{-1}; **MP**: 156.2-157.9 °C.

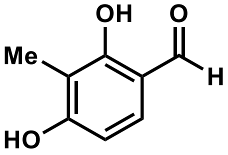

2,4-dihydroxy-3-methylbenzaldehyde (2.49)

13.4 mL DMF was added to a flame-dried round bottom flask equipped with a stir bar. The vessel was cooled to 0 °C and $POCl_3$ (3.04 mL, 32.6 mmol, 1.5 equiv) was slowly added over the course of 10 min. The mixture was stirred for 30 min before 2,5-dimethylbenzene-1,3-diol (3.00 g, 21.7 mmol, 1.0 equiv in 13.4 mL DMF) was added dropwise. The mixture was then warmed to rt. After 2 h, the reaction was quenched by the addition of ice (approx. 5 g) followed by addition of 10% $NaOH_{(aq)}$ until a pH of 13 was achieved. The mixture was then refluxed for 10 min before cooling to rt. Acidification to pH 3 induced the precipitation of a yellow crystalline solid which was isolated by vacuum filtration to yield 3.24 g (98% yield) of the title compound. **^{1}H NMR** (600 MHz, $CDCl_3$) δ 11.66 (d, J = 1.4 Hz, 1H), 9.69 (s, 1H), 7.29 (d, J = 8.5 Hz, 1H), 6.47 (d, J = 8.4 Hz, 1H), 5.72 (s, 1H), 2.14 (s, 3H). All spectra obtained were consistent with literature values.[26]

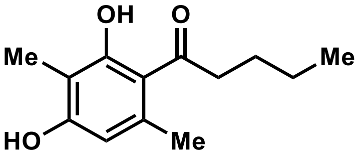

1-(2,4-Dihydroxy-3,6-dimethylphenyl)butan-1-one (22.2d)

$AlCl_3$ (44.0 mg, 0.330 mmol, 1.1 equiv) and 0.5 mL of nitroethane were added to a flame-dried vial equipped with a stir bar. A solution of 1,3-dimethoxy-2,5-dimethylbenzene (50 mg, 0.30 mmol, 1.0 equiv) in 0.2 mL nitroethane was added followed by butyryl chloride (46.7 μL, 0.450 mmol,1.5 equiv). The mixture was then stirred overnight before the reaction was quenched by the addition of water (3 mL). The mixture was then extracted three times with EtOAc (3 x 15 mL). The combined organic layers were washed with brine, dried over magnesium sulfate and filtered. The solvent was removed under reduced pressure to afford a dark brown oil. The oil was then taken up in hexanes and EtOAc (1:1) and filtered through a silica gel plug. This crude material was transferred to an oven-dried vial, dissolved in DCM (3.75 mL) and cooled to -78 °C. BBr_3 (1.20 mL, 1 M in DCM, 4.0 equiv) was added dropwise. After 20 h, the reaction mixture was quenched by the slow addition of water (10 mL). The solution was extracted three times with DCM. The combined organic layers were washed with brine and dried over magnesium sulfate. The solvent was removed under reduced pressure to afford a dark brown oil. Purification on silica gel (100% hexanes to 15% EtOAc in hexanes) afforded 38.9 mg (53% yield over two steps) of the title compound as a colorless solid. **^{1}H NMR** (600 MHz, $CDCl_3$) δ 13.56 (s, 1H), 6.21 (s, 1H), 5.70 (s, 1H), 2.89 (t, J = 8.5 Hz, 2H), 2.52 (s, 3H), 2.09 (s, 3H), 1.70 (m, 2H), 1.38 (m, 2H), 0.94 (t, J = 8.5 Hz, 3H); **^{13}C NMR** (150 MHz, $CDCl_3$) δ 207.7, 164.0, 158.4, 138.4, 115.4, 111.1, 109.1, 43.7, 27.2, 24.8, 22.5, 13.9, 7.5 ; **HR-ESI-MS**: *m/z* calculated for $C_{13}H_{17}O_3$ $[M-H]^-$: 221.1183, found: 221.1183; **IR** (thin film)**:** 2927, 1574, 1439, 1296, 1127 cm^{-1}; **MP**: 156.2-157.9°C.

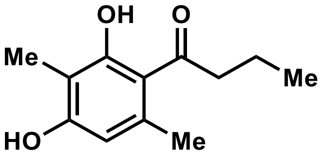

1-(2,4-Dihydroxy-3,6-dimethylphenyl)butan-1-one (2.22c)

$AlCl_3$ (44.0 mg, 0.3 mmol, 1.1 equiv) and 0.5 mL of nitroethane were added to a flame-dried vial equipped with a stir bar. A solution of 1,3-dimethoxy-2,5-dimethylbenzene (50 mg, 0.30 mmol, 1.0 equiv) in 0.2 mL of nitroethane was added followed by propionyl chloride (39.3 μL, 0.450 mmol, 1.5 equiv). The mixture was stirred overnight, and then the reaction was quenched by the addition of water (3 mL). The mixture was extracted with EtOAc (3 x 15 mL). The combined organic layers were washed with brine, dried over magnesium sulfate and filtered. The solvent was removed under reduced pressure to afford a dark brown oil. The oil was then taken up in hexanes and EtOAc (1:1) and filtered through a silica gel plug. This crude material was transferred to an oven-dried vial, dissolved in DCM (3.75 mL) and cooled to -78 °C. BBr_3 (1.20 mL, 1 M in DCM, 4.0 equiv) was added dropwise. After 24 h, the reaction mixture was quenched by the slow addition of water (10 mL). The solution was extracted with EtOAc (3 x 15 mL). The combined organic layers were washed with brine (10 mL) and dried over magnesium sulfate. The solvent was removed under reduced pressure to afford a dark brown oil. Purification on silica gel (100% hexanes to 15% EtOAc in hexanes) afforded 44.4 mg (71% yield over two steps) of the title compound as a pale yellow solid. **^{1}H NMR** (400 MHz, $CDCl_3$) δ 13.56 (s 1H), 6.21 (s, 1H), 5.39 (s, 1H), 2.88 (t, J = 8, 2H), 2.53 (s, 3H), 2.09 (s, 3H), 1.76 (m, 2H), 0.98 (t, 3H, J = 8 Hz). All spectra obtained were consistent with literature values.[15]

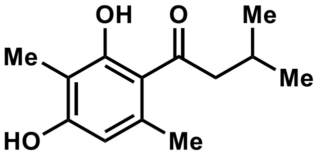

1-(2,4-Dihydroxy-3,6-dimethylphenyl)-3-methylbutan-1-one (2.22e)

$AlCl_3$ (44.0 mg, 0.330 mmol, 1.1 equiv) and 0.5 mL nitroethane were added to a flame-dried vial equipped with a stir bar. A solution of 1,3-dimethoxy-2,5-dimethylbenzene (50.0 mg, 0.300 mmol, 1.0 equiv) in 0.2 mL nitroethane was then added followed by isobutyryl chloride (39.3 µL, 0.450 mmol, 1.5 equiv). The mixture was stirred overnight before the reaction was quenched by the addition of water (3 mL). The mixture was extracted with EtOAc (3 x 15 mL). The combined organic layers were washed with brine (1 x 10 mL), dried over magnesium sulfate and filtered. The solvent was removed under reduced pressure to afford a dark brown oil. The oil was taken up in hexanes and EtOAc (1:1) and filtered through a silica gel plug. The crude material was transferred to an oven-dried vial, dissolved in DCM (3.75 mL) and cooled to -78 °C. BBr_3 (1.20 mL, 1 M in DCM, 4.0 equiv) was added dropwise. After 4 h, the reaction mixture was quenched by the slow addition of water (10 mL). The solution was extracted with EtOAc (3 x 15 mL). The combined organic layers were washed with brine (1 x 10 mL) and dried over magnesium sulfate. The solvent was removed under reduced pressure to afford a dark brown oil. Purification on silica gel (100% hexanes to 15% EtOAc in hexanes) afforded 41.3 mg (62% yield over two steps) of the title compound as a tan solid. **^{1}H NMR** (400 MHz, $CDCl_3$) δ 13.34 (s, 1H), 6.20 (s, 1H), 5.10 (s, 1H), 2.78 (d, J = 6.6 Hz, 1H), 2.53 (s, 3H), 2.27 (m, 1H), 2.09 (s, 3H), 0.96 (d, J = 6.6 Hz, 6H).**^{13}C NMR** (150 MHz, $CDCl_3$) δ 207.6, 163.7, 158.6, 138.3, 115.7, 111.2, 109.3, 52.8, 25.9, 24.7, 22.7, 7.6; **HR-ESI-MS**: *m/z* calculated for $C_{13}H_{17}O_3$ $[M-H]^-$: 221.1183, found: 221.1185; **IR** (thin film)**:** 3377, 2959, 1589, 1400, 1110 cm^{-1}; **MP**: 69.2-71.8 °C.

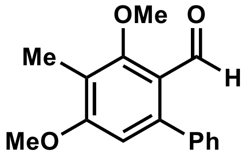

3,5-dimethoxy-4-methyl-[1,1'-biphenyl]-2-carbaldehyde (2.52)

6-Bromo-2,4-dimethoxy-3-methylbenzaldehyde (100 mg, 0.433 mmol, 1.0 equiv), Pd(PPh)$_4$ (50.0 mg, 0.0430 mmol, 0.1 equiv), and K_2CO_3 (138 mg, 0.693 mmol, 1.6 equiv) were added to a flame-dried vial which was then backfilled with N_2. DMF (3.0 mL) was added followed by phenylboronic acid (79.0 mg, 0.649 mmol, 1.5 equiv), and the mixture was sparged with N_2 for 15 min. The mixture was capped and stirred at 100 °C for 10 h at which time the reaction mixture was allowed to cool to rt. The reaction was diluted with EtOAc (10 mL) and washed with water (3 x 10 mL) and brine (1 x 10 mL). The organic layer was dried over magnesium sulfate and concentrated under reduced pressure to afford a brown oil. Purification on silica gel (10% EtOAc in hexanes) afforded 81.3 mg (73% yield) of biphenyl **2.52** as a colorless oil. **^{1}H NMR** (400 MHz, $CDCl_3$) δ 9.91 (s, 1H), 7.40 (m, 3H), 7.32 (m, 2H), 6.60 (s, 1H), 3.89 (s, 3H), 2.19 (s, 3H); **^{13}C NMR** (151 MHz, $CDCl_3$) δ 190.3, 161.9, 160.6, 146.4, 139.4, 129.6, 128.1, 127.8, 121.1, 120.1, 108.6, 62.3, 55.8, 8.4; **HR-ESI-MS:** m/z calculated for $C_{16}H_{17}O_3$ [M+Na]$^+$: 279.0992, found: 279.0994; **IR** (thin film): 3060, 2959, 1603, 1582 cm^{-1}.

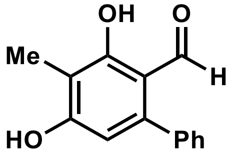

3,5-dihydroxy-4-methyl-[1,1'-biphenyl]-2-carbaldehyde (2.53)

3,5-dimethoxy-4-methyl-[1,1'-biphenyl]-2-carbaldehyde (83.1 mg, 0.317 mmol, 1.0 equiv) in DCM (4.0 mL) was cooled to -78 °C, and BBr_3 (1.27 mL, 1 M in DCM, 4.0 equiv) was added dropwise. The mixture was then warmed to rt and stirred for 24 h. The reaction mixture was quenched by the slow addition of water (10 mL). The solution was extracted with EtOAc (3 x 15 mL). The combined organic layers were washed with brine, dried over sodium sulfate and concentrated under reduced pressure to afford a brown oil. Purification on silica gel (10% to 20% EtOAc in hexanes) afforded 61.5 mg (85% yield) of the title compound as a white solid. **^{1}H NMR** (400 MHz, $CDCl_3$) δ 12.66 (s, 1H), 9.63 (s, 1H), 7.45 (m, 3H), 7.34 (m, 2H), 6.36 (s, 1H), 5.49 (s, 1H), 2.18 (s, 3H); **^{13}C NMR** (100 MHz, $CDCl_3$) δ 195.3, 163.6, 160.2, 146.8, 137.3, 129.8, 128.3, 128.2, 112.7, 110.2, 109.5, 7.1; **HR-ESI-MS:** m/z calculated for $C_{14}H_{11}O_3$ $[M-H]^-$: 227.0714, found: 227.0715; **IR** (thin film): 2922, 1597, 1289, 1252, 1222, 1115 cm^{-1}; **MP**: 121.5-123.7 °C.

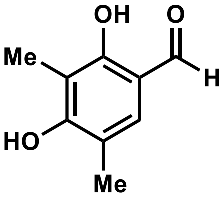

2,4-dihydroxy-3,5-dimethylbenzaldehyde (2.58)

0.45 mL DMF was added to a flame-dried round-bottom flask equipped with a stir bar. The vessel was cooled to 0 °C and $POCl_3$ (0.081 mL, 0.86 mmol, 1.2 equiv) was slowly added. The mixture was stirred for 30 min before 2,4-dimethylbenzene-1,3-diol (100 mg, 0.72 mmol in 0.45 mL DMF) was added dropwise. The mixture was warmed to rt. After 2 h, the reaction was quenched by the addition of ice (approx. 250 mg) followed by 10% $NaOH_{(aq)}$ until a pH of 13 was achieved at which time a precipitate formed. A white crystalline solid was isolated by vacuum filtration to yield 45.3 mg (41% yield) of the title compound. **^{1}H NMR** (400 MHz, $CDCl_3$) δ 11.54 (s, 1H), 9.66 (s, 1H), 7.14 (s, 1H), 5.39 (s, 1H), 2.23 (s, 3H), 2.14 (s, 3H). All spectra obtained were consistent with literature values.[13]

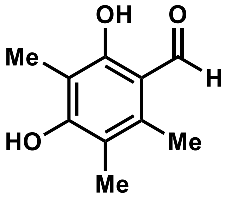

2,4-dihydroxy-3,5,6-trimethylbenzaldehyde (2.59)

2.50 mL DMF was added to a flame-dried round-bottom flask equipped with a stir bar. The vessel was cooled to 0 °C and $POCl_3$ (0.50 mL, 4.4 mmol, 1.1 equiv) was slowly added over 10 min. The mixture was stirred for 30 min before 2,4,5-trimethylbenzene-1,3-diol (0.55 g, 4.0 mmol in 2.5 mL DMF) was added dropwise. The mixture was then warmed to rt. After 2 h, the reaction was quenched by the addition of ice (approx. 1 g) followed by 10% $NaOH_{(aq)}$ until a pH of 13 was achieved. The mixture was refluxed for 10 min before cooling to rt. Acidification to pH 3 induced precipitation of a white crystalline solid, which was isolated by vacuum filtration to yield 0.44 g (66% yield) of the title compound. **^{1}H NMR** (400 MHz, $CDCl_3$) δ 12.79 (s, 1H), 10.18 (s, 1H), 5.46 (s, 1H), 2.46 (s, 3H), 2.14 (s, 3H), 2.11 (s, 3H). All spectra obtained were consistent with literature values.[27]

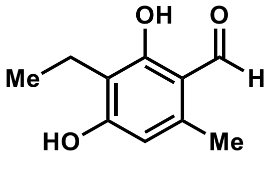

3-ethyl-2,4-dihydroxy-6-methylbenzaldehyde (2.47)

To a flame-dried round-bottomed flask equipped with a stir bar was added 2.5 mL DMF. The vessel was cooled to 0 °C and $POCl_3$ (0.50 mL, 1.1 equiv) was slowly added over 10 min. 2-ethyl-

5-methylbenzene-1,3-diol (0.61 g, 4.0 mmol, 1.0 equiv) as a solution in 2.50 mL DMF was added dropwise. The mixture was warmed to rt. After 2 h, the reaction was quenched by the addition of ice followed by 10% $NaOH_{(aq)}$ to a pH of 13. The mixture was refluxed for 10 min before being cooling to rt and acidified to a pH of 3. A white crystalline solid precipitated and was isolated by vacuum filtration to yield 0.42 g (58% yield) of the title compound. **^{1}H NMR** (600 MHz, CD_3CN) δ 12.73 (s, 1H), 10.07 (s, 1H), 7.72 (s, 1H), 6.28 (s, 1H), 2.58 (q, J = 7.5 Hz, 2H), 2.25 (s, 3H), 1.08 (t, J = 7.5 Hz, 3H);**^{13}C NMR** (150 MHz, CD_3CN) δ 194.0, 163.6, 162.1, 142.2, 115.0, 112.8, 110.0, 17.0, 15.0, 12.6; **HRMS** (ESI) *m/z* calculated for $C_{14}H_{11}O_3$ $[M-H]^-$ 179.0714, found: 179.0713; **IR** (thin film) 2965, 1607, 1234, 1113 cm^{-1}; **MP**: 152.0-154.6 °C.

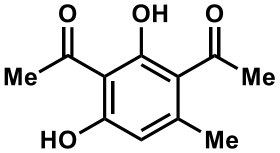

1,1'-(2,4-dihydroxy-6-methyl-1,3-phenylene)bis(ethan-1-one) (2.60)

A mixture of 1,3-diacetoxy-5-methylbenzene (50 mg, 0.24 mmol) and $AlCl_3$ (100 mg, 0.72 mmol, 3.0 equiv) in chlorobenzene (2.5 mL) was stirred at 90 °C for 24 h. After cooling to rt, ice (3 g) was added to the reaction mixture. The mixture was extracted with EtOAc (3 x 10 mL). The combined organic layers were washed with brine (1 x 5 mL), dried over sodium sulfate and concentrated under reduced pressure to give crude 2,6-diacetyl-5-methylresorcinol (53 mg). Purification on silica gel (20% EtOAc in hexanes) afforded 43 mg (85% yield) of the diketone as a colorless solid. **^{1}H NMR** (600 MHz, $CDCl_3$): δ 6.29 (s, 1H), 2.74 (s, 3H), 2.65 (s, 3H), 2.57 (s, 3H). All spectra obtained were consistent with literature values.[28]

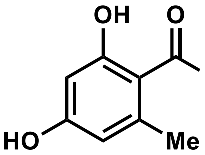

2,4-dihydroxy-6-methylbenzaldehyde (2.61)

10 mL DMF was added to a flame-dried round-bottomed flask equipped with a stir bar. The vessel was cooled to 0 °C and $POCl_3$ (0.82 mL, 8.9 mmol, 1.1 equiv) was slowly added over 10 min. 5-methyl resorcinol (1.0 g, 8.1 mmol, 1.0 equiv) as a solution in 5.0 mL DMF was added dropwise. The mixture was warmed to rt. After 2 h, the reaction was quenched by the addition of ice followed by 10% $NaOH_{(aq)}$ to a pH of 13. The mixture was refluxed for 10 min before being cooling to rt and acidified to pH 3. A white crystalline solid precipitated and was isolated by vacuum filtration to yield 1.1 g (87% yield) of the aldehyde. **^{1}H NMR** (400 MHz, $CDCl_3$) δ 12.38 (s, 1H), 10.10 (s, 1H), 6.25 (overlapping s, 2H), 5.46 (s, 1H), 2.53 (s, 3H). All spectra obtained were consistent with literature values.[29]

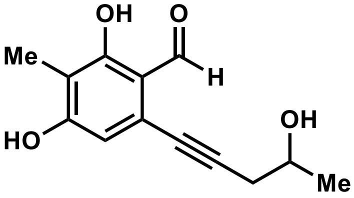

2,4-dihydroxy-6-(4-hydroxypent-1-yn-1-yl)-3-methylbenzaldehyde ((±)-2.95)

6-Bromo-2,4-dihydroxy-3-methylbenzaldehyde (**2.55**) (140 mg, 0.649 mmol, 1.0 equiv), $PdCl_2(PPh_3)_2$ (46.1 mg, 0.065 mmol, 0.1 equiv) and CuI (12.4 mg, 0.065 mmol, 0.1 equiv) in 4.7 mL anhydrous DMF were added to a flame-dried round-bottomed flask. ± 4-Pentyn-2-ol (73.5 μL, 0.779 mmol, 1.2 equiv) and Et_3N (298 μL, 2.14 mmol, 3.3 equiv) were then added, and the mixture was sparged with N_2 for 15 min. The mixture was heated at 60 °C for 14 h. The reaction mixture was cooled to rt, diluted with water (5 mL) and acidified to a pH of 2. The mixture was extracted with EtOAc (3 x 15 mL) and the combined organic layers were washed with water (10 mL) and brine (10 mL), dried over sodium sulfate, filtered, and concentrated under reduced pressure to afford crude **2.95**. Purification on silica gel (50% EtOAc in hexanes) provided 121 mg (80% yield) of alkynylbenzaldehyde **2.95** as a yellow solid. **^{1}H NMR** (400 MHz, CD_3OD) δ 10.16 (s, 1H), 6.49 (s, 1H), 3.98 (h, J = 6.1 Hz, 1H), 2.59 (d, J = 6.0 Hz, 2H), 2.01 (s, 3H), 1.29 (d, J = 6.2 Hz, 3H); **^{13}C NMR** (150 MHz, $(CD_3)_2SO$) δ 194.9, 163.4, 162.6, 126.8, 113.3, 112.4, 111.5, 95.4, 77.3, 65.3, 29.8, 23.3, 7.8; **HR-ESI-MS:** *m/z* calculated for $C_{13}H_{13}O_4$ $[M-H]^-$ 233.0819, found: 233.0820; **IR** (thin film) 2965, 1607, 1234, 113 cm^{-1}; **MP**: 89.4-90.3 °C.

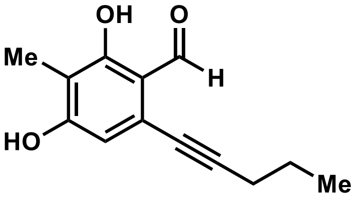

2,4-dihydroxy-3-methyl-6-(pent-1-yn-1-yl)benzaldehyde (2.96)

6-Bromo-2,4-dihydroxy-3-methylbenzaldehyde (**2.55**) (100 mg, 0.433 mmol, 1.0 equiv), $PdCl_2(PPh_3)_2$ (30.4 mg, 0.043 mmol, 0.1 equiv) and CuI (8.25 mg, 0.043 mmol, 0.1 equiv) in 3.1 mL anhydrous DMF were added to a flame-dried round-bottom flask. 1-Pentyne (85.0 μL, 0.866 mmol, 2.0 equiv) and Et_3N (197 μL, 1.41 mmol, 3.3 equiv) were added, and the resulting mixture was heated at 60 °C for 14 h. The reaction mixture was cooled to rt, diluted with water (5 mL), and neutralized with 1.0 N aqueous HCl (2 mL). The mixture was extracted with EtOAc (3 x 15 mL) and the combined organic layers were washed with water (10 mL), brine (10 mL), dried over sodium sulfate, filtered, and concentrated under reduced pressure afford **2.96**. Purification on silica gel (15% EtOAc in hexanes) provided 93.8 mg (99% yield) of the alkynylbenzaldehyde as a yellow solid. **^{1}H NMR** (600 MHz, $(CD_3)_2SO$) δ 12.26 (s, 1H), 10.93 (s, 1H), 10.05 (s, 1H), 6.53 (s, 1H), 2.44 (t, J = 7.0 Hz, 2H), 1.94 (s, 3H), 1.56 (h, J = 7.2 Hz, 2H), 0.98 (t, J = 7.4 Hz, 3H); **^{13}C NMR** (150 MHz, $(CD_3)_2SO$) δ 194.6, 163.4, 162.6, 126.8, 113.3, 112.5, 111.5, 97.5, 76.4, 21.9, 21.1, 13.8, 7.8; **HR-ESI-MS** (ESI) *m/z* calculated for $C_{13}H_{13}O_3$ $[M-H]^-$ 217.0870, found: 217.0870; **IR** (thin film) 2965, 1607, 1234, 1098 cm^{-1}; **MP**: 89.4-90.3 °C.

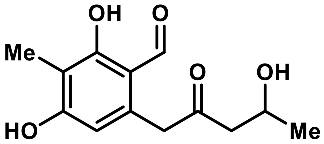

2,4-dihydroxy-6-(4-hydroxy-2-oxopentyl)-3-methylbenzaldehyde ((±)-2.18)

2,4-dihydroxy-3-methyl-6-(pent-1-yn-1-yl)benzaldehyde (121 mg, 0.519 mmol, 1.0 equiv) and $AgNO_3$ (8.8 mg, 0.052 mmol, 0.1 equiv) were added to a flame-dried round-bottom flask followed by DCE (5 mL) and TFA (198 μL, 2.60 mmol, 5.0 equiv). The resulting mixture was stirred at rt for 45 min. MeCN and water (10 mL, 10:1) was added, and the mixture was stirred for 1 h. The mixture was concentrated under reduced pressure and the residue was diluted with EtOAc (10 mL), washed with water (5 mL) and brine (5 mL). The organic layer was dried over sodium sulfate, filtered and concentrated under reduced pressure. Purification on silica gel (40% EtOAc in hexanes) provided 55.0 mg (42% yield) of aldehyde **25** as a colorless solid. **^{1}H NMR** (400 MHz, CD_3OD) δ 10.16 (s, 1H), 6.49 (s, 1H), 3.99 (m, 1H), 2.60 (m, 2H), 2.01 (s, 3H), 1.29 (d, *J* = 8.0 Hz, 3H) ppm. All spectra obtained were consistent with literature values.[30]

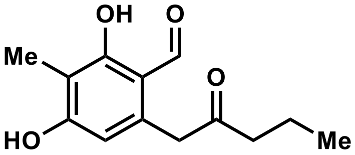

2,4-dihydroxy-3-methyl-6-(2-oxopentyl)benzaldehyde (2.62)

2,4-dihydroxy-3-methyl-6-(pent-1-yn-1-yl)benzaldehyde (99.8 mg, 0.430 mmol, 1.0 equiv) and $AgNO_3$ (7.3 mg, 0.043 mmol, 0.1 equiv) were added to a flame-dried round bottom flask followed by DCE (5 mL) and TFA (165 μL, 2.15 mmol, 5.0 equiv), and the resulting mixture was stirred at rt for 45 min. MeCN and water (10 mL, 10:1) was added and the mixture was stirred for 1 h. The mixture was then concentrated, and the residue was diluted with EtOAC (10 mL), washed with water (5 mL) and brine (5 mL). The organic layer was dried over sodium sulfate, filtered and concentrated under reduced pressure. Purification on silica gel (30% EtOAc in hexanes) provided 29.5 mg (29% yield) of the dicarbonyl as a tan solid. **^{1}H NMR** (400 MHz, $CDCl_3$) δ 12.65 (s, 1H), 9.86 (s, 1H), 6.19 (s, 1H), 3.89 (s, 2H), 2.51 (t, J = 7.3 Hz, 2H), 1.62 (q, J = 7.3 Hz, 2H), 0.91 (t, J = 7.4 Hz, 3H) ppm; **^{13}C NMR** (150 MHz, CD_3CN) δ 207.5, 194.1, 163.7, 162.2, 138.4, 112.7, 110.4, 110.0, 45.1, 44.0, 21.9, 6.4; **HR-ESI-MS**: *m/z* calcd. for $C_{13}H_{15}O_4$ $[M-H]^-$: 235.0976, found: 235.0975; **IR** (thin film) 2962, 1713, 1620, 1494 cm^{-1}; **MP**: 122.1-123.6 °C.

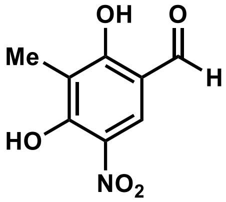

2,4-Dihydroxy-3-methyl-5-nitrobenzaldehyde (2.63)

A solution of 2,4-dihydroxy-3-methylbenzaldehyde (260 mg, 1.71 mmol, 1.0 equiv) in acetic anhydride (210 μL, 1.90 mmol, 1.1 equiv) was added to a round-bottom flask and cooled to 0 °C. $Cu(NO_3)_2{\bullet}3H_2O$ (546 mg, 2.22 mmol, 1.3 equiv) was added to the solution over 5 min. The reaction mixture was stirred for 2 h at 0 °C. The reaction was quenched by the addition of ice (4 g) and extracted with EtOAc (3 x 5 mL). The combined organic layers were washed with brine (5 mL), dried over sodium sulfate, filtered, and concentrated under reduced pressure. Purification on silica gel (30% EtOAc in hexanes) provided 211 mg (73% yield) of the nitrobenzaldehyde as a pale yellow solid. **^{1}H NMR** (400 MHz, $CDCl_3$) δ 11.88 (s, 1H), 11.53 (s, 1H), 9.80 (s, 1H), 8.36 (s, 1H), 2.19 (s, 3H); **^{13}C NMR** (100 MHz, $CDCl_3$) δ 194.4, 165.5, 159.3, 130.7, 127.7, 115.2, 114.3, 7.4; **IR** (thin film): 2922, 1597, 1289, 1252, 1222, 1115 cm^{-1}; **HR-ESI-MS:** m/z calculated for $C_8H_6NO_5$ $[M-H]^-$: 196.0251, found: 196.0250; **MP**: 144.0-144.7 °C.

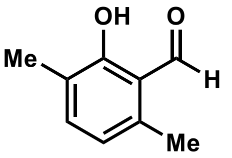

2-hydroxy-3,6-dimethylbenzaldehyde (2.64)

2,5-dimethylphenol (1.04 g, 8.18 mmol, 1.0 equiv), in a 1 M solution of $NaOH_{(aq)}$ (13 mL) was heated to 60 °C. $CHCl_3$ (1.64 mL, 20.4 mmol, 2.5 equiv) was added dropwise. The mixture was allowed to stir for 5 h, and then the reaction was quenched by the addition of HCl (2 M, 7 mL). The mixture was extracted with EtOAc (3 x 30 mL). The combined organic layers were washed with brine (1 x 15 mL), dried over sodium sulfate, filtered and concentrated under reduced pressure. Purification on silica gel (100% hexanes to 30% EtOAc in hexanes) afforded 163 mg (13% yield) of the *ortho*-hydroxybenzaldehyde as a colorless solid. **^{1}H NMR** (400 MHz, $CDCl_3$): δ 12.18 (s, 1H), 10.30 (s, 1H), 7.24 (d, J = 7.5 Hz, 1H), 6.61 (d, J = 7.5 Hz, 1H), 2.57 (s, 3H), 2.21 (s, 3H). All spectra obtained were consistent with literature values.[31] The structural isomer **2.68** eluted in 50% EtOAc/hexanes. **^{1}H NMR** (400 MHz, $CDCl_3$): 10.08 (s, 1H), 7.60 (s, 1H), 6.67 (s, 1H), 6.18 (s, 1H), 2.59 (s, 3H). All spectra obtained were consistent with literature values.[32]

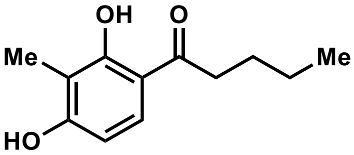

1-(2,4-dihydroxy-3-methylphenyl)pentan-1-one (2.79)

2-methylresorcinol (100 mg, 0.805 mmol, 1.0 equiv) and valeric acid (87.6 μL, 0.805 mmol, 1.0 equiv), were added to a flame-dried vial equipped with a stir bar. BF_3•OEt_2 (0.199 mL, 1.61 mmol, 2 equiv) was added, and the reaction mixture was heated to 120 °C for 4 h. The reaction was quenched at 0 °C by the addition of water (1 mL) and extracted with EtOAc (3 x 10 mL). The combined organic layers were dried over magnesium sulfate, and the filtrate was concentrated under reduced pressure to afford a brown solid. The resulting material was refluxed in THF/water (1:1, 0.07 M) for 3 h. The mixture was extracted with EtOAc (3 x 25 mL). The organic layers were combined, dried over magnesium sulfate and concentrated under reduced pressure. Purification on silica gel (100% hexanes to 30% EtOAc in hexanes) afforded 122 mg (73% yield over two steps) of ketone **2.79** as a white solid. **^{1}H NMR** (600 MHz, $CDCl_3$): δ 13.17 (s, 1H), 7.54 (d, J = 8.8 Hz, 1H), 6.38 (d, J = 8.8 Hz, 1H), 5.97 (s, 1H), 2.90 (t, J = 6.0 Hz, 2H), 2.13 (s, 3H), 1.72 (m, 2H), 1.41 (m, 2H), 0.94 (t, J = 7.4 Hz, 3H); **^{13}C NMR** (150 MHz, $CDCl_3$): δ 205.8, 163.2, 160.3, 129.1, 113.3, 111.4, 106.9, 37.8, 27.3, 22.5, 13.8, 7.3; **HR-ESI-MS:** m/z calculated for $C_{12}H_{15}O_3$ [M-H]$^-$: 207.1027, found: 207.1026; **IR** (thin film): 2922, 1597, 1289, 1252, 1222, 1115 cm^{-1}; **MP**: 144.0-144.7 °C.

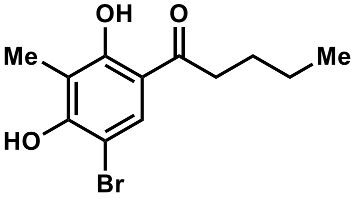

1-(5-bromo-2,4-dihydroxy-3-methylphenyl)pentan-1-one (2.67)

1-(2,4-dihydroxy-3-methylphenyl)pentan-1-one (50.0 mg, 0.240 mmol, 1.0 equiv) and 2.4 mL of MeOH were added to a flame-dried round-bottom flask equipped with a stir bar. NBS (57.8 mg, 0.325 mmol, 1.3 equiv) was added, and the mixture was stirred at rt for 1 h. The solution was concentrated and extracted with EtOAc (3 x 15 mL). The combined organic layers were washed with brine, dried over sodium sulfate, filtered, and concentrated under reduced pressure to afford an orange oil. Purification on silica gel (100% hexanes to 15% EtOAc in hexanes) afforded 34.1 mg (49% yield) of the aryl bromide as a pale yellow solid. **^{1}H NMR** (400 MHz, $CDCl_3$): δ 12.94 (s, 1H), 7.74 (s, 1H), 5.96 (s, 1H), 2.87 (t, J = 7.5 Hz, 2H), 2.17 (s, 3H), 1.68 (m, 2H), (m, 2H), 0.94 (t, J = 7.4 Hz, 3H); **^{13}C NMR** (150 MHz, $CDCl_3$): δ 205.8, 163.2, 160.3, 129.1, 113.3, 111.4, 106.9, 37.8, 27.3, 22.5, 13.8, 7.3; **HR-ESI-MS:** m/z calculated for $C_{12}H_{14}BrO_3$ $[M-H]^-$: 285.0132, found: 285.0135; **IR** (thin film): 3408, 2955, 2867, 1617, 1083 cm^{-1}; **MP**: 59.5-60.9 °C.

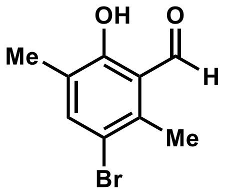

3-bromo-6-hydroxy-2,5-dimethylbenzaldehyde (2.73)

2-hydroxy-3,6-dimethylbenzaldehyde (100 mg, 0.609 mmol, 1.0 equiv), and NBS (141 mg, 0.792 mmol, 1.3 equiv) were added to a vial and stirred at rt for 3 h. The solvent was then removed under reduced pressure and diluted with water. The mixture was extracted with EtOAc (3 x 10 mL). The combined organic layers were washed with brine (1 x 15 mL), dried over sodium sulfate, filtered and concentrated under reduced pressure. Purification on silica gel (100% hexanes to 10% Et_2O in hexanes) afforded 139 mg (99% yield) of the aryl bromide as a pale yellow solid. **^{1}H NMR** (400

MHz, $CDCl_3$) δ; 12.20 (s, 1H), 10.18 (s, 1H), 7.37 (s, 1H), 2.49 (s, 3H), 2.05 (s, 3H); **^{13}C NMR** (100 MHz, $CDCl_3$) δ 195.3, 160.8, 141.1, 137.4, 126.7, 118.5, 114.0, 17.0, 14.3; **IR** (thin film): 3043, 2953, 2922, 1632, 1609, 1451 cm^{-1}; **HR-ESI-MS:** m/z calculated for $C_9H_7BrO_2$ $[M+H]^+$: 228.9859, 230.9838, found: 228.9826, 230.9837; **MP**: 83- 85 °C.

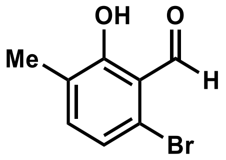

6-bromo-2-hydroxy-3-methylbenzaldehyde (2.74)

BBr_3 (2.79 mL, 2.79 mmol, 1.2 equiv, 1 M in DCM) and $FeCl_3$ (452 mg, 2.79 mmol, 1.2 equiv) in 3 mL chlorobenzene was cooled to -15 °C. 5-bromo-2-methylphenyl formate (500 mg, 2.32 mmol, 1.0 equiv) in 1 mL chlorobenzene was added dropwise and allowed to stir at 0 °C overnight. The reaction was warmed to rt and quenched by the addition of water. The mixture was extracted with EtOAc (3 x 10 mL). The combined organic layers were washed with brine (1 x 15 mL), dried over sodium sulfate, filtered and concentrated under reduced pressure. Purification on silica gel (100% hexanes to 10% Et_2O in hexanes) afforded 360 mg (72% yield) of the aryl bromide as a pale yellow solid. **^{1}H NMR** (600 MHz, $CDCl_3$) δ 12.16 (s, 1H), 10.19 (s, 1H), 7.08 (d, J = 7.9 Hz, 1H), 6.95 (d, J = 7.9 Hz, 1H), 2.11 (3H); **^{13}C NMR** (100 MHz, $CDCl_3$) δ 197.9, 162.3, 138.0, 127.1, 124.1, 123.6, 116.8, 14.9 cm^{-1}; **IR** (thin film): 2924, 2855, 1632, 1600, 1452, 1381 cm^{-1}; **HR-ESI-MS:** m/z calculated for $C_8H_7BrO_2$ $[M+H]^+$: 213.9629, 215.9609, found: 213.9318, 215.9841; **MP**: 68-70 °C.

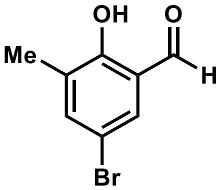

5-bromo-2-hydroxy-3-methylbenzaldehyde (2.73)

2-hydroxy-3-methylbenzaldehyde (200 mg, 1.47 mmol, 1.0 equiv), and NBS (340 mg, 1.91 mmol, 1.3 equiv) were added to a vial and stirred at rt for 3 h. The solvent was then removed under reduced pressure and diluted with water. The mixture was extracted with EtOAc (3 x 10 mL). The combined organic layers were washed with brine (1 x 15 mL), dried over sodium sulfate, filtered and concentrated under reduced pressure. Purification on silica gel (100% hexanes to 10% Et_2O in hexanes) afforded 111 mg (35% yield) of the aryl bromide as a colorless solid. **^{1}H NMR** (600 MHz, $CDCl_3$) δ 11.22 (s, 1H), 9.85 (s, 1H), 7.54 (s 1H), 7.53 (s, 1H), 2.29 (s, 3H). All spectra obtained were consistent with literature values.[33]

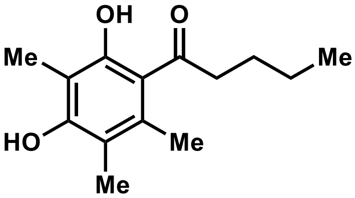

1-(2,4-dihydroxy-3,5,6-trimethylphenyl)pentan-1-one (2.75)

2,4,5-trimethylbenzene-1,3-diol (173 mg, 1.14 mmol, 1.0 equiv) and valeric acid (124 μL, 1.14 mmol, 1.0 equiv) were added to a flame-dried vial equipped with a stir bar. BF_3•OEt_2 (4.89 mL, 38.6 mmol, 10.7 equiv) was added and the reaction mixture was heated to 120 °C for 4 h. The reaction was quenched at 0 °C by the addition of water (10 mL) and extracted with EtOAc (3 x 20 mL). The combined organic layers were dried over magnesium sulfate, filtered and concentrated under reduced pressure to afford a brown solid. The resulting material was refluxed in THF/water

(1:1, 0.07 M) for 3 h. The mixture was extracted with EtOAc (3 x 25 mL). The organic layers were combined, dried over magnesium sulfate and concentrated under reduced pressure. Purification on silica gel (100% hexanes to 30% EtOAc in hexanes) afforded 83.9 mg (31% yield over two steps) of the ketone as a pale yellow solid. **^{1}H NMR** (400 MHz, $CDCl_3$): δ 11.79 (s, 1H), 5.23 (s, 1H), 2.82 (t, J = 8.0 Hz, 2H), 2.38 (s, 3H), 2.11 (s, 3H), 2.10 (s, 3H), 1.68 (m, 2H), 1.33 (m, 2H), 0.89 (t, J = 8.0 Hz, 3H); **^{13}C NMR** (150 MHz, $CDCl_3$): δ 205.7, 161.5, 158.5, 132.1, 113.9, 113.4, 101.4, 37.4, 26.6, 22.1, 14.2, 9.3; **HR-ESI-MS:** m/z calculated for $C_{14}H_{20}O_3$ $[M-H]^-$: 235.1340, found: 235.1339; **IR** (thin film): 3405, 2902, 2866, 1617 cm^{-1}.

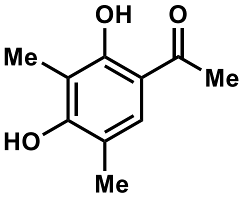

1-(2,4-dihydroxy-3,5-dimethylphenyl)ethan-1-one (2.25a)

2,4-dimethylbenzene-1,3-diol (50.0 mg, 0.362 mmol, 1.0 equiv) and acetic acid (20.7 μL, 0.362 mmol, 1.0 equiv) were added to a flame-dried vial equipped with a stir bar. $BF_3•OEt_2$ (4.89 mL, 38.6 mmol, 10.7 equiv) was added, and the reaction mixture was heated to 120 °C for 4 h. The reaction was quenched at 0 °C by the addition of water (2 mL) and extracted with EtOAc (3 x 10 mL). The combined organic layers were dried over magnesium sulfate, filtered and concentrated under reduced pressure to afford a dark orange solid. The resulting material was refluxed in THF/water (1:1, 0.07 M) for 3 h. The mixture was extracted with EtOAc (3 x 10 mL). The organic layers were combined, dried over magnesium sulfate and concentrated under reduced pressure. Purification on silica gel (100% hexanes to 50% EtOAc in hexanes) afforded 17.5 mg (27% yield over two steps) of the ketone as a white solid. **^{1}H NMR** (600 MHz, $CDCl_3$): δ 12.87 (s, 1H), 7.37

(s, 1H), 5.28 (s, 1H), 2.55 (s, 3H), 2.21 (s, 3H), 2.13 (s, 3H). All spectra obtained were consistent with literature values.[13]

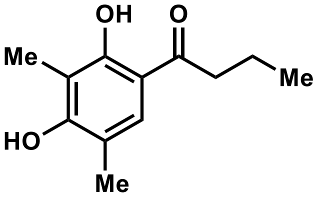

1-(2,4-dihydroxy-3,5-dimethylphenyl)butan-1-one (2.25b)

2,4-dimethylbenzene-1,3-diol (500 mg, 3.62 mmol, 1.0 equiv) and butyric acid (398 μL, 4.34 mmol, 1.2 equiv), were added to a flame-dried vial equipped with a stir bar. BF_3•OEt_2 (4.89 mL, 38.6 mmol, 10.7 equiv) was added, and the reaction mixture was heated to 120 °C for 4 h. The reaction was quenched at 0 °C by the addition of water (10 mL) and extracted with EtOAc (3 x 20 mL). The combined organic layers were dried over magnesium sulfate, filtered and concentrated under reduced pressure to afford a brown solid. The resulting material was refluxed in THF/water (1:1, 0.07 M) for 3 h. The mixture was extracted with EtOAc (3 x 25 mL). The organic layers were combined, dried over magnesium sulfate and concentrated under reduced pressure. Purification on silica gel (100% hexanes to 30% EtOAc in hexanes) afforded 528 mg (70% yield over two steps) of the propylketone as a pale yellow solid. **^{1}H NMR** (600 MHz, $CDCl_3$) δ 13.04 (s, 1H), 7.40 (s, 1H), 5.30 (s, 1H), 2.88 (t, J = 7.4 Hz, 2H), 2.21 (s, 3H), 2.14 (s, 3H), 1.76 (m, 2H), 1.01 (t, J = 7.4 Hz, 3H);**^{13}C NMR** (150 MHz, $CDCl_3$): δ 207.5, 163.7, 158.4, 138.2, 115.7, 111.1, 109.1, 52.8, 25.8, 24.8, 7.6. **HR-ESI-MS:** m/z calculated for $C_{12}H_{15}O_3$ $[M-H]^-$: 207.1027, found: 207.1027; **IR** (thin film): 3419, 2964, 1633, 1603, 1156 cm^{-1}; **MP**: 118.4-120.3 °C.

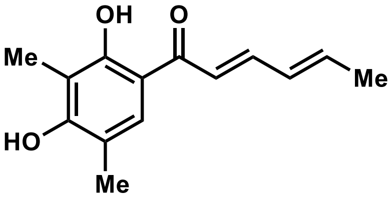

(2E,4E)-1-(2,4-dihydroxy-3,5-dimethylphenyl)hexa-2,4-dien-1-one (sorbicillin, 2.15)

2,4-dimethylbenzene-1,3-diol (500 mg, 3.62 mmol, 1.0 equiv) and butyric acid (398 μL, 4.34 mmol, 1.2 equiv), were added to a flame-dried vial equipped with a stir bar. BF_3•OEt_2 (4.89 mL, 38.6 mmol, 10.7 equiv) was added, and the reaction mixture was heated to 120 °C for 4 h. The reaction was quenched at 0 °C by the addition of water (10 mL) and extracted with EtOAc (3 x 20 mL). The combined organic layers were dried over magnesium sulfate, filtered and concentrated under reduced pressure to afford a brown solid. The resulting material was refluxed in THF/water (1:1, 0.07 M) for 3 h. The mixture was extracted with EtOAc (3 x 25 mL). The organic layers were combined, dried over magnesium sulfate and concentrated under reduced pressure. Purification on silica gel (100% hexanes to 30% EtOAc in hexanes) afforded 528 mg (70% yield over two steps) of sorbicillin (**2.15**) as a pale yellow solid. **^{1}H NMR** (600 MHz, $CDCl_3$) δ 13.59 (s, 1H), 7.46 (m, 2H), 6.95 (d, *J* = 14.8 Hz, 1H), 6.31 (m, 2H), 5.27 (s, 1H), 2.22 (s, 3H), 2.15 (s, 3H), 1.91 (d, *J* = 6.0 Hz, 3H). All spectra obtained were consistent with literature values.[13]

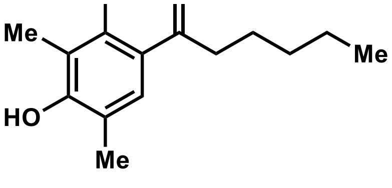

1-(2,4-dihydroxy-3,5-dimethylphenyl)hexan-1-one (2.25d)

2,4-dimethylbenzene-1,3-diol (500 mg, 3.62 mmol, 1.0 equiv) and hexanoic acid (544 μL, 3.62 mmol, 1.0 equiv), were added to a flame-dried vial equipped with a stir bar. BF_3•OEt_2 (4.89 mL, 38.6 mmol, 10.7 equiv) was added, and the reaction mixture was heated to 120 °C for 4 h. The reaction was quenched at 0 °C by the addition of water (10 mL) and extracted with EtOAc (3 x 20 mL). The combined organic layers were dried over magnesium sulfate, filtered and concentrated under reduced pressure to afford a brown solid. The resulting material was refluxed in THF/water (1:1, 0.07 M) for 3 h. The mixture was extracted with EtOAc (3 x 25 mL). The organic layers were combined, dried over magnesium sulfate and concentrated under reduced pressure. Purification on silica gel (100% hexanes to 30% EtOAc in hexanes) afforded 667 mg (78% yield over two steps) of the ketone as a pale yellow solid. **^{1}H NMR** (600 MHz, $CDCl_3$) δ 13.04 (s, 1H), 7.38 (s, 1H), 5.47 (s, 1H), 2.88 (t, *J* = 7.5 Hz, 2H), 2.21 (s, 3H), 2.13 (s, 3H), 1.72 (m, 2H), 1.36 (m, 4H), 0.91 (m, 3H). All spectra obtained were consistent with literature values.[13]

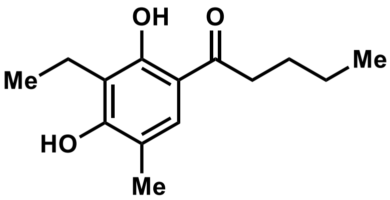

1-(3-ethyl-2,4-dihydroxy-5-methylphenyl)pentan-1-one (2.76)

2-Ethyl-4-methylbenzene-1,3-diol (82.3 mg, 0.541 mmol, 1.0 equiv) and valeric acid (71.0 μL, 0.649 mmol, 1.2 equiv) were added to a flame-dried vial equipped with a stir bar. BF_3•OEt_2 (0.730 mL, 4.59 mmol, 7.0 equiv) was added, and the reaction mixture was heated to 120 °C for 4 h. The reaction was quenched at 0 °C by the addition of water (1 mL) and extracted with EtOAc (3 x 10 mL). The combined organic layers were dried over magnesium sulfate, filtered and concentrated under reduced pressure to afford a brown solid. The resulting material was refluxed in THF/water (1:1, 0.07 M) for 3 h. The mixture was extracted with EtOAc (3 x 25 mL). The organic layers were combined, dried over magnesium sulfate and concentrated under reduced pressure. Purification on silica gel (100% hexanes to 30% EtOAc in hexanes) afforded 30.6 mg (24% yield over two steps) of the ketone as a pale yellow solid. **^{1}H NMR** (400 MHz, $CDCl_3$) δ 13.01 (s, 1H), 7.39 (s, 1H), 5.34 (s, 1H), 2.89 (t, *J* = 7.5 Hz, 2H), 2.67 (q, *J* = 7.5 Hz, 2H), 2.21 (s, 3H), 1.72 (m, 2H), 1.42 (m, 2H), 1.15 (t, *J* = 7.5 Hz, 3H), 0.96 (t, *J* = 7.3 Hz, 3H); **^{13}C NMR** (100 MHz, $CDCl_3$): δ 205.4, 161.3, 158.2, 127.6, 120.7, 113.0, 110.2, 37.7, 27.1, 22.8, 22.5, 14.1, 13.9, 7.4. **HR-ESI-MS:** m/z calculated for $C_{14}H_{19}O_3$ $[M-H]^-$: 235.1340, found: 235.1341; **IR** (thin film): 3419, 2964, 1633, 1603, 1156 cm^{-1}; **MP**: 118.4-120.3 °C.

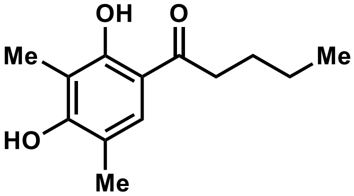

1-(2,4-dihydroxy-3,5-dimethylphenyl)pentan-1-one (2.25b)

2,4-dimethylbenzene-1,3-diol (100 mg, 0.805 mmol, 1.0 equiv) and valeric acid (87.6 μL, 0.805 mmol, 1.0 equiv) were added to a flame-dried vial equipped with a stir bar. $BF_3•OEt_2$ (1.09 mL, 8.58 mmol, 10.7 equiv) was added, and the reaction mixture was heated to 120 °C for 4 h. The reaction was quenched at 0 °C by the addition of water (1 mL) and extracted with EtOAc (3 x 10 mL). The combined organic layers were dried over magnesium sulfate, filtered and concentrated under reduced pressure to afford a brown solid. The resulting material was refluxed in THF/water (1:1, 0.07 M) for 3 h. The mixture was extracted with EtOAc (3 x 25 mL). The organic layers were combined, dried over magnesium sulfate and concentrated under reduced pressure. Purification on silica gel (100% hexanes to 30% EtOAc in hexanes) afforded 100 mg (62% yield over two steps) of the ketone as a white solid. **^{1}H NMR** (600 MHz, $CDCl_3$) δ 13.04 (s, 1H), 7.40 (s, 1H), 5.25 (s, 1H), 2.93 – 2.87 (t, J = 6.0 Hz, 2H), 2.21 (s, 3H), 2.13 (s, 3H), 1.71 (m, 2H), 1.45 – 1.38 (m, 2H), 0.96 (t, J = 7.4 Hz, 3H); **^{13}C NMR** (150 MHz, $CDCl_3$): δ 205.3, 161.4, 158.5, 129.1, 114.3, 113.0, 110.3, 37.7, 27.1, 22.5, 15.6, 13.9, 7.4; **HR-ESI-MS:** m/z calculated for $C_{13}H_{17}O_3$ $[M-H]^-$: 221.1183, found: 221.1182; **IR** (thin film): 2924, 1640, 1572, 1115, 798 cm^{-1}; **MP**: 82.5-84.9 °C.

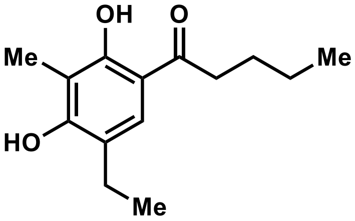

1-(5-ethyl-2,4-dihydroxy-3-methylphenyl)pentan-1-one (2.77)

4-Ethyl-2-methylbenzene-1,3-diol (455 mg, 2.99 mmol, 1.0 equiv) and valeric acid (394 μL, 3.59 mmol, 1.2 equiv) were added to a flame-dried vial equipped with a stir bar. BF_3•OEt_2 (4.27 mL, 26.2 mmol, 8.8 equiv) was added, and the reaction mixture was heated to 120 °C for 4 h. The reaction was quenched at 0 °C by the addition of water (1 mL) and extracted with EtOAc (3 x 10 mL). The combined organic layers were dried over magnesium sulfate, filtered and concentrated under reduced pressure to afford a brown solid. The resulting material was refluxed in THF/water (1:1, 0.07 M) for 3 h. The mixture was extracted with EtOAc (3 x 25 mL). The organic layers were combined, dried over magnesium sulfate and concentrated under reduced pressure. Purification on silica gel (100% hexanes to 30% EtOAc in hexanes) afforded 257 mg (36% yield over two steps) of the ketone as a white solid. **^{1}H NMR** (400 MHz, $CDCl_3$) δ 13.06 (s, 1H), 7.40 (s, 1H), 5.29 (s, 1H), 2.94 (m, 2H), 2.59 (q, J = 7.4 Hz, 2H), 2.14 (s, 3H), 1.70 (m, 2H), 1.42 (m, 2H), 1.24 (t, J = 7.5 Hz, 3H), 0.96 (t, J = 7.3 Hz, 3H); **^{13}C NMR** (100 MHz, $CDCl_3$): δ 205.4, 161.3, 158.2, 127.6, 120.7, 113.0, 110.2, 37.7, 27.1, 22.8, 22.5, 14.1, 13.9, 7.4; **HR-ESI-MS:** m/z calculated for $C_{14}H_{19}O_3$ $[M-H]^-$: 235.1340, found: 235.1339; **IR** (thin film): 3429, 1962, 1632, 1603, 1110 cm^{-1}; **MP**: 87.0- 89.1°C.

Synthesis of racemic product standards

Note: full characterization of products provided for products isolated from biocatalytic reactions in Chapter 2.6.3.

General procedure for IBX-mediated oxidative dearomatization: Adapted from reference 5. Substrate (20 mg, 1.0 equiv), IBX (1.2 equiv) and TBAI (0.05 equiv) were added to an oven-dried vial. DCE (1.5 mL) and TFA (5.0 equiv) were added and the mixture was allowed to stir at rt until full consumption of starting material by TLC analysis. The reaction was quenched by the addition of water and concentrated to dryness. Preparative HPLC purification afforded the racemic *o*-quinol product.

General procedure for lead tetraacetate (LTA)-mediated oxidative dearomatization: Adapted from reference 20. Substrate (50 mg, 1 equiv, 0.04 M) was dissolved in AcOH and DCM (5:1). LTA (1.2 equiv) was added and the reaction was allowed to stir at rt for 1 h. The reaction was quenched by the addition of water (10 mL) and the mixture was extracted with EtOAc (3 x 15 mL). The combined organic layers were washed with water (1 x 20 mL) and brine (1 x 20 mL), dried over sodium sulfate, and concentrated under reduced pressure to afford a yellow oil. Purification on silica gel afforded the O-acylated *o*-quinol product.

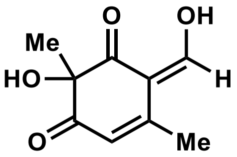

(Z)-2-hydroxy-6-(hydroxymethylene)-2,5-dimethylcyclohex-4-ene-1,3-dione, (±)-2.13

The title compound was synthesized according to the general procedure for IBX-mediated oxidative dearomatization. Purification by preparative HPLC using a Phenomenex Kinetex 5 µm C18, 150 x 21.2 mm column under the following conditions: mobile phase A = deionized water + 0.1% formic acid and B = acetonitrile + 0.1% formic acid; method = 5% to 100% B over 13 min, 100% B for 4 min; flow rate, 15 mL/min afforded 4.4 mg (20% yield) of the title compound as a dark orange oil. **^{1}H NMR** (600 MHz, CD_3CN) δ 8.09 (s, 1H), 5.81 (s, 1H), 2.15 (s, 3H), 1.47 (s, 3H).

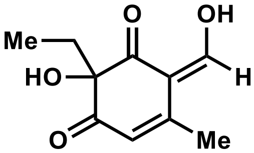

(*Z*)-2-ethyl-2-hydroxy-6-(hydroxymethylene)-5-methylcyclohex-4-ene-1,3-dione, (±)-2.81

The title compound was synthesized according to the general procedure for IBX-mediated oxidative dearomatization. Purification by preparative HPLC using a Phenomenex Kinetex 5 µm C18, 150 x 21.2 mm column under the following conditions: mobile phase A = deionized water + 0.1% formic acid and B = acetonitrile + 0.1% formic acid; method = 5% to 100% B over 13 min, 100% B for 4 min; flow rate, 15 mL/min afforded 3.0 mg (14% yield) of the racemic *o*-quinol as a yellow oil. **^{1}H NMR** (400 MHz, $CDCl_3$) δ 7.88 (s, 1H), 5.86 (s, 1H), 3.67 (s, 1H), 2.13 (s, 2H), 1.86 (q, J = 7.1 Hz, 3H), 0.90 (t, J = 7.5, 3H).

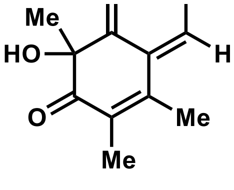

(*Z*)-2-hydroxy-6-(hydroxymethylene)-2,4,5-trimethylcyclohex-4-ene-1,3-dione, (±)-2.97

The title compound was synthesized according to the general procedure for IBX-mediated oxidative dearomatization. Purification by preparative by preparative HPLC using a Phenomenex Kinetex 5 µm C18, 150 x 21.2 mm column under the following conditions: mobile phase A = deionized water + 0.1% formic acid and B = acetonitrile + 0.1% formic acid; method = 5% to 100% B over 13 min, 100% B for 4 min; flow rate, 15 mL/min afforded 6.7 mg (31% yield) of the racemic *o*-quinol as a yellow oil. **^{1}H NMR** (600 MHz, CD_3CN) δ 8.06 (s, 1H), 2.10 (s, 3H), 1.94 (s, 3H), 1.45 (s, 3H).

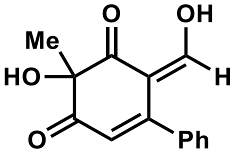

(*Z*)-4-hydroxy-2-(hydroxymethylene)-4-methyl-[1,1'-biphenyl]-3,5(2H,4H)-dione, (±)-2.80

The title compound was synthesized according to the general procedure for IBX-mediated oxidative dearomatization. Purification by preparative HPLC using a Phenomenex Kinetex 5 µm C18, 150 x 21.2 mm column under the following conditions: mobile phase A = deionized water + 0.1% formic acid and B = acetonitrile + 0.1% formic acid; method = 5% to 70% B over 10 min, 70% to 100% B for 10 min; flow rate, 15 mL/min afforded 3.9 mg (18% yield) of the title compound as a yellow oil. **^{1}H NMR** (600 MHz, CD_3CN): δ 7.73 (s, 1H), 7.51 (m, 3H), 7.44 (m, 2H), 5.85 (s, 1H), 3.95 (s, 1H), 1.60 (s, 3H).

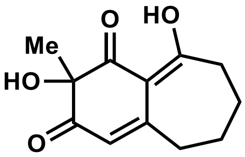

2,8-dihydroxy-2-methyl-6,7-dihydronaphthalene-1,3(2H,5H)-dione, (±)-2.84

The title compound was synthesized according to the general procedure for IBX-mediated oxidative dearomatization. Purification by preparative HPLC using a Phenomenex Kinetex 5 µm C18, 150 x 21.2 mm column under the following conditions: mobile phase A = deionized water + 0.1% formic acid and B = acetonitrile + 0.1% formic acid; method = 5% to 70% B over 10 min, 70% to 100% B for 10 min; flow rate, 15 mL/min afforded 3.6 mg (26% yield) of the title compound as a yellow oil. **^{1}H NMR** (600 MHz, $CDCl_3$) δ 5.76 (s, 1H), 3.66 (s, 1H), 2.72 (m, 2H), 2.70 (m, 2H), 1.86 (m, 4H), 1.57 (s, 3H).

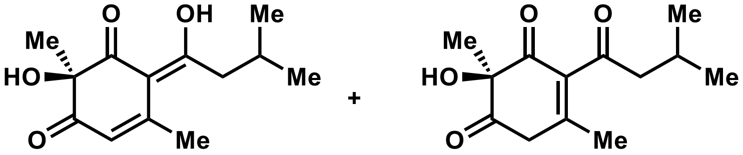

(*Z*)-2-hydroxy-6-(1-hydroxy-3-methylbutylidene)-2,5-dimethylcyclohex-4-ene-1,3-dione, (±)-2.98

The title compound was synthesized according to the general procedure for IBX-mediated oxidative dearomatization. Purification by preparative HPLC using a Phenomenex Kinetex 5 µm C18, 150 x 21.2 mm column under the following conditions: mobile phase A = deionized water + 0.1% formic acid and B = acetonitrile + 0.1% formic acid; method = 5% to 70% B over 15 min, 70% to 100% B for 10 min; flow rate, 15 mL/min afforded 2.6 mg (11% yield) of the title compound as a yellow oil. **^{1}H NMR** (600 MHz, CD_3CN) δ 3.91 (s, 1H), 3.74 (d, J = 21.3 Hz, 1H), 3.24 (d, J = 21.3 Hz, 1H), 2.54 (m, 2H), 1.56 (s, 3H), 0.99 (m, 1H), 0.96 (d, J = 6 Hz, 6H).

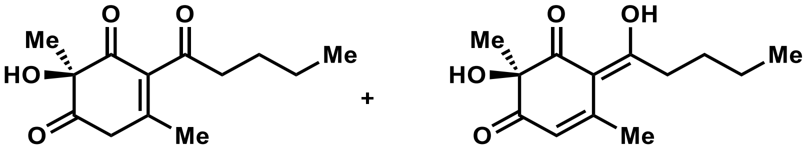

(*Z*)-2-hydroxy-6-(1-hydroxypentylidene)-2,5-dimethylcyclohex-4-ene-1,3-dione, (±)-2.83

The title compound was synthesized according to the general procedure for IBX-mediated oxidative dearomatization. Purification by preparative HPLC using a Phenomenex Kinetex 5 µm C18, 150 x 21.2 mm column under the following conditions: mobile phase A = deionized water + 0.1% formic acid and B = acetonitrile + 0.1% formic acid; method = 5% to 70% B over 15 min, 70% to 100% B for 10 min; flow rate, 15 mL/min afforded 2.8 mg (12% yield) of the title compound as a dark orange oil. **^{1}H NMR** (600 MHz, CD_3CN) δ 3.90 (s, 1H), 3.75 (d, J = 18 Hz, 1H), 3.25 (d, J = 18 Hz, 1H), 2.62 (t, J = 7.2, 2H), 1.98 (s, 3H), 1.60 (m, 2H), 1.56 (s, 3H), 1.47 (m, 2H), 0.92 (t, J = 6H, 3H).

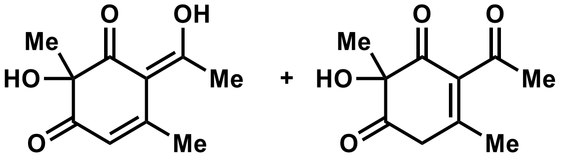

(*Z*)-2-hydroxy-6-(1-hydroxyethylidene)-2,5-dimethylcyclohex-4-ene-1,3-dione, (±)-2.82

The title compound was synthesized according to the general procedure for IBX-mediated oxidative dearomatization Purification by preparative HPLC using a Phenomenex Kinetex 5 µm C18, 150 x 21.2 mm column under the following conditions: mobile phase A = deionized water + 0.1% formic acid and B = acetonitrile + 0.1% formic acid; method = 5% to 100% B over 13 min, 100% B for 4 min; flow rate, 15 mL/min afforded 2.9 mg (13% yield) of the title compound as a dark orange oil as a mixture of the keto-enol tautomers. **^{1}H NMR** (400 MHz, CD_3CN) δ 8.10 (s, 1H), 5.54 (s, 1H), 3.75 (d, J = 22.2 Hz, 1H), 3.26 (d, J = 22.1 Hz, 1H), 2.46 (s, 3H), 2.34 (s, 3H), 2.31 (s, 3H), 2.00 (s, 3H), 1.56 (s, 3H), 1.45 (s, 3H).

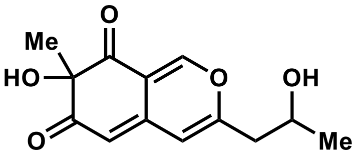

7-hydroxy-3-(2-hydroxypropyl)-7-methyl-6H-isochromene-6,8(7H)-dione, (±)-2.20

The title compound was prepared according to the general procedure for IBX-mediated oxidative dearomatization. Purification by preparative HPLC using a Phenomenex Kinetex 5 µm C18, 150 x 21.2 mm column under the following conditions: mobile phase A = deionized water + 0.1% formic acid and B = acetonitrile + 0.1% formic acid; method = 5% to 100% B over 13 min, 100% B for 4 min; flow rate, 15 mL/min afforded 6.3 mg (55% yield) of the beta-hydroxyazaphilone as a dark red oil. ^{1}**H NMR** (400 MHz, $CDCl_3$) δ 8.04 (s, 1H), 6.40 (s, 1H), 5.48 (d, J = 1.1 Hz, 1H), 4.12 – 4.07 (m, 1H), 2.61 (dd, J = 14.6, 4.6 Hz, 1H), 2.53 (dd, J = 14.6, 8.2 Hz, 1H), 1.49 (s, 3H), 1.25 (d, J = 6.2 Hz, 3H).

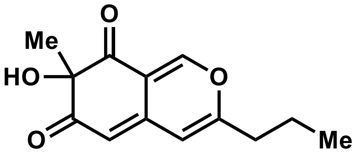

7-hydroxy-7-methyl-3-propyl-6H-isochromene-6,8(7H)-dione, (±)-2.85

The title compound was prepared according to the general procedure for IBX-mediated oxidative dearomatization. Purification by preparative HPLC using a Phenomenex Kinetex 5 µm C18, 150 x 21.2 mm column under the following conditions: mobile phase A = deionized water + 0.1% formic acid and B = acetonitrile + 0.1% formic acid; method = 5% to 100% B over 13 min, 100% B for 4 min; flow rate, 15 mL/min afforded 14 mg (71% yield) of the azaphilone as a dark orange oil. ^{1}**H NMR** (700 MHz, $CDCl_3$): δ 7.90 (s, 1H), 6.12 (s, 1H), 5.52 (s, 1H), 2.73 (s, 1H), 2.41 (t, J = 7.5 Hz, 2H), 1.67 (m, 2H), 1.55 (s, 3H), 1.00 (t, J = 7.5 Hz, 3H).

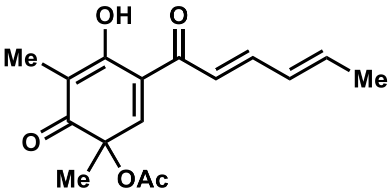

3-((2E,4E)-hexa-2,4-dienoyl)-4-hydroxy-1,5-dimethyl-6-oxocyclohexa-2,4-dien-1-yl acetate, (±)-2.87

The title compound was prepared according to the general procedure for LTA-mediated oxidative dearomatization. Purification on silica gel (20% to 50% EtOAc in hexanes) afforded 12 mg (20% yield) of the *o*-quinol as a yellow oil. ^{1}**H NMR** (700 MHz, $CDCl_3$) δ 11.83 (s, 1H), 7.46 (dd, J = 14.7, 10.6 Hz, 1H), 7.25 (s, 1H), 6.66 (d, J = 14.8 Hz, 1H), 6.35 (m, 2H), 2.15 (s, 3H), 1.93 (d, J = 6.4 Hz, 3H), 1.86 (s, 3H), 1.49 (s, 3H). All spectra obtained were consistent with literature values.[13]

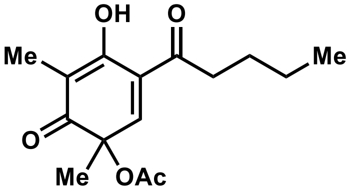

4-hydroxy-1,5-dimethyl-6-oxo-3-pentanoylcyclohexa-2,4-dien-1-yl acetate, (±)-2.89

The title compound was prepared according to the general procedure for LTA-mediated oxidative dearomatization. Purification on silica gel (30% to 50% EtOAc in hexanes) afforded 14 mg (23% yield) of the *o*-quinol as a yellow oil. ^{1}**H NMR** (700 MHz, $CDCl_3$) δ 11.53 (s, 1H), 7.29 (s, 1H), 2.81 (t, J = 7.3, 2H), 2.14 (s, 3H), 1.84 (s, 3H), 1.65 (m, 2H), 1.48 (s, 3H), 1.36 (m, 2H), 0.94 (t, J = 6.9 Hz, 3H).

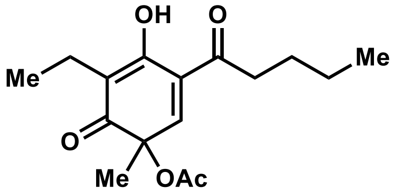

5-ethyl-4-hydroxy-1-methyl-6-oxo-3-pentanoylcyclohexa-2,4-dien-1-yl acetate, (±)-2.88

The title compound was prepared according to the general procedure for LTA-mediated oxidative dearomatization. Purification on silica gel (20% to 40% EtOAc in hexanes) afforded 5.2 mg (8.0% yield) of the *o*-quinol as a yellow oil. **^{1}H NMR** (400 MHz, $CDCl_3$) δ 11.48 (s, 1H), 7.28 (s, 1H), 2.82 (t, J = 8.6 Hz, 2H), 2.40 (m, 2H), 2.15 (s, 3H), 1.65 (p, J = 7.5 Hz, 2H), 1.49 (s, 3H), 1.38 (h, J = 7.6 Hz, 3H), 1.00 (t, J = 0.97 (t, 3H).

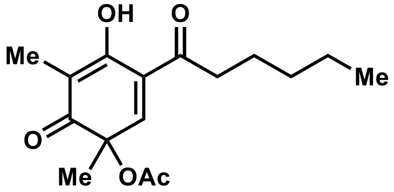

3-hexanoyl-4-hydroxy-1,5-dimethyl-6-oxocyclohexa-2,4-dien-1-yl acetate, (±)-2.99

The title compound was prepared according to the general procedure for LTA-mediated oxidative dearomatization. Purification on silica gel (20% to 40% EtOAc in hexanes) afforded 6.2 mg (10% yield) of the *o*-quinol as a yellow oil. **^{1}H NMR** (400 MHz, $CDCl_3$) δ 11.53 (s, 1H), 7.29 (s, 1H), 2.81 (td, J = 7.3, 3.1 Hz, 2H), 2.13 (s, 3H), 1.83 (s, 3H), 1.65 (p, J = 7.3 Hz, 2H), 1.48 (s, 3H), 1.35 (m, 4H), 0.90 (t, J = 6.9 Hz, 3H). All spectra obtained were consistent with literature values.[13]

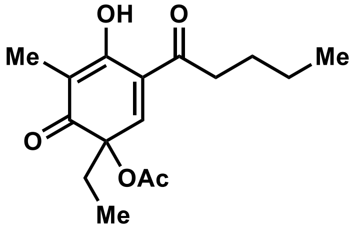

1-ethyl-4-hydroxy-5-methyl-6-oxo-3-pentanoylcyclohexa-2,4-dien-1-yl acetate, (±)-2.89

The title compound was prepared according to the general procedure for LTA-mediated oxidative dearomatization. Purification on silica gel (20% to 40% EtOAc in hexanes) afforded 11 mg (17% yield) of the *o*-quinol as a yellow oil. **^{1}H NMR** (700 MHz, $CDCl_3$) δ 11.50 (d, J = 1.1 Hz, 1H), 7.28 (s, 1H), 2.81 (t, J = 8 Hz, H), 2.15 (s, 3H), 1.88 (m, 2H), 1.82 (s, 3H), 1.64 (m, 2H), 1.37 (m, 2H), 0.94 (overlapping t, 6H).

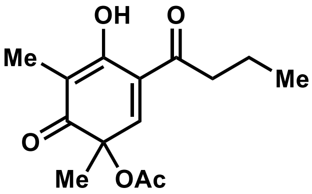

3-butyryl-4-hydroxy-1,5-dimethyl-6-oxocyclohexa-2,4-dien-1-yl acetate, (±)-2.91

The title compound was prepared according to the general procedure for LTA-mediated oxidative dearomatization. Purification on silica gel (20% to 40% EtOAc in hexanes) afforded 11 mg (18% yield) of the *o*-quinol as a yellow oil. **^{1}H NMR** (400 MHz, $CDCl_3$) δ 11.53 (t, J = 1.2 Hz, 1H), 7.29 (s, 1H), 2.81 (m, 2H), 2.14 (s, 3H), 1.84 (s, 3H), 1.71 (m, 2H), 1.48 (s, 3H), 0.98 (t, J = 7.4, 3H).

Chapter 2.6.2: Plasmids and Proteins

Plasmids: Genes encoding *tropB* (DAA64700.1) and *sorbC* (XP_002567552) were codon-optimized for overexpression in *E. coli* and synthesized by GeneArt (Thermofisher). The synthesized sequences were cloned by GeneArt into pET151 vectors conferring the T7 expression system, ampicillin resistance, and N-terminal 6xHis-tags encoded upstream from the insert genes. The plasmid encoding *azaH* (G3XMC2.1), in a modified pET28 vector to afford protein with both C- and N-terminal 6xHis-tags and is hereby referred to as pAZ83, was a generous gift from Professor Yi Tang's lab at the University of California, Los Angeles.[11] No further modifications to any of these plasmid constructs were necessary.

Codon-Optimized *tropB* Sequence

ATGCCTGGTAGCCTGATTGATACCCGTCAGCAGCCGCTGAGCGTTGGTATTGTTGGTGGTGGTA
TTATTGGCGTTATTCTGGCAGCAGGTCTGGTTCGTCGTGGTATTGATGTTAAAGTTTTTGAACA
GGCACGTGGCTTTCGTGAAATTGGTGCAGGTATGGCATTTACCGCAAATGCAGTTCGTTGTATG
GAAATGCTGGATCCGGCAATTGTTTGGGCACTGCGTAGCAGCGGTGCAGTTCCGATTAGCATTG
GTGATCATCAGGCCGAAGCACGTGATTATCTGCGTTGGGTTGATGGTTATCATGAAAGCAGCAA
ACGTCTGTATCAGCTGGATGCAGGTATTCGTGGTTTTGAAGCATGTCGTCGTGATCAGTTTCTG
GAAGCACTGGTTAAAGTTCTGCCGGAAGGTATTGTGGAATGTCAGAAACGTCTGCAGAAAATCC
ACGAAAAAAACGAAACCGAAAAAGTGACCCTGGAATTTGCAGATGGCACCTTTGCACATGTTGA
TTGTGTTATTGGTGCCGATGGTATTCGTAGCCGTGTTCGTCAGCACCTGTTTGGTGAAGATAGC
CCGTATAGCCATCCGCATTATAGCCATAAATTTGCATTTCGTGGTCTGATCACCATGGAAAATG
CAATTAGCGCACTGGGCGAAGATAAAGCACGTACCCTGAATATGCATGTTGGTCCGAATGCACA
TCTGATTCATTATCCGGTTGCAAATGAAACCATGGTGAATATTGCAGCCTTTGTTAGCGATCCG
GAAGAATGGCCTGATAAACTGAGCCTGGTTGGTCCGGCAACCCGTGAAGAAGCAATGGGTTATT
TTGCAAATTGGAATCCGGGTCTGCGTGCAGTTCTGGGTTTTATGCCGGAAAATATTGATCGTTG
GGCAATGTTCGATACCTATGATTATCCGGCACCGTTTTTTAGCCGTGGTAAAATTTGTCTGGTT
GGTGATGCAGCACATGCAGCAGTTCCGCATCATGGTGCCGGTGCATGTATTGGTATTGAAGATG
CACTGTGTGCAACCGTTCTGCTGGCAGAAGTTTTTGTTAGCACCCGTGGCAAAAGCAGCATTGT
TCGTAATCGTGCAATTGCCGCAGCATTTGGTAGCTTTAATGCAGTGCGTCGTGTTCGTGCACAG
TGGTTTGTTGATAGCAGCCGTCGTGTTTGTGATCTGTATCAACAGCCGGAATGGGCAGATCCGC
AGAAACGTATTAAAGCCGAAAATTGCTTCGAAGAGATTAAAGATCGCAGCCATAAAATCTGGCA
CTTCGATTATAACTCCATGCTGCAAGAAGCCATCGAAAAATATCGTCATAATATGGGCAGCTAA

TropB Protein Sequence

MPGSLIDTRQQPLSVGIVGGGIIGVILAAGLVRRGIDVKVFEQARGFREIGAGMAFTANAVRCM
EMLDPAIVWALRSSGAVPISIGDHQAEARDYLRWVDGYHESSKRLYQLDAGIRGFEACRRDQFL

EALVKVLPEGIVECQKRLQKIHEKNETEKVTLEFADGTFAHVDCVIGADGIRSRVRQHLFGEDS
PYSHPHYSHKFAFRGLITMENAISALGEDKARTLNMHVGPNAHLIHYPVANETMVNIAAFVSDP
EEWPDKLSLVGPATREEAMGYFANWNPGLRAVLGFMPENIDRWAMFDTYDYPAPFFSRGKICLV
GDAAHAAVPHHGAGACIGIEDALCATVLLAEVFVSTRGKSSIVRNRAIAAAFGSFNAVRRVRAQ
WFVDSSRRVCDLYQQPEWADPQKRIKAENCFEEIKDRSHKIWHFDYNSMLQEAIEKYRHNMGS

Codon-Optimized *sorbC* Sequence

ATGACCCGTAGCGCAAATAGCCCGTTTGAAGTTGCAATTGTTGGTGGTGGTATTACCGGTCTGG
CACTGGCAGTTGGTCTGCTGAAACGTAATGTTAGCTTTACCATTTATGAACGTGCCGAAAATTT
TGGTGAACTGGGTGTGGGTATTACCTTTACCCCGAATGCACAGCGTGCAATGGAAGCACTGGAT
CCGTGTGTTCTGCAGAGTTTTACCAATGTTGCAAGCGCACCGAGCGGTGGCACCATTAACTTTG
TTGATGGTGTTCGTGAACAGGGTAGCGAAGATCCGCGTACCAGCACCGCAGCACTGCTGTTTCA
GCTGCATGTTAAAGGTGGTTATAAAGCATGTCGTCGTTGCGATTTTGTTGATCAGATTGTTCAG
CATATCCCGAAAGATTGTGTGCAGTATCGTAAATGGCTGGATAGCATTGAAACCGATCATGAAA
GCGGTCGTGCAGTTCTGAAATTTCGTGATGGTGAAATTGCACATGCCGATGTTGTTATTGGTTG
TGATGGTATTCGTAGCCAGGTTCGTGCAAGCATGTTTGGCACCGATGAACTGTGTCCGCGTGCA
CAGTATAGCCATCAGCTGGGTTATCGTGGTATGGTTCCGCTGGCACAGGCAACCGCAGTTCTGG
GTCCGGAAAAAACCAGCTCAGCAGTTCTGCATACCGGTCCGGGTGCATTTGTTCTGACCATCCC
GCTGGCCGAAGTTCATGCAATGCATATTGAAGCCTTCATCATGGATAAAGAAGAATGGCCTGAA
GTACAGACCAGCAGCGATAGCAAACGTTATGTTCTGCCTGCAACCCGTAATGAAGCAACCAAAG
CATTTGCAGAATTTGGTCCGACCGTTCGTAGCGCAGTTAGCATGTTTCCTGAAAAACTGGAAAA
ATGGGCAGTGTTCGATATGCTGGAAGCACCGGTTCCGACCTTTGCAAAAGGCCGTGTTTGTCTG
GCTGGTGATGCAGCACATGCAAGCACCCCGAATCAGGGTGGTGGTGCAGGTTTTGGTATTGAAG
ATGCACTGGTTCTGGCAGAAGTTCTGGCCGTTCTGGCTGAAGCACCGAATGTTAGCGGTATTGT
TGCCAGCGAAGCCCTGGCAGTTTATAGCGAAGTTCGTTATGAACGCAGCCAGTGGCTGGTGCGT
AGCAGCCGTCGTACAGGTGAACTGTGCACCTGGAAAGATCGTGATTGGGGTCTGGCAGCCGAAG
AACTGAGCCGTGATATTATCAGCCGTAGTCATCAGCTGTGGGATCATGATACCGCAGGTATGGT
TAGTGATGCCCTGGCAATTCTGGGTGAACGTGTTCGTGGTGCAGATACCGCATTTTAA

SorbC Protein Sequence

MTRSANSPFEVAIVGGGITGLALAVGLLKRNVSFTIYERAENFGELGVGITFTPNAQRAMEALD
PCVLQSFTNVASAPSGGTINFVDGVREQGSEDPRTSTAALLFQLHVKGGYKACRRCDFVDQIVQ
HIPKDCVQYRKWLDSIETDHESGRAVLKFRDGEIAHADVVIGCDGIRSQVRASMFGTDELCPRA
QYSHQLGYRGMVPLAQATAVLGPEKTSSAVLHTGPGAFVLTIPLAEVHAMHIEAFIMDKEEWPE
VQTSSDSKRYVLPATRNEATKAFAEFGPTVRSAVSMFPEKLEKWAVFDMLEAPVPTFAKGRVCL
AGDAAHASTPNQGGGAGFGIEDALVLAEVLAVLAEAPNVSGIVASEALAVYSEVRYERSQWLVR
SSRRTGELCTWKDRDWGLAAEELSRDIISRSHQLWDHDTAGMVSDALAILGERVRGADTAF

Non-optimized *azaH* Sequence

ATGAGTACAGACTCGATCGAAGTTGCCATTATAGGCGCCGGGATCACGGGAATCACCCTGGCCC
TGGGCCTCCTGTCTCGCGGCATTCCCGTCCGCGTCTACGAGCGAGCCCGCGACTTTCACGAAAT

TGGAGCCGGTATCGGTTTCACCCCCAACGCCGAATGGGCGATGAAAGTCGTCGACCCGCGCATT
CAAGCTGCTTTCAAACGCGTCGCTACCCCCAATGCCTCCGACTGGTTCCAGTGGGTGGACGGAT
TCAACGAGTCCGGTACCGACCCGCGCGAGACCGAGGAACAGCTACTCTTCAAGATCTACCTCGG
CGAGCGTGGATTTGAGGGCTGCCACCGTGCCGACTTCCTAGGTGAGCTGGCACGTCTACTACCG
GAAGGTGTGGTGACATTCCAGAAGGCGCTGGATACCGTGGAGCCTGCAGCAGATAATAGCCTCG
GCCAGCTTCTTCGATTCCAAGATGGCACGACAGCTACCGCCCACGCGGTGATCGGCTGCGATGG
CATTCGGTCGCGCGTTCGTCAGATCCTCCTAGGTGAAGACCATCCGACAGCATCAGCCCATTAC
AGTCATAAATATGCAGCACGCGGCCTTATTCCCATGGACCGCGCCCGGGAGGCGCTGGGCGAAG
ATAAAGTGGCGACACGCTTCATGCATCTCGGTCCGGATGCCCATGCCCTGACCTTCCCCGTTAG
CCATGGGTCCTTGTTGAACGTCGTCGCCTTCGTCACGGACCCTAACCCTTGGCCATATGCTGAT
CGCTGGACGGCGCAGGGGCCCAAGAAAGACGTGACGGCTGCCTTTTCCCGCTTTGGTCCGACCA
TGCGCACCATAATTGACCTCTTGCCTGATCCTATTGATCAATGGGCCGTTTTTGATACATACGA
CCATCCCCCAAATACGTATTCCCGGGGAGCTGTCTGTATAGCAGGGGATGCTGCTCATGCCGCG
GCTCCGCATCACGGTGCAGGTGCAGGTTGTGGTGTGGAAGACGCGGCTGTGCTGTGCGCTGTGC
TTCATATGGCTGCGAAAAAAGTTAACACCGCAAAAACTGGTTCTGAGGGGAAAGCCGCTCTTAT
CACGGCCGCATTCGAAACCTATGATTCGGTTTGTCGCGAGCGTGCGCAGTGGCTGGTGGAAAGT
AGTCGCGTTATCGGTAATCTGTATGAGTGGCAGGATAAGGAGGTAGGGTCGGATGCTTCCAGGT
GCCACGATGAGGTGTATTGGCGCTCTCATCGCATTTGGGACTATGATATTGATGCGATGATGAG
AGAGACAGCTGAGGTGTTTGAGGCGCAGGTAGCTGGGGTGGCGAGAAAT

AzaH Protein Sequence

MSTDSIEVAIIGAGITGITLALGLLSRGIPVRVYERARDFHEIGAGIGFTPNAEWAMKVVDPRI
QAAFKRVATPNASDWFQWVDGFNESGTDPRETEEQLLFKIYLGERGFEGCHRADFLGELARLLP
EGVVTFQKALDTVEPAADNSLGQLLRFQDGTTATAHAVIGCDGIRSRVRQILLGEDHPTASAHY
SHKYAARGLIPMDRAREALGEDKVATRFMHLGPDAHALTFPVSHGSLLNVVAFVTDPNPWPYAD
RWTAQGPKKDVTAAFSRFGPTMRTIIDLLPDPIDQWAVFDTYDHPPNTYSRGAVCIAGDAAHAA
APHHGAGAGCGVEDAAVLCAVLHMAAKKVNTAKTGSEGKAALITAAFETYDSVCRERAQWLVES
SRVIGNLCHDEVYWRSHRIWDYDIDAMMRETAEVFEAQVAGVARN

Protein overexpression and purification: Plasmids containing *tropB*, *sorbC*, and *azaH* were transformed using standard heat-shock protocols for chemically competent *E. coli* into BL21(DE3) cells. Overexpression of TropB and SorbC was achieved in 500 mL 4% glycerol (v/v) Terrific Broth (TB) in 2.8 L flasks. 500 mL portions of media were inoculated with 5 mL overnight culture prepared from a single colony in Luria Broth (LB) and 100 μg/mL ampicillin (Gold Biotechnology). Cultures were grown at 37 °C and 250 rpm until the optical density at 600 nm reached 0.8. The cultures were then cooled to 20 °C for 1 h and protein expression was induced with 0.1 mM isopropyl-β-D-1-thiogalactopyranoside (IPTG, Gold Biotechnology). Expression continued at 20 °C overnight (approx. 18 h) at 200 rpm. The typical yield for one 500 mL culture cell pellet was ~25 g. Overexpression of AzaH followed the same protocol as described above, except 1 L cultures were grown in 2.8 L flasks and kanamycin was used at 50 μg/mL (Gold Biotechnology) in place of ampicillin. The typical yield for one 1 L culture cell pellet was ~30 g.

General purification procedure: 25 – 30 g of cell pellet was resuspended in 100 mL of lysis buffer containing 50 mM Tris HCl pH 7.4, 300 mM NaCl, 10 mM imidazole, and 10% glycerol. Protease inhibitors were added to lysis buffer of AzaH only and consisted of 1 mM phenylmethane sulfonyl fluoride (v), 0.1 mg/mL benzamidine HCl, 0.5 mg/mL leupeptin, and 0.5 mg/mL pepstatin. Approximatley 1 mg/mL lysozyme was added prior to incubating on a rocker held at 4 °C for 30 min. Cells were lysed by passing the total cell lysate through an Avestin pressure homogenizer at 15000 psi. The total lysate was centrifuged at 40,000 x g for 30 min and the supernatant was filtered through 0.45 μm syringe filters. The crude cell lysate was loaded onto a 5 mL HisTrap HP column (General Electric) on an ÄKTA Pure FPLC system (General Electric) at a flow rate of 2.5 mL/min. Buffer A = the lysis buffer listed above, and Buffer B = 50 mM Tris HCl pH 7.4, 300 mM NaCl, 10% glycerol, and 400 mM imidazole. The column was washed with 25 mM imidazole (6.3% Buffer B) for 6 CV and eluted in a gradient to 100% Buffer B over 8 CV. Fractions containing TropB, SorbC, or AzaH were visibly yellow and pooled for desalting by dialysis. TropB and SorbC were dialyzed into 50 mM Tris HCl pH 7.4 and 10% glycerol buffer, while AzaH was dialyzed into 50 mM Tris HCl pH 7.4, 300 mM NaCl, and 10% glycerol buffer due to instability upon dialysis into the TropB/SorbC storage buffer. Average yields: 100 mg from 1 L TropB, 100 mg from 1 L SorbC, and 20 mg from 1 L AzaH. Molecular weights including

6xHis-tags for each protein were estimated by the ProtParam tool on the Expasy server to be 50.8 kDa for TropB, 49.2 kDa for SorbC, and 47.6 kDa for AzaH. These molecular weights are consistent with the proteins observed by SDS-PAGE analysis (Figure 2.8). The purified proteins were aliquoted into 0.6 mL tubes and frozen in liquid nitrogen before long-term storage at -80 °C.

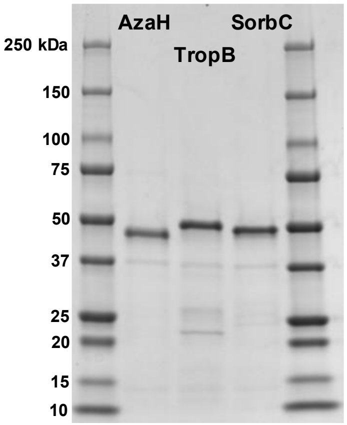

Figure 2.8: Purified AzaH, TropB, and SorbC. Approximately 5 µL of 1.25 µM each protein was loaded onto an MiniPROTEAN TGX Precast 4-15% SDS-PAGE gel (Bio-Rad). The gel was stained with Quick Coomassie stain (Anatrace) and visualized with the Azure Gel Imaging System. The relative apparent masses are consistent with the predicted estimates.

Determination of flavin incorporation and extinction coefficients (Experiments performed by April Lukowski): Samples of each protein were diluted to 10 µM in 1 mL using dialysis buffer for UV-vis analysis using a disposable poly(methyl 2-methylpropenoate) cuvette. The absorbance spectrum for each protein was taken from 300 nm to 700 nm in 2 nm increments (blue traces in Figure 2.9). A 20 µL aliquot of fresh 10% sodium dodecyl sulfate (w/v) was added to each 1 mL solution and mixed. Samples were incubated at room temperature for 10 min before reading the absorbance spectra again under the same conditions (red traces in Figure 2.9). The absorbance at 450 nm for the denatured enzymes and the extinction coefficient of free FAD (11300 M^{-1} cm^{-1}) was used to calculate the concentration of FAD in each protein sample using Beer's law. The typical FAD incorporation was 82% for AzaH, 88% for TropB, and 89% for SorbC. Extinction coefficients were calculated using the concentrations of free flavin obtained and the absorbance at 450 nm of the native enzymes. At 450 nm, the extinction coefficients of the proteins are 17490 M^{-1} cm^{-1} for AzaH, 16180 M^{-1} cm^{-1} for TropB, and 11970 M^{-1} cm^{-1} for SorbC.

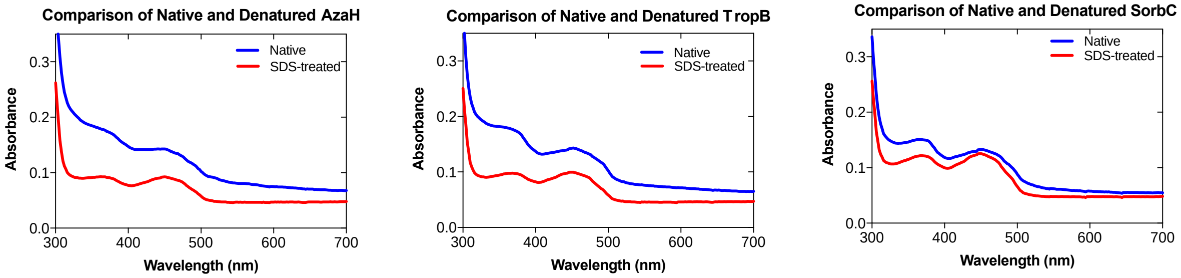

Figure 2.9: Native enzyme absorbance spectra compared to denatured enzyme absorbance spectra exposing free FAD to solution.

Chapter 2.6.3: Biocatalytic Reactions

Stock solutions: Stock solutions of each substrate (50 mM) were prepared by dissolving the substrate in DMSO (analytical grade). Stock solutions of $NADP^+$ (100 mM) and glucose-6-phosphate (G6P, 500mM) were stored at -20 °C. Aliquots of TropB (127 μM), SorbC (62 μM), AzaH (40 μM) and glucose-6-phosphate dehydrogenase (G6PDH, 100 U/mL) were stored at -80 °C.

Analytical-scale reactions: Each reaction contained 25 μL 100 mM potassium phosphate buffer, pH 8.0, 2.5 mM substrate (2.5 μL of a 50 mM stock solution in DMSO), 2.5 μM FAD-dependent monooxygenase, 5 mM G6P (0.5 μL, 500 mM), 1 mM $NADP^+$ (0.5 μL, 100 mM), 1 U/mL G6P-DH (0.5 μL, 100 U/mL), and Milli-Q water to a final volume of 50 μL. The reaction was carried out at 30 °C for 1 h and quenched by addition of 75 μL acetonitrile with 25 mM pentamethylbenzene as an internal standard. Precipitated biomolecules were pelleted by centrifugation (16,000 x *g*, 12 min). The supernatant was analyzed by UPLC-DAD and conversion obtained by comparison to calibration curves of each substrate.

Determination of total turnover number (TTN): Total turnover number was determined by analyzing (# of moles of starting material consumed)/(# of moles of enzyme) under the following conditions: 2.5 μM FAD-dependent monooxygenase, 2.5 mM substrate, 1 mM $NADP^+$, 0.05 U G6PDH, and 5 mM G6P for NADPH regeneration in 50 μL of reaction buffer (50 mM potassium phosphate, pH 8.0). The reaction was carried out at 30 °C for 1 h and quenched by addition of 75 μL acetonitrile with 2.5 mM pentamethylbenzene as an internal standard. Precipitated biomolecules were pelleted by centrifugation (16,000 x *g*, 12 min). The subsequent liquid chromatography PDA spectrometry (UPLC) analysis was performed on a Waters Aquity H-Class UPLC-PDA using a Phenomenex Kinetex 1.7 µm C18, 2.1x150 mm column under the following conditions: Method A: mobile phase (A = deionized water + 0.1% formic acid, B = acetonitrile + 0.1% formic acid), 5% to 100% B over 6 min, 100% B for 4 min; flow rate, 0.5 mL/min; Method B: mobile phase (A = deionized water + 0.1% formic acid, B = acetonitrile + 0.1% formic acid), 5% to 100% B over 2 min, 100% B for 1 min; flow rate, 0.5 mL/min. Based on calibration curves of the starting materials, the percent conversion of the substrate to dearomatized product was calculated with $AUC_{substrate}/AUC_{internal\ standard}$ at 270 nm. All reactions were performed and analyzed in triplicate.

General procedure for *in vitro* milligram-scale reactions: Preparative–scale enzymatic reactions were conducted on 10 mg of each substrate under the following conditions: 2.5 µM flavin-dependent monooxygenase, 2.5 mM substrate, 1 mM $NADP^+$, 1 U/mL G6PDH, and 5 mM G6P for NADPH generation in reaction buffer (50 mM potassium phosphate buffer, pH 8.0). The reaction mixture was added to a crystallizing dish and incubated at 30 °C for 2 h. The increased surface area afforded by the crystalizing dish as reaction vessel allowed for higher conversions with some substrates due to increased oxygen concentration. After 2 h, a 50 µL aliquot was removed and processed in an identical manner to the analytical-scale reactions escribed above to determine substrate conversion. The remaining reaction mixture was diluted with acetonitrile (2 x total reaction volume). Precipitated biomolecules were pelleted by centrifugation (4,000 x *g*, 12 min). **Isolation procedure A:** The supernatant was concentrated under reduced pressure to a final volume of approximately 2 mL. The resulting mixture was filtered through a 0.22 µm filter and purified by preparative HPLC using a Phenomenex Kinetex 5 µm C18, 150 x 21.2 mm column under the following conditions: mobile phase A = deionized water + 0.1% formic acid and B = acetonitrile + 0.1% formic acid; method = 5% to 100% B over 13 min, 100% B for 4 min; flow rate, 15 mL/min. **Isolation procedure B:** The reaction mixture was cooled to 0 °C and pyridine (14.0 µL, 0.173 mmol) was added followed by Ac_2O (10.4 µL, 0.110 mmol). The resulting mixture was stirred at rt for 2 h. The reaction was then acidified to pH 2 and the mixture was extracted with EtOAc (3 x 70 mL). The combined organic layers were washed with brine (1 x 50 mL), dried over sodium sulfate and concentrated under reduced pressure. Purification on silica gel (30% hexanes to 50% EtOAc in hexanes) afforded the acylated *o*-quinol products.

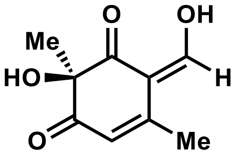

(*R*,*Z*)-2-hydroxy-6-(hydroxymethylene)-2,5-dimethylcyclohex-4-ene-1,3-dione (2.13)

The title compound was synthesized according to the general procedure for milligram-scale *in vitro* enzymatic oxidative dearomatization using isolation method A. Purification by preparative HPLC afforded 6.1 mg (56% yield) of the title compound as a dark orange oil. **^{1}H NMR** (400 MHz, CD_3CN) δ 8.09 (s, 1H), 5.81 (s, 1H), 2.15 (s, 3H), 1.47 (s, 3H). All spectra obtained were consistent with literature values.[2]

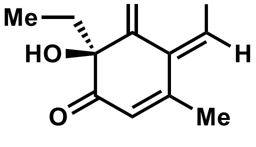

(*R*,*Z*)-2-ethyl-2-hydroxy-6-(hydroxymethylene)-5-methylcyclohex-4-ene-1,3-dione (2.81)

The title compound was synthesized according to the general procedure for milligram-scale *in vitro* enzymatic oxidative dearomatization using isolation method A. Purification by preparative HPLC afforded 4.2 mg (39% yield) of the title compound as a yellow oil. **^{1}H NMR** (400 MHz, $CDCl_3$) δ 7.88 (s, 1H), 5.86 (s, 1H), 3.67 (s, 1H), 2.13 (s, 2H), 1.86 (q, J = 7.1 Hz, 3H), 0.90 (m, J = 7.5, 1.9 Hz, 3H); **^{13}C NMR** (150 MHz, CD_3CN): δ 203.3, 197.0, 169.7, 152.0, 118.4, 110.8, 84.5, 35.3, 35.0, 18.2, 7.2, 6.9; **HR-ESI-MS:** m/z calculated for $C_{10}H_{11}O_4$ $[M-H]^-$: 195.0663, found: 195.0664; **IR** (thin film): 3256, 2917, 1729, 1676 cm^{-1}.

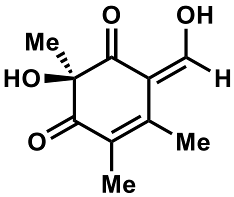

(*R,Z*)-2-hydroxy-6-(hydroxymethylene)-2,4,5-trimethylcyclohex-4-ene-1,3-dione (2.97)

The title compound was synthesized according to the general procedure for milligram-scale *in vitro* enzymatic oxidative dearomatization using isolation method A. Purification by preparative HPLC afforded 2.6 mg (24% yield) of the title compound as a yellow oil. **^{1}H NMR** (400 MHz, $CDCl_3$) δ 8.07 (s, 1H), 2.10 (s, 3H), 1.94 (s, 3H), 1.45 (s, 3H); **^{13}C NMR** (150 MHz, CD_3CN): δ 203.1, 198.1, 169.1, 145.4, 123.6, 110.8, 80.5, 28.7, 14.3, 11.1; **HR-ESI-MS:** m/z calculated for $C_{10}H_{11}O_4$ $[M-H]^-$: 195.0663, found: 195.0663; **IR** (thin film): 3275, 2951, 2929, 1758, 1655, 1498 cm^{-1}.

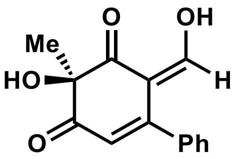

(*R,Z*)-4-hydroxy-2-(hydroxymethylene)-4-methyl-[1,1'-biphenyl]-3,5(2H,4H)-dione (2.80)

The title compound was synthesized according to the general procedure for milligram-scale *in vitro* enzymatic oxidative dearomatization using isolation method A. Purification by preparative HPLC afforded 2.8 mg (26% yield) of the title compound as a yellow oil. **^{1}H NMR** (600 MHz, CD_3CN): δ 7.73 (s, 1H), 7.51 (m, 3H), 7.44 (m, 2H), 5.85 (s, 1H), 3.95 (s, 1H), 1.60 (s, 3H); **^{13}C NMR** (151 MHz, CD_3CN): δ 204.0, 197.3, 172.9, 154.8, 136.1, 129.5, 128.8, 127.9, 118.2, 110.1, 81.2, 28.4; **HR-ESI-MS:** m/z calculated for $C_{14}H_{11}O_4$ $[M-H]^-$: 243.0663, found: 243.0661; **IR** (thin film) 3325, 2961, 1632, 1596 cm^{-1}.

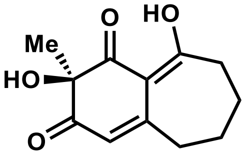

(*R*)-2,8-dihydroxy-2-methyl-6,7-dihydronaphthalene-1,3(2H,5H)-dione (2.84)

The title compound was synthesized according to the general procedure for milligram-scale *in vitro* enzymatic oxidative dearomatization using isolation method A. Purification by preparative HPLC afforded 2.8 mg (26% yield) of the title compound as a yellow oil. **^{1}H NMR** (600 MHz, $CDCl_3$) δ 5.76 (s, 1H), 3.66 (s, 1H), 2.72 (m, 2H), 2.70 (m, 2H), 1.86 (m, 4H), 1.57 (s, 3H); **^{13}C NMR** (150 MHz, $CDCl_3$): δ 201.6, 197.8, 192.1, 158.0, 116.0, 108.0, 80.1, 34.6, 34.4, 30.3, 23.9, 22.8; **HR-ESI-MS:** m/z calculated for $C_{12}H_{13}O_4$ $[M-H]^-$: 221.0819, found: 221.0819; **IR** (thin film): 3425, 2929, 1671, 1628, 1591 cm^{-1}.

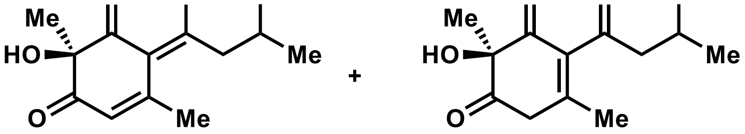

(*R,Z*)-2-hydroxy-6-(1-hydroxy-3-methylbutylidene)-2,5-dimethylcyclohex-4-ene-1,3-dione (2.98)

The title compound was synthesized according to the general procedure for milligram-scale *in vitro* enzymatic oxidative dearomatization using isolation method A. Purification by preparative HPLC afforded 8.0 mg (68% yield) of the title compound as a yellow oil. **^{1}H NMR** (600 MHz, CD_3CN) δ 3.91 (s, 1H), 3.74 (d, J = 21.3 Hz, 1H), 3.24 (d, J = 21.3 Hz, 1H), 2.54 (m, 2H), 1.97 (s, 3H), 1.56 (s, 3H), 0.99 (m, 1H), 0.96 (d, J = 6 Hz, 6H); **^{13}C NMR** (150 MHz, CD_3CN): δ 204.0, 202.5, 196.2, 154.4, 137.0, 84.2, 52.0, 44.7, 25.1, 23.8, 21.7, 20.1; **HR-ESI-MS:** $C_{13}H_{17}O_4$ [M-H]$^-$: 237.1132, found: 237.1131; **IR** (thin film): 3411, 2959, 1725, 1682 cm^{-1}.

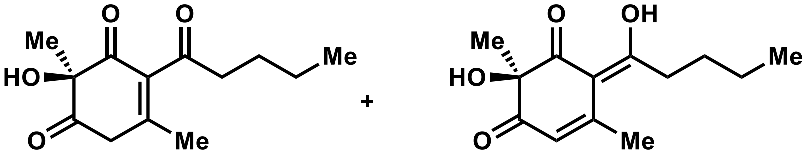

(*R,Z*)-2-hydroxy-6-(1-hydroxypentylidene)-2,5-dimethylcyclohex-4-ene-1,3-dione (2.83)

The title compound was synthesized according to the general procedure for milligram-scale *in vitro* enzymatic oxidative dearomatization using isolation method A. Purification by preparative HPLC afforded 7.8 mg (68% yield) of the title compound as a dark orange oil. **^{1}H NMR** (600 MHz, CD_3CN) δ 3.90 (s, 1H), 3.75 (d, J = 18 Hz, 1H), 3.25 (d, J = 18 Hz, 1H), 2.62 (t, J = 7.2, 2H), 1.98 (s, 3H), 1.60 (m, 2H), 1.56 (s, 3H), 1.47 (m, 2H), 0.92 (t, J = 6H, 3H); **^{13}C NMR** (150 MHz, CD_3CN): δ 204.6, 202.6, 196.2, 154.3, 137.0, 84.1, 44.6, 43.0, 25.2, 25.1, 21.9, 20.1, 13.1; **HR-ESI-MS:** m/z calculated for $C_{13}H_{17}O_4$ [M-H]$^-$: 237.1132, found: 237.1131; **IR** (thin film): 3348, 3120, 2959, 1703, 1686, 1624 cm^{-1}.

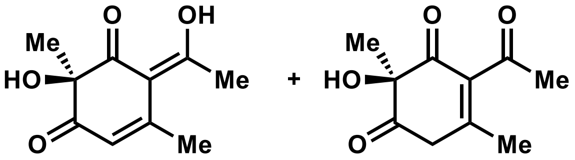

(*R*,*Z*)-2-hydroxy-6-(1-hydroxyethylidene)-2,5-dimethylcyclohex-4-ene-1,3-dione (2.82)

The title compound was synthesized according to the general procedure for milligram-scale *in vitro* enzymatic oxidative dearomatization using isolation method A. Purification by preparative HPLC afforded 10.1 mg (93% yield) of the title compound as a dark orange oil as a 1:1 mixture of keto-enol tautomers. **^{1}H NMR** (400 MHz, CD$_3$CN) δ 8.10 (s, 1H), 5.54 (s, 1H), 3.75 (d, J = 22.2 Hz, 1H), 3.26 (d, J = 22.1 Hz, 1H), 2.46 (s, 3H), 2.34 (s, 3H), 2.31 (s, 3H), 2.00 (s, 3H), 1.56 (s, 3H), 1.45 (s, 3H); **^{13}C NMR** (150 MHz, CD$_3$CN) δ 202.6, 201.9, 196.2, 154.7, 136.9, 84.1, 44.7, 30.4, 29.1, 25.1, 24.7, 20.1; **HR-ESI-MS:** m/z calculated for C$_{10}$H$_{11}$O$_4$ [M-H]$^-$: 195.0663, found: 195.0664; **IR** (thin film): 3264, 2963, 2952, 1722, 1624, 1538 cm^{-1}.

A) In CD$_3$CN ratio of keto-enol tautomers = 1:1

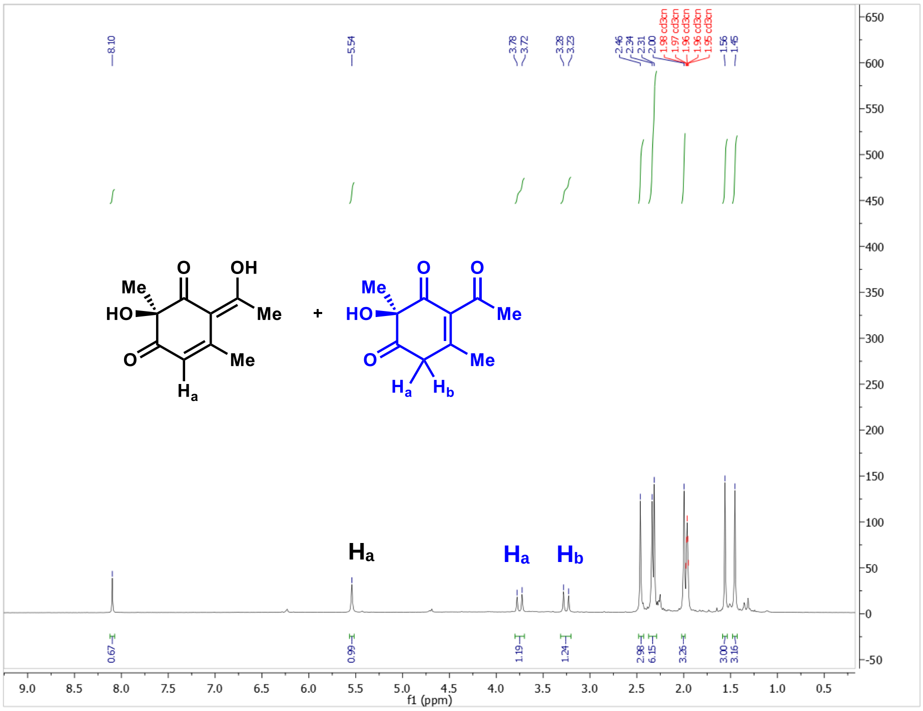

B) In CD_3Cl ratio of tautomers = 5:1

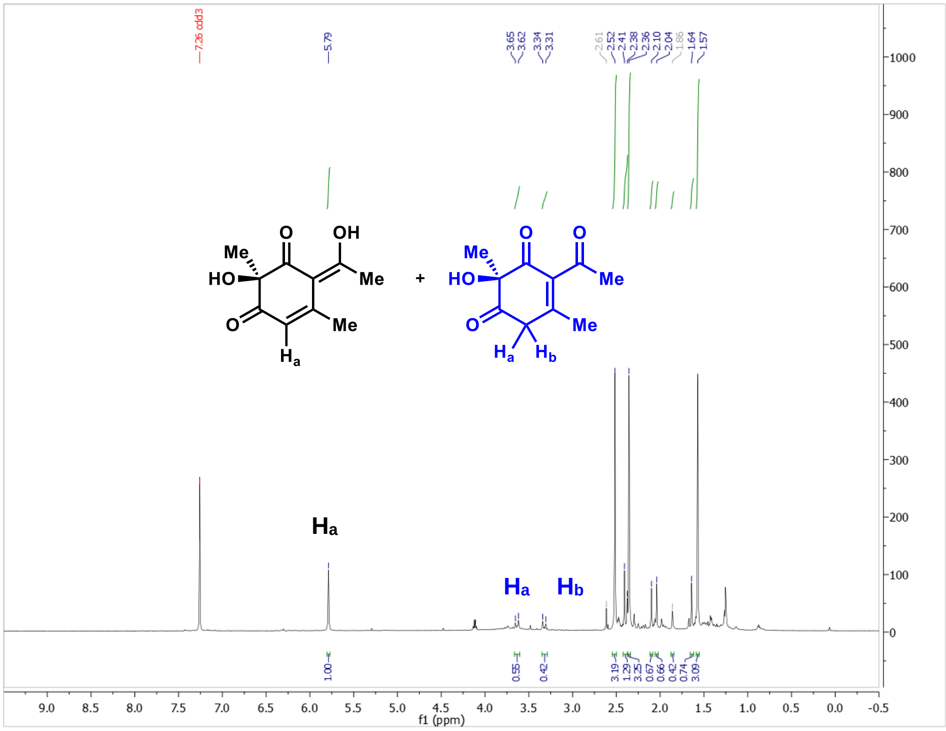

C) In CD_3CN with 10% D_2O alpha-protons exchange with deuterium.

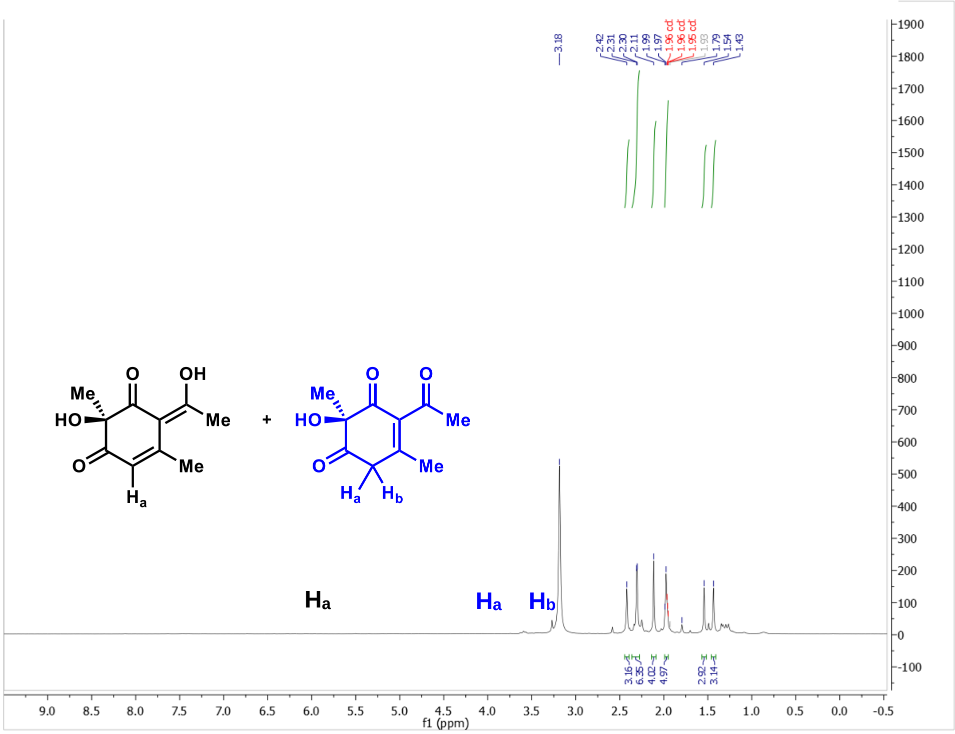

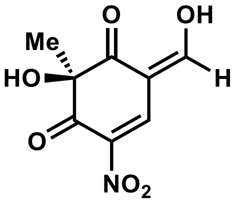

(*S*,*Z*)-2-hydroxy-6-(hydroxymethylene)-2-methyl-4-nitrocyclohex-4-ene-1,3-dione (2.86)

The title compound was synthesized according to the general procedure for milligram-scale *in vitro* enzymatic oxidative dearomatization using isolation method A. Purification by preparative HPLC afforded 2.6 mg (24% yield) of the title compound as a yellow oil. ^{1}**H NMR** (600 MHz, $(CD_3)_2SO$) δ 9.63 (s, 1H), 8.75 (s, 1H), 1.25 (s, 3H); ^{13}**C NMR** (150 MHz, $(CD_3)_2SO$): δ 197.6, 189.2, 186.0, 145.0, 125.2, 111.0, 83.1, 28.9; **HR-ESI-MS:** m/z calculated for $C_8H_6NO_6$ $[M-H]^-$: 212.0201, found: 212.0202; **IR** (thin film): 3296, 2255, 1776, 1658, 1523 cm^{-1}.

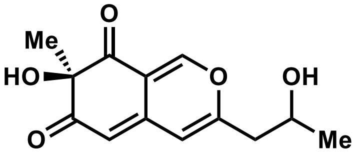

(*7R*)-7-hydroxy-3-(2-hydroxypropyl)-7-methyl-6H-isochromene-6,8(7H)-dione (2.20)

The title compound was prepared according to the general procedure for milligram-scale *in vitro* enzymatic oxidative dearomatization using isolation method A. Purification by preparative HPLC afforded 5.4 mg (55% yield) of the title compound as a dark red oil. ^{1}**H NMR** (400 MHz, $CDCl_3$) δ 8.04 (s, 1H), 6.40 (s, 1H), 5.48 (d, J = 1.1 Hz, 1H), 4.12 – 4.07 (m, 1H), 2.61 (dd, J = 14.6, 4.6 Hz, 1H), 2.53 (dd, J = 14.6, 8.2 Hz, 1H), 1.49 (s, 3H), 1.25 (d, J = 6.2 Hz, 3H) ppm; ^{13}**C NMR** (150 MHz, CD_3OD): δ 199.0, 198.6, 162.1, 154.9, 117.1, 111.2, 84.5, 66.1, 43.5, 28.0, 23.4 ppm;

HR-ESI-MS: m/z calcd. for $C_{13}H_{13}O_5H^+$ $[M+H]^+$: 251.0914, found: 251.0904. All spectra obtained were consistent with literature values.[30]

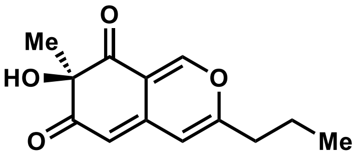

(*R*)-7-hydroxy-7-methyl-3-propyl-6H-isochromene-6,8(7H)-dione (2.85)

The title compound was prepared according to the general procedure for milligram-scale *in vitro* enzymatic oxidative dearomatization using isolation method A. Purification by preparative HPLC afforded 8.1 mg (82% yield) of the title compound as a dark orange oil. **^{1}H NMR** (700 MHz, $CDCl_3$): δ 7.90 (s, 1H), 6.12 (s, 1H), 5.52 (s, 1H), 2.73 (s, 1H), 2.41 (t, J = 7.5 Hz, 2H), 1.67 (m, 2H), 1.55 (s, 3H), 1.00 (t, J = 7.5 Hz, 3H); **^{13}C NMR** (175 MHz, $CDCl_3$): δ 196.5, 196.0, 163.0, 153.2, 144.4, 115.7, 108.5, 104.9, 83.5, 35.1, 28.4, 19.9, 13.4; **HR-ESI-MS:** m/z calculated for $C_{13}H_{13}O_4$ $[M-H]^-$: 233.0819, found: 233.0819; **IR** (thin film): 3262, 2963, 2925, 1722, 1624 cm^{-1}.

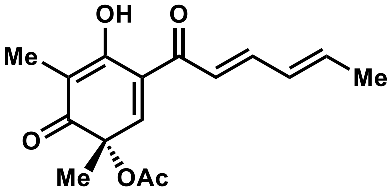

(*S*)-3-((2E,4E)-hexa-2,4-dienoyl)-4-hydroxy-1,5-dimethyl-6-oxocyclohexa-2,4-dien-1-yl acetate (2.87)

The title compound was prepared according to the general procedure for milligram-scale *in vitro* enzymatic dearomatization using isolation method B. Purification on silica gel (20% to 50% EtOAc in hexanes) afforded 5.4 mg (43%) of the *o*-quinol as a yellow oil. **^{1}H NMR** (700 MHz, $CDCl_3$) δ 11.83 (s, 1H), 7.46 (dd, J = 14.7, 10.6 Hz, 1H), 7.25 (s, 1H), 6.66 (d, J = 14.8 Hz, 1H), 6.35 (m, 2H), 2.15 (s, 3H), 1.93 (d, J = 6.4 Hz, 3H), 1.86 (s, 3H), 1.49 (s, 3H). All spectra obtained were consistent with literature values.[13]

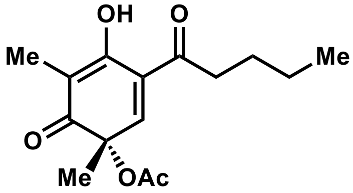

(*S*)-4-hydroxy-1,5-dimethyl-6-oxo-3-pentanoylcyclohexa-2,4-dien-1-yl acetate (2.90)

The title compound was prepared according to the general procedure for milligram-scale *in vitro* enzymatic oxidative dearomatization using isolation method B. Purification on silica gel (30% to 50% EtOAc in hexanes) afforded 3.0 mg (24%) of the *o*-quinol as a yellow oil. **^{1}H NMR** (700 MHz, $CDCl_3$) δ 11.53 (s, 1H), 7.29 (s, 1H), 2.81 (t, J = 7.3, 2H), 2.14 (s, 3H), 1.84 (s, 3H), 1.65 (m, 2H), 1.48 (s, 3H), 1.36 (m, 2H), 0.94 (t, J = 6.9 Hz, 3H); **^{13}C NMR** (100 MHz, $CDCl_3$): δ 206.1, 194.8, 170.0, 162.1, 152.9, 124.6, 111.8, 78.0, 37.6, 26.1, 24.0, 22.1, 20.5, 13.8, 7.1; **HR-ESI-MS:** m/z calculated for $C_{15}H_{19}O_5$ $[M-H]^-$: 279.1238, found: 279.1239; **IR** (thin film): 3280, 2937, 1647, 1640 cm^{-1}.

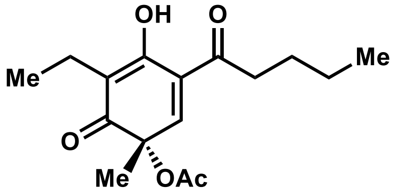

(*S*)-5-ethyl-4-hydroxy-1-methyl-6-oxo-3-pentanoylcyclohexa-2,4-dien-1-yl acetate (2.88)

The title compound was prepared according to the general procedure for milligram-scale *in vitro* enzymatic oxidative dearomatization using isolation method B. Purification on silica gel (20% to 40% EtOAc in hexanes) afforded 1.0 mg (8.0% yield) of the *o*-quinol as a yellow oil. **^{1}H NMR** (400 MHz, $CDCl_3$) δ 11.48 (s, 1H), 7.28 (s, 1H), 2.82 (t, J = 8.6 Hz, 2H), 2.40 (m, 2H), 2.15 (s, 3H), 1.65 (p, J = 7.5 Hz, 2H), 1.49 (s, 3H), 1.38 (h, J = 7.6 Hz, 3H), 1.00 (t, J = 0.97 (t, 3H); **^{13}C**

NMR (100 MHz, $CDCl_3$): δ 205.4, 161.3, 158.2, 127.6, 120.7, 113.0, 110.2, 37.7, 27.1, 22.8, 22.5, 14.1, 13.9, 7.4; **HR-ESI-MS:** m/z calculated for $C_{16}H_{21}O_5$ $[M-H]^-$: 293.1394, found: 293.1395; **IR** (thin film): 2965, 1740, 1673, 1652, 1408 cm^{-1}.

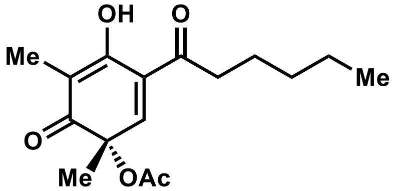

(*S*)-3-hexanoyl-4-hydroxy-1,5-dimethyl-6-oxocyclohexa-2,4-dien-1-yl acetate (2.99)

The title compound was prepared according to the general procedure for milligram-scale *in vitro* enzymatic oxidative dearomatization using isolation method B. Purification on silica gel (20% to 40% EtOAc in hexanes) afforded 7.8 mg (63% yield) of the *o*-quinol as a yellow oil. **^{1}H NMR** (700 MHz, $CDCl_3$) δ 11.53 (s, 1H), 7.29 (s, 1H), 2.81 (td, J = 7.3, 3.1 Hz, 2H), 2.13 (s, 3H), 1.83 (s, 3H), 1.65 (p, J = 7.3 Hz, 2H), 1.48 (s, 3H), 1.35 (m, 4H), 0.90 (t, J = 6.9 Hz, 3H). All spectra obtained were consistent with literature values.[13]

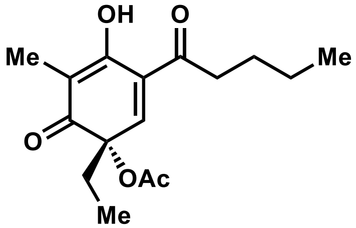

(*S*)-1-ethyl-4-hydroxy-5-methyl-6-oxo-3-pentanoylcyclohexa-2,4-dien-1-yl acetate (2.89)

The title compound was prepared according to the general procedure for milligram-scale *in vitro* enzymatic oxidative dearomatization using isolation method B. Purification on silica gel (20% to 40% EtOAc in hexanes) afforded 3.4 mg (27% yield) of the *o*-quinol as a yellow oil. **^{1}H NMR** (700 MHz, $CDCl_3$) δ 11.50 (s, 1H), 7.28 (s, 1H), 2.81 (t, J = 8 Hz, H), 2.15 (s, 3H), 1.88 (m, 2H), 1.82 (s, 3H), 1.64 (m, 2H), 1.37 (m, 2H), 0.94 (overlapping t, 6H); **^{13}C NMR** (100 MHz, CDCl$_3$): δ 206.1, 194.8, 170.0, 162.1, 153.0, 124.6, 111.8, 78.0, 37.9, 31.1, 24.0, 23.7, 22.4, 20.4, 13.8, 7.1; **HR-ESI-MS:** m/z calculated for $C_{14}H_{19}O_3$ [M-H]$^-$: 235.1340, found: 235.1339; **IR** (thin film): 2961, 1740, 1675, 1650, 1403 cm^{-1}.

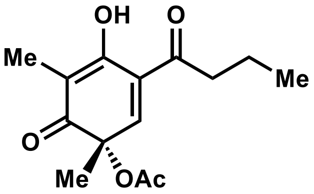

(*S*)-3-butyryl-4-hydroxy-1,5-dimethyl-6-oxocyclohexa-2,4-dien-1-yl acetate (2.91)

The title compound was prepared according to the general procedure for milligram-scale *in vitro* enzymatic oxidative dearomatization using isolation method B. Purification on silica gel (20% to 40% EtOAc in hexanes) afforded 2.8 mg (22% yield) of the *o*-quinol as a yellow oil. **^{1}H NMR** (400 MHz, CDCl$_3$) δ 11.53 (t, J = 1.2 Hz, 1H), 7.29 (s, 1H), 2.81 (m, 2H), 2.14 (s, 3H), 1.84 (s, 3H), 1.71 (m, 2H), 1.48 (s, 3H), 0.98 (t, J = 7.4, 3H); **^{13}C NMR** (100 MHz, CDCl$_3$): δ 205.9, 194.8, 167.0, 162.0, 153.0, 124.6, 111.8, 78.0, 39.8, 24.0, 20.5, 17.6, 13.6, 7.1; **HR-ESI-MS:** m/z calculated for $C_{14}H_{17}O_5$ [M-H]$^-$: 265.1081, found: 265.1081; **IR** (thin film): 2961, 2932, 1737, 1703, 1650 cm^{-1}.

Chapter 2.6.4: Substrate Calibration Curves

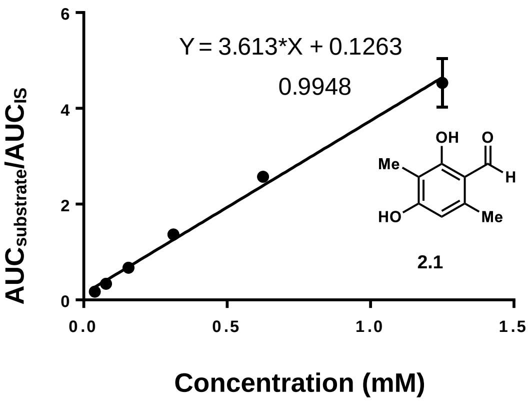

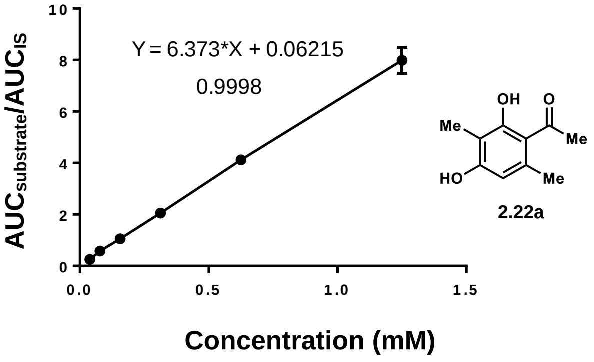

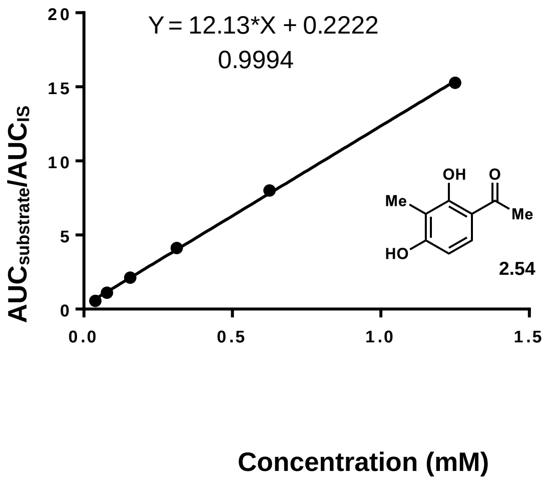

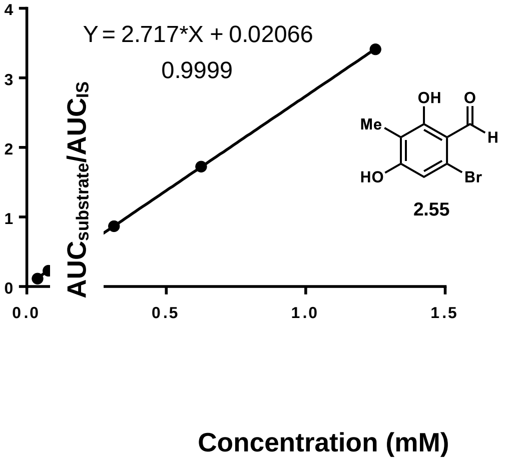

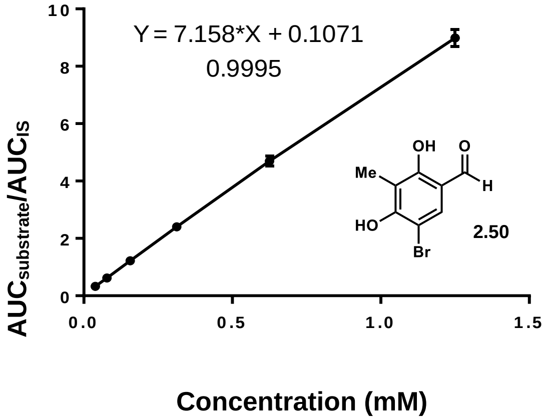

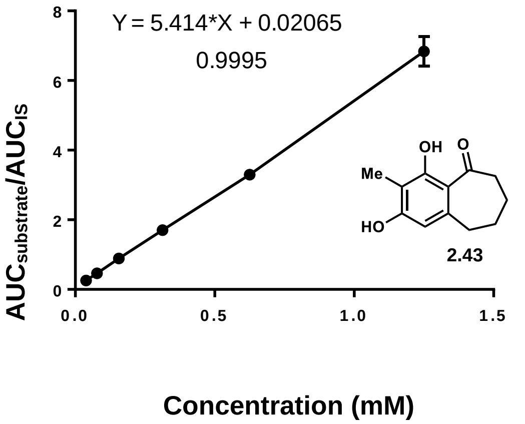

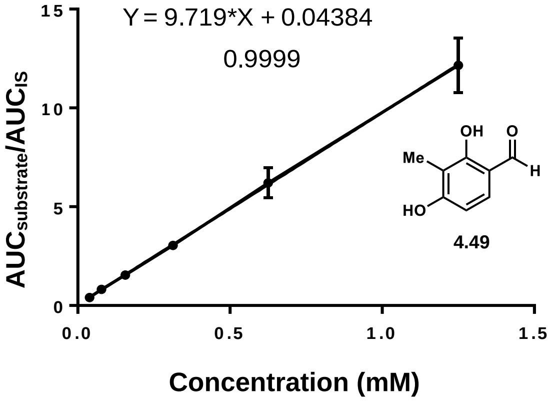

Y = 9.719*X + 0.04384
0.9999
AUCsubstrate/AUCIS
15
10
5
0
0.0
0.5
1.0
1.5
Concentration (mM)
OH
O
Me
H
HO
4.49

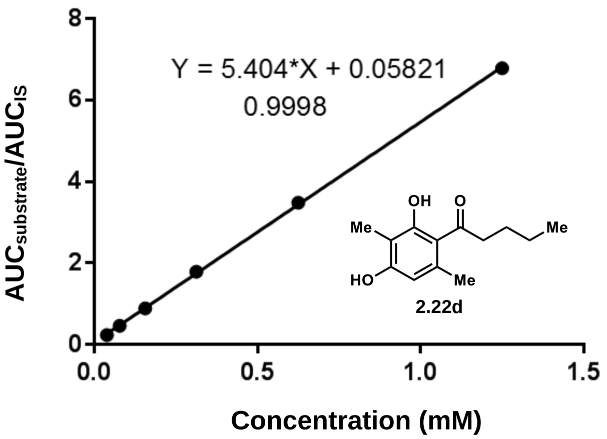

Y = 5.404*X + 0.05821
0.9998
AUCsubstrate/AUCIS
8
6
4
2
0
0.0
0.5
1.0
1.5
Concentration (mM)
OH
O
Me
Me
HO
Me
2.22d

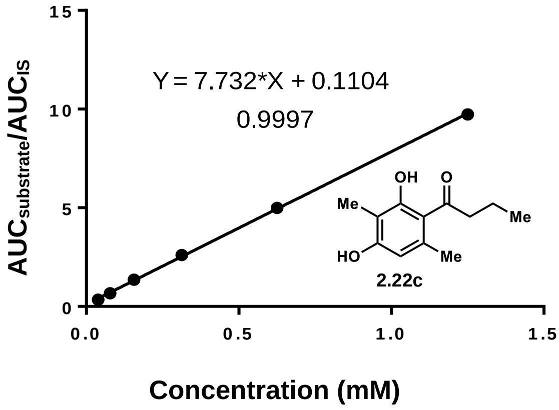

Y = 7.732*X + 0.1104
0.9997
AUCsubstrate/AUCIS
15
10
5
0
0.0
0.5
1.0
1.5
Concentration (mM)
OH
O
Me
Me
HO
Me
2.22c

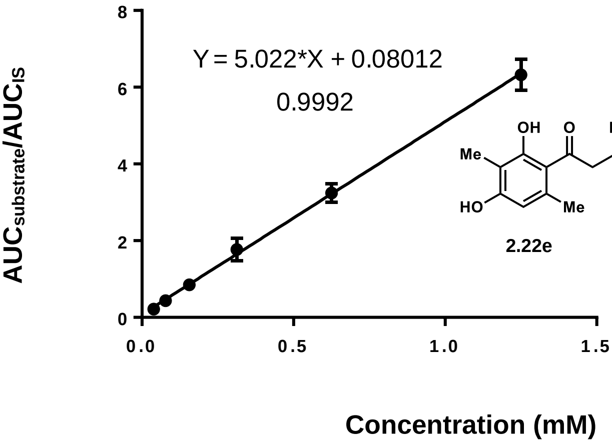

Y = 5.022*X + 0.08012
0.9992
AUCsubstrate/AUCIS
8
6
4
2
0
0.0
0.5
1.0
1.5
Concentration (mM)
OH
O
Me
Me
Me
HO
Me
2.22e

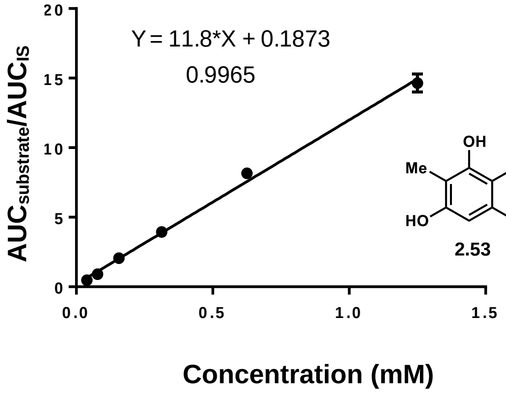

Y = 11.8*X + 0.1873
0.9965
AUCsubstrate/AUCIS
20
15
10
5
0
0.0
0.5
1.0
1.5
Concentration (mM)
OH
O
Me
H
HO
Ph
2.53

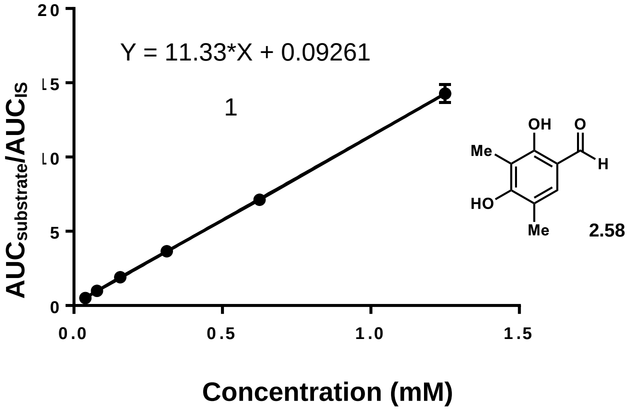

Y = 11.33*X + 0.09261
1
AUCsubstrate/AUCIS
20
15
10
5
0
0.0
0.5
1.0
1.5
Concentration (mM)
OH
O
Me
H
HO
Me
2.58

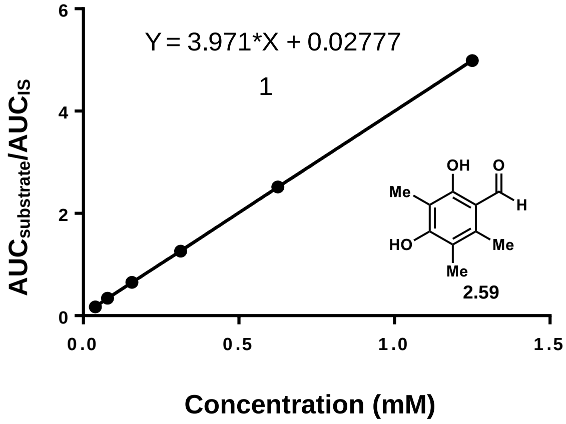
Y = 3.971*X + 0.02777
1
AUCsubstrate/AUCIS
Concentration (mM)
6
4
2
0
0.0
0.5
1.0
1.5
OH
O
Me
H
HO
Me
Me
2.59

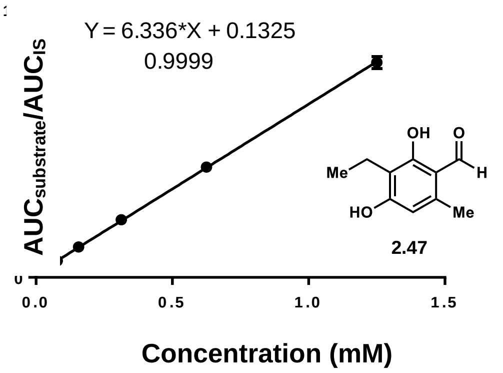
Y = 6.336*X + 0.1325
0.9999
AUCsubstrate/AUCIS
Concentration (mM)
0
0.0
0.5
1.0
1.5
OH
O
Me
H
HO
Me
2.47

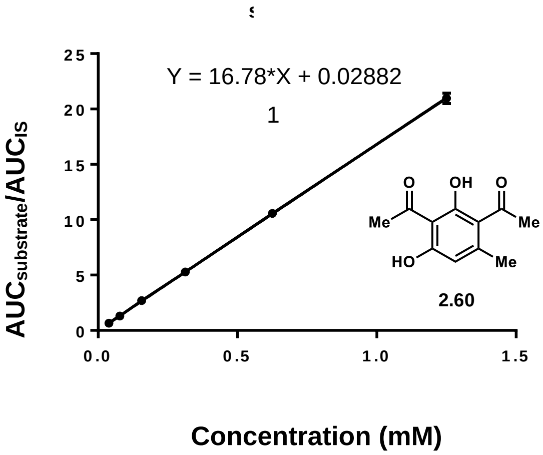
Y = 16.78*X + 0.02882
1
AUCsubstrate/AUCIS
Concentration (mM)
25
20
15
10
5
0
0.0
0.5
1.0
1.5
O
OH
O
Me
Me
HO
Me
2.60

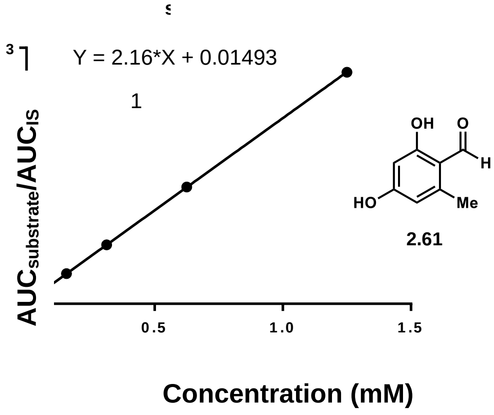
Y = 2.16*X + 0.01493
1
3
AUCsubstrate/AUCIS
Concentration (mM)
0.5
1.0
1.5
OH
O
H
HO
Me
2.61

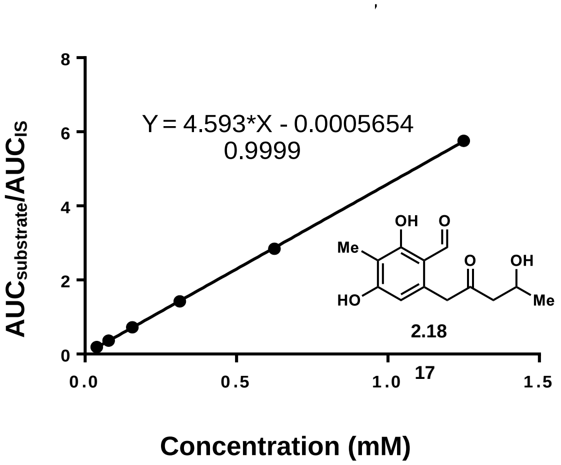
Y = 4.593*X - 0.0005654
0.9999
AUCsubstrate/AUCIS
Concentration (mM)
8
6
4
2
0
0.0
0.5
1.0
17
1.5
OH
O
Me
O
OH
HO
Me
2.18

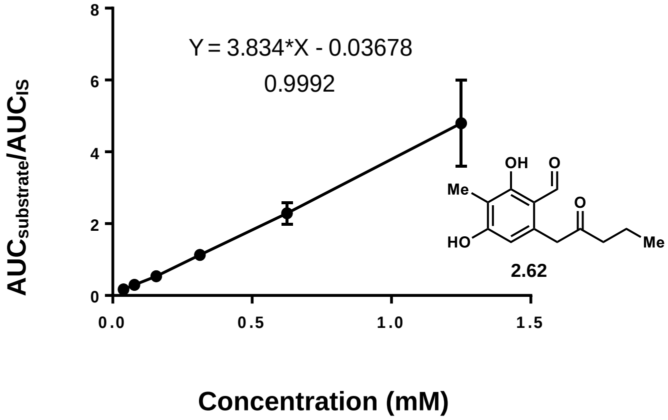
Y = 3.834*X - 0.03678
0.9992
AUCsubstrate/AUCIS
Concentration (mM)
8
6
4
2
0
0.0
0.5
1.0
1.5
OH
O
Me
O
HO
Me
2.62

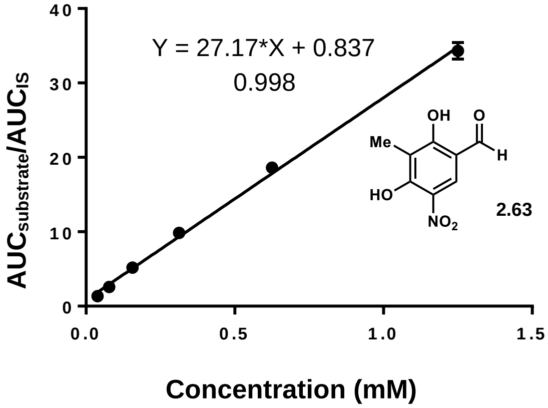
Y = 27.17*X + 0.837
0.998
AUCsubstrate/AUCIS
Concentration (mM)
0
10
20
30
40
0.0
0.5
1.0
1.5
OH
O
Me
H
HO
NO2
2.63

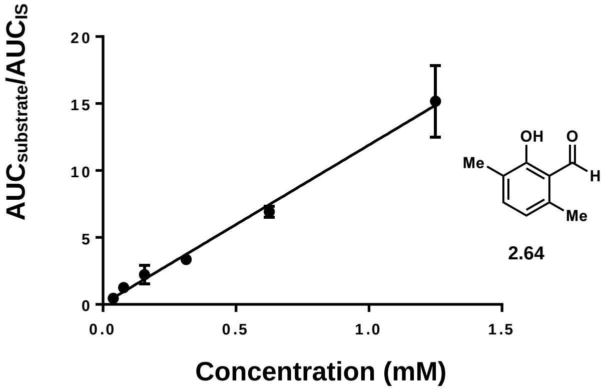
AUCsubstrate/AUCIS
Concentration (mM)
0
5
10
15
20
0.0
0.5
1.0
1.5
OH
O
Me
H
Me
2.64

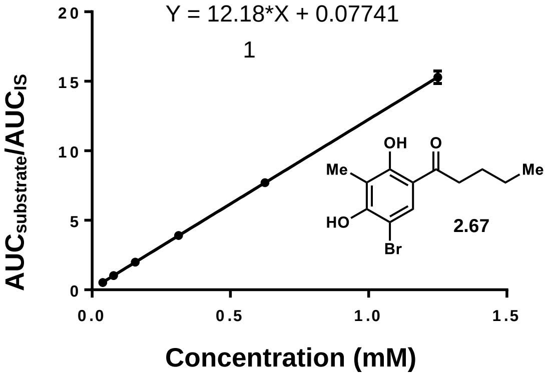
Y = 12.18*X + 0.07741
1
AUCsubstrate/AUCIS
Concentration (mM)
0
5
10
15
20
0.0
0.5
1.0
1.5
OH
O
Me
Me
HO
Br
2.67

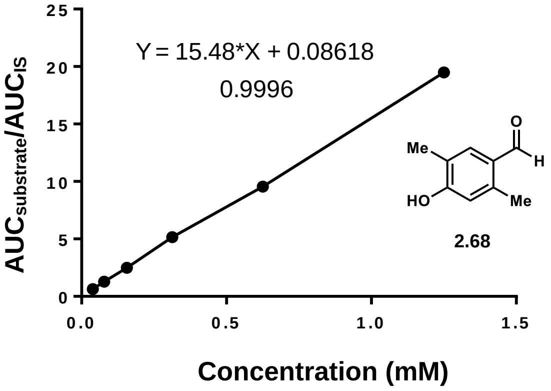
Y = 15.48*X + 0.08618
0.9996
AUCsubstrate/AUCIS
Concentration (mM)
0
5
10
15
20
25
0.0
0.5
1.0
1.5
O
Me
H
HO
Me
2.68

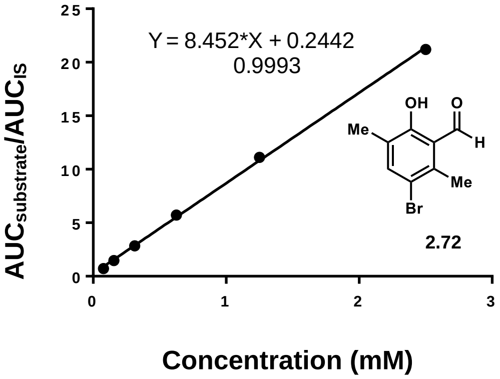
Y = 8.452*X + 0.2442
0.9993
AUCsubstrate/AUCIS
Concentration (mM)
0
5
10
15
20
25
0
1
2
3
OH
O
Me
H
Me
Br
2.72

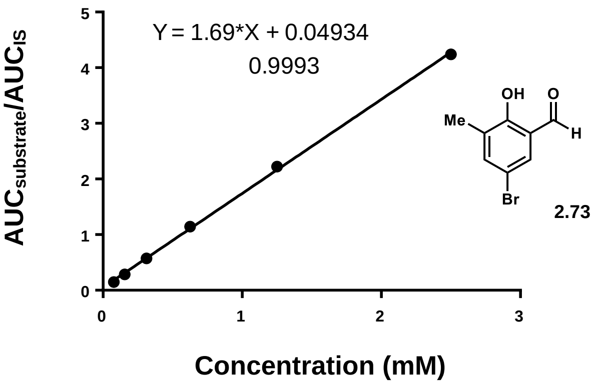
Y = 1.69*X + 0.04934
0.9993
AUCsubstrate/AUCIS
Concentration (mM)
0
1
2
3
4
5
0
1
2
3
OH
O
Me
H
Br
2.73

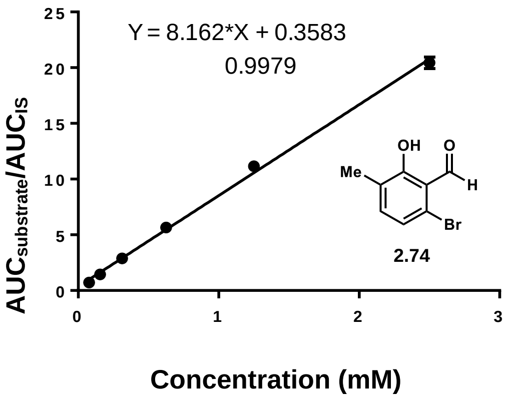

Y = 8.162*X + 0.3583
0.9979
AUCsubstrate/AUCIS
25
20
15
10
5
0
0
1
2
3
Concentration (mM)
OH
O
Me
H
Br
2.74

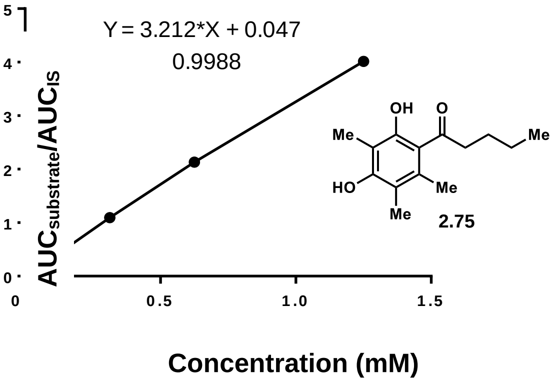

Y = 3.212*X + 0.047
0.9988
AUCsubstrate/AUCIS
5
4
3
2
1
0
0
0.5
1.0
1.5
Concentration (mM)
OH
O
Me
Me
HO
Me
Me
2.75

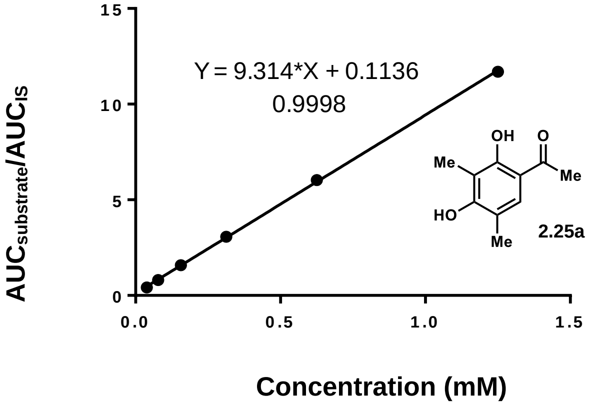

Y = 9.314*X + 0.1136
0.9998
AUCsubstrate/AUCIS
15
10
5
0
0.0
0.5
1.0
1.5
Concentration (mM)
OH
O
Me
Me
HO
Me
2.25a

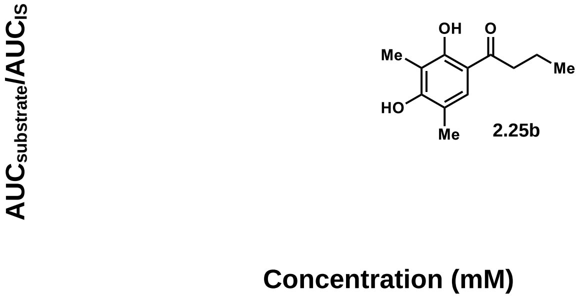

AUCsubstrate/AUCIS
OH
O
Me
Me
HO
Me
2.25b
Concentration (mM)

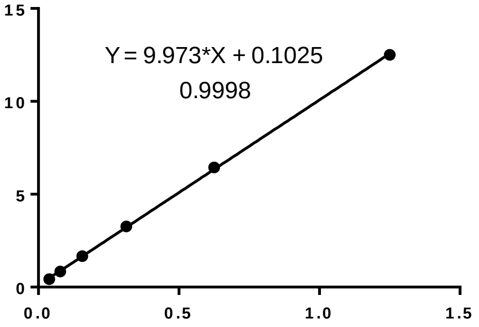

Y = 9.973*X + 0.1025
0.9998
15
10
5
0
0.0
0.5
1.0
1.5

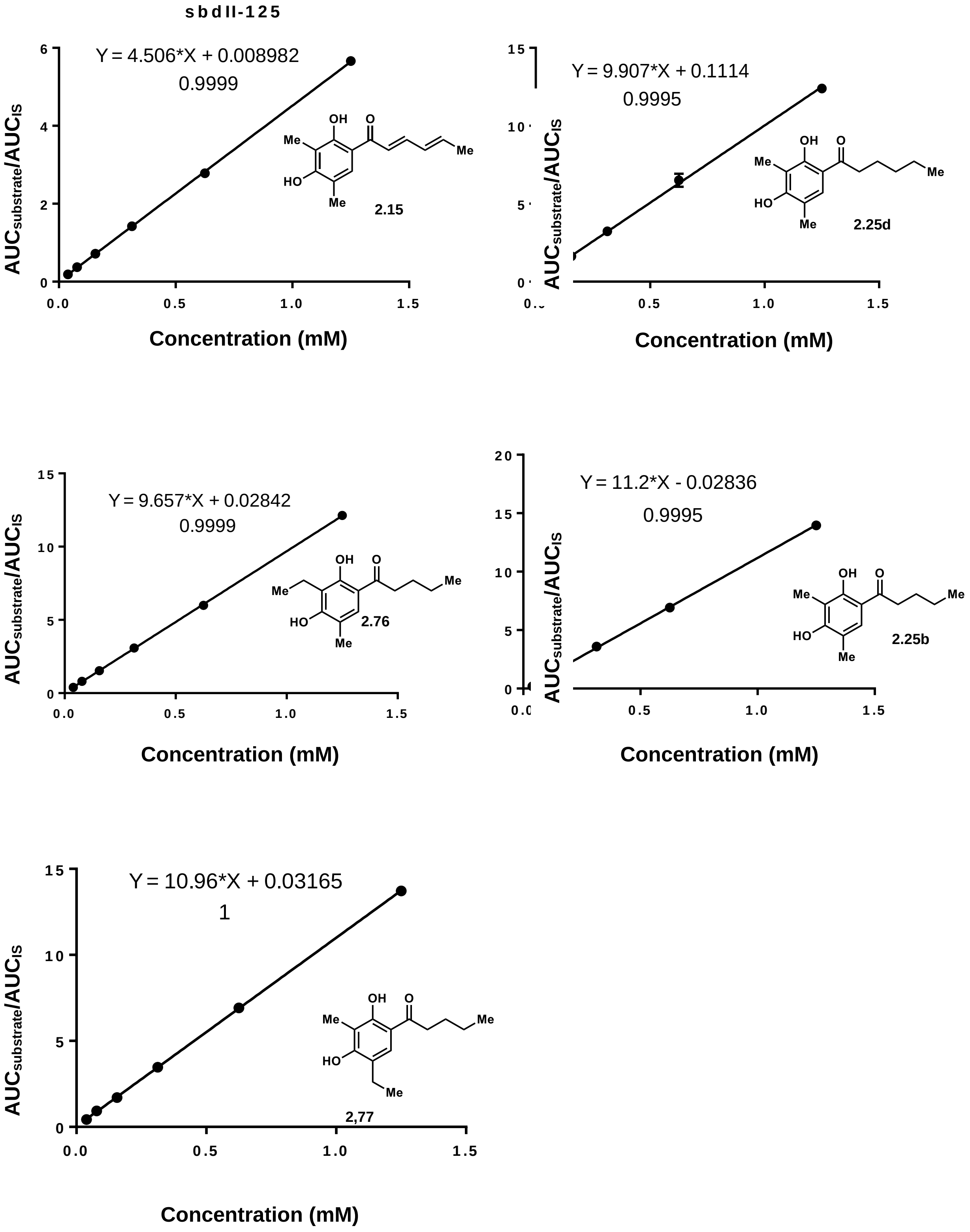

Figure 2.11: Calibration curves of substrates.

Chapter 2.6.5: UPLC Traces of Biocatalytic Reactions

With TropB

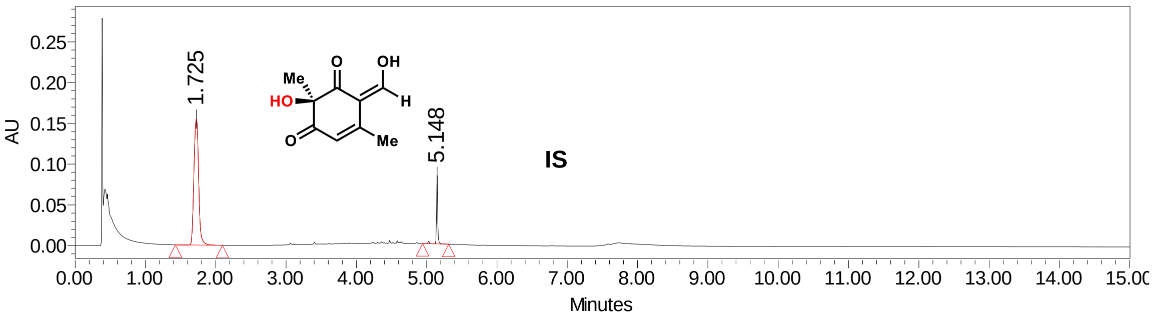

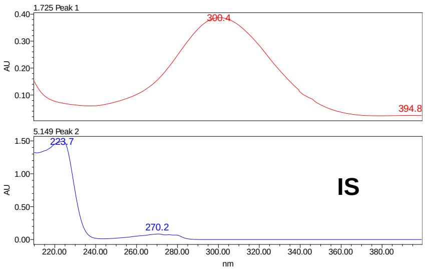

	Retention Time	Area	% Area	Height
1	1.725	721031	87.98	154590
2	5.148	98519	12.02	84071

No enzyme control

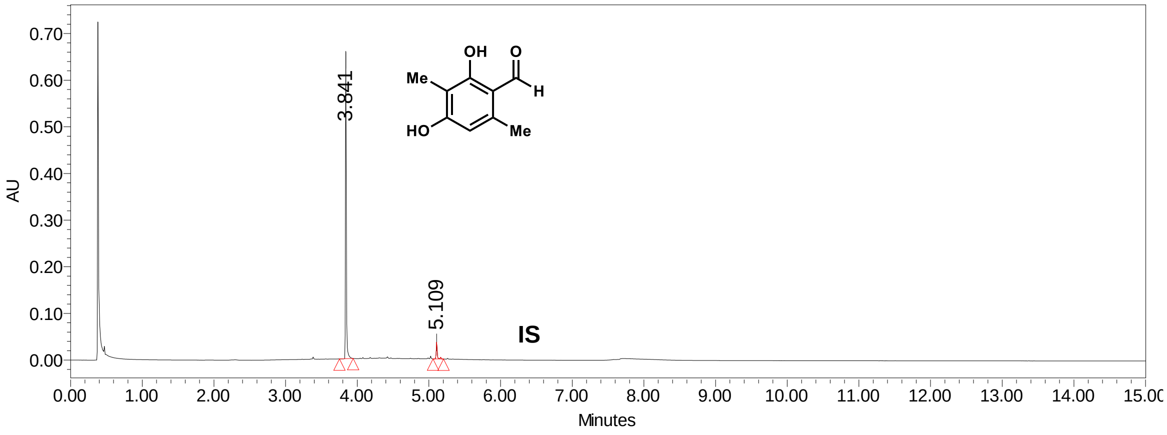

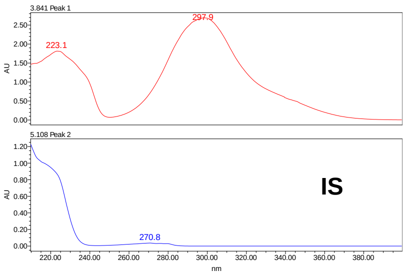

	Retention Time	Area	% Area	Height
1	3.841	539715	93.46	659310
2	5.109	37786	6.54	35891

Figure 2.12: Oxidative dearomatization of **2.12** by TropB. PDA traces of enzymatic reaction and control reaction.

With TropB

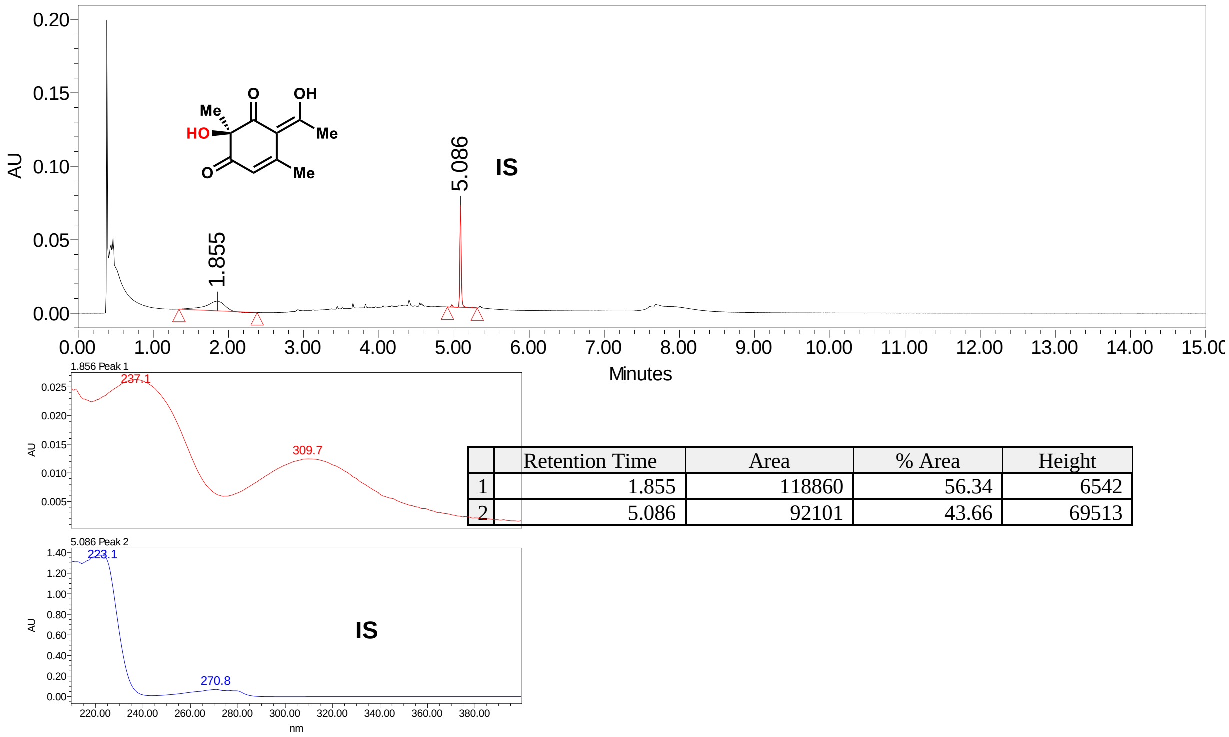

	Retention Time	Area	% Area	Height
1	1.855	118860	56.34	6542
2	5.086	92101	43.66	69513

No enzyme control

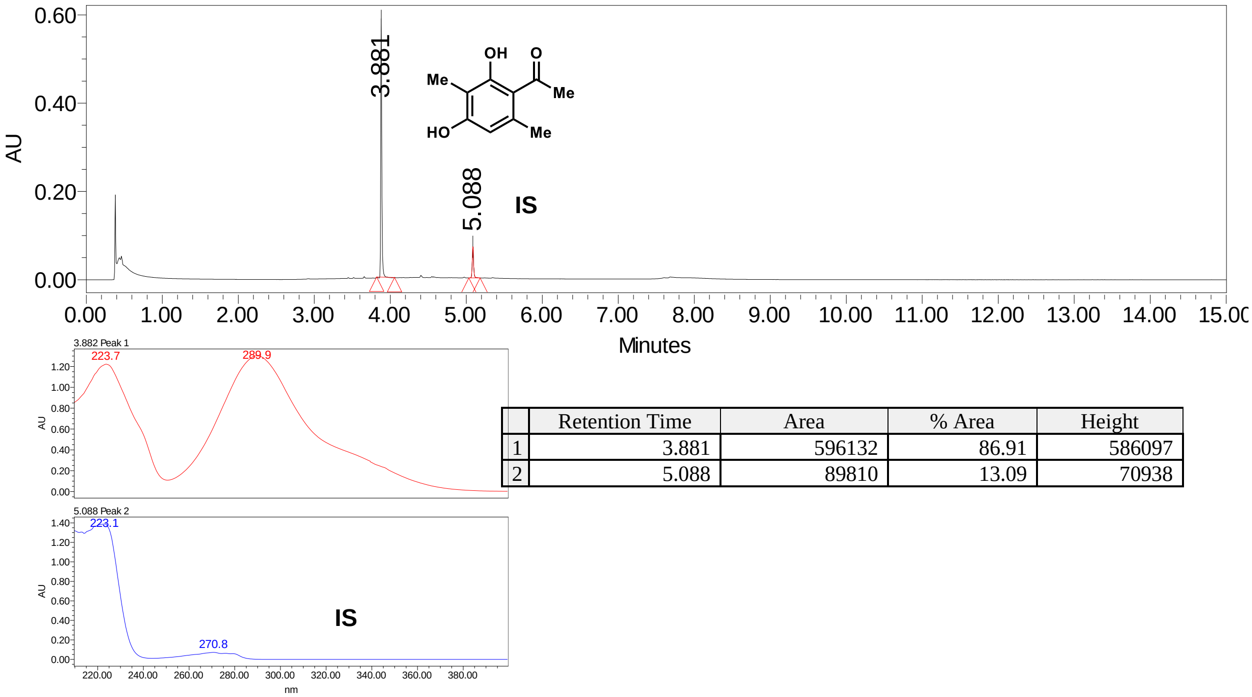

	Retention Time	Area	% Area	Height
1	3.881	596132	86.91	586097
2	5.088	89810	13.09	70938

With TropB

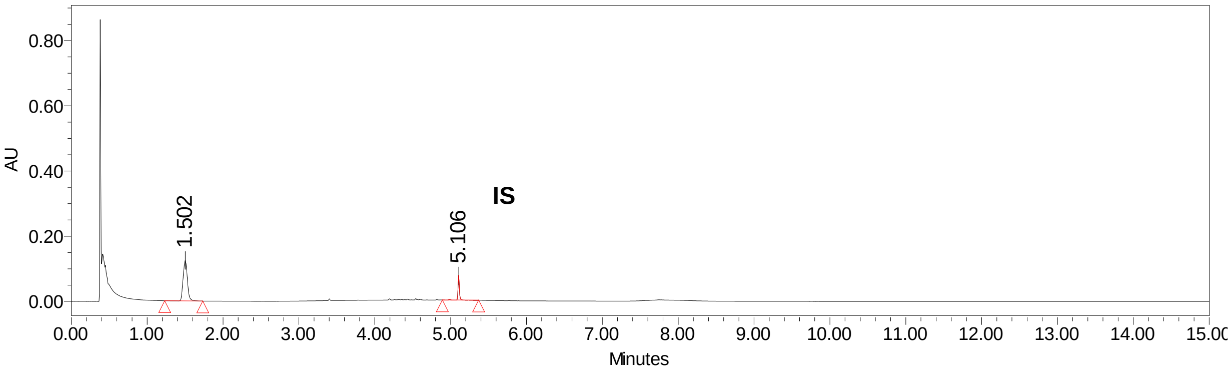

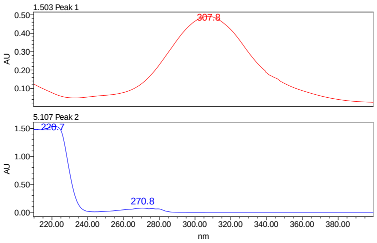

	Retention Time	Area	% Area	Height
1	1.502	484359	83.13	124361
2	5.106	98277	16.87	76056

No enzyme control

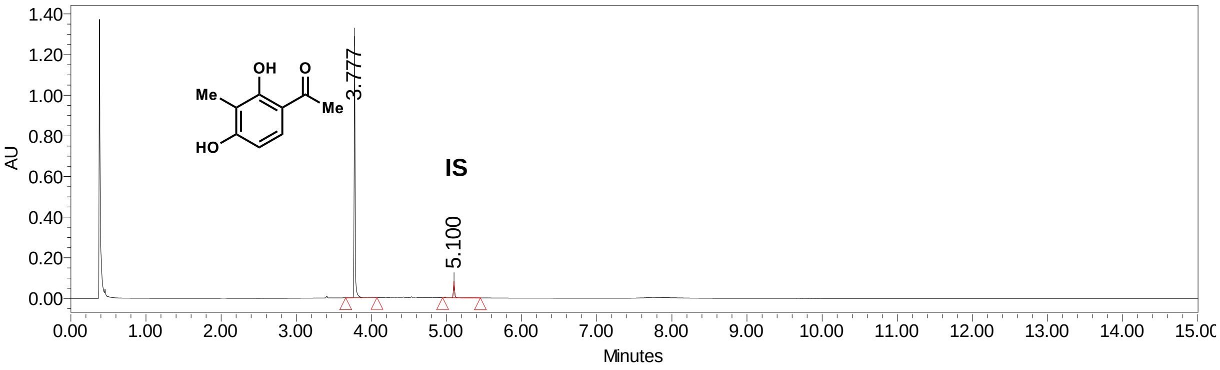

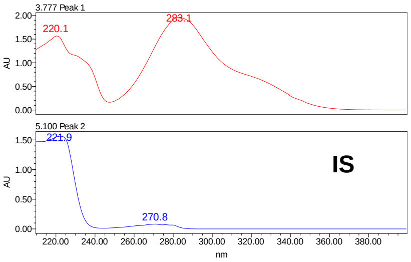

	Retention Time	Area	% Area	Height
1	3.777	1136190	92.71	1285582
2	5.100	89389	7.29	80322

Figure 2.14: Oxidative dearomatization of **2.54** by TropB. PDA traces of enzymatic reaction and control reaction.

With TropB

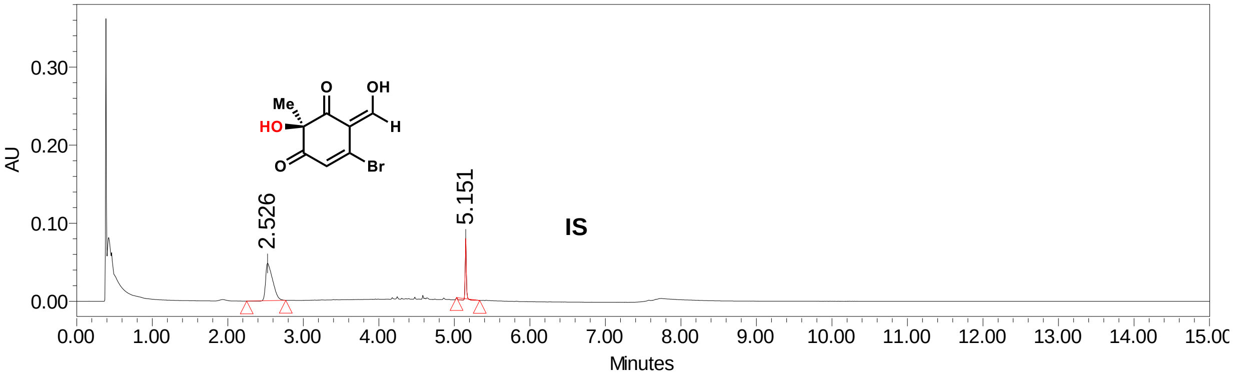

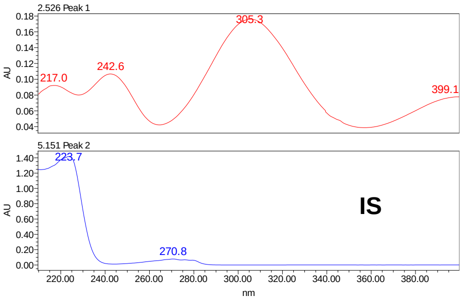

	Retention Time	Area	% Area	Height
1	2.526	310271	76.01	47820
2	5.151	97939	23.99	77097

No enzyme control

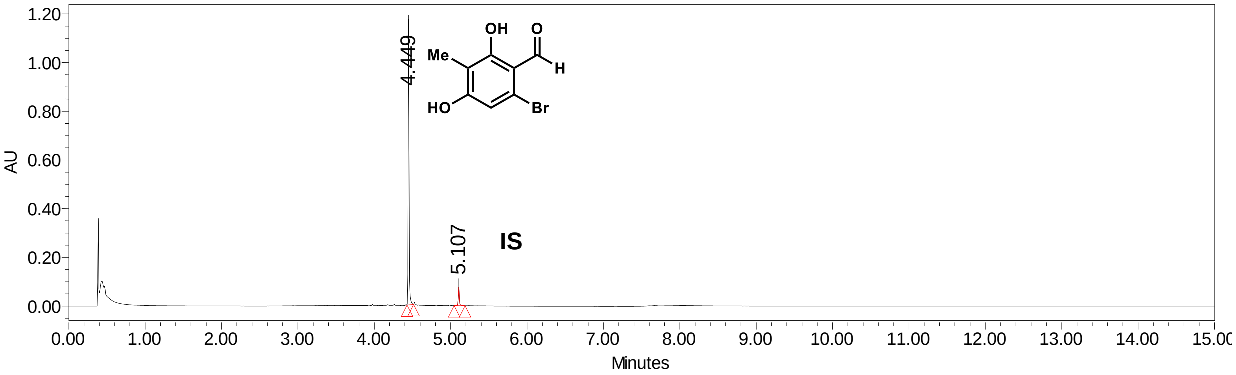

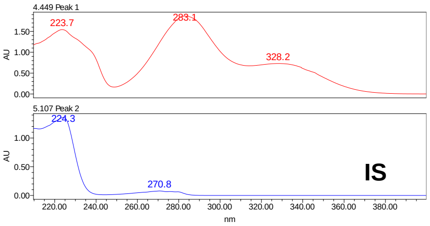

	Retention Time	Area	% Area	Height
1	4.449	925130	92.77	1175806
2	5.107	72062	7.23	76922

Figure 2.15: Oxidative dearomatization of **2.55** by TropB. PDA traces of enzymatic reaction and control reaction

With TropB

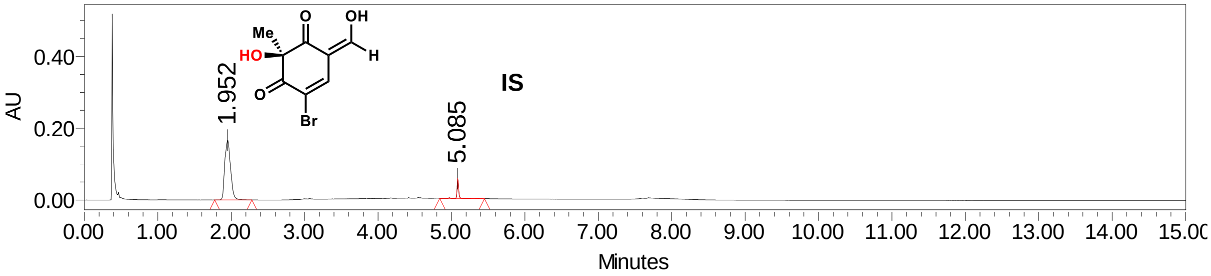

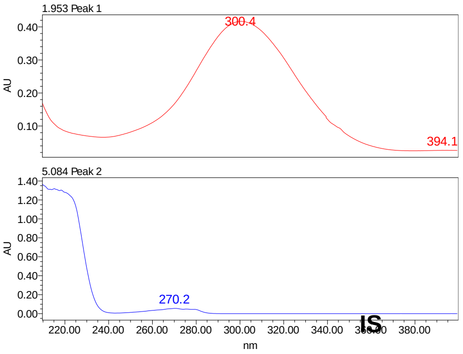

	Retention Time	Area	% Area	Height
1	1.952	909010	90.96	166861
2	5.085	90292	9.04	55477

No enzyme control

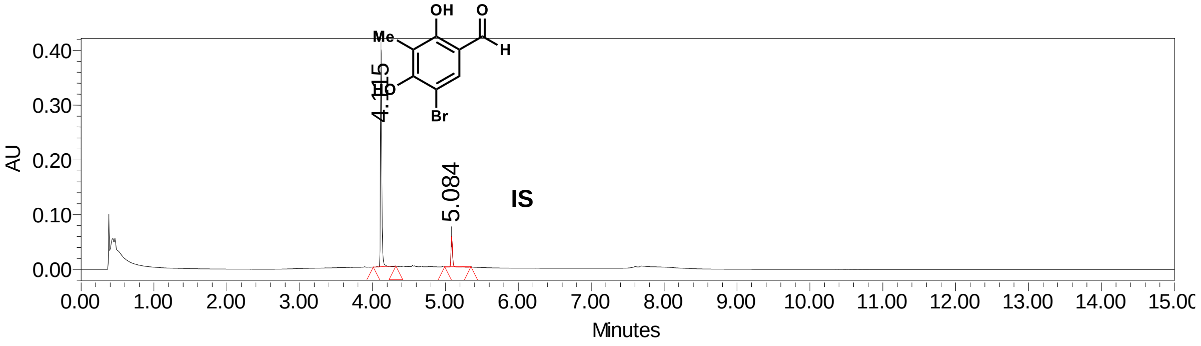

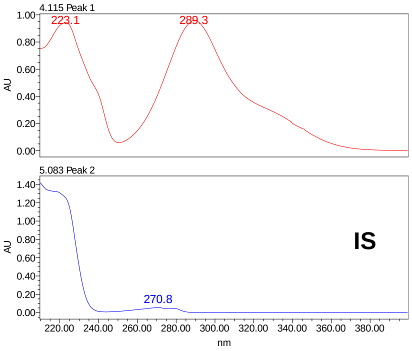

	Retention Time	Area	% Area	Height
1	4.115	484839	85.17	396843
2	5.084	84395	14.83	54993

Figure 2.16: Oxidative dearomatization of **2.50** by TropB. PDA traces of enzymatic reaction and control reaction.

With TropB

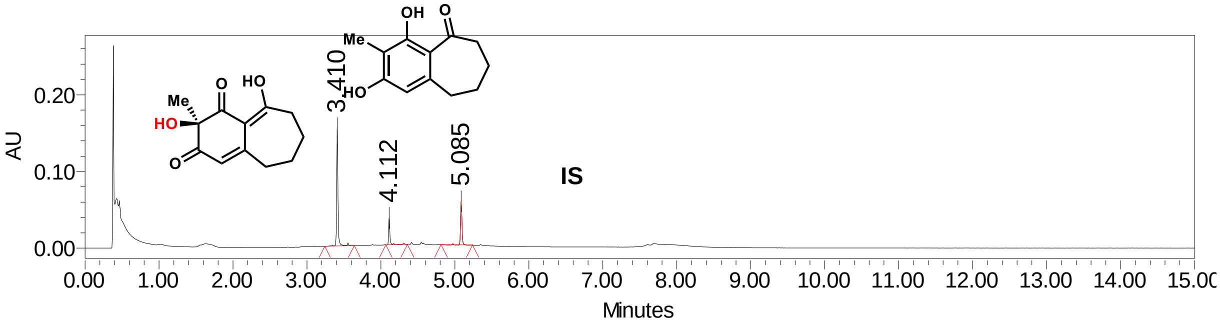

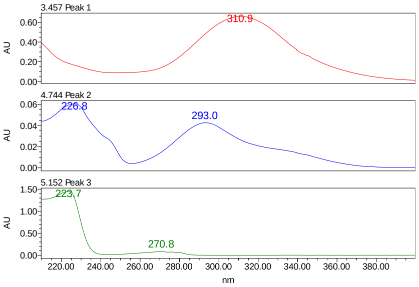

	Retention Time	Area	% Area	Height
1	3.410	181356	59.21	154254
2	4.112	43890	14.33	35524
3	5.085	81051	26.46	56795

No enzyme control

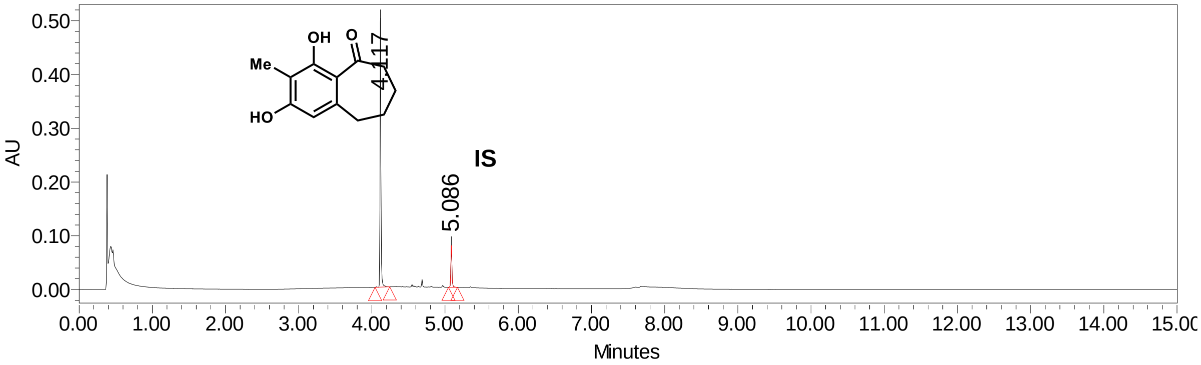

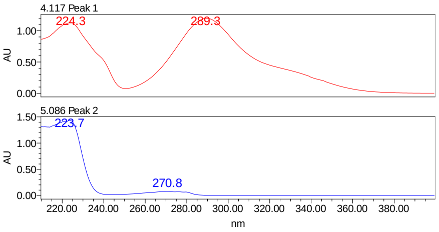

	Retention Time	Area	% Area	Height
1	4.117	429008	84.07	500038
2	5.086	81283	15.93	78207

Figure 2.17: Oxidative dearomatization of **2.43** by TropB. PDA traces of enzymatic reaction and control reaction.

With TropB

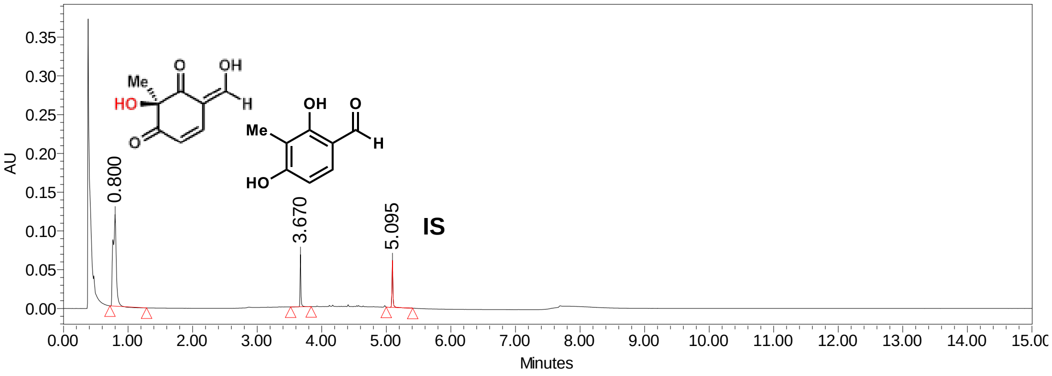

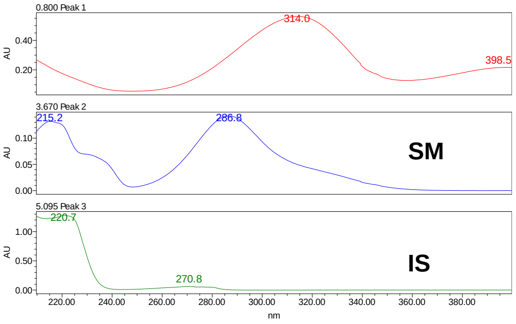

	Retention Time	Area	% Area	Height
1	0.800	418978	77.69	118420
2	3.670	57521	10.67	67315
3	5.095	62803	11.65	60631

No enzyme control

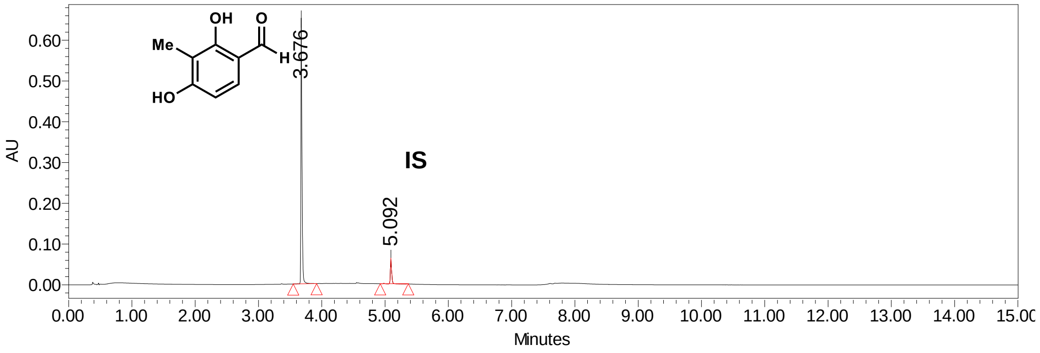

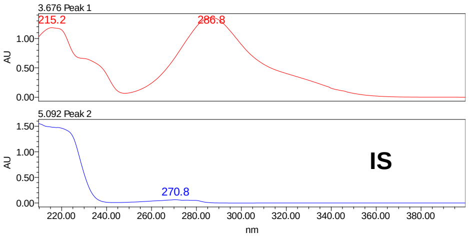

	Retention Time	Area	% Area	Height
1	3.676	782521	89.67	652406
2	5.092	90136	10.33	62812

Figure 2.18: Oxidative dearomatization of **2.49** by TropB. PDA traces of enzymatic reaction and control reaction.

With TropB

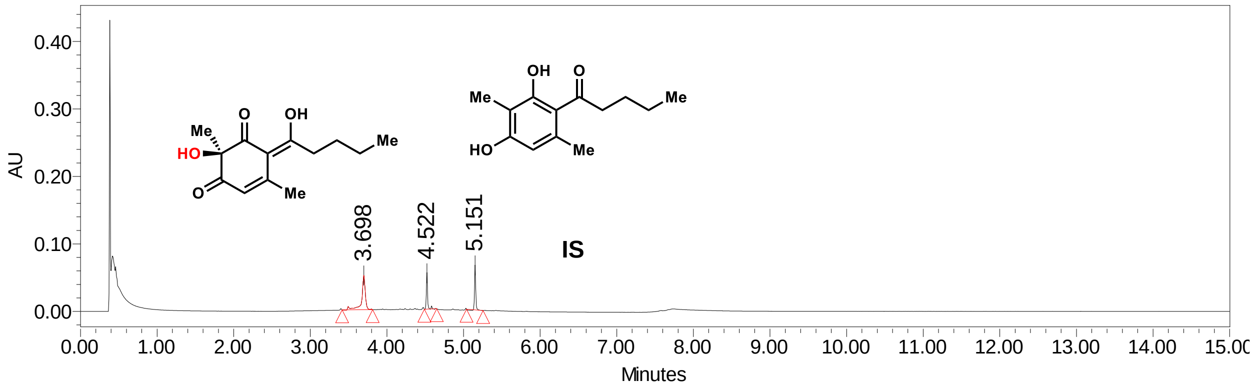

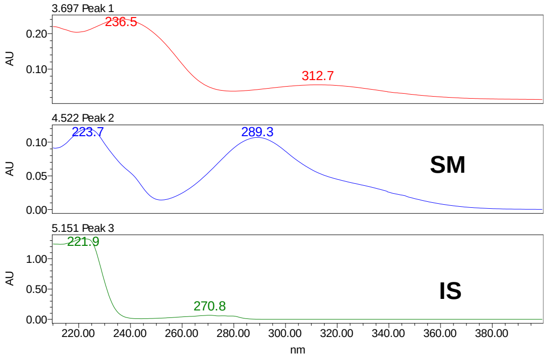

	Retention Time	Area	% Area	Height
1	3.698	166835	54.48	51045
2	4.522	61034	19.93	54287
3	5.151	78337	25.58	66344

No enzyme control

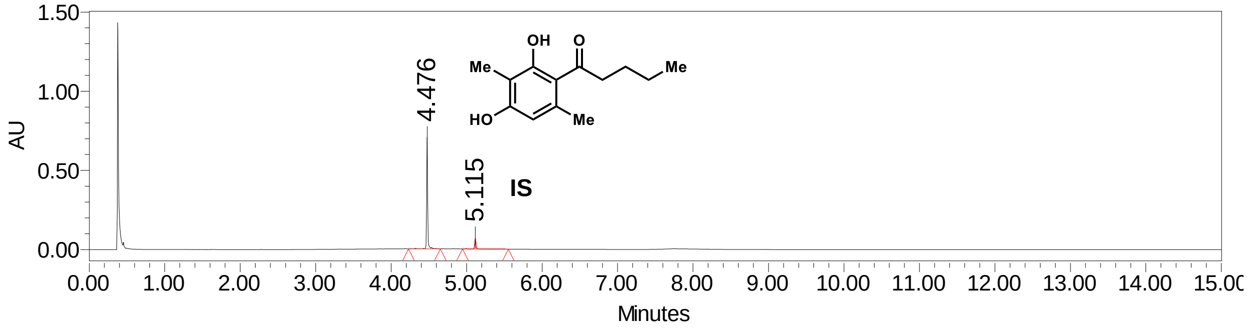

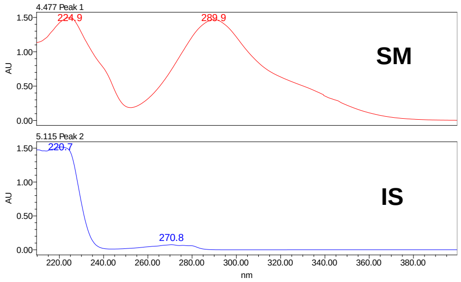

	Retention Time	Area	% Area	Height
1	4.476	669825	88.45	706595
2	5.115	87429	11.55	73777

Figure 2.19: Oxidative dearomatization of **2.22d** by TropB. PDA traces of enzymatic reaction and control reaction.

With TropB

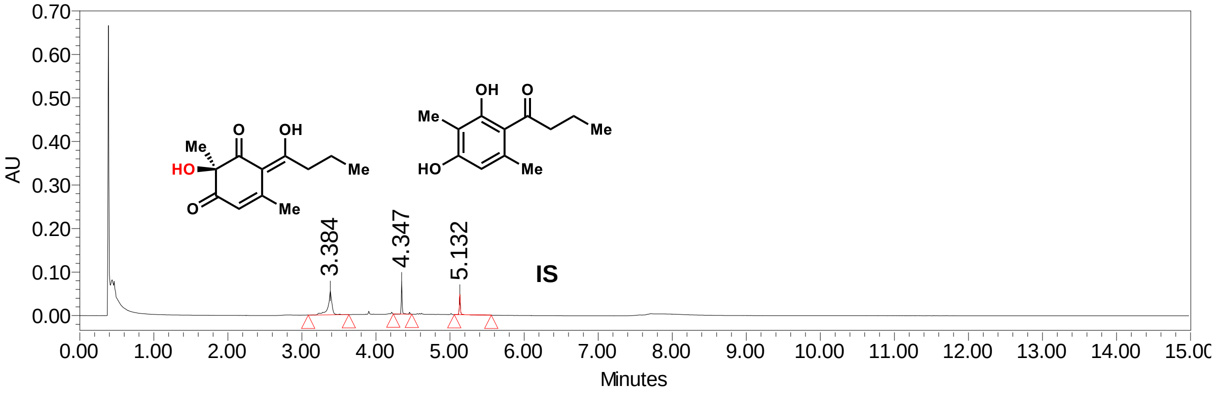

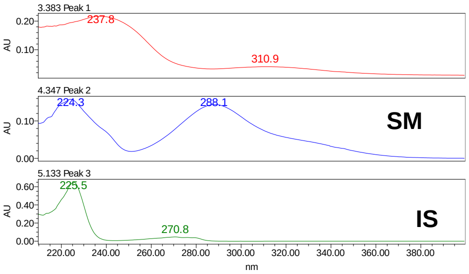

	Retention Time	Area	% Area	Height
1	3.384	204823	63.33	54734
2	4.347	66909	20.69	75822
3	5.132	51715	15.99	46843

No enzyme control

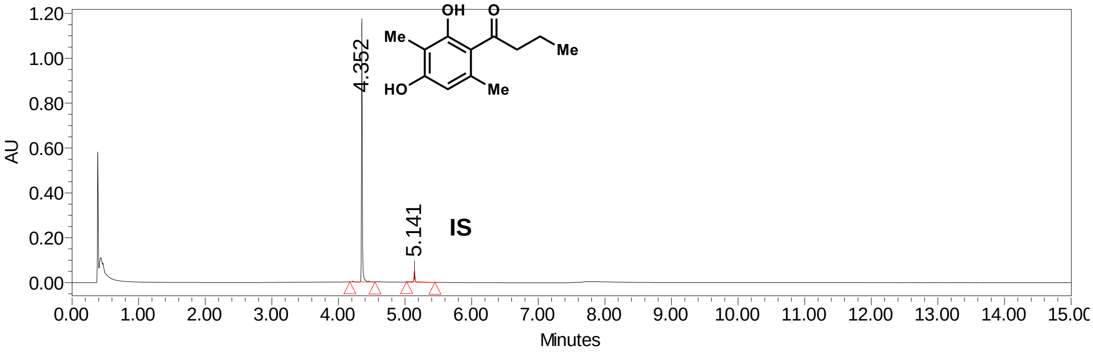

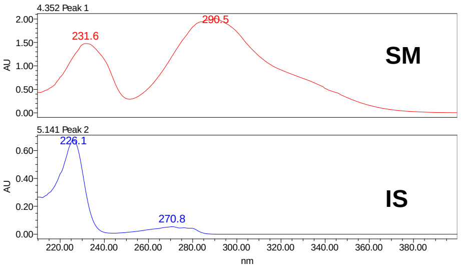

	Retention Time	Area	% Area	Height
1	3.841	539715	93.46	659310
2	5.109	37786	6.54	35891

Figure 2.20: Oxidative dearomatization of **2.22c** by TropB. PDA traces of enzymatic reaction and control reaction.

With TropB

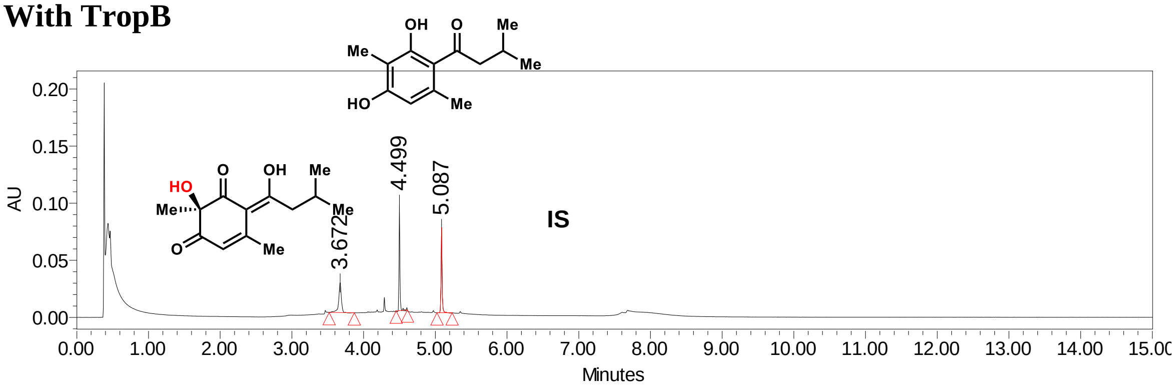

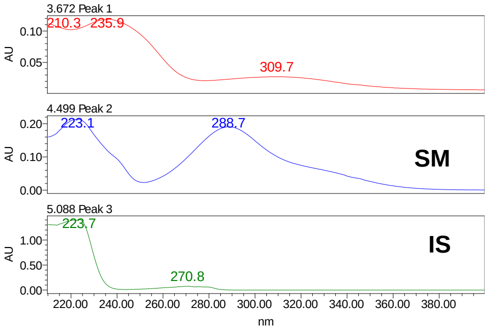

	Retention Time	Area	% Area	Height
1	3.672	83136	25.70	25063
2	4.499	148552	45.93	132589
3	5.087	91747	28.37	73036

No enzyme control

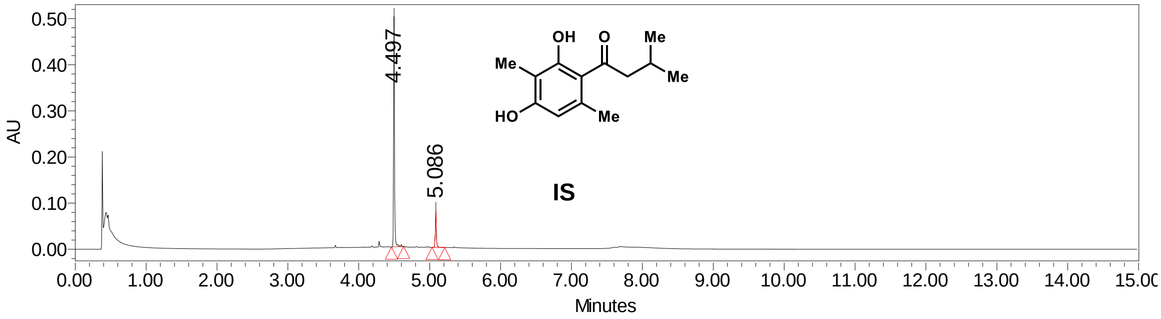

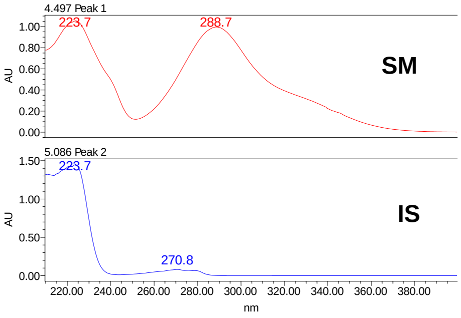

	Retention Time	Area	% Area	Height
1	4.497	237495	71.30	255312
2	5.086	95581	28.70	81318

Figure 2.21: Oxidative dearomatization of **2.22e** by TropB. PDA traces of enzymatic reaction and control reaction.

With TropB

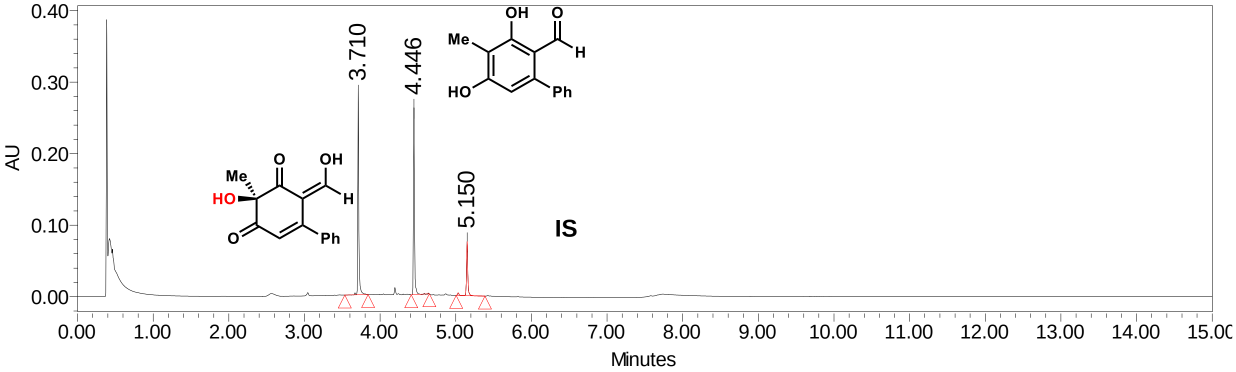

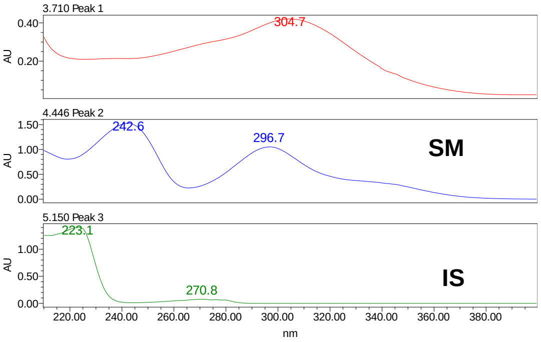

	Retention Time	Area	% Area	Height
1	3.710	270021	44.33	288410
2	4.446	247233	40.59	261165
3	5.150	91864	15.08	75650

No enzyme control

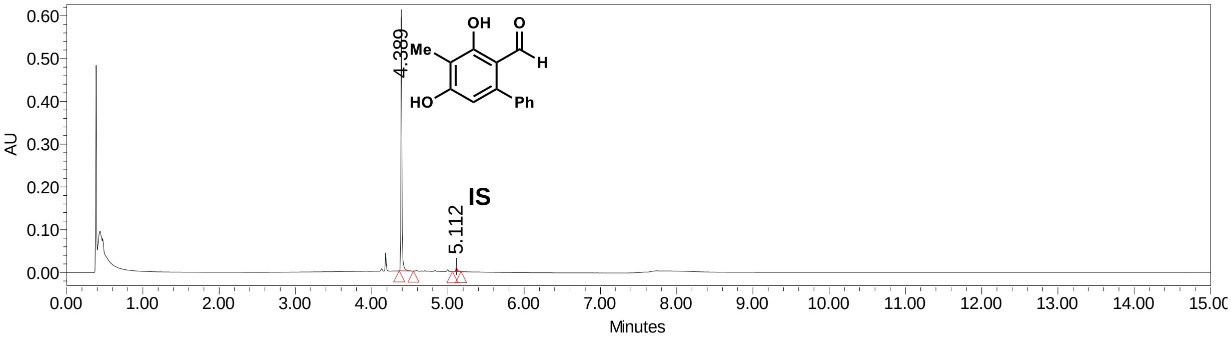

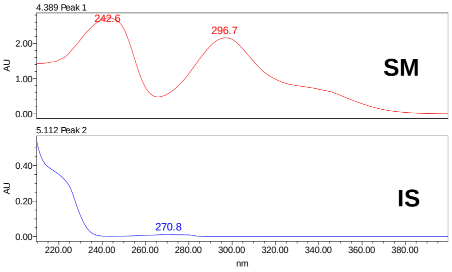

	Retention Time	Area	% Area	Height
1	4.389	527040	97.59	592278
2	5.112	13039	2.41	12346

Figure 2.22: Oxidative dearomatization of **2.53** by TropB. PDA traces of enzymatic reaction and control reaction.

With TropB

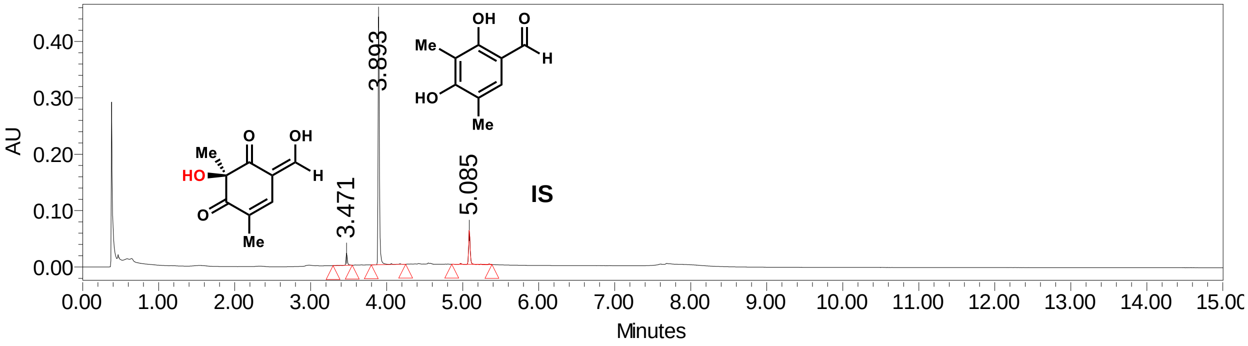

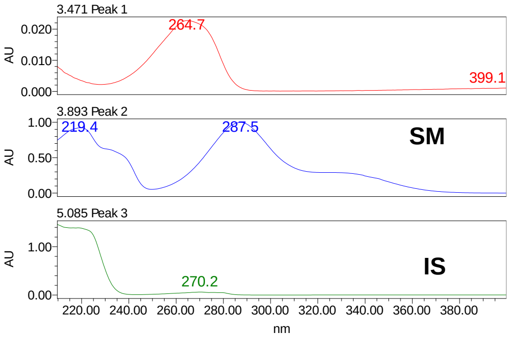

	Retention Time	Area	% Area	Height
1	3.471	28222	4.31	21589
2	3.893	536506	81.92	439714
3	5.085	90190	13.77	60686

No enzyme control

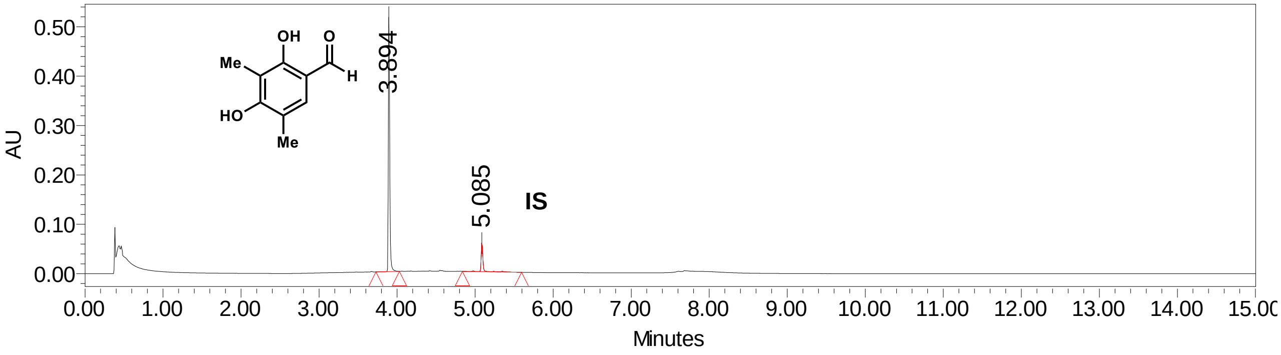

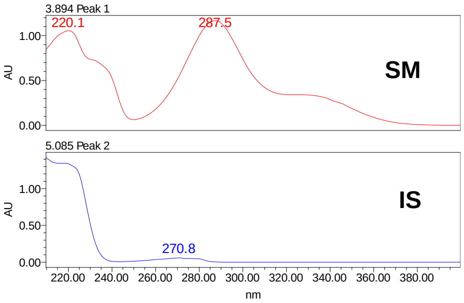

	Retention Time	Area	% Area	Height
1	3.894	638837	86.57	515355
2	5.085	99072	13.43	58303

Figure 2.23: Oxidative dearomatization of **2.58** by TropB. PDA traces of enzymatic reaction and control reaction.

With TropB

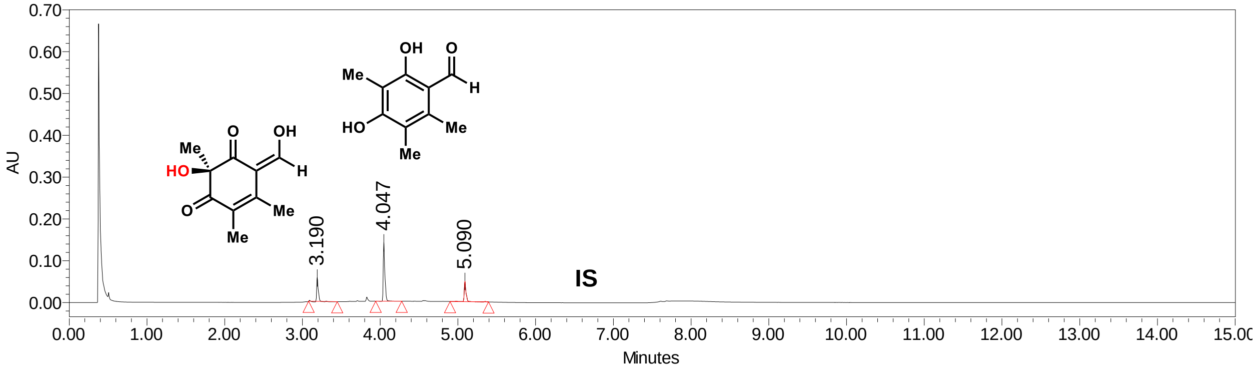

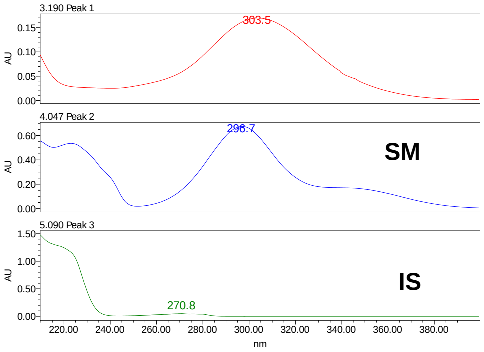

	Retention Time	Area	% Area	Height
1	3.190	89444	23.96	56539
2	4.047	204672	54.84	140734
3	5.090	79126	21.20	48989

No enzyme control

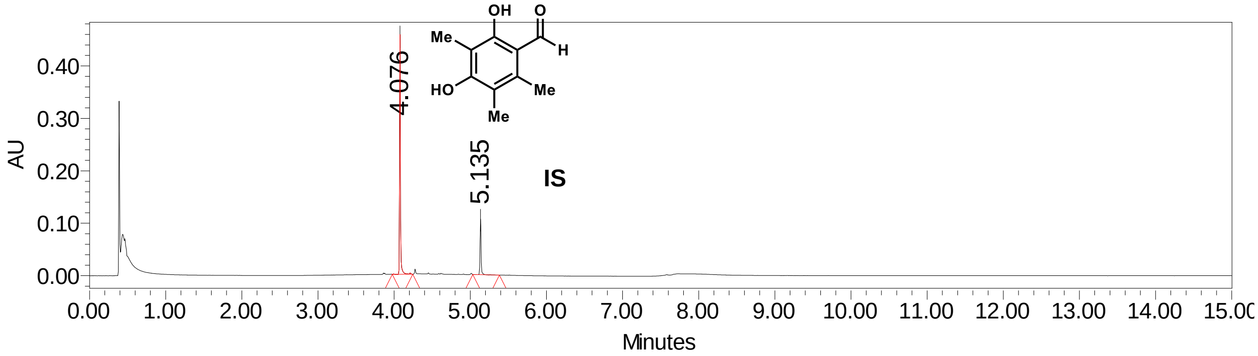

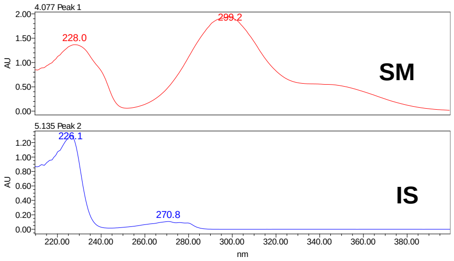

	Retention Time	Area	% Area	Height
1	4.076	367055	78.47	457278
2	5.135	100729	21.53	106230

Figure 2.24: Oxidative dearomatization of **2.59** by TropB. PDA traces of enzymatic reaction and control reaction.

With TropB

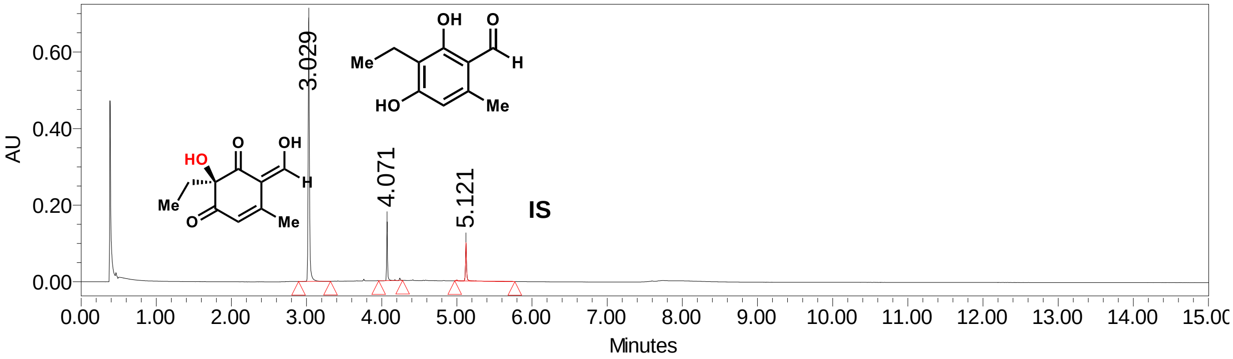

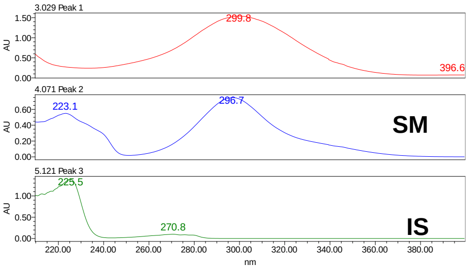

	Retention Time	Area	% Area	Height
1	3.029	841812	78.19	689175
2	4.071	129334	12.01	153712
3	5.121	105509	9.80	100119

No enzyme control

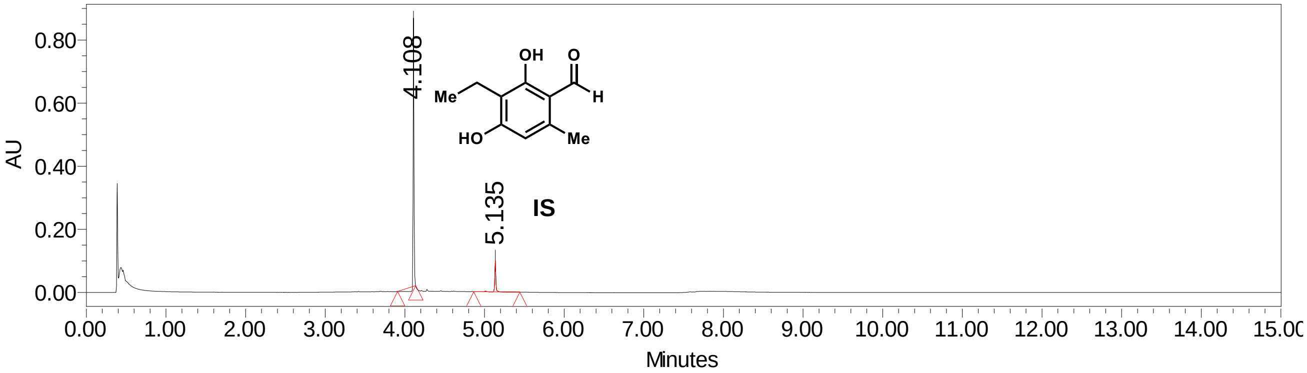

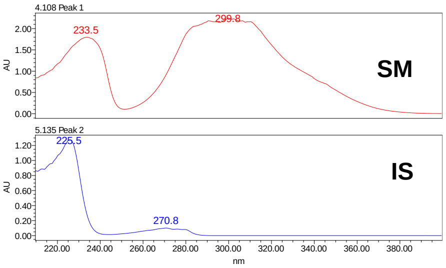

	Retention Time	Area	% Area	Height
1	4.108	703952	87.74	850433
2	5.135	98354	12.26	99761

Figure 2.25: Oxidative dearomatization of **2.47** by TropB. PDA traces of enzymatic reaction and control reaction.

With TropB

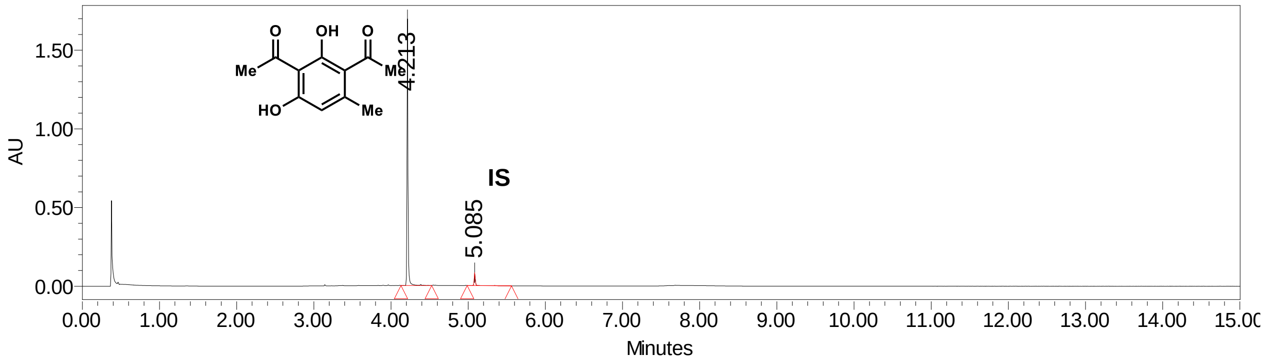

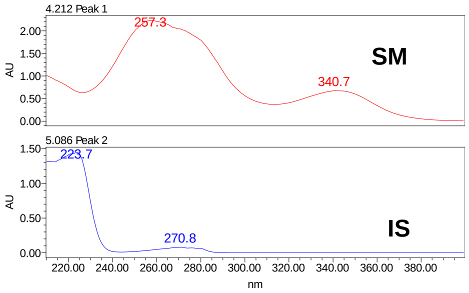

	Retention Time	Area	% Area	Height
1	4.213	1225257	92.16	1434429
2	5.085	104244	7.84	105774

No enzyme control

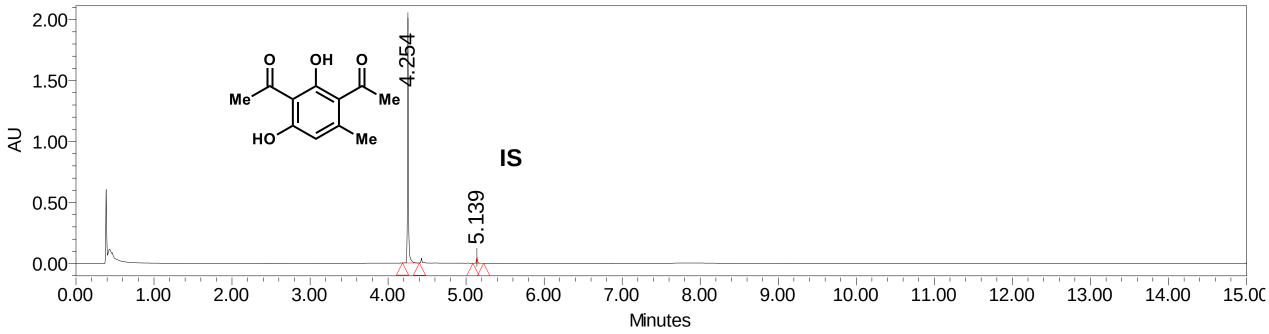

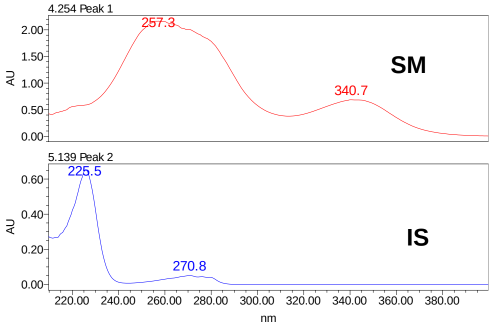

	Retention Time	Area	% Area	Height
1	4.254	1759860	97.37	2011893
2	5.139	47612	2.63	50138

Figure 2.26: Oxidative dearomatization of **2.50** by TropB. PDA traces of enzymatic reaction and control reaction.

With TropB

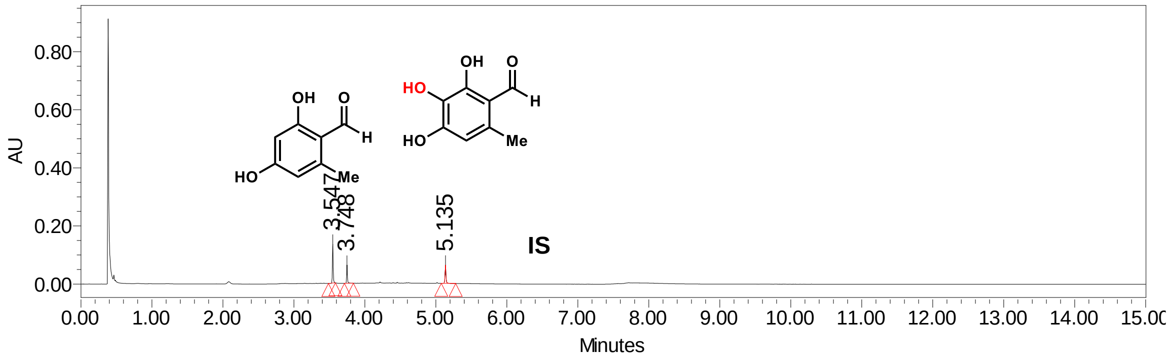

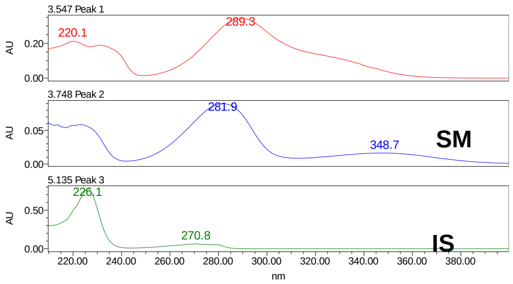

	Retention Time	Area	% Area	Height
1	3.547	90667	37.38	108949
2	3.748	40487	16.69	48434
3	5.135	111429	45.93	103871

No enzyme control

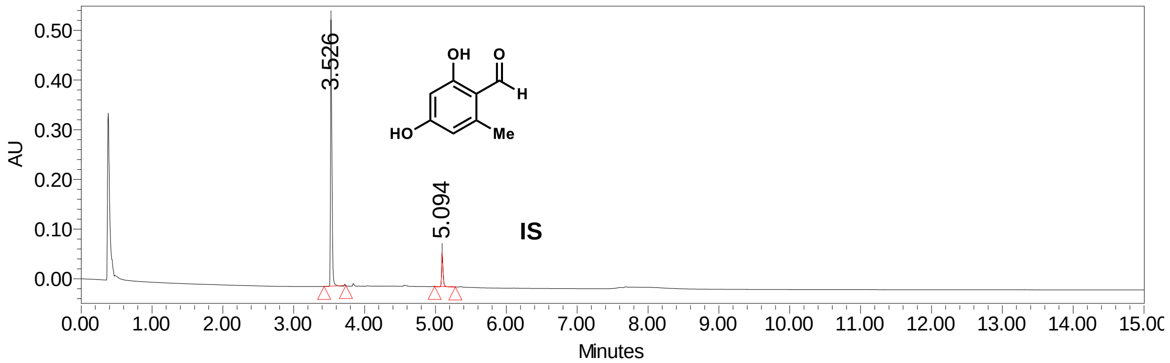

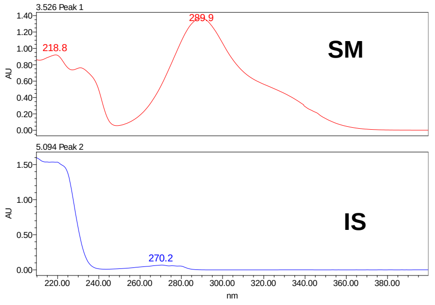

	Retention Time	Area	% Area	Height
1	3.526	700523	87.89	536023
2	5.094	96562	12.11	67674

Figure 2.27: Oxidative dearomatization of **2.61** by TropB. PDA traces of enzymatic reaction and control reaction.

With AzaH

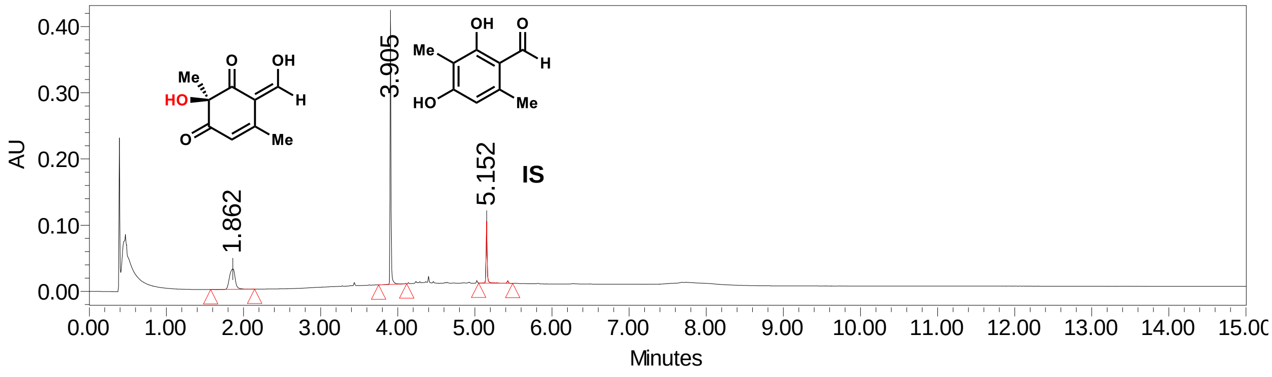

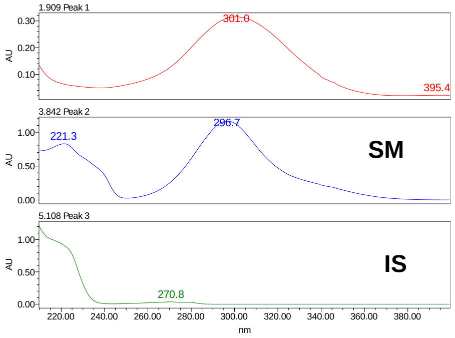

	Retention Time	Area	% Area	Height
1	1.862	159582	26.76	30989
2	3.905	333733	55.96	400936
3	5.152	103014	17.27	93779

No enzyme control

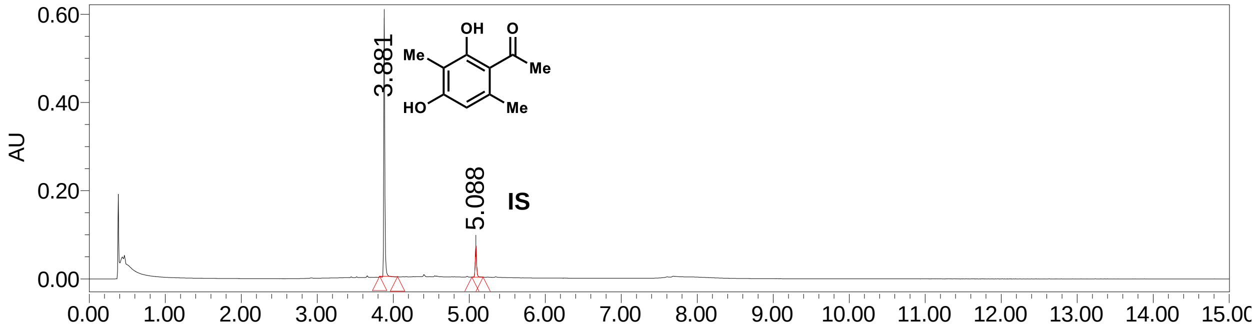

Minutes

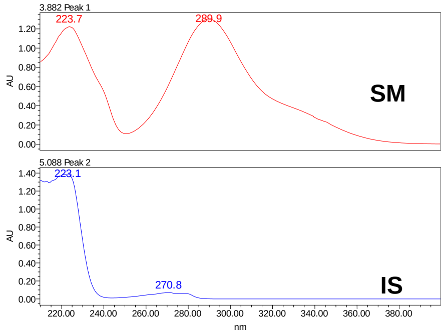

	Retention Time	Area	% Area	Height
1	3.881	596132	86.91	586097
2	5.088	89810	13.09	70938

With AzaH

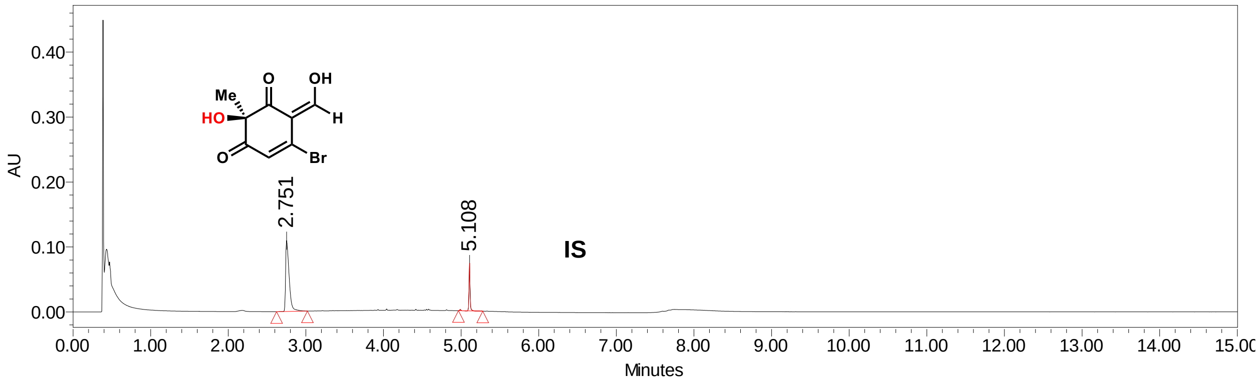

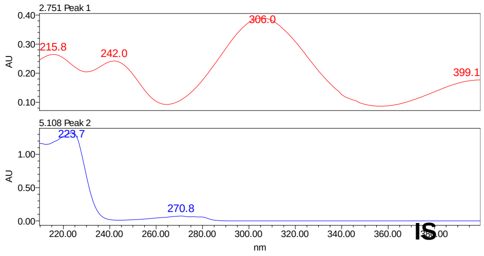

	Retention Time	Area	% Area	Height
1	2.751	340680	82.70	109193
2	5.108	71281	17.30	73345

No enzyme control

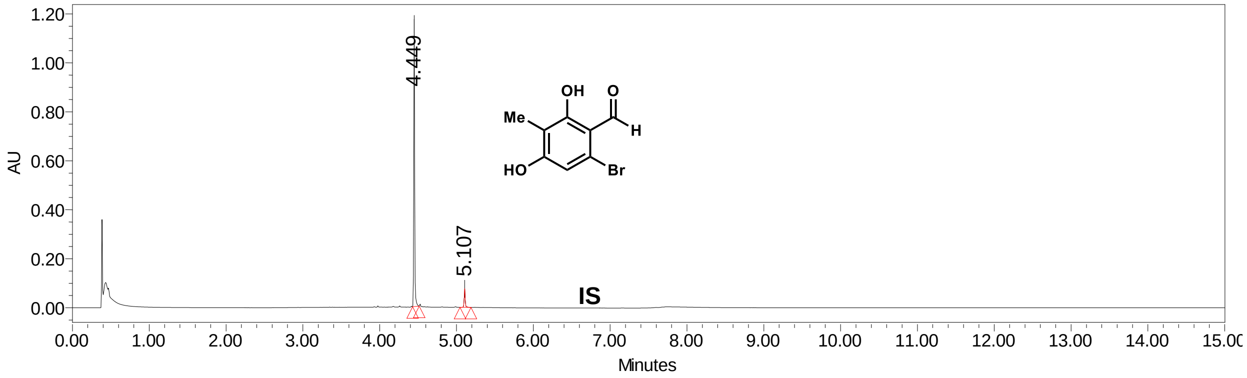

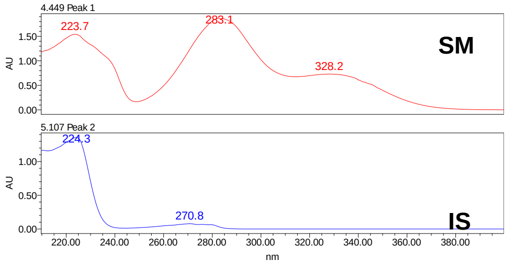

	Retention Time	Area	% Area	Height
1	4.449	925130	92.77	1175806
2	5.107	72062	7.23	76922

Figure 2.29: Oxidative dearomatization of **2.55** by TropB. PDA traces of enzymatic reaction and control reaction.

With AzaH

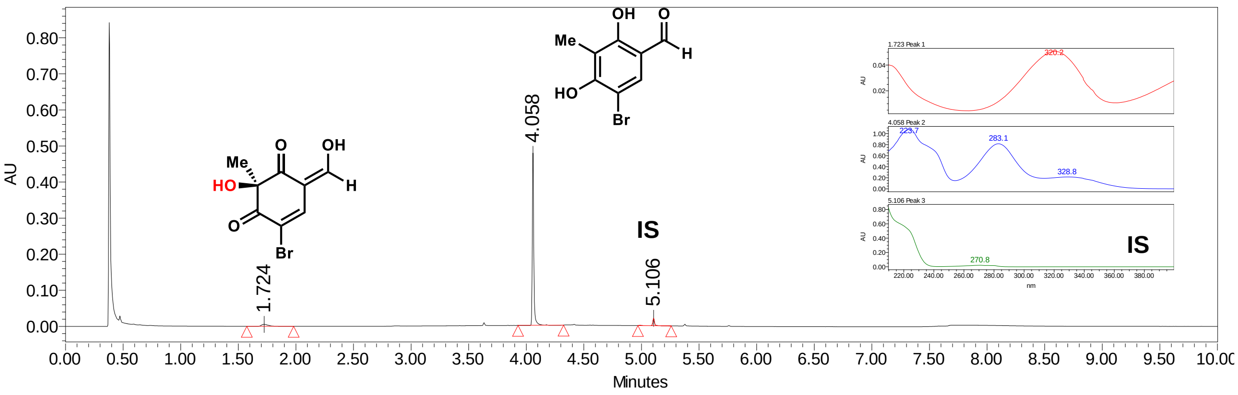

The product of the AzaH reaction (rt = 1.724 min) absorbs weakly at 270 nm but can be seen clearly at 300 nm.

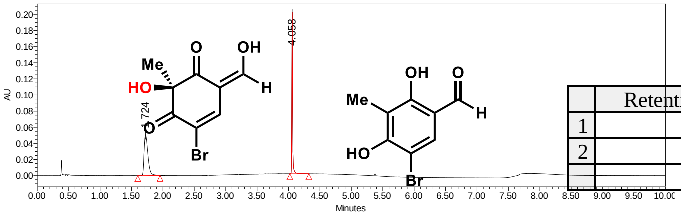

	Retention Time	Area	% Area	Height
1	1.724	35678		43654
2	4.087	387692	79.63	467090
	5.128	99150	20.37	97478

No enzyme control

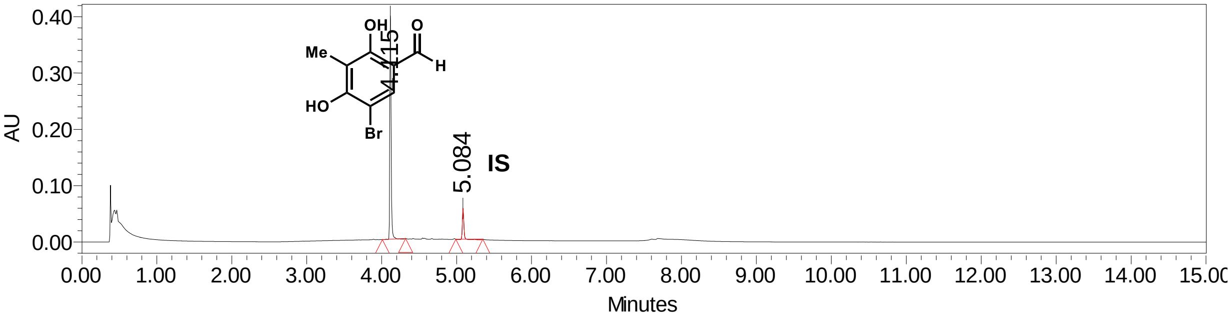

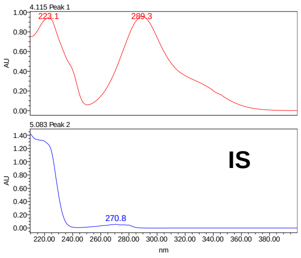

	Retention Time	Area	% Area	Height
1	4.115	484839	85.17	396843
2	5.084	84395	14.83	54993

With AzaH

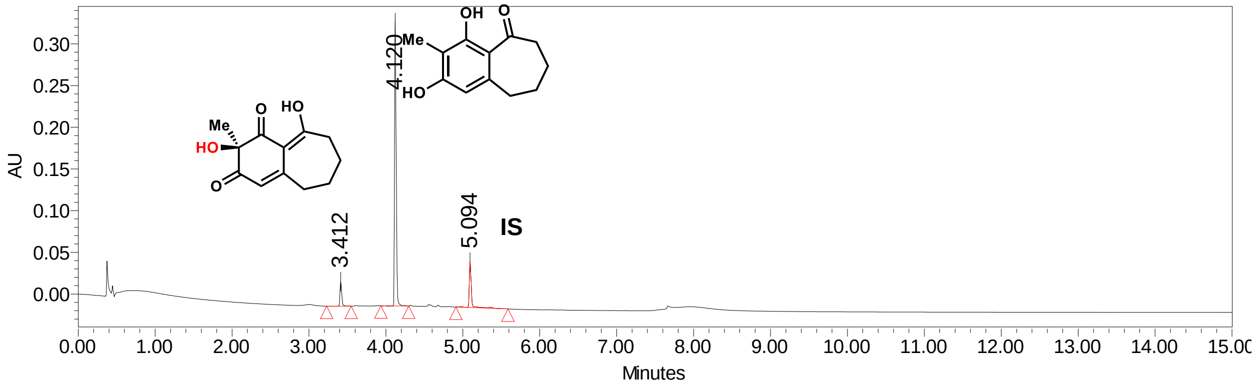

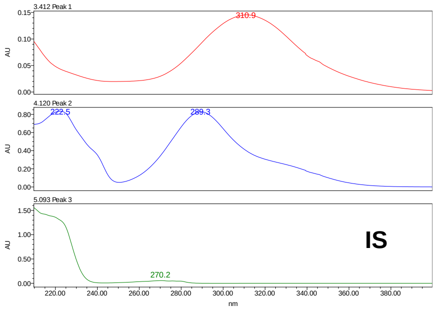

	Retention Time	Area	% Area	Height
1	3.412	47614	7.15	29718
2	4.120	511990	76.92	341787
3	5.094	105983	15.92	54970

No enzyme control

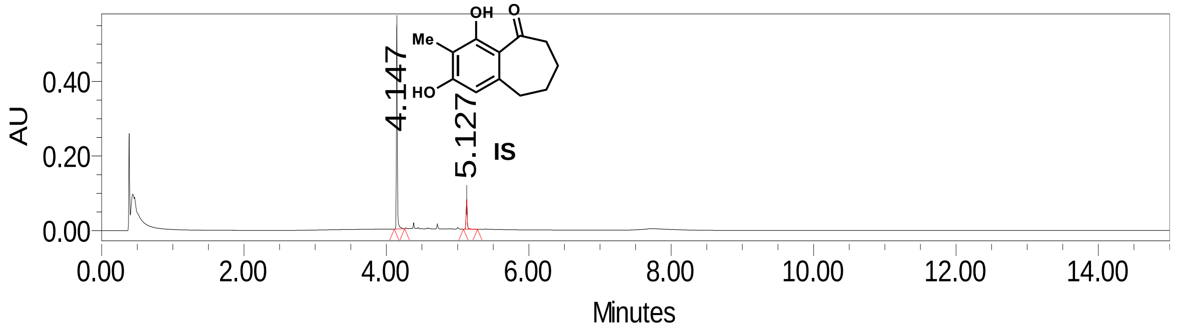

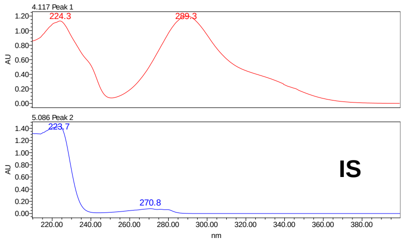

	Retention Time	Area	% Area	Height
1	4.117	429008	84.07	500038
2	5.086	81283	15.93	78207

Figure 2.31: Oxidative dearomatization of **2.43** by TropB. PDA traces of enzymatic reaction and control reaction.

With AzaH

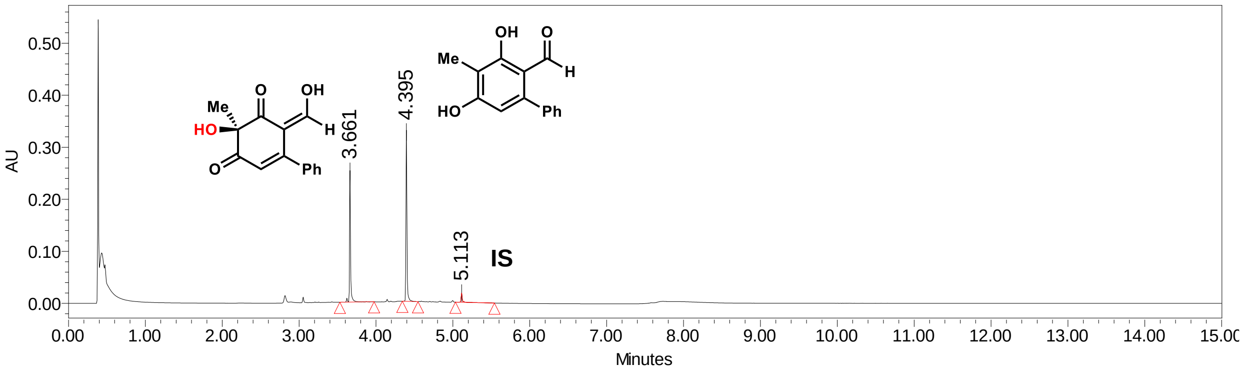

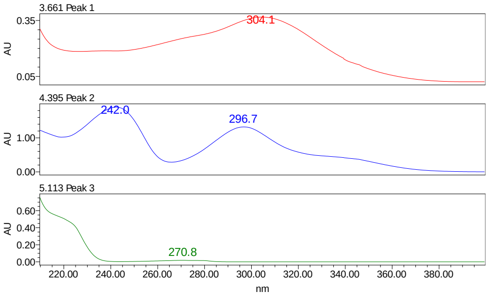

	Retention Time	Area	% Area	Height
1	3.661	217106	39.80	254795
2	4.395	308640	56.58	349462
3	5.113	19743	3.62	18314

No enzyme control

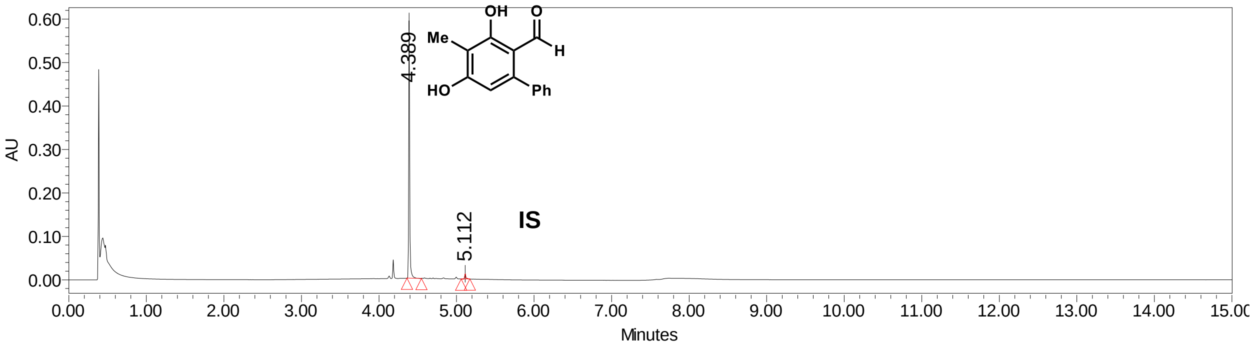

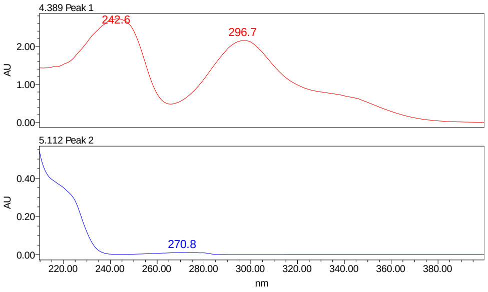

	Retention Time	Area	% Area	Height
1	4.389	527040	97.59	592278
2	5.112	13039	2.41	12346

Figure 2.32: Oxidative dearomatization of **2.53** by TropB. PDA traces of enzymatic reaction and control reaction.

With AzaH

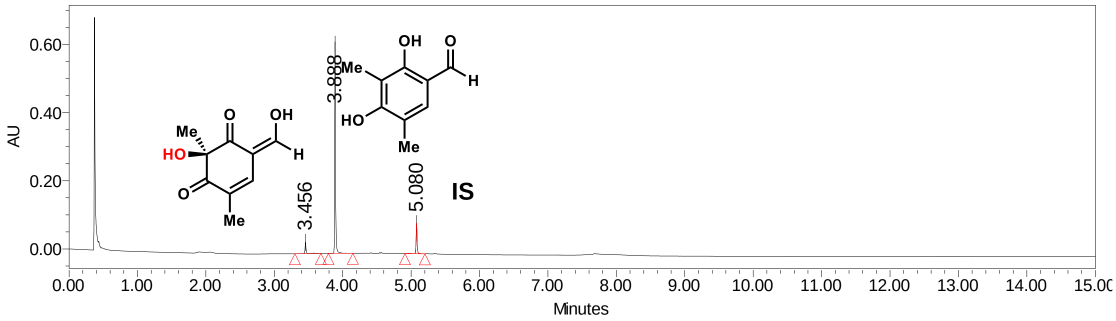

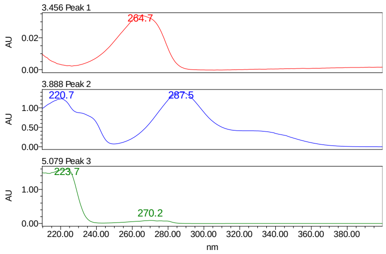

	Retention Time	Area	% Area	Height
1	3.456	36206	5.68	32252
2	3.888	513051	80.43	620848
3	5.080	88600	13.89	89590

No enzyme control

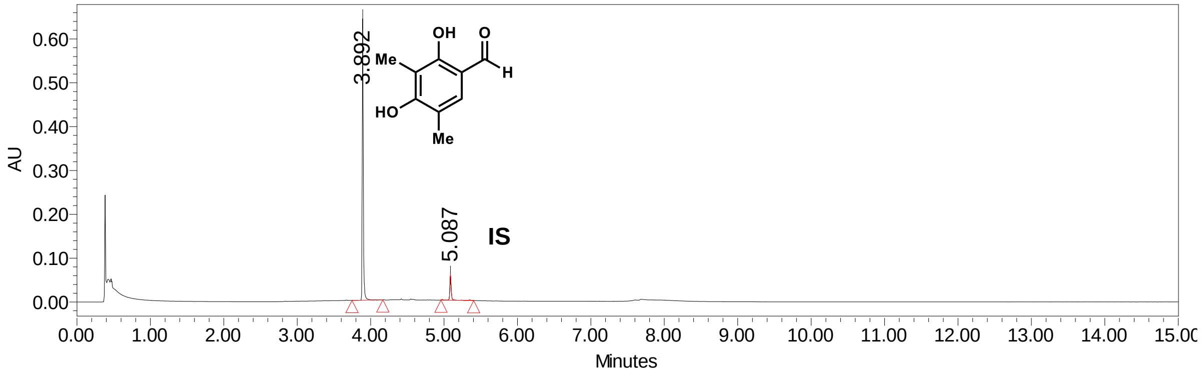

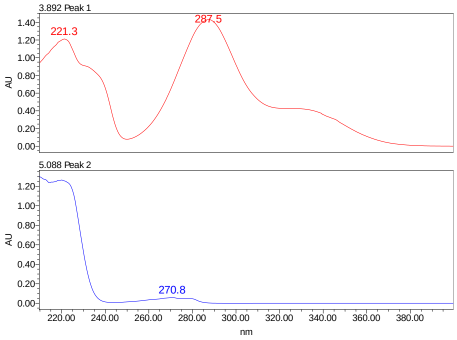

	Retention Time	Area	% Area	Height
1	3.892	678875	89.78	641975
2	5.087	77288	10.22	57379

Figure 2.33: Oxidative dearomatization of **2.58** by AzaH. PDA traces of enzymatic reaction and control reaction.

With AzaH

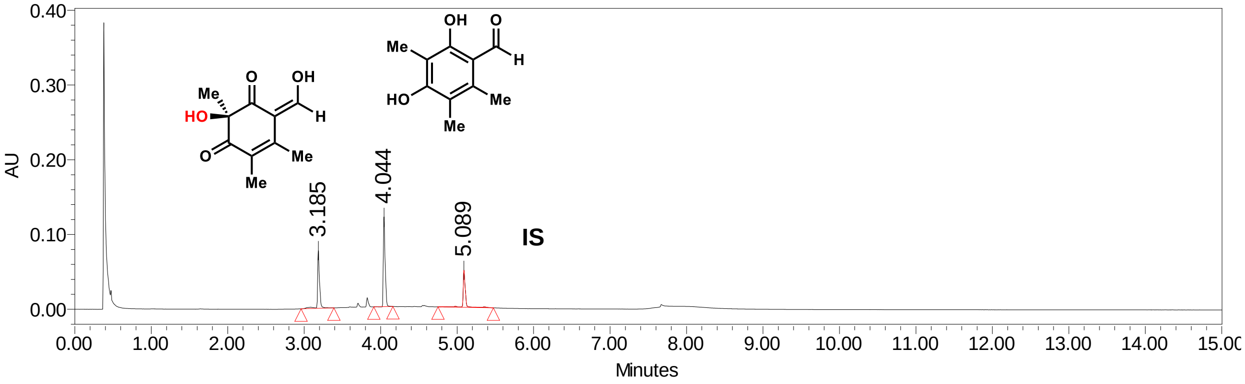

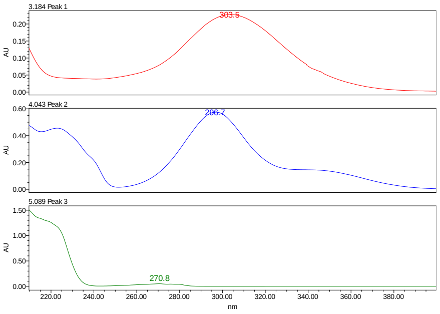

	Retention Time	Area	% Area	Height
1	3.185	142178	32.27	77677
2	4.044	198204	44.99	120265
3	5.089	100184	22.74	49523

No enzyme control

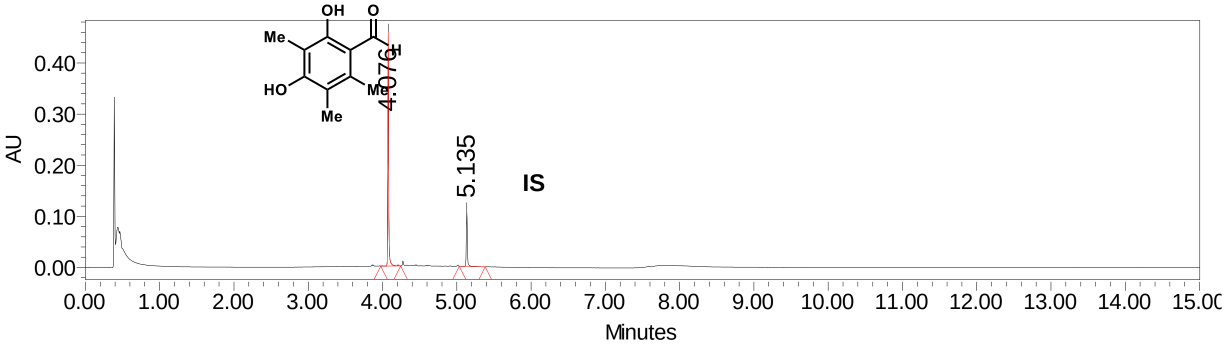

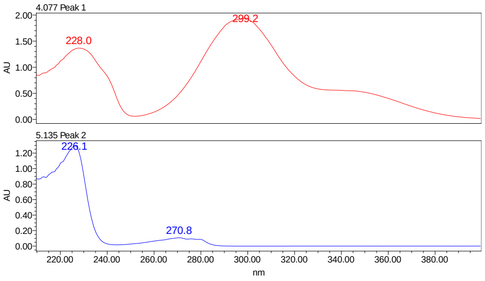

	Retention Time	Area	% Area	Height
1	4.076	367055	78.47	457278
2	5.135	100729	21.53	106230

Figure 2.34: Oxidative dearomatization of **2.59** by AzaH. PDA traces of enzymatic reaction and control reaction.

With AzaH

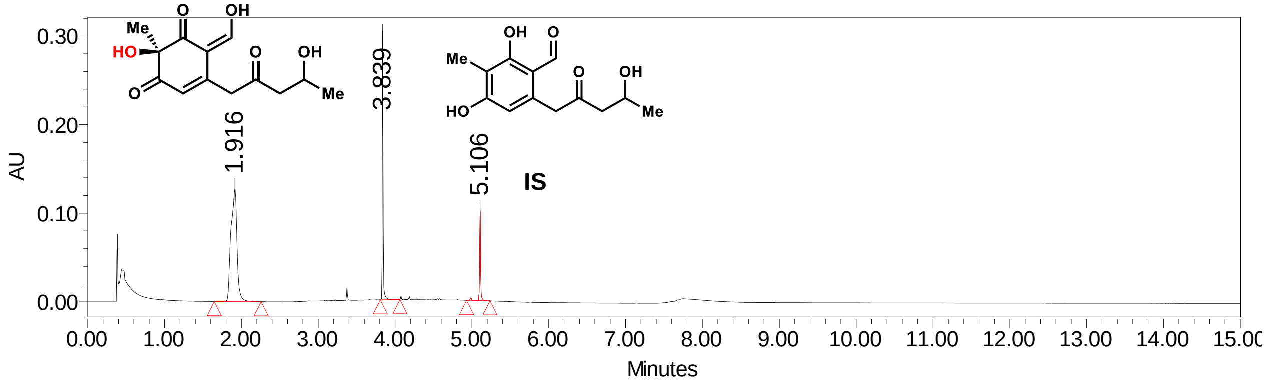

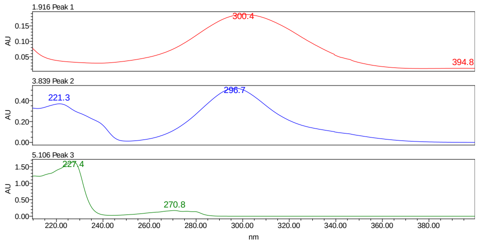

	Retention Time	Area	% Area	Height
1	1.916	691128	68.43	127188
2	3.839	221794	21.96	303367
3	5.106	97016	9.61	102058

No enzyme control

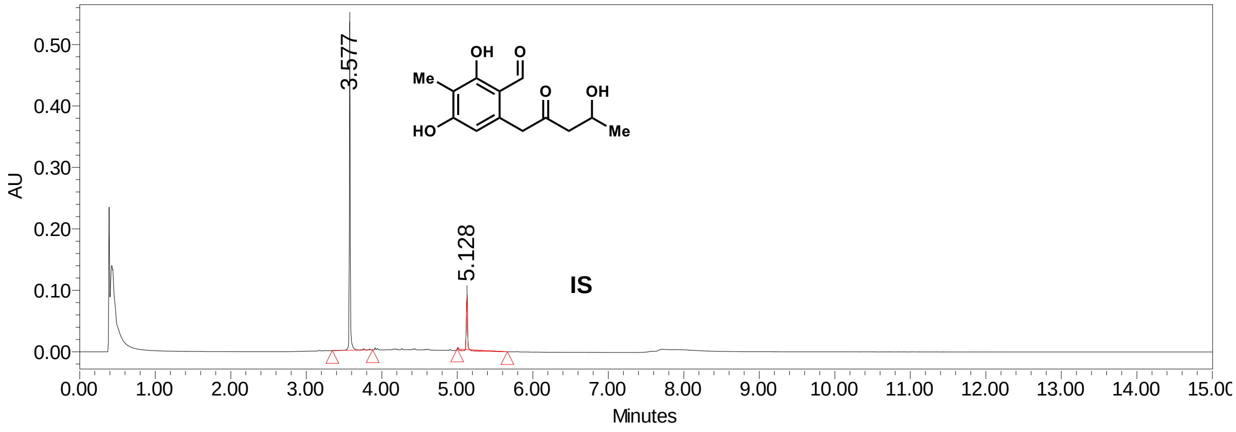

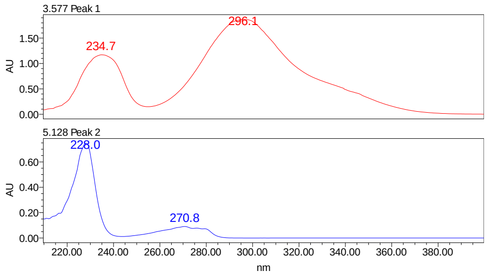

	Retention Time	Area	% Area	Height
1	3.577	446940	81.21	535164
2	5.128	103350	18.78	89796

Figure 2.35: Oxidative dearomatization of **17** (**2.18**) by AzaH. PDA traces of enzymatic reaction and control reaction.

With AzaH

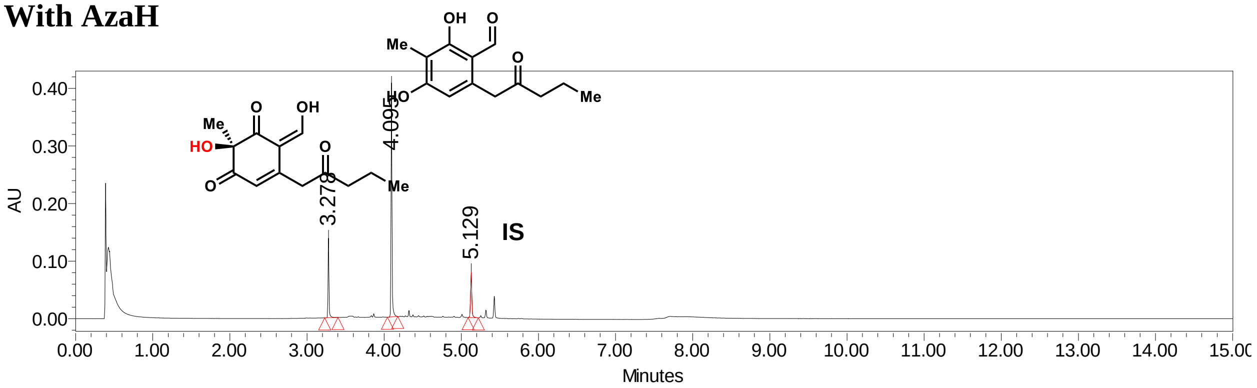

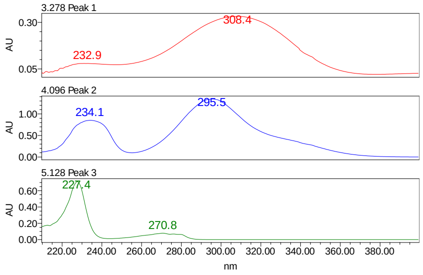

	Retention Time	Area	% Area	Height
1	3.278	112683	20.08	138423
2	4.095	356300	63.50	406913
3	5.129	92110	16.42	78498

No enzyme control

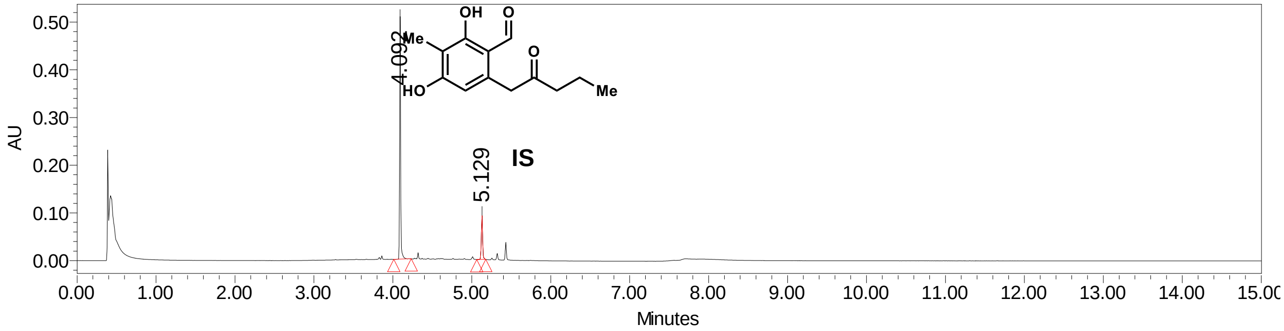

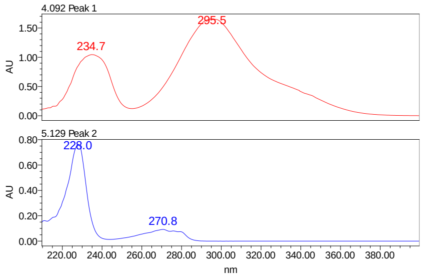

	Retention Time	Area	% Area	Height
1	4.092	441680	80.91	508946
2	5.129	104212	19.09	91868

With AzaH

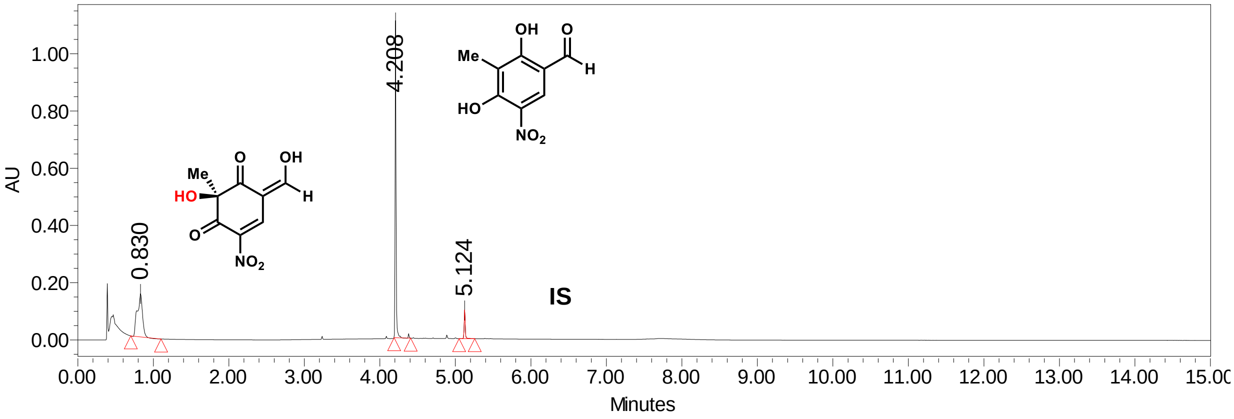

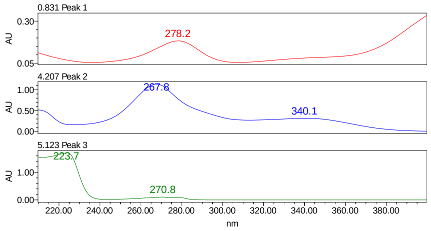

	Retention Time	Area	% Area	Height
1	0.830	731105	40.71	150972
2	4.208	966490	53.81	1108286
3	5.124	98423	5.48	100786

No enzyme control

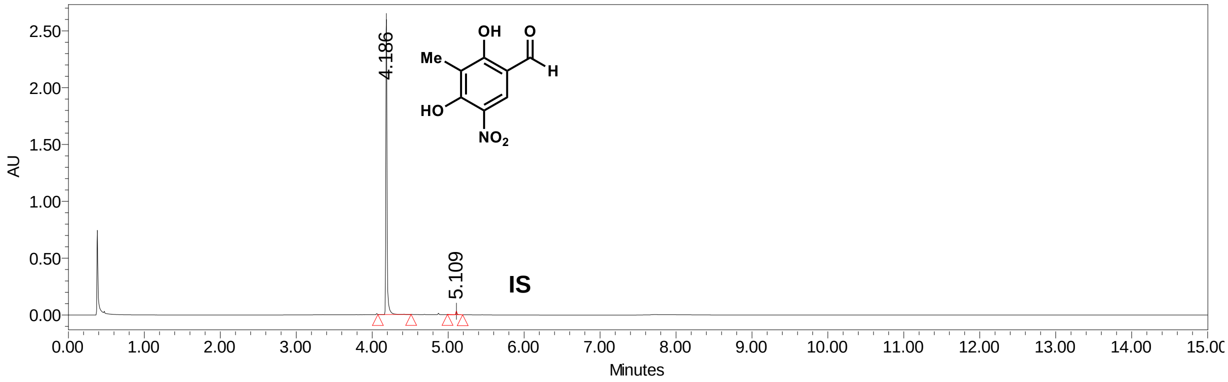

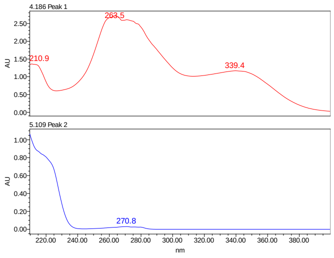

	Retention Time	Area	% Area	Height
1	4.182	2422938	96.79	2515618
2	5.106	80257	3.21	83005

Figure 2.37: Oxidative dearomatization of **17** (**2.63**) by AzaH. PDA traces of enzymatic reaction and control reaction.

With AzaH

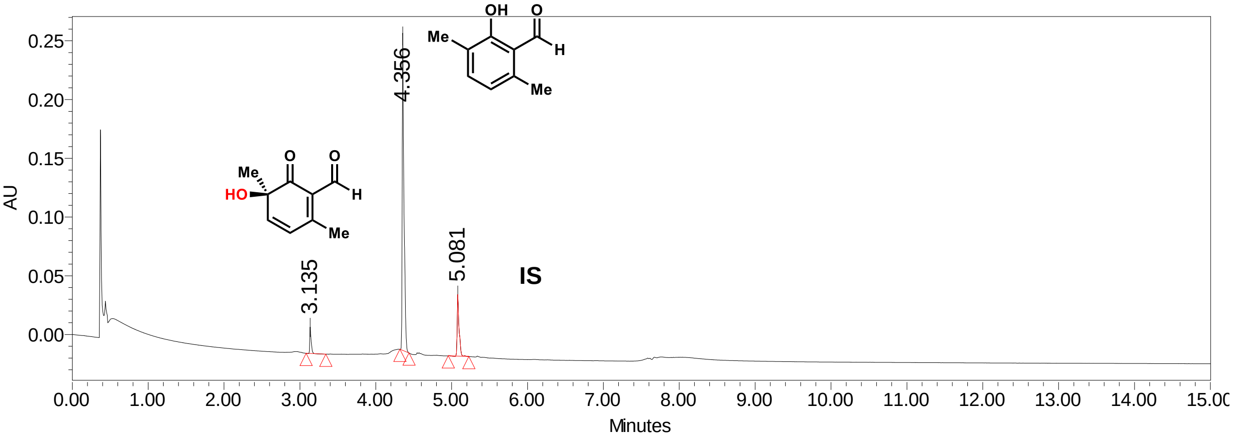

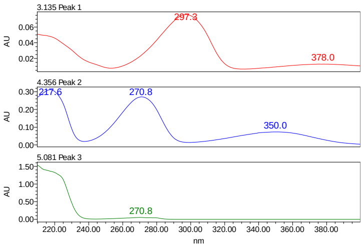

	Retention Time	Area	% Area	Height
1	3.135	28843	5.24	22549
2	4.356	430957	78.35	270100
3	5.081	90268	16.41	52523

No enzyme control

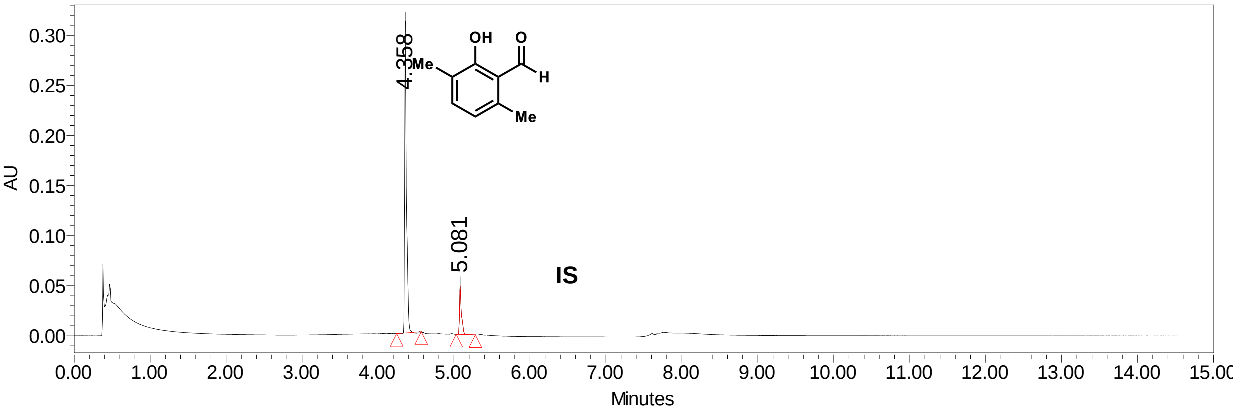

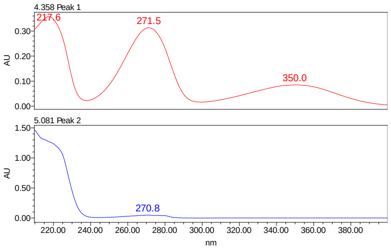

	Retention Time	Area	% Area	Height
1	4.358	508333	85.80	311590
2	5.081	84161	14.20	48366

Figure 2.38: Oxidative dearomatization of **2.64** by AzaH. PDA traces of enzymatic reaction and control reaction.

With AzaH

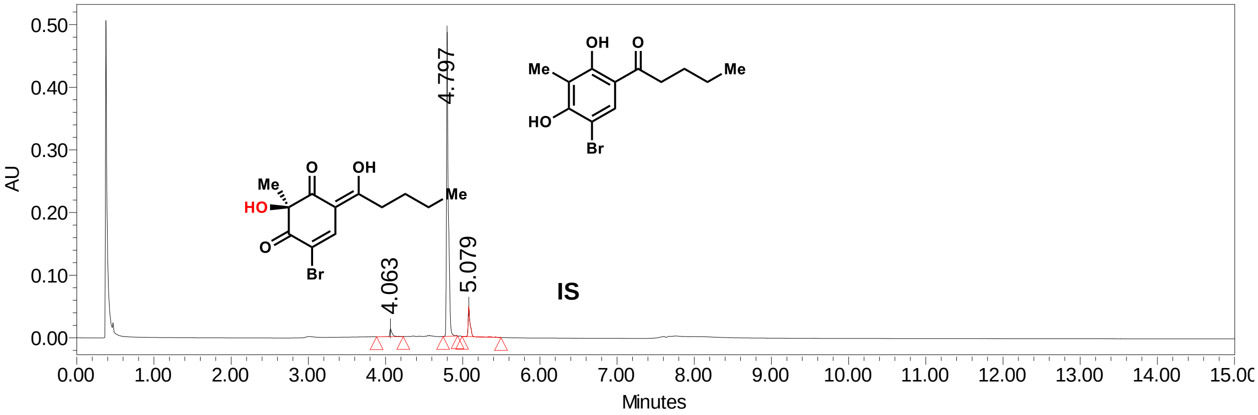

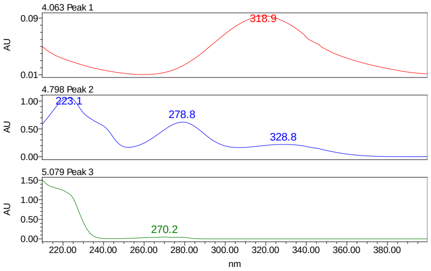

	Retention Time	Area	% Area	Height
1	4.063	26667	2.99	13325
2	4.797	779733	87.42	485933
3	5.079	85564	9.59	48080

No enzyme control

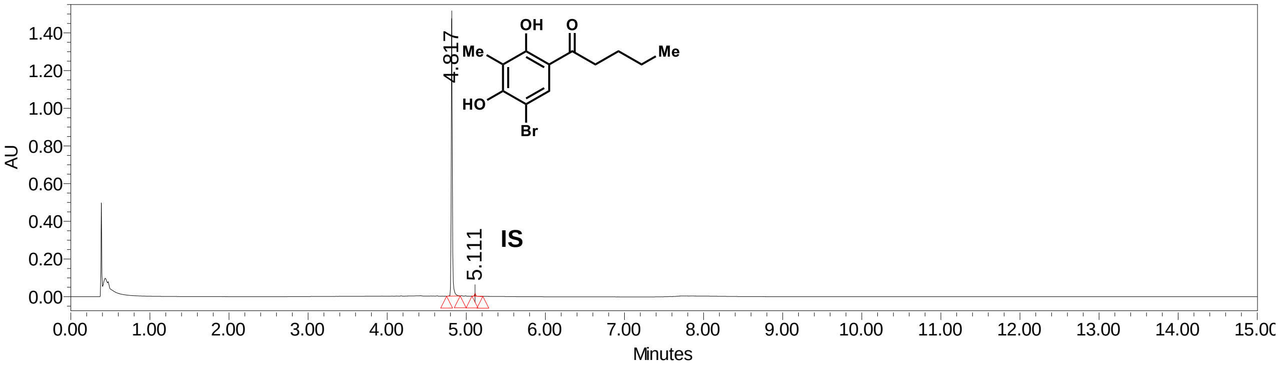

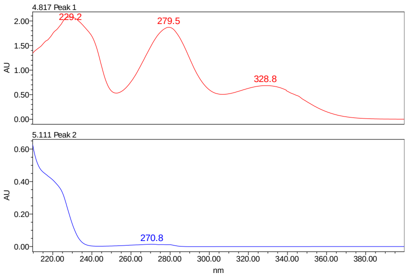

	Retention Time	Area	% Area	Height
1	4.832	1030970	91.78	1079052
2	5.126	92373	8.22	87104

Figure 2.39: Oxidative dearomatization of **2.57** by AzaH. PDA traces of enzymatic reaction and control reaction.

With AzaH

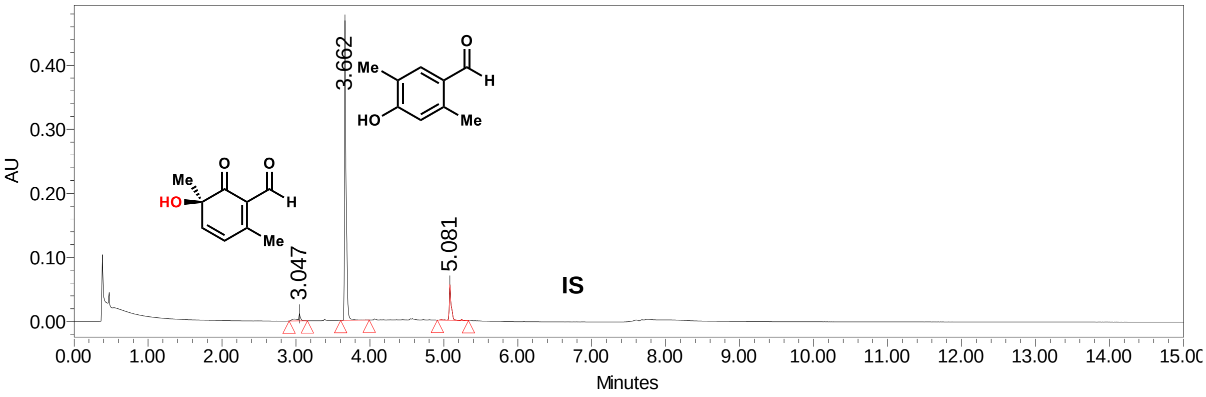

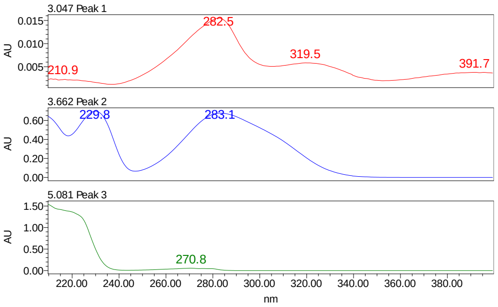

	Retention Time	Area	% Area	Height
1	3.047	30565	3.72	11190
2	3.662	689187	83.94	468888
3	5.081	101288	12.34	55561

No enzyme control

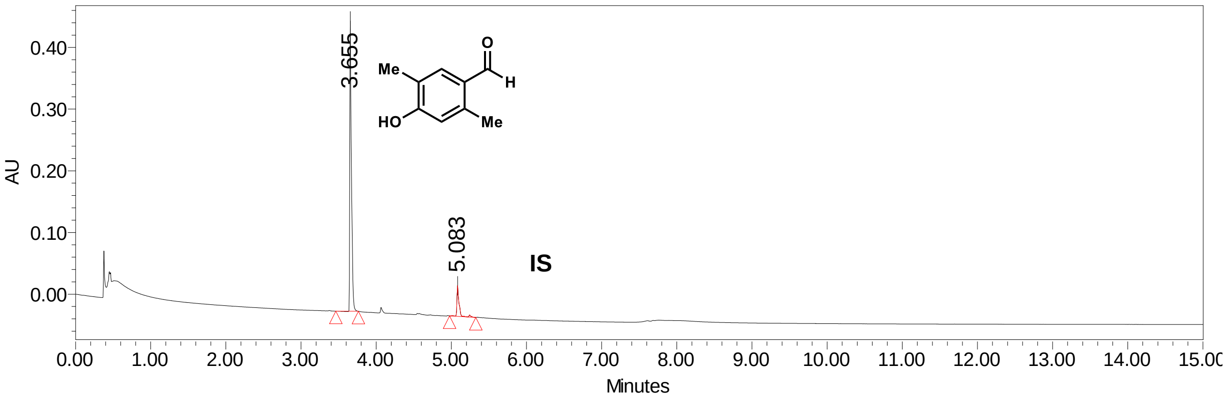

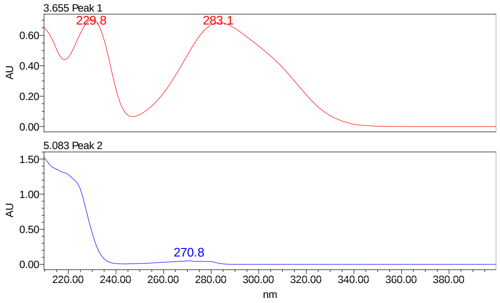

	Retention Time	Area	% Area	Height
1	3.655	711564	88.14	470658
2	5.083	95753	11.86	49802

With AzaH

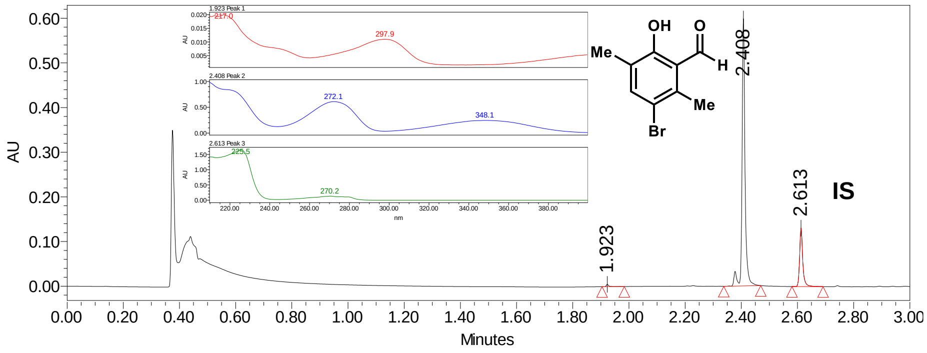

	Retention Time	Area	% Area	Height
1	1.923	3085	0.56	5193
2	2.408	447438	80.97	597906
3	2.613	102101	18.48	131261

The product of the AzaH reaction (rt = 1.923 min) absorbs weakly at 270 nm but can be visualized at 300 nm.

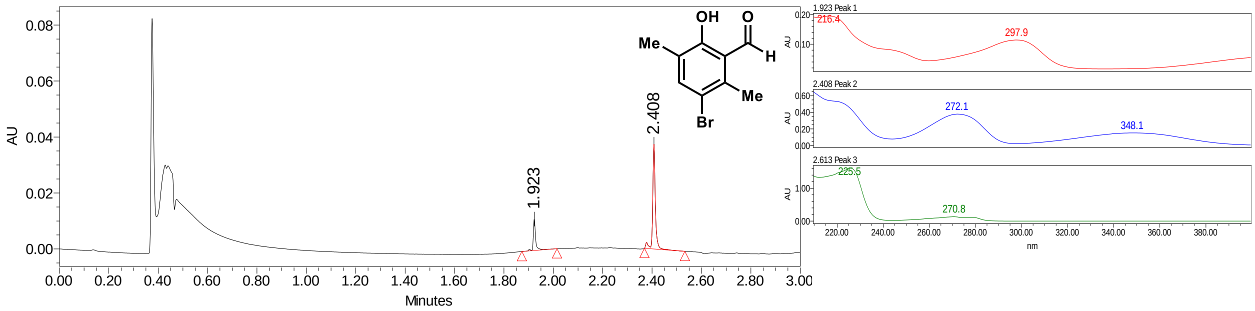

	Retention Time	Area	% Area	Height
1	1.923	7249	20.46	11308
2	2.408	28184	79.54	37395

No enzyme control

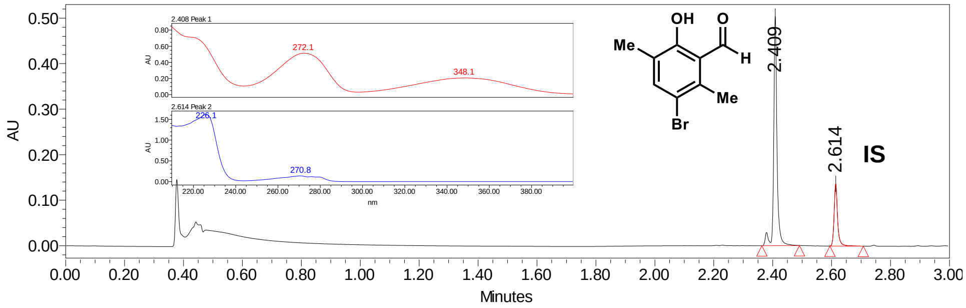

	Retention Time	Area	% Area	Height
1	2.409	395329	77.95	505198
2	2.614	111829	22.05	137119

Figure 2.41: Oxidative dearomatization of **2.72** by AzaH. PDA traces of enzymatic reaction and control reaction analyzed using UPLC Method B.

With AzaH

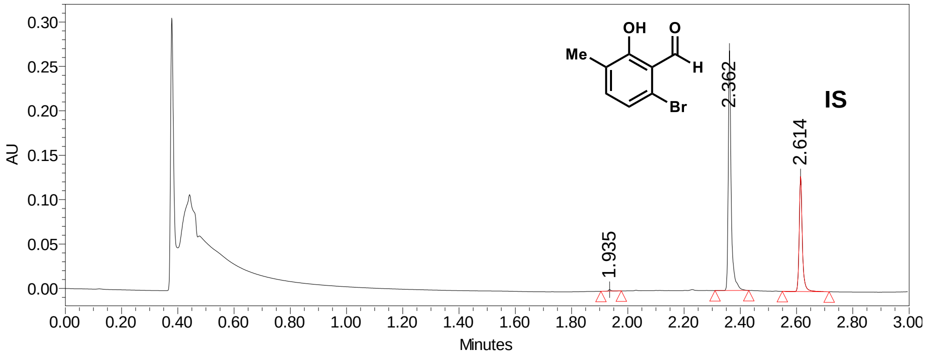

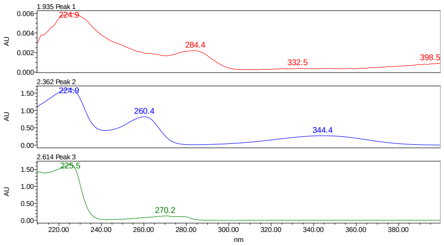

	Retention Time	Area	% Area	Height
1	1.935	1078	0.36	1675
2	2.362	193428	65.42	270165
3	2.614	101186	34.22	129354

No enzyme control

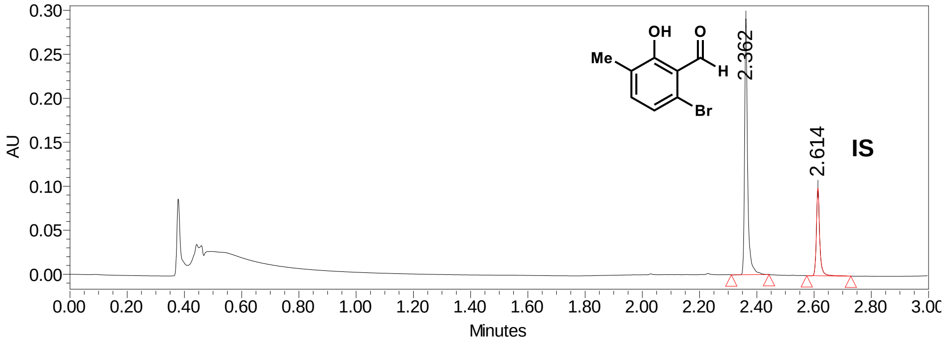

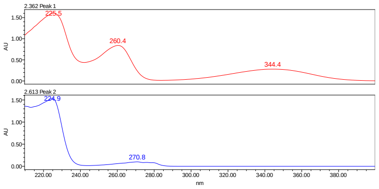

	Retention Time	Area	% Area	Height
1	2.362	213306	72.72	291165
2	2.614	80009	27.28	99226

Figure 2.42: Oxidative dearomatization of **2.73** by AzaH. PDA traces of enzymatic reaction and control reaction analyzed using UPLC Method B.

With AzaH

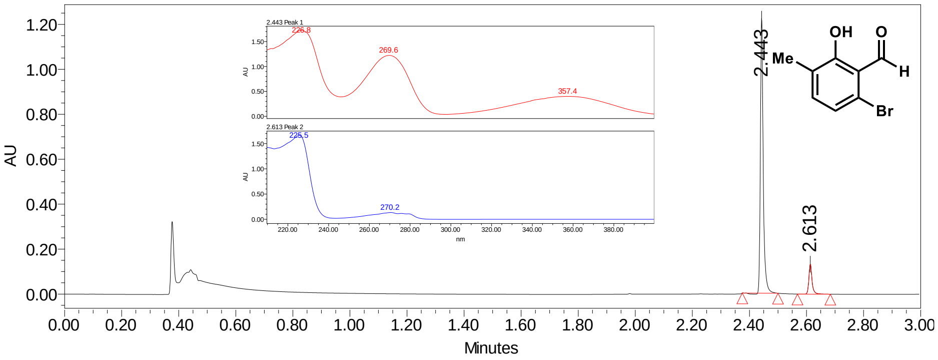

The product of the AzaH reaction (rt = 1.960 min) absorbs weakly at 270 nm but can be visualized at 300 nm.

	Retention Time	Area	% Area	Height
1	2.443	860640	89.29	1223636
2	2.613	103236	10.71	133581

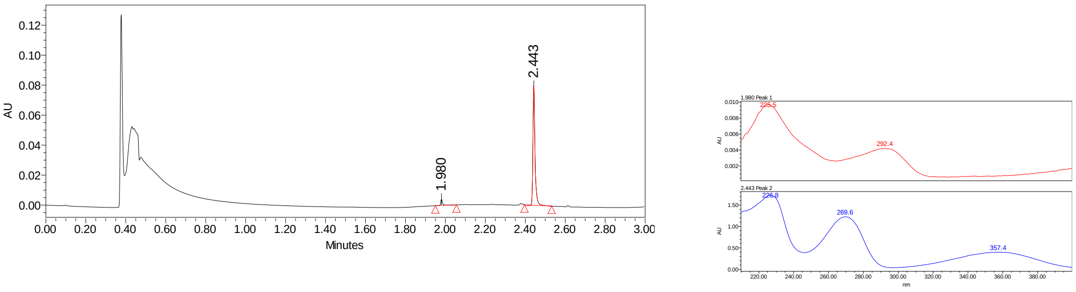

No enzyme control

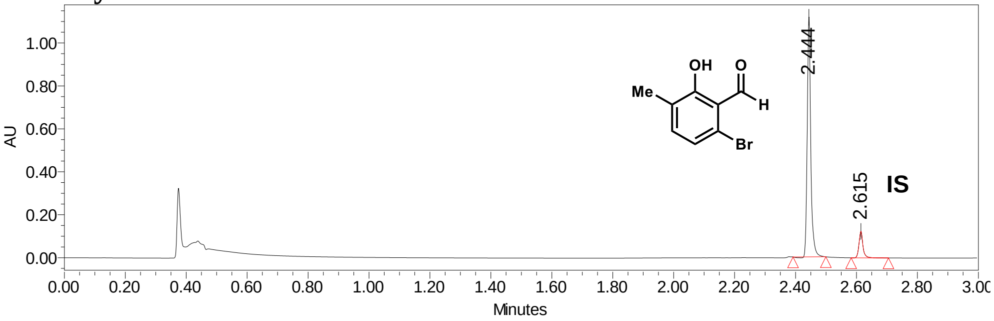

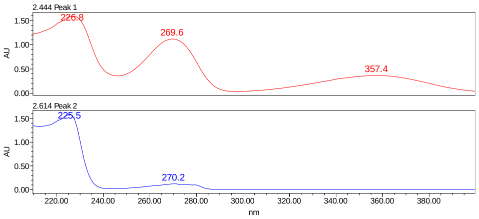

	Retention Time	Area	% Area	Height
1	2.444	911364	89.04	1119379
2	2.615	112213	10.96	123376

Figure 2.43: Oxidative dearomatization of **2.74** by AzaH. PDA traces of enzymatic reaction and control reaction analyzed using UPLC Method B. Note that 25 μM enzyme was used to visualize product formation.

With AzaH

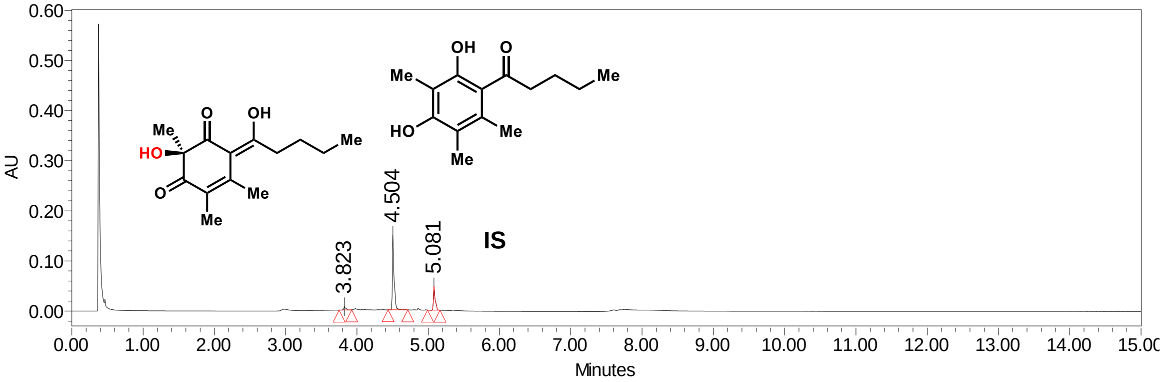

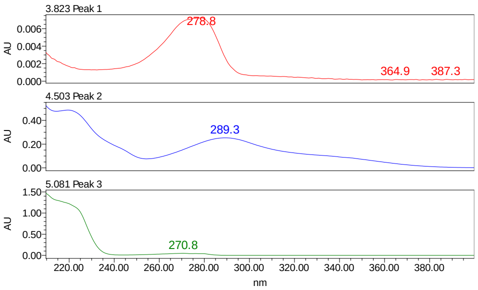

	Retention Time	Area	% Area	Height
1	3.823	13657	4.01	6727
2	4.504	245318	72.11	149424
3	5.081	81230	23.88	47193

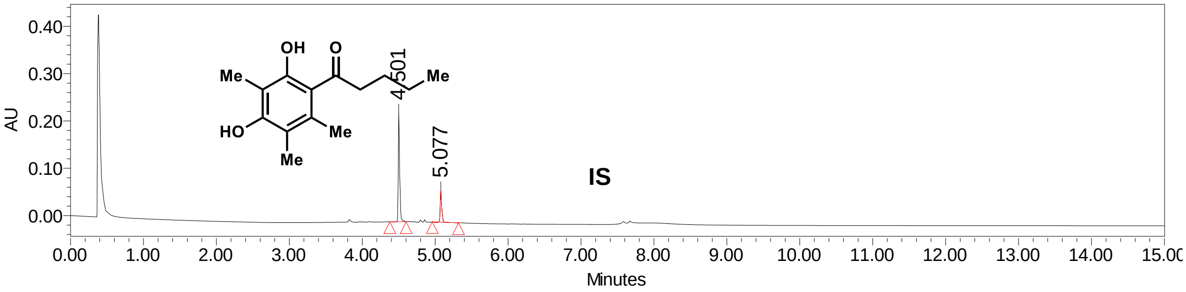

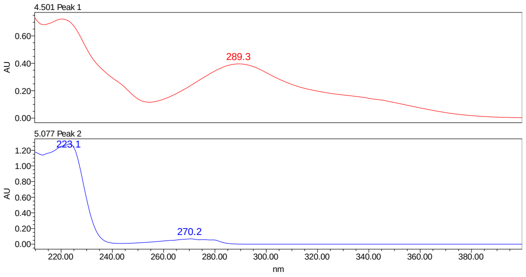

	Retention Time	Area	% Area	Height
1	4.501	313207	75.59	231850
2	5.077	101116	24.41	66793

Figure 2.44: Oxidative dearomatization of **2.75** by AzaH. PDA traces of enzymatic reaction and control reaction.

With AzaH

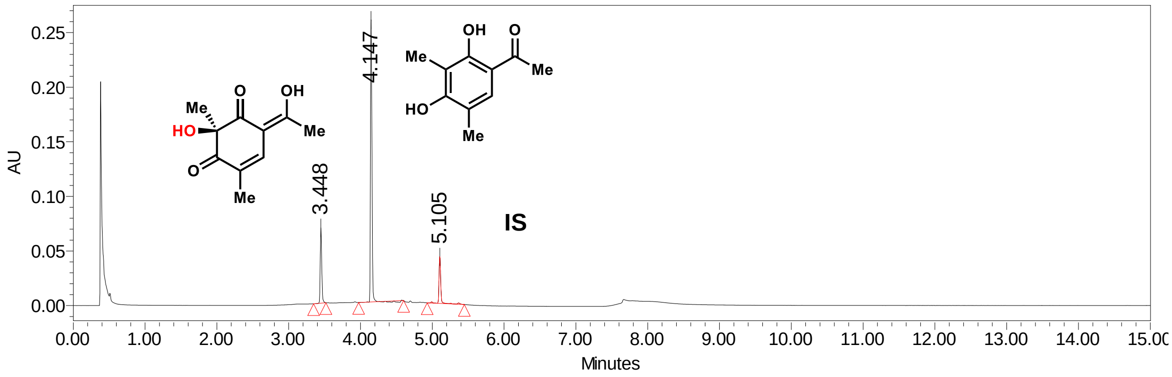

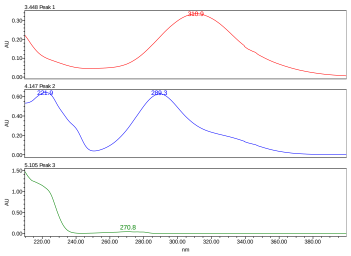

	Retention Time	Area	% Area	Height
1	3.448	99988	17.77	69219
2	4.147	388393	69.02	258431
3	5.105	74309	13.21	42896

No enzyme control

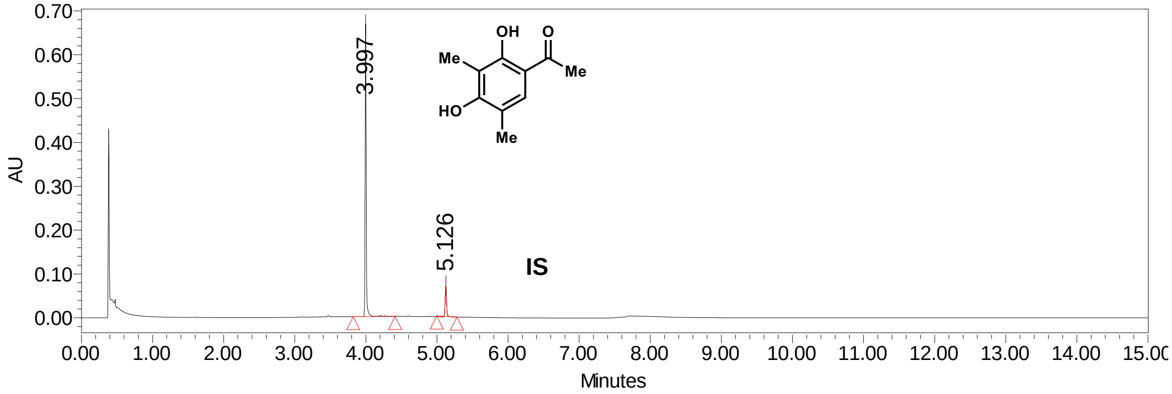

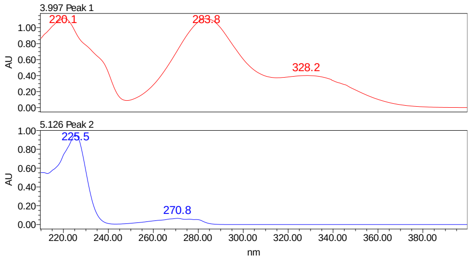

	Retention Time	Area	% Area	Height
1	3.997	724401	87.86	667824
2	5.126	100134	12.14	71008

Figure 2.45: Oxidative dearomatization of **2.25a** by AzaH. PDA traces of enzymatic reaction and control reaction.

With AzaH

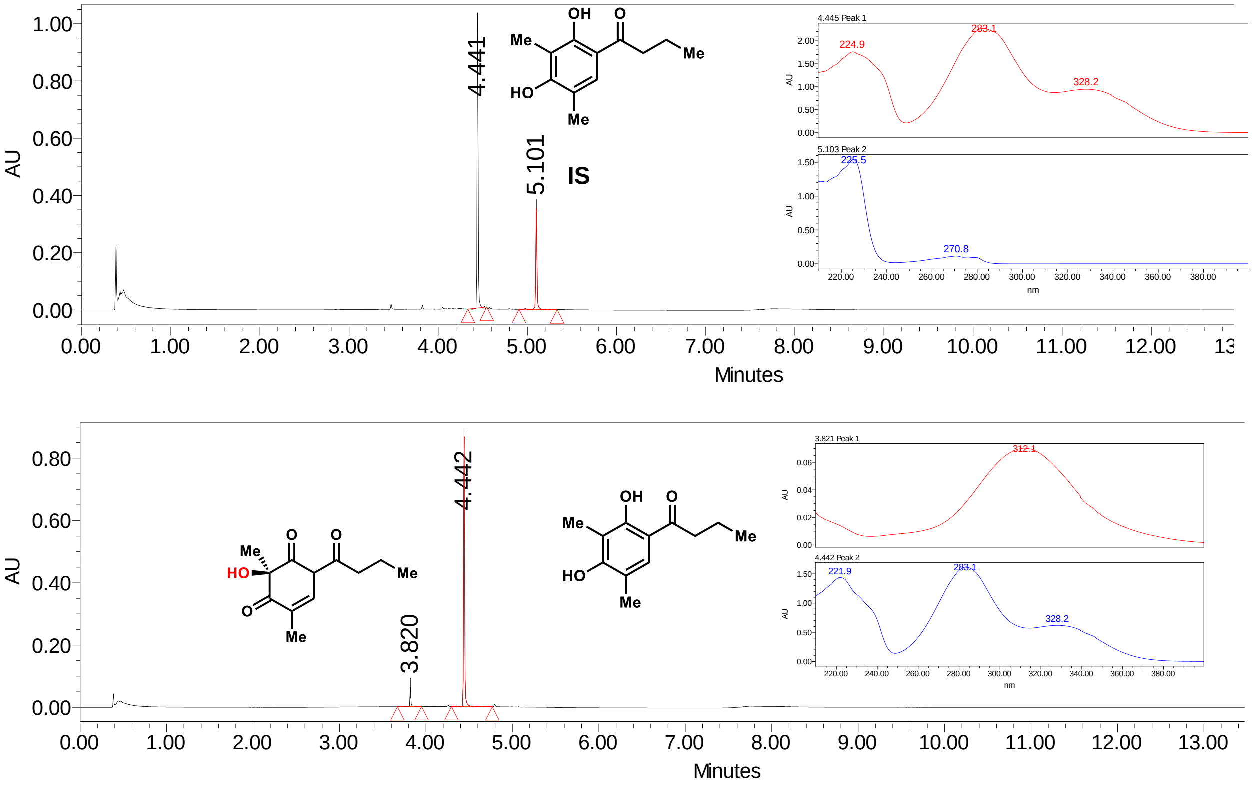

No enzyme control

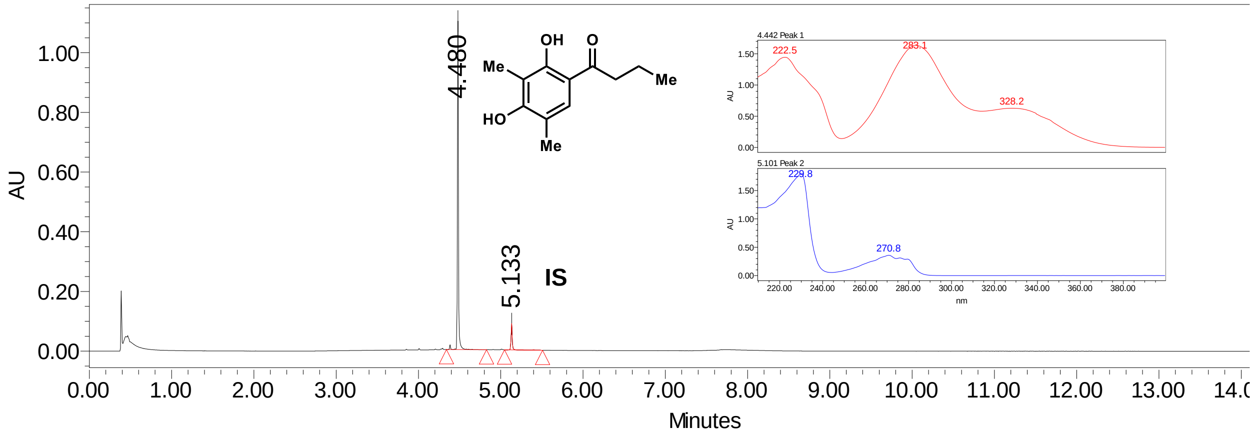

	Retention Time	Area	% Area	Height
1	4.480	971633	91.20	1100819
2	5.133	93772	8.80	88619

Figure 2.46: Oxidative dearomatization of **2.25b** by AzaH. PDA traces of enzymatic reaction and control reaction.

.

With AzaH

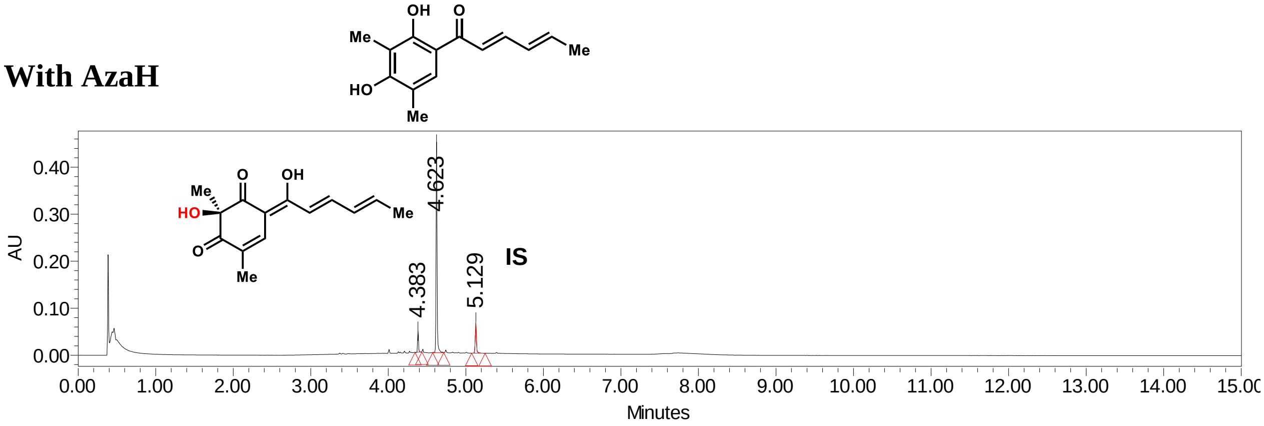

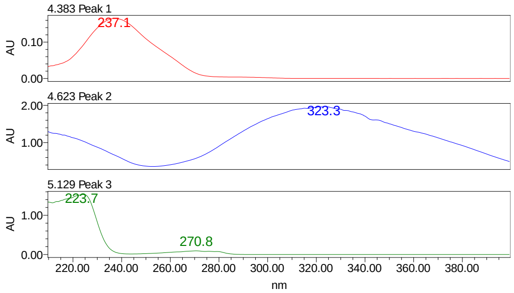

	Retention Time	Area	% Area	Height
1	4.383	55863	12.49	69790
2	4.623	341471	76.32	386499
3	5.129	50087	11.19	48911

No enzyme control

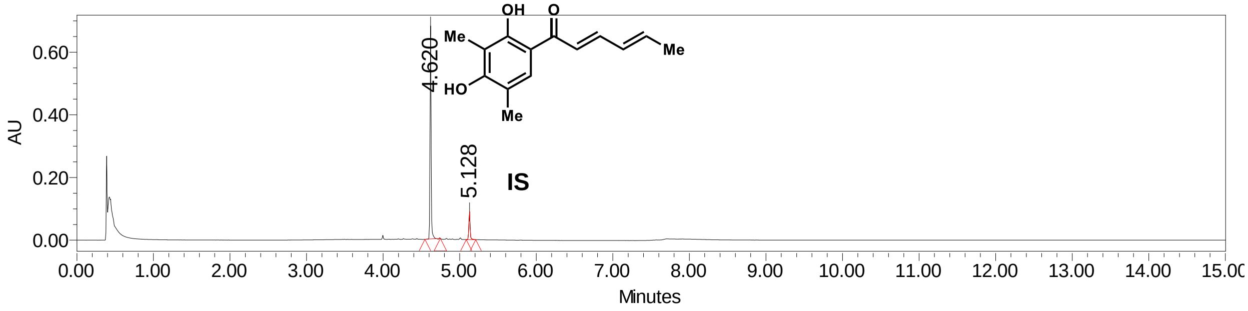

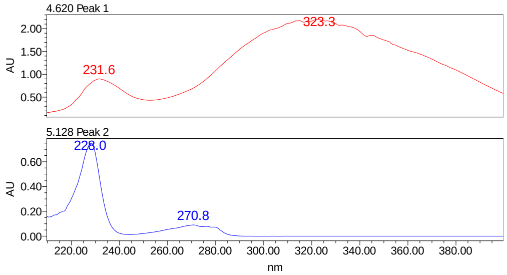

	Retention Time	Area	% Area	Height
1	4.620	683943	86.80	680347
2	5.128	103967	13.20	89310

Figure 2.47: Oxidative dearomatization of sorbicillin (**2.15**) by AzaH. PDA traces of enzymatic reaction and control reaction.

With AzaH

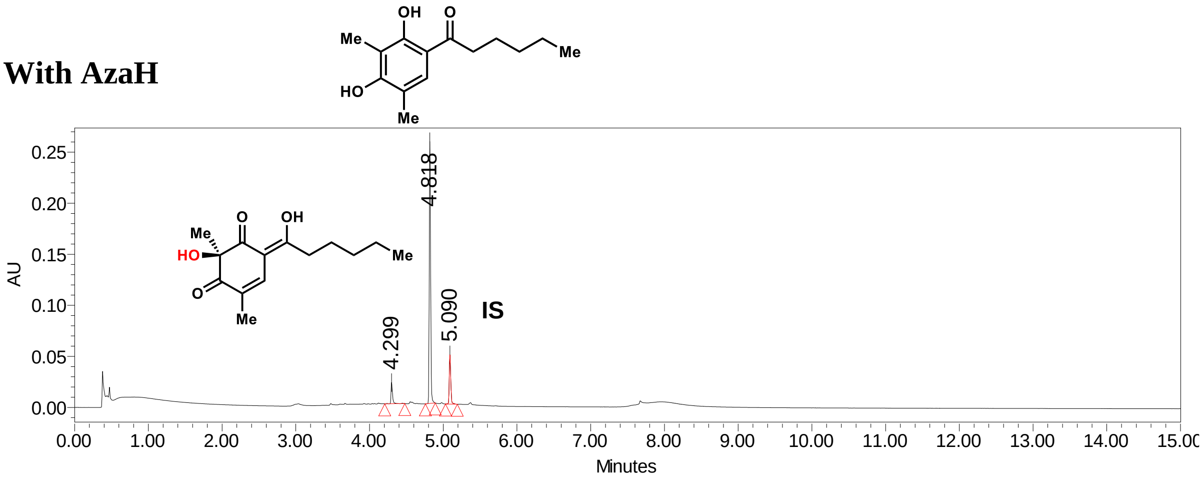

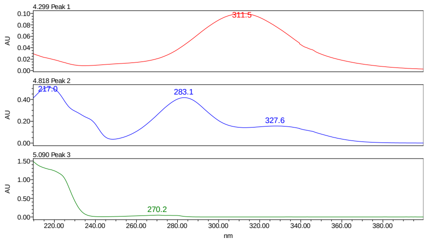

	Retention Time	Area	% Area	Height
1	4.299	29866	6.92	20712
2	4.818	333555	77.33	256926
3	5.090	67925	15.75	48221

No enzyme control

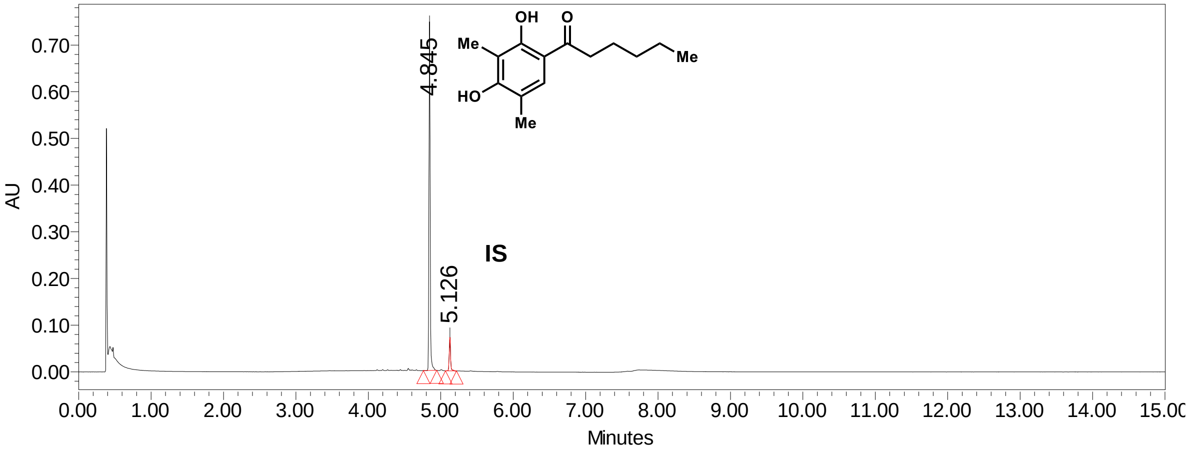

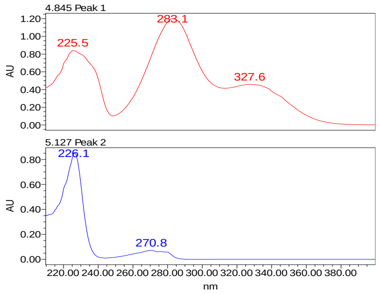

	Retention Time	Area	% Area	Height
1	4.845	869112	90.18	747186
2	5.126	94651	9.82	71763

Figure 2.48: Oxidative dearomatization of **2.25d** by AzaH. PDA traces of enzymatic reaction and control reaction.

With AzaH

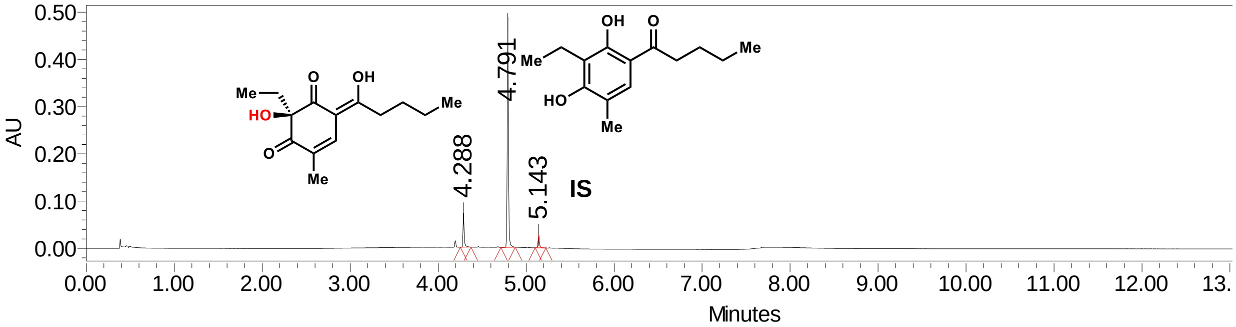

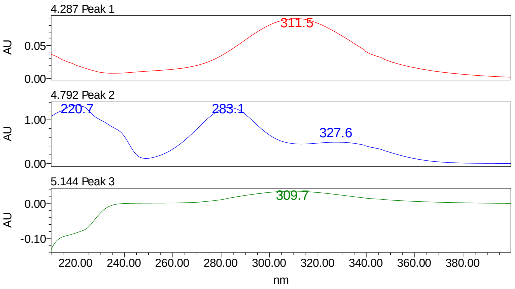

	Retention Time	Area	% Area	Height
1	4.288	65507	12.40	72216
2	4.791	435710	82.50	488324
3	5.143	26915	5.10	27481

No enzyme control

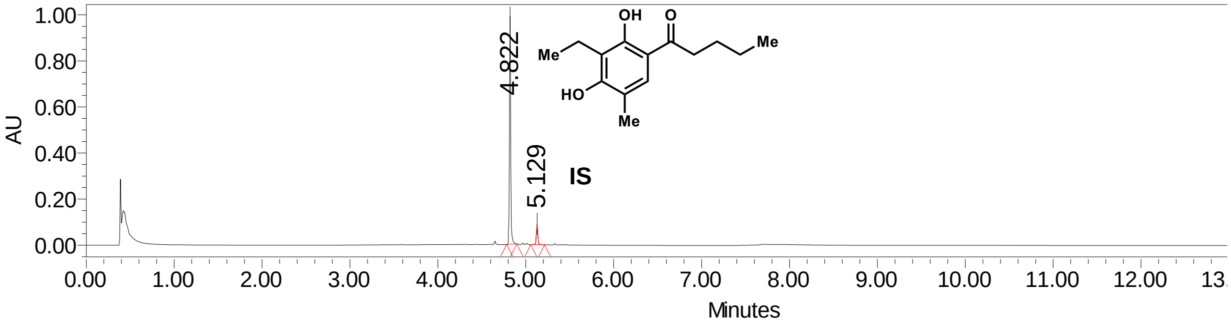

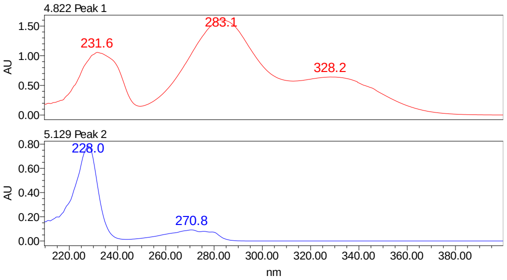

	Retention Time	Area	% Area	Height
1	4.822	997907	90.39	990194
2	5.129	106038	9.61	90938

Figure 2.49: Oxidative dearomatization of **2.76** by AzaH. PDA traces of enzymatic reaction and control reaction.

With AzaH

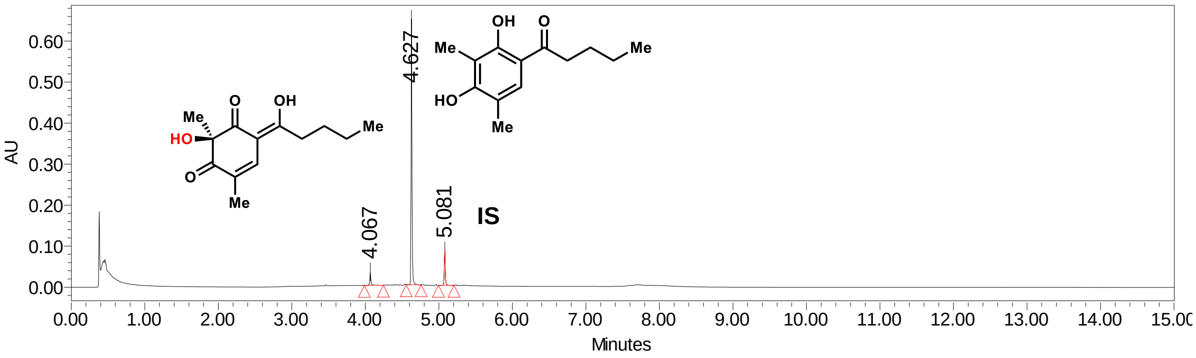

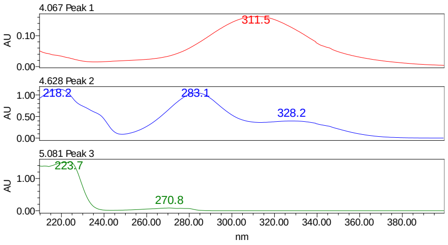

	Retention Time	Area	% Area	Height
1	4.067	31731	4.67	33355
2	4.627	560059	82.51	648065
3	5.081	87010	12.82	84948

No enzyme control

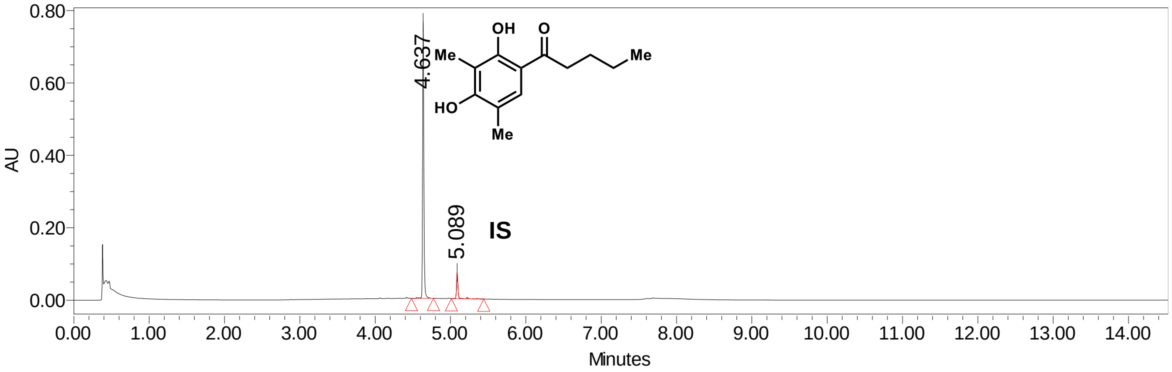

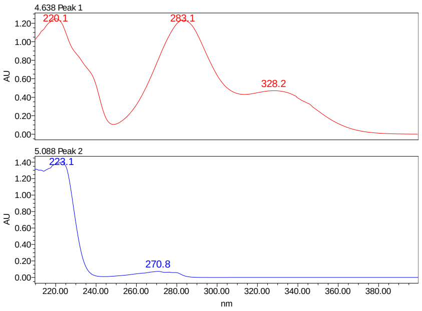

	Retention Time	Area	% Area	Height
1	4.637	877248	89.55	763969
2	5.089	102374	10.45	72349

Figure 2.50: Oxidative dearomatization of **2.25b** by AzaH. PDA traces of enzymatic reaction and control reaction.

With AzaH

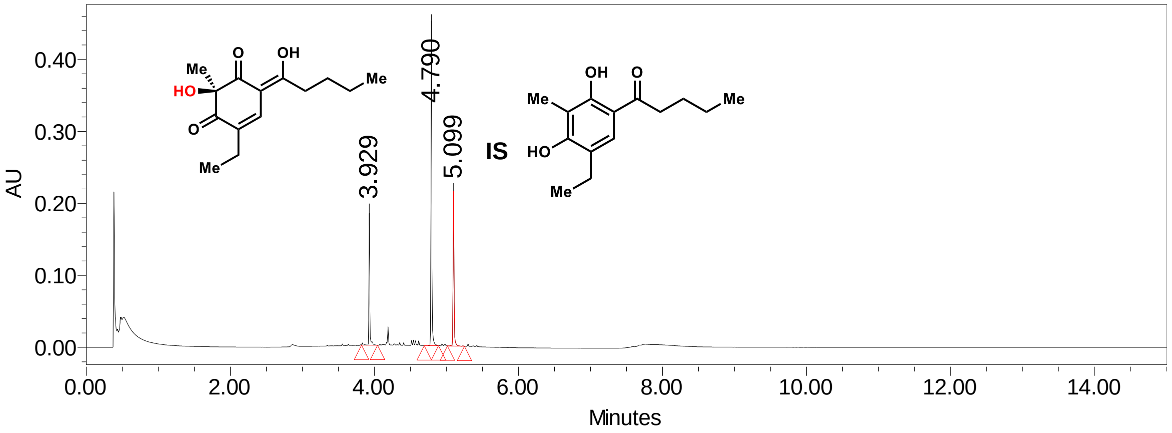

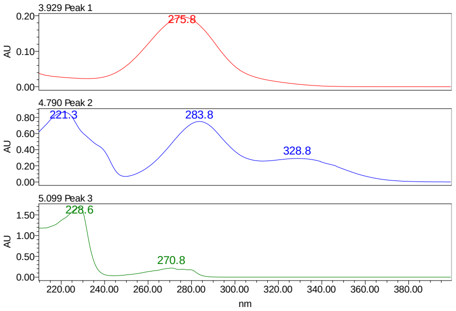

	Retention Time	Area	% Area	Height
1	3.929	148271	20.93	182824
2	4.790	368151	51.98	452041
3	5.099	191872	27.09	215767

No enzyme control

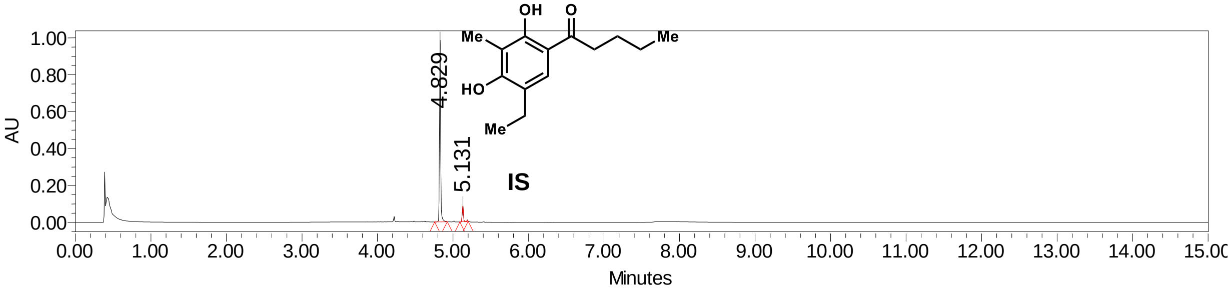

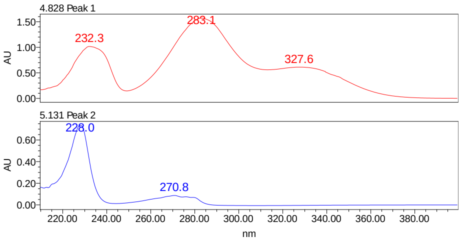

	Retention Time	Area	% Area	Height
1	4.829	1024234	91.07	985786
2	5.131	100432	8.93	85905

Figure 2.51: Oxidative dearomatization of **2.77** by AzaH. PDA traces of enzymatic reaction and control reaction

With SorbC

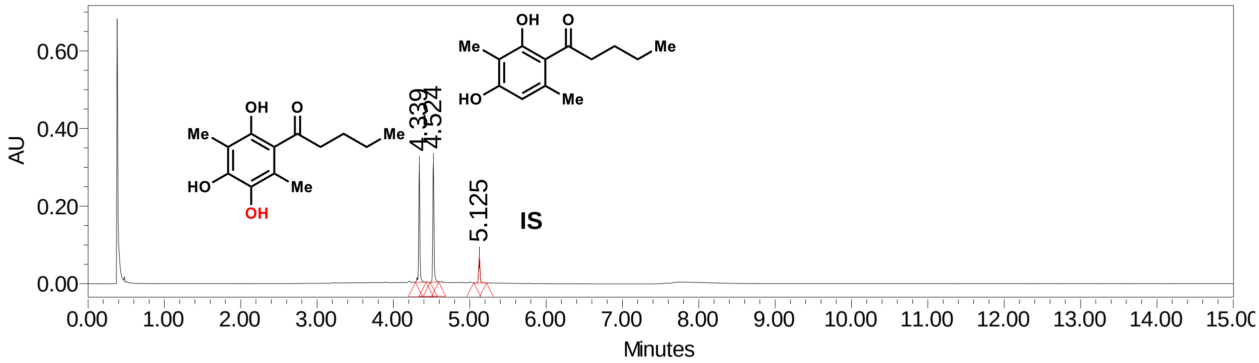

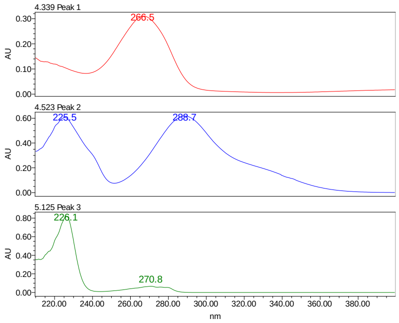

	Retention Time	Area	% Area	Height
1	4.339	308173	42.32	301769
2	4.524	336046	46.15	308969
3	5.125	83974	11.53	66040

No enzyme control

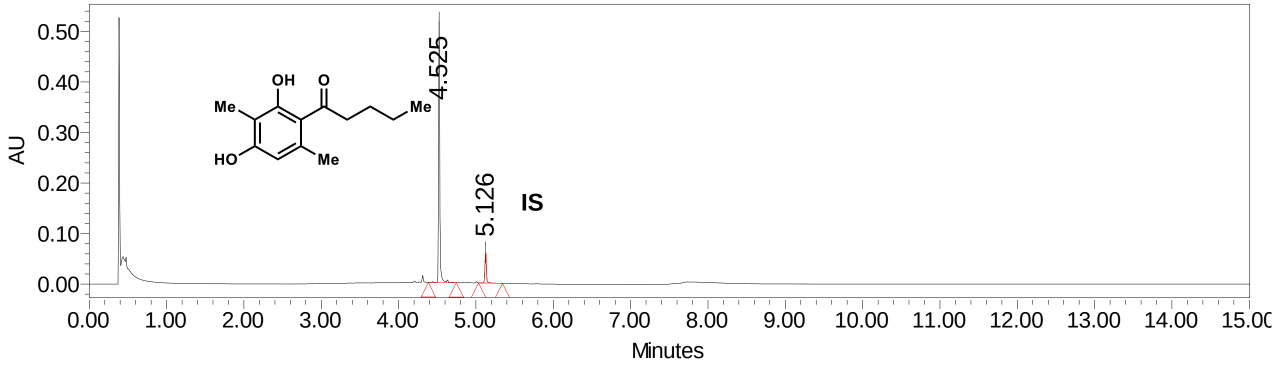

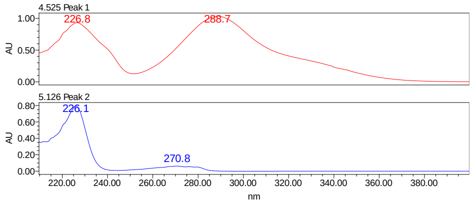

	Retention Time	Area	% Area	Height
1	4.525	569864	87.66	517315
2	5.126	80243	12.34	61491

Figure 2.52: Oxidative Dearomatization of **2.22d** by SorbC. PDA traces of enzymatic reaction and control reaction.

With SorbC

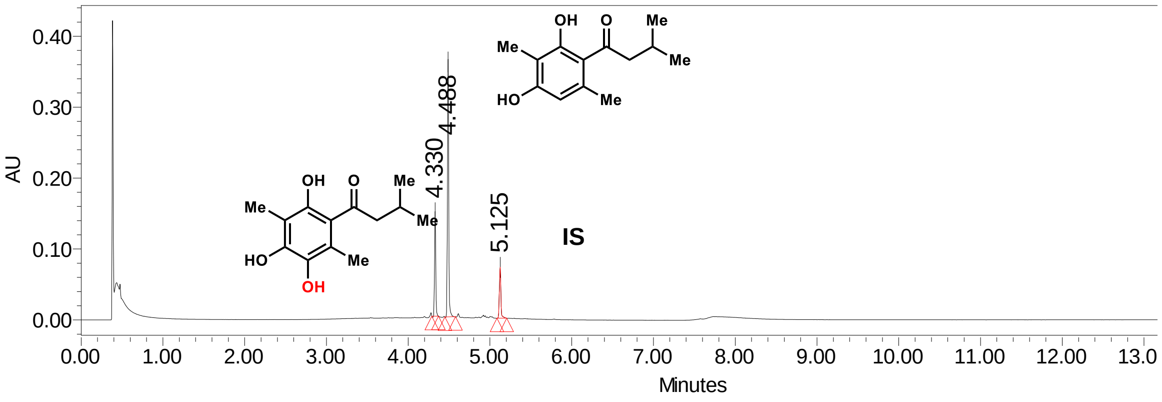

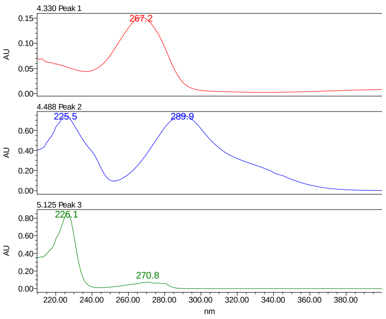

	Retention Time	Area	% Area	Height
1	4.330	149076	23.64	147864
2	4.488	388674	61.63	363526
3	5.125	92871	14.73	71874

No enzyme control

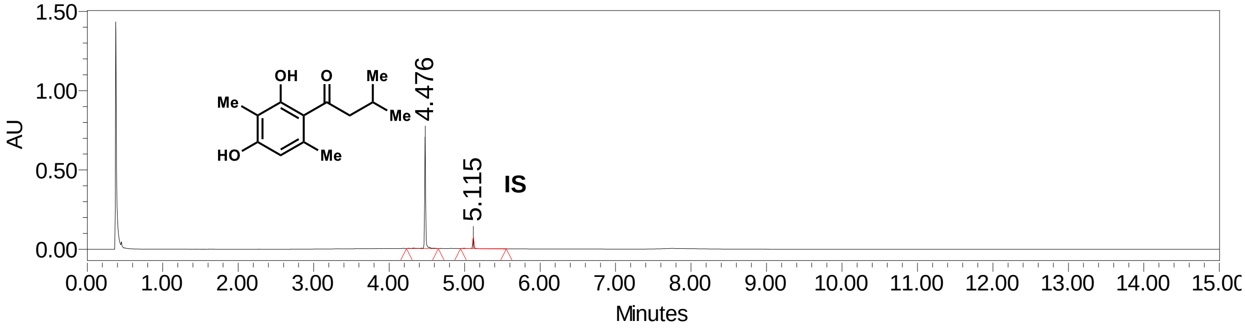

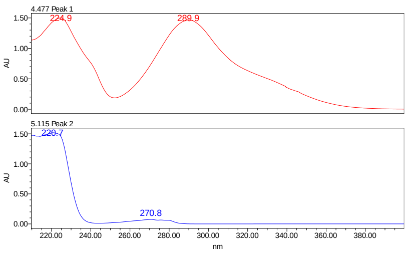

	Retention Time	Area	% Area	Height
1	4.476	669825	88.45	706595
2	5.115	87429	11.55	73777

Figure 2.53: Oxidative Dearomatization of **2.22e** by SorbC. PDA traces of enzymatic reaction and control reaction.

With SorbC

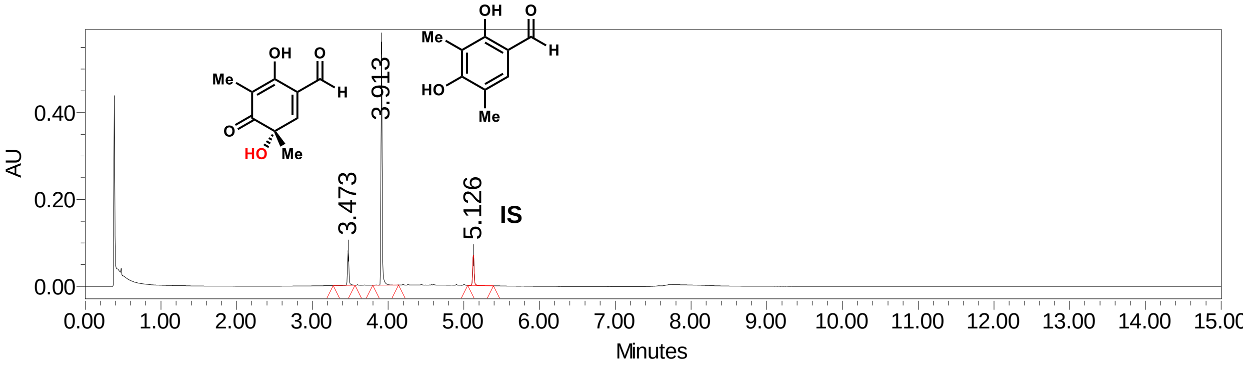

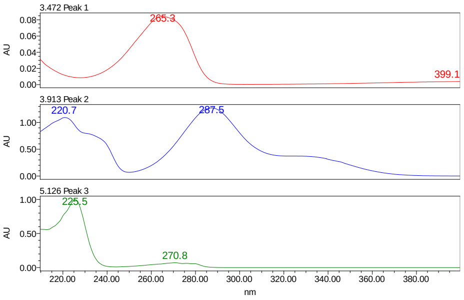

	Retention Time	Area	% Area	Height
1	3.473	104135	12.96	80180
2	3.913	604255	75.20	559715
3	5.126	95092	11.84	70041

No enzyme control

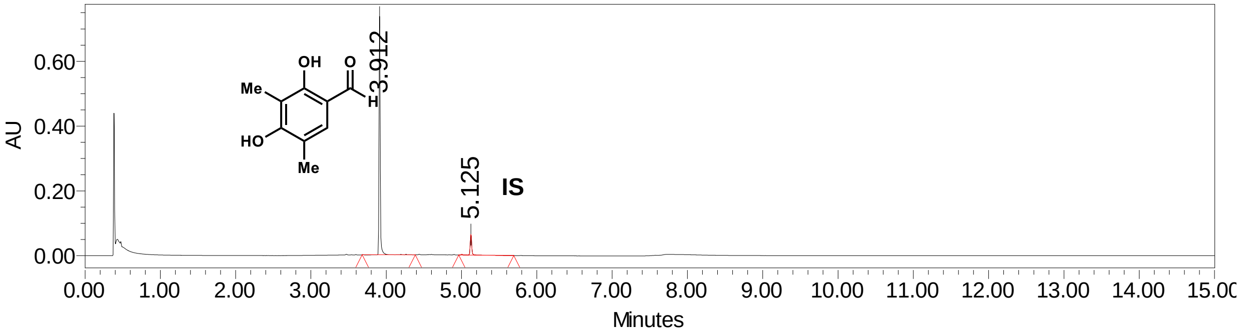

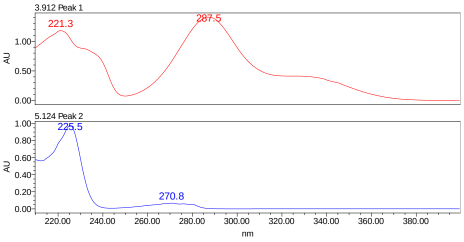

	Retention Time	Area	% Area	Height
1	3.912	809530	89.41	736129
2	5.125	95863	10.59	64246

Figure 2.54: Oxidative dearomatization of **2.58** by SorbC. PDA traces of enzymatic reaction and control reaction.

With SorbC

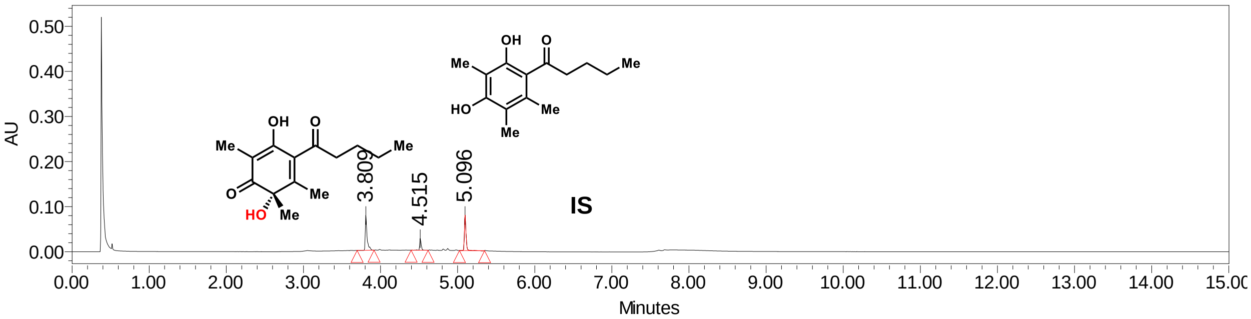

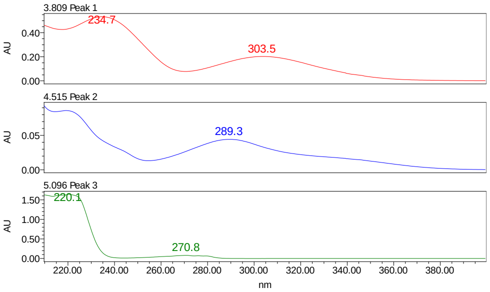

	Retention Time	Area	% Area	Height
1	3.809	126396	46.23	78348
2	4.515	33751	12.35	25916
3	5.096	113236	41.42	78706

No enzyme control

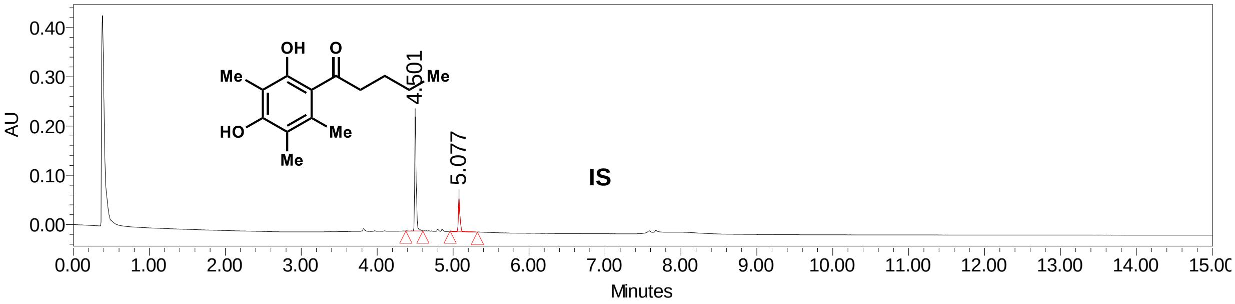

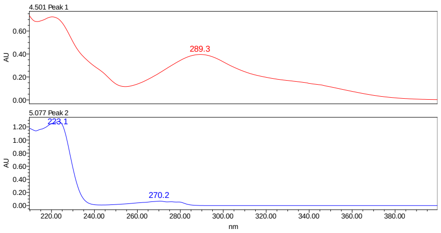

	Retention Time	Area	% Area	Height
1	4.501	313207	75.59	231850
2	5.077	101116	24.41	66793

Figure 2.55: Oxidative dearomatization of **2.75** by SorbC. PDA traces of enzymatic reaction and control reaction.

With SorbC

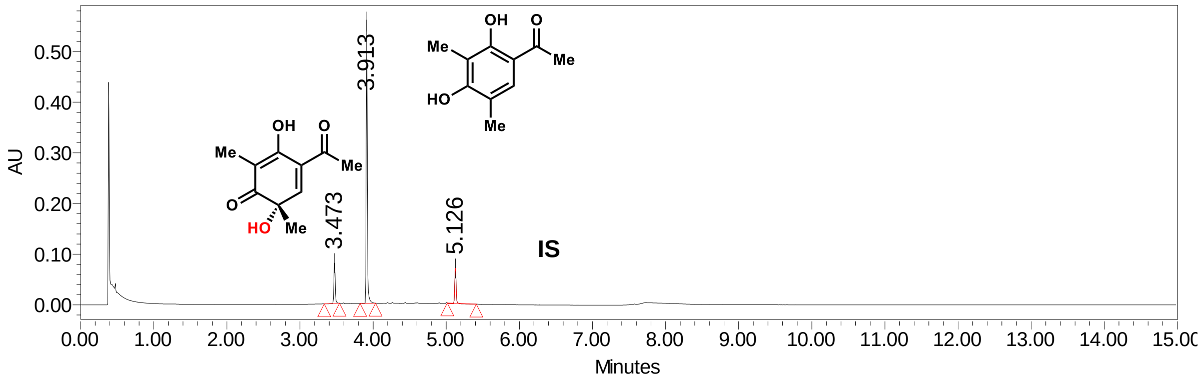

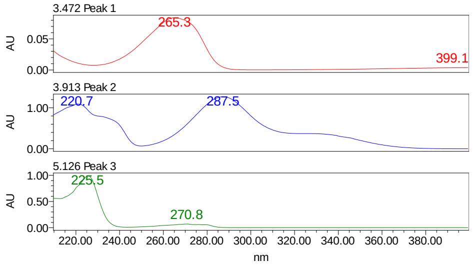

	Retention Time	Area	% Area	Height
1	3.473	101663	12.64	79764
2	3.913	602274	74.90	559609
3	5.126	100144	12.45	69007

No enzyme control

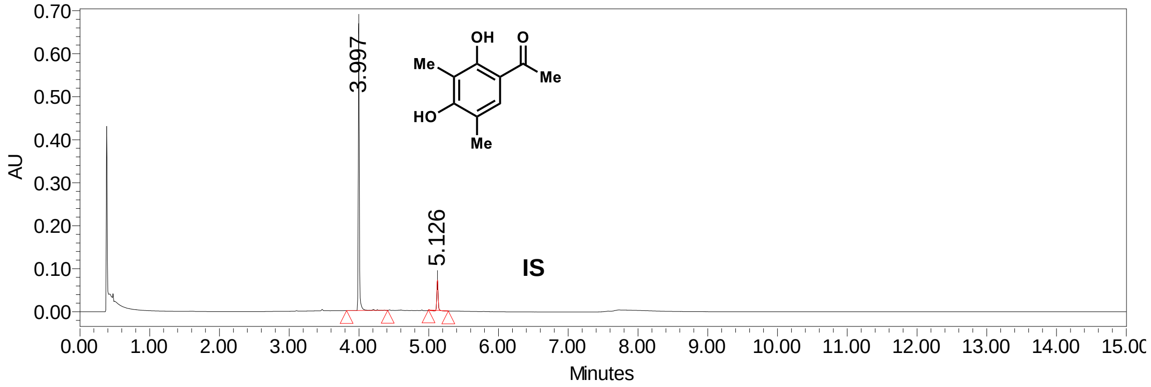

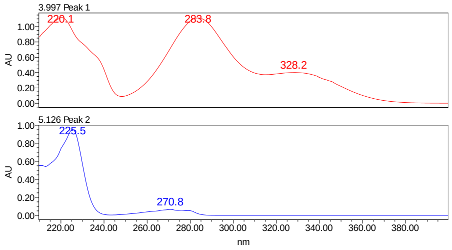

	Retention Time	Area	% Area	Height
1	3.997	724401	87.86	667824
2	5.126	100134	12.14	71008

Figure 2.56: Oxidative dearomatization of **2.25a** by SorbC. PDA traces of enzymatic reaction and control reaction.

With SorbC: Note the formation of a second product (rt= 3.490). The immediate product of the reaction is converted to **B** over time after quenching the reaction. The addition of 1,000 u/mL of catalase prevents this side product from forming. Likely the second product is the result of oxidation of the dearomatized product by hydrogen peroxide which is formed from disproportionation of the hydroperoxy flavin intermediate.

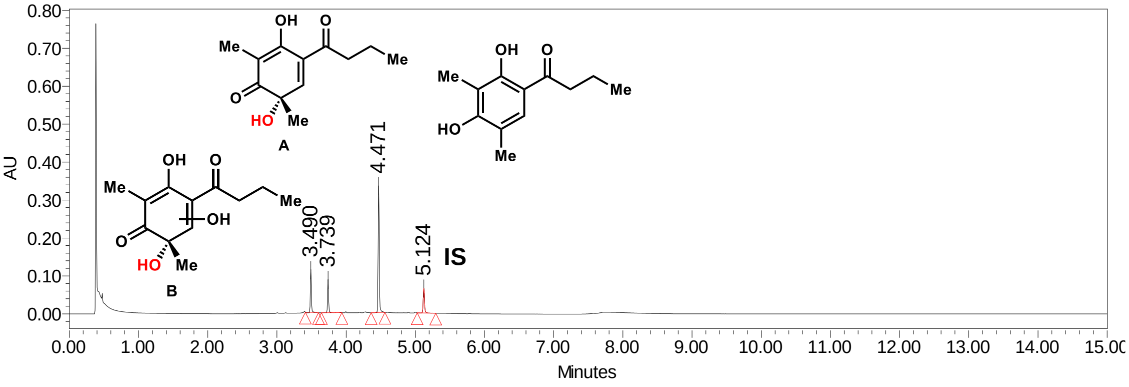

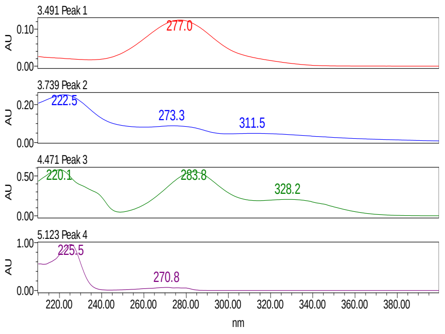

	Retention Time	Area	% Area	Height
1	3.490	115556	17.23	113576
2	3.739	89353	13.32	87093
3	4.471	377486	56.27	334338
4	5.124	88436	13.18	65003

With SorbC and catalase

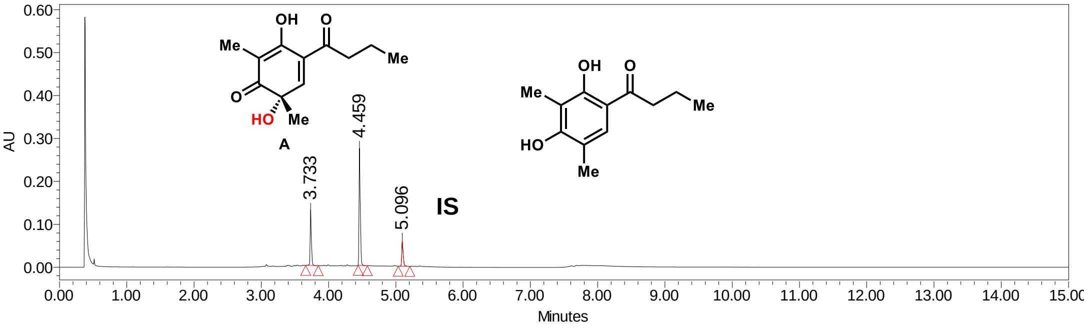

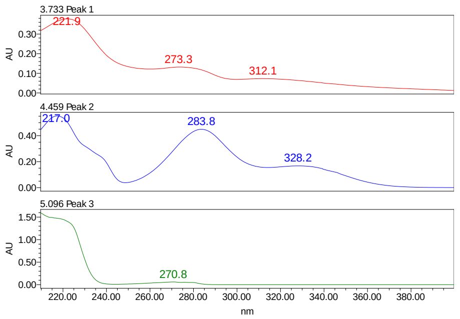

	Retention Time	Area	% Area	Height
1	3.733	161363	27.72	130068
2	4.459	336440	57.80	272397
3	5.096	84258	14.48	60310

No enzyme control

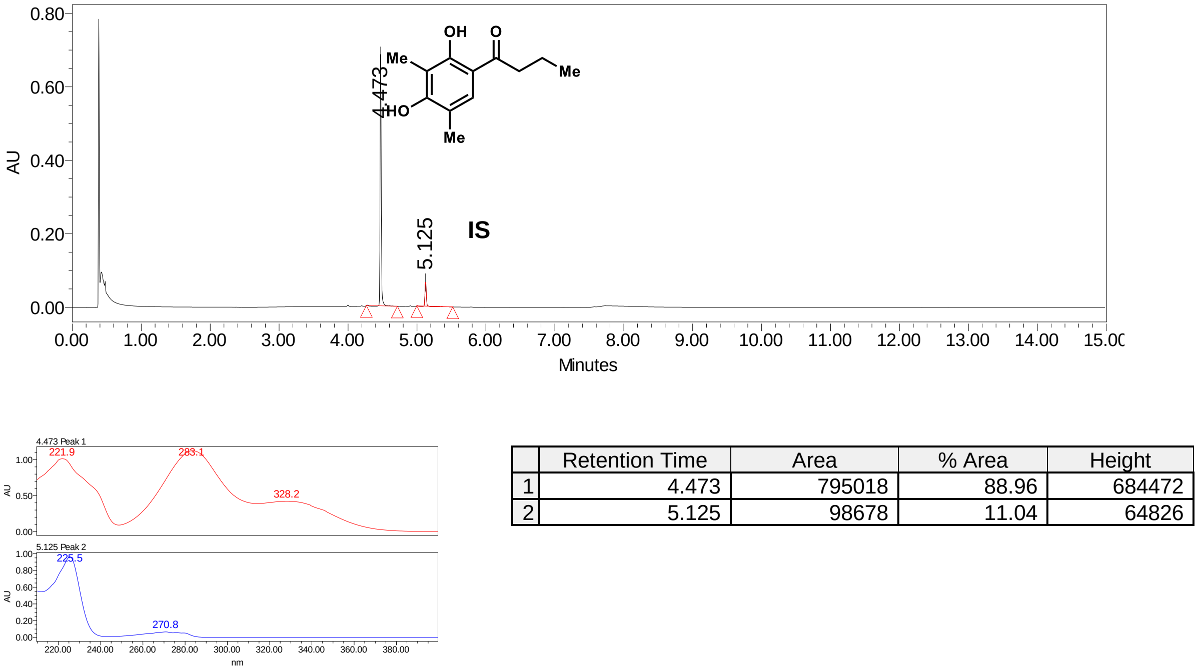

	Retention Time	Area	% Area	Height
1	4.473	795018	88.96	684472
2	5.125	98678	11.04	64826

Figure 2.57: Oxidative dearomatization of **2.25b** by SorbC. PDA traces of enzymatic reaction and control reaction.

With SorbC:

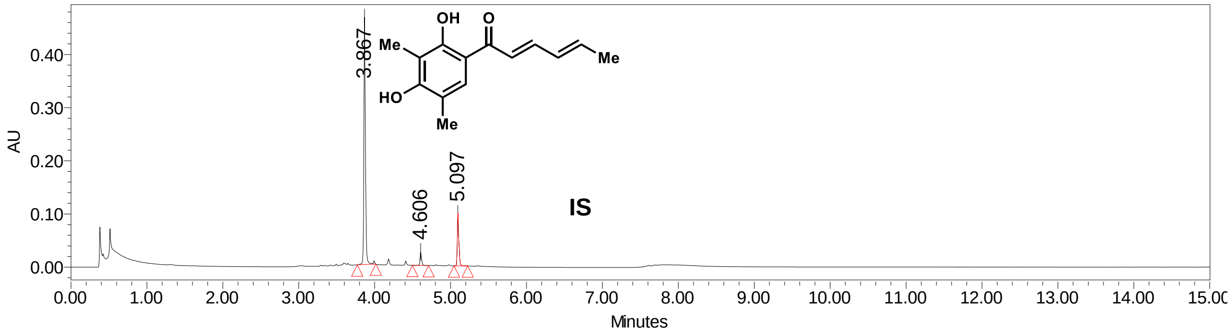

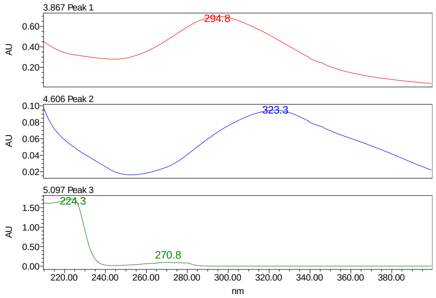

	Retention Time	Area	% Area	Height
1	3.867	664888	79.45	465219
2	4.606	34647	4.14	25663
3	5.097	137322	16.41	98940

No enzyme control

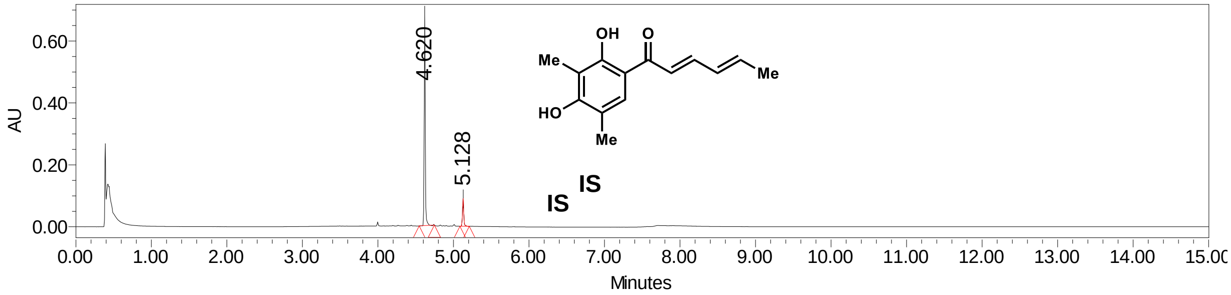

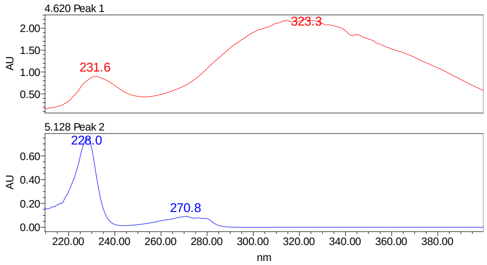

	Retention Time	Area	% Area	Height
1	4.620	683943	86.80	680347
2	5.128	103967	13.20	89310

Figure 2.58: Oxidative dearomatization of **2.15** by SorbC. PDA traces of enzymatic reaction and control reaction.

With SorbC: Note the formation of a second product (rt= 3.992). The immediate product of the reaction (**A**) is converted to **B** (mass = +32 of starting material) over time after quenching the reaction. The addition of 1,000 u/mL of catalase prevents this side product from forming. Likely the second product is the result of oxidation of the dearomatized product by hydrogen peroxide which is formed from disproportionation of the hydroperoxy flavin intermediate.

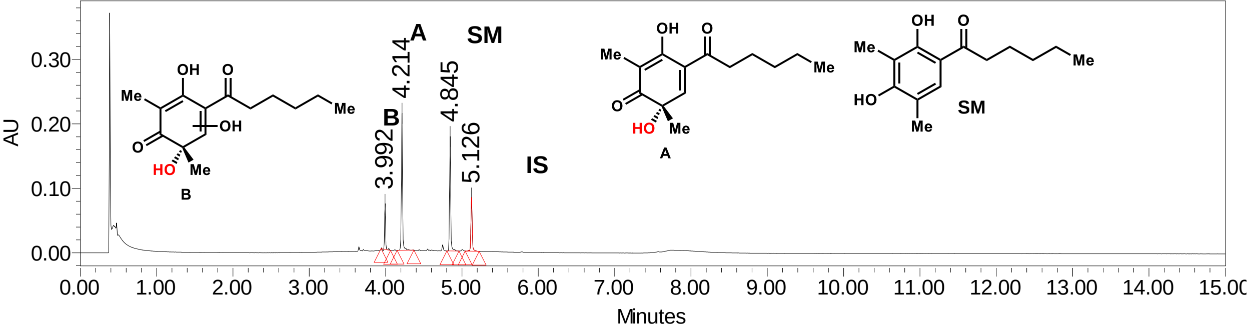

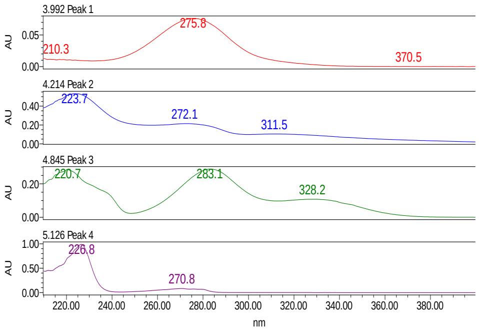

	Retention Time	Area	% Area	Height
1	3.992	66049	11.44	71240
2	4.214	219320	37.99	212829
3	4.845	190823	33.05	177612
4	5.126	101193	17.53	83294

After quenching the enzymatic reaction prd A converts fully to B in 2 h.

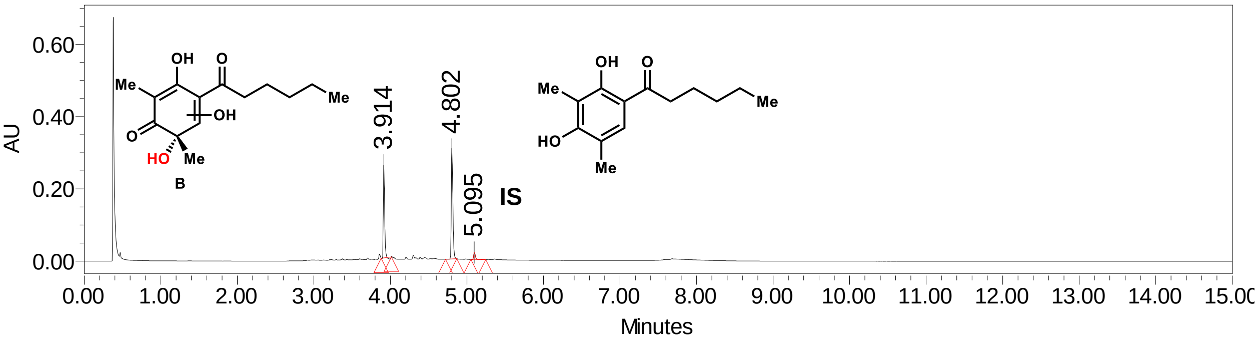

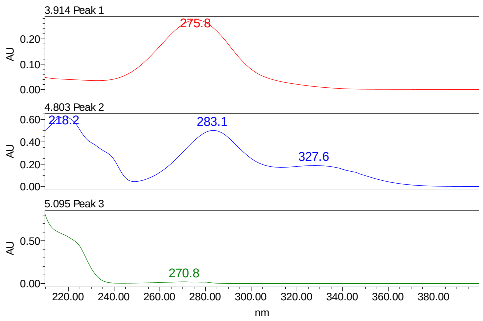

	Retention Time	Area	% Area	Height
1	3.914	324746	41.41	256800
2	4.802	428228	54.60	306790
3	5.095	31285	3.99	19412

With SorbC and catalase

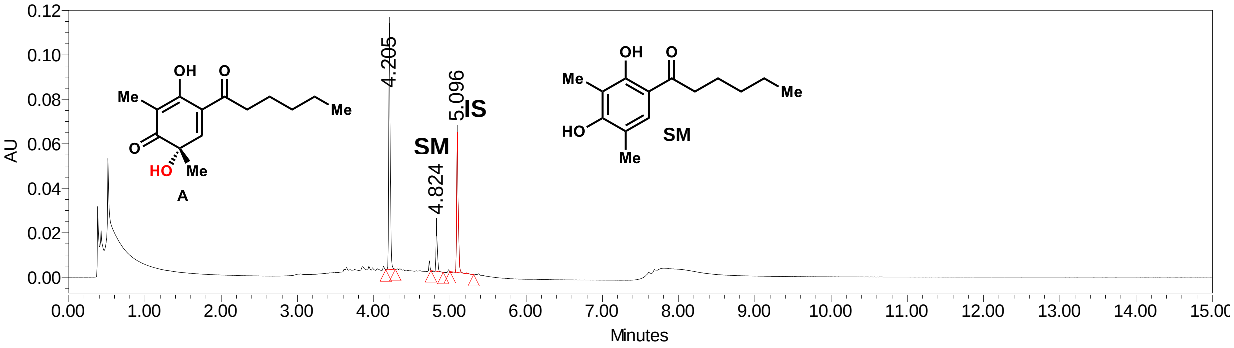

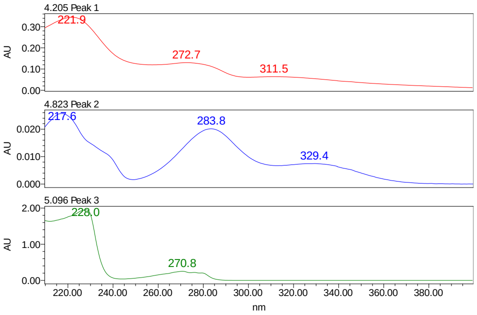

	Retention Time	Area	% Area	Height
1	4.205	143931	55.29	110819
2	4.824	26347	10.12	20112
3	5.096	90024	34.58	63055

No enzyme control

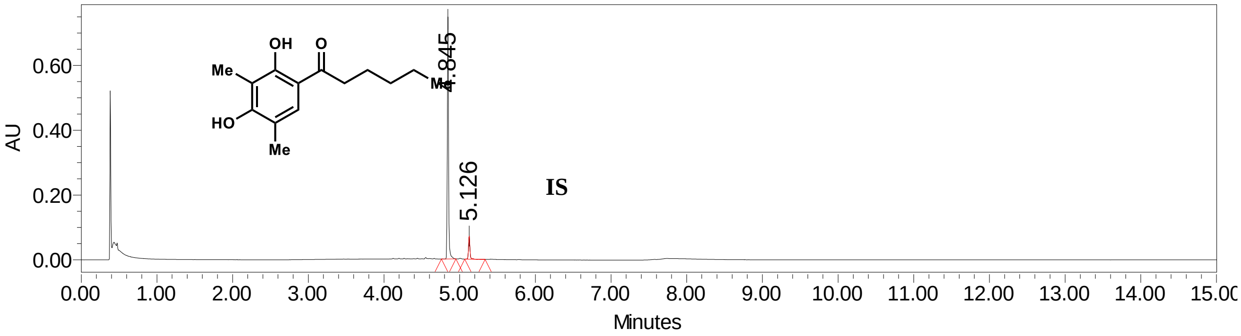

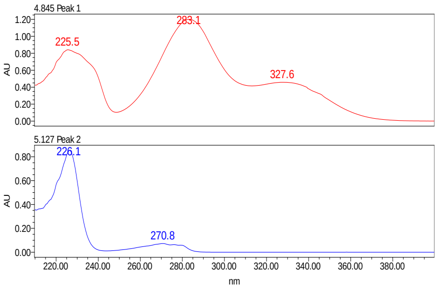

	Retention Time	Area	% Area	Height
1	4.845	869112	90.18	747186
2	5.126	94651	9.82	71763

Figure 2.59: Oxidative dearomatization of **2.25d** by SorbC. PDA traces of enzymatic reaction and control reaction.

With SorbC: Note the formation of a second product (rt= 3.763). The immediate product of the reaction is converted to C (mass = +32 of starting material) over time after quenching the reaction. The addition of 1,000 u/mL of catalase prevents this side product from forming. Likely the second product is the result of oxidation of the dearomatized product by hydrogen peroxide which is formed from disproportionation of the hydroperoxy flavin intermediate

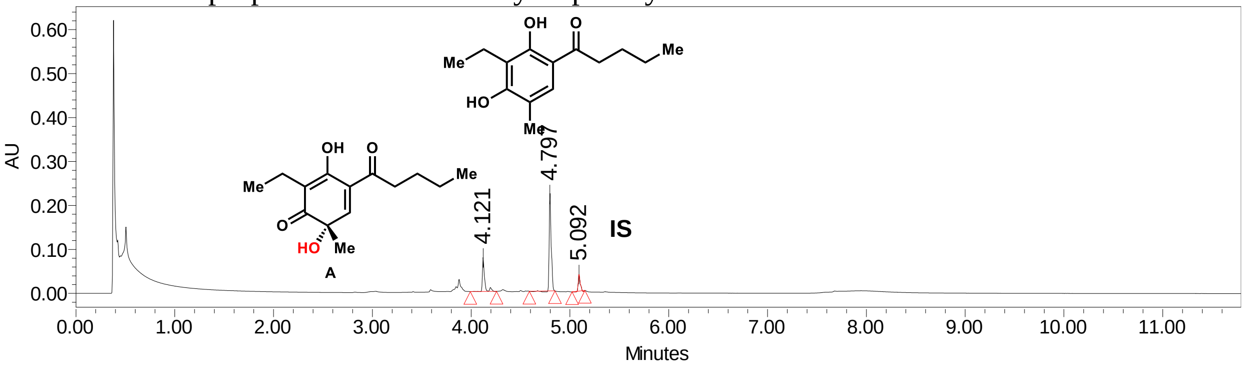

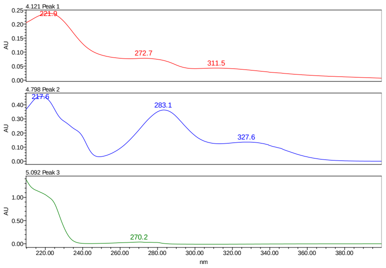

	Retention Time	Area	% Area	Height
1	4.121	116168	23.76	77525
2	4.797	317027	64.85	221984
3	5.092	55683	11.39	37959

No enzyme control

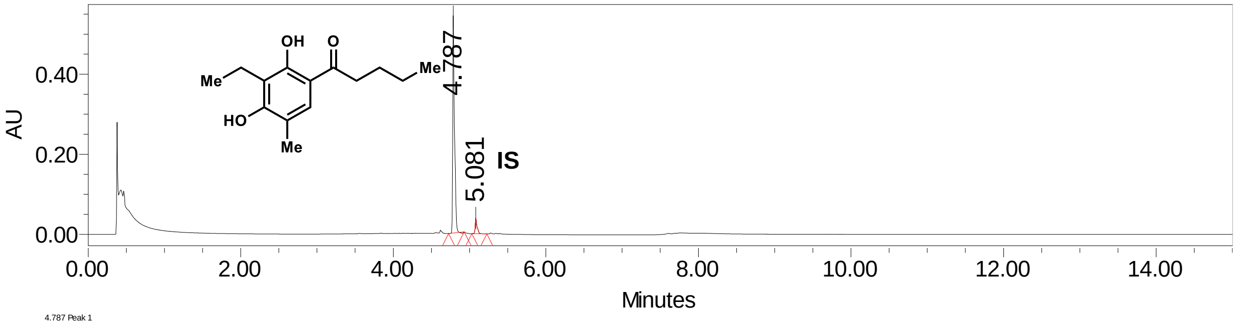

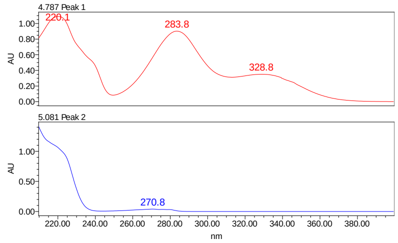

	Retention Time	Area	% Area	Height
1	4.787	874906	92.62	543140
2	5.081	69750	7.38	39630

Figure 2.60: Oxidative dearomatization of **2.76** by SorbC. PDA traces of enzymatic reaction and control reaction.

With SorbC: Note the formation of a second product (rt= 3.763). The immediate product of the reaction (**A**) is converted to **B** (mass = +32 of starting material) over time after quenching the reaction. The addition of 1,000 u/mL of catalase prevents this side product from forming. Likely the second product is the result of oxidation of the dearomatized product by hydrogen peroxide which is formed from disproportionation of the hydroperoxy flavin intermediate

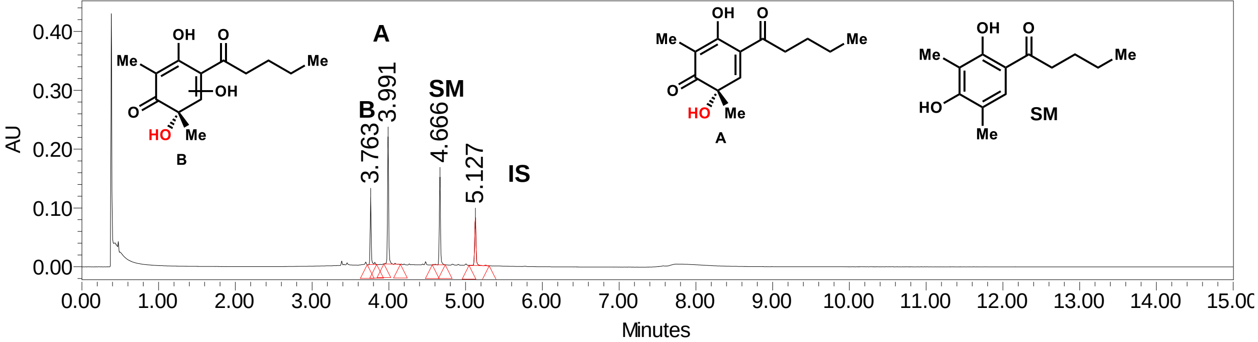

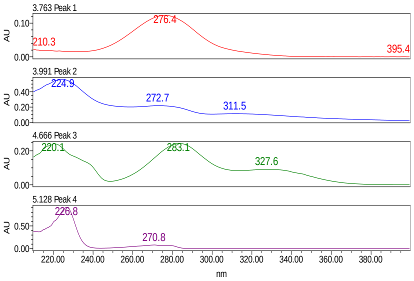

	Retention Time	Area	% Area	Height
1	3.763	106922	18.07	114375
2	3.991	219339	37.06	216484
3	4.666	162404	27.44	149164
4	5.127	103181	17.43	81174

With SorbC and catalase

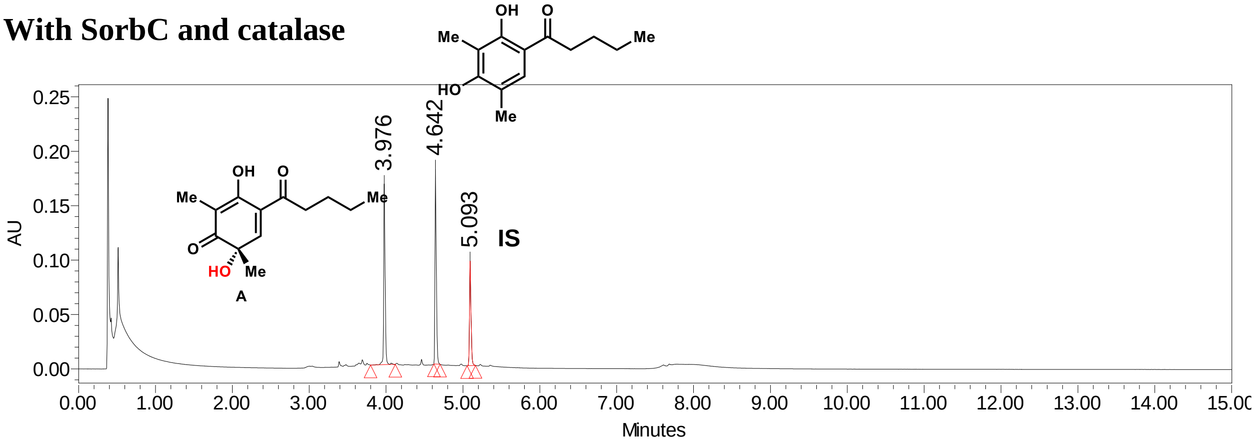

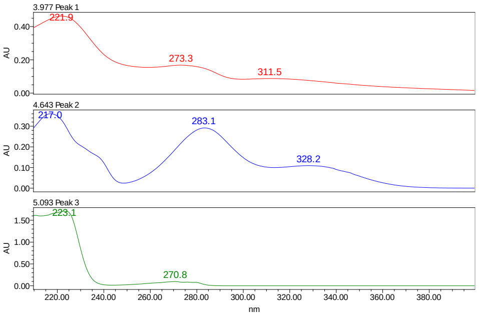

	Retention Time	Area	% Area	Height
1	3.976	217360	38.08	166133
2	4.642	221882	38.87	178801
3	5.093	131550	23.05	95956

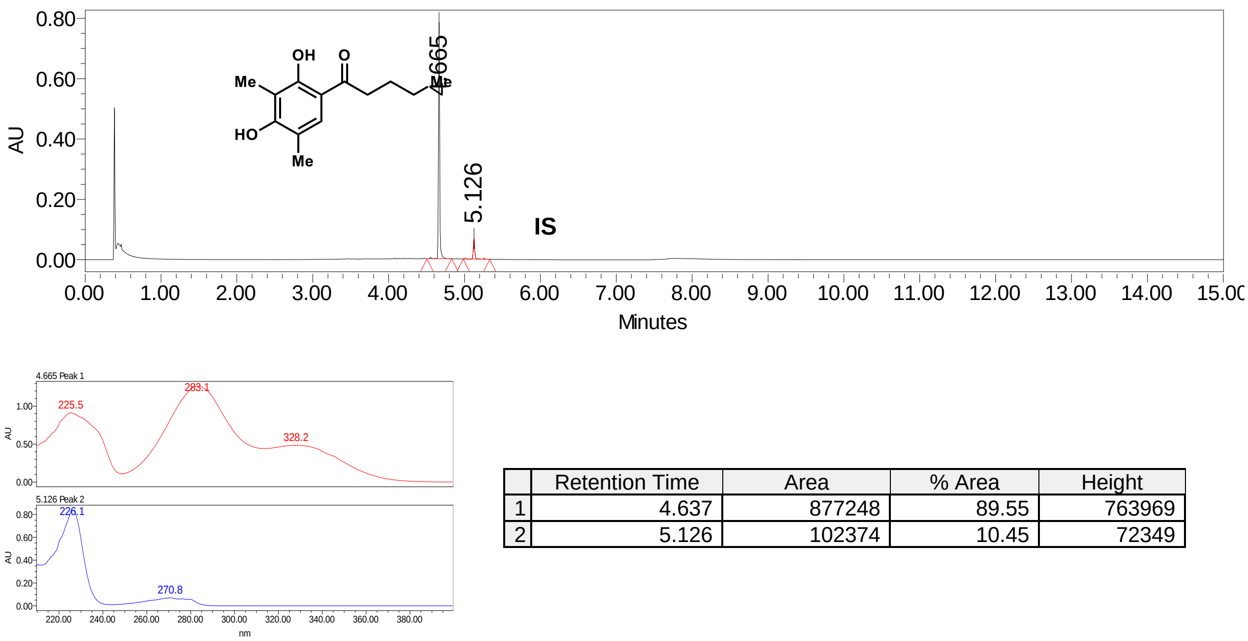

	Retention Time	Area	% Area	Height
1	4.637	877248	89.55	763969
2	5.126	102374	10.45	72349

Figure 2.61: Oxidative dearomatization of **2.25c** by SorbC. PDA traces of enzymatic reaction and control reaction.

With SorbC:

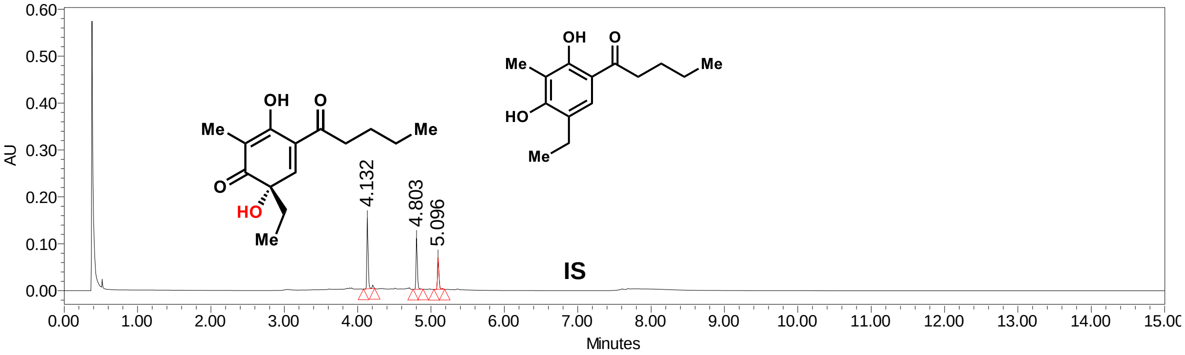

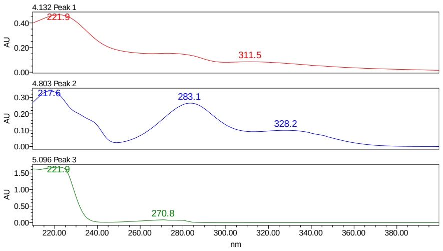

	Retention Time	Area	% Area	Height
1	4.132	190388	45.50	150883
2	4.803	135918	32.48	108578
3	5.096	92126	22.02	67077

No enzyme control

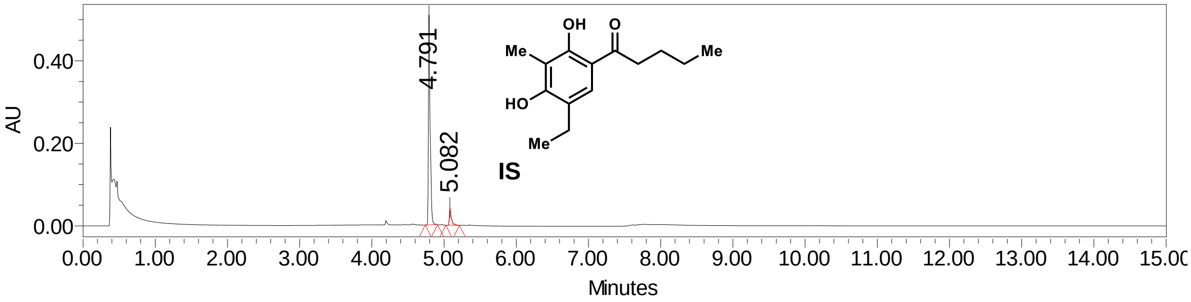

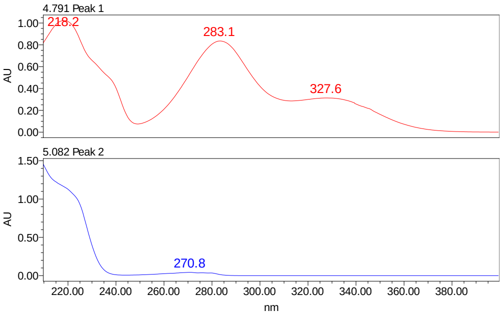

	Retention Time	Area	% Area	Height
1	4.791	821742	91.32	508753
2	5.082	78067	8.68	42294

Figure 2.62: Oxidative dearomatization of **2.77** by SorbC. PDA traces of enzymatic reaction and control reaction.

Chapter 2.6.6: HPLC and SFC Traces

HPLC traces: Note in reverse phase the *S* enantiomer elutes first.

Racemic standard

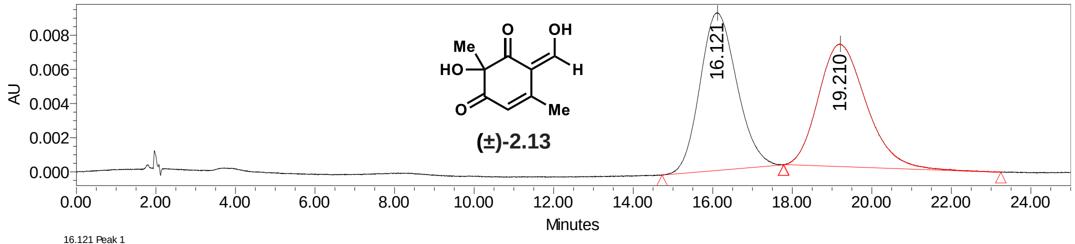

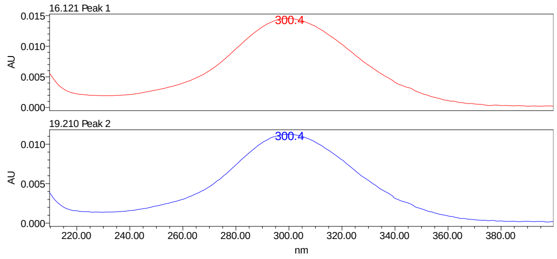

	Retention Time	Area	% Area	Height
1	16.121	594177	49.82	9235
2	19.210	598376	50.18	7181

2.13 from TropB reaction

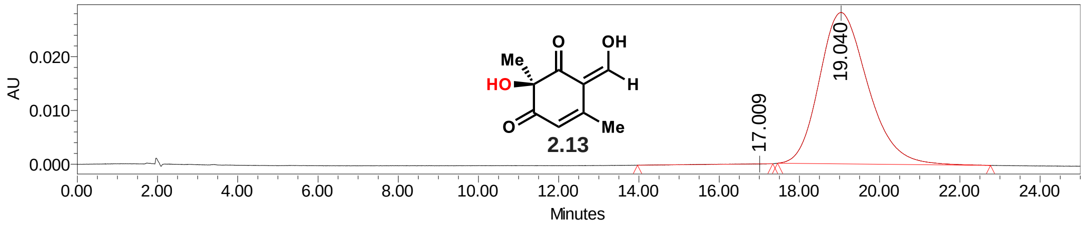

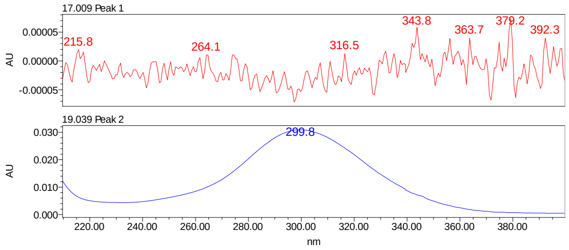

	Retention Time	Area	% Area	Height
1	17.009	2207	0.09	-47
2	19.040	2360932	99.91	28174

Racemic standard

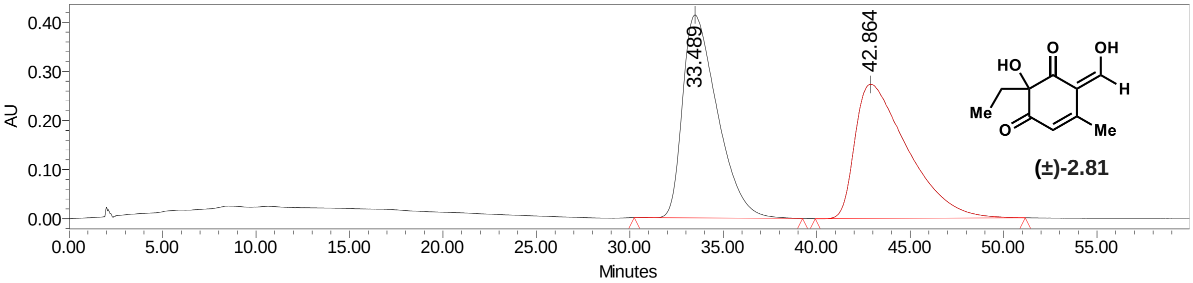

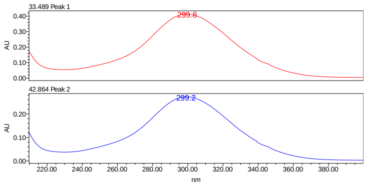

	Retention Time	Area	% Area	Height
1	33.489	53482643	49.97	413483
2	42.864	53540926	50.03	273030

2.81 from TropB reaction

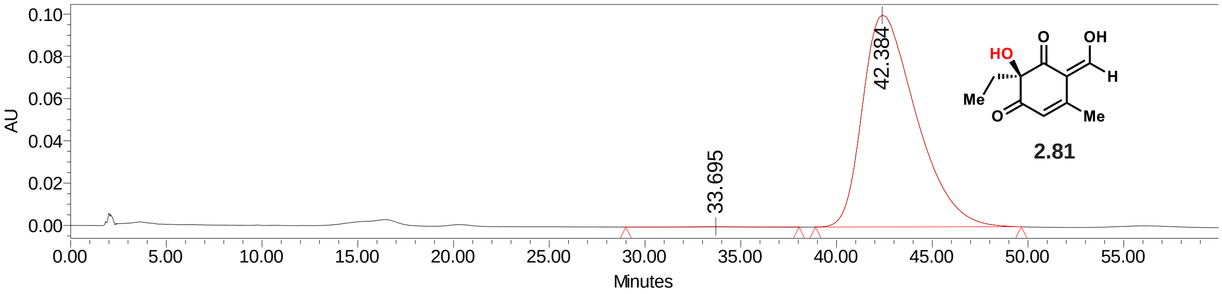

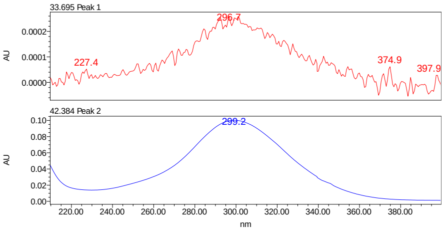

	Retention Time	Area	% Area	Height
1	33.695	32608	0.17	249
2	42.384	19618969	99.83	100190

Racemic standard

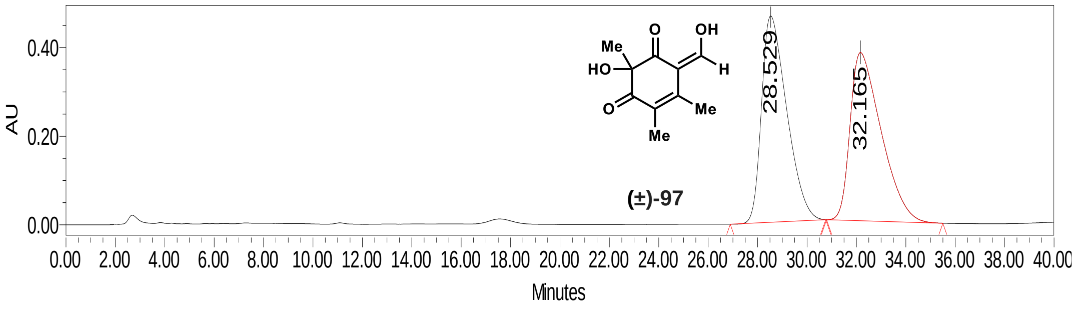

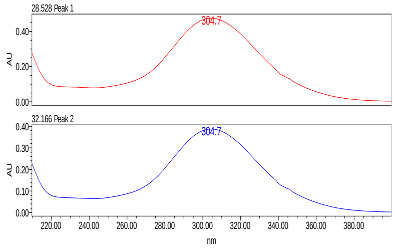

	Retention Time	Area	% Area	Height
1	28.529	33044792	49.85	465816
2	32.165	33250255	50.15	379831

2.97 from TropB reaction

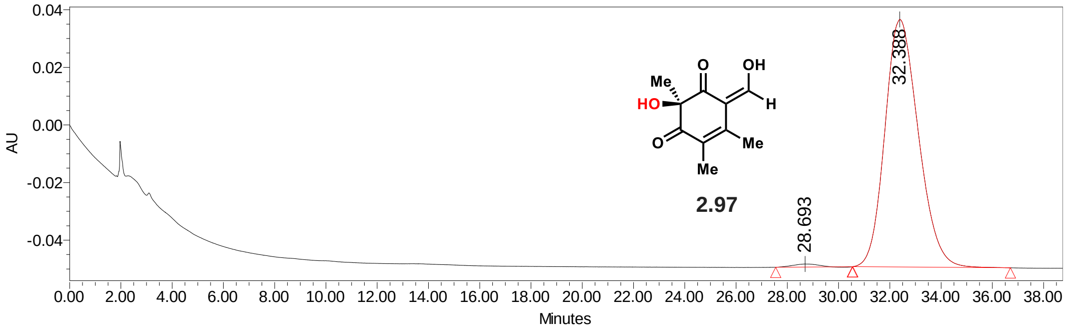

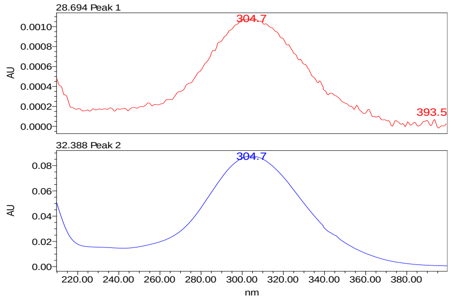

	Retention Time	Area	% Area	Height
1	28.693	77788	0.99	1072
2	32.388	7819254	99.01	85938

SFC traces: Note in normal phase the *(R)* enantiomer elutes first.

Racemic stand

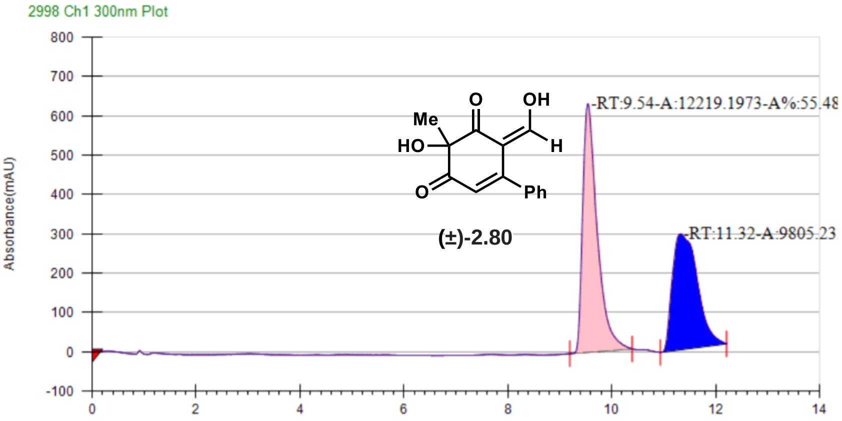

Run Information

Instrument Method	Inj. Vol.	Solvent	Column	Sample	Well Location	Temp.	Flow	% Modifier	Pressure
AD-H_8%	5	iPrOH	AD-H Chiral Analytical	sbdIV-116_8%	11A	40	3.5	8	120

Peak Information

Peak No	% Area	Area	Ret. Time	Height	Cap. Factor
1	55.4802	12219.1973	9.54 min	632.3805	9540.6667
2	44.5198	9805.233	11.32 min	295.027	11324

2.80 from TropB reaction

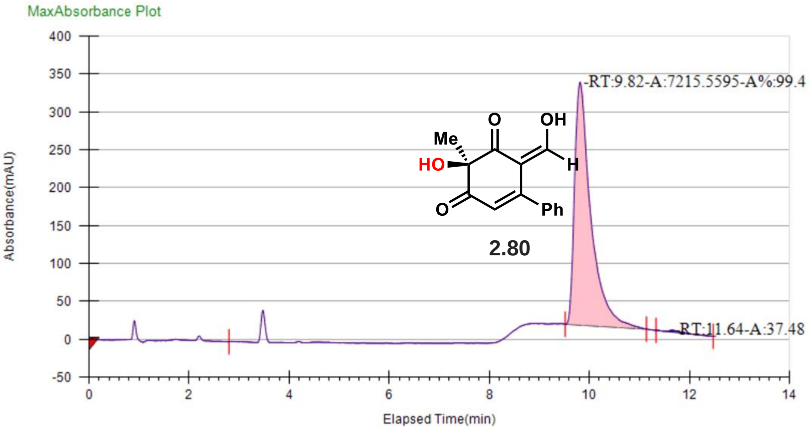

Run Information

Instrument Method	Inj. Vol.	Solvent	Column	Sample	Well Location	Temp.	Flow	% Modifier	Pressure
AD-H_8%	6	iPrOH	AD-H Chiral Analytical	sbdIV-106_8%	13A	40	3.5	8	120

Peak Information

Peak No	% Area	Area	Ret. Time	Height	Cap. Factor
1	99.4832	7215.5595	9.82 min	320.5403	0
2	0.5168	37.4819	11.64 min	2.2183	0

Racemic standard

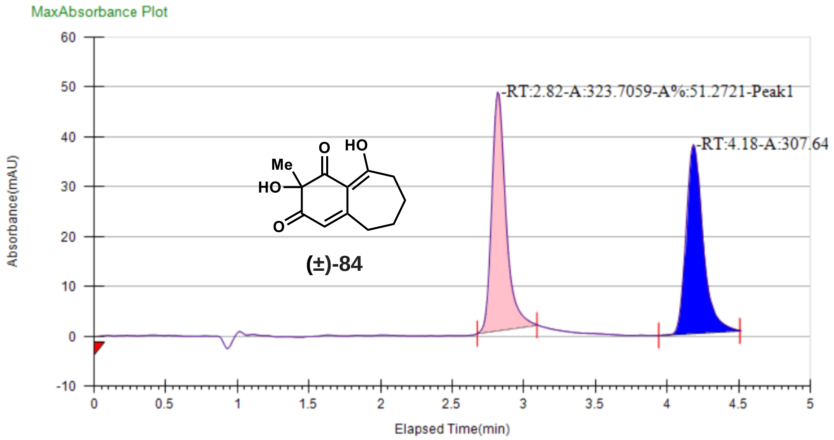

Run Information

Instrument Method	Inj. Vol.	Solvent	Column	Sample	Well Location	Temp.	Flow	% Modifier	Pressure
AD-H_30%_300-330	10	iPrOH	AD-H Chiral Analytical	sbdIV-105 40iPrOH	12A	40	3.5	30	120

Peak Information

Peak No	% Area	Area	Ret. Time	Height	Cap. Factor
1	51.2721	323.7059	2.82 min	47.8595	2815.6333
2	48.7279	307.6434	4.18 min	37.9302	4182.2833

2.84 from TropB reaction

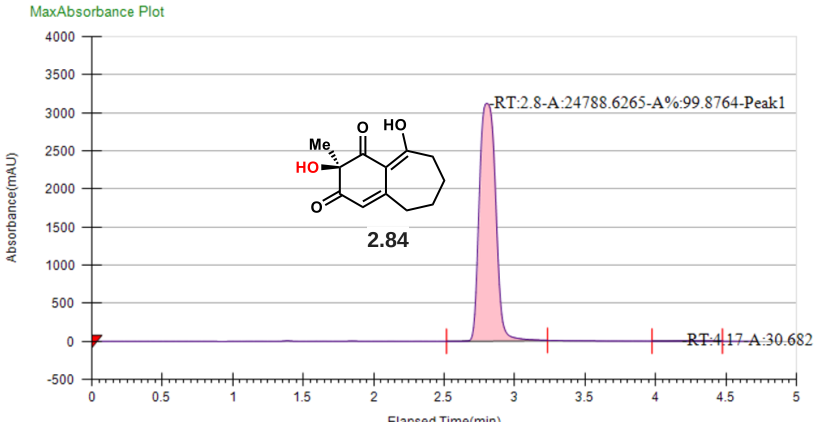

Run Information

Instrument Method	Inj. Vol.	Solvent	Column	Sample	Well Location	Temp.	Flow	% Modifier	Pressure
AD-H_30%_300-330	10	iPrOH	AD-H Chiral Analytical	sbdIV-107_30iPrOH	11A	40	3.5	30	120

Peak Information

Peak No	% Area	Area	Ret. Time	Height	Cap. Factor
1	99.8764	24788.6265	2.8 min	3117.8111	0
2	0.1236	30.6821	4.17 min	2.9908	0

Racemic standard

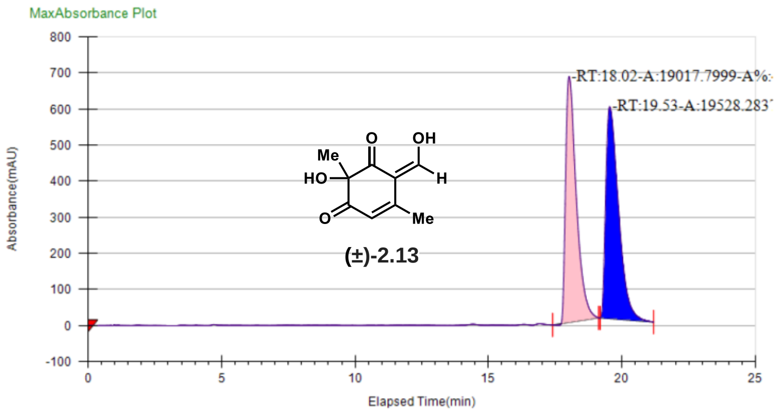

Run Information

Instrument Method	Inj. Vol.	Solvent	Column	Sample	Well Location	Temp.	Flow	% Modifier	Pressure
AD-H_4.5%	5	iPrOH	AD-H Chiral Analytical	sbdIII-034_4.5%	11B	40	3.5	4.5	120

Peak Information

Peak No	% Area	Area	Ret. Time	Height	Cap. Factor
1	49.3378	19017.7999	18.02 min	681.9914	18015.4
2	50.6622	19528.2837	19.53 min	587.5899	19532.05

2.13 from AzaH reaction

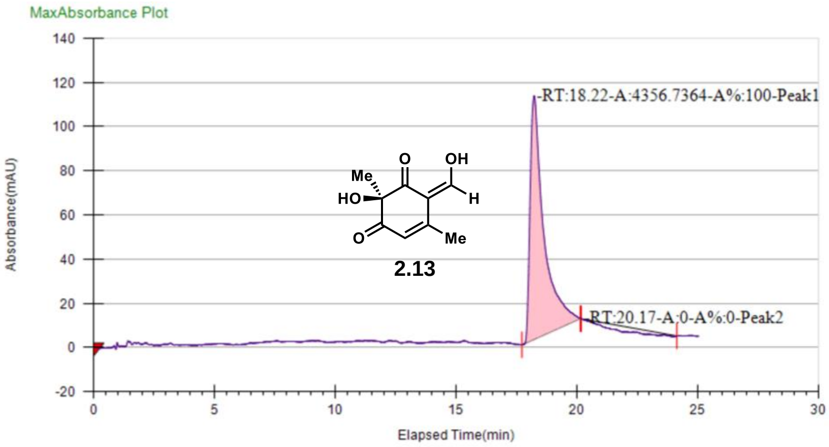

Run Information

Instrument Method	Inj. Vol.	Solvent	Column	Sample	Well Location	Temp.	Flow	% Modifier	Pressure
AD-H_4.5%	5	iPrOH	AD-H Chiral Analytical	sbdIV-082_4.5%	12A	40	3.5	4.5	120

Peak Information

Peak No	% Area	Area	Ret. Time	Height	Cap. Factor
1	100	4356.7364	18.22 min	110.3373	18223.8
2	0	0	20.17 min	0	20173.7833

Racemic standard

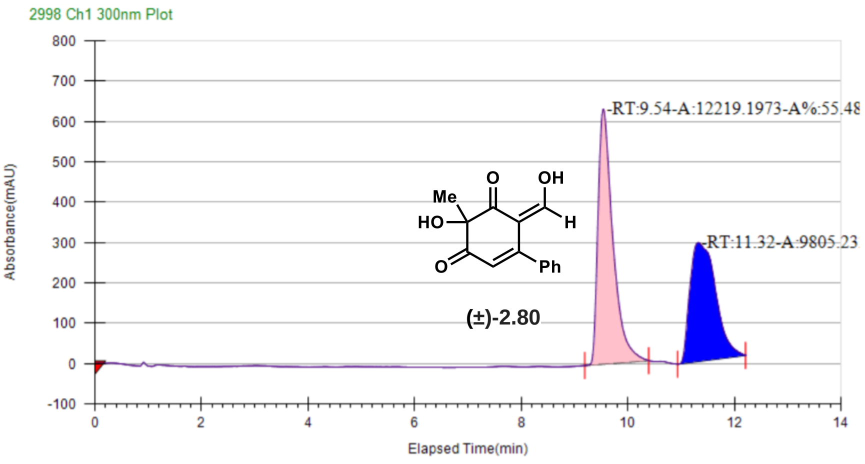

Run Information

Instrument Method	Inj. Vol.	Solvent	Column	Sample	Well Location	Temp.	Flow	% Modifier	Pressure
AD-H_8%	5	iPrOH	AD-H Chiral Analytical	sbdIV-116_8%	11A	40	3.5	8	120

Peak Information

Peak No	% Area	Area	Ret. Time	Height	Cap. Factor
1	55.4802	12219.1973	9.54 min	632.3805	9540.6667
2	44.5198	9805.233	11.32 min	295.027	11324

2.80 from AzaH reaction

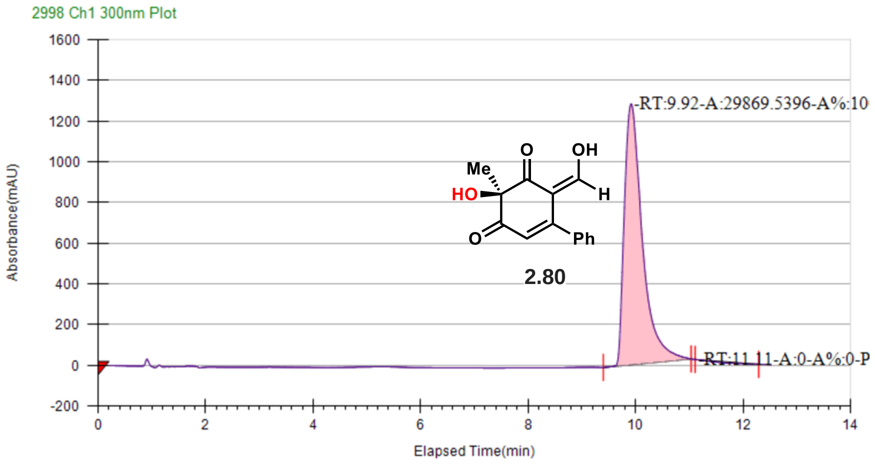

Run Information

Instrument Method	Inj. Vol.	Solvent	Column	Sample	Well Location	Temp.	Flow	% Modifier	Pressure
AD-H_8%	10	iPrOH	AD-H Chiral Analytical	sbdIV-134_8%	12A	40	3.5	8	120

Peak Information

Peak No	% Area	Area	Ret. Time	Height	Cap. Factor
1	100	29869.5396	9.92 min	1282.7466	9915.6667
2	0	0	11.11 min	0	11107.3333

Racemic standard

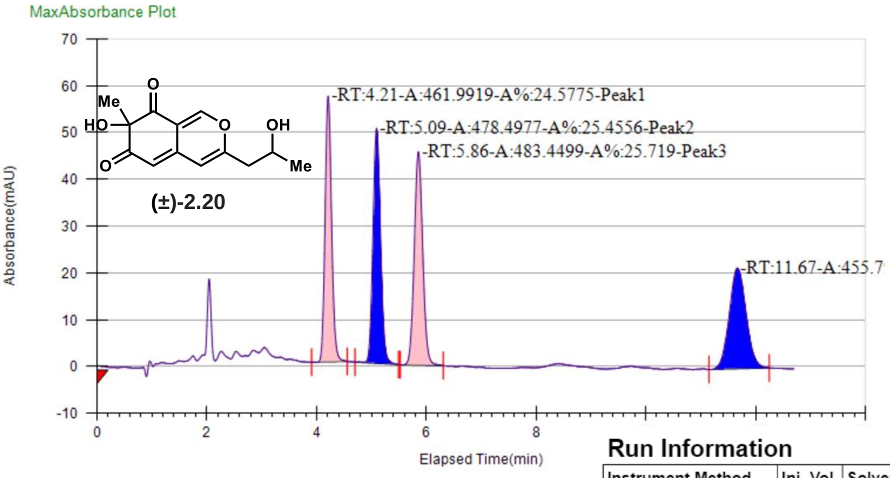

Run Information

Instrument Method	Inj. Vol.	Solvent	Column	Sample
AD-H_30%_300-330	5	iPrOH	AD-H Chiral Analytical	sbdIV-087

Peak Information

Peak No	% Area	Area	Ret. Time	Height
1	24.5775	461.9919	4.21 min	56.8468
2	25.4556	478.4977	5.09 min	50.282
3	25.719	483.4499	5.86 min	45.5769
4	24.248	455.798	11.67 min	21.5286

2.20 from AzaH reaction

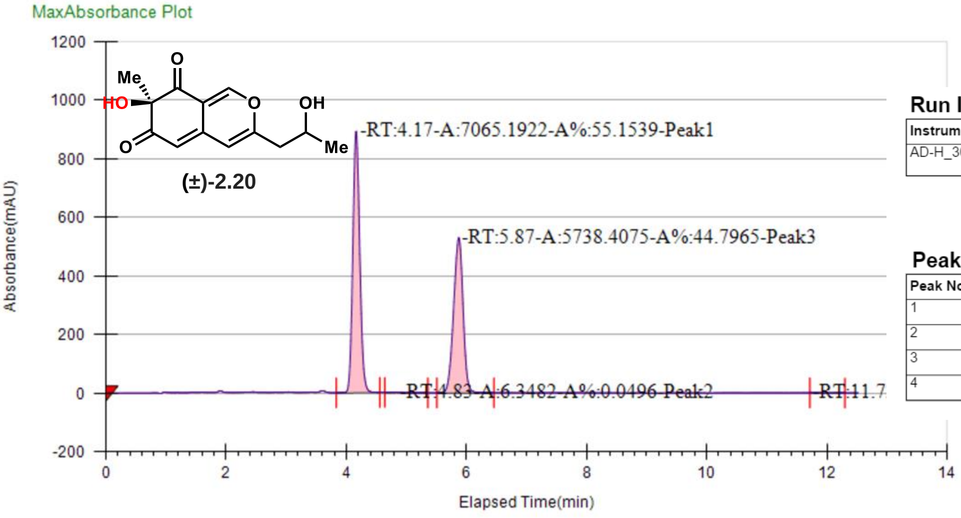

Run Information

Instrument Method	Inj. Vol.	Solvent	Column	Sample	W
AD-H_30%_300-330	5	iPrOH	AD-H Chiral Analytical	sbdIV-090	13

Peak Information

Peak No	% Area	Area	Ret. Time	Height	Ca
1	55.1539	7065.1922	4.17 min	892.6999	0
2	0.0496	6.3482	4.83 min	0.8265	0
3	44.7965	5738.4075	5.87 min	530.3277	0
4	2.1E-07	2.7E-05	11.72 min	4.1E-05	0

Figure 2.70: PDA traces of racemic **2.20** obtained from IBX oxidative dearomatization, and **2.20** obtained from AzaH-mediated oxidative dearomatization (CHIRALPAK® AD-H, 30% iPrOH, CO2, 3.5 mL/min). Note two pairs of diastereomers were formed from the IBX dearomatization of ±**2.18**.

Racemic standard

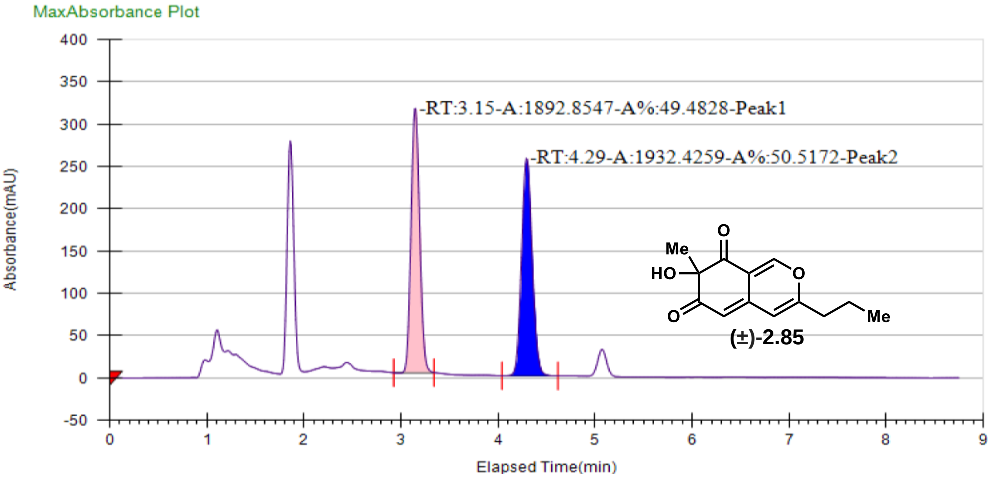

Run Information

Instrument Method	Inj. Vol.	Solvent	Column	Sample	Well Location	Temp.	Flow	% Modifier	Pressure
AD-H_30%	5	iPrOH	AD-H Chiral Analytical	sbdIV-087_30%	12A	40	3.5	30	120

Peak Information

Peak No	% Area	Area	Ret. Time	Height	Cap. Factor
1	49.4828	1892.8547	3.15 min	312.2806	3148.9667
2	50.5172	1932.4259	4.29 min	257.0694	4290.6167

2.85 from AzaH reaction

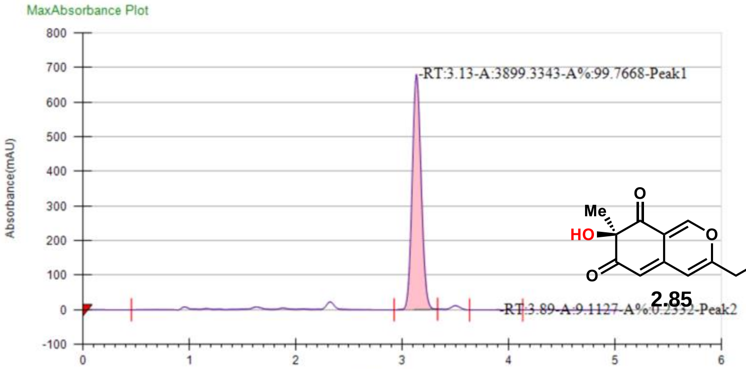

Run Information

Instrument Method	Inj. Vol.	Solvent	Column	Sample	Well Location	Temp.	Flow	% Modifier	Pressure
AD-H_30%	2	iPrOH	AD-H Chiral Analytical	sbdIV-89_ADH	11B	40	3.5	30	120

Peak Information

Peak No	% Area	Area	Ret. Time	Height	Cap. Factor
1	99.7668	3899.3343	3.13 min	679.6491	0
2	0.2332	9.1127	3.89 min	0.5864	0

Racemic standard

Racemic standard

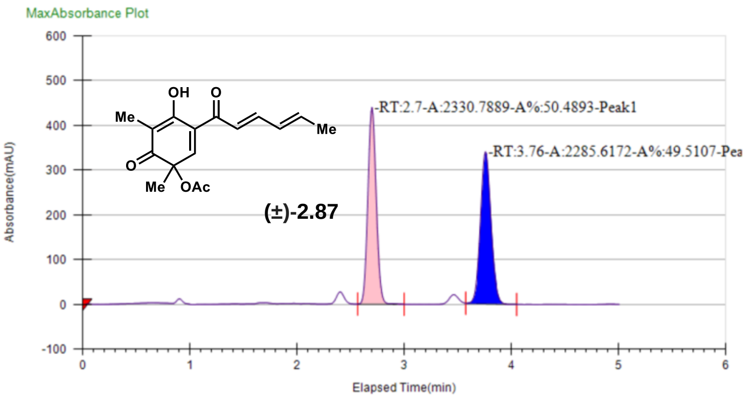

Run Information

Instrument Method	Inj. Vol.	Solvent	Column	Sample	Well Location	Temp.	Flow	% Modifier	Pressure
AD-H_10%	1	iPrOH	AD-H Chiral Analytical	sbdIV-096_ADH	13A	40	3.5	10	120

Peak Information

Peak No	% Area	Area	Ret. Time	Height	Cap. Factor
1	50.4893	2330.7889	2.7 min	439.8615	2698.9667
2	49.5107	2285.6172	3.76 min	339.9273	3757.2833

2.87 from SorbC reaction

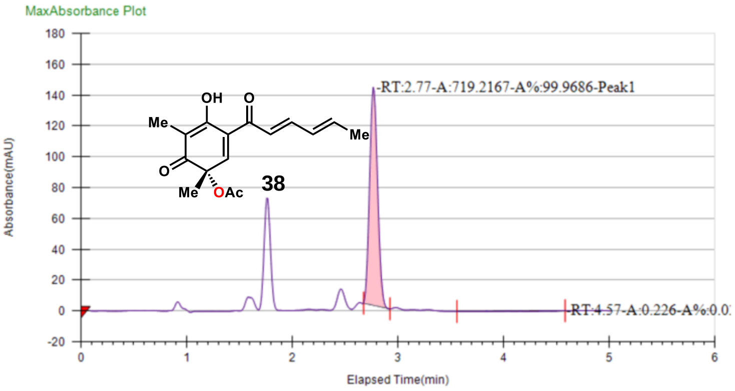

Run Information

Instrument Method	Inj. Vol.	Solvent	Column	Sample	Well Location	Temp.	Flow	% Modifier	Pressure
AD-H_10%	1	iPrOH	AD-H Chiral Analytical	sbdIV-097_ADH	14A	40	3.5	10	120

Peak Information

Peak No	% Area	Area	Ret. Time	Height	Cap. Factor
1	99.9686	719.2167	2.77 min	141.3126	2765.6333
2	0.0314	0.226	4.57 min	0.0412	4573.9333

Racemic standard

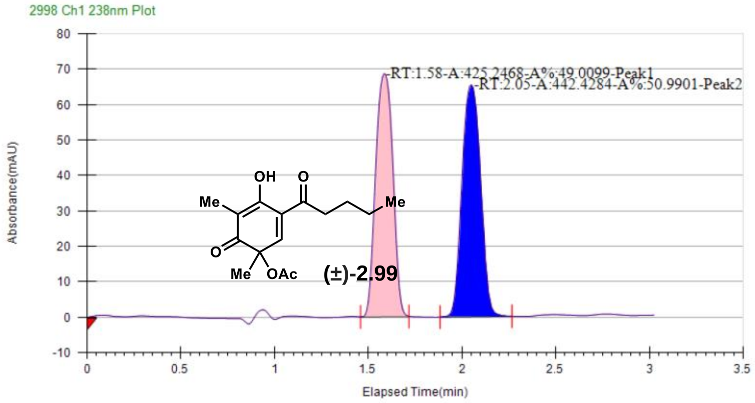

Run Information

Instrument Method	Inj. Vol.	Solvent	Column	Sample	Well Location	Temp.	Flow	% Modifier	Pressure
Jim	10	iPrOH	AD-H Chiral Analytical	sbd-III-198	11B	40	3.5	10	100

Peak Information

Peak No	% Area	Area	Ret. Time	Height	Cap. Factor
1	49.0099	425.2468	1.58 min	68.6443	1582.3333
2	50.9901	442.4284	2.05 min	65.5046	2049

2.99 from SorbC reaction

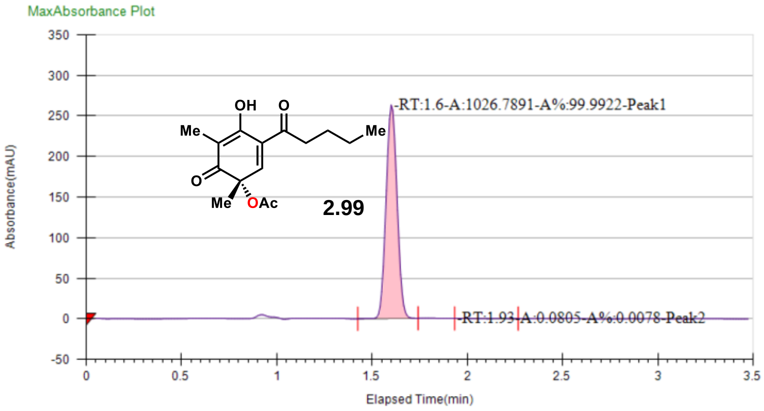

Run Information

Instrument Method	Inj. Vol.	Solvent	Column	Sample	Well Location	Temp.	Flow	% Modifier	Pressure
AD-H_10%	10	iPrOH	AD-H Chiral Analytical	sbdIII-057_ADH	14A	40	3.5	10	120

Peak Information

Peak No	% Area	Area	Ret. Time	Height	Cap. Factor
1	100	445.1886	1.61 min	94.8111	1607.3167
2	0	0	1.8 min	0	1798.9833

Racemic standard

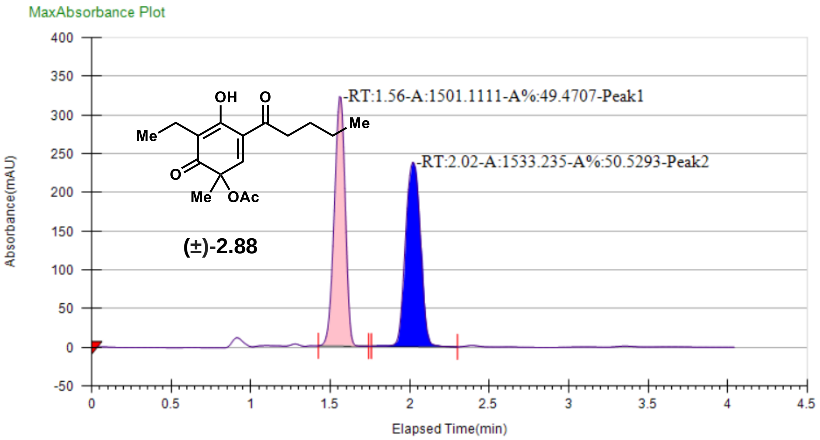

Run Information

Instrument Method	Inj. Vol.	Solvent	Column	Sample	Well Location	Temp.	Flow	% Modifier	Pressure
AD-H_10%	10	iPrOH	AD-H Chiral Analytical	sbdIV-003_ADH	15A	40	3.5	10	120

Peak Information

Peak No	% Area	Area	Ret. Time	Height	Cap. Factor
1	49.4707	1501.1111	1.56 min	321.7827	1557.3167
2	50.5293	1533.235	2.02 min	237.5026	2015.65

2.88 from SorbC reaction

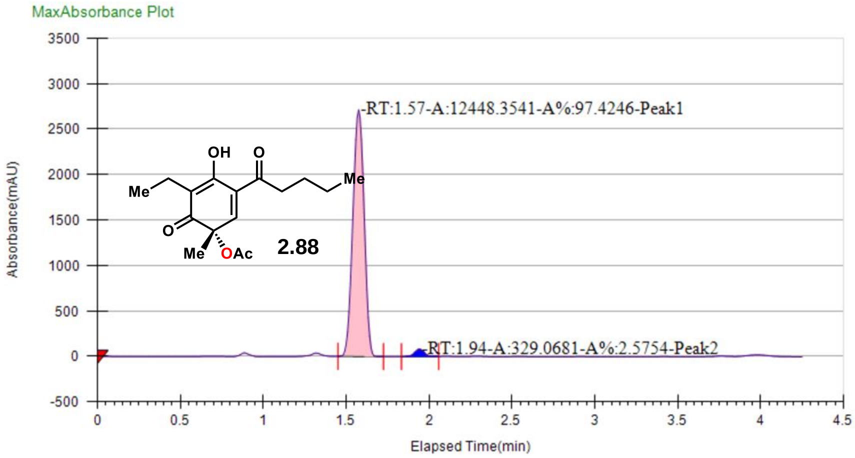

Run Information

Instrument Method	Inj. Vol.	Solvent	Column	Sample	Well Location	Temp.	Flow	% Modifier	Pressure
AD-H_10%	5	iPrOH	AD-H Chiral Analytical	sbdIV-096_ADH	12A	40	3.5	10	120

Peak Information

Peak No	% Area	Area	Ret. Time	Height	Cap. Factor
1	97.4246	12448.3541	1.57 min	2716.7156	1573.9833
2	2.5754	329.0681	1.94 min	82.1367	1940.65

Racemic standard

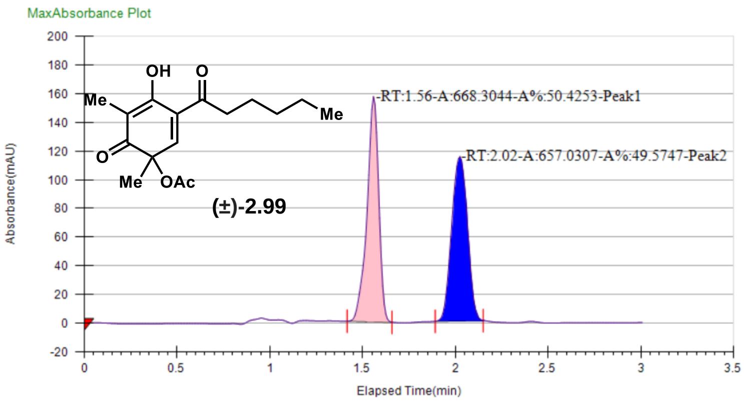

Run Information

Instrument Method	Inj. Vol.	Solvent	Column	Sample	Well Location	Temp.	Flow	% Modifier	Pressure
Jim	10	iPrOH	AD-H Chiral Analytical	198	11A	40	3.5	10	120

Peak Information

Peak No	% Area	Area	Ret. Time	Height	Cap. Factor
1	50.4253	668.3044	1.56 min	157.0425	1557.3167
2	49.5747	657.0307	2.02 min	114.6003	2023.9833

2.98 from SorbC reaction

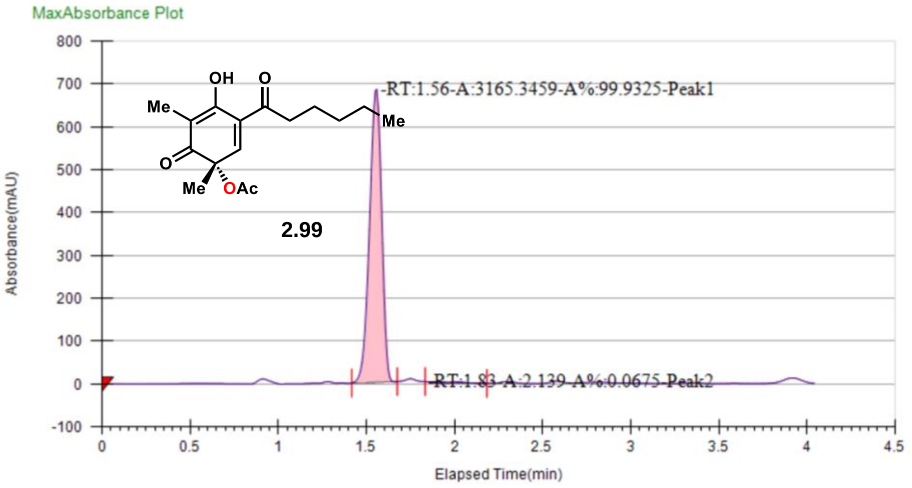

Run Information

Instrument Method	Inj. Vol.	Solvent	Column	Sample	Well Location	Temp.	Flow	% Modifier	Pressure
AD-H_10%	10	iPrOH	AD-H Chiral Analytical	sbdIV-034_ADH	16A	40	3.5	10	120

Peak Information

Peak No	% Area	Area	Ret. Time	Height	Cap. Factor
1	99.9325	3165.3459	1.56 min	683.6869	1557.3167
2	0.0675	2.139	1.83 min	0.8753	1832.3167

Racemic standard

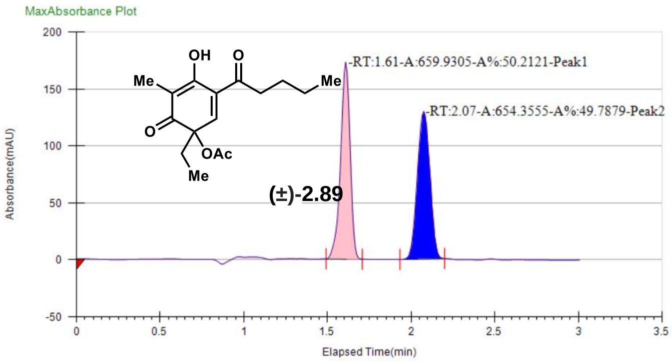

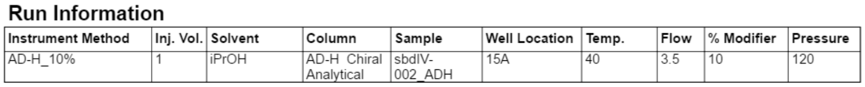

Run Information

Instrument Method	Inj. Vol.	Solvent	Column	Sample	Well Location	Temp.	Flow	% Modifier	Pressure
AD-H_10%	1	iPrOH	AD-H Chiral Analytical	sbdIV-002_ADH	15A	40	3.5	10	120

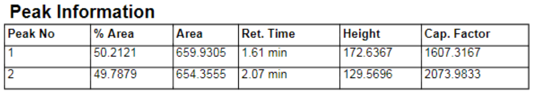

Peak Information

Peak No	% Area	Area	Ret. Time	Height	Cap. Factor
1	50.2121	659.9305	1.61 min	172.6367	1607.3167
2	49.7879	654.3555	2.07 min	129.5696	2073.9833

2.89 from SorbC reaction

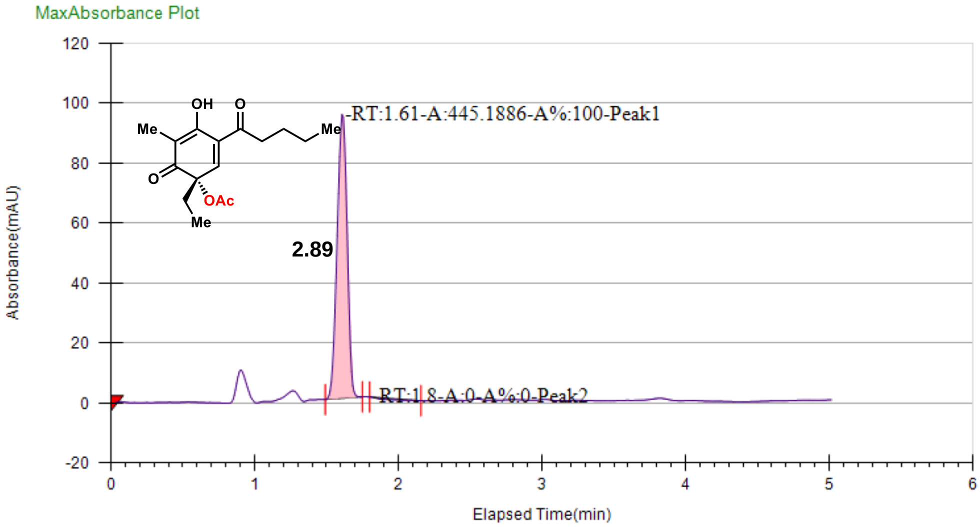

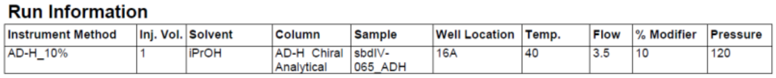

Run Information

Instrument Method	Inj. Vol.	Solvent	Column	Sample	Well Location	Temp.	Flow	% Modifier	Pressure
AD-H_10%	1	iPrOH	AD-H Chiral Analytical	sbdIV-065_ADH	16A	40	3.5	10	120

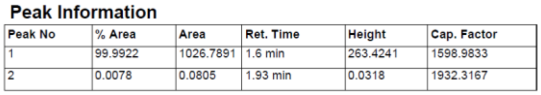

Peak Information

Peak No	% Area	Area	Ret. Time	Height	Cap. Factor
1	99.9922	1026.7891	1.6 min	263.4241	1598.9833
2	0.0078	0.0805	1.93 min	0.0318	1932.3167

Figure 2.75: PDA traces of racemic **2.89** obtained from LTA oxidative dearomatization, and **2.89** (>99% ee) obtained from SorbC-mediated oxidative dearomatization (CHIRALPAK® AD-H, 10% *i*PrOH, CO_2, 3.5 mL/min).

Racemic standard

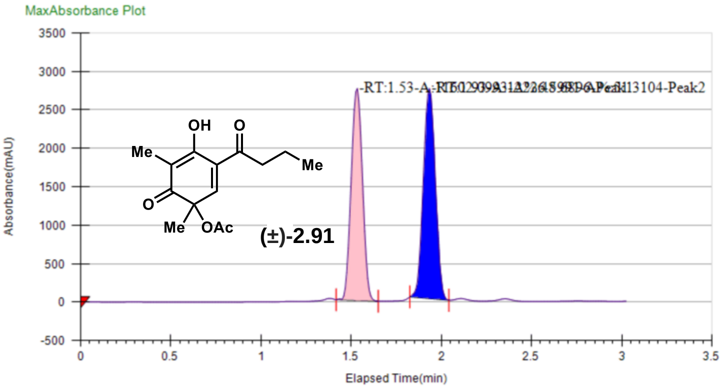

(±)-2.91

Run Information

Instrument Method	Inj. Vol.	Solvent	Column	Sample	Well Location	Temp.	Flow	% Modifier	Pressure
AD-H_9.5%	2	iPrOH	AD-H Chiral Analytical	sbdIV-102_ADH	14A	40	3.5	9.5	120

Peak Information

Peak No	% Area	Area	Ret. Time	Height	Cap. Factor
1	48.6896	11602.0993	1.53 min	2757.7154	0
2	51.3104	12226.5991	1.93 min	2731.7356	0

2.91 from SorbC reaction

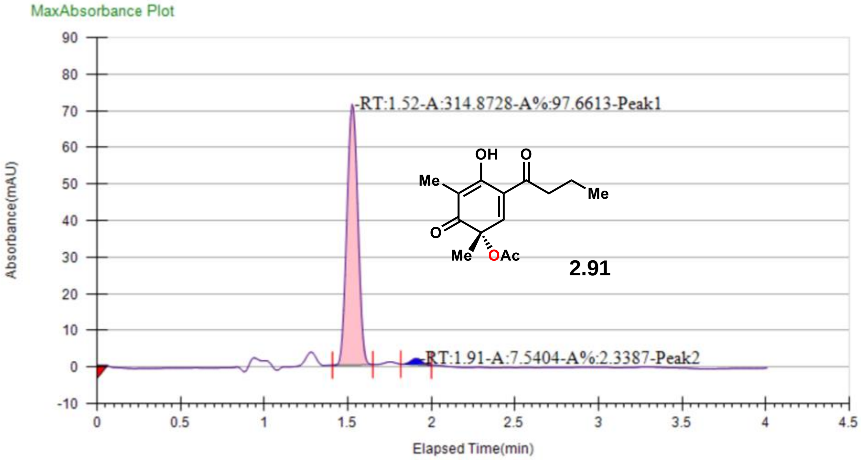

2.91

Run Information

Instrument Method	Inj. Vol.	Solvent	Column	Sample	Well Location	Temp.	Flow	% Modifier	Pressure
AD-H_9.5%	2	iPrOH	AD-H Chiral Analytical	sbdIV-101_ADH	13A	40	3.5	9.5	120

Peak Information

Peak No	% Area	Area	Ret. Time	Height	Cap. Factor
1	97.6613	314.8728	1.52 min	71.1886	0
2	2.3387	7.5404	1.91 min	1.7274	0

Chapter 2.6.7: NMR Spectra of Synthetic Compounds

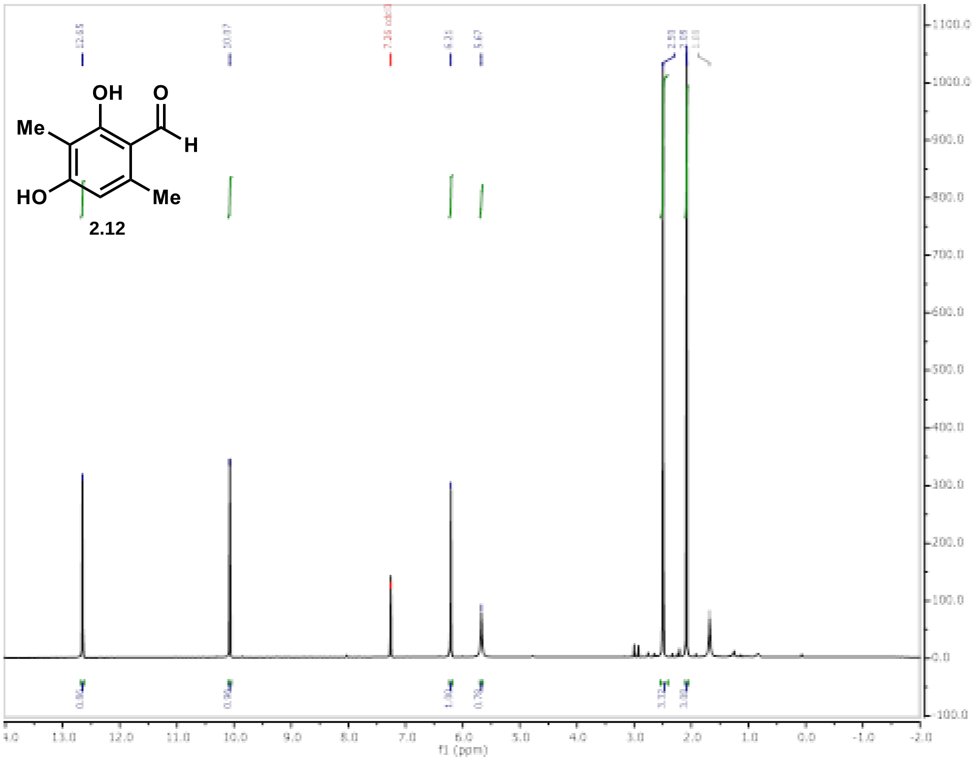

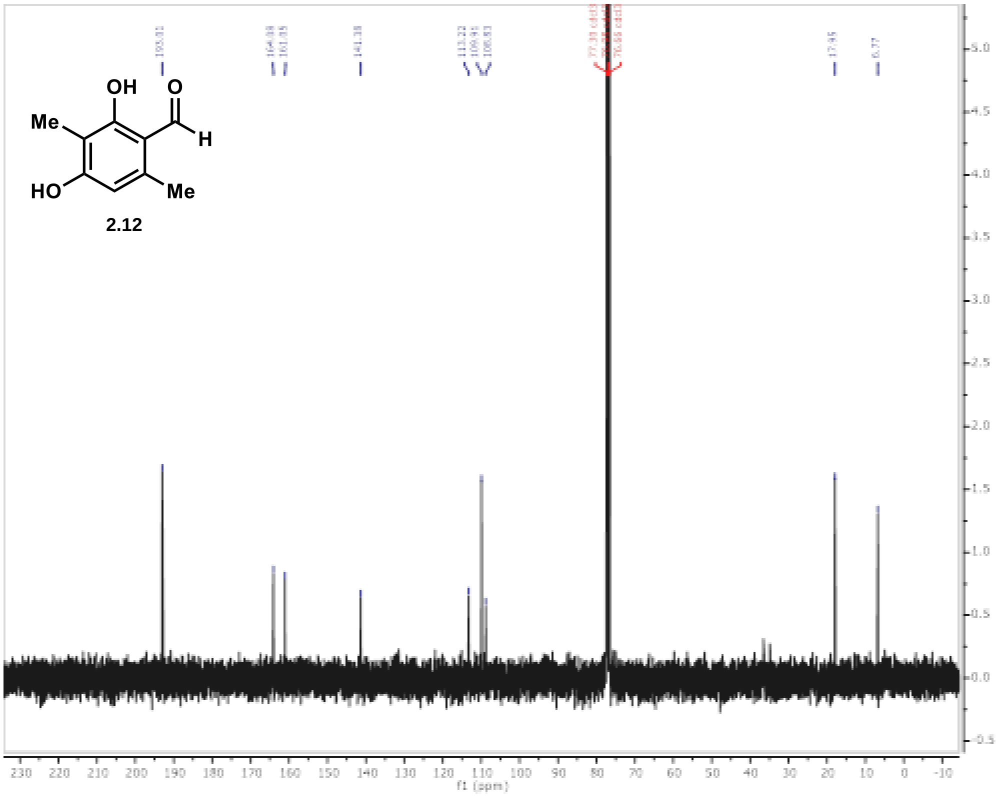

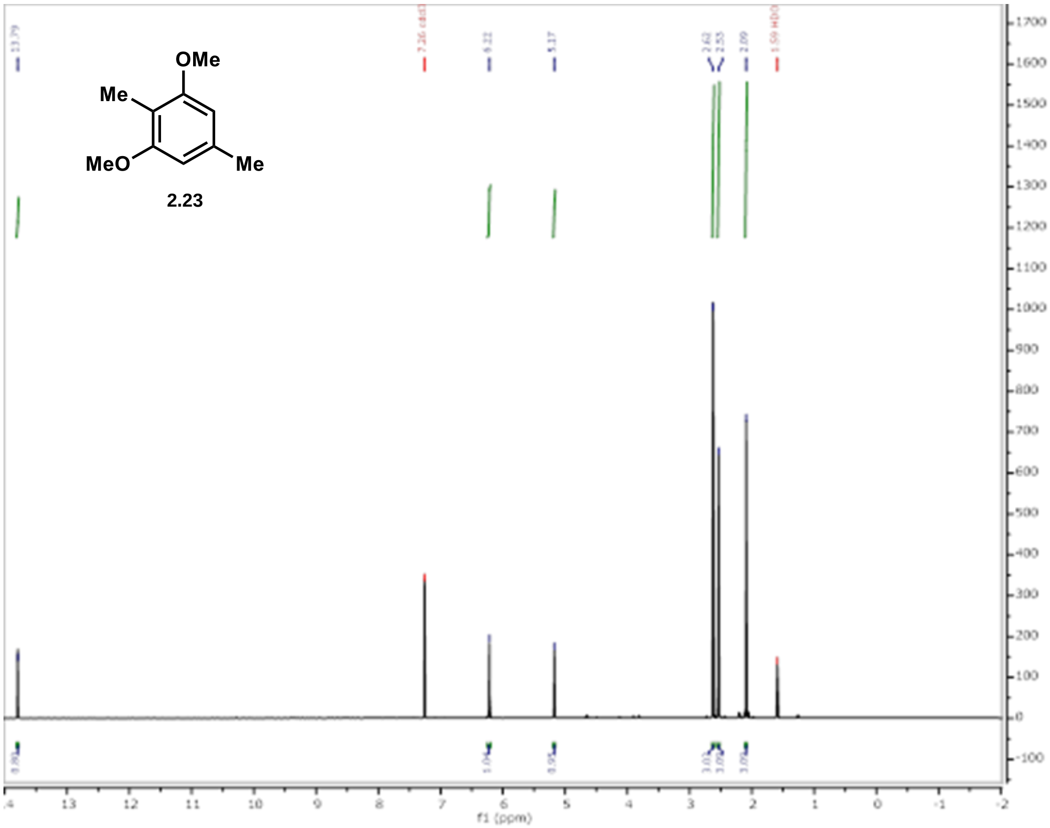
2.23

13.79
7.26 cdcl3
6.22
5.17
2.62
2.55
2.09
1.59 H2O
OMe
Me
MeO
Me
0.80
1.04
0.95
3.01
3.02
3.09
1700
1600
1500
1400
1300
1200
1100
1000
900
800
700
600
500
400
300
200
100
0
-100
14
13
12
11
10
9
8
7
6
5
4
3
2
1
0
-1
-2
f1 (ppm)

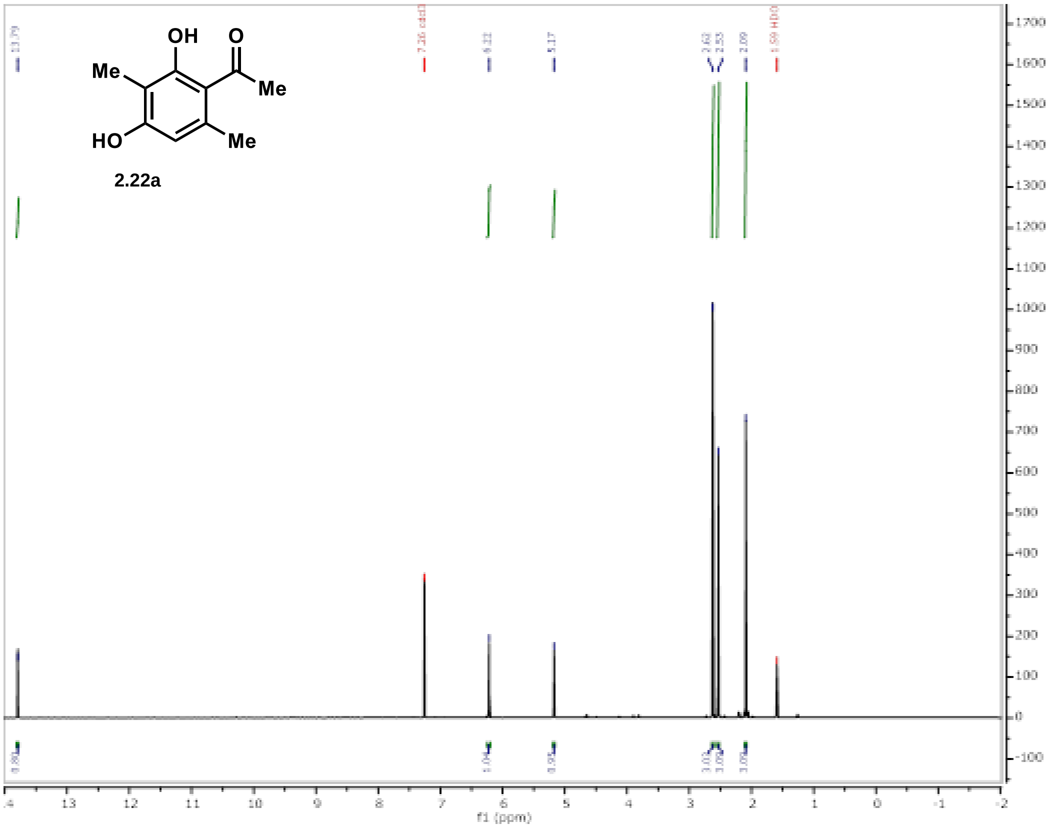
OH
O
Me
Me
HO
Me
2.22a
13.79
7.26 cdcl3
6.22
5.17
2.62
2.53
2.09
1.59 HDO
0.80
1.04
0.95
3.03
3.05
3.09
f1 (ppm)

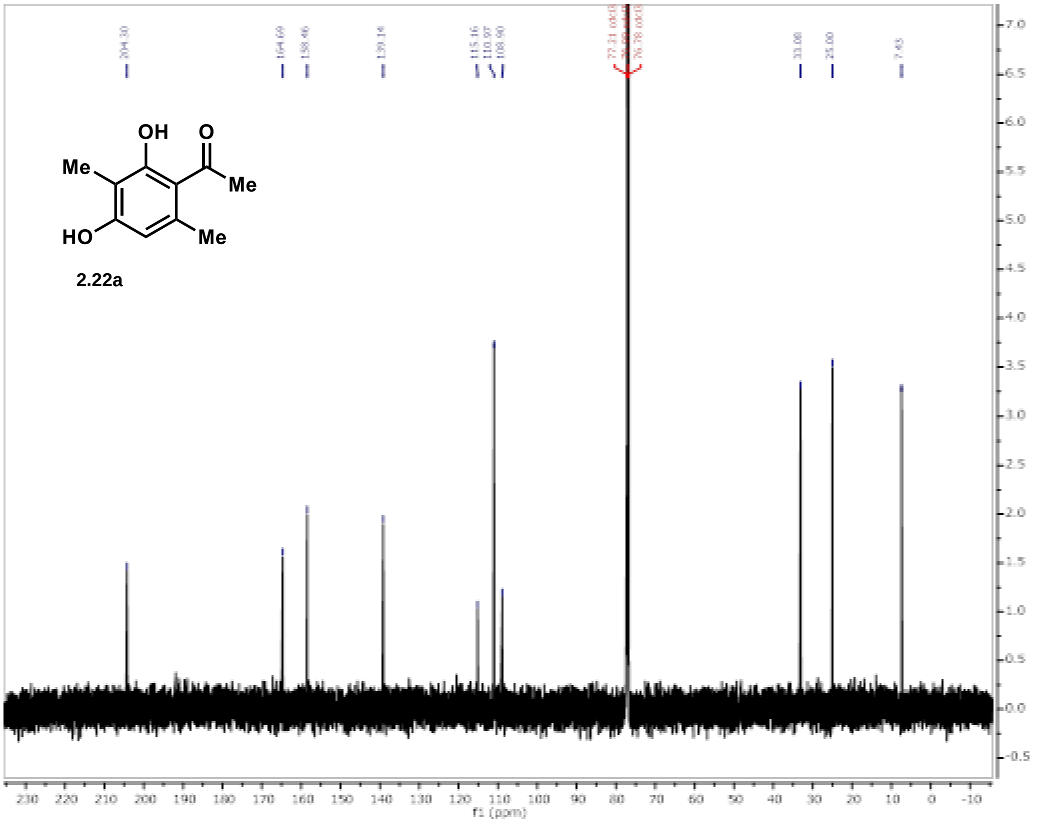
OH
O
Me
Me
HO
Me
2.22a
204.30
164.69
158.46
139.14
115.16
110.97
108.90
77.21 cdcl3
77.00 cdcl3
76.78 cdcl3
33.08
25.00
7.43
f1 (ppm)

.

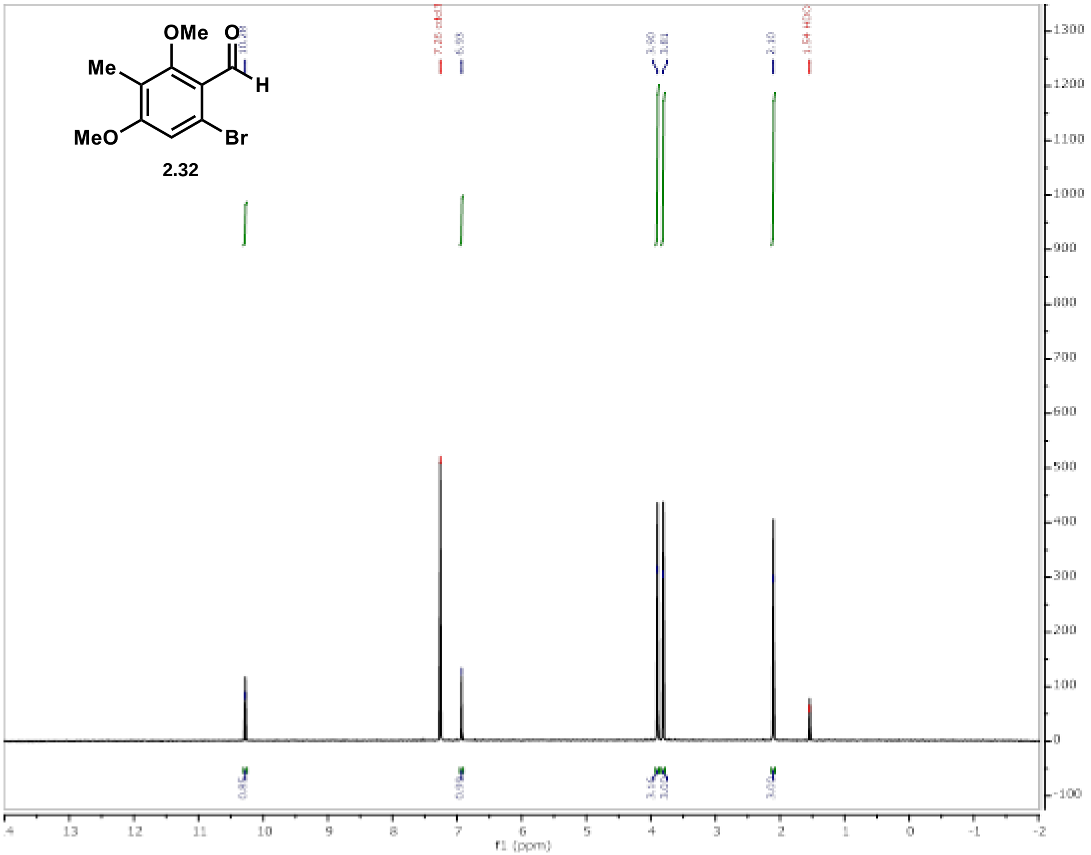
2.32
OMe
O
Me
H
MeO
Br
7.26 cdcl3
6.93
3.90
3.81
2.10
f1 (ppm)
14
13
12
11
10
9
8
7
6
5
4
3
2
1
0
-1
-2
1300
1200
1100
1000
900
800
700
600
500
400
300
200
100
0
-100

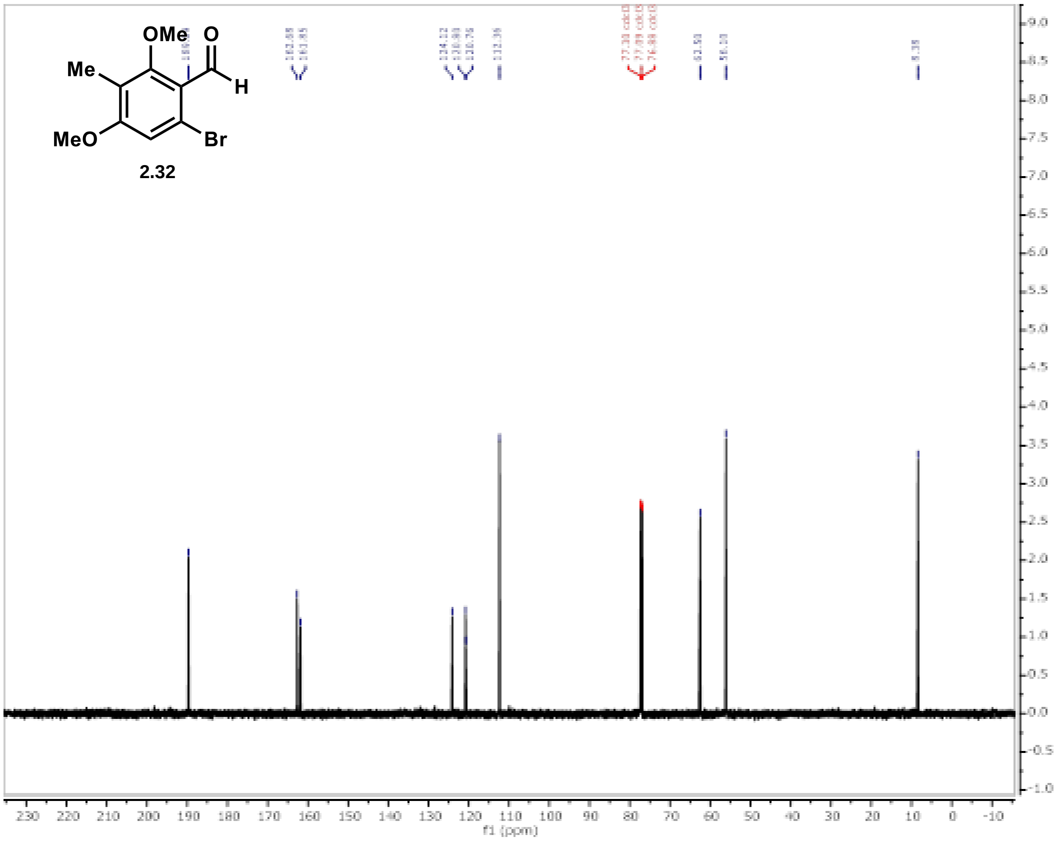
2.32
OMe
O
Me
H
MeO
Br
f1 (ppm)
230
220
210
200
190
180
170
160
150
140
130
120
110
100
90
80
70
60
50
40
30
20
10
0
-10
9.0
8.5
8.0
7.5
7.0
6.5
6.0
5.5
5.0
4.5
4.0
3.5
3.0
2.5
2.0
1.5
1.0
0.5
0.0
-0.5
-1.0

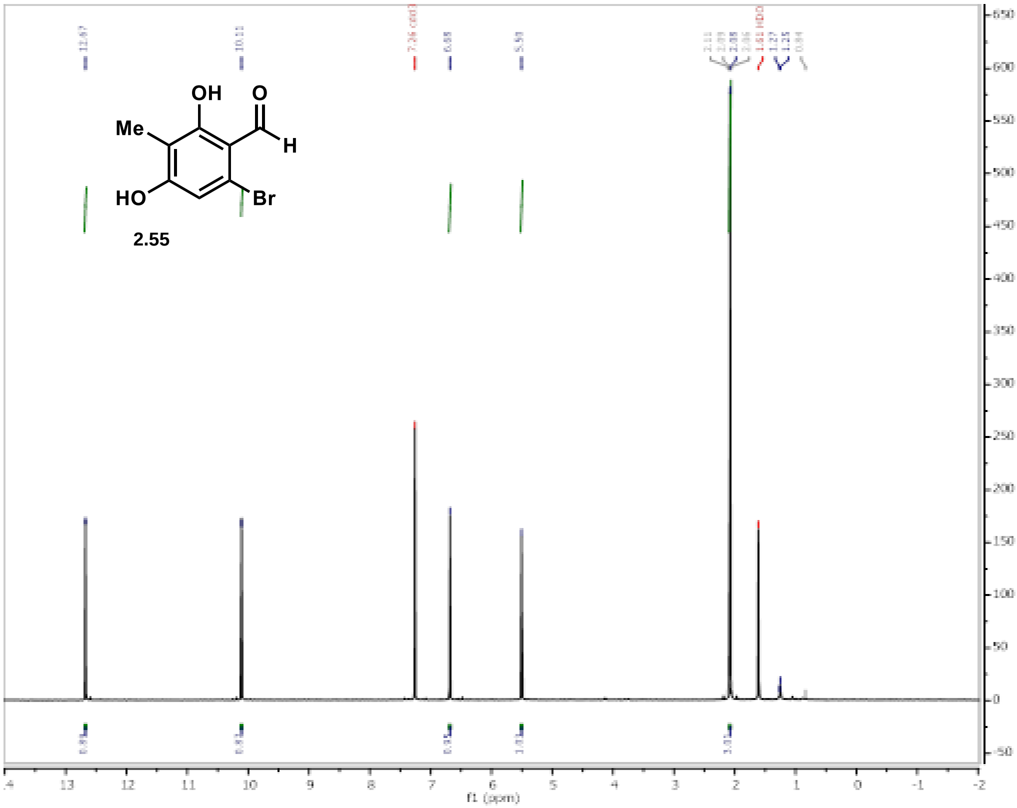
2.55

12.67
10.11
7.26 cdcl3
6.68
5.50
2.11
2.09
2.08
2.06
1.61 HDO
1.27
1.25
0.84
OH
O
Me
H
HO
Br
f1 (ppm)

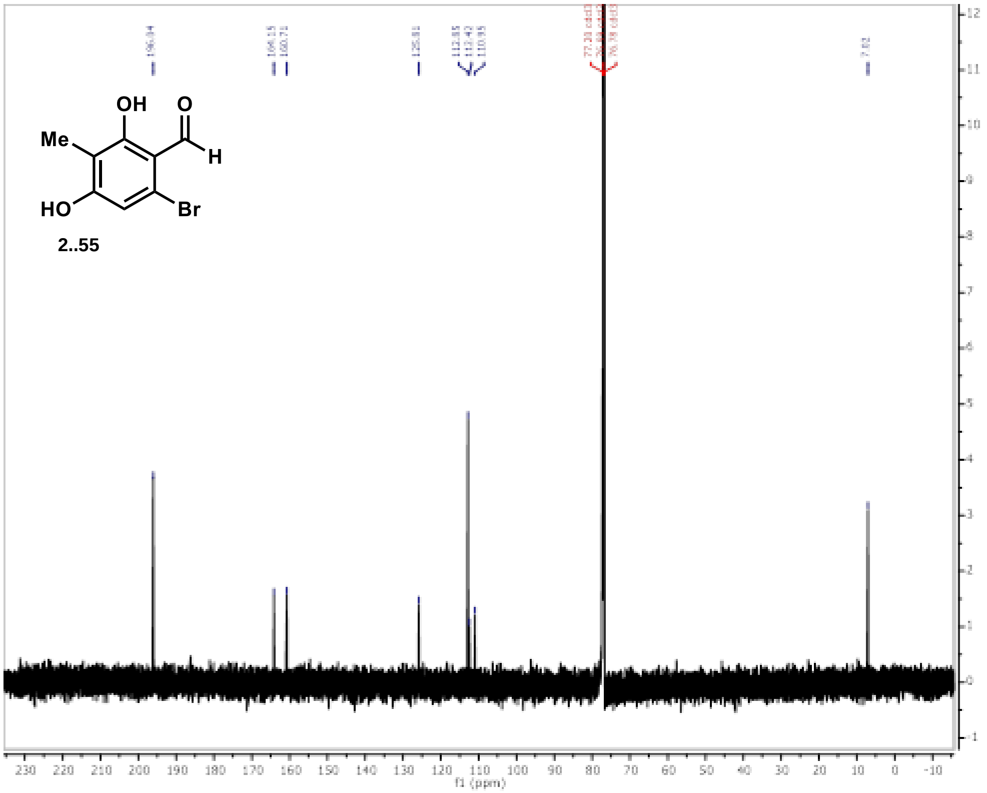
2..55

196.34
164.15
160.71
125.81
112.85
112.42
110.95
77.20 cdcl3
76.58 cdcl3
7.52
OH
O
Me
H
HO
Br
f1 (ppm)

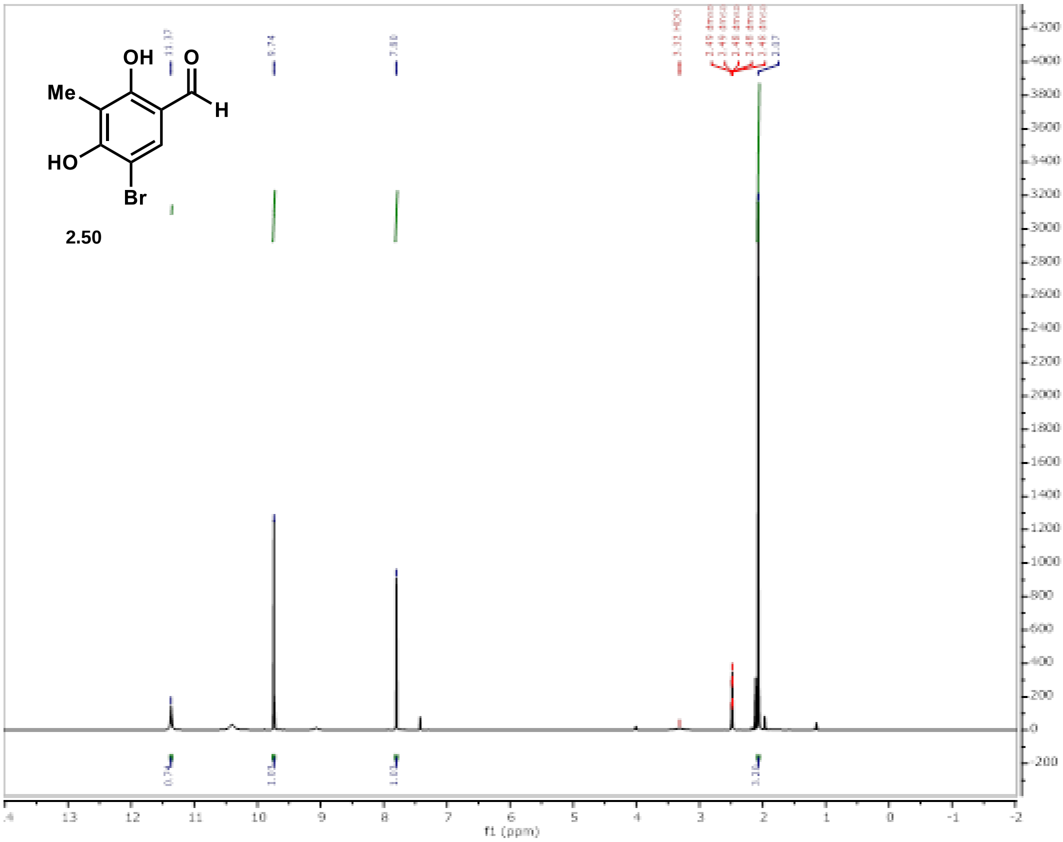

OH
O
Me
H
HO
Br
2.50
11.37
9.74
7.80
3.32 HDO
2.50 dmso
2.49 dmso
2.49 dmso
2.48 dmso
2.48 dmso
2.07
0.74
1.01
1.01
3.10
f1 (ppm)

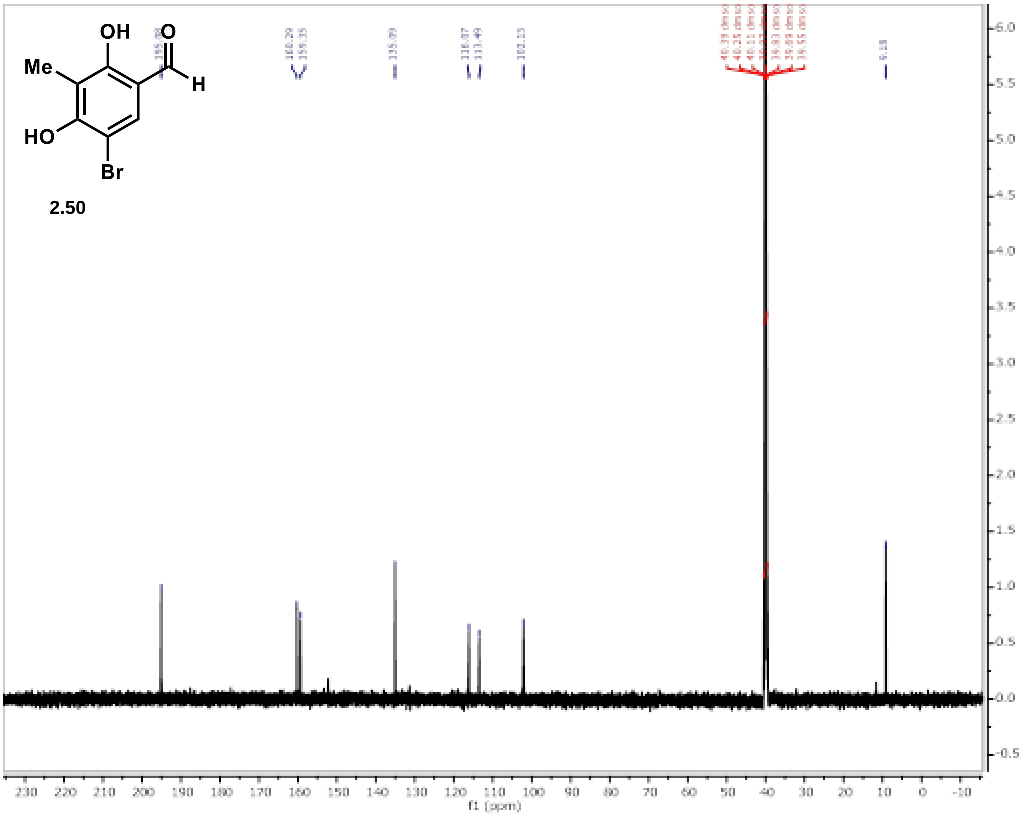

OH
O
Me
H
HO
Br
2.50
195.88
160.29
159.35
135.89
116.07
113.49
102.13
40.39 dmso
40.25 dmso
40.11 dmso
39.97 dmso
39.83 dmso
39.69 dmso
39.55 dmso
9.18
f1 (ppm)

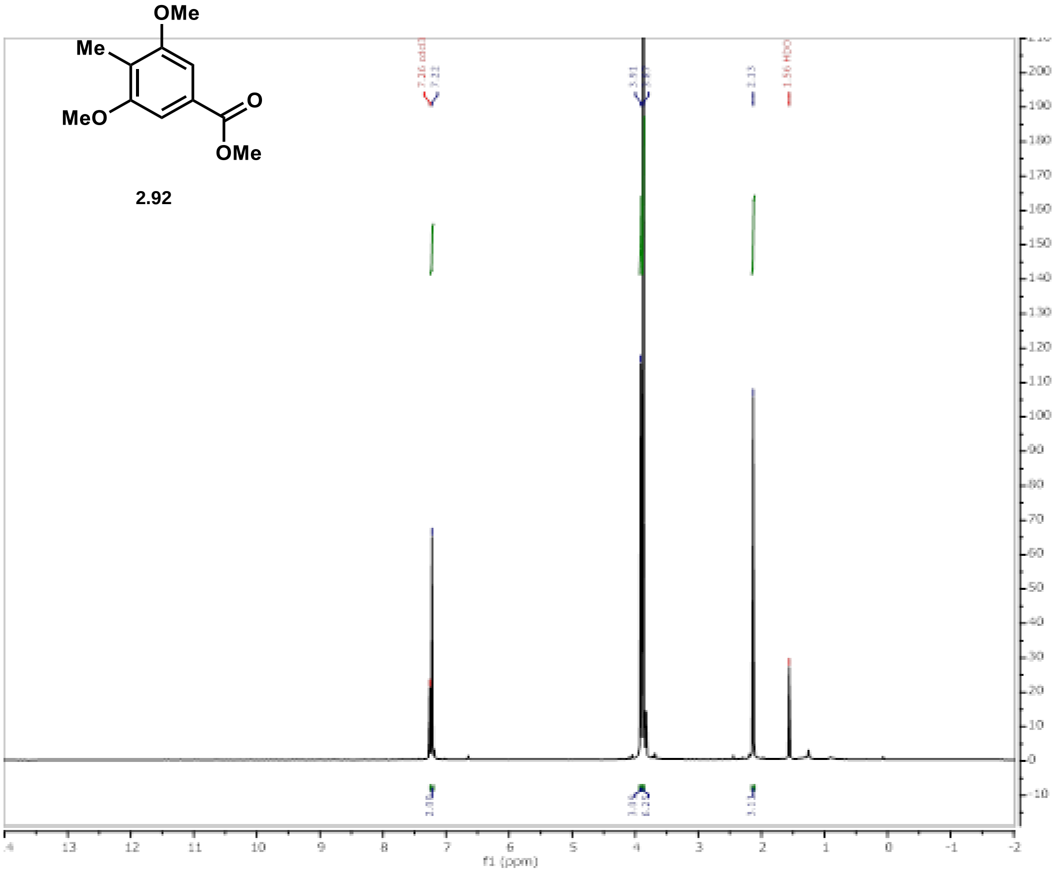

2.92

OMe
Me
MeO
O
OMe
7.26 cdcl3
7.21
3.91
3.87
2.13
1.56 H2O
2.00
3.05
6.22
3.11
14
13
12
11
10
9
8
7
6
5
4
3
2
1
0
-1
-2
f1 (ppm)
210
200
190
180
170
160
150
140
130
120
110
100
90
80
70
60
50
40
30
20
10
0
-10

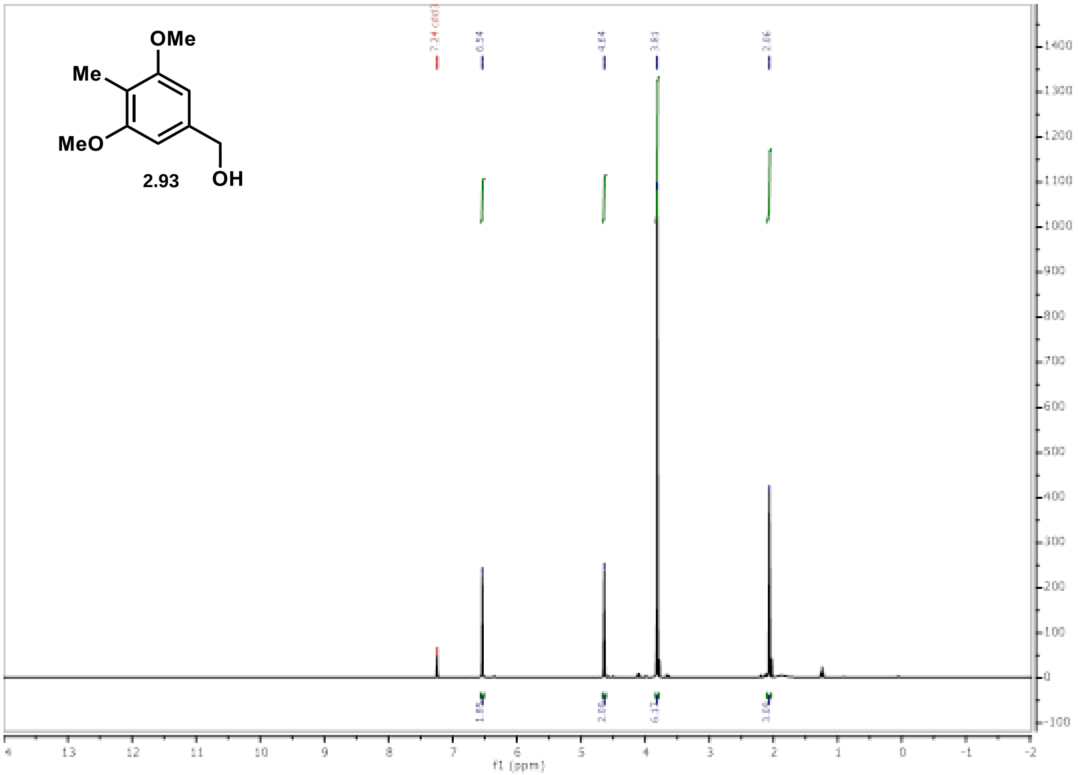
OMe
Me
MeO
OH
7.24 cdcl3
6.54
4.64
3.81
2.06
1.85
2.00
6.17
3.06
1400
1300
1200
1100
1000
900
800
700
600
500
400
300
200
100
0
-100
14
13
12
11
10
9
8
7
6
5
4
3
2
1
0
-1
-2
f1 (ppm)

2.93

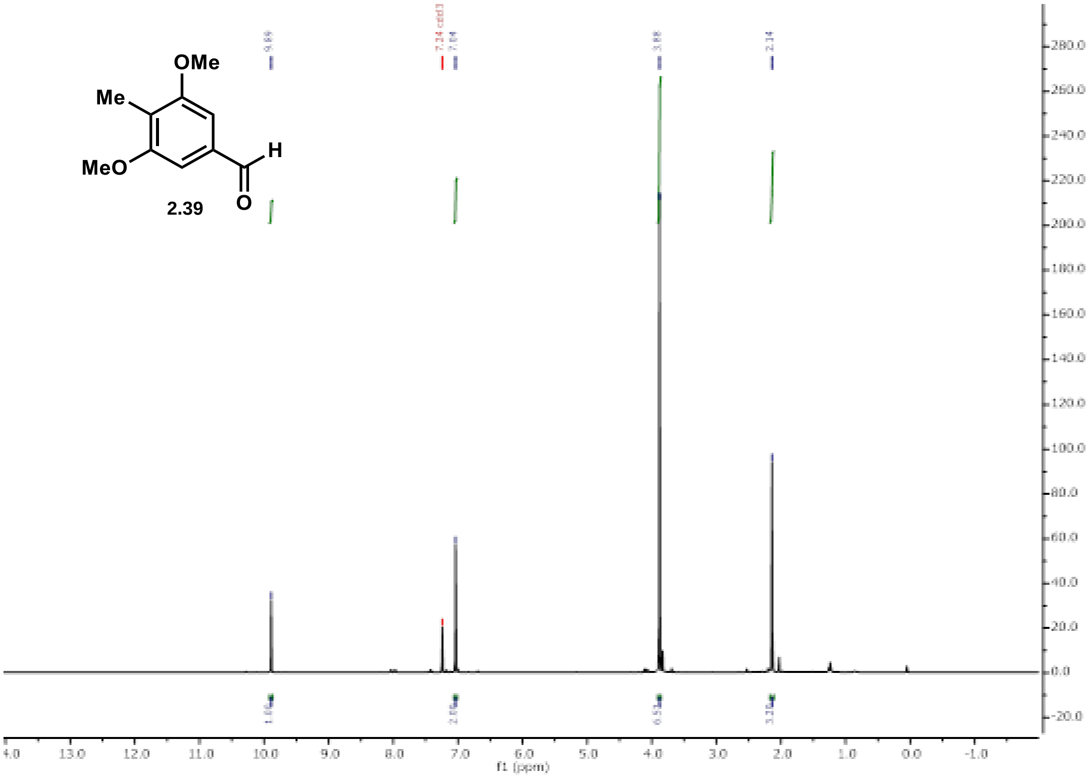
OMe
Me
MeO
H
O
9.89
7.24 cdcl3
7.04
3.88
2.14
1.00
2.00
6.51
3.21
280.0
260.0
240.0
220.0
200.0
180.0
160.0
140.0
120.0
100.0
80.0
60.0
40.0
20.0
0.0
-20.0
14.0
13.0
12.0
11.0
10.0
9.0
8.0
7.0
6.0
5.0
4.0
3.0
2.0
1.0
0.0
-1.0
f1 (ppm)

2.39

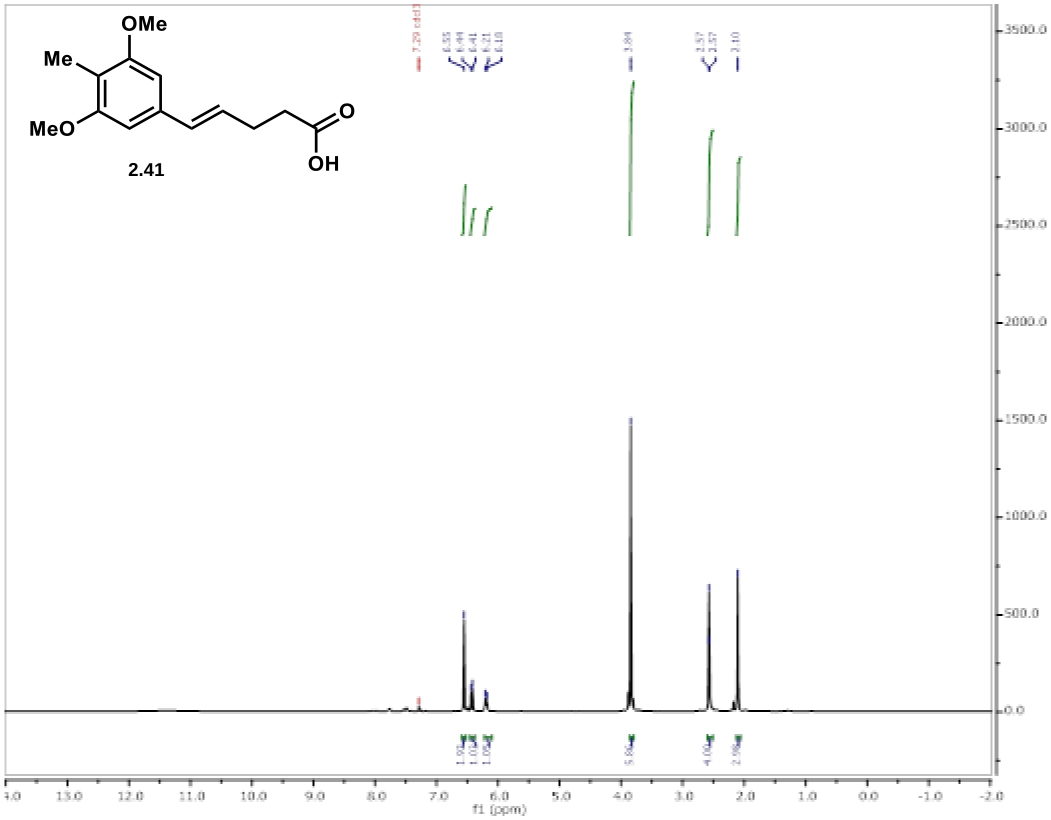
OMe
Me
MeO
O
OH
2.41
7.29 cdcl3
6.55
6.49
6.41
6.21
6.18
3.84
2.57
2.57
2.10
1.92
1.03
1.05
5.86
4.00
2.98
3500.0
3000.0
2500.0
2000.0
1500.0
1000.0
500.0
0.0
14.0
13.0
12.0
11.0
10.0
9.0
8.0
7.0
6.0
5.0
4.0
3.0
2.0
1.0
0.0
-1.0
-2.0
f1 (ppm)

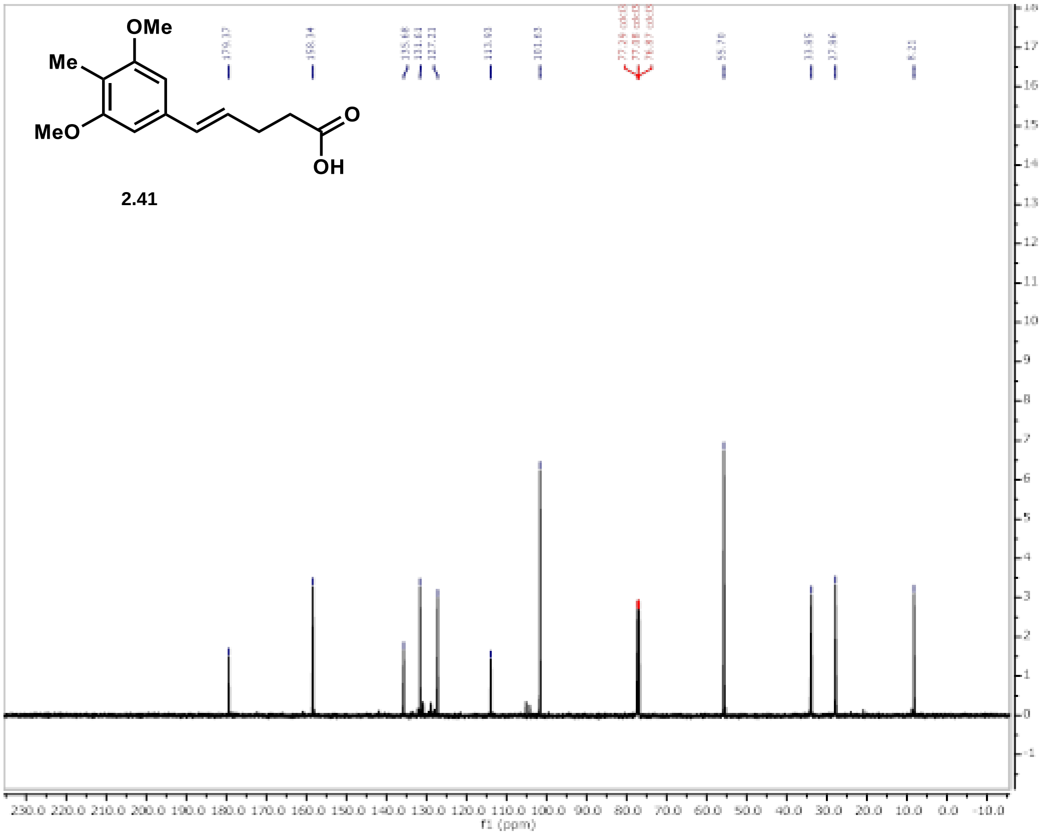
OMe
Me
MeO
O
OH
2.41
179.37
158.34
135.68
131.61
127.21
113.63
101.63
77.29 cdcl3
77.08 cdcl3
76.87 cdcl3
55.76
33.85
27.86
8.21
18
17
16
15
14
13
12
11
10
9
8
7
6
5
4
3
2
1
0
-1
230.0
220.0
210.0
200.0
190.0
180.0
170.0
160.0
150.0
140.0
130.0
120.0
110.0
100.0
90.0
80.0
70.0
60.0
50.0
40.0
30.0
20.0
10.0
0.0
-10.0
f1 (ppm)

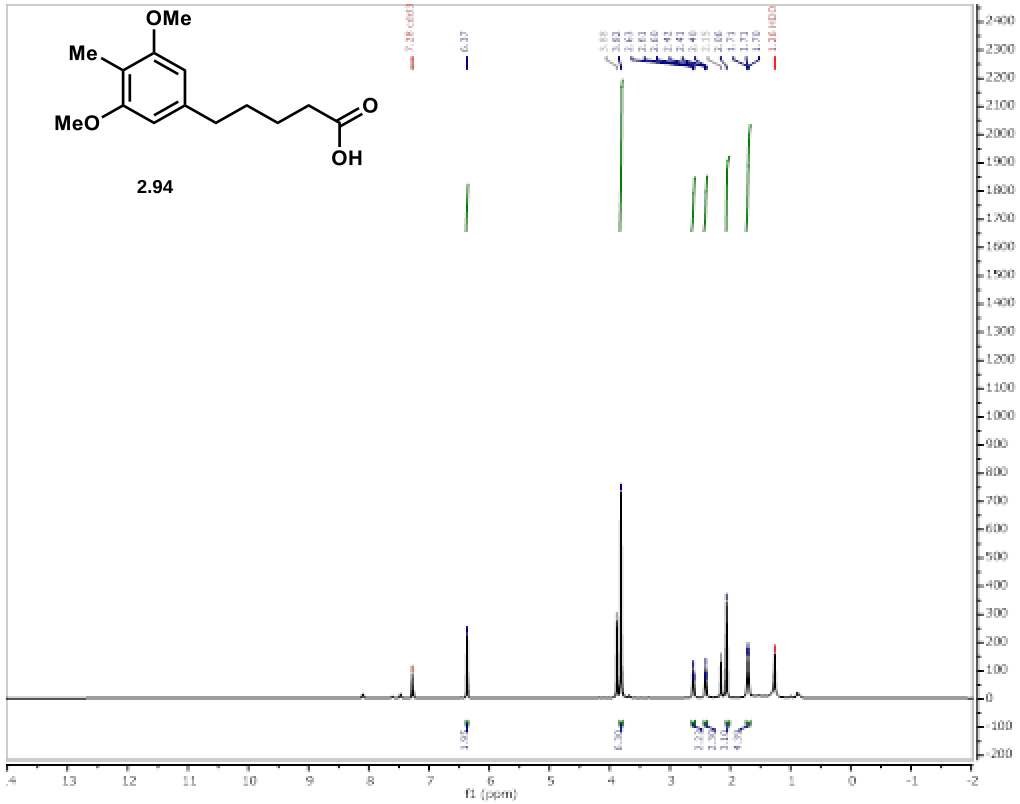
OMe
Me
MeO
O
OH
2.94
7.28 cdcl3
6.37
3.88
3.82
1.26 HDO
1.93
6.30
f1 (ppm)

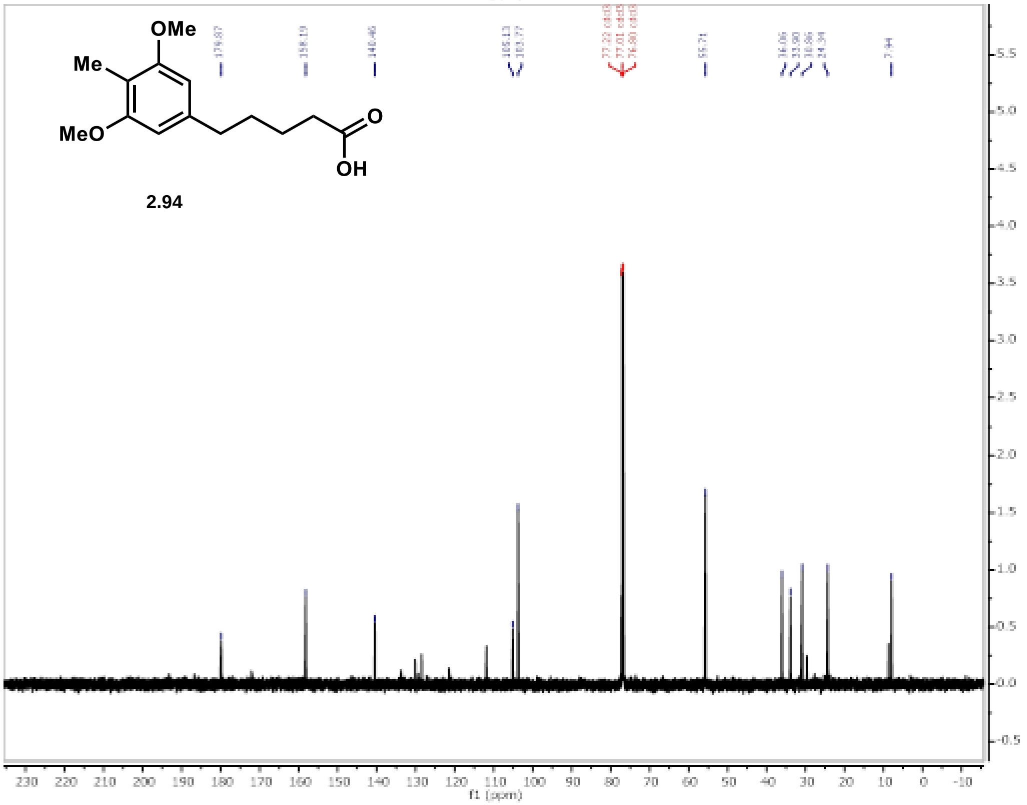
OMe
Me
MeO
O
OH
2.94
179.87
158.19
140.46
105.13
103.77
77.22 cdcl3
77.01 cdcl3
76.80 cdcl3
55.71
36.06
33.90
30.86
24.39
7.94
f1 (ppm)

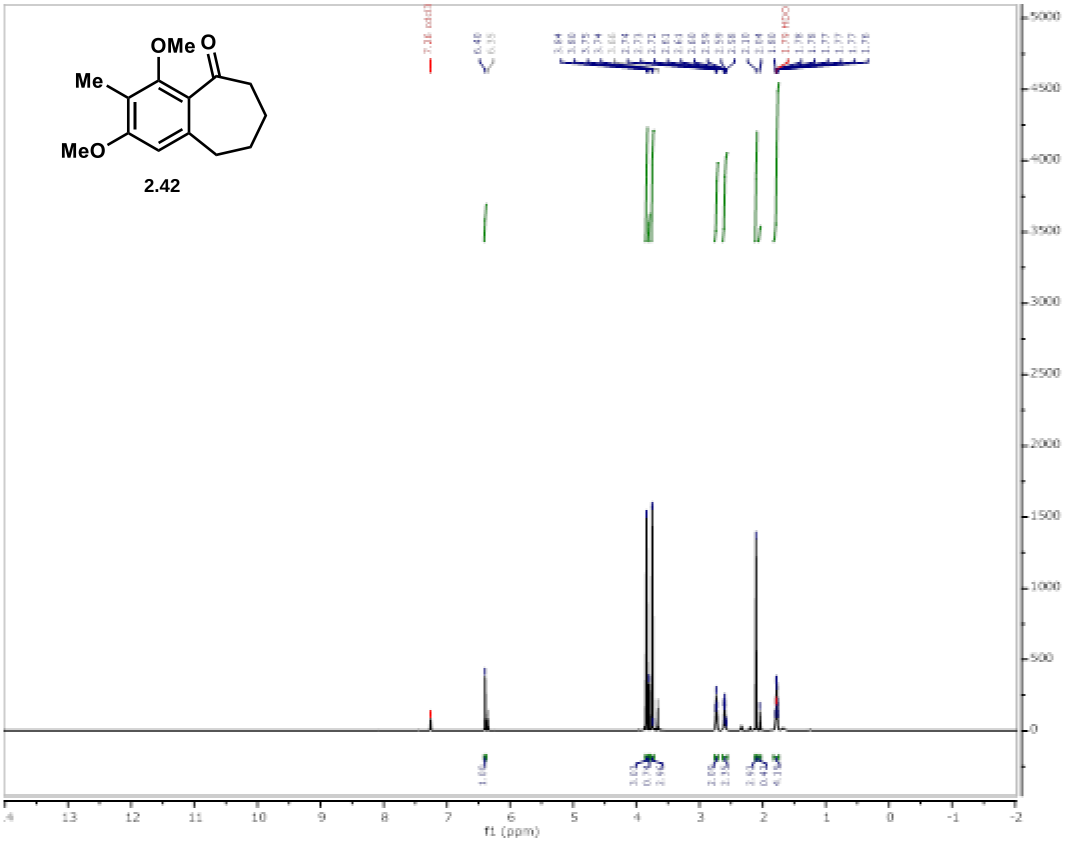

OMe
O
Me
MeO
7.26 cdcl3
6.40
6.35
1.79 HDO
5000
4500
4000
3500
3000
2500
2000
1500
1000
500
0
14
13
12
11
10
9
8
7
6
5
4
3
2
1
0
-1
-2
f1 (ppm)

2.42

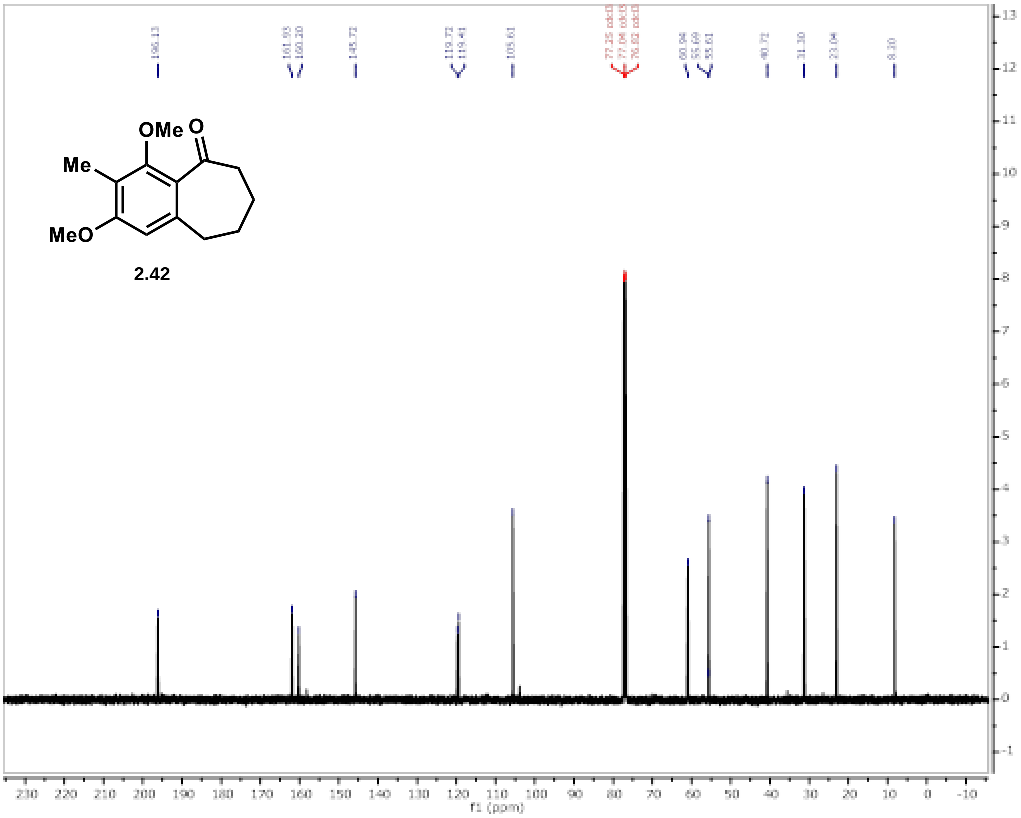

196.13
161.93
160.20
145.72
119.72
119.41
105.61
77.35 cdcl3
77.04 cdcl3
76.82 cdcl3
60.94
55.69
55.61
40.72
31.30
23.04
8.20
OMe
O
Me
MeO
13
12
11
10
9
8
7
6
5
4
3
2
1
0
-1
230
220
210
200
190
180
170
160
150
140
130
120
110
100
90
80
70
60
50
40
30
20
10
0
-10
f1 (ppm)

2.42

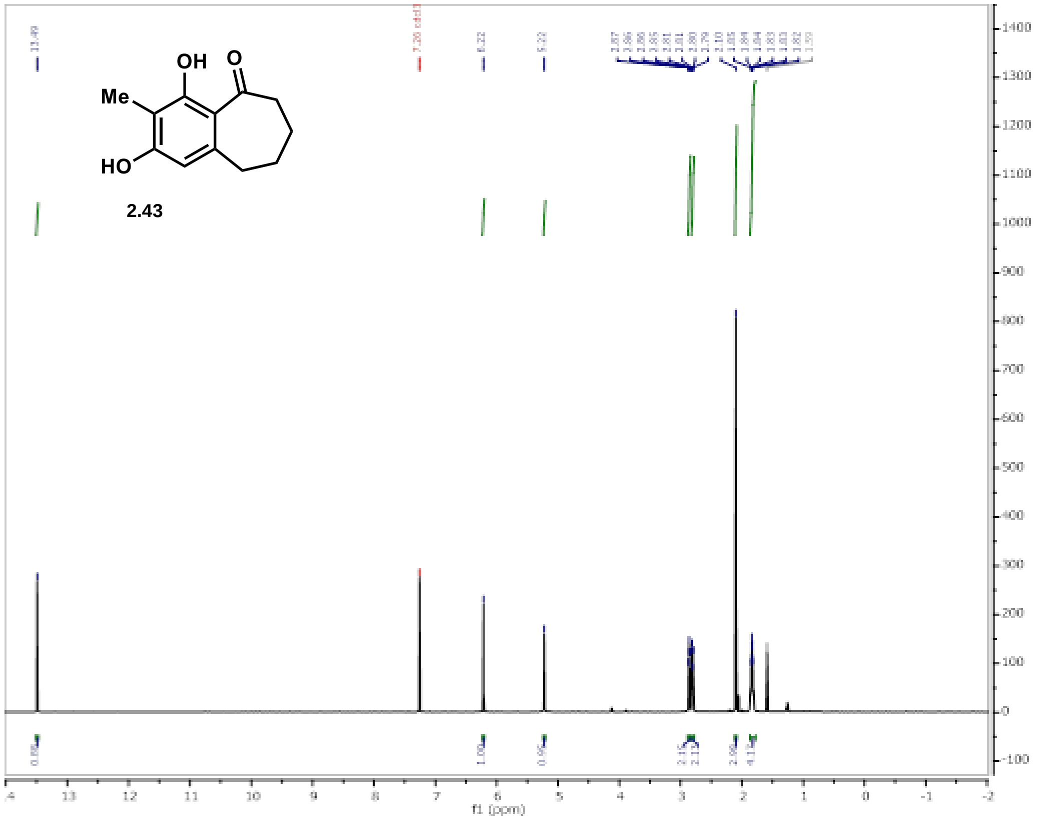
13.49
7.26 cdcl3
6.22
5.22
2.87
2.86
2.86
2.85
2.81
2.81
2.80
2.79
2.10
1.85
1.84
1.84
1.83
1.83
1.82
1.59
OH
O
Me
HO
2.43
0.89
1.00
0.96
2.15
2.13
2.99
4.13
1400
1300
1200
1100
1000
900
800
700
600
500
400
300
200
100
0
-100
14
13
12
11
10
9
8
7
6
5
4
3
2
1
0
-1
-2
f1 (ppm)

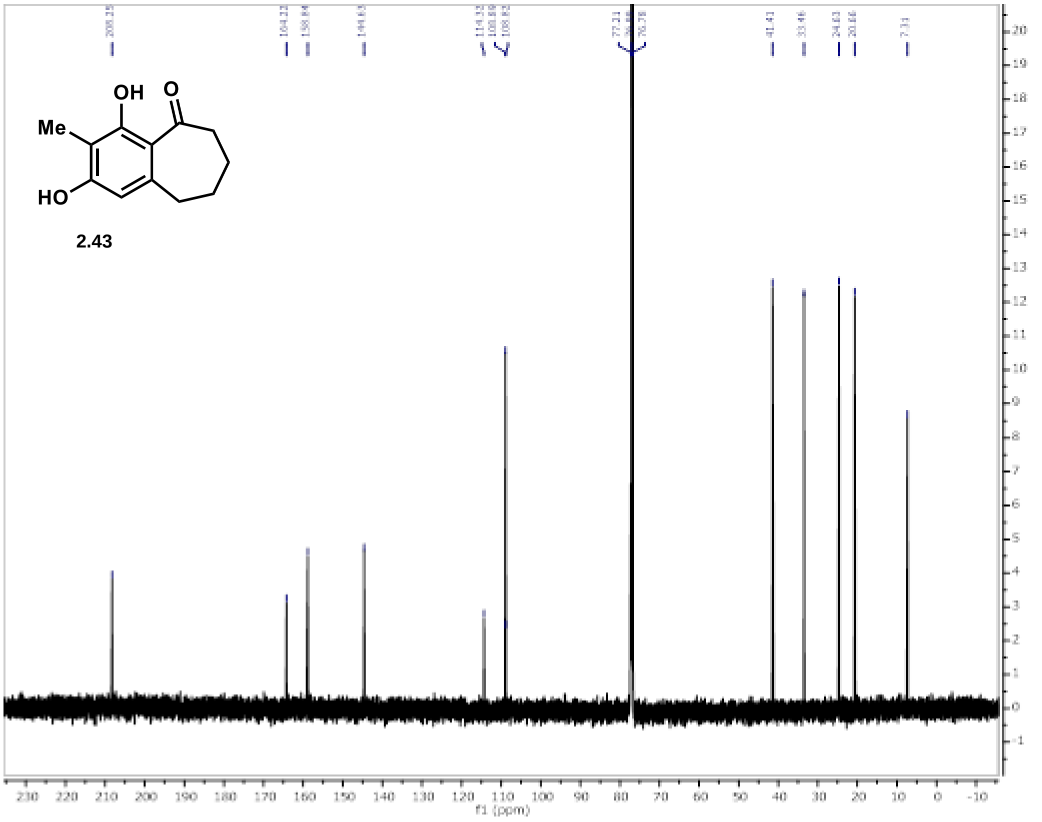
208.25
164.22
158.84
144.63
114.33
108.89
108.82
77.21
76.96
76.70
41.41
33.46
24.63
20.66
7.31
OH
O
Me
HO
2.43
20
19
18
17
16
15
14
13
12
11
10
9
8
7
6
5
4
3
2
1
0
-1
230
220
210
200
190
180
170
160
150
140
130
120
110
100
90
80
70
60
50
40
30
20
10
0
-10
f1 (ppm)

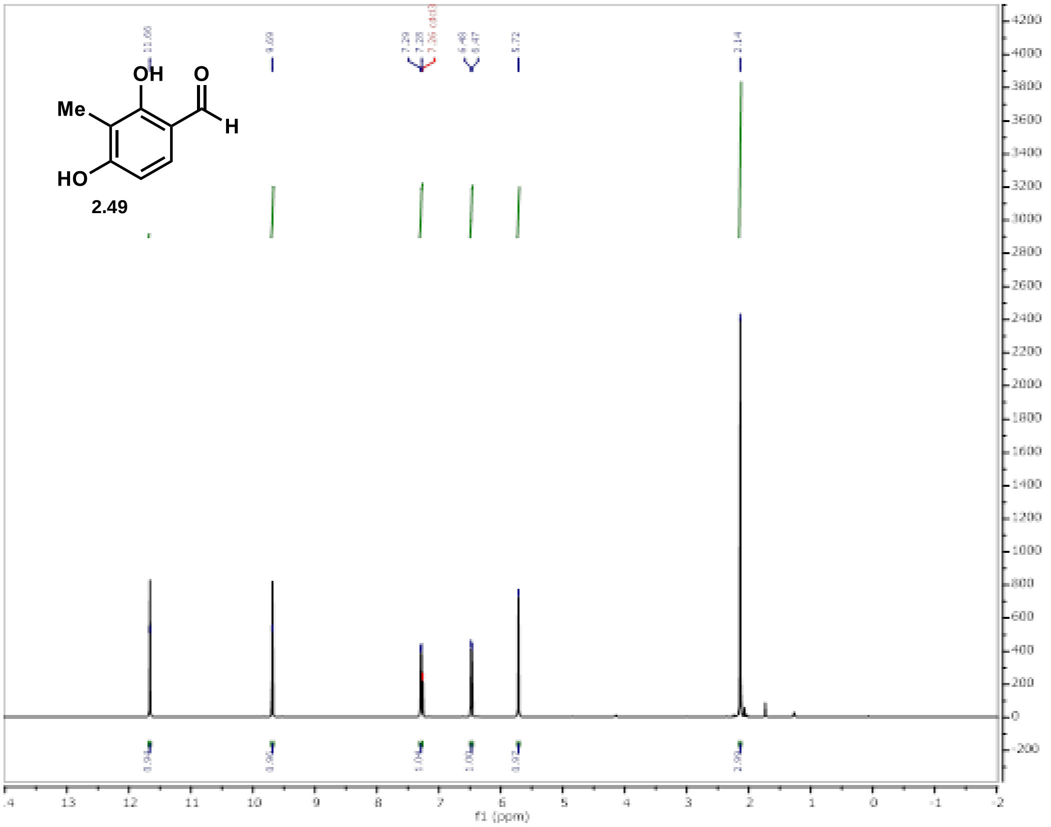
11.69
9.69
7.29
7.28
7.26 cdcl3
6.48
6.47
5.72
2.14
OH
O
Me
H
HO
0.94
0.96
1.04
1.00
0.97
2.99
f1 (ppm)

2.49

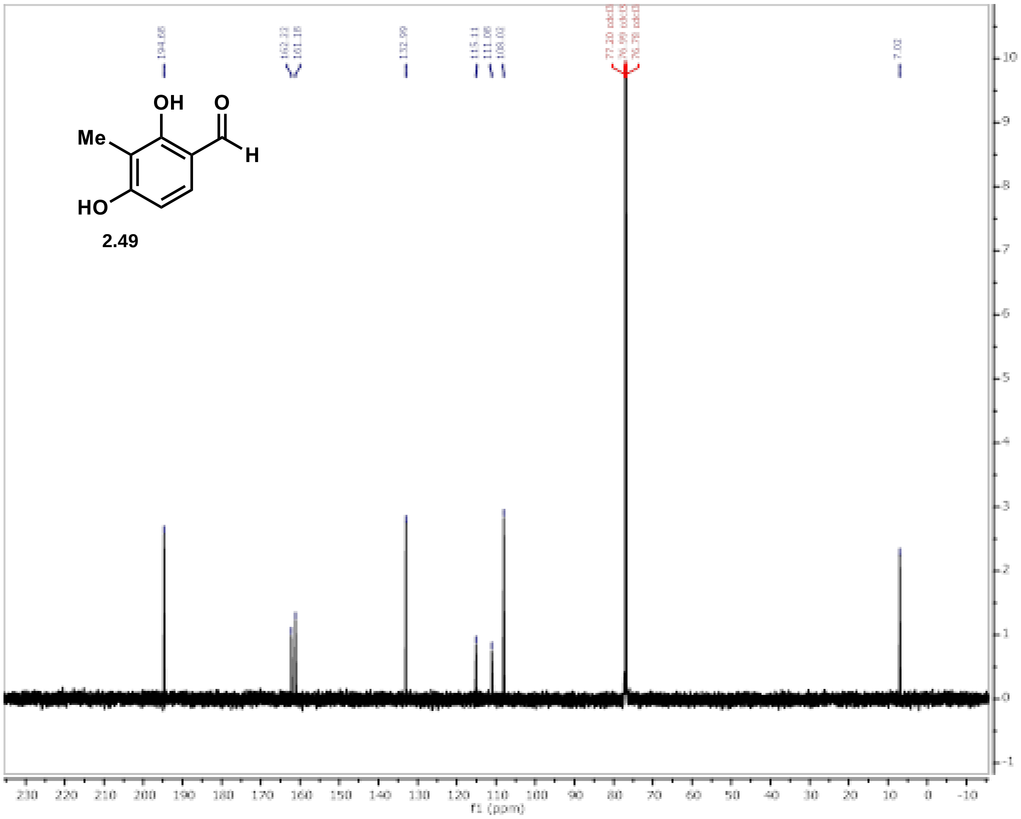
194.65
162.13
161.18
132.99
115.11
111.06
108.02
77.20 cdcl3
76.99 cdcl3
76.78 cdcl3
7.01
OH
O
Me
H
HO
f1 (ppm)

2.49

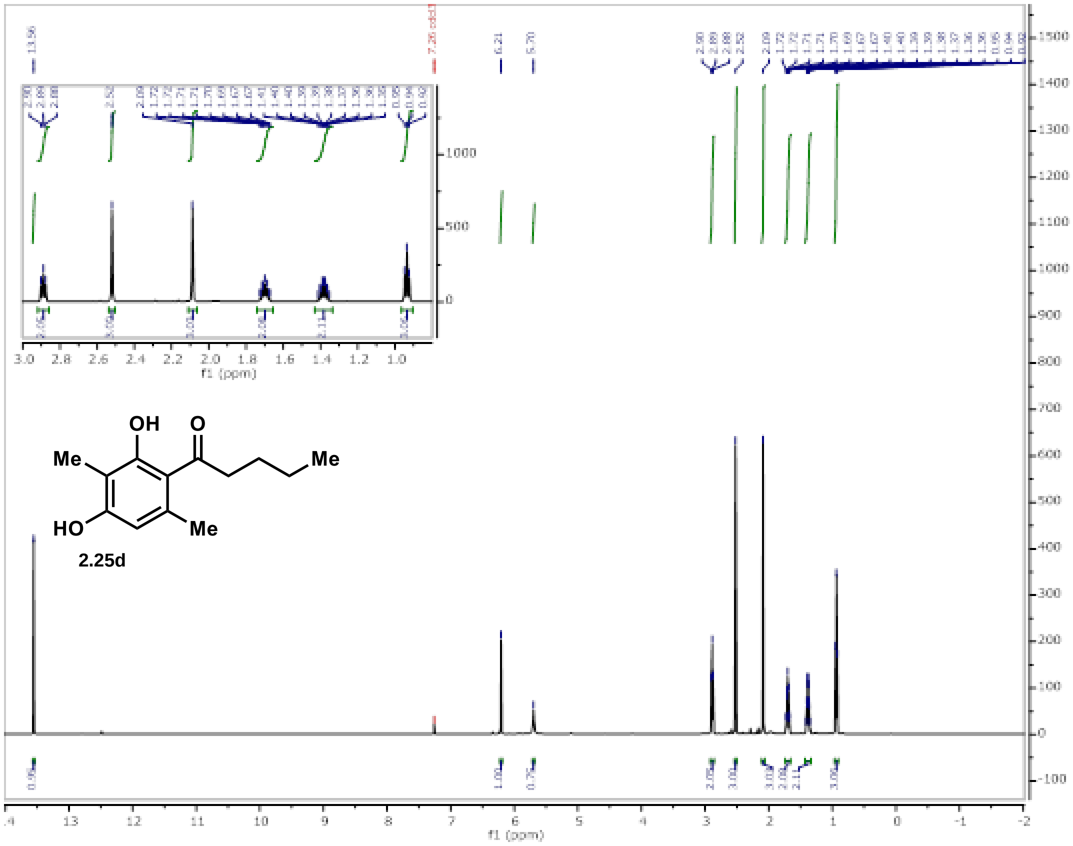

13.56
7.26 cdcl3
6.21
5.70
2.90
2.89
2.88
2.52
2.09
1.72
1.71
1.70
1.69
1.67
1.41
1.40
1.39
1.38
1.37
1.36
0.95
0.94
0.92
OH
O
Me
Me
HO
Me
2.25d
0.95
1.00
0.75
2.05
3.00
3.02
2.08
2.11
3.06
f1 (ppm)

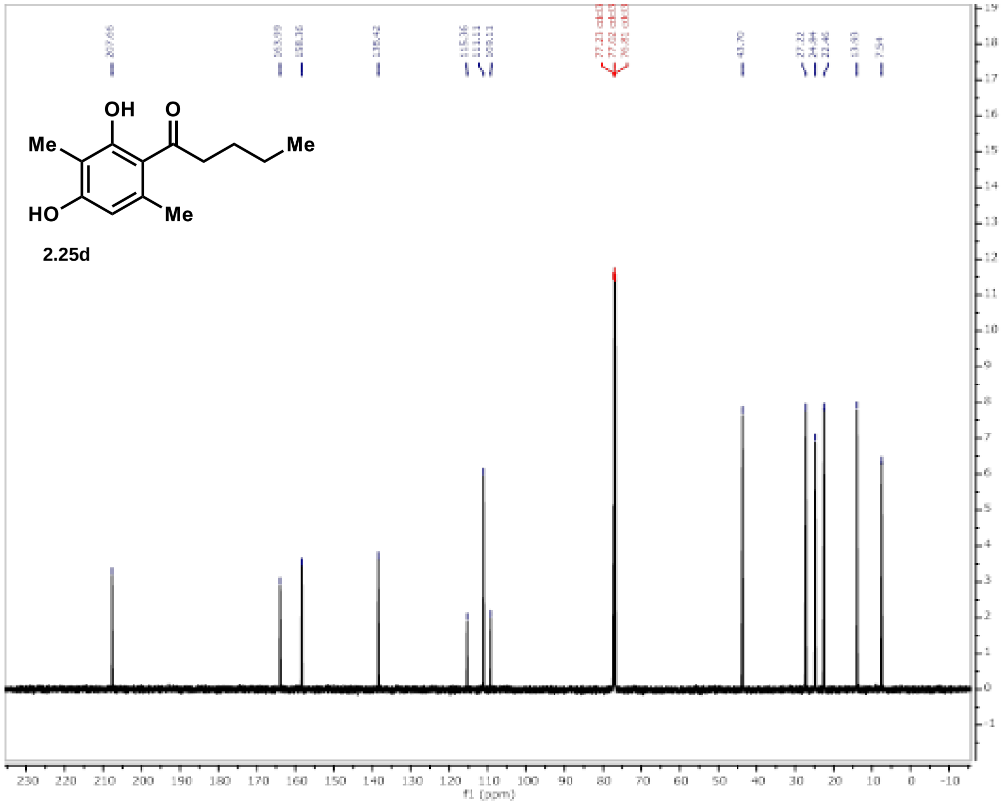

207.66
163.99
158.36
138.42
115.36
111.11
109.11
77.23 cdcl3
77.02 cdcl3
76.81 cdcl3
43.70
27.22
24.84
22.46
13.93
7.54
OH
O
Me
Me
HO
Me
2.25d
f1 (ppm)

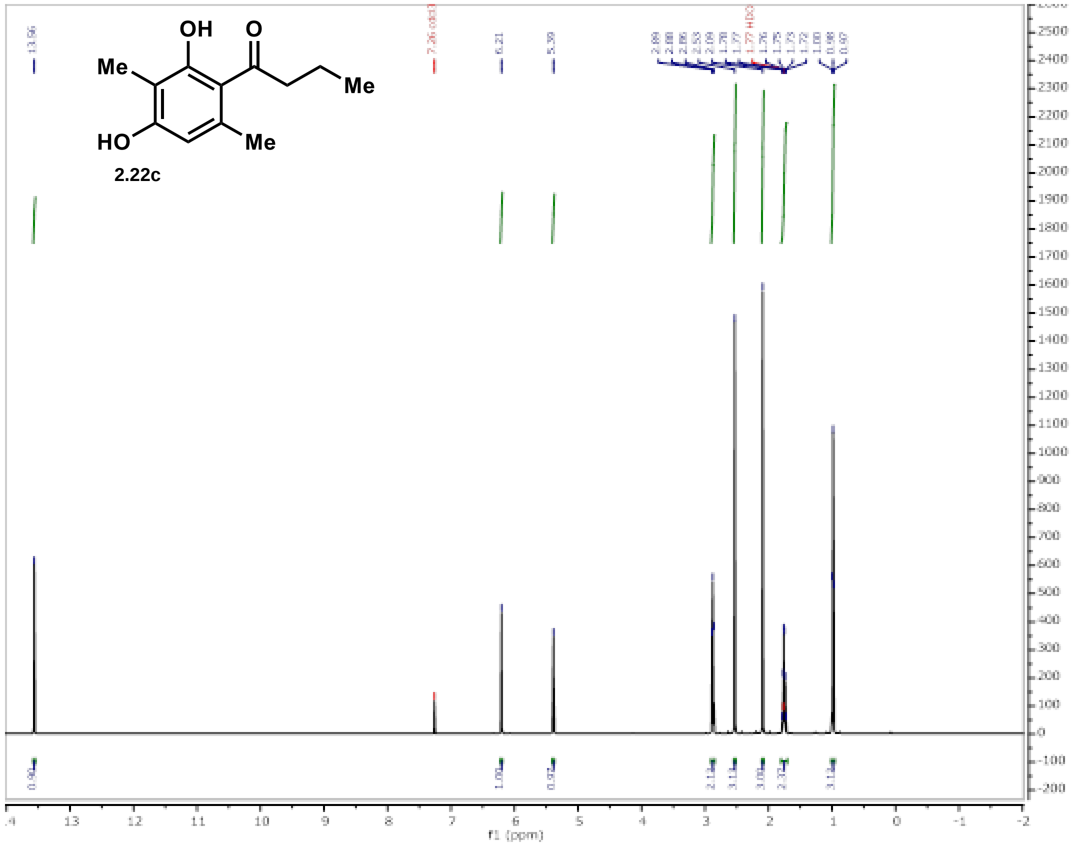
OH
O
Me
Me
HO
Me
2.22c
13.56
7.26 cdcl3
6.21
5.39
2.89
2.88
2.86
2.53
2.09
1.78
1.77
1.77 HDO
1.76
1.75
1.73
1.72
1.00
0.98
0.97
0.90
1.00
0.97
2.14
3.14
3.00
2.32
3.14
f1 (ppm)

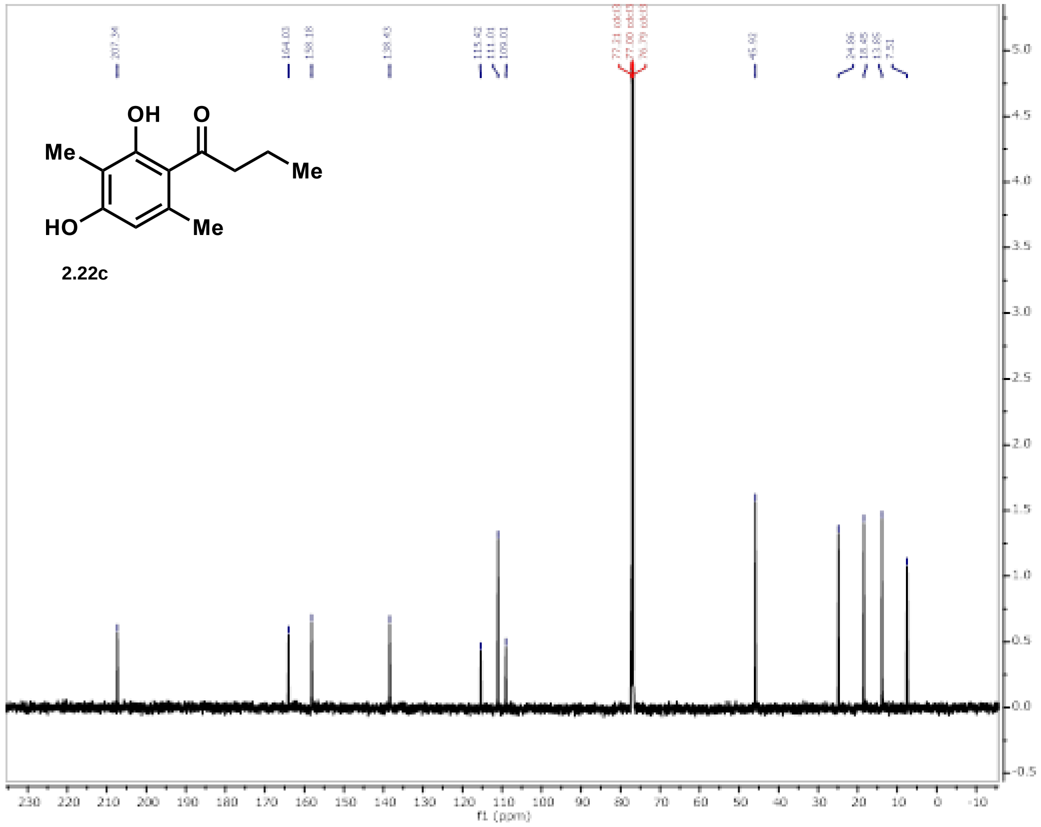
OH
O
Me
Me
HO
Me
2.22c
207.34
164.03
158.18
138.45
115.42
111.01
109.01
77.21 cdcl3
77.00 cdcl3
76.79 cdcl3
45.90
24.66
18.45
13.86
7.51
f1 (ppm)

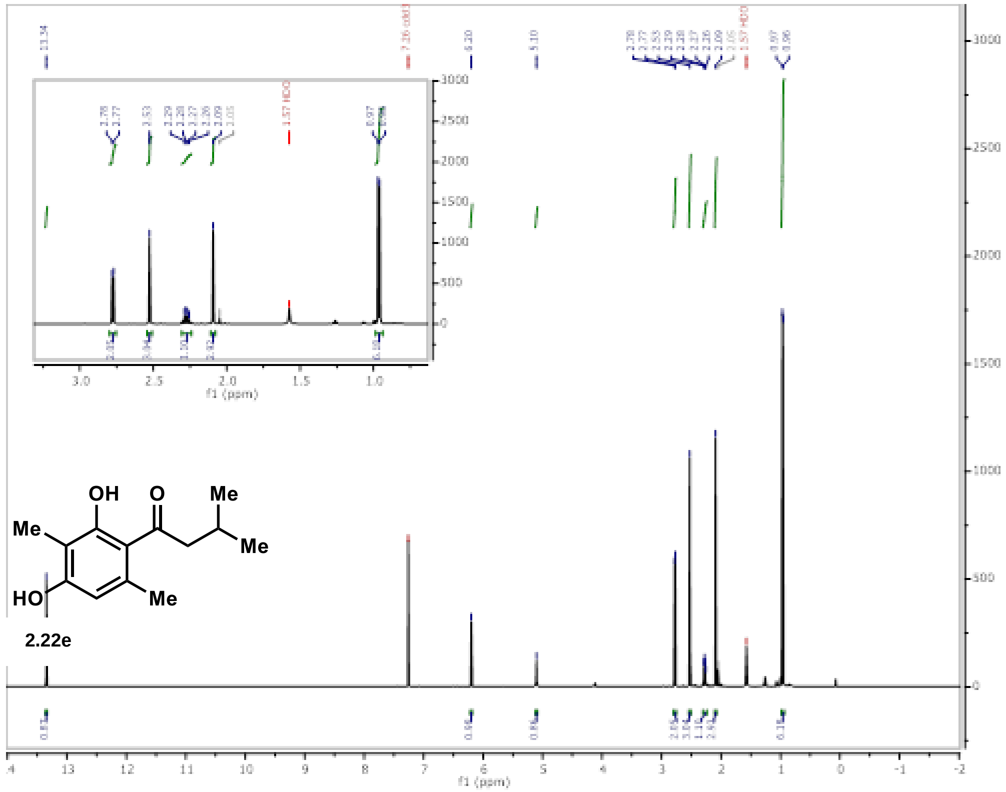
2.22e

OH
O
Me
Me
Me
HO
Me
13.34
7.26 cdcl3
6.20
5.10
2.78
2.77
2.53
2.29
2.28
2.27
2.26
2.09
2.05
1.57 H2O
0.97
0.96
0.87
0.92
0.86
2.05
3.04
1.12
2.92
6.10
f1 (ppm)

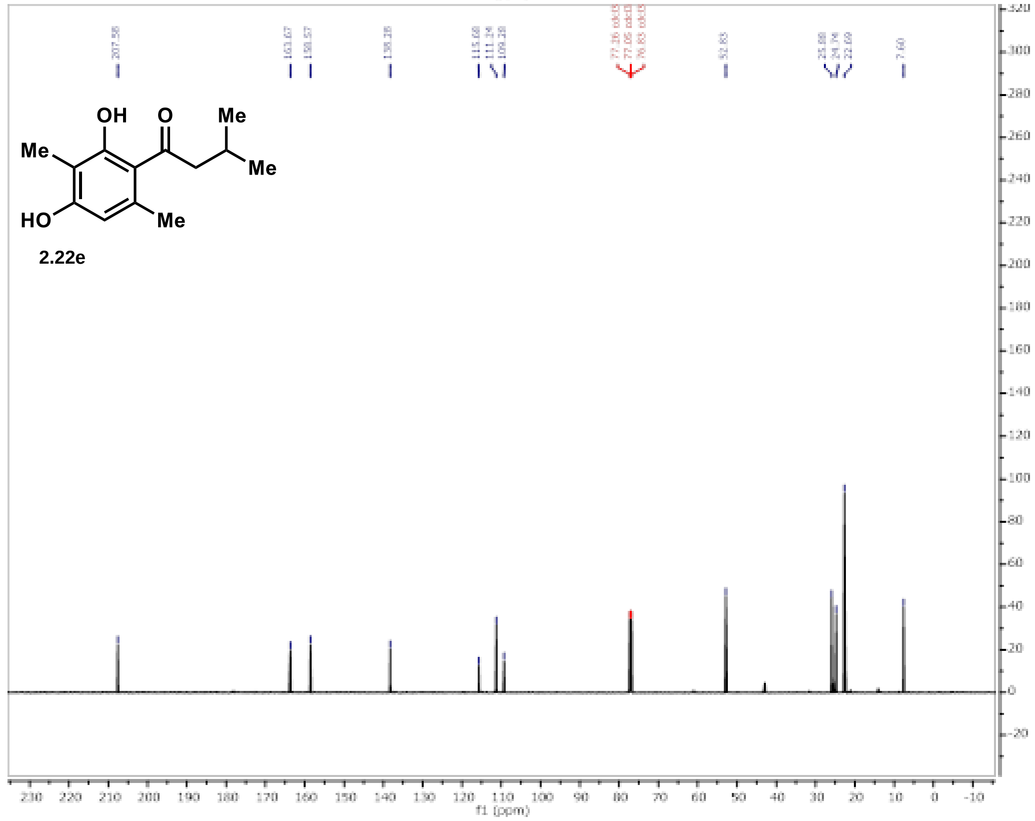
2.22e

OH
O
Me
Me
Me
HO
Me
207.58
163.67
158.57
138.28
115.68
111.24
109.28
77.16 cdcl3
77.05 cdcl3
76.83 cdcl3
52.83
25.88
24.74
22.69
7.60
f1 (ppm)

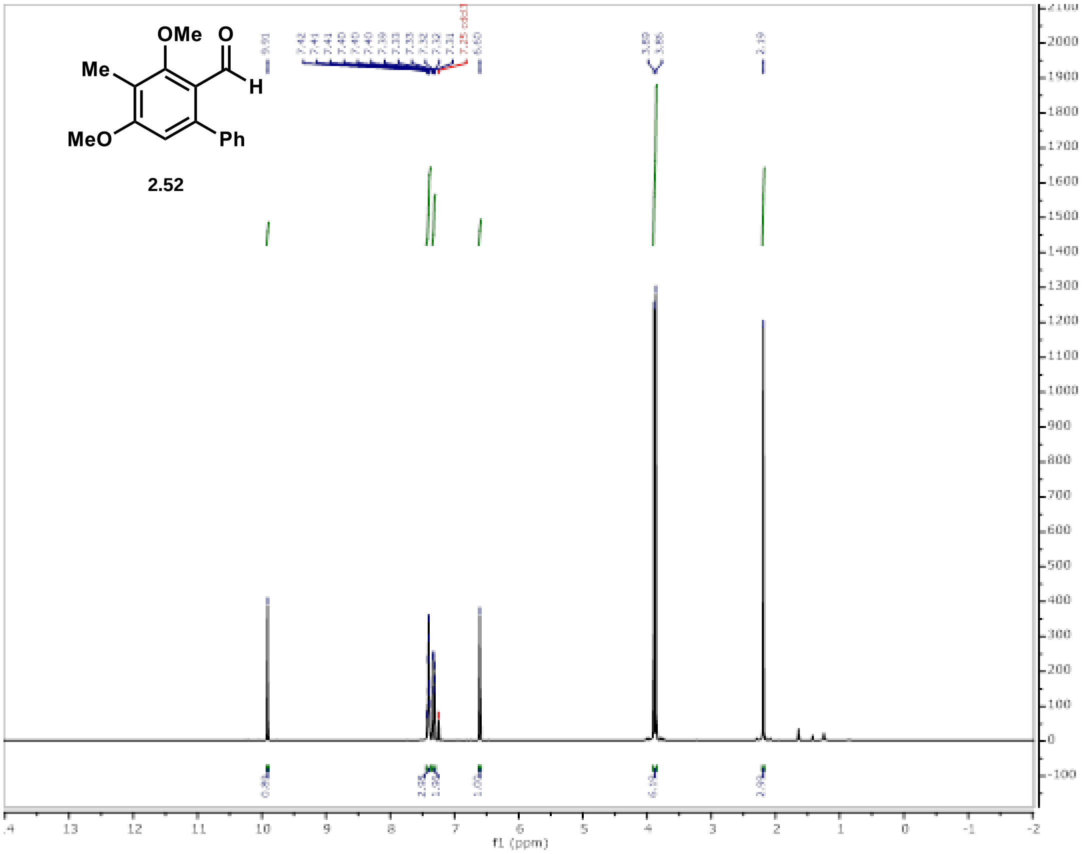
OMe
O
Me
H
MeO
Ph
2.52
9.91
7.42
7.41
7.41
7.40
7.40
7.40
7.39
7.33
7.33
7.32
7.32
7.31
7.25 cdcl3
6.60
3.89
3.86
2.19
f1 (ppm)

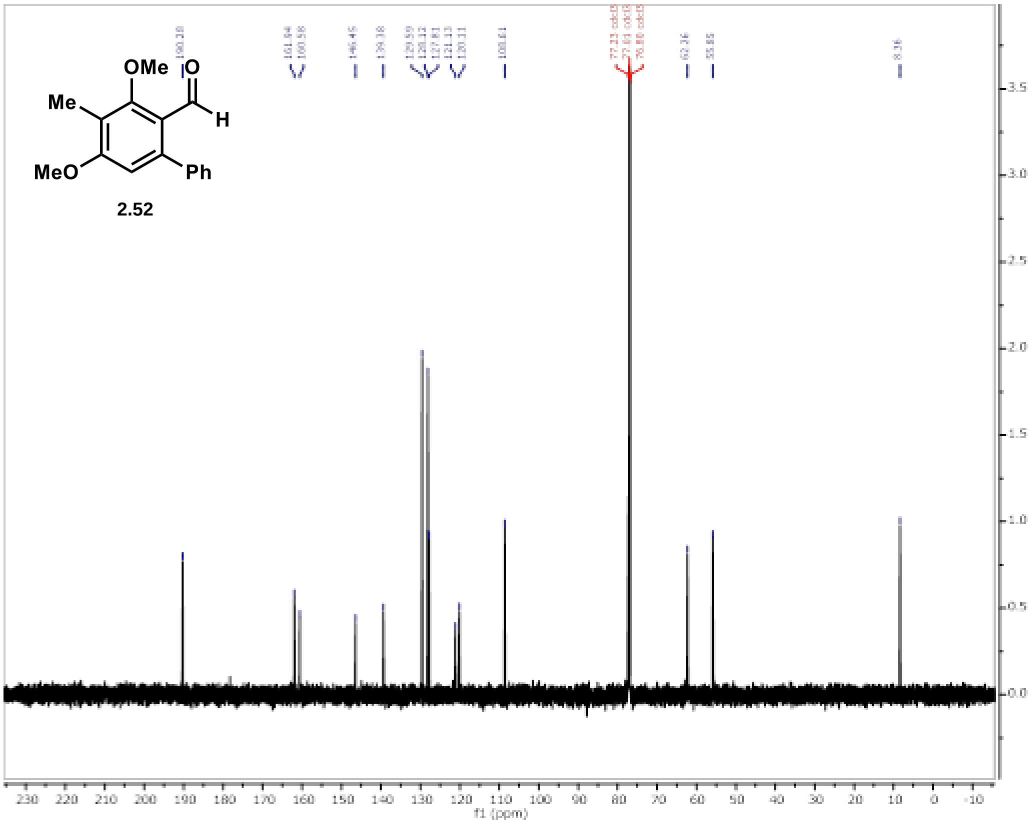
OMe
O
Me
H
MeO
Ph
2.52
190.18
161.84
160.58
146.45
139.18
129.59
128.12
127.81
121.13
120.11
108.61
77.23 cdcl3
77.01 cdcl3
76.80 cdcl3
62.36
55.85
8.36
f1 (ppm)

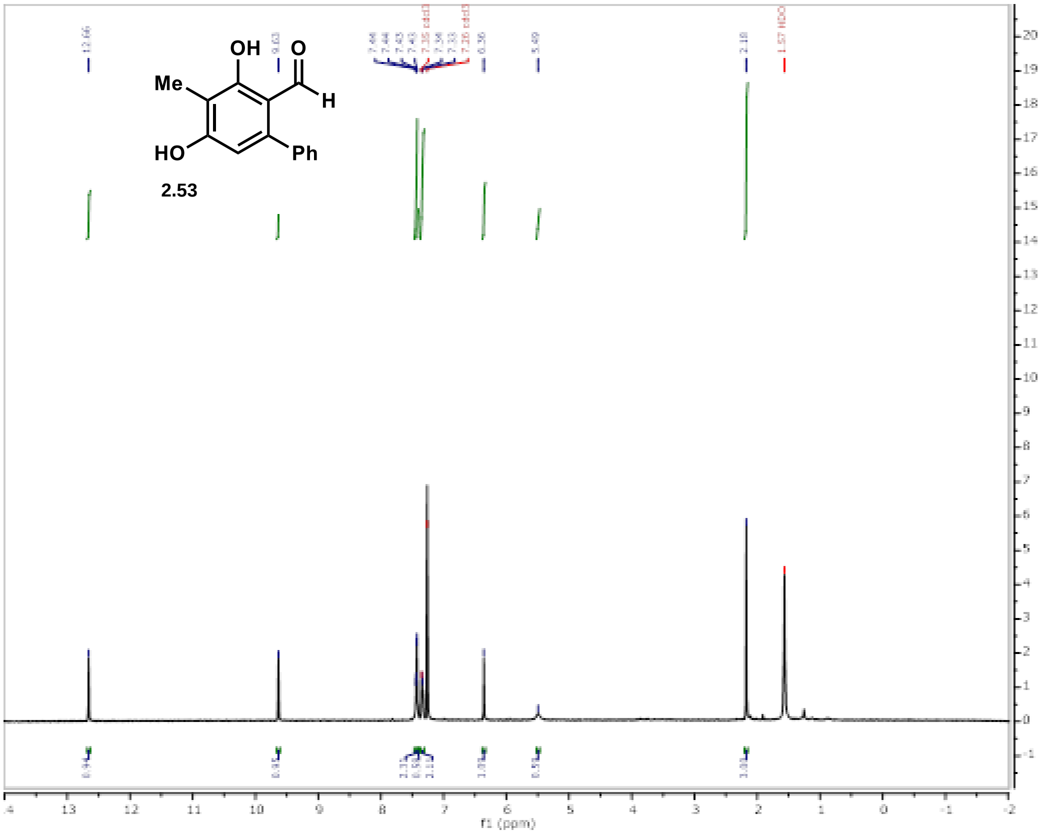
OH
O
Me
H
HO
Ph
12.66
9.63
7.44
7.44
7.43
7.43
7.35 cdcl3
7.34
7.33
7.26 cdcl3
6.36
5.49
2.18
1.57 HDO
0.94
0.92
2.15
0.59
2.13
1.01
0.51
3.01
f1 (ppm)

2.53

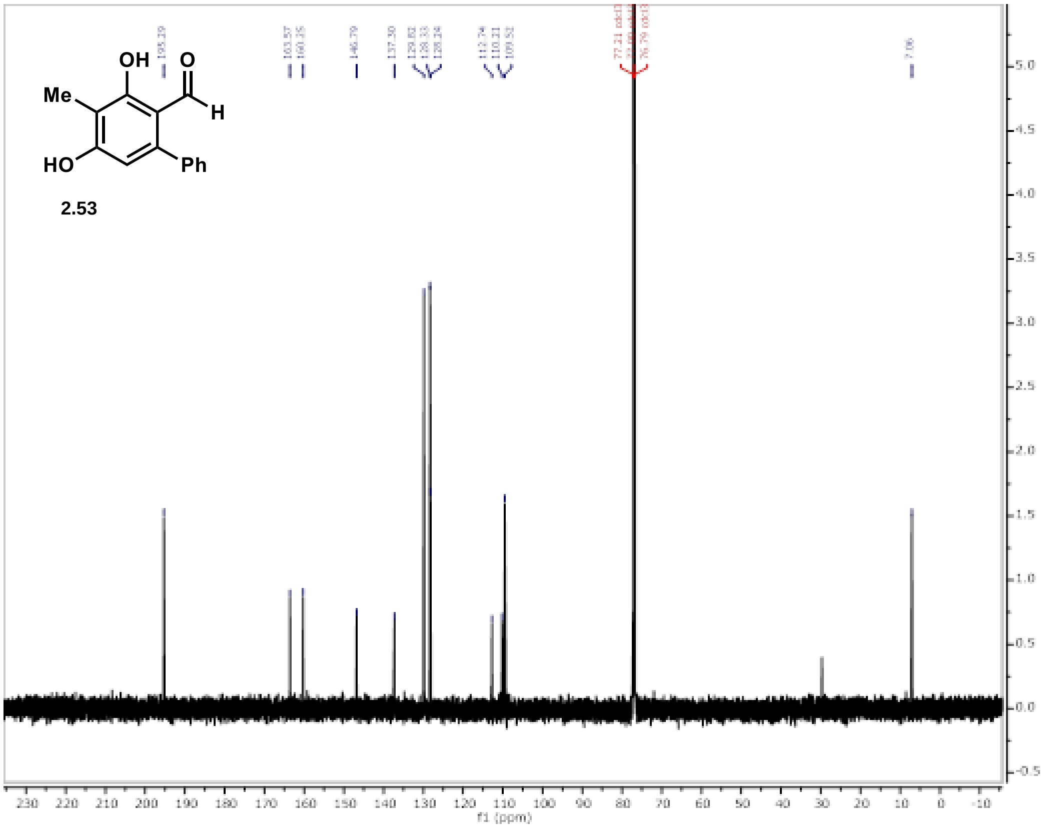
OH
O
Me
H
HO
Ph
195.29
163.57
160.35
146.79
137.30
129.82
128.33
128.24
112.74
110.21
109.52
77.21 cdcl3
76.79 cdcl3
7.06
f1 (ppm)

2.53

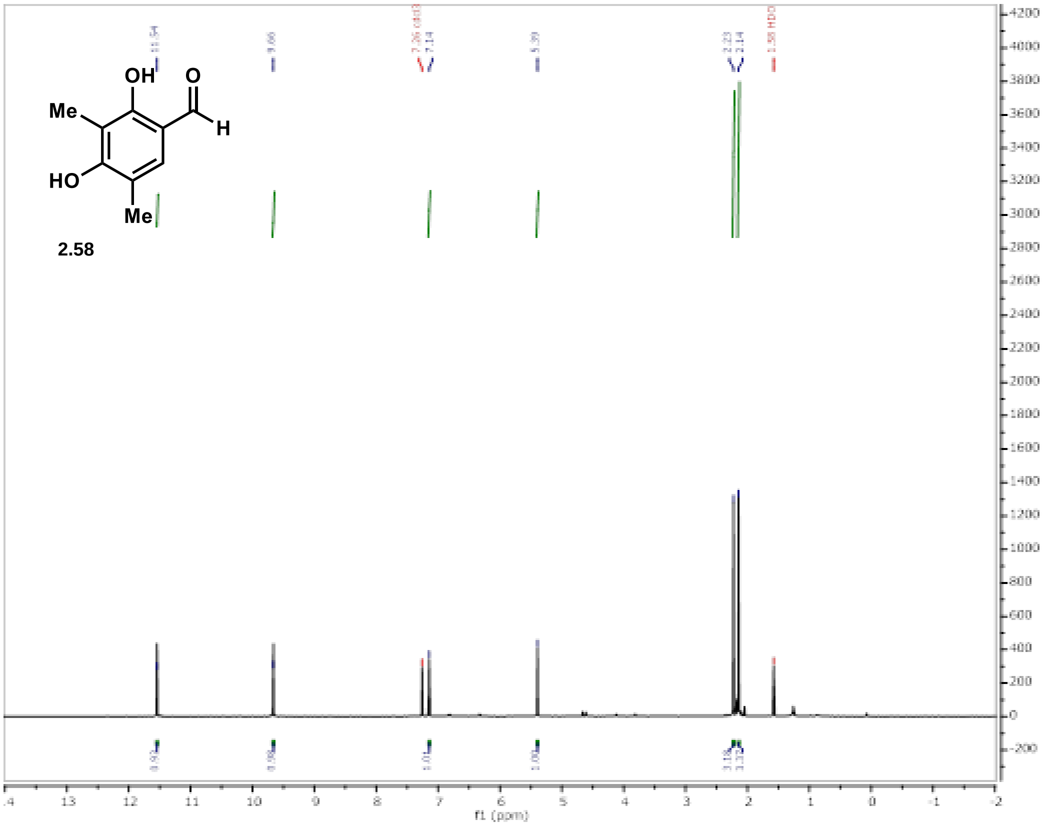
OH
O
Me
H
HO
Me
2.58
11.54
9.66
7.26 cdcl3
7.14
5.39
2.23
2.14
1.58 HDO
0.92
0.98
1.01
1.00
3.18
3.13
f1 (ppm)

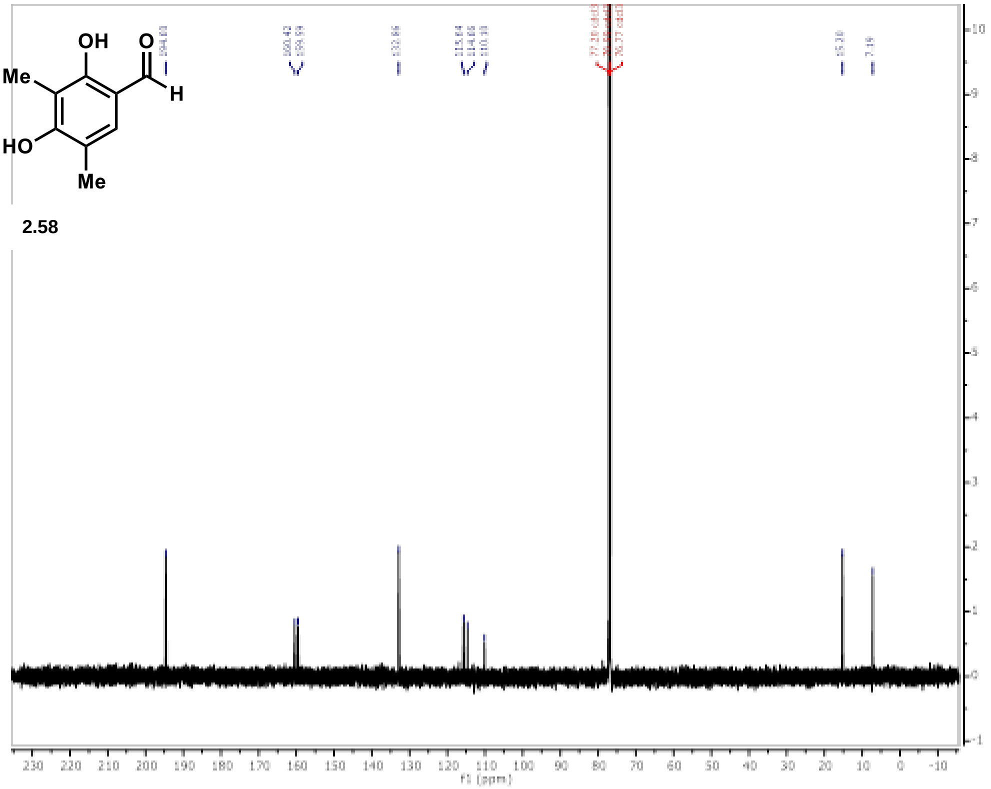
OH
O
Me
H
HO
Me
2.58
194.03
160.42
159.59
132.86
115.64
114.66
110.18
77.28 cdcl3
76.77 cdcl3
15.26
7.19
f1 (ppm)

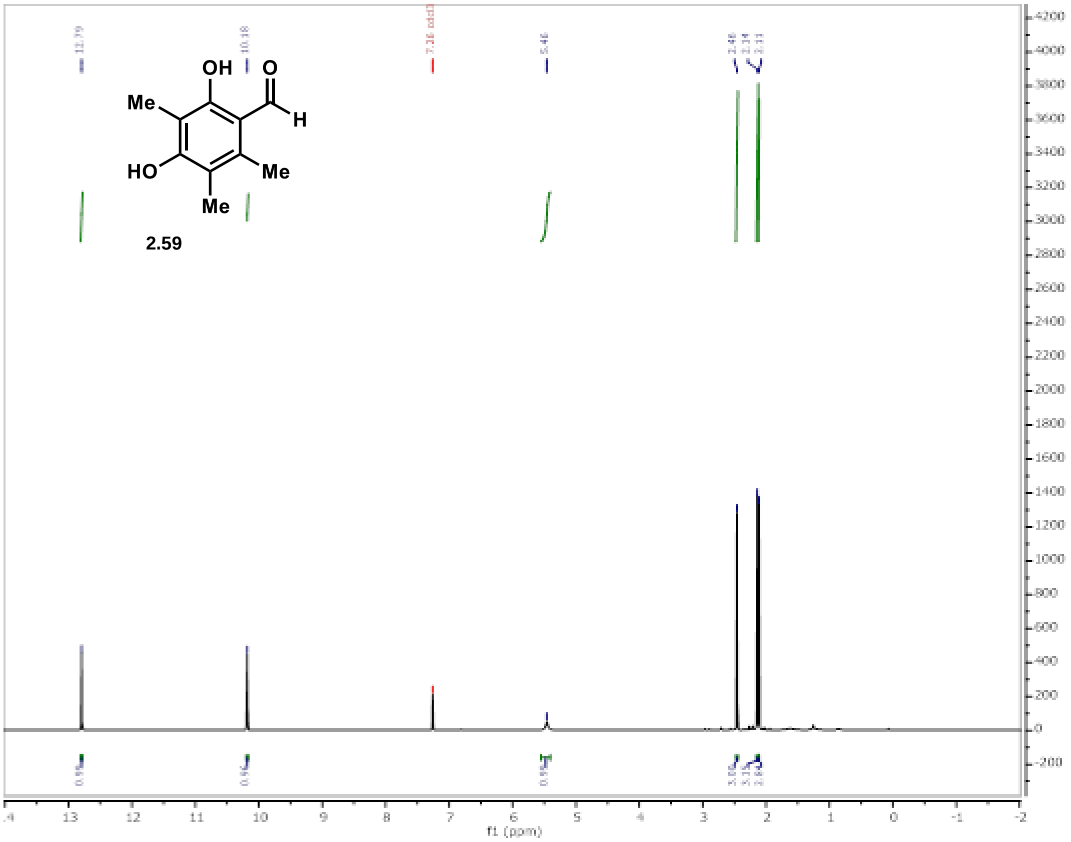
12.79
10.18
7.26 cdcl3
5.46
2.48
2.14
2.13
OH
O
H
Me
HO
Me
Me
0.99
0.96
0.95
3.00
3.15
2.84
f1 (ppm)
4200
4000
3800
3600
3400
3200
3000
2800
2600
2400
2200
2000
1800
1600
1400
1200
1000
800
600
400
200
0
-200
13
12
11
10
9
8
7
6
5
4
3
2
1
0
-1
-2

2.59

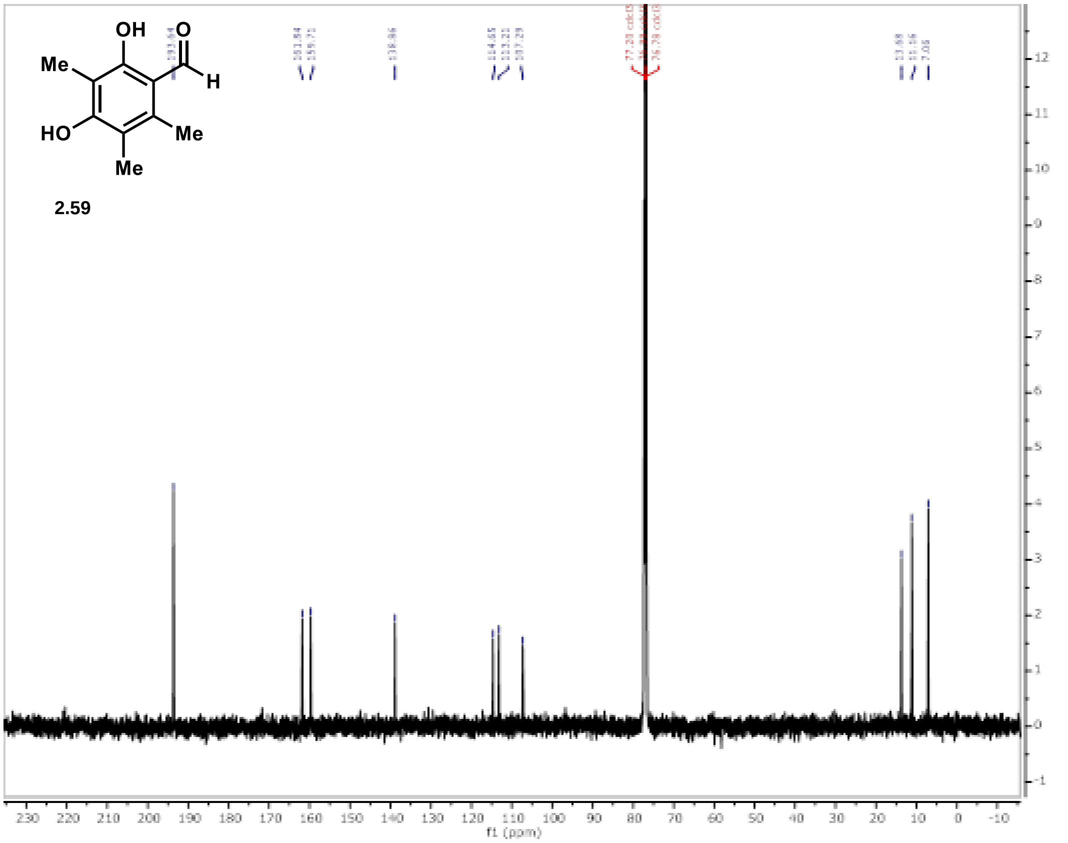
193.64
161.84
159.71
138.86
114.65
113.21
107.29
77.23 cdcl3
77.00 cdcl3
76.78 cdcl3
13.68
11.56
7.05
OH
O
H
Me
HO
Me
Me
f1 (ppm)
230
220
210
200
190
180
170
160
150
140
130
120
110
100
90
80
70
60
50
40
30
20
10
0
-10
12
11
10
9
8
7
6
5
4
3
2
1
0
-1

2.59

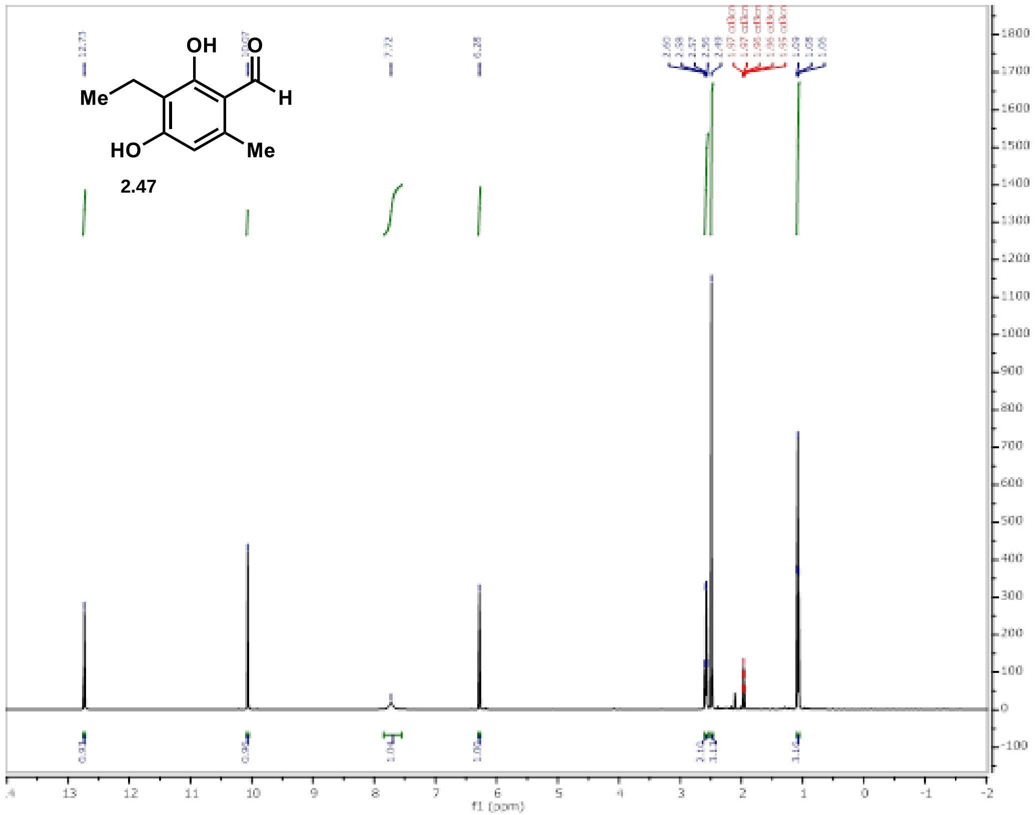
OH
O
Me
H
HO
Me
2.47
12.73
10.07
7.72
6.28
2.60
2.58
2.57
2.56
2.49
1.09
1.08
1.06
0.91
0.96
1.04
1.00
2.10
3.11
3.14
f1 (ppm)

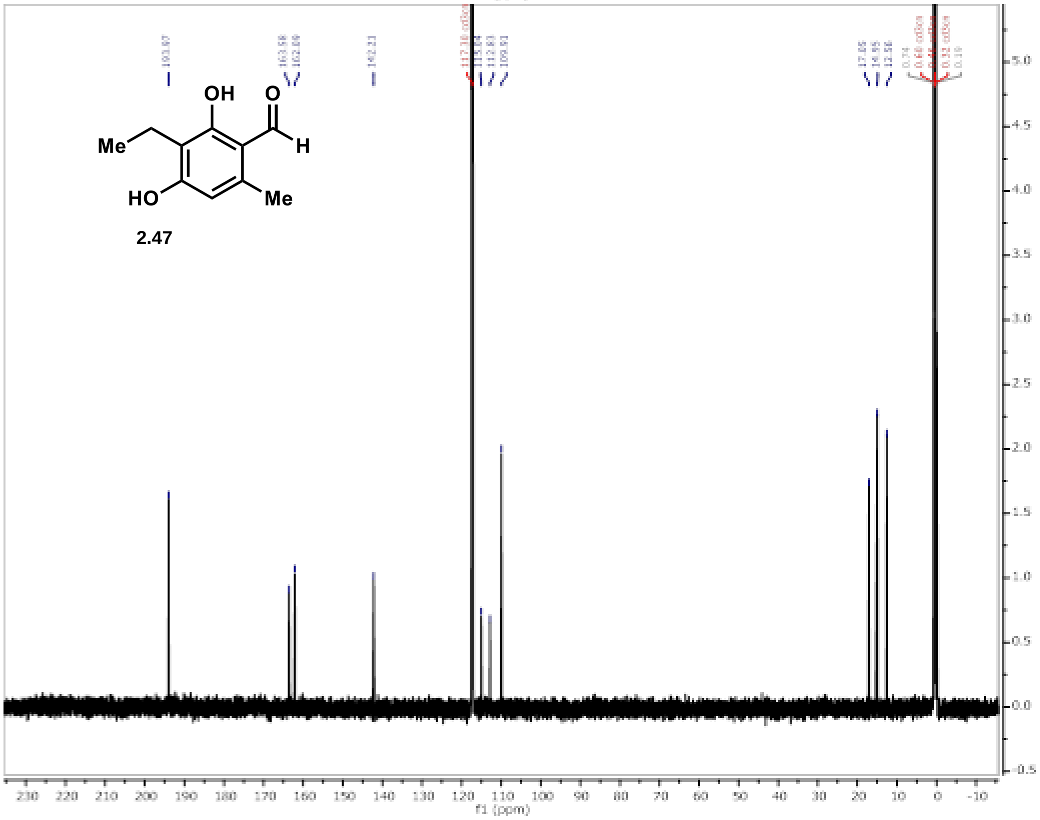
OH
O
Me
H
HO
Me
2.47
193.97
163.58
162.86
142.21
117.16
115.04
112.83
109.91
17.65
14.86
12.56
f1 (ppm)

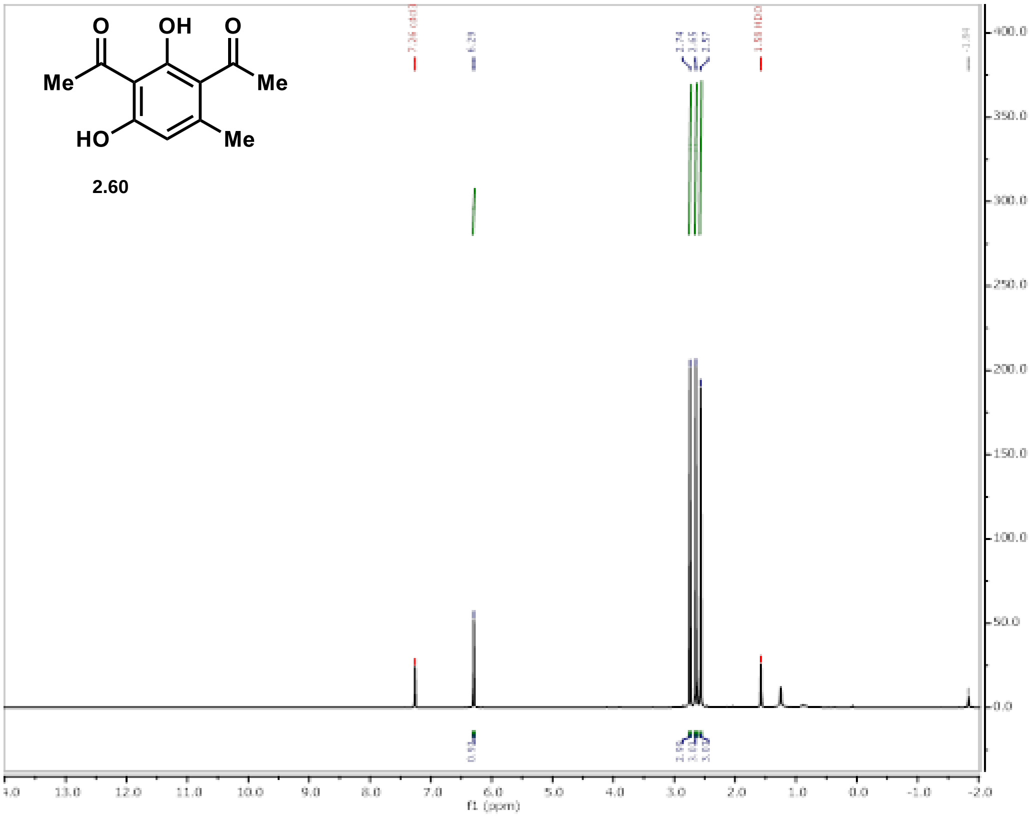
O
OH
O
Me
Me
HO
Me
2.60
7.26 cdcl3
6.29
2.74
2.65
2.57
1.58 HDO
-1.84
0.91
1.95
3.04
3.07
400.0
350.0
300.0
250.0
200.0
150.0
100.0
50.0
0.0
13.0
12.0
11.0
10.0
9.0
8.0
7.0
6.0
5.0
4.0
3.0
2.0
1.0
0.0
-1.0
-2.0
f1 (ppm)

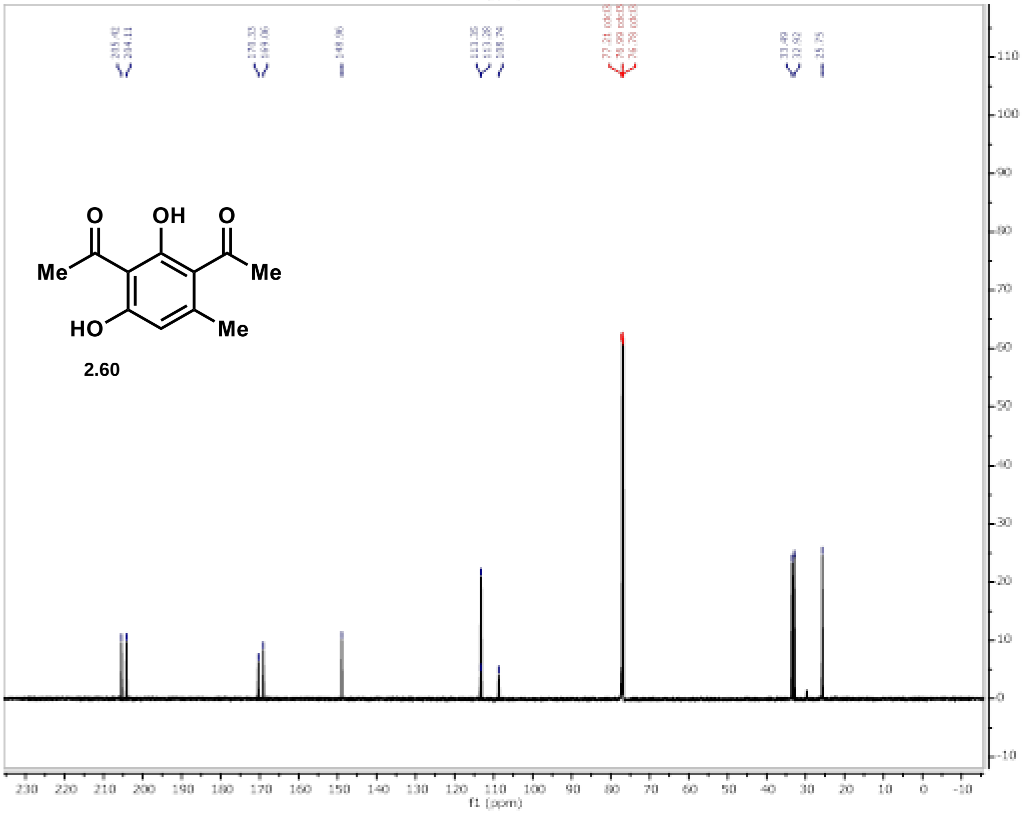
205.42
204.11
170.33
169.06
148.96
113.36
113.28
108.74
77.21 cdcl3
76.99 cdcl3
76.78 cdcl3
33.49
32.92
25.75
O
OH
O
Me
Me
HO
Me
2.60
110
100
90
80
70
60
50
40
30
20
10
0
-10
230
220
210
200
190
180
170
160
150
140
130
120
110
100
90
80
70
60
50
40
30
20
10
0
-10
f1 (ppm)

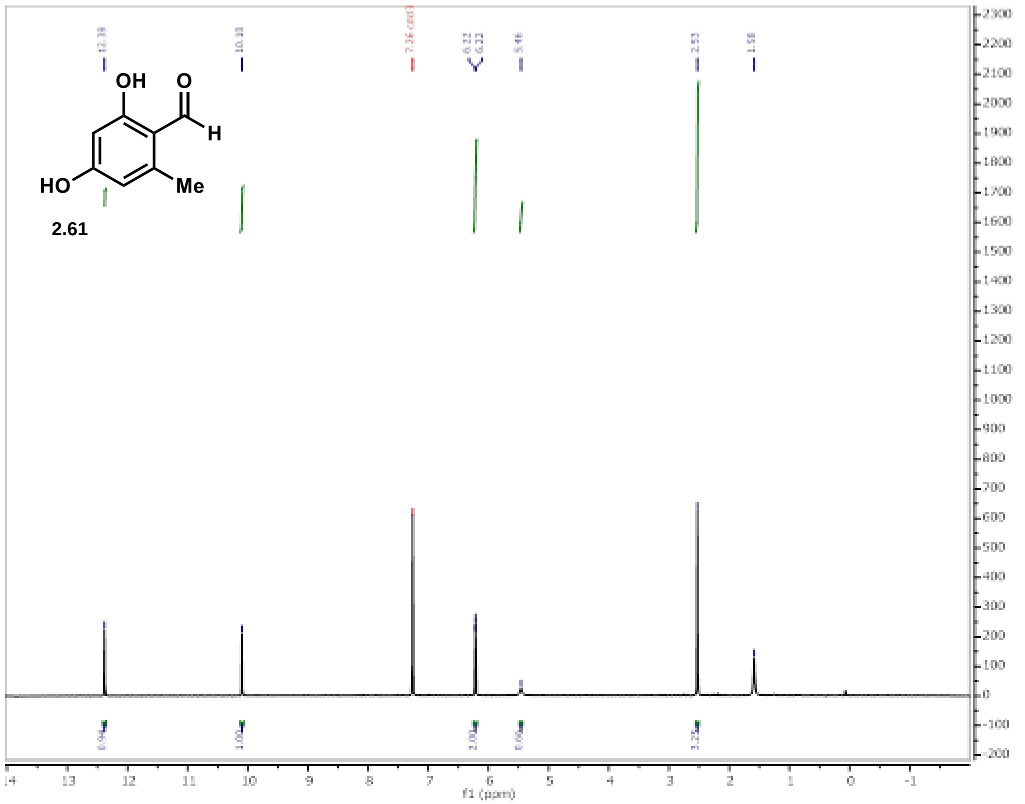
12.38
10.13
7.26 cdcl3
6.22
6.21
5.46
2.53
1.58
OH
O
H
HO
Me
2.61
0.94
1.00
2.00
0.66
3.25
f1 (ppm)

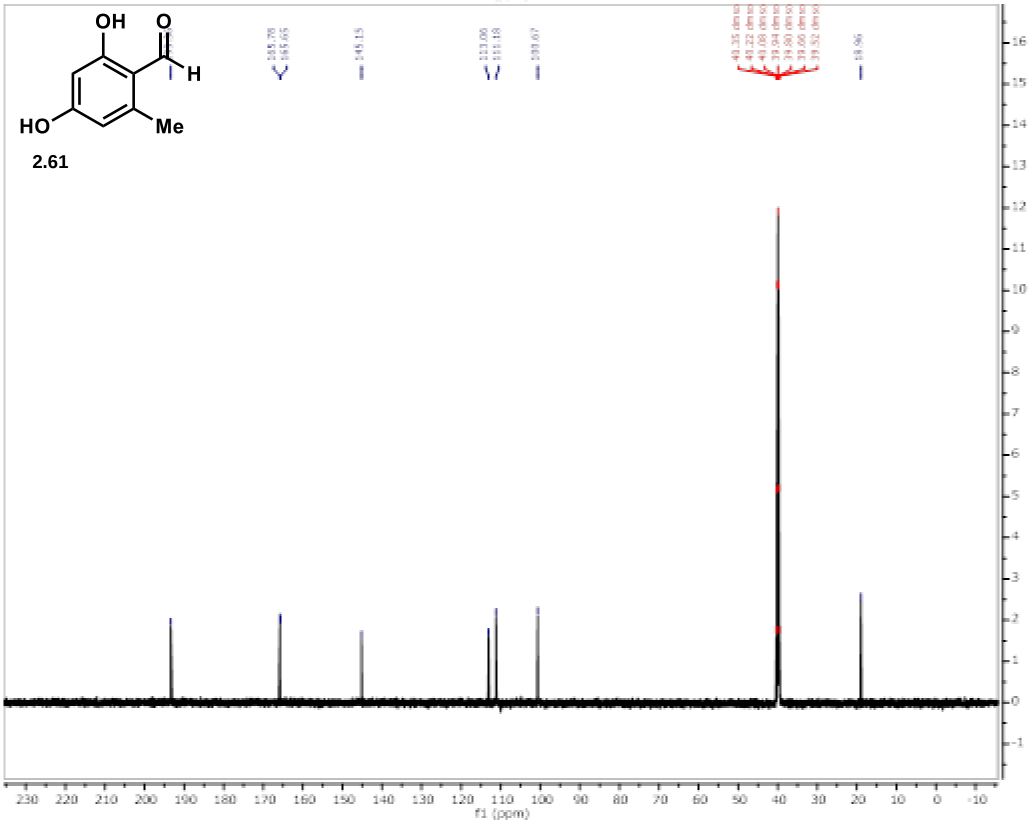
165.78
165.65
145.15
113.06
111.18
100.67
41.35 dmso
41.22 dmso
41.08 dmso
39.94 dmso
39.80 dmso
39.66 dmso
39.52 dmso
18.96
OH
O
H
HO
Me
2.61
f1 (ppm)

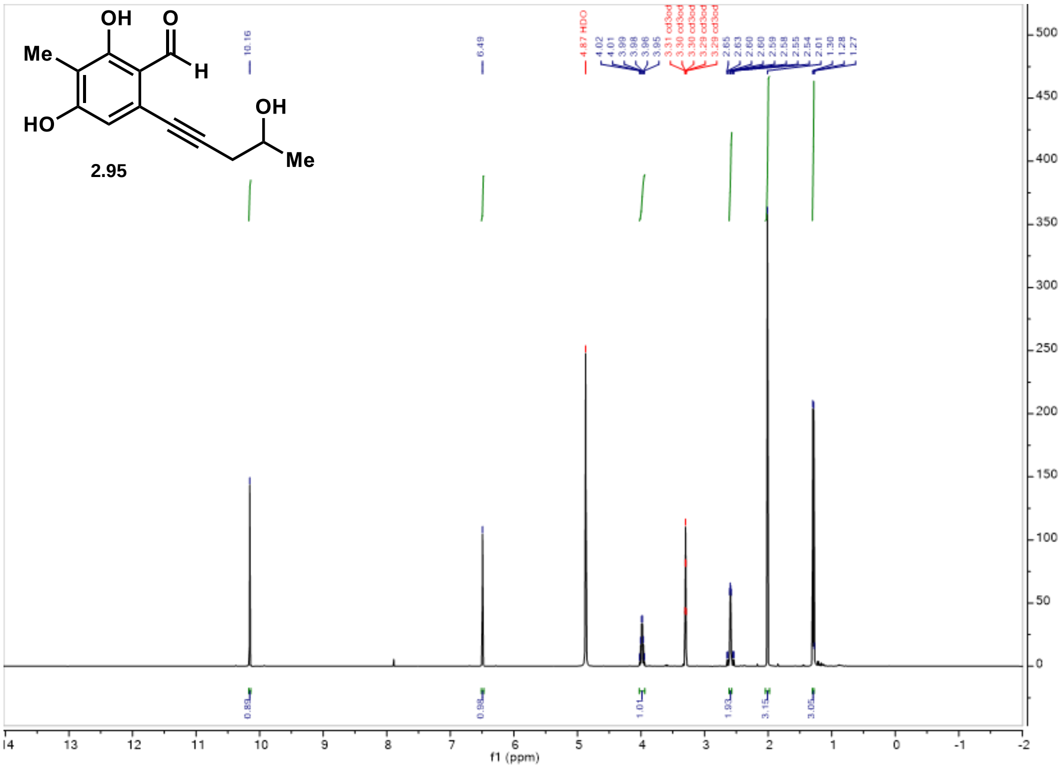
2.95

OH
O
Me
H
HO
OH
Me
10.16
6.49
4.87 HDO
4.02
4.01
3.99
3.98
3.96
3.95
3.31 cd3od
3.30 cd3od
3.30 cd3od
3.29 cd3od
3.29 cd3od
2.65
2.63
2.60
2.60
2.59
2.58
2.55
2.54
2.01
1.30
1.28
1.27
0.89
0.98
1.01
1.93
3.15
3.05
14
13
12
11
10
9
8
7
6
5
4
3
2
1
0
-1
-2
f1 (ppm)
500
450
400
350
300
250
200
150
100
50
0

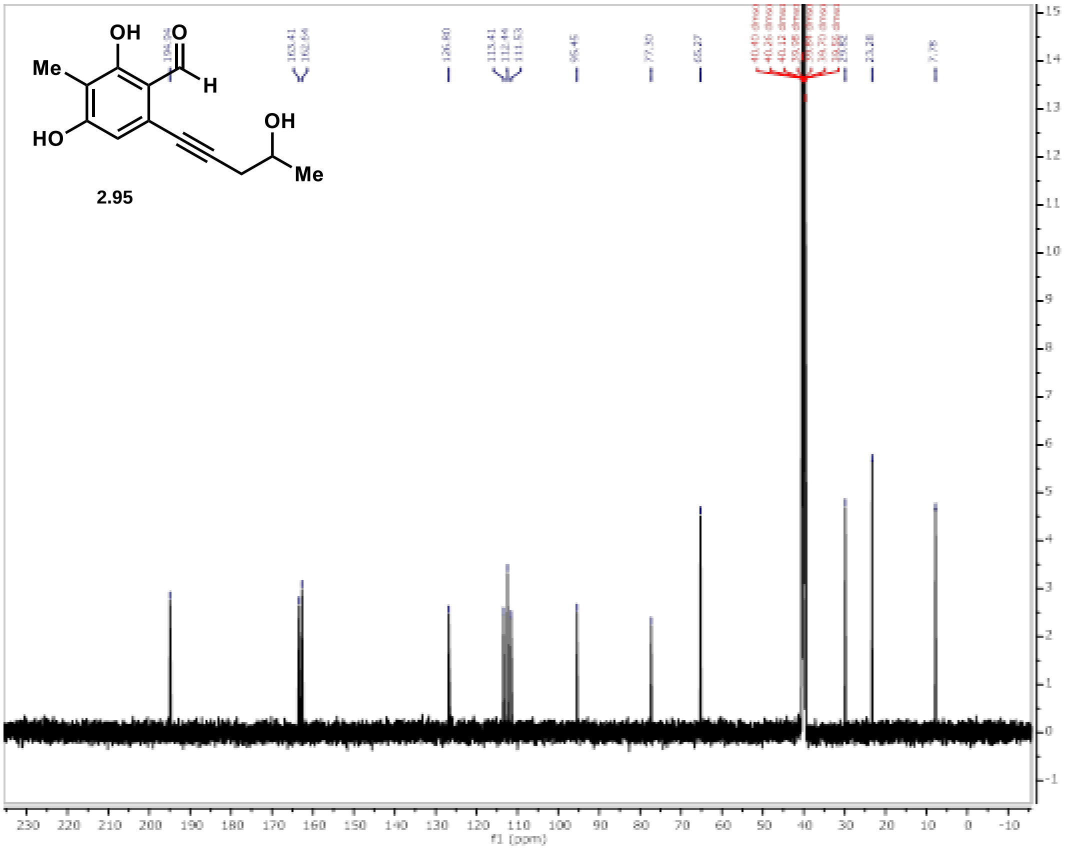
2.95

OH
O
Me
H
HO
OH
Me
194.94
163.41
162.64
126.80
113.41
112.44
111.53
95.45
77.30
65.27
40.40 dmso
40.26 dmso
40.12 dmso
39.98 dmso
39.84 dmso
39.70 dmso
39.56 dmso
29.82
23.28
7.76
230
220
210
200
190
180
170
160
150
140
130
120
110
100
90
80
70
60
50
40
30
20
10
0
-10
f1 (ppm)
15
14
13
12
11
10
9
8
7
6
5
4
3
2
1
0
-1

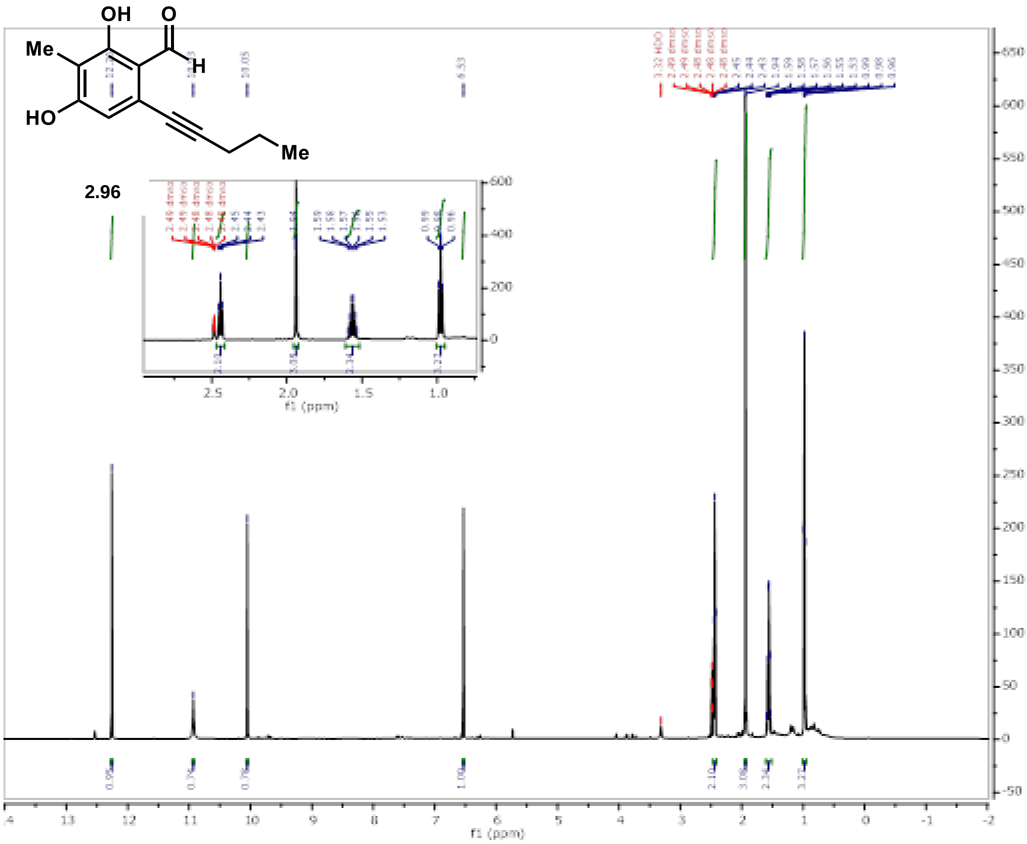

2.96

OH
O
Me
H
HO
Me
3.32 HDO
2.49 dmso
f1 (ppm)
0.95
0.79
0.79
1.00
2.10
3.06
2.34
3.27

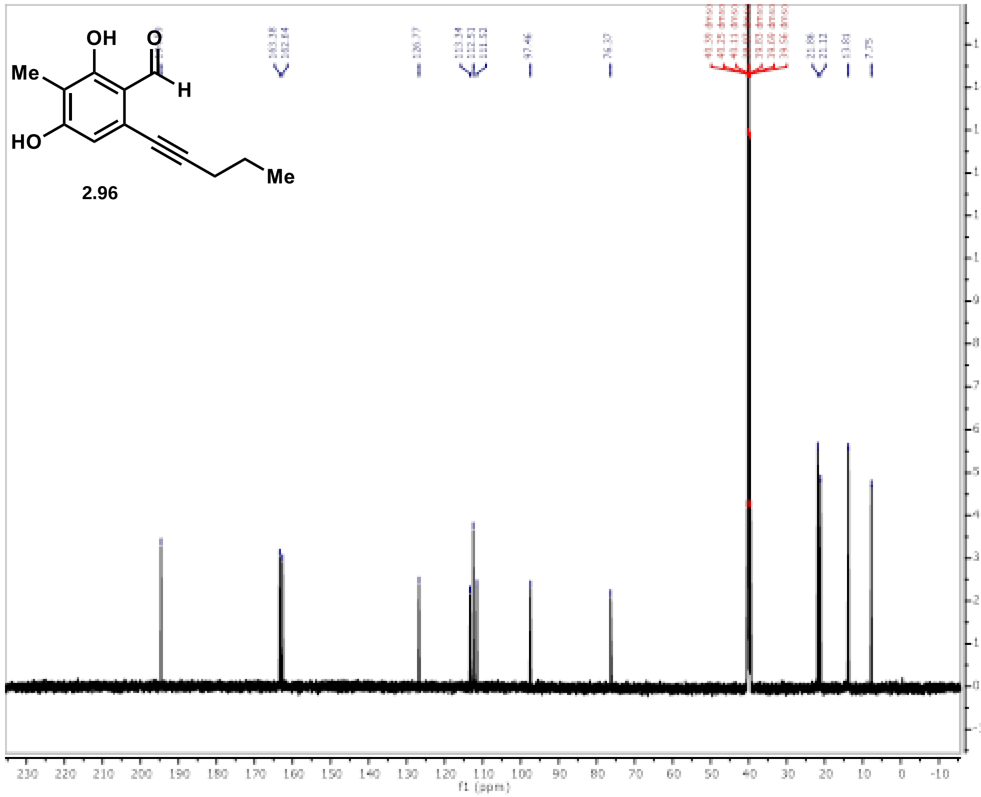

2.96

OH
O
Me
H
HO
Me
163.18
162.64
126.77
113.34
112.53
111.52
97.46
76.37
21.86
21.12
13.81
7.75
f1 (ppm)

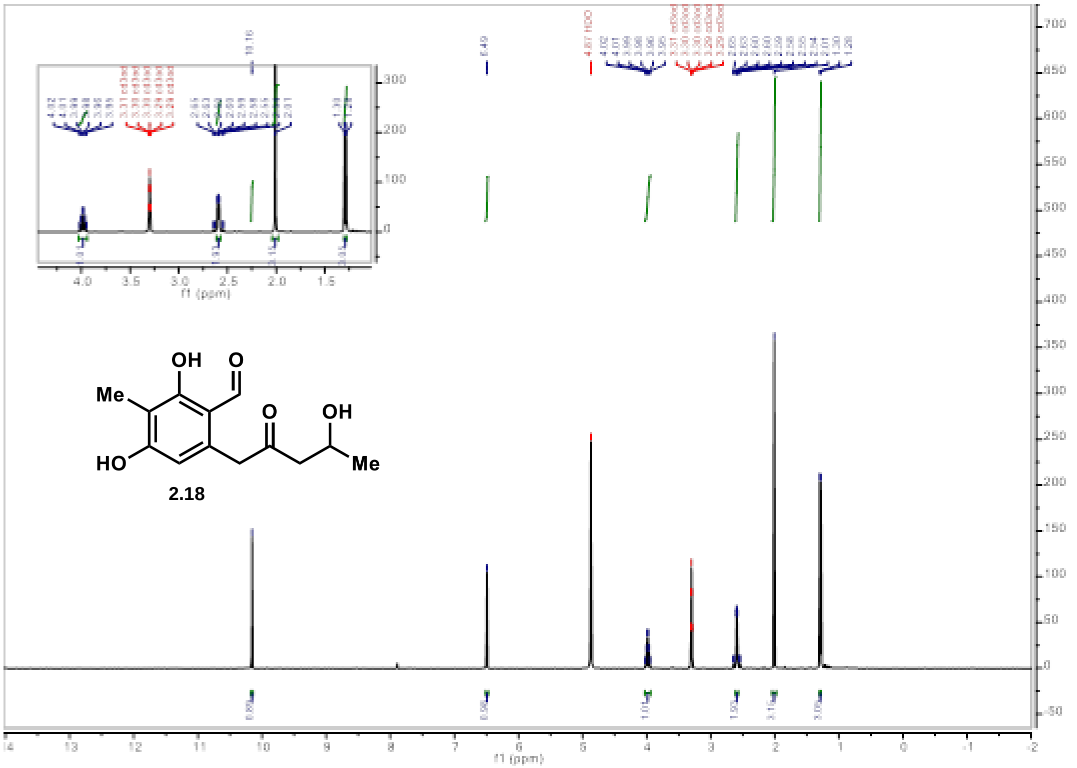10.16
6.49
4.87 HDO
4.02
4.01
3.99
3.98
3.96
3.95
3.31 cd3od
3.30 cd3od
3.30 cd3od
3.29 cd3od
3.29 cd3od
2.65
2.63
2.60
2.59
2.58
2.55
2.54
2.01
1.30
1.28
0.80
0.96
1.01
1.90
3.15
3.05
f1 (ppm)
OH
O
Me
O
OH
HO
Me
2.18

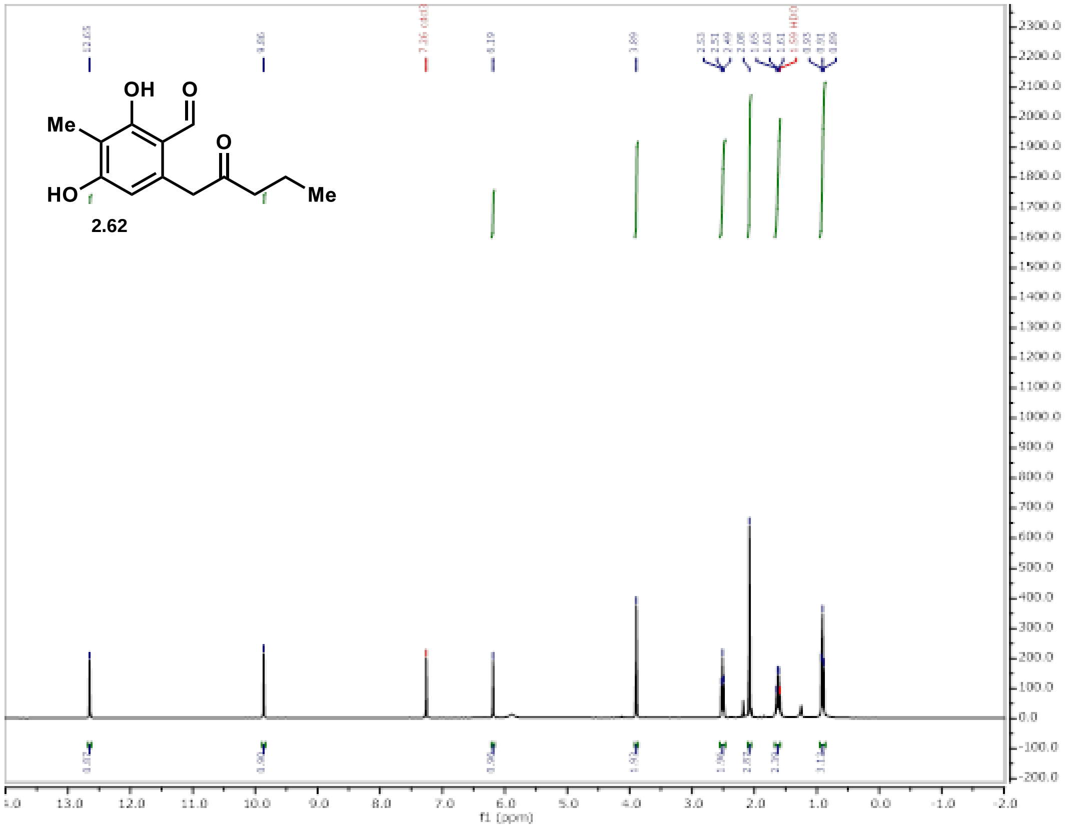
OH
O
Me
O
HO
Me
2.62
12.65
9.86
7.26 cdcl3
6.19
3.89
2.53
2.51
2.49
2.08
1.65
1.63
1.61
1.59 HDO
0.93
0.91
0.89
f1 (ppm)

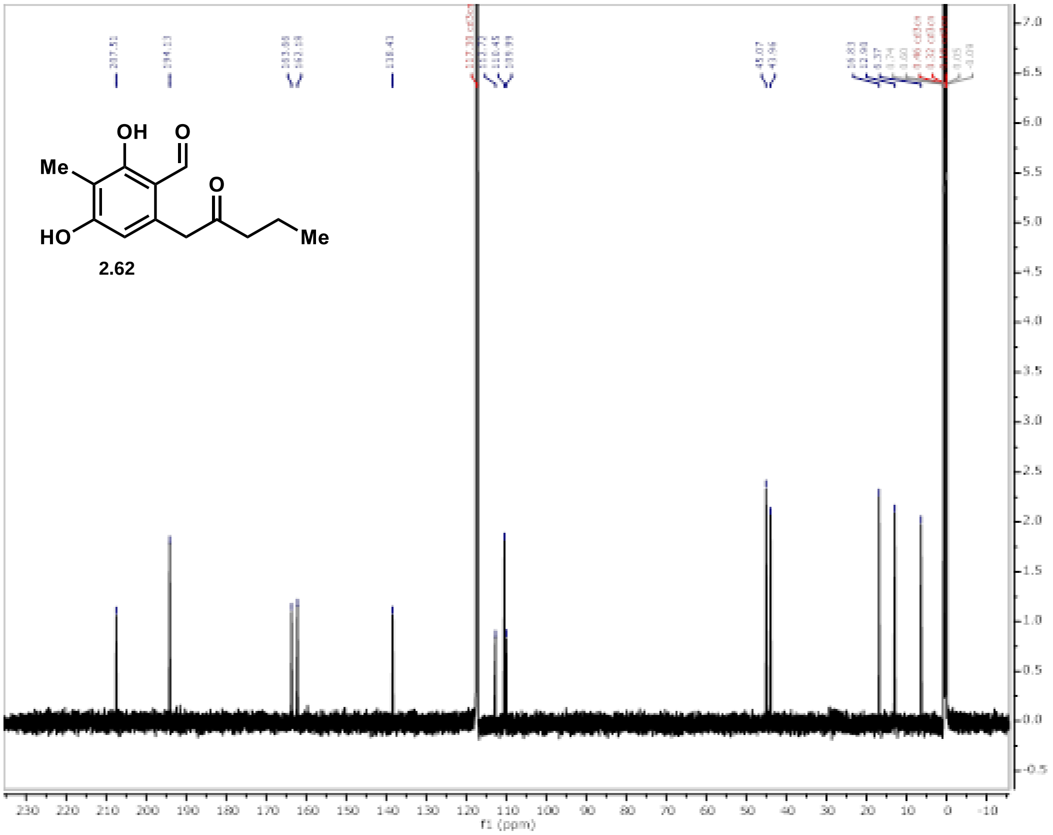
OH
O
Me
O
HO
Me
2.62
207.51
194.13
163.88
162.59
138.43
117.33 cd3cn
112.72
110.45
109.99
45.07
43.96
f1 (ppm)

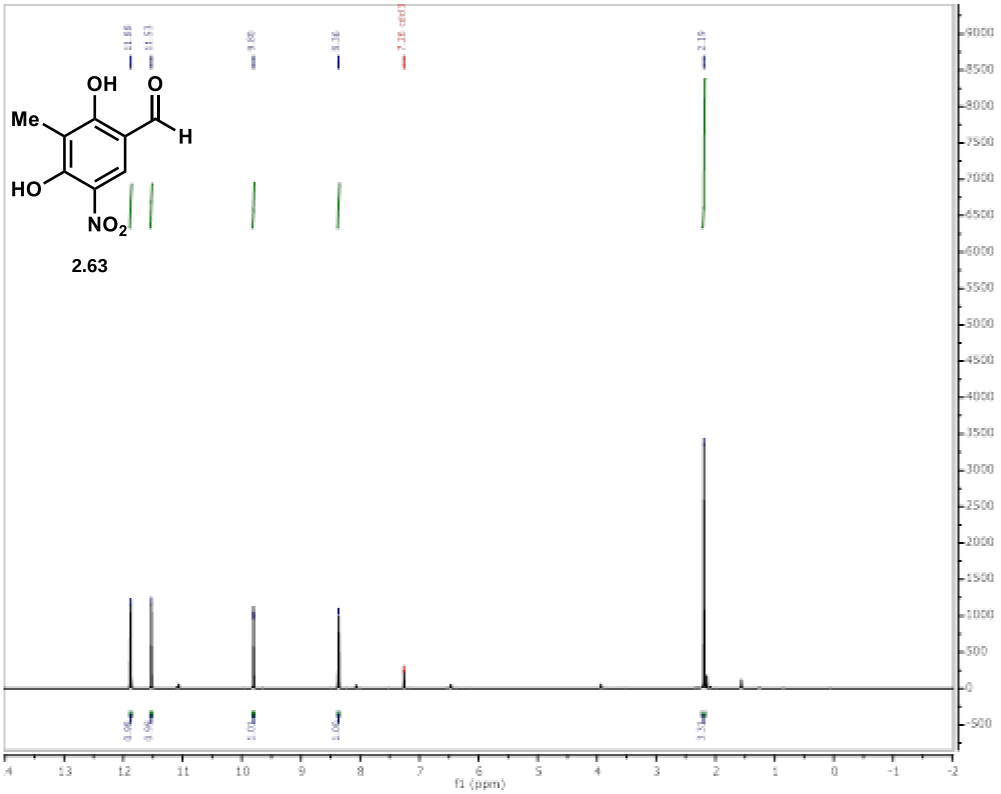
2.63
11.88
11.53
9.80
8.36
7.28 cdcl3
2.19
OH
O
Me
H
HO
NO2
0.96
0.96
1.00
1.06
3.51
9000
8500
8000
7500
7000
6500
6000
5500
5000
4500
4000
3500
3000
2500
2000
1500
1000
500
0
-500
14
13
12
11
10
9
8
7
6
5
4
3
2
1
0
-1
-2
f1 (ppm)

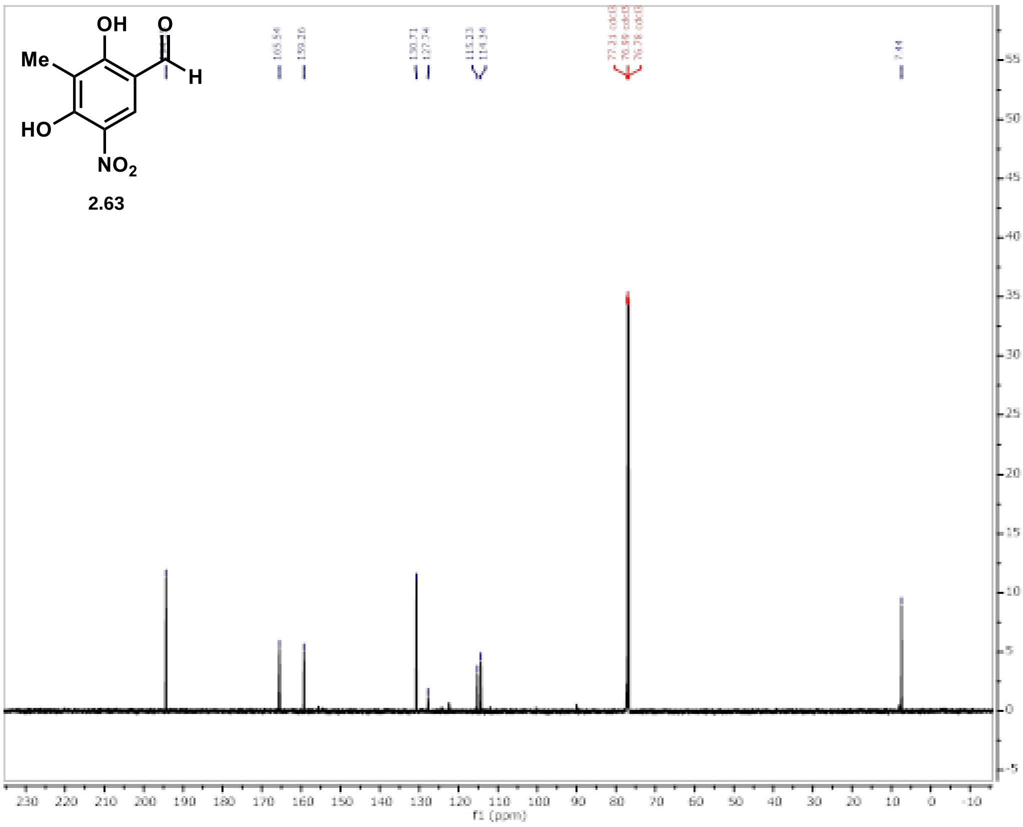
2.63
165.54
159.26
130.71
127.74
115.23
114.34
77.31 cdcl3
76.99 cdcl3
76.78 cdcl3
7.44
OH
O
Me
H
HO
NO2
55
50
45
40
35
30
25
20
15
10
5
0
-5
230
220
210
200
190
180
170
160
150
140
130
120
110
100
90
80
70
60
50
40
30
20
10
0
-10
f1 (ppm)

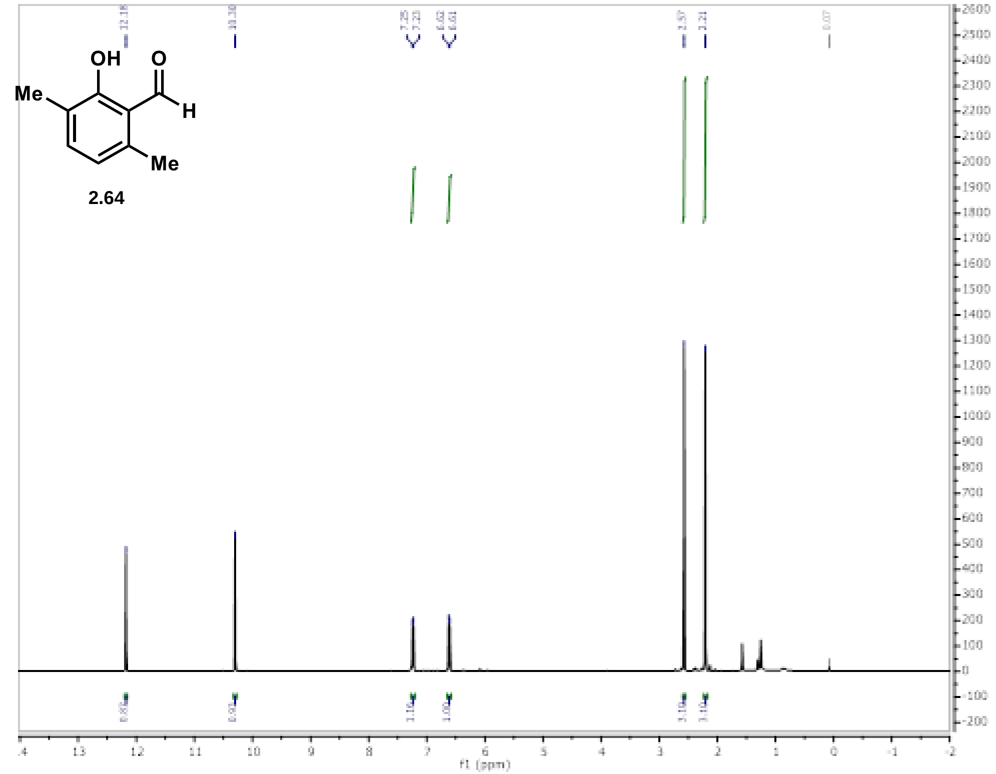
12.18
10.30
7.25
7.23
6.62
6.61
2.57
2.21
0.07
OH
O
Me
H
Me
2.64
0.88
0.91
1.16
1.00
3.18
3.10
2600
2500
2400
2300
2200
2100
2000
1900
1800
1700
1600
1500
1400
1300
1200
1100
1000
900
800
700
600
500
400
300
200
100
0
-100
-200
14
13
12
11
10
9
8
7
6
5
4
3
2
1
0
-1
-2
f1 (ppm)

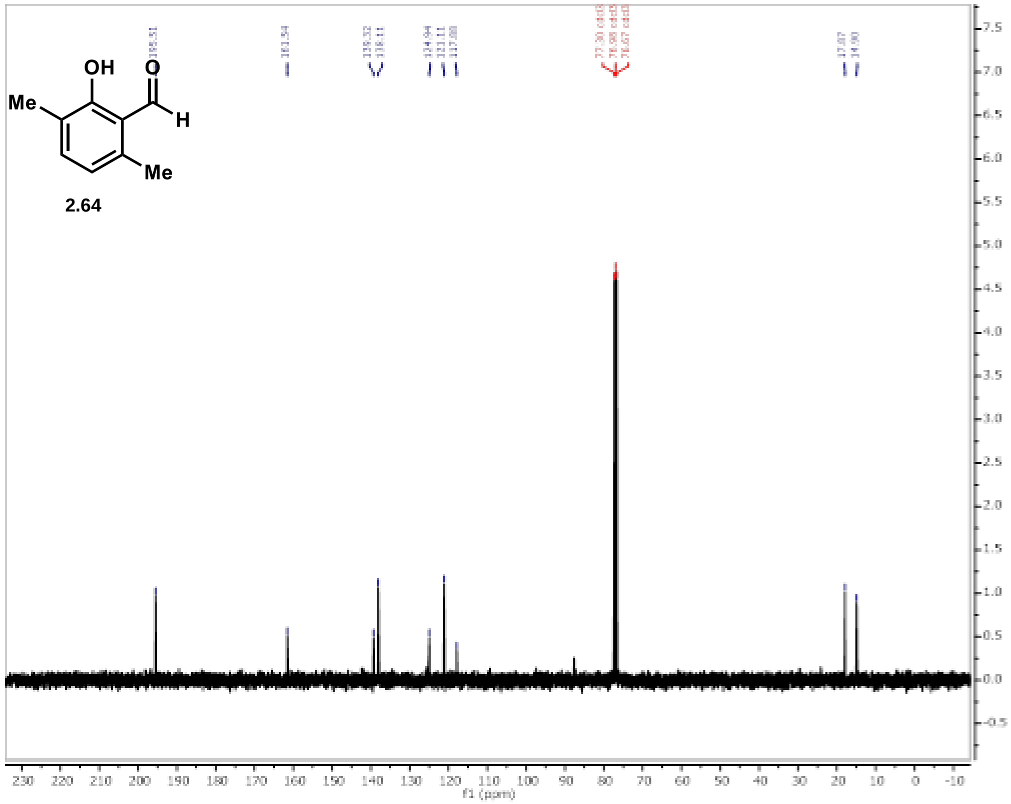
195.51
161.54
139.32
138.11
124.94
121.11
117.88
77.30 cdcl3
76.98 cdcl3
76.67 cdcl3
17.87
14.90
OH
O
Me
H
Me
2.64
7.5
7.0
6.5
6.0
5.5
5.0
4.5
4.0
3.5
3.0
2.5
2.0
1.5
1.0
0.5
0.0
-0.5
230
220
210
200
190
180
170
160
150
140
130
120
110
100
90
80
70
60
50
40
30
20
10
0
-10
f1 (ppm)

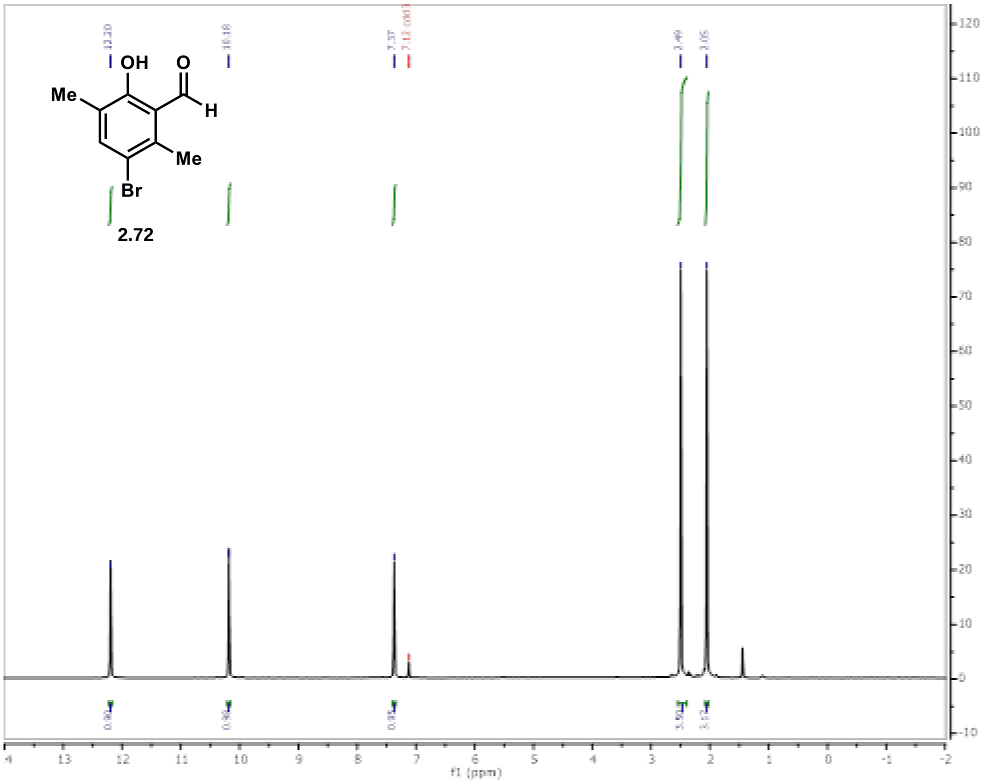
12.20
10.18
7.37
7.12 cdcl3
2.49
2.05
OH
O
Me
H
Me
Br
2.72
f1 (ppm)

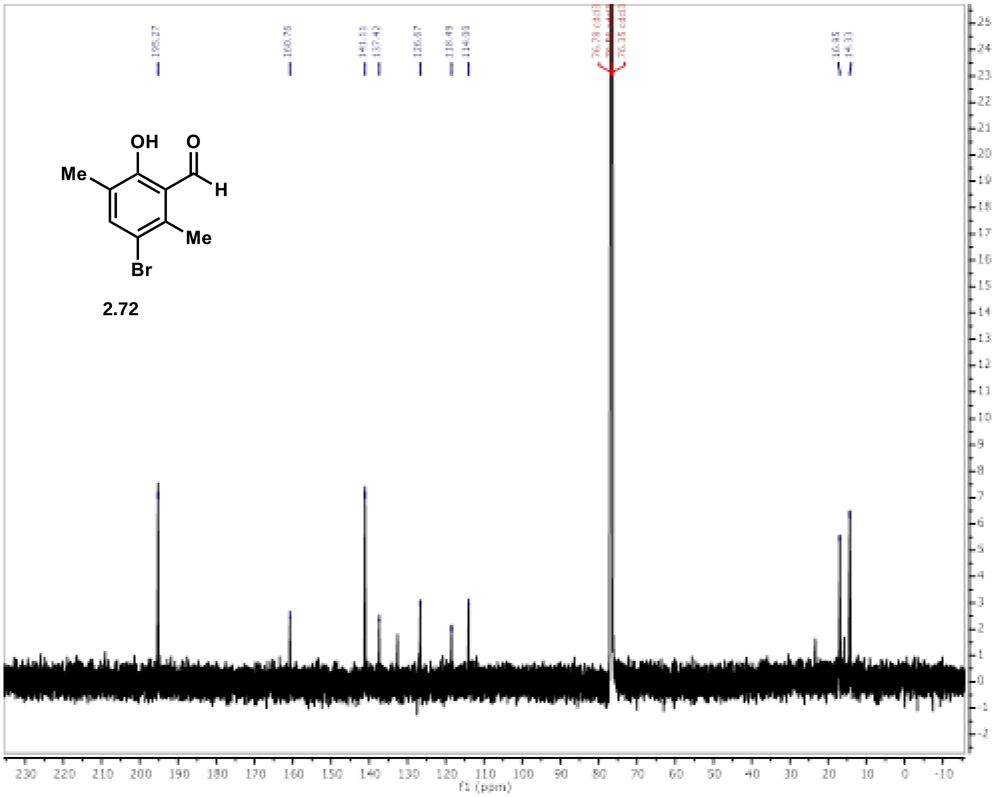
195.27
160.78
141.11
137.42
126.87
118.49
114.01
76.78 cdcl3
76.46 cdcl3
76.15 cdcl3
16.85
14.33
OH
O
Me
H
Me
Br
2.72
f1 (ppm)

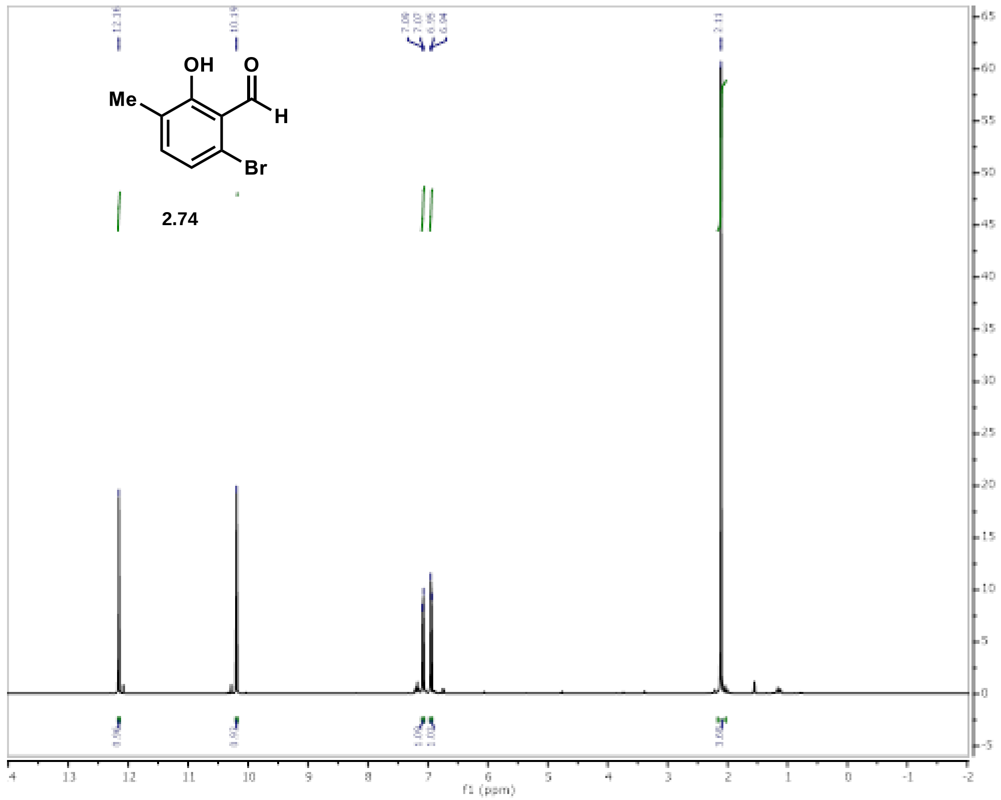
12.16
10.19
7.09
7.07
6.95
6.94
2.11
OH
O
Me
H
Br
0.96
0.91
1.00
1.03
3.04
f1 (ppm)

2.74

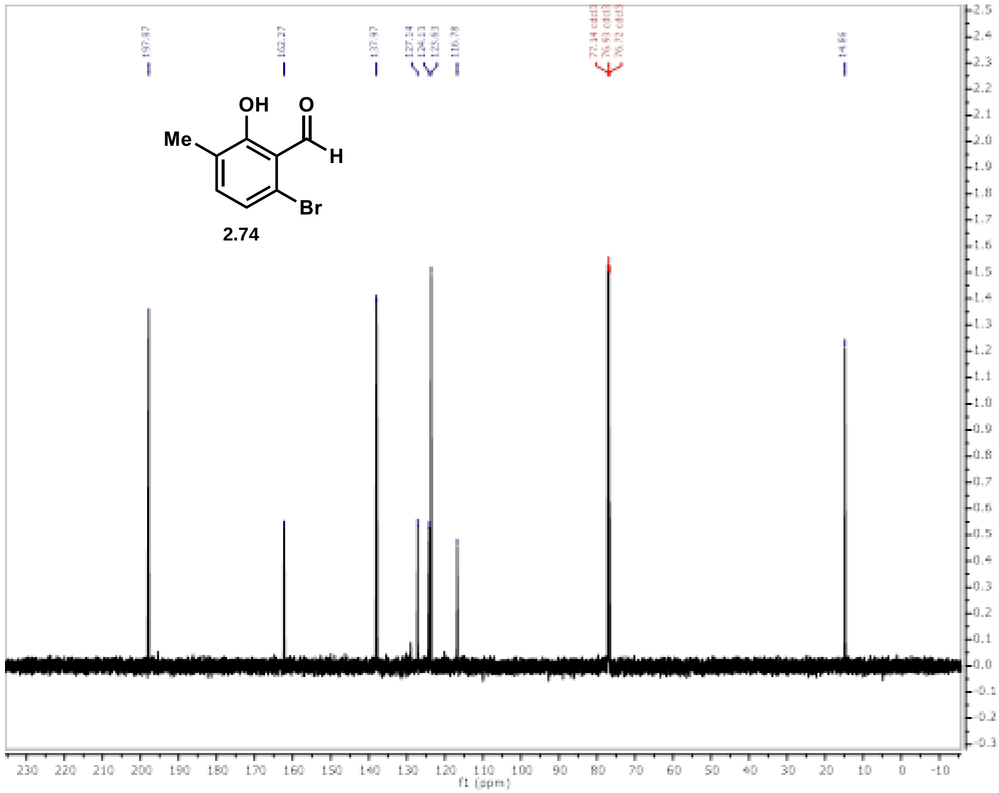
197.87
162.27
137.97
127.54
124.13
123.93
116.78
77.34 cdcl3
76.93 cdcl3
76.72 cdcl3
14.86
OH
O
Me
H
Br
f1 (ppm)

2.74

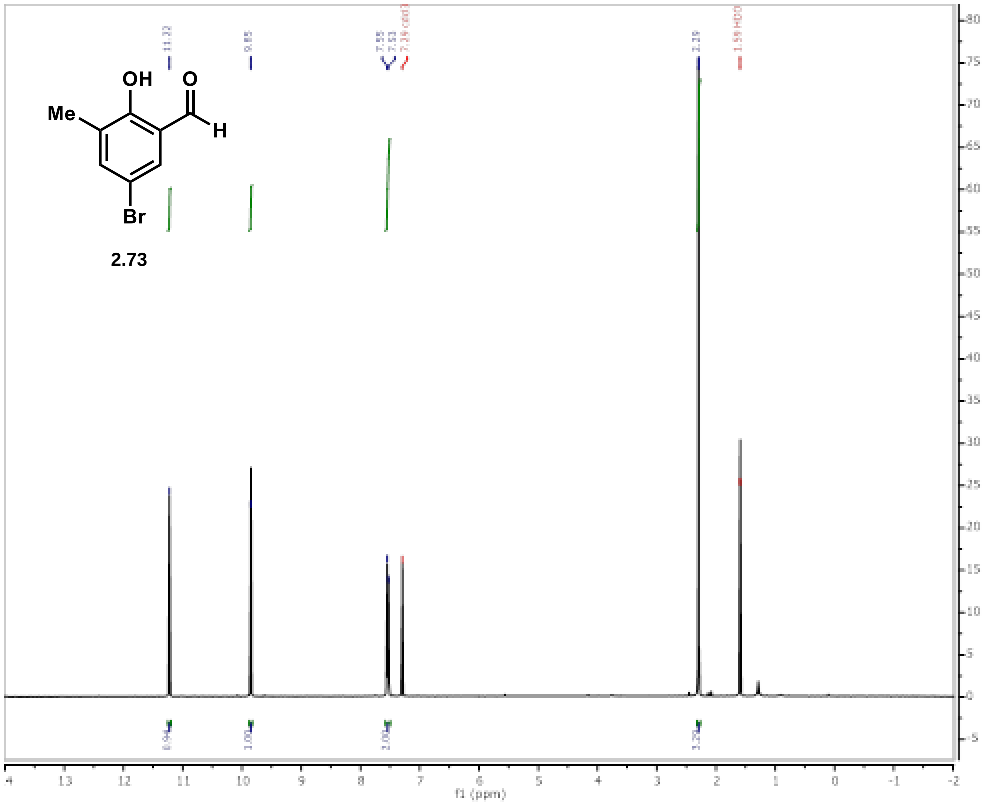
OH
O
Me
H
Br
2.73
11.22
9.85
7.55
7.53
7.29 cdcl3
2.29
1.59 HDO
0.94
1.00
2.00
3.29
f1 (ppm)

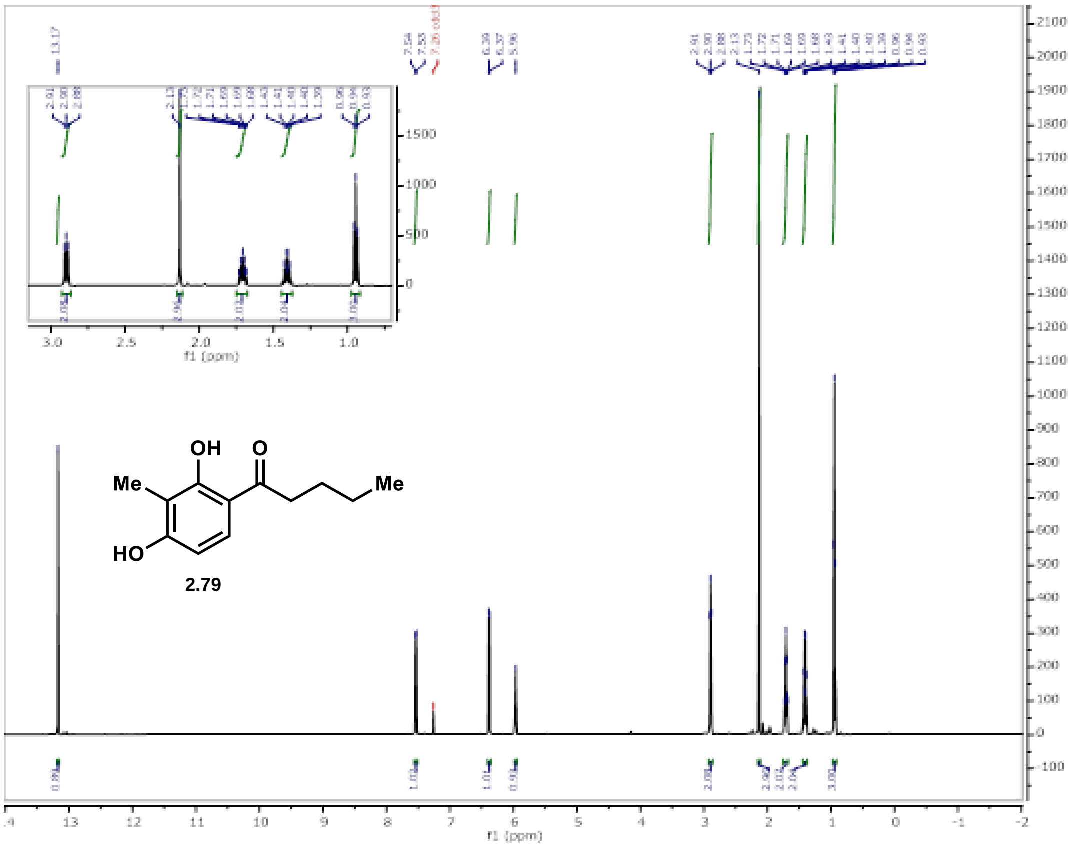
13.17
7.54
7.53
7.26 cdcl3
6.39
6.37
5.96
2.91
2.90
2.88
2.13
1.73
1.72
1.71
1.69
1.69
1.68
1.43
1.41
1.40
1.40
1.39
0.96
0.94
0.93
0.89
1.03
1.01
0.93
2.08
2.96
2.01
2.04
3.00
OH
O
Me
Me
HO
f1 (ppm)

2.79

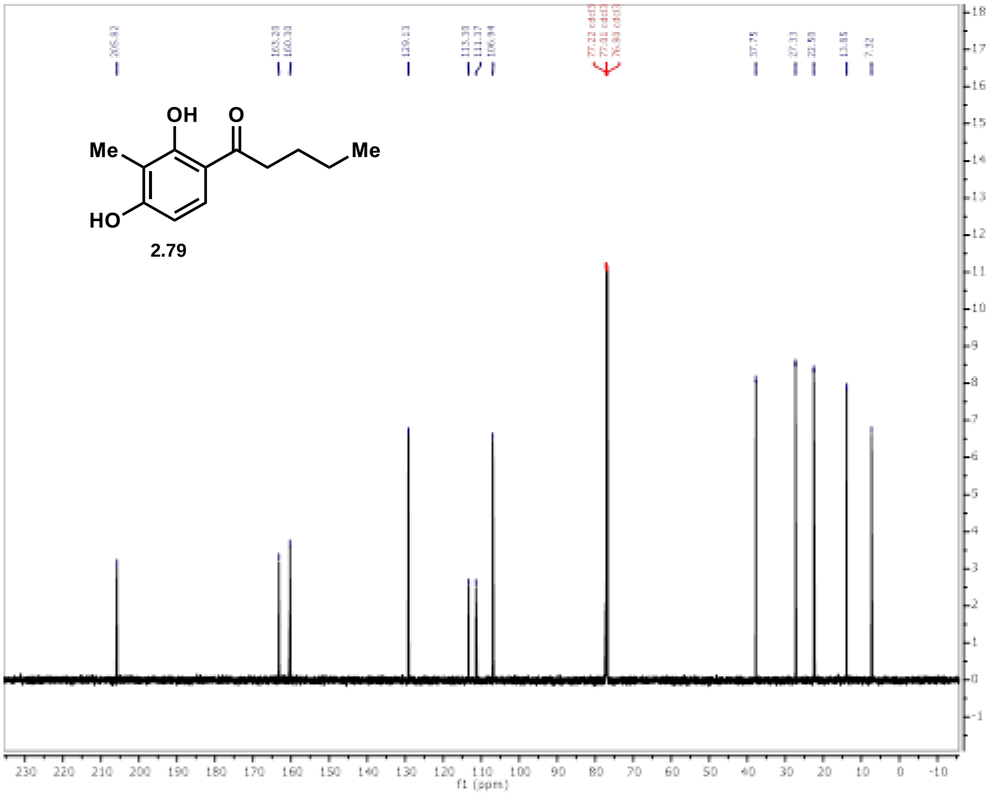
205.82
163.20
160.33
129.13
113.33
111.37
106.94
77.32 cdcl3
77.01 cdcl3
76.69 cdcl3
37.75
27.33
22.53
13.85
7.32
OH
O
Me
Me
HO
f1 (ppm)

2.79

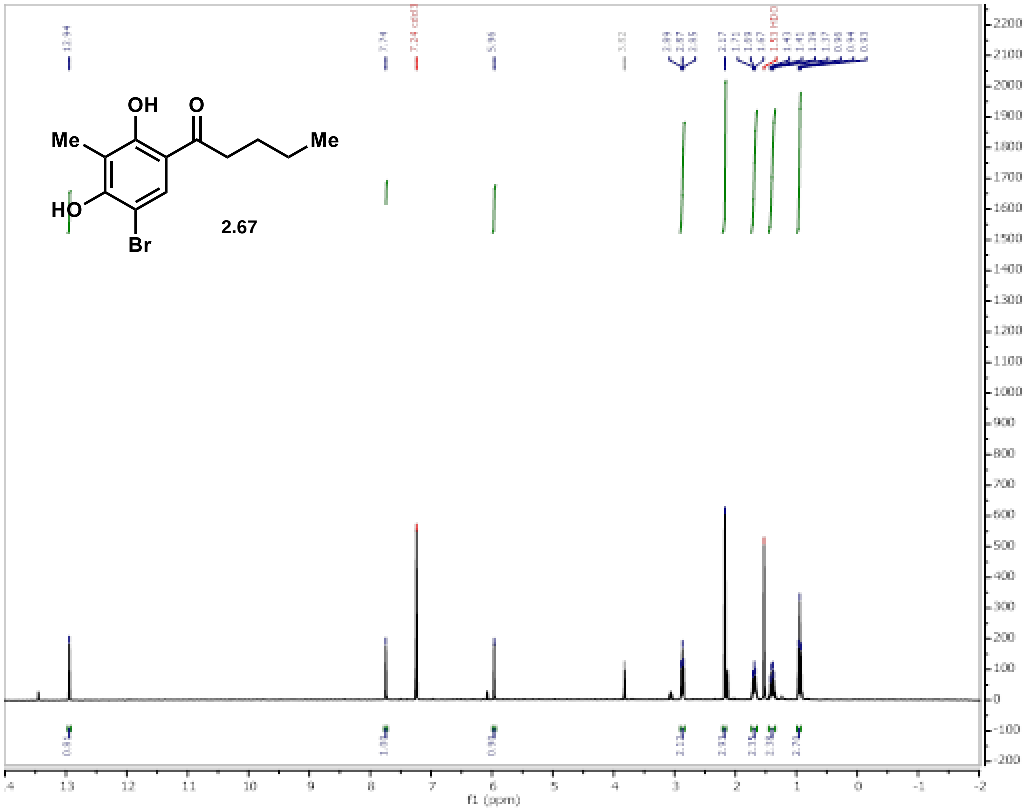
12.94
7.74
7.24 cdcl3
5.96
3.82
2.89
2.87
2.85
2.17
1.71
1.69
1.67
1.53 HDO
1.43
1.41
1.39
1.37
0.96
0.94
0.93
OH
O
Me
Me
HO
Br
2.67
f1 (ppm)

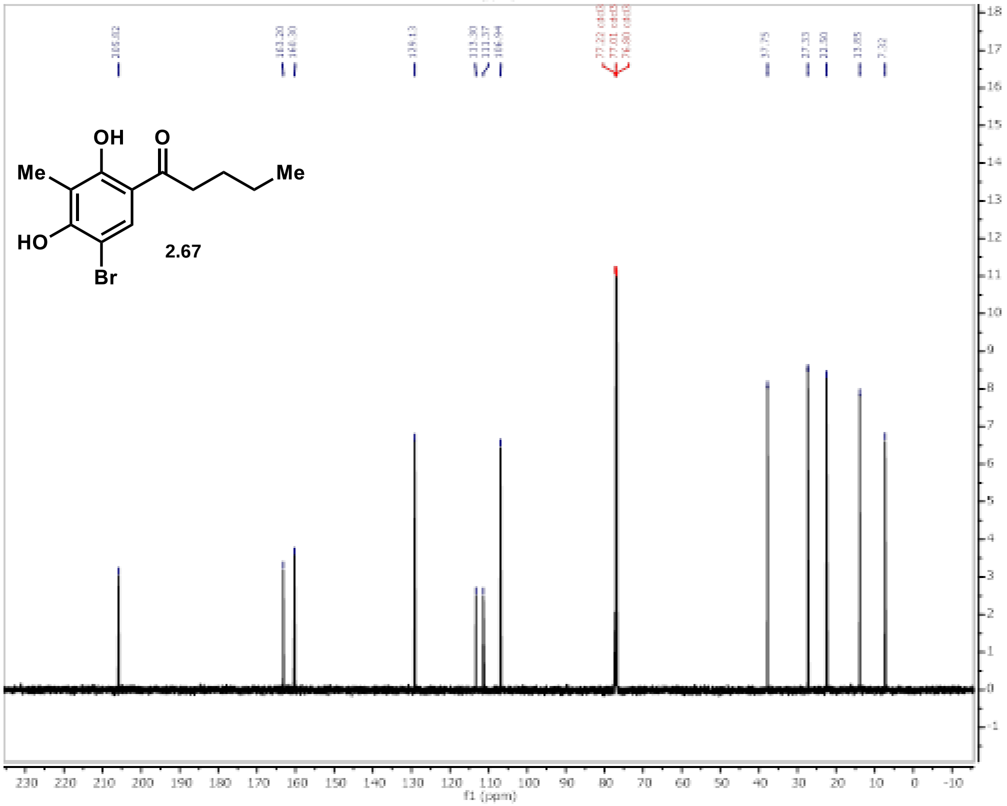
205.82
163.20
160.30
129.13
113.30
111.37
106.94
77.22 cdcl3
77.01 cdcl3
76.80 cdcl3
37.75
27.33
22.50
13.85
7.32
OH
O
Me
Me
HO
Br
2.67
f1 (ppm)

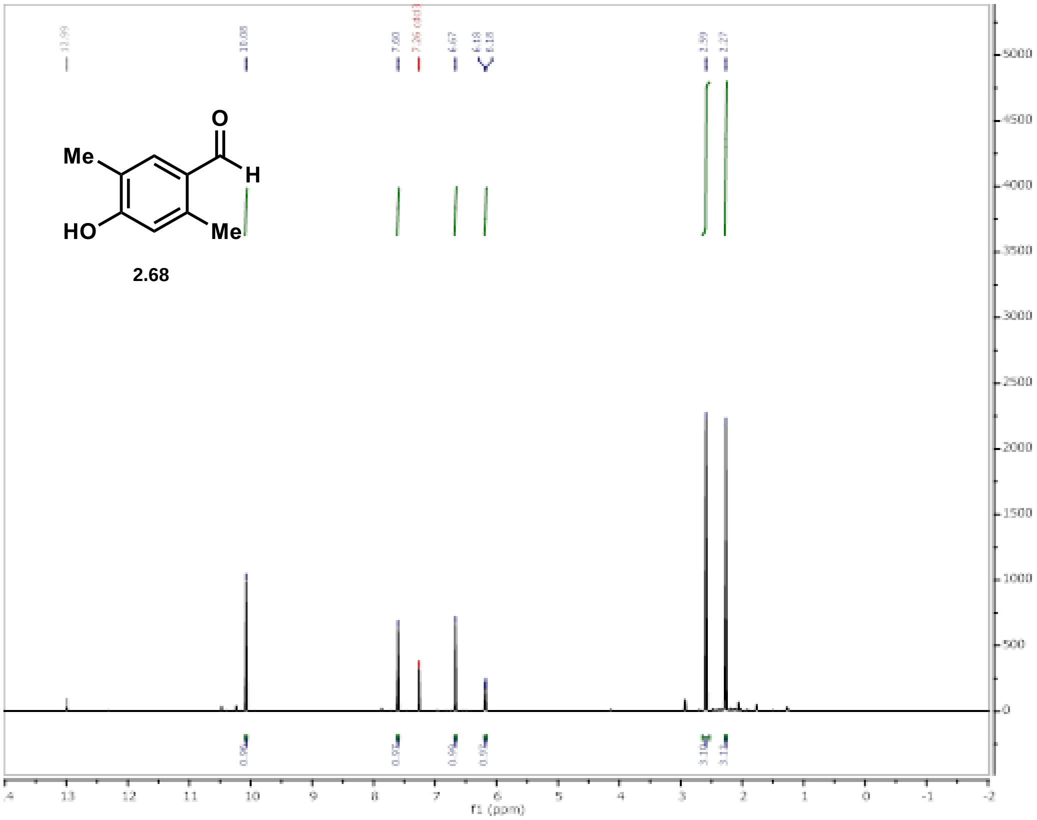
13.99
10.08
7.60
7.26 cdcl3
6.67
6.18
6.18
2.59
2.27
O
Me
H
HO
Me
2.68
0.96
0.97
0.99
0.96
3.10
3.11
5000
4500
4000
3500
3000
2500
2000
1500
1000
500
0
14
13
12
11
10
9
8
7
6
5
4
3
2
1
0
-1
-2
f1 (ppm)

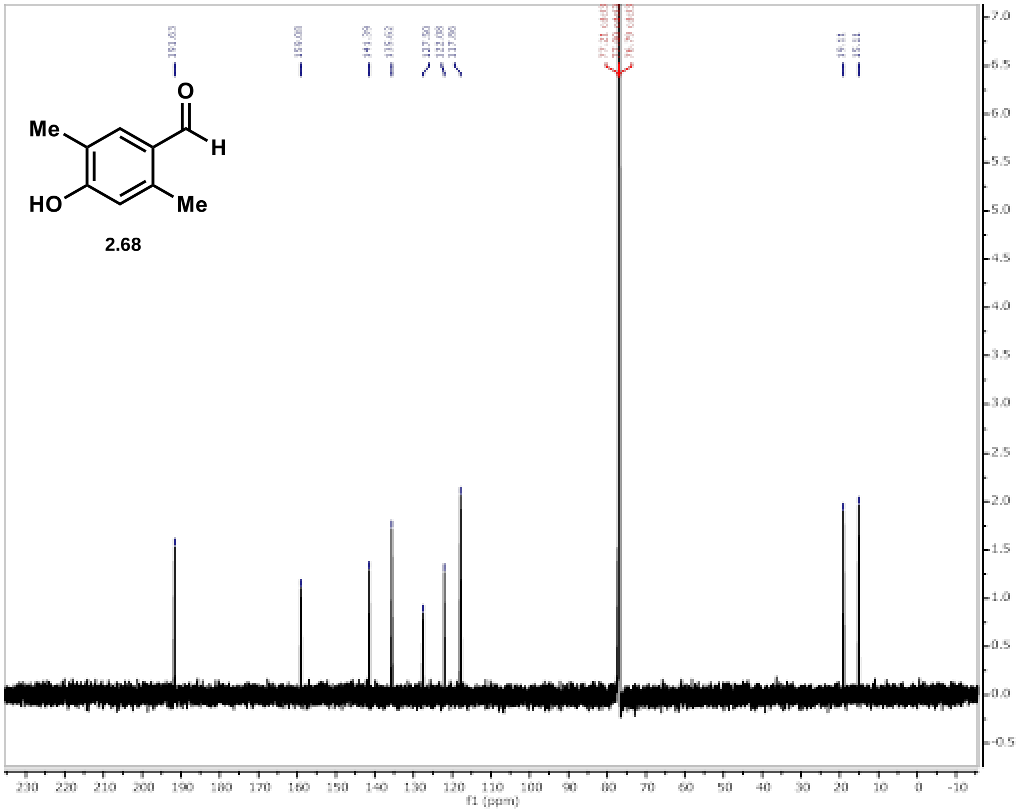
191.63
159.08
141.39
135.62
127.50
122.08
117.86
77.21 cdcl3
77.00 cdcl3
76.79 cdcl3
19.11
15.11
O
Me
H
HO
Me
2.68
7.0
6.5
6.0
5.5
5.0
4.5
4.0
3.5
3.0
2.5
2.0
1.5
1.0
0.5
0.0
-0.5
230
220
210
200
190
180
170
160
150
140
130
120
110
100
90
80
70
60
50
40
30
20
10
0
-10
f1 (ppm)

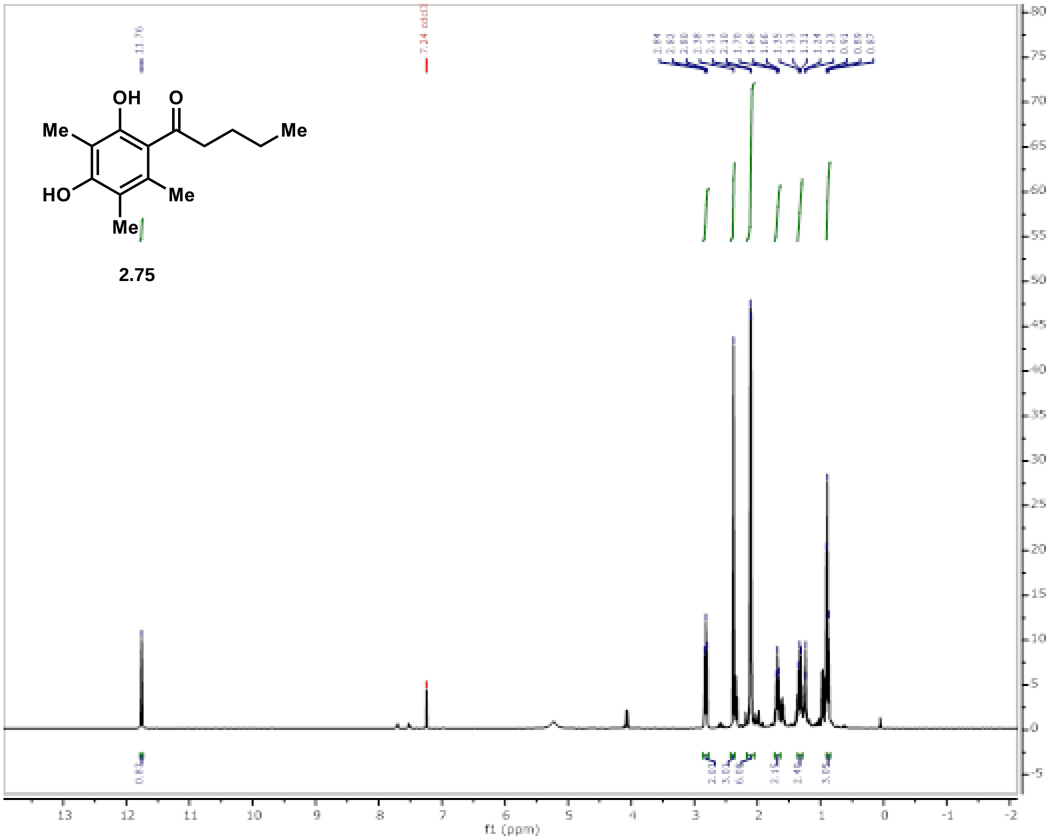
11.76
7.24 cdcl3
2.84
2.82
2.80
2.38
2.31
2.10
1.70
1.68
1.66
1.35
1.33
0.93
0.89
0.87
OH
O
Me
Me
HO
Me
Me
0.83
2.02
3.01
6.00
2.15
2.16
3.05
13
12
11
10
9
8
7
6
5
4
3
2
1
0
-1
-2
f1 (ppm)
80
75
70
65
60
55
50
45
40
35
30
25
20
15
10
5
0
-5

2.75

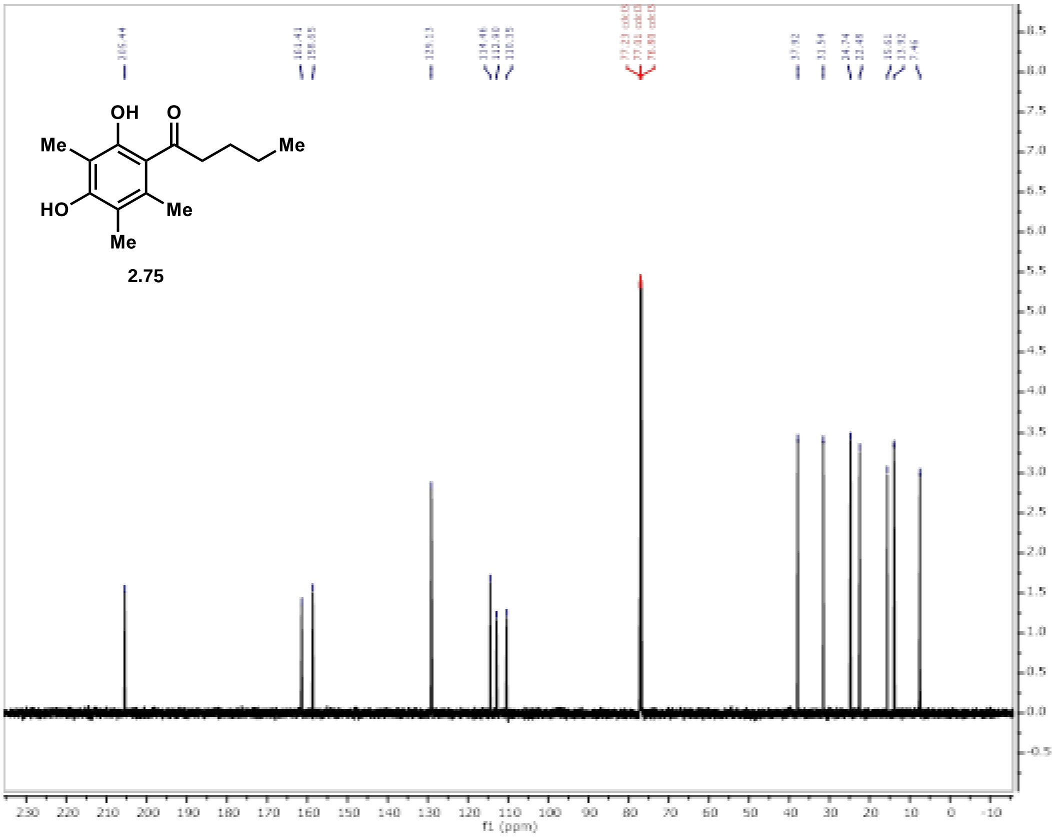
205.44
161.41
158.65
129.13
114.46
112.90
110.35
77.23 cdcl3
77.01 cdcl3
76.80 cdcl3
37.92
31.54
24.74
22.48
15.61
13.92
7.46
OH
O
Me
Me
HO
Me
Me
230
220
210
200
190
180
170
160
150
140
130
120
110
100
90
80
70
60
50
40
30
20
10
0
-10
f1 (ppm)
8.5
8.0
7.5
7.0
6.5
6.0
5.5
5.0
4.5
4.0
3.5
3.0
2.5
2.0
1.5
1.0
0.5
0.0
-0.5

2.75

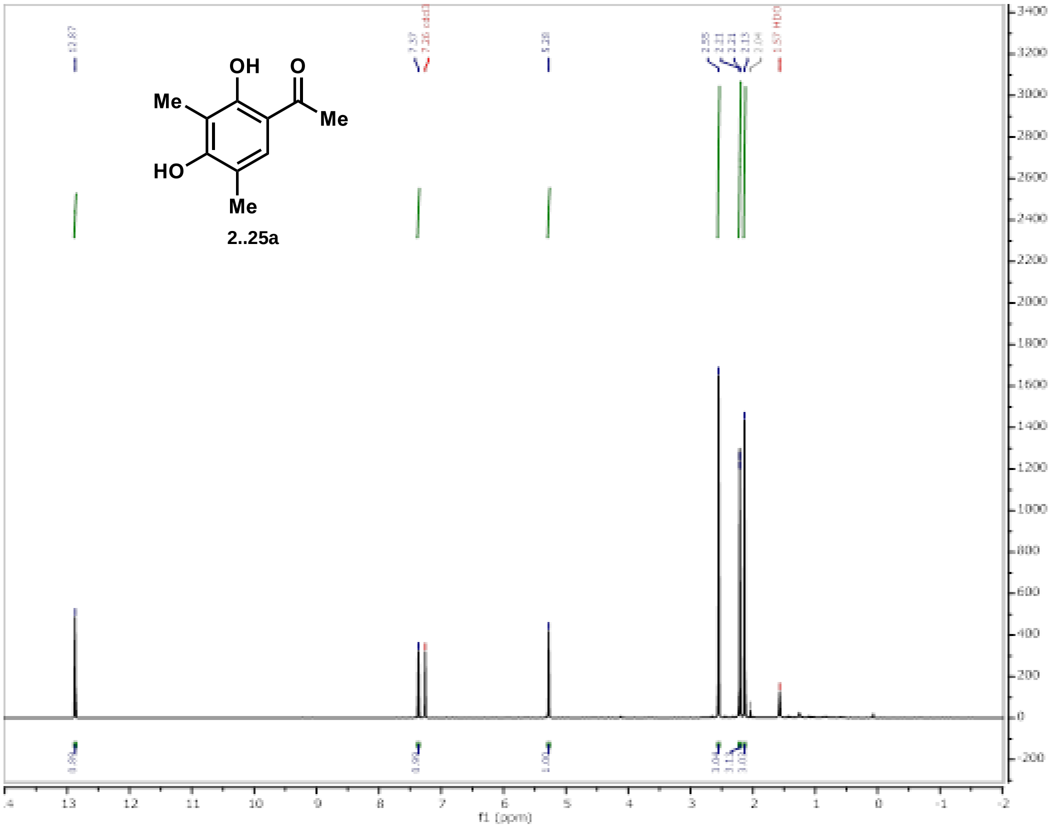
12.87
7.37
7.26 cdcl3
5.28
2.55
2.21
2.21
2.13
2.04
1.57 HDO
OH
O
Me
Me
HO
Me
2..25a
0.89
0.90
1.00
3.04
3.11
3.02
f1 (ppm)

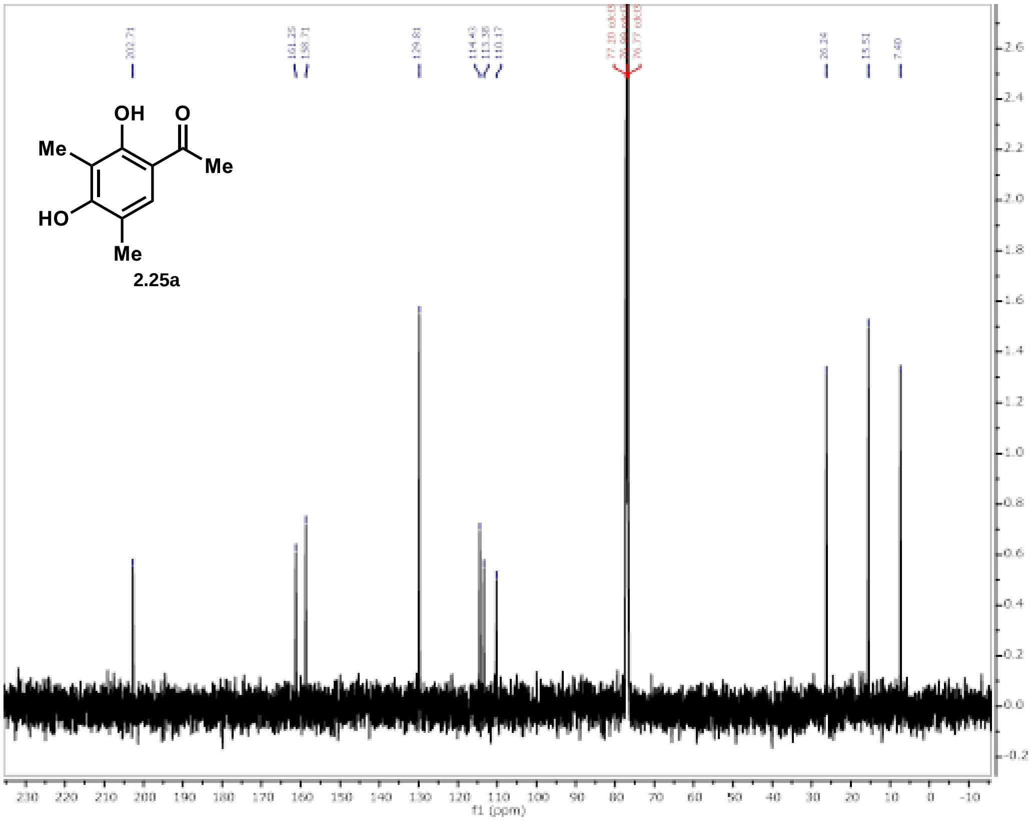
202.71
161.25
158.71
129.81
114.43
113.38
110.17
77.20 cdcl3
76.99 cdcl3
76.77 cdcl3
26.24
15.51
7.40
OH
O
Me
Me
HO
Me
2.25a
f1 (ppm)

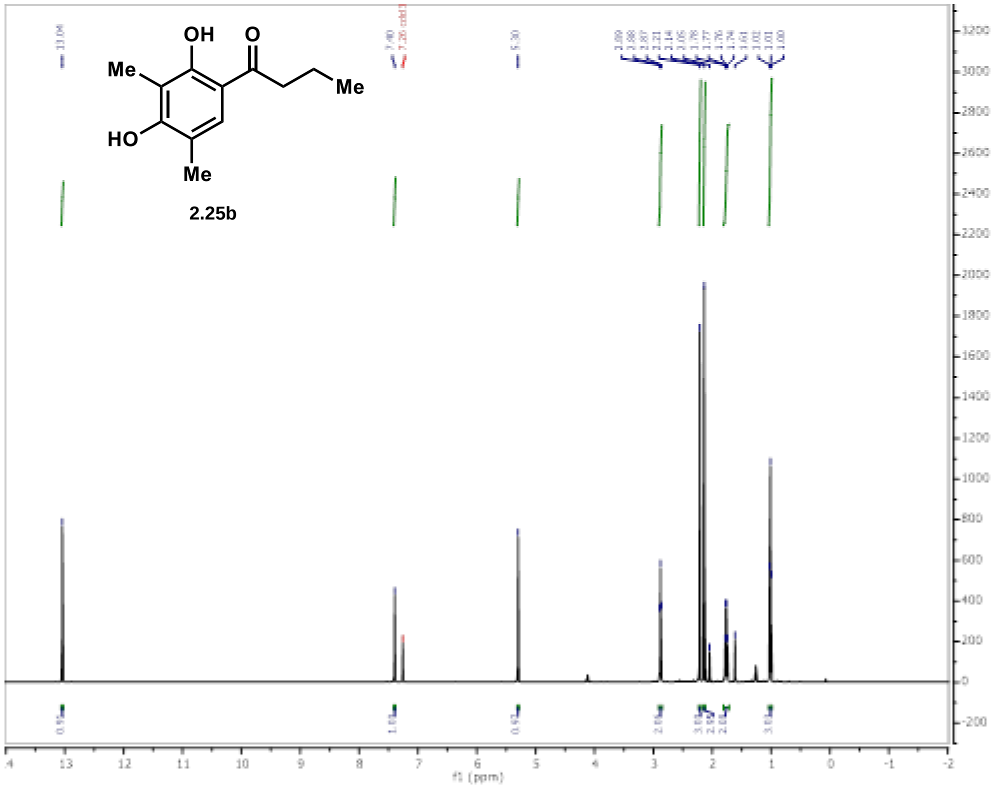
13.04
7.40
7.26 cdcl3
5.30
2.89
2.88
2.87
2.21
2.14
2.05
1.78
1.77
1.76
1.74
1.61
1.02
1.01
1.00
OH
O
Me
Me
HO
Me
0.95
1.01
0.92
2.06
3.00
2.92
2.04
3.01
f1 (ppm)

2.25b

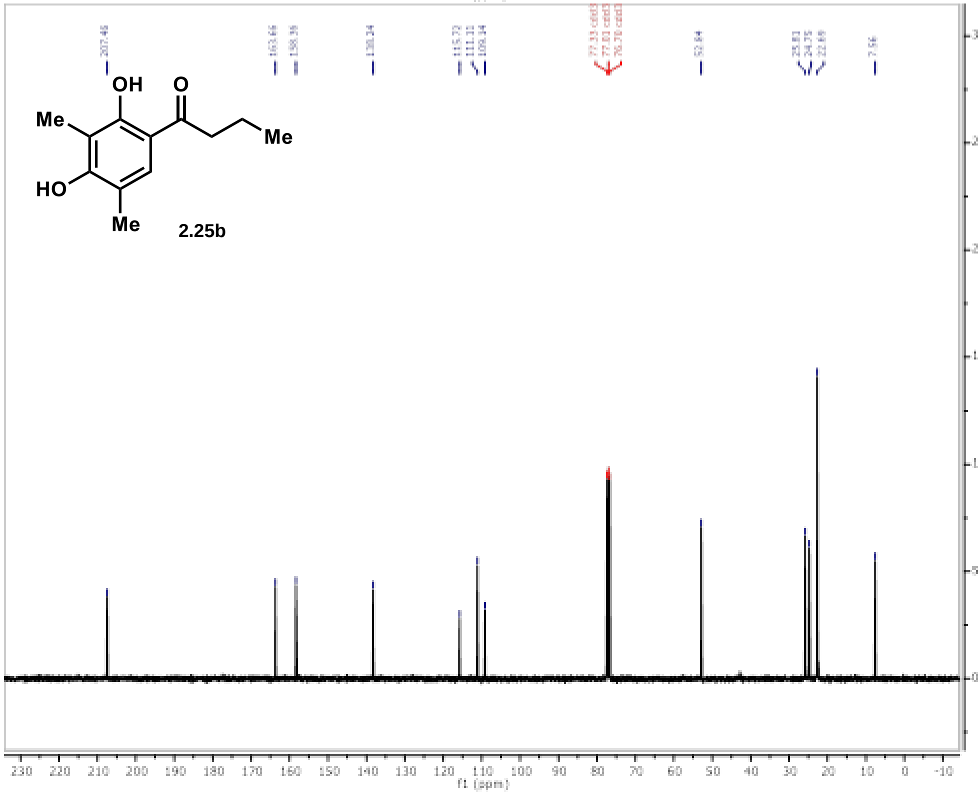
207.46
163.66
158.36
138.24
115.73
111.11
109.14
77.33 cdcl3
77.01 cdcl3
76.70 cdcl3
52.84
25.83
24.75
22.89
7.56
OH
O
Me
Me
HO
Me
f1 (ppm)

2.25b

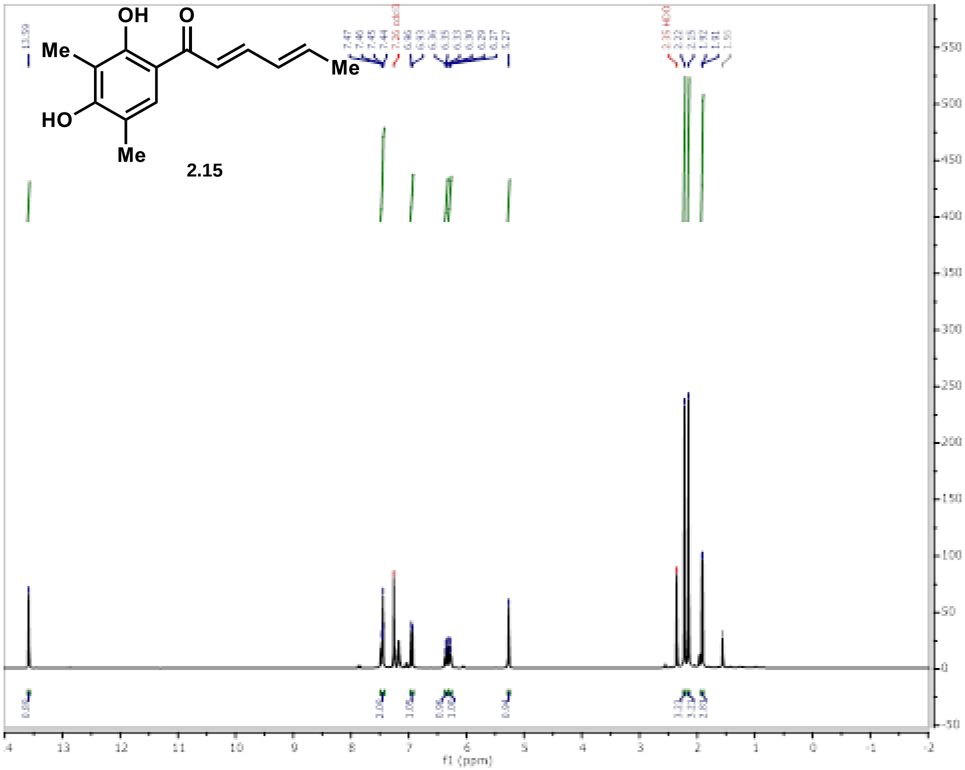
OH
O
Me
HO
Me
Me
13.59
7.47
7.46
7.45
7.44
7.26 cdcl3
6.96
6.93
6.36
6.35
6.33
6.30
6.29
6.27
5.27
2.35 HOD
2.22
2.15
1.92
1.91
1.55
550
500
450
400
350
300
250
200
150
100
50
0
-50
14
13
12
11
10
9
8
7
6
5
4
3
2
1
0
-1
-2
f1 (ppm)

2.15

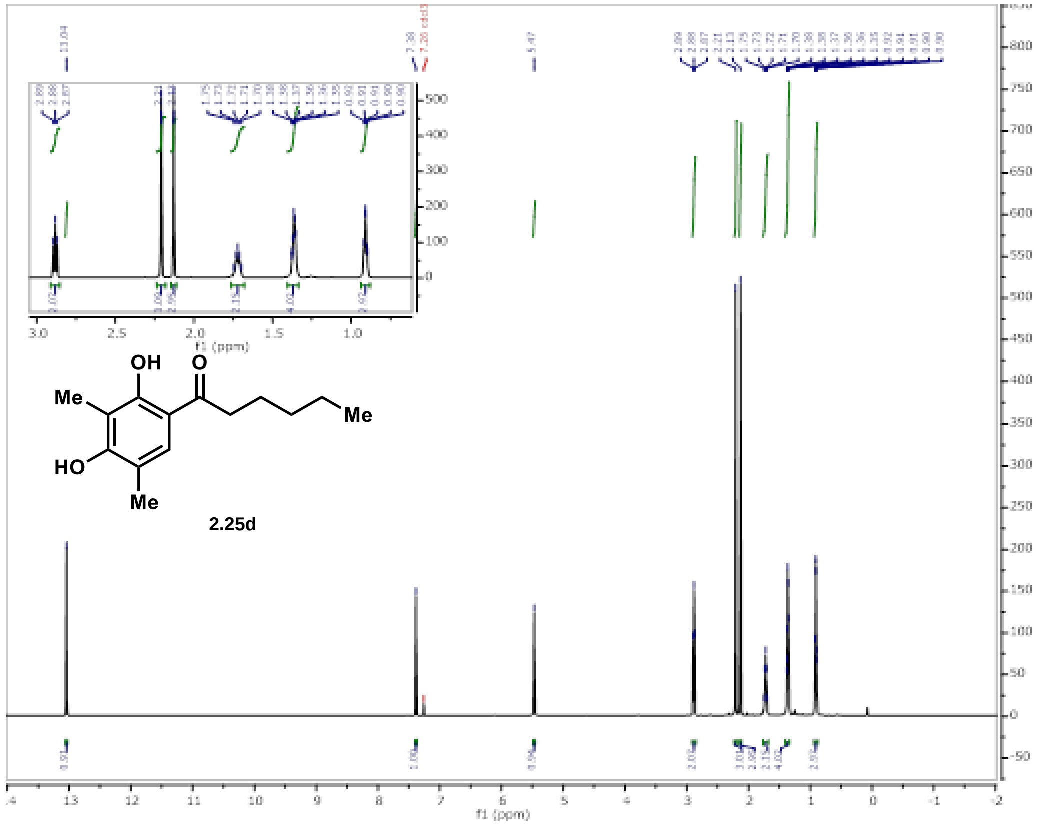
13.04
7.38
7.26 cdcl3
5.47
2.89
2.88
2.87
2.21
2.13
0.91
1.00
0.96
2.03
3.01
2.96
2.15
4.02
2.93
f1 (ppm)
OH
O
Me
HO
Me
Me

2.25d

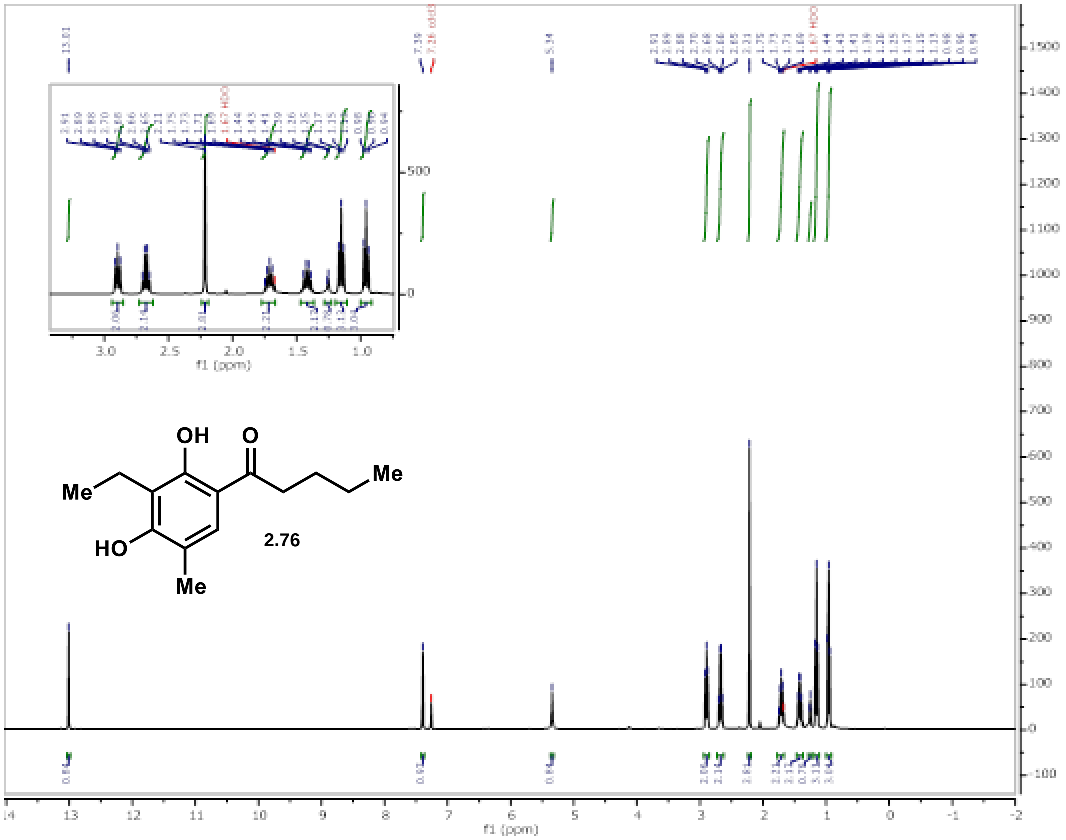
13.01
7.39
7.26 cdcl3
5.34
2.91
2.89
2.88
2.70
2.68
2.66
2.65
2.21
1.75
1.73
1.71
1.69
1.67 HDO
1.44
1.43
1.41
1.39
1.36
1.35
1.17
1.15
1.13
0.98
0.96
0.94
0.84
0.87
0.84
2.06
2.14
2.81
2.21
2.17
0.78
3.14
3.04
OH
O
Me
Me
HO
Me
2.76
f1 (ppm)

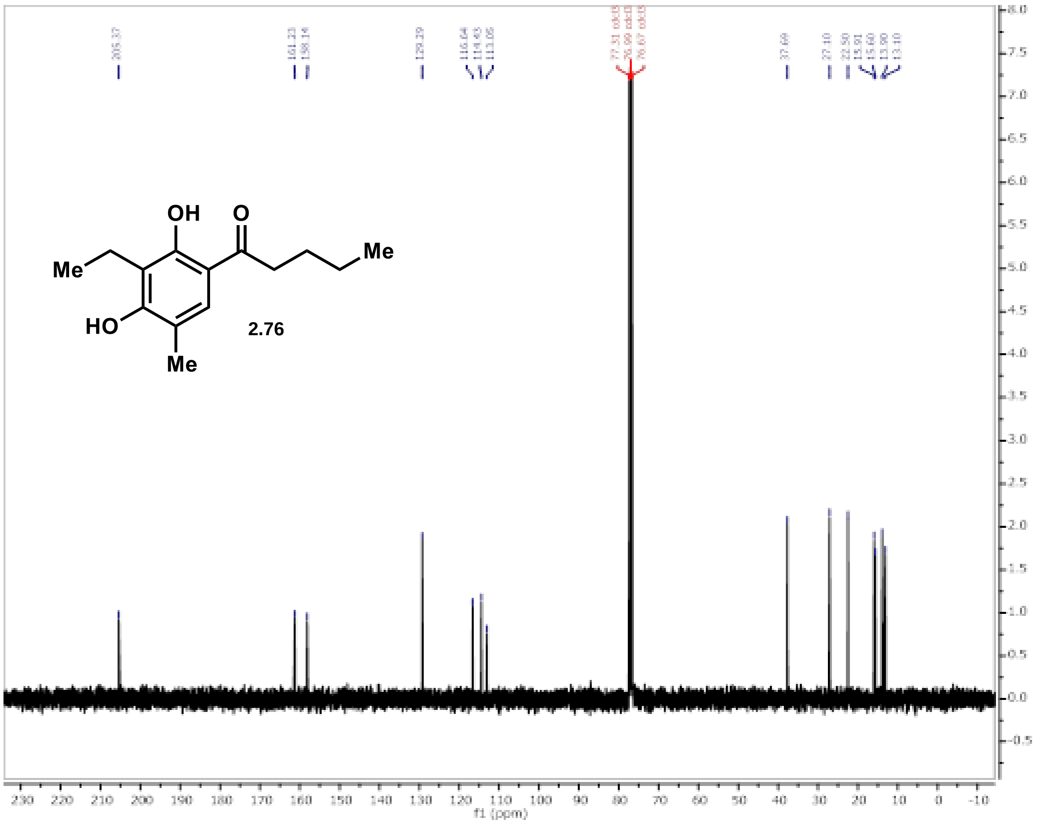
205.37
161.23
158.14
129.29
116.64
114.43
113.06
77.31 cdcl3
76.99 cdcl3
76.67 cdcl3
37.69
27.10
22.50
15.91
15.60
13.90
13.10
OH
O
Me
Me
HO
Me
2.76
f1 (ppm)

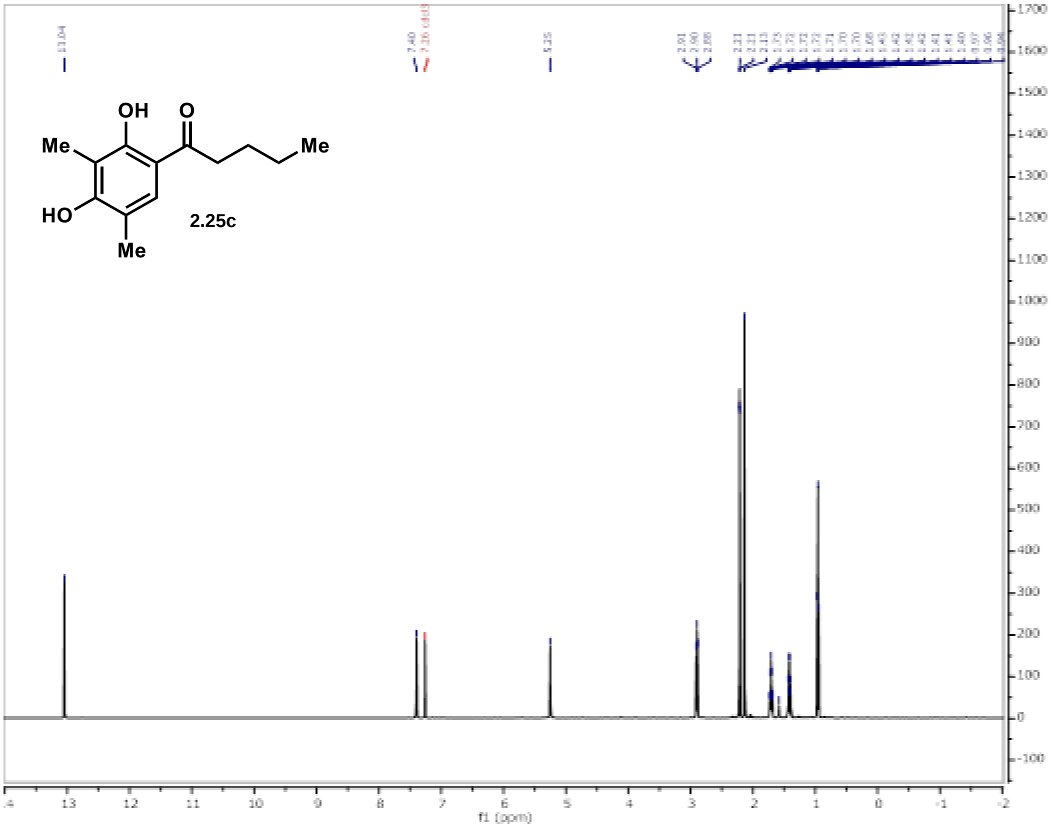

13.04
7.40
7.26 cdcl3
5.25
2.91
2.90
2.88
2.21
2.21
2.13
1.73
1.72
1.72
1.72
1.71
1.70
1.70
1.68
1.43
1.42
1.42
1.42
1.41
1.41
1.40
0.97
0.96
0.96
OH
O
Me
Me
HO
Me
2.25c
14
13
12
11
10
9
8
7
6
5
4
3
2
1
0
-1
-2
f1 (ppm)
1700
1600
1500
1400
1300
1200
1100
1000
900
800
700
600
500
400
300
200
100
0
-100

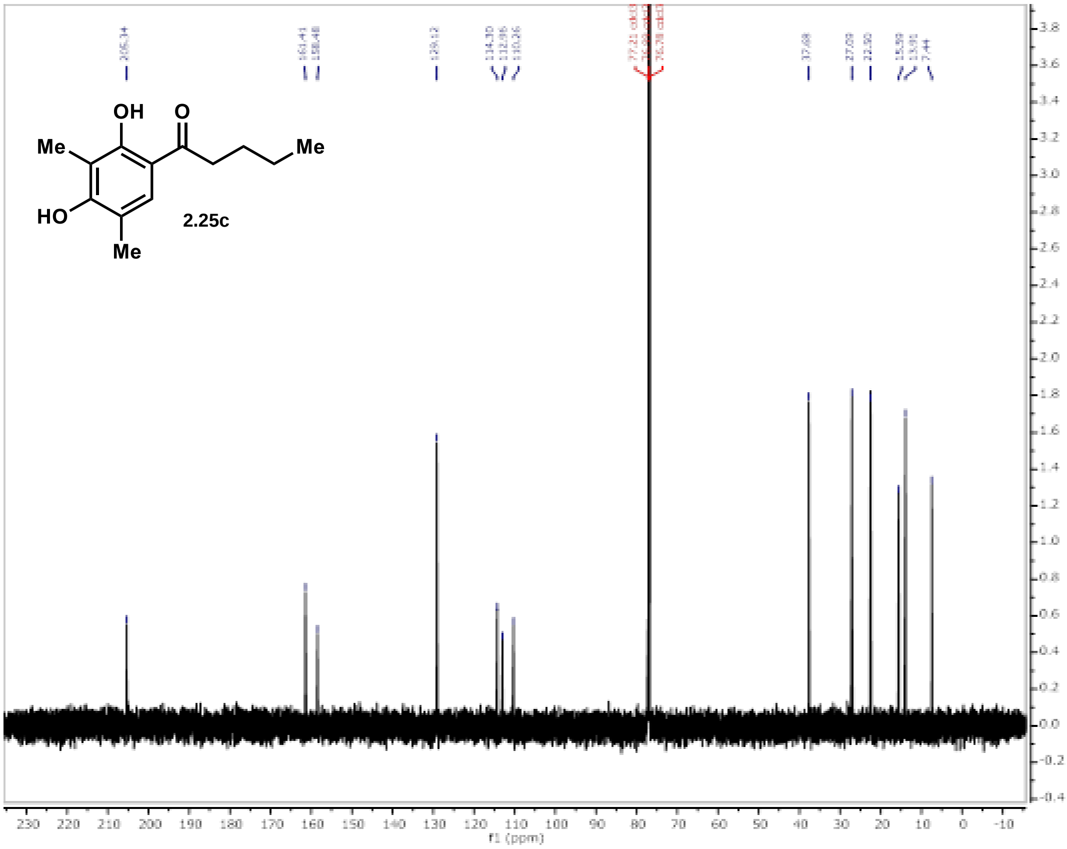

205.34
161.41
158.48
129.12
114.30
112.95
110.26
77.21 cdcl3
76.99 cdcl3
76.78 cdcl3
37.68
27.09
22.90
15.59
13.91
7.44
OH
O
Me
Me
HO
Me
2.25c
230
220
210
200
190
180
170
160
150
140
130
120
110
100
90
80
70
60
50
40
30
20
10
0
-10
f1 (ppm)
3.8
3.6
3.4
3.2
3.0
2.8
2.6
2.4
2.2
2.0
1.8
1.6
1.4
1.2
1.0
0.8
0.6
0.4
0.2
0.0
-0.2
-0.4

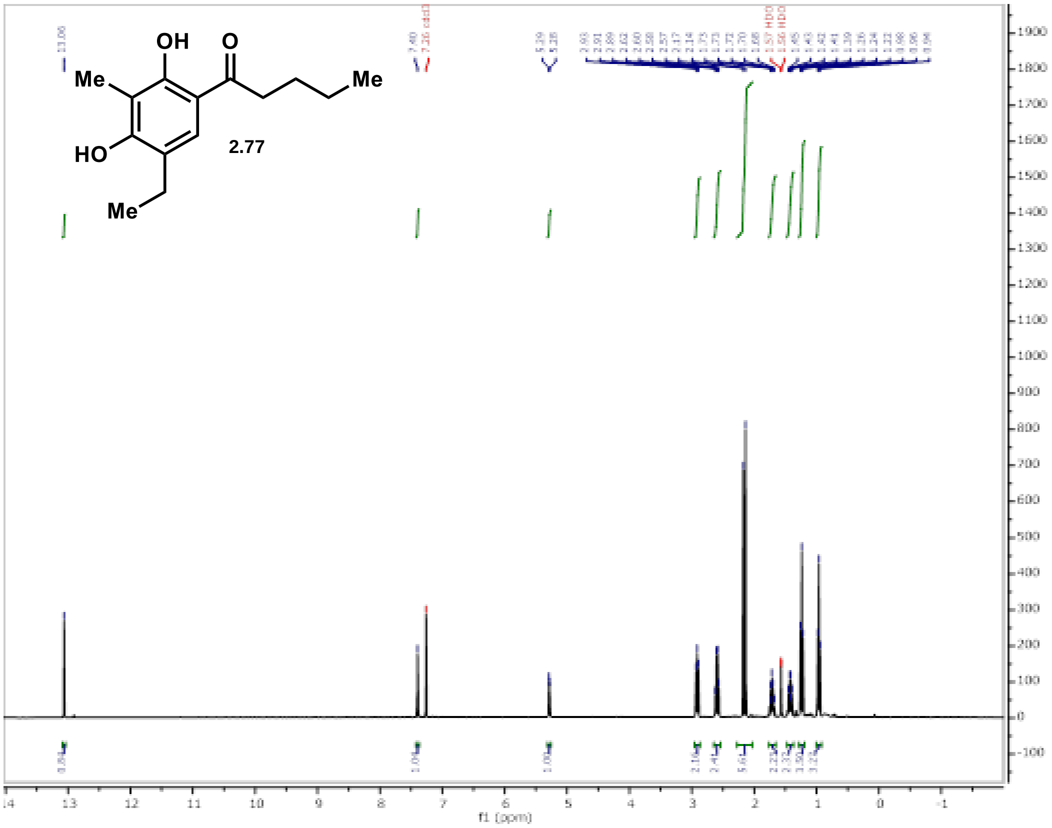

OH
O
Me
Me
HO
Me
2.77
13.06
7.40
7.26 cdcl3
5.29
5.28
1.57 HDO
1.56 HDO
0.84
1.04
1.00
2.10
2.41
5.61
f1 (ppm)
14
13
12
11
10
9
8
7
6
5
4
3
2
1
0
-1
1900
1800
1700
1600
1500
1400
1300
1200
1100
1000
900
800
700
600
500
400
300
200
100
0
-100

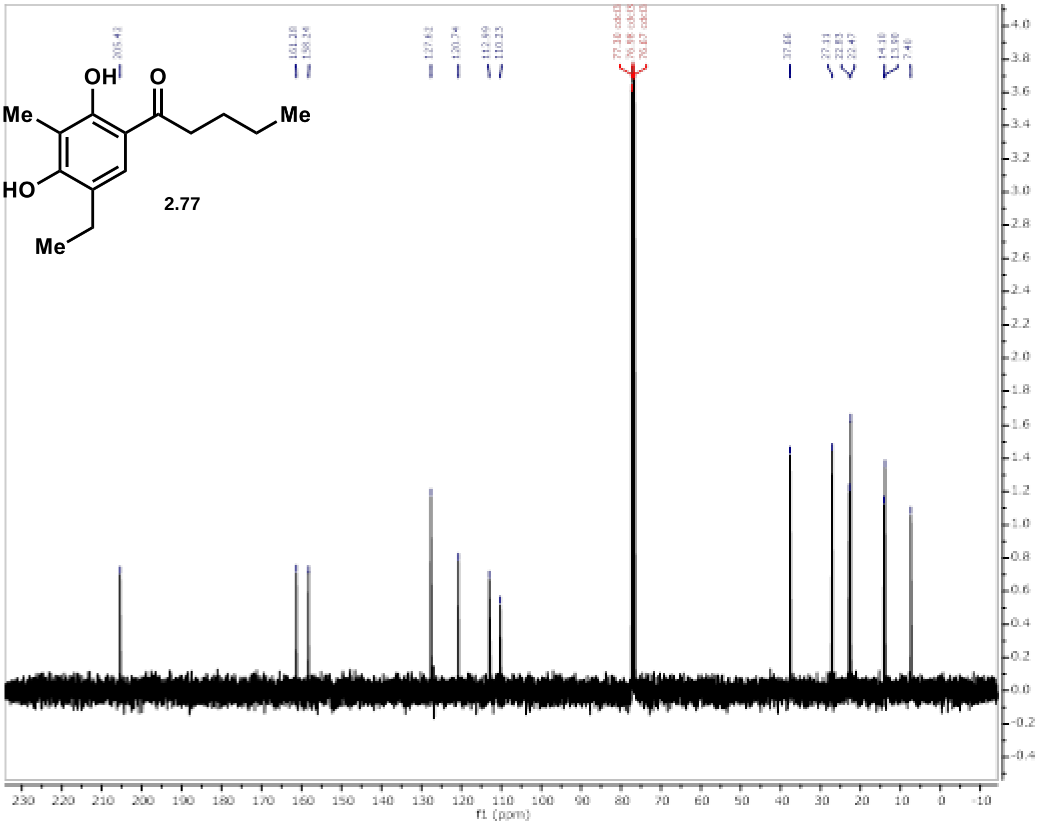

OH
O
Me
Me
HO
Me
2.77
205.42
161.28
158.24
127.61
120.74
112.69
110.23
77.38 cdcl3
76.98 cdcl3
76.67 cdcl3
37.66
27.11
22.83
22.47
14.18
13.88
7.48
f1 (ppm)
230
220
210
200
190
180
170
160
150
140
130
120
110
100
90
80
70
60
50
40
30
20
10
0
-10
4.0
3.8
3.6
3.4
3.2
3.0
2.8
2.6
2.4
2.2
2.0
1.8
1.6
1.4
1.2
1.0
0.8
0.6
0.4
0.2
0.0
-0.2
-0.4

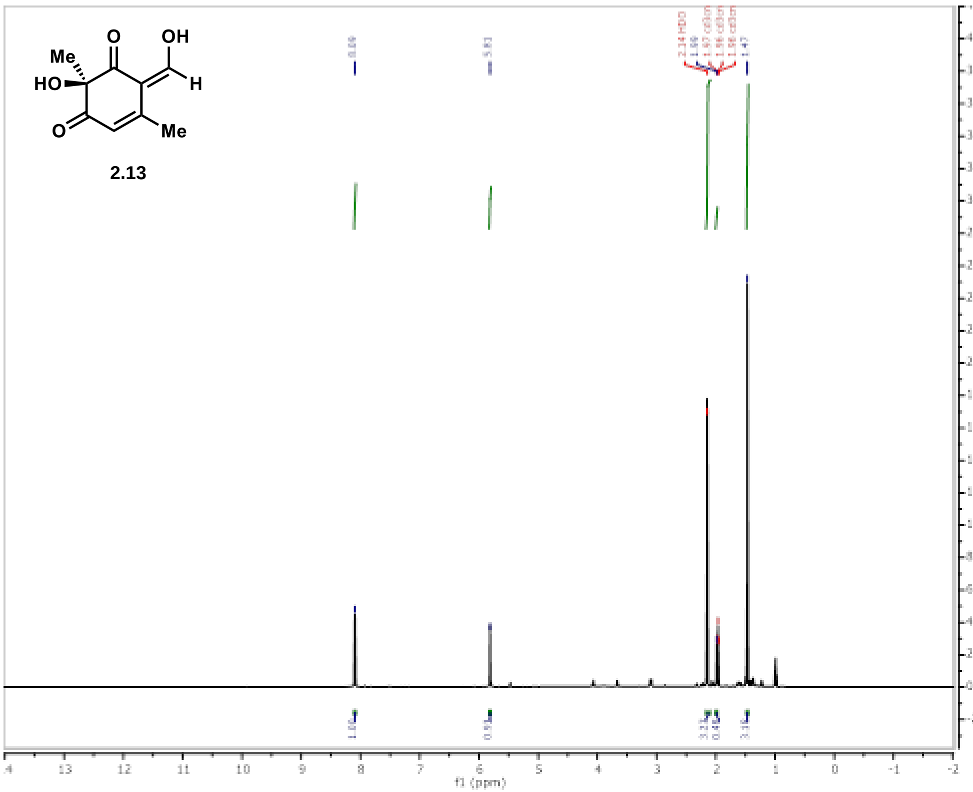
O
OH
Me
HO
H
O
Me
2.13
8.09
5.81
2.14 HDO
1.99
1.97 cd3cn
1.96 cd3cn
1.96 cd3cn
1.47
1.00
0.91
3.11
0.42
3.16
4000
3800
3600
3400
3200
3000
2800
2600
2400
2200
2000
1800
1600
1400
1200
1000
800
600
400
200
0
-200
14
13
12
11
10
9
8
7
6
5
4
3
2
1
0
-1
-2
f1 (ppm)

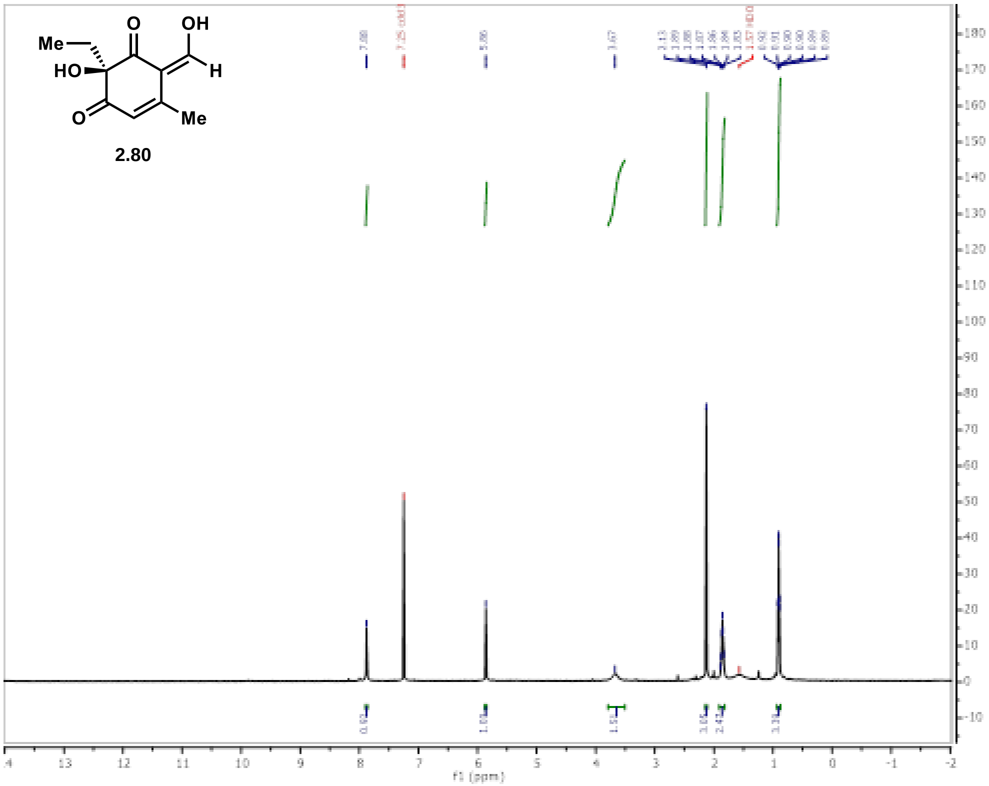
2.80
Me
HO
O
OH
H
O
Me
7.88
7.25 cdcl3
5.86
3.67
2.13
1.89
1.88
1.87
1.86
1.84
1.83
1.57 HDO
0.92
0.91
0.90
0.90
0.89
0.89
0.92
1.03
1.54
3.05
2.41
3.34
f1 (ppm)

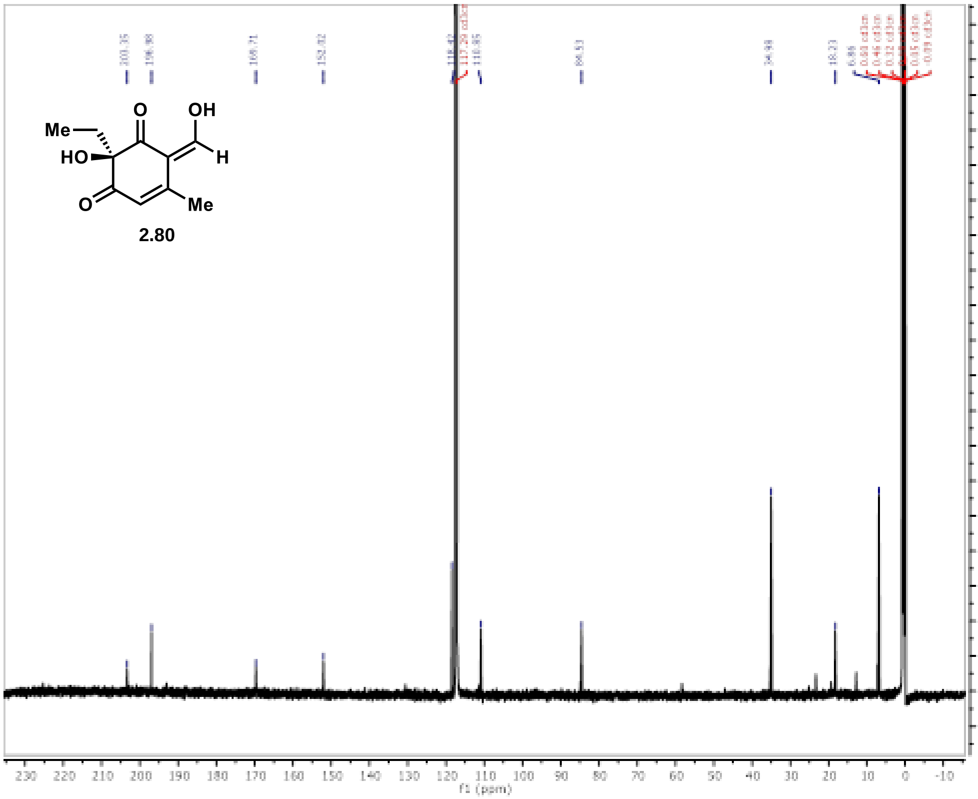
2.80
Me
HO
O
OH
H
O
Me
203.35
196.98
169.71
152.02
118.42
117.29 cd3cn
110.95
84.53
34.98
18.23
6.86
0.83 cd3cn
0.46 cd3cn
0.32 cd3cn
0.05 cd3cn
-0.09 cd3cn
f1 (ppm)

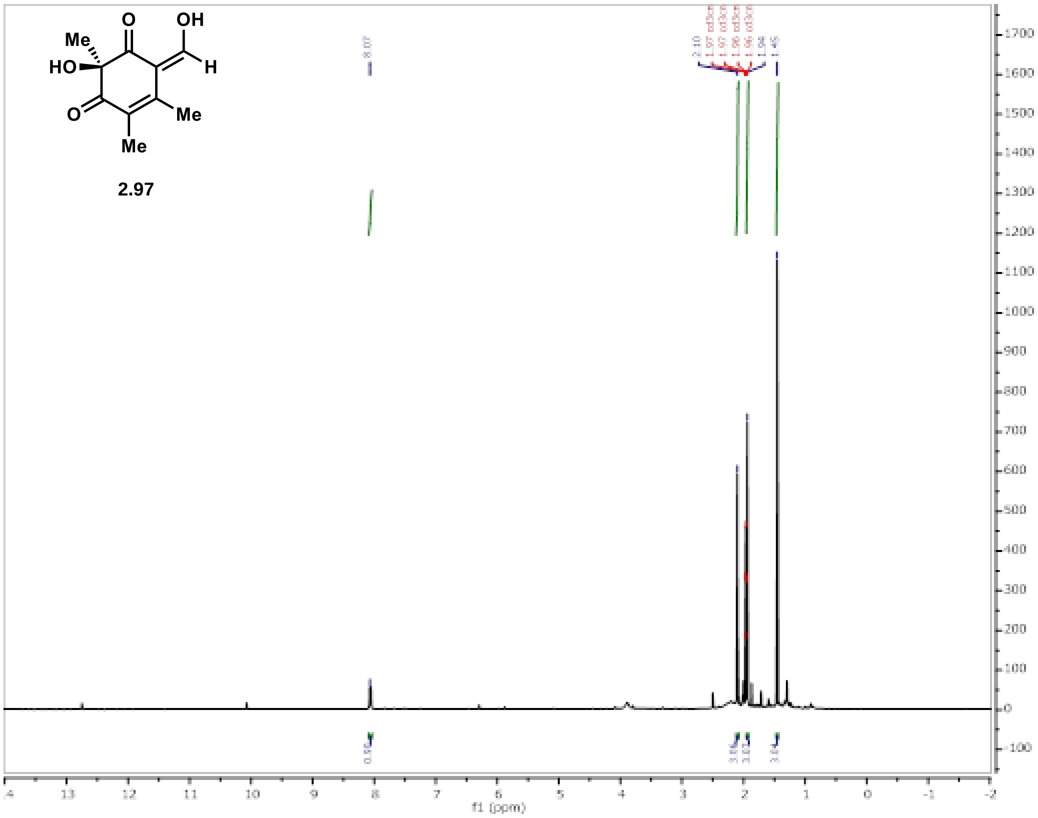
O
OH
Me
HO
H
O
Me
Me
2.97
8.07
2.10
1.45
0.56
3.06
3.02
3.64
f1 (ppm)

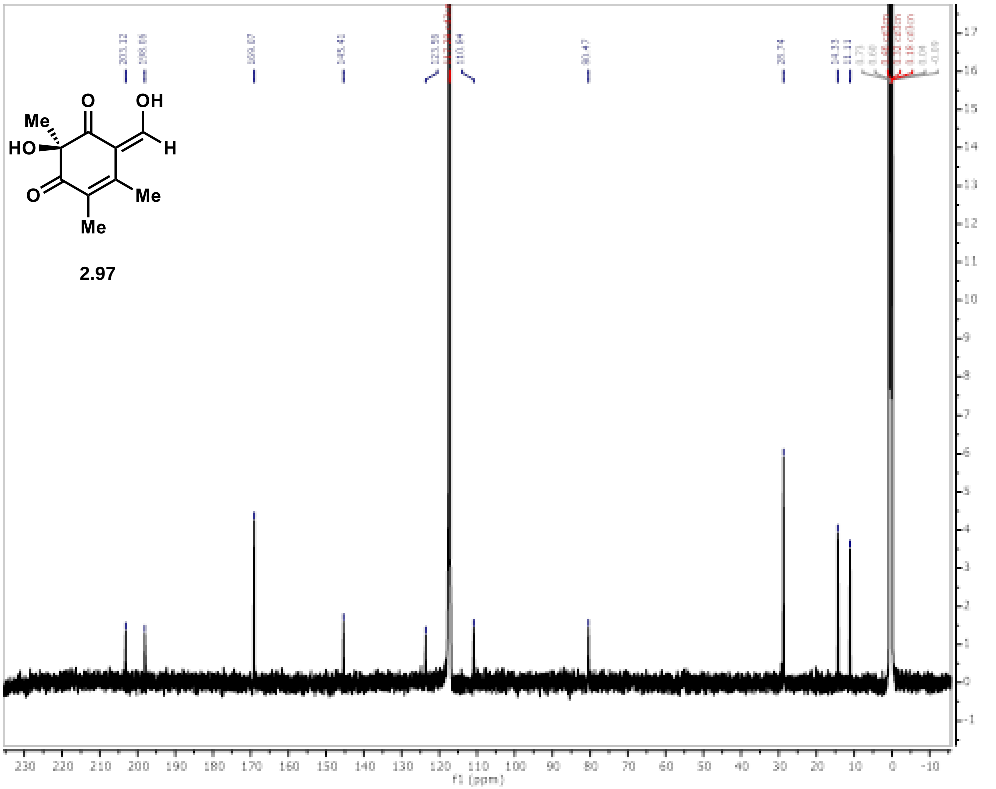
O
OH
Me
HO
H
O
Me
Me
2.97
203.12
198.69
169.67
145.41
123.55
110.64
80.47
28.74
14.33
11.11
f1 (ppm)

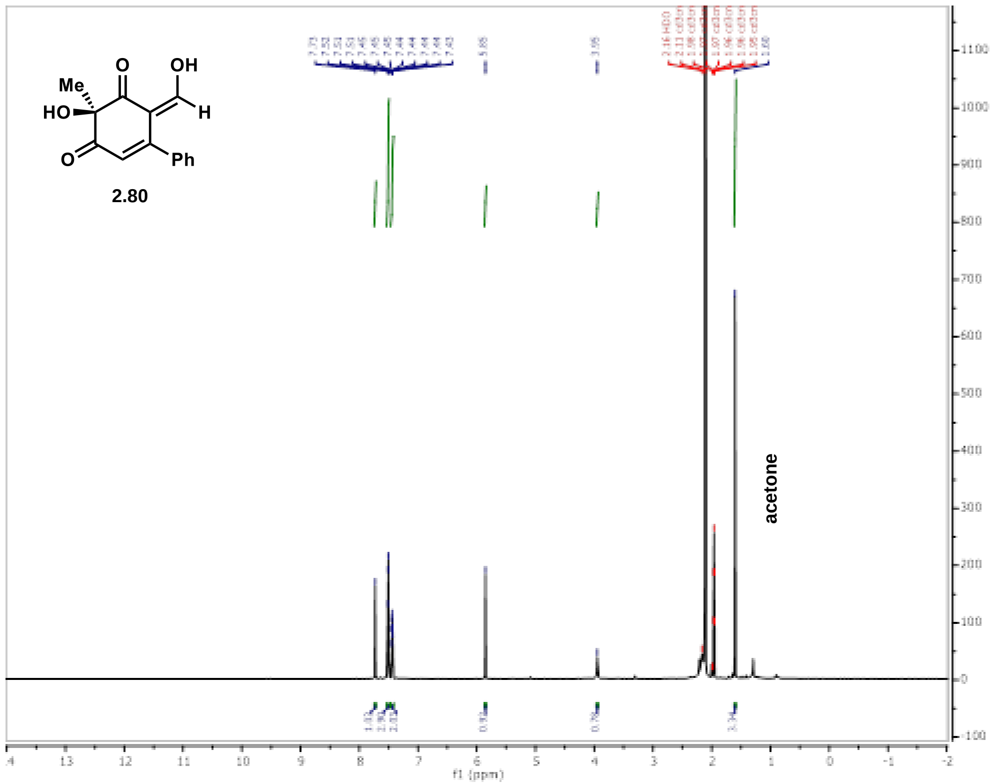
Me
HO
O
OH
H
O
Ph
7.73
5.88
3.95
1.66
acetone
f1 (ppm)

2.80

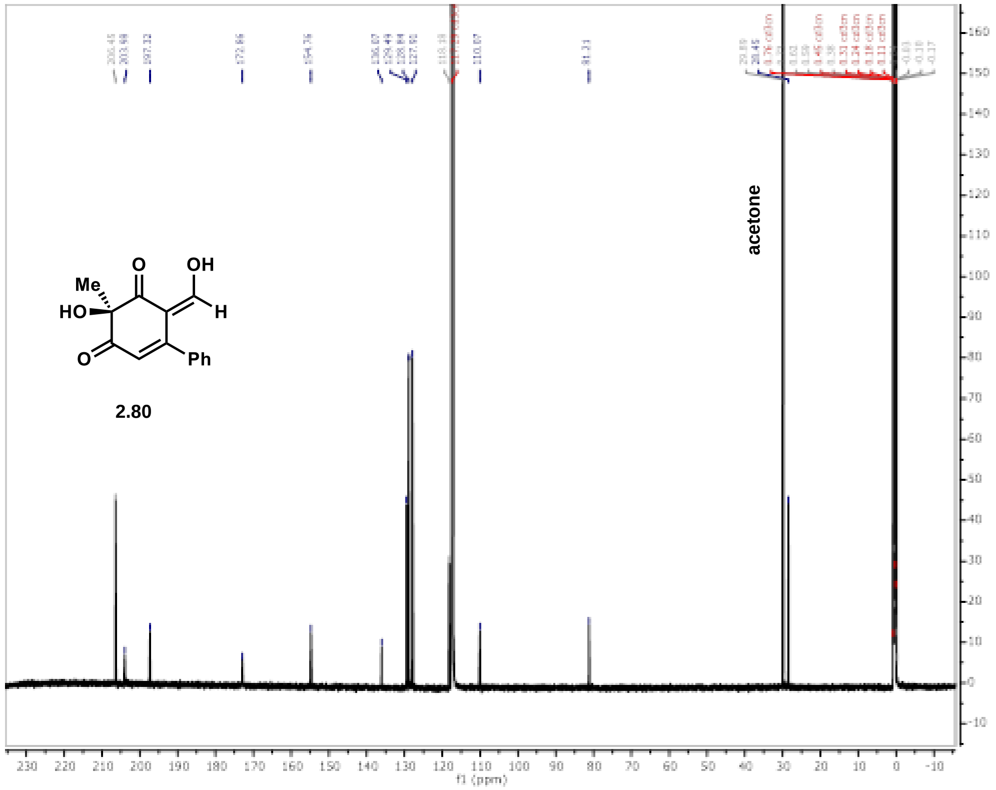
Me
HO
O
OH
H
O
Ph
206.45
203.98
197.32
172.86
154.36
136.07
129.49
128.84
127.91
110.07
81.21
acetone
f1 (ppm)

2.80

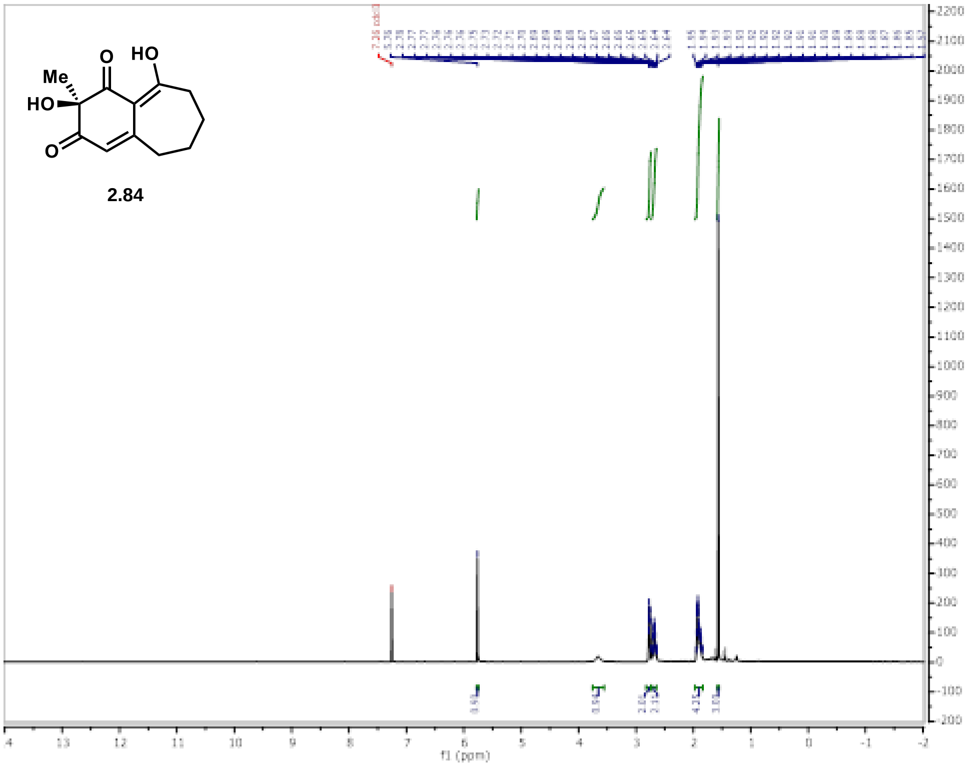
2.84

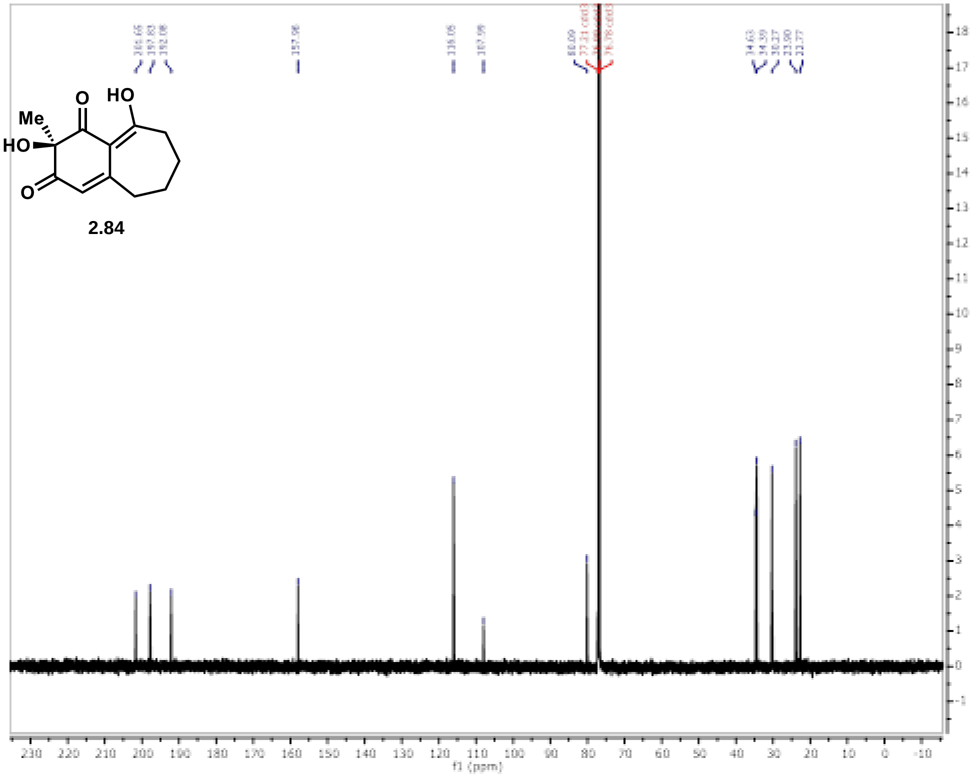
2.84

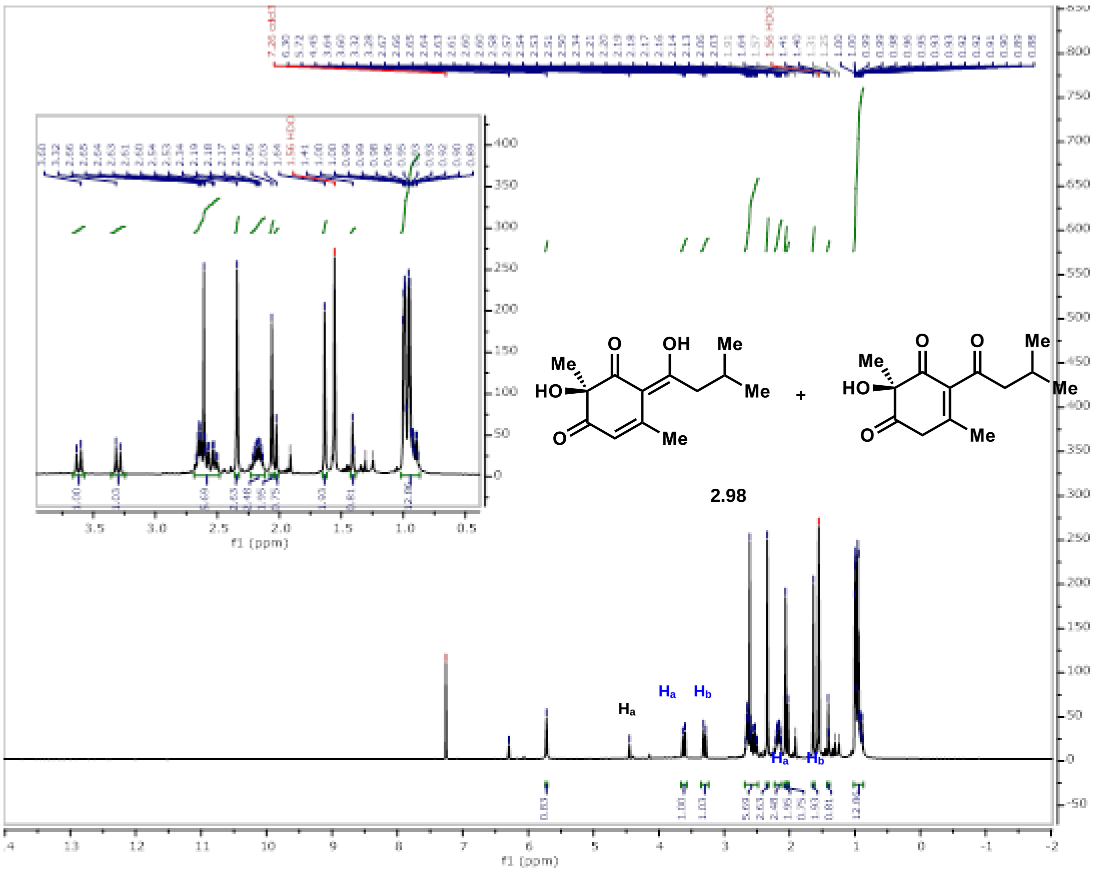
H_a

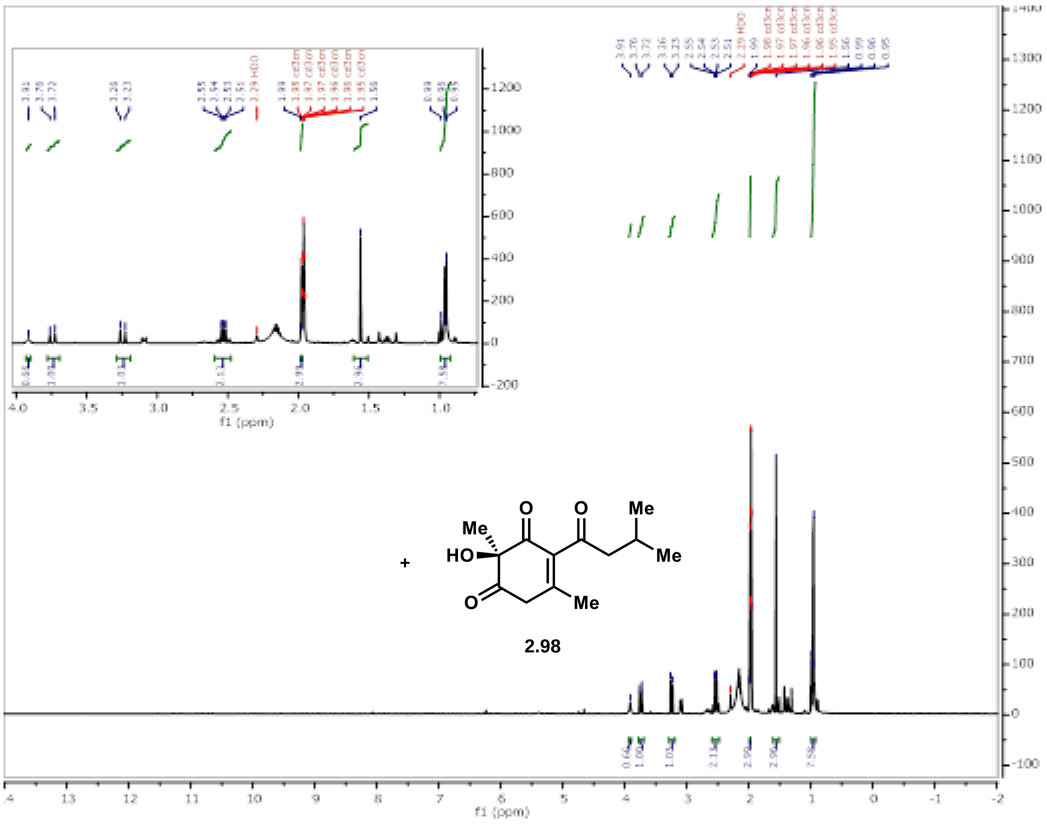
+
2.98
f1 (ppm)

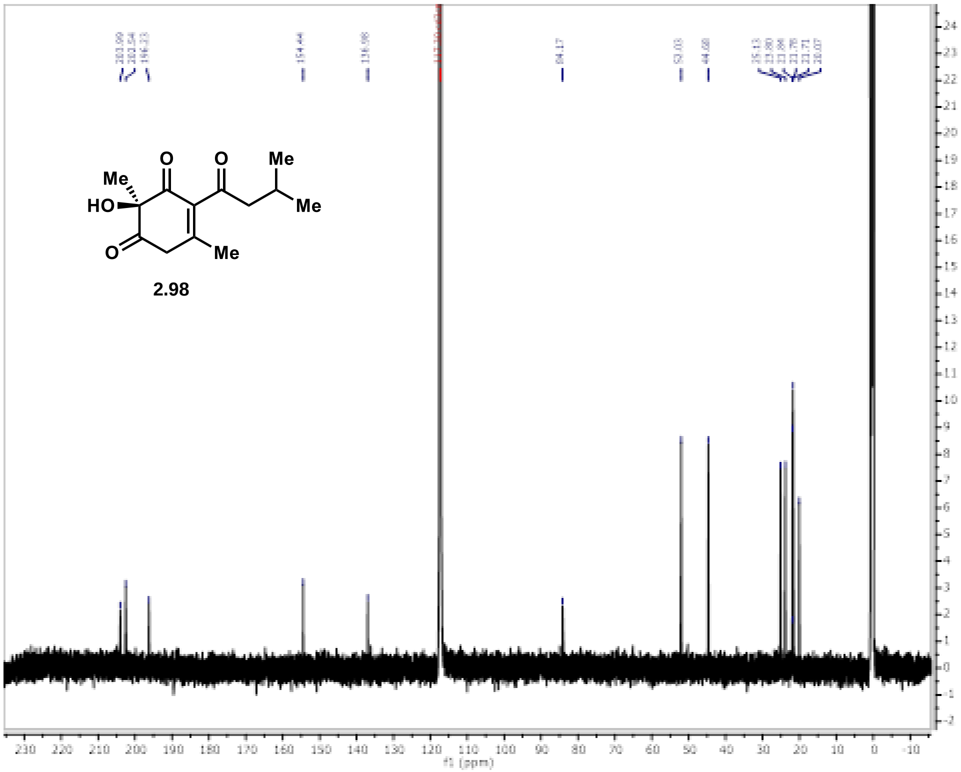
203.99
202.54
196.13
154.44
136.98
84.17
52.03
44.68
25.13
23.80
22.88
21.76
21.71
20.07
Me
HO
O
O
Me
Me
O
Me
230 220 210 200 190 180 170 160 150 140 130 120 110 100 90 80 70 60 50 40 30 20 10 0 -10
f1 (ppm)
24 23 22 21 20 19 18 17 16 15 14 13 12 11 10 9 8 7 6 5 4 3 2 1 0 -1 -2

2.98

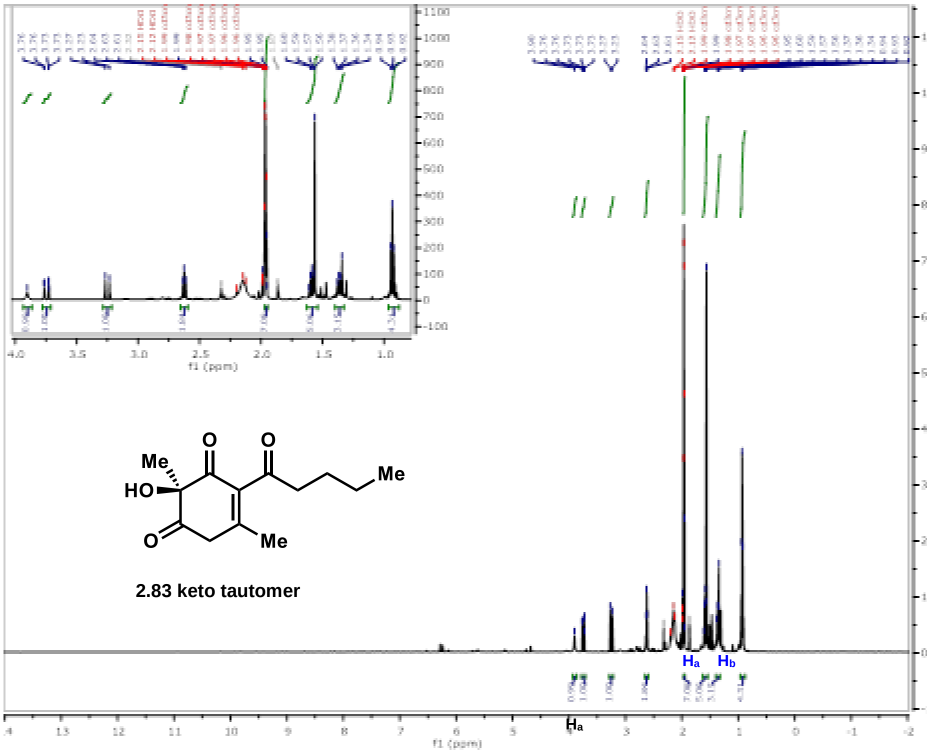

2.83 keto tautomer

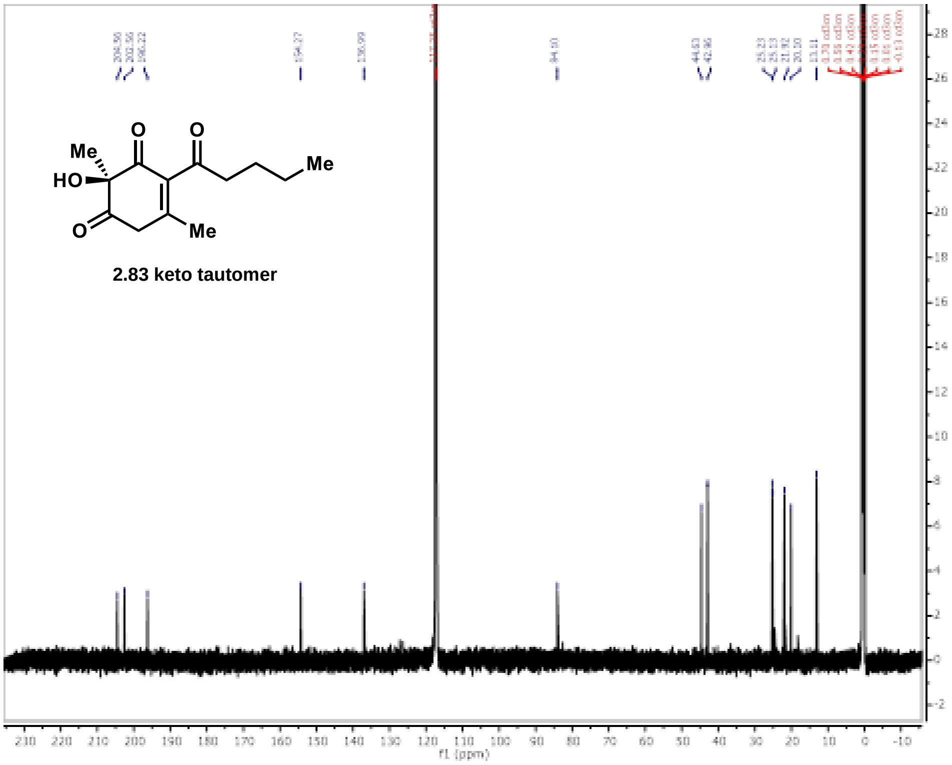

2.83 keto tautomer

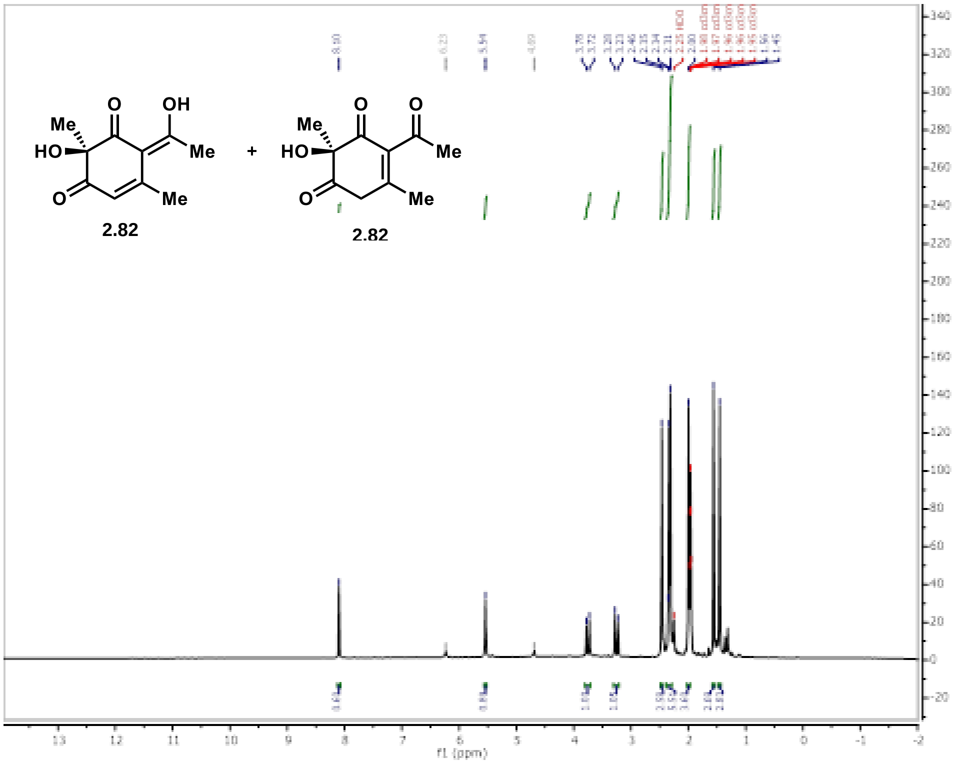
Me
HO
O
O
OH
Me
Me
2.82
+
Me
HO
O
O
O
Me
Me
2.82
f1 (ppm)

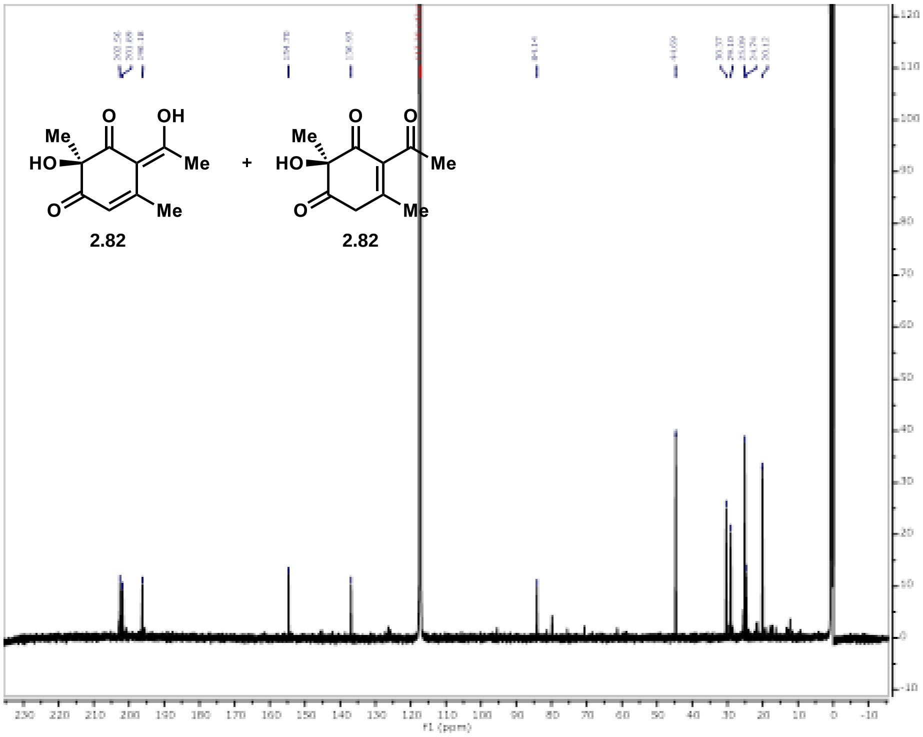
Me
HO
O
O
OH
Me
Me
2.82
+
Me
HO
O
O
O
Me
Me
2.82
f1 (ppm)

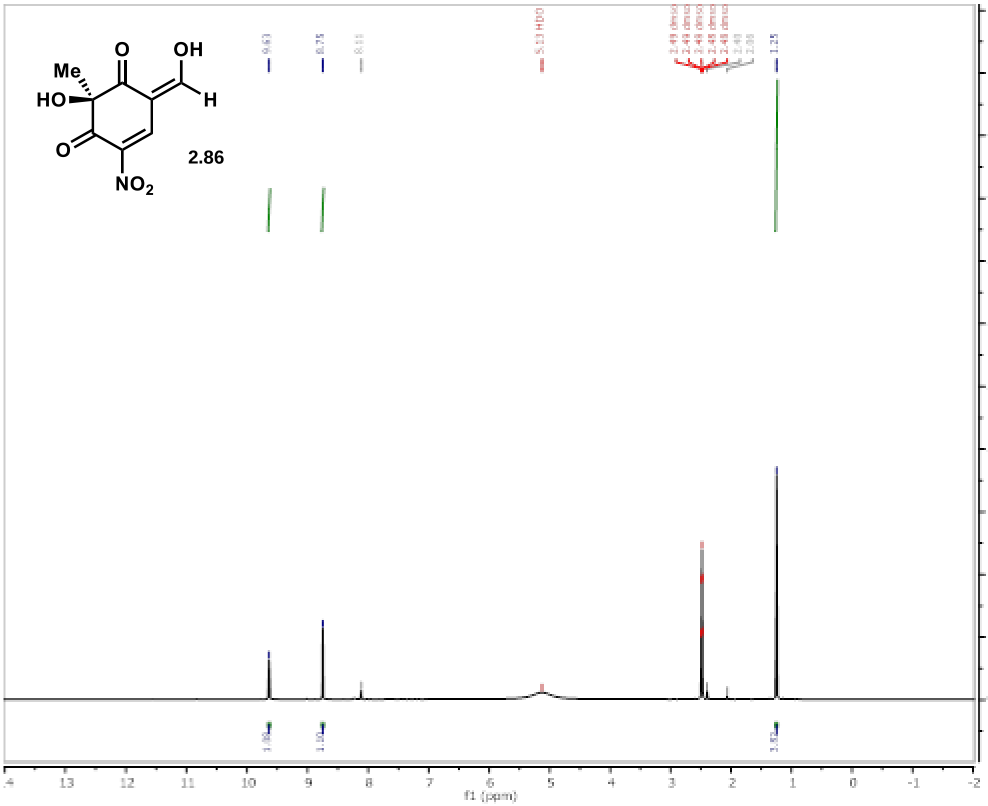
9.63
8.75
8.11
5.13 HDO
2.49 dmso
2.49 dmso
2.48 dmso
2.48 dmso
2.48 dmso
2.40
2.08
1.25
1.00
1.00
3.02
Me
HO
O
O
OH
H
NO2
2.86
f1 (ppm)

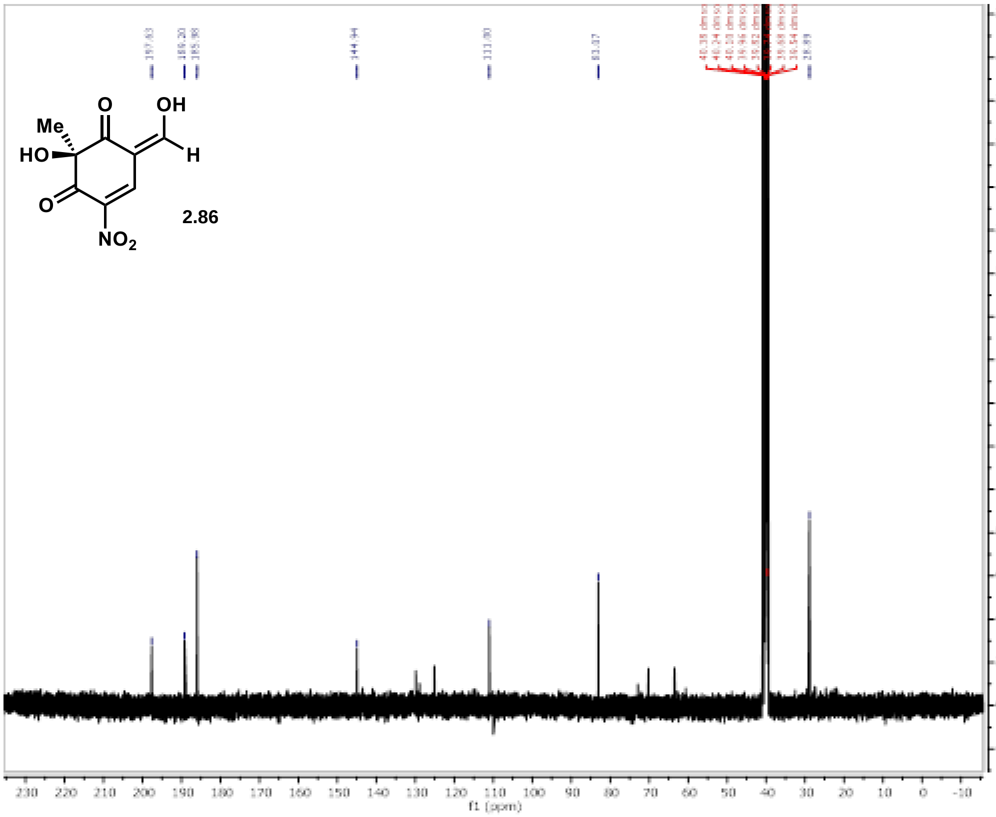
197.63
189.20
185.88
144.94
111.00
83.07
40.35 dmso
40.24 dmso
40.13 dmso
39.96 dmso
39.82 dmso
39.74 dmso
39.68 dmso
39.54 dmso
28.89
Me
HO
O
O
OH
H
NO2
2.86
f1 (ppm)

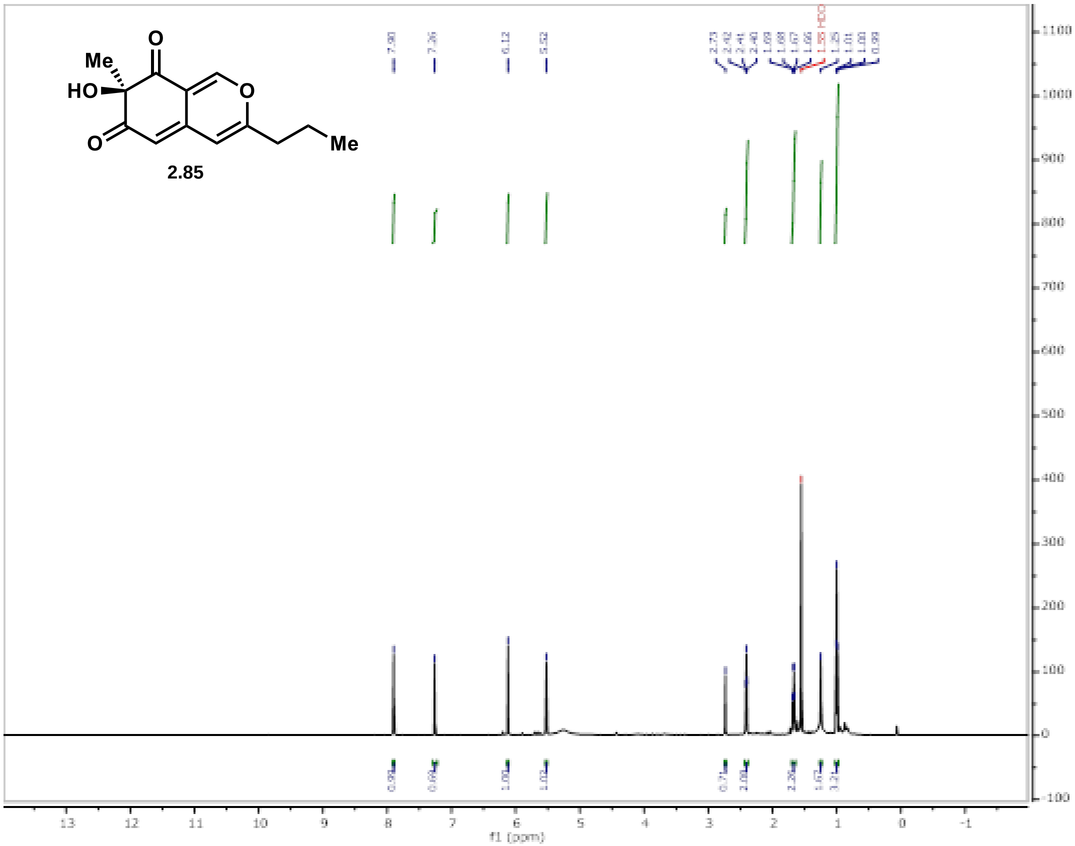
Me
HO
O
O
O
Me
2.85
7.90
7.26
6.12
5.52
2.73
2.42
2.41
2.40
1.69
1.68
1.67
1.66
1.58 HDO
1.25
1.01
1.00
0.99
0.90
0.60
1.00
1.02
0.71
2.00
2.26
1.67
3.21
1100
1000
900
800
700
600
500
400
300
200
100
0
-100
13
12
11
10
9
8
7
6
5
4
3
2
1
0
-1
f1 (ppm)

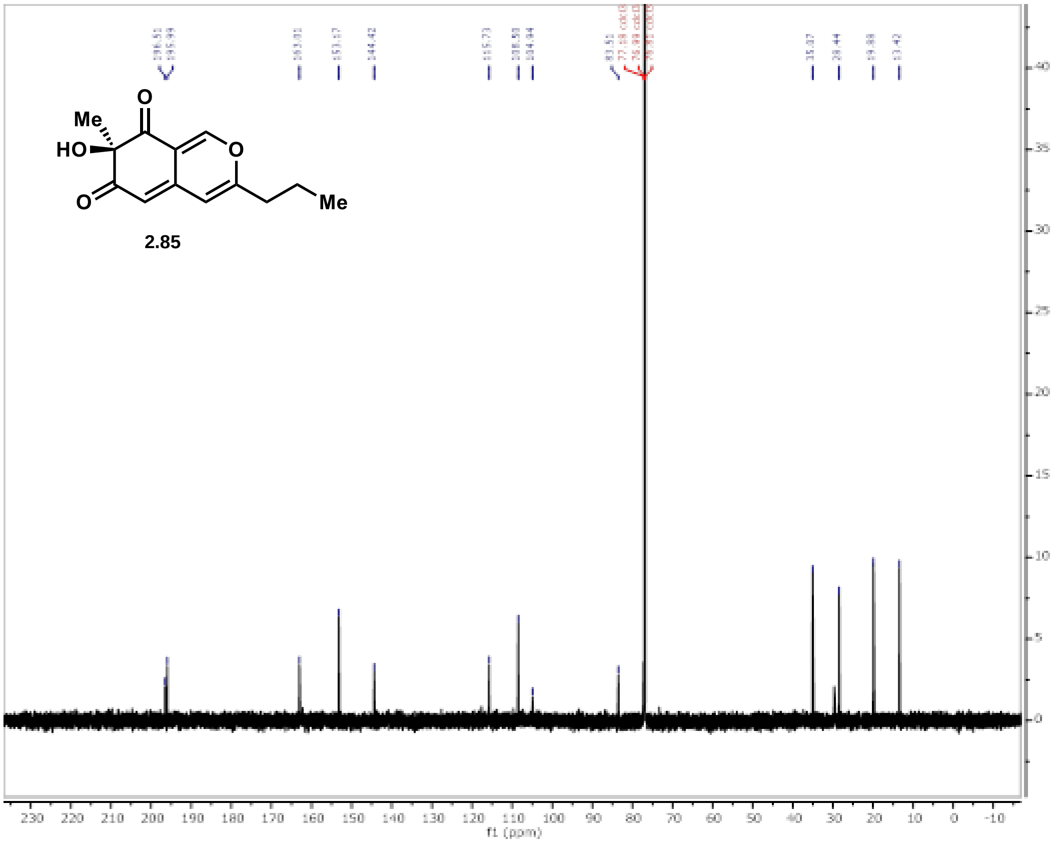
196.51
195.99
163.01
153.17
144.42
115.73
108.53
104.94
83.51
77.38 cdcl3
76.99 cdcl3
76.81 cdcl3
35.07
28.44
19.88
13.42
Me
HO
O
O
O
Me
2.85
40
35
30
25
20
15
10
5
0
230
220
210
200
190
180
170
160
150
140
130
120
110
100
90
80
70
60
50
40
30
20
10
0
-10
f1 (ppm)

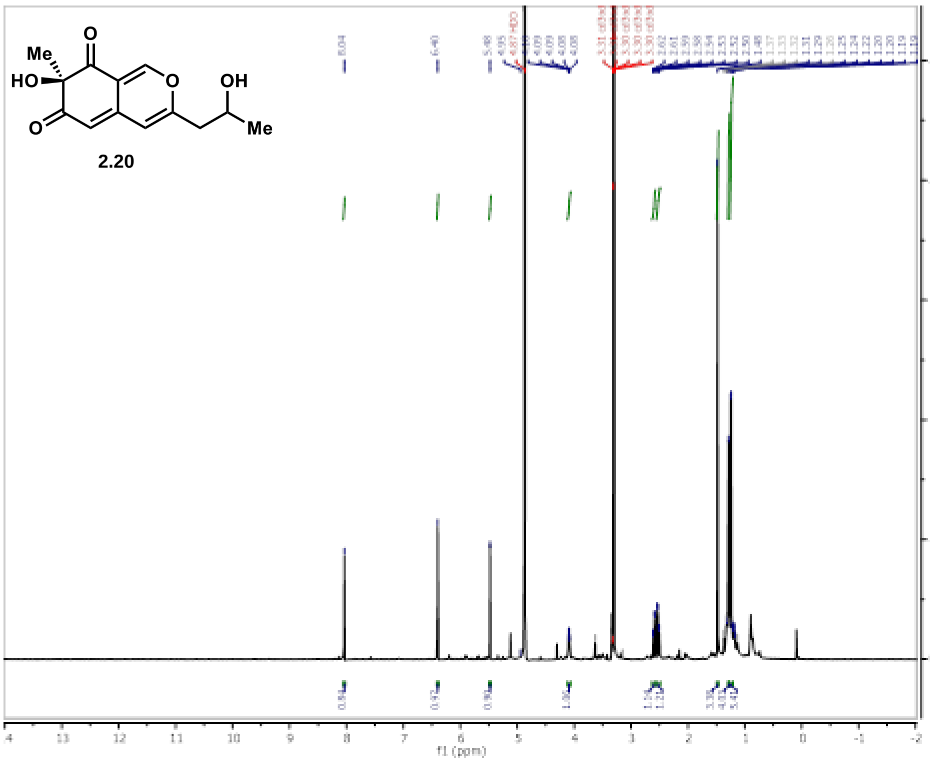

2.20

Me
HO
O
O
O
OH
Me
f1 (ppm)
250
200
150
100
50
0
14
13
12
11
10
9
8
7
6
5
4
3
2
1
0
-1
-2

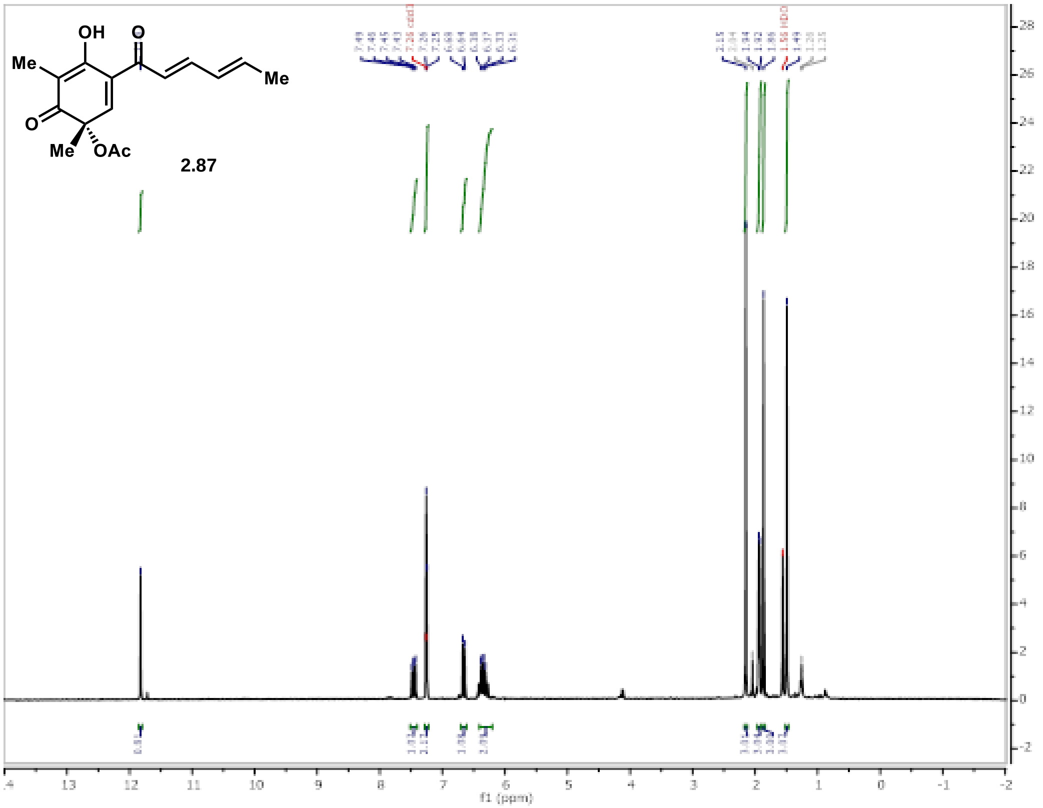
OH
O
Me
Me
O
Me
OAc
2.87
7.49
7.46
7.45
7.43
7.26 cdcl3
7.26
7.25
6.68
6.64
6.38
6.37
6.33
6.31
2.15
2.04
1.94
1.92
1.89
1.56 HDO
1.49
1.28
1.25
0.81
f1 (ppm)

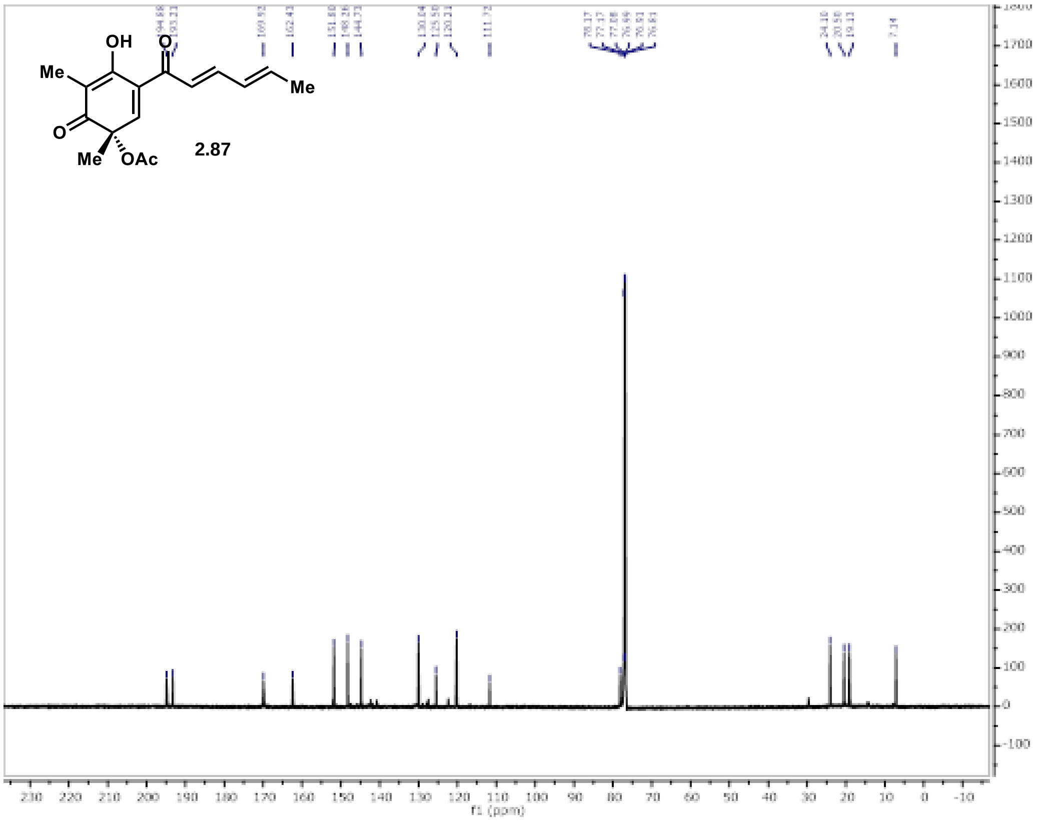
OH
O
Me
Me
O
Me
OAc
2.87
194.68
193.11
169.92
162.43
151.80
148.26
144.21
130.04
125.50
120.21
111.73
24.10
20.58
19.13
7.34
f1 (ppm)

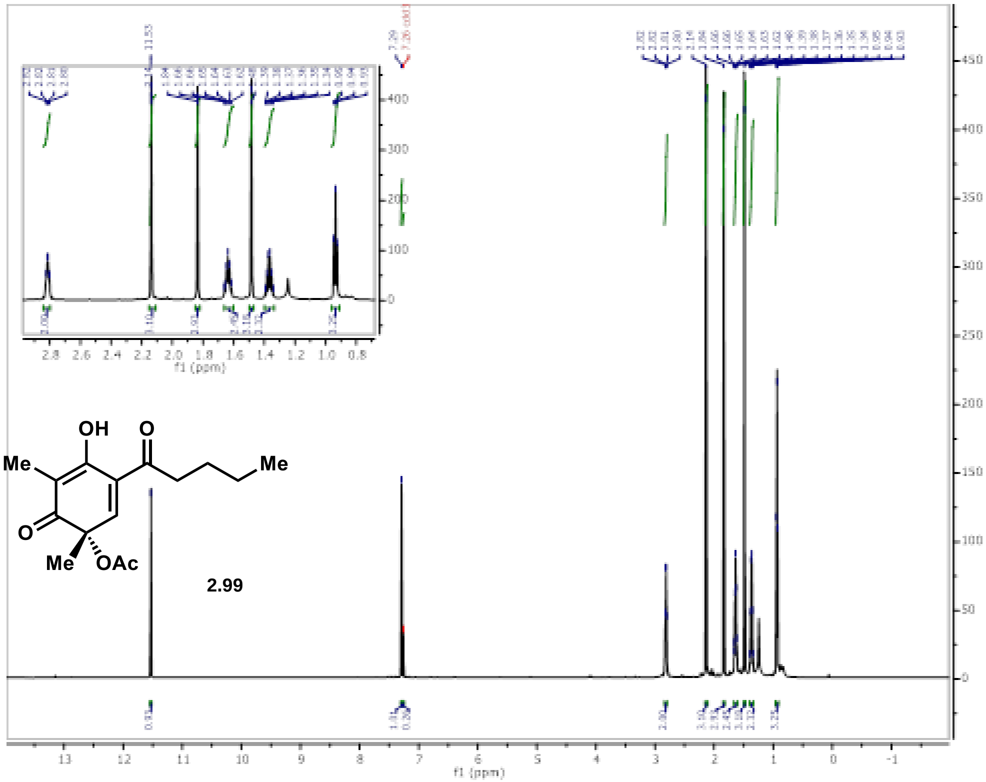

2.99

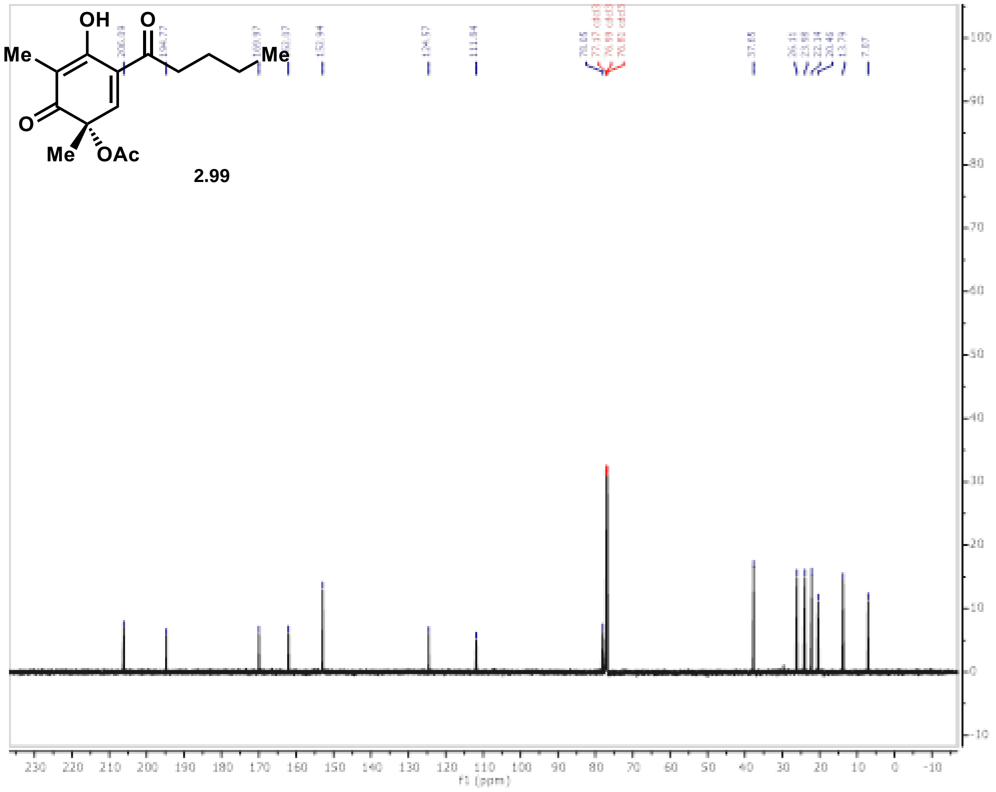

2.99

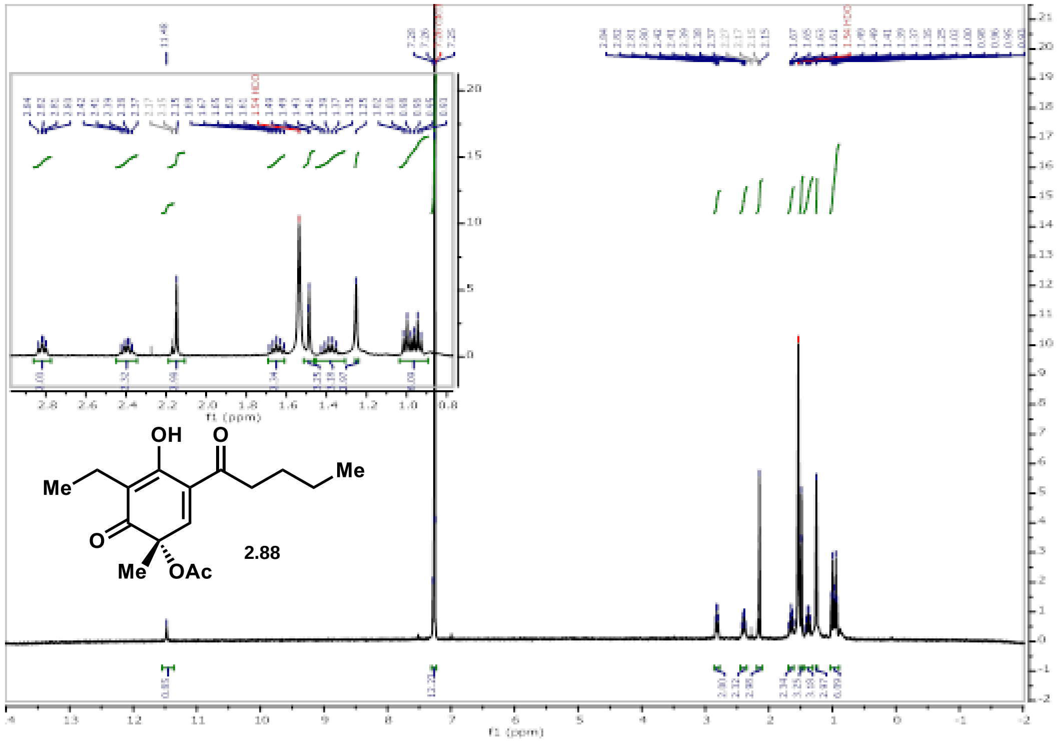
OH
O
Me
Me
O
Me
OAc
2.88
f1 (ppm)
f1 (ppm)

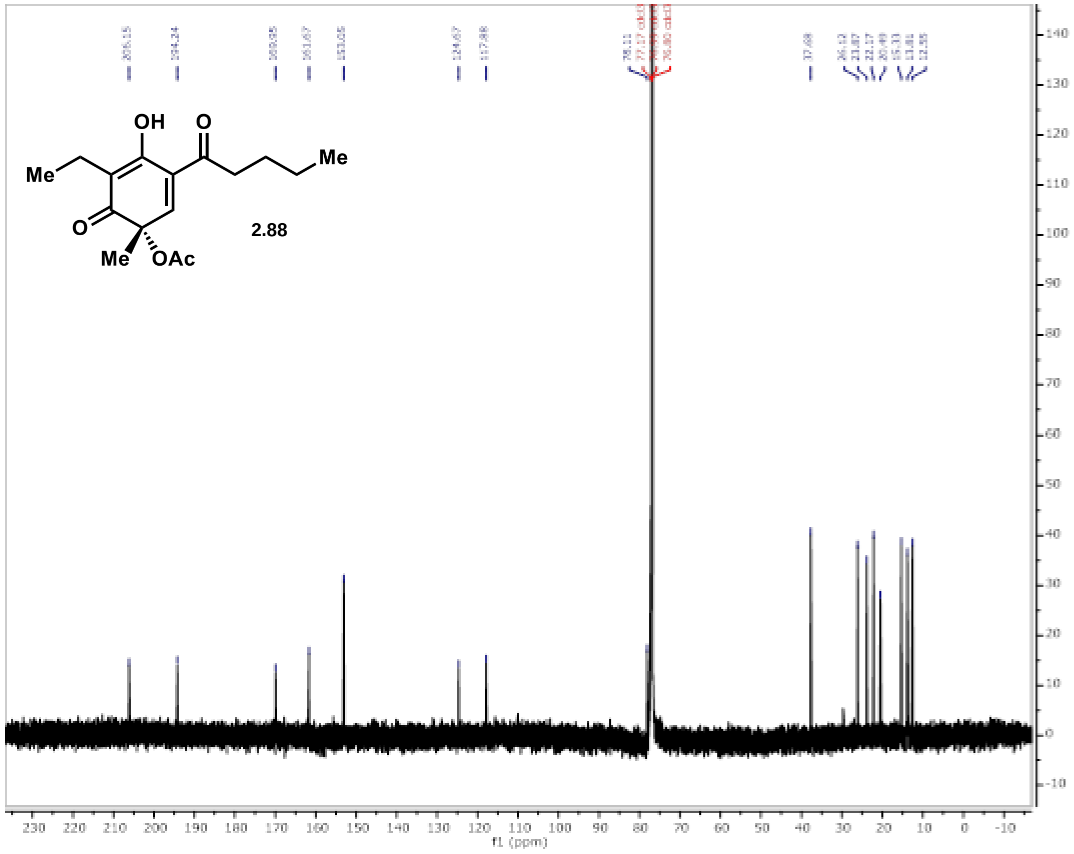
OH
O
Me
Me
O
Me
OAc
2.88
f1 (ppm)

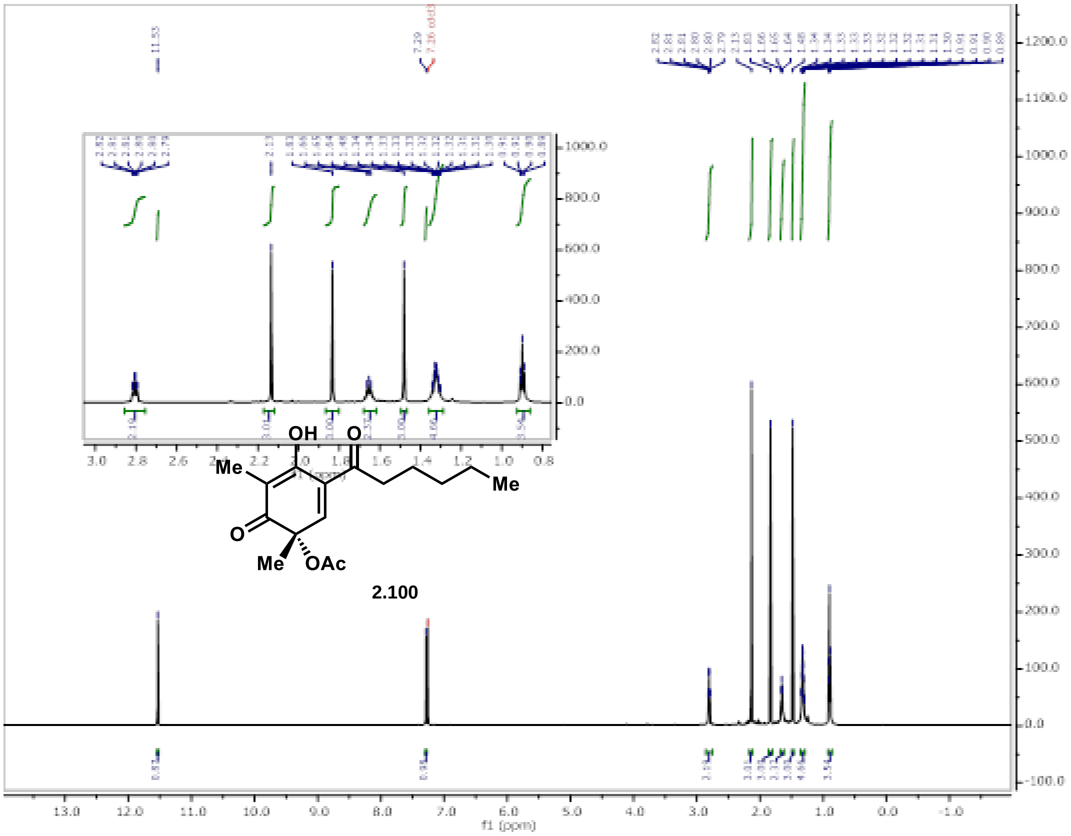

11.53
7.29
7.26 cdcl3
2.82
2.81
2.81
2.80
2.80
2.79
2.13
1.83
1.66
1.65
1.64
1.48
1.34
1.34
1.33
1.33
1.33
1.32
1.32
1.32
1.31
1.31
1.30
0.91
0.91
0.90
0.89
0.51
0.38
2.19
3.01
3.06
2.52
3.00
4.66
3.54
OH
O
Me
O
Me
OAc
Me
1200.0
1100.0
1000.0
900.0
800.0
700.0
600.0
500.0
400.0
300.0
200.0
100.0
0.0
-100.0
13.0
12.0
11.0
10.0
9.0
8.0
7.0
6.0
5.0
4.0
3.0
2.0
1.0
0.0
-1.0
f1 (ppm)
1000.0
800.0
600.0
400.0
200.0
0.0
3.0
2.8
2.6
2.4
2.2
2.0
1.8
1.6
1.4
1.2
1.0
0.8
f1 (ppm)

2.100

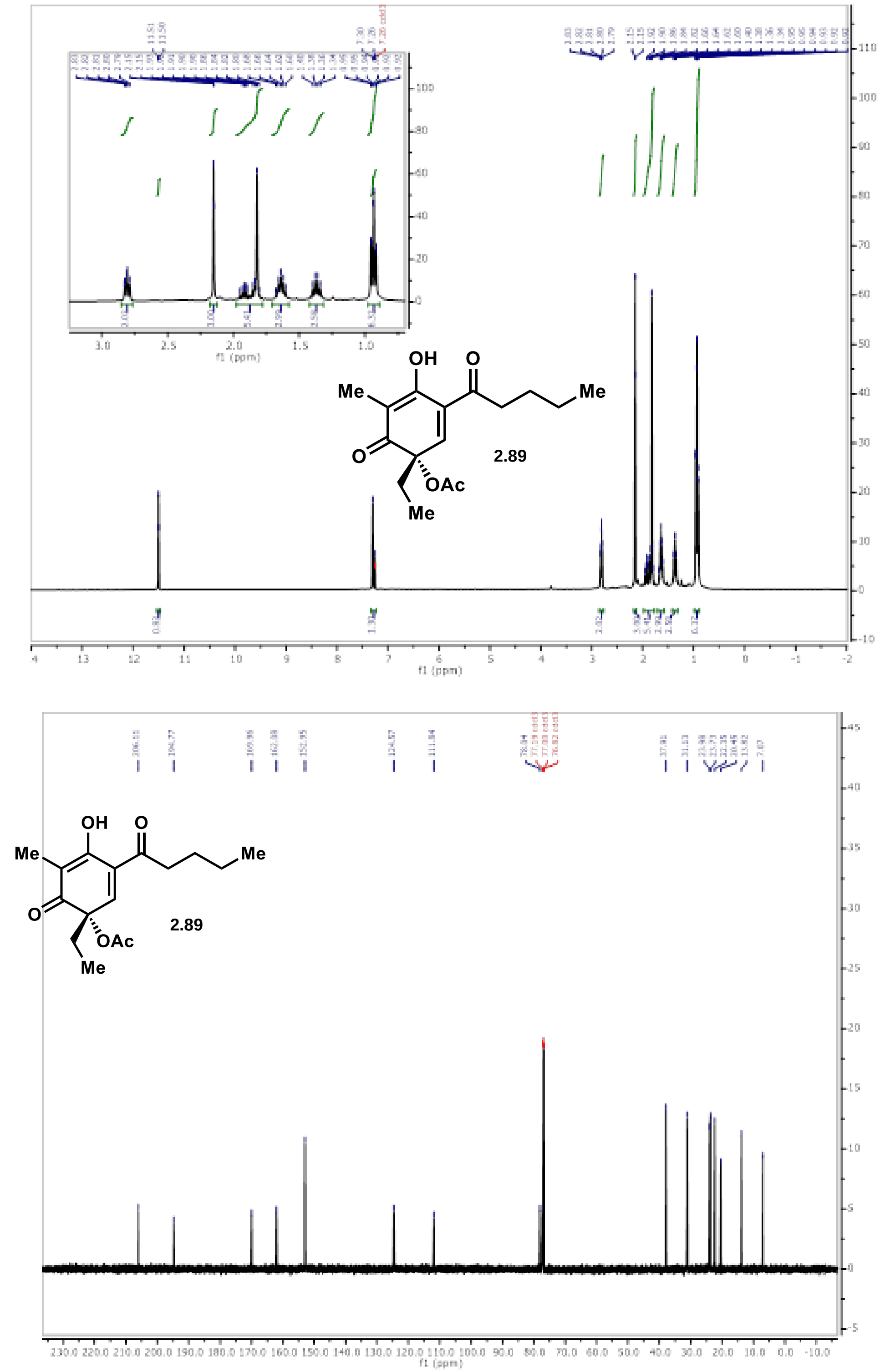

Figure 2.77: NMR spectra of synthetic compounds.

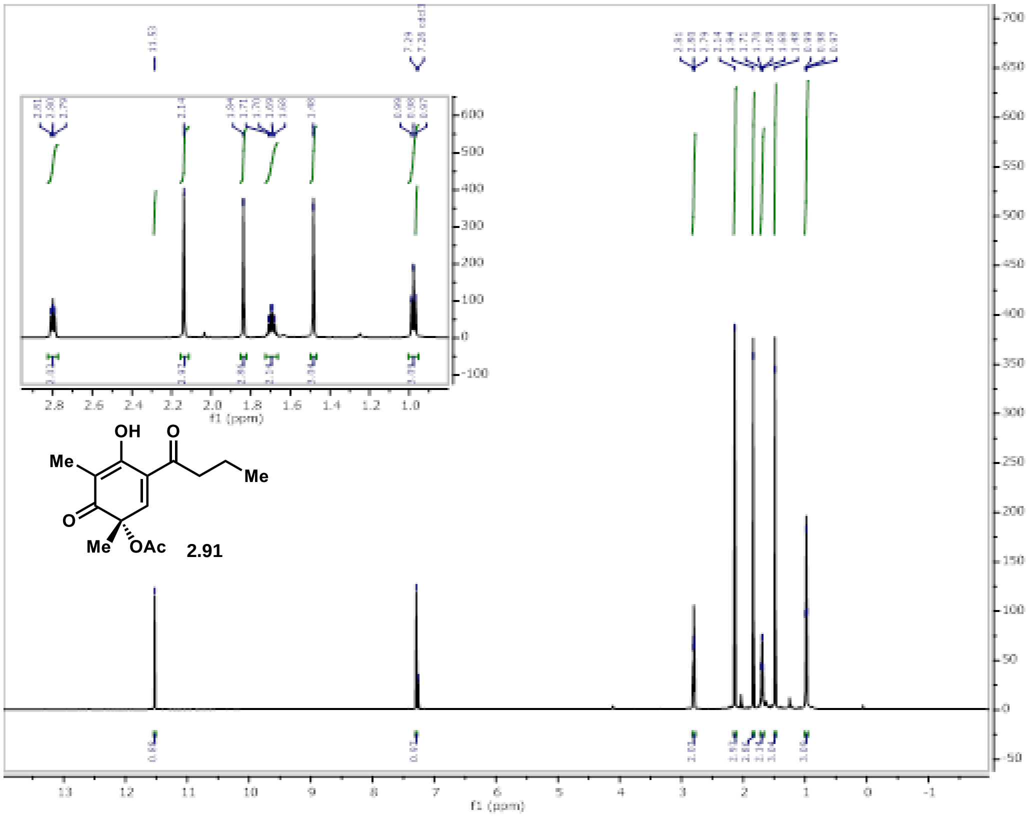
11.53
7.29
7.28 cdcl3
2.81
2.80
2.79
2.14
1.84
1.71
1.70
1.69
1.68
1.48
0.99
0.98
0.97
0.86
0.92
2.01
2.91
2.86
2.14
3.04
3.06
f1 (ppm)
OH
O
Me
Me
O
Me
OAc
2.91

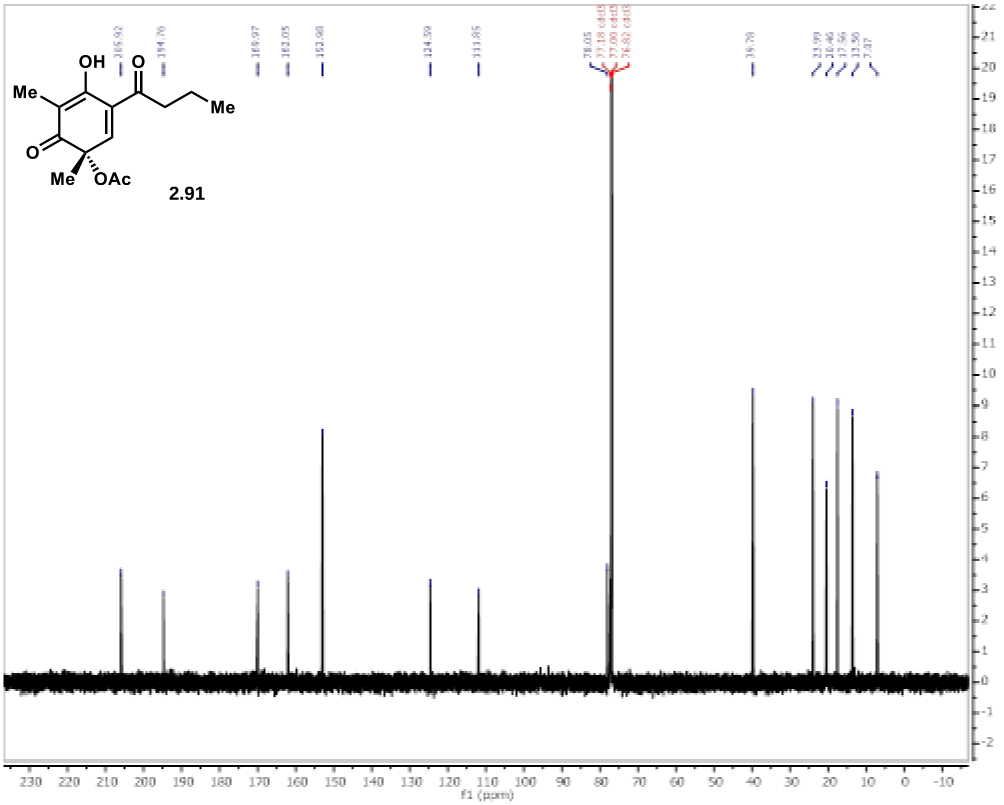
205.92
194.76
169.97
162.05
152.98
124.59
111.85
78.05
77.18 cdcl3
77.00 cdcl3
76.82 cdcl3
39.78
23.99
20.46
17.96
13.50
7.87
f1 (ppm)
OH
O
Me
Me
O
Me
OAc
2.91

Chapter 2.7: References

1) For a review: Roche, S. P.; Porco, J. A. *Angew. Chem. Int. Ed.* **2011**, *50,* 4068. a.) Zhang, C. *J. Am. Chem. Soc.* **2014**, *136*, 17750. b.) Zhu, J. et. al. *J. Am. Chem. Soc.* **2005**, *127*, 9342. c.) Hsu, D.-S. et al *Org. Lett.* **2007**, *9*, 4563. d.) Frie, J. L. *J. Am. Chem. Soc.* **2009**, *131*, 6674. Wu, W.-T.; Zhang, L.; You, S.-L. *Chem. Soc. Rev.*, **2016**, *45*, 1570.
2) a) Wessely, F.; Lauterbach-Keil, G.; Schmid, F. Monatsh. Chem. **1950**, *81*, 811. b) Wessely, F. and Sinwel, F. Monatsh. Chem. **1950**, *81*, 1055.
3) a) Bosset, C.; Coffinier, R.; Peixoto, P.A.; El Assal, M.; Miqueu, K.; Sotiropoulos; J.-M.; Pouységu, L.; Quideau,S.: *Angew. Chem. Int. Ed*. **2014**, *53*, 9860. b) Zhu, J.; Germain, A. R.; Porco, J. A., Jr. *Angew. Chem. Int. Ed. Engl.* **2004**, *43*, 1239-1243.
4) Zhu, J.; Grigoriadis, N. P.; Lee, J. P: Porco, J. A. Jr. *J. Am. Chem. Soc*. **2005**, *127*, 9342.
5) a) Volp, K. A.; Harned, A. M. *Chem. Commun*. **2013**, 3001. b) Boppisetti, J. K; Birman, V. B. *Org. Lett.* **2009**, *11*, 1221.
6) Hasimoto, T.; Shimazaki, Y.; Omatsu, Y.; Maruoka, K. *Angew. Chem. Int. Ed. Engl.* **2018**, *57*, 7200-7204.
7) van Berkel, W. J. H.; Kamerbeek, N. M.; Fraajie, M. W. J. Biotechnol. **2006**, *124*, 670.
8) Turner, N. J. *Nat. Chem. Biol*. **2009**, *5*, 567.
9) Davison, J.; Al Fahad, A.; Cai, M.; Song, Z.; Yehia, S. Y.; Lazarus, C. M.; Bailey, A. M.; Simpson, T. J.; Cox, R. J. *Proc Natl Acad Sci U S A.* **2012**, *109*, 7642.
10) al Fahad, A.; Abood, A.; Fisch, K.; Osipow, A.; Davison, J.; Avramovic, M.; Butts, C. P.; Piel, J.; Simpson, T. J.; Cox, R. J. *Chem. Sci.* **2014**, *5*, 523.
11) Zabala, A. O.; Xu, W.; Chooi, Y.-H.; Tang, Y. *Chem. Biol.* **2012**, *19*, 1049.
12) Wen-Hau, J.; Qian-Shan, G.; Yun-Liang, L.; Hong-Mei, G.; Xiao, W.; Yan-Ling, G. *Synth. Commun.* **2014**, *44*, 450.
13) Nicolaou, K. C.; Vassilikogiannakis, G.; Simonsen, K. B.; Baran, P. S.; Zhong, Y.-L.; Vidali, V. P.; Pitsinos, E. N.; Couladouros, E. A. *J. Am. Chem. Soc.* **2000**, *122*, 3071.
14) I. Jeon, I. K. Mangion, *Synlett*, **2012**, *23*, 1927-1930.
15) Abood, A.; Al-Fahad, A.; Scott, A.; Hosny, A. E.-D. M. S.; Hashem, A. M.; Fattah, A. M. a.; Race, P. R.; Simpson, T. J.; Cox, R. J. *RSC Adv*. **2015**, *5*, 49987.
16) Zhang, J.; Witholt, B.; Li, Z. *Adv. Synth. Catal.*, **2006**, *348*, 429–433.
17) a) Rodríguez Benítez, A.; Tweedy, S.; Baker Dockrey, S.; Lukowski, A.; Wymore, T.; Khare, D.; Brooks, C. III.; Palfey, B. A.; Smith, J.; Narayan, A. *ACS Catal.* **2019**, *9*, 3633. b) Tweedy, S. E.; Rodríguez Benítez, A.; Narayan, A. R. H.; Zimmerman, P. M.; Brooks, C. L., III; Wymore, T. *J. Phys. Chem. B.* **2019**, *123*, 38, 8065.
18) Baker Dockrey, S. A.; Lukowski, A. L.; Becker, M. R., Narayan, A. R. H. *Nat. Chem.* **2018**, *10,* 119.
19) Hoye, T. R.; Jeffery, S. C.; Feng, S. *Nat. Protoc.* **2007**, *2*, 2451.
20) Barnes-Seeman, D., Corey, E. J. *Org. Lett.* **1999**, *1*, 1503-1504.
21) Frigerio, M., Santagostino, M., Sputore, S. *J. Org. Chem.* **1999**, *64*, 4537-4537.
22) Blangetti, M., Fleming, P., O'Shea, D. F. *J. Org. Chem.* **2012**, *77*, 2870-2877.
23) Mizutani, T., Wada, K., Kitagawa, S. *J. Org. Chem.* **2000**, *65*, 6097-6106.
24) Harmata, M., Ying, W., Barnes, C. L. *Tetrahedron Lett.* **2009**, *50*, 2326-2328.
25) Saa, J. M., Martorell, G. *J. Org. Chem.* **1993**, *58*, 1963-1966.
26) Volp, K. A.; Johnson, D. M.; Harned, A. M. *J. Org. Chem*. **2011**, *13*, 3001.
27) Yeh, H.-H. et al. *Org. Lett*. **2013**, *15*, 756-759.
28) Tangestaninejad, S., Habibi, M. H., Mirkhani, V., Moghadam, M. *Synth. Commun.* **2002** *32,* 1337-1343.
29) Kang, Y., Mei, Y., Du, Y., Jin, Z. *Org. Lett.* **2003**, *5*, 4481-4483.

30) Lee, Y. M., Li, H., Hong, J., Cho, H. Y., Bae, K. S., Kim, M. A., Kim, D.-K., Jung, J. H. *Arch. Pharm. Res.* **2010**, *33*, 231-235.
31) Dhankher, P., Sheppard, T. D. *Synlett.* **2014,** *25*, 381-283.
32) Konakahara, T., Kiran, Y. B., Okuno, Y., Ikeda, R., Sakai, N. *Tetrahedron Lett.* **2010**, *51*, 2335-2338.
33) Baleizão, C.; Gigante, B.; Garcia, H.; Corma, A. *J. Catal.* **2004**, *221*, 77-84.

CHAPTER 3: Positioning-group Enabled Biocatalytic Oxidative Dearomatization

Portions adapted with permission from "Positioning-group enabled biocatalytic oxidative dearomatization" *ACS Central Sci.* **2019**, *5*, 1010-1016.

Chapter 3.1: Introduction

Protein engineering is a powerful tool to alter the substrate scope of a given biocatalyst, in which the structure of the catalyst is altered to accommodate a targeted non-native substrate;[1,2] however, this approach requires expertise and equipment not uniformly available in synthetic chemistry laboratories. Classical chemical methods rely not only on tuning the catalysts, but also an orthogonal strategy to engineer interactions between a catalyst and substrate by altering the substrates to contain a functional group that possesses a high affinity for the catalyst. Using this

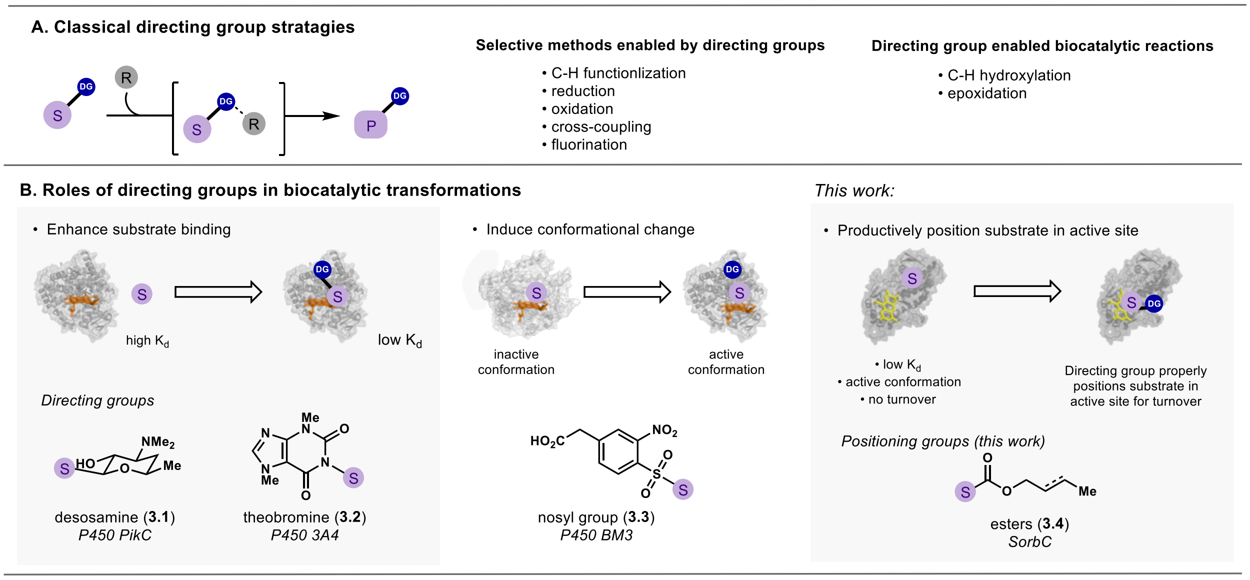
A. Classical directing group stratagies
DG
S
R
DG
S
R
P
DG
Selective methods enabled by directing groups
• C-H functionlization
• reduction
• oxidation
• cross-coupling
• fluorination
Directing group enabled biocatalytic reactions
• C-H hydroxylation
• epoxidation
B. Roles of directing groups in biocatalytic transformations
• Enhance substrate binding
S
high K_d
DG
S
low K_d
Directing groups
S
HO
O
NMe$_2$
Me
desosamine (3.1)
P450 PikC
Me
N
O
N
N
N
Me
O
S
theobromine (3.2)
P450 3A4
• Induce conformational change
S
inactive conformation
DG
S
active conformation
HO$_2$C
NO$_2$
S
O
O
S
nosyl group (3.3)
P450 BM3
This work:
• Productively position substrate in active site
S
• low K_d
• active conformation
• no turnover
S
DG
Directing group properly positions substrate in active site for turnover
Positioning groups (this work)
S
O
O
Me
esters (3.4)
SorbC

Figure 3.1: (A) Classical and biocatalytic methods enabled by directing groups. S = substrate, R = chemical reagent, DG = directing group. (B) Roles of directing groups in biocatalytic transformations including enhanced substrate binding, impact on conformation and substrate positioning within active site.

approach, high levels of site- and stereoselectivity have been obtained in a wide variety of chemical transformations (Figure 3.1).[3,4]

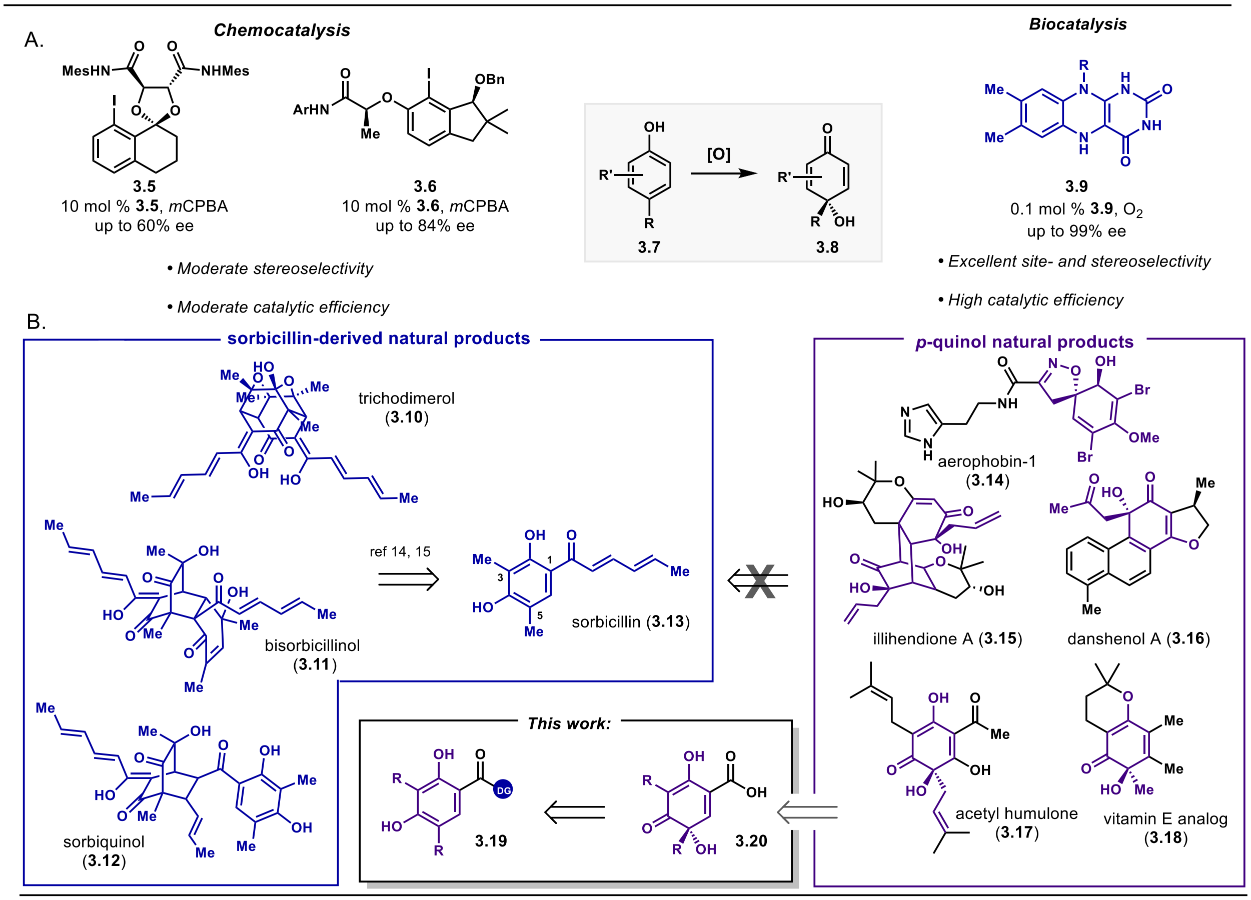
A.
Chemocatalysis
MesHN
NHMes
3.5
10 mol % 3.5, mCPBA
up to 60% ee
ArHN
OBn
Me
3.6
10 mol % 3.6, mCPBA
up to 84% ee
• Moderate stereoselectivity
• Moderate catalytic efficiency
OH
R'
R
[O]
R' OH
3.7
3.8
Biocatalysis
3.9
0.1 mol % 3.9, O2
up to 99% ee
• Excellent site- and stereoselectivity
• High catalytic efficiency
B.
sorbicillin-derived natural products
trichodimerol
(3.10)
bisorbicillinol
(3.11)
ref 14, 15
sorbicillin (3.13)
sorbiquinol
(3.12)
This work:
DG
3.19
3.20
p-quinol natural products
aerophobin-1
(3.14)
illihendione A (3.15)
danshenol A (3.16)
acetyl humulone
(3.17)
vitamin E analog
(3.18)

Figure 3.2: (A) Chemo- and biocatalytic methods for asymmetric oxidative dearomatization. (B) Sorbicillin derived natural products accessible by previous methodology and examples of *p*-quinol natural products that can be accessed via a directing-group strategy.

In contrast to the widespread use of directing groups in organic synthesis with chemical reagents and catalysts, the analogous strategy of substrate engineering has remained under-utilized in biocatalysis. Reported examples of substrate engineering for the purpose of synthetic chemistry have been restricted to a single class of enzymes, cytochromes P450.[5-12] However, we anticipate that substrate engineering can radically expand the utility of a range of enzyme classes in biocatalysis. Substrate engineering can impact various aspects of a biocatalytic reaction. For example, approaches to substrate engineering have included the installation of a directing group to anchor a substrate through a specific protein-substrate interaction (Figure 3.2).[6,8-10] Using this strategy, substrates with low binding affinity for a biocatalyst's active site are transformed into substrates with an increased affinity for the catalyst. Both Auclair and Sherman have demonstrated this anchoring group approach, identifying heterocycles that can enhance the binding of non-native substrates with P450s, and allow for predictable hydroxylation of engineered substrates.[6,9,10] Substrate engineering can also be targeted toward inducing a conformational change upon binding to shift from an inactive protein conformation to a catalytically productive conformation, thus initiating substrate turnover.[13] By contrast, we have demonstrated a strategy in which a tightly bound but unreactive substrate is engineered to include a functional group that poses the substrate within the enzyme active site for a productive reaction (Figure 3.1B). This approach addresses a problem distinct from substrate binding, which we have shown occurs with substrates which lack the positioning group but do not undergo conversion. We have applied this positioning group strategy to expand the synthetic utility of the flavin-dependent monooxygenase SorbC, which mediates oxidative dearomatization with site- and stereoselectivity which exceed existing chemical methods.

Like cytochromes P450, flavin-dependent enzymes mediate a broad array of chemical transformations encompassing both reductive and oxidative processes.[14] Within the category of oxidative transformations, flavin-dependent enzymes are capable of catalyzing highly selective hydroxylation,[15] epoxidation,[16] halogenation,[17] and Baeyer-Villiger[18] reactions among others, and have found application in a number of commercial processes.[19] Recently, we explored the synthetic potential of a panel of flavin-dependent monooxygenases which mediate the highly site- and stereoselective oxidative dearomatization of phenolic substrates.[20] While several wild-type biocatalysts investigated demonstrated an impressive substrate scope, an enzyme with unique site-selectivity, SorbC, operated on a limited range of substrates.[20] The site-selectivity achieved in reactions with SorbC is difficult to access with chemical reagents and catalysts, often requiring specific substitution patterns to bias the site of hydroxylation. Controlling the stereochemical outcome in this transformation has also challenged chemists with state-of-the-art methods employing hypervalent iodine catalysts providing products in 60-84% ee (Figure 2A).[21,22] In the biocatalytic mechanism, molecular oxygen reacts with reduced flavin adenine dinucleotide ($FADH_2$, **3.5**) to form C4a-hydroperoxy flavin, an electrophilic source of oxygen.[23] The site- and stereoselectivity of hydroxylation arises from the pose of the substrate in the enzyme active site relative to the flavin cofactor (**3.9**). This strategy for stereocontrol allows for perfect selectivity in the native reaction.

Our initial investigations indicated that SorbC is capable of mediating oxidative dearomatization with exceptional stereoselectivity, generating products such as **3.8** in >99% ee, solidifying SorbC as the catalyst with the highest reported site- and enantioselectivity for this transformation (Figure 2.5).[20] However, the limited substrate scope demonstrated by SorbC presents a challenge in applying this biocatalyst to the synthesis of structurally diverse target molecules. For example, profiling the substrate promiscuity of SorbC revealed the requirement of an alkyl chain extending from the C1 position (see **3.24**, Table 2.1). Thus, while SorbC has been used in the synthesis of complex molecules derived from sorbicillin (**3.13**), [20,24,25] it is limited to the synthesis of compounds containing long alkyl chains (compounds in blue, Figure 3.2B) and does not provide access to the full breadth of biologically active molecules that could arise from *para*-quinol precursors (see compounds in purple, Figure 3.2B). For example, the native substrate of SorbC, **3.13**, bears a linear six-carbon chain at this position with a carbonyl at the benzylic position and one or two carbon-carbon double bonds. Truncation of this six-carbon chain resulted in lower conversion to dearomatized products in reactions with SorbC (Figure 3.4, entries 4 and 5). Additionally, an erosion in the enantioenrichment of the product was observed as this C1 chain was truncated or the C3 methyl group was extended to an ethyl substituent (see **21** and **22**, respectively). Based on these data, we hypothesized that the six-carbon chain plays a critical role in substrate binding and orientation within SorbC's active site. Herein, we demonstrate how this finding can be leveraged in a structure-guided substrate engineering approach to expand the synthetic utility of SorbC in the enantioselective oxidative dearomatization of phenolic substrates to enable access to a much broader array of quinol-containing natural products (see Figure 3.2B). Ultimately, this work will enable the syntheses of a variety of complex targets employing wild-type SorbC in the enantiodetermining step.

Chapter 3.2: Substrate Synthesis

Several substrates were designed to probe the promiscuity of the FDMO SorbC towards substrates with varying C1 functional groups, including amides and esters of different chain length and saturation. Carolyn Suh completed the synthesis of the key carboxylic acid intermediate 3.23 through a Kolbe-Schmitt carboxylation of dimethyl resorcinol 3.22.26 Alternate routes to carboxylic acid 3.23 were attempted but were unsuccessful. For example, Pinnick oxidation of the unprotected aldehyde resulted in low conversion or oxidation of the aromatic ring. Although the

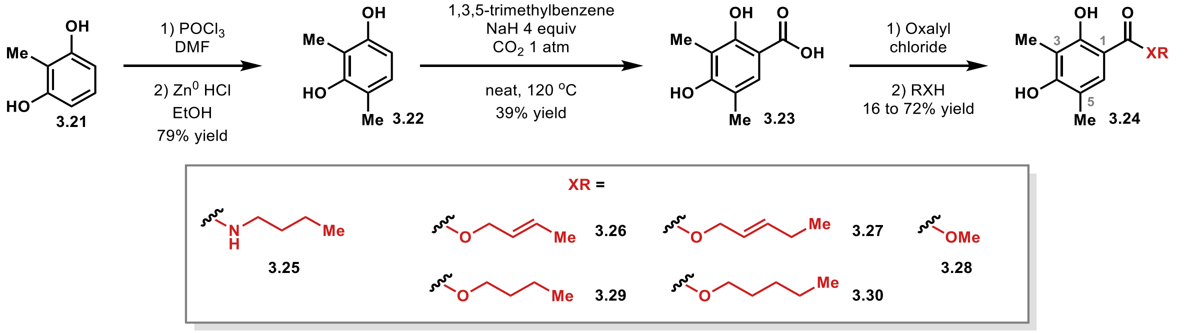
OH
Me
HO
3.21
1) POCl3
DMF
2) Zn0 HCl
EtOH
79% yield
OH
Me
HO
Me 3.22
1,3,5-trimethylbenzene
NaH 4 equiv
CO2 1 atm
neat, 120 °C
39% yield
OH O
Me
OH
HO
Me 3.23
1) Oxalyl
chloride
2) RXH
16 to 72% yield
OH O
Me 3 1
XR
HO 5
Me 3.24
XR =
N
H
Me
3.25
O
Me
3.26
O
Me
3.27
OMe
3.28
O
Me
3.29
O
Me
3.30

Figure 3.3: Synthetic route to ester and amide sorbicillin derivatives.

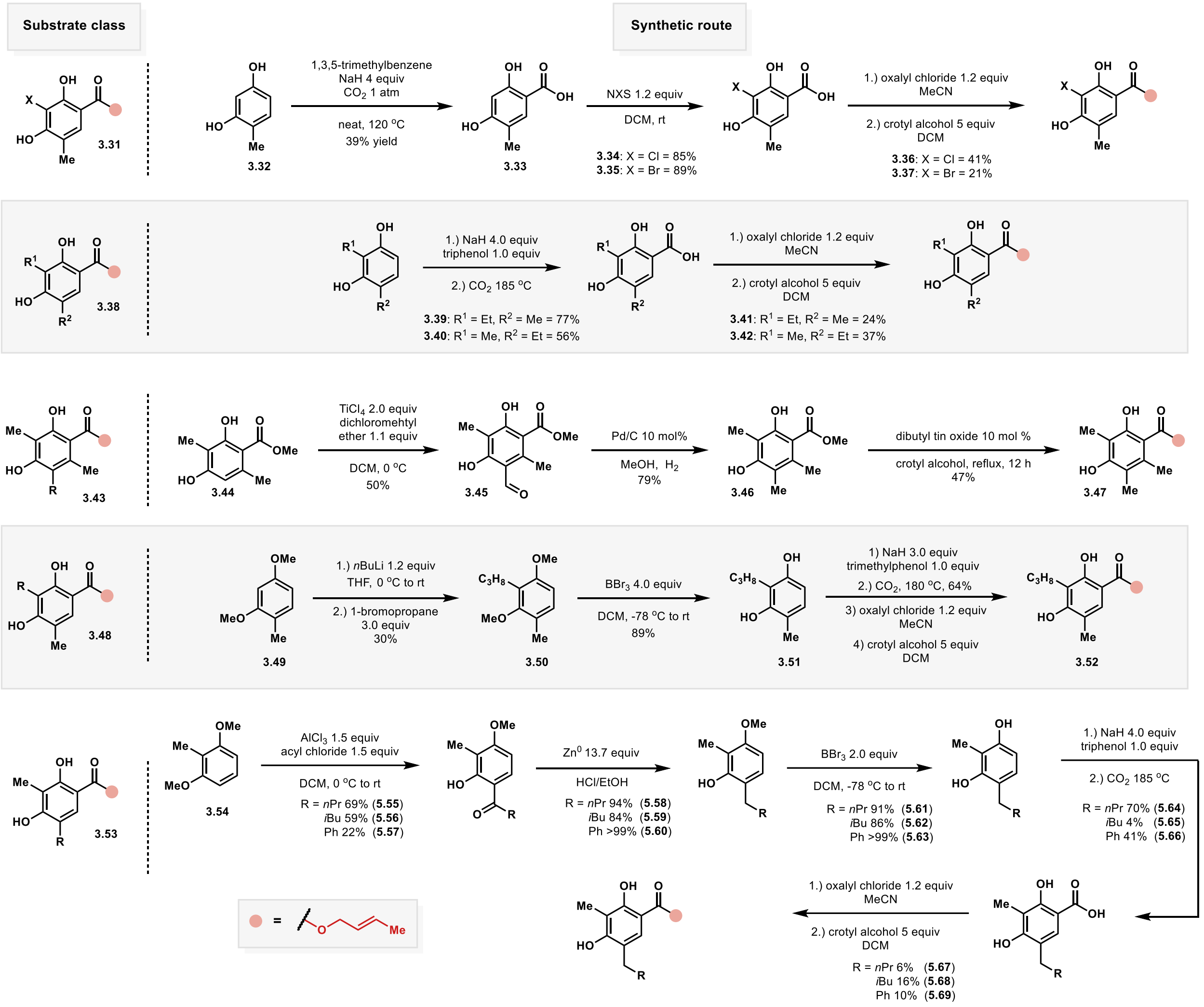
Substrate class
Synthetic route
3.31
3.32
1,3,5-trimethylbenzene
NaH 4 equiv
CO2 1 atm
neat, 120 °C
39% yield
3.33
NXS 1.2 equiv
DCM, rt
3.34: X = Cl = 85%
3.35: X = Br = 89%
1.) oxalyl chloride 1.2 equiv
MeCN
2.) crotyl alcohol 5 equiv
DCM
3.36: X = Cl = 41%
3.37: X = Br = 21%
3.38
1.) NaH 4.0 equiv
triphenol 1.0 equiv
2.) CO2 185 °C
3.39: R1 = Et, R2 = Me = 77%
3.40: R1 = Me, R2 = Et = 56%
1.) oxalyl chloride 1.2 equiv
MeCN
2.) crotyl alcohol 5 equiv
DCM
3.41: R1 = Et, R2 = Me = 24%
3.42: R1 = Me, R2 = Et = 37%
3.43
3.44
TiCl4 2.0 equiv
dichloromehtyl
ether 1.1 equiv
DCM, 0 °C
50%
3.45
Pd/C 10 mol%
MeOH, H2
79%
3.46
dibutyl tin oxide 10 mol %
crotyl alcohol, reflux, 12 h
47%
3.47
3.48
1.) nBuLi 1.2 equiv
THF, 0 °C to rt
2.) 1-bromopropane
3.0 equiv
30%
3.49
3.50
BBr3 4.0 equiv
DCM, -78 °C to rt
89%
3.51
1) NaH 3.0 equiv
trimethylphenol 1.0 equiv
2.) CO2, 180 °C, 64%
3) oxalyl chloride 1.2 equiv
MeCN
4) crotyl alcohol 5 equiv
DCM
3.52
3.53
3.54
AlCl3 1.5 equiv
acyl chloride 1.5 equiv
DCM, 0 °C to rt
R = nPr 69% (5.55)
iBu 59% (5.56)
Ph 22% (5.57)
Zn0 13.7 equiv
HCl/EtOH
R = nPr 94% (5.58)
iBu 84% (5.59)
Ph >99% (5.60)
BBr3 2.0 equiv
DCM, -78 °C to rt
R = nPr 91% (5.61)
iBu 86% (5.62)
Ph >99% (5.63)
1.) NaH 4.0 equiv
triphenol 1.0 equiv
2.) CO2 185 °C
R = nPr 70% (5.64)
iBu 4% (5.65)
Ph 41% (5.66)
1.) oxalyl chloride 1.2 equiv
MeCN
2.) crotyl alcohol 5 equiv
DCM
R = nPr 6% (5.67)
iBu 16% (5.68)
Ph 10% (5.69)
● =

Figure 3.4: Routes to crotyl ester resorcinol compounds with varying functional groups at C2, C4 and C5.

Kolbe-Schmitt carboxylation was typically low-yielding, this route was more direct than formylation followed by oxidation and so was used in the synthesis of substrates with alternative substitution of the ring (Figure 3.4). With carboxylic acid **3.23** in hand, we were able to access ester and amide derivatives via *in situ* acyl chloride generation followed by addition of the appropriate nucleophile. Alcohols and amides were chosen to give carbonyl products of the same length as the native substrate (see **3.25**, **3.26**, and **3.29**), as well as increased length (see **3.27** and **3.30**) and decreased lengths (**3.28**).

We next synthesized a number of salicylic acid derivatives varying the steric bulk and electronics of the C3, C5, and C6 position (Figure 3.4). C3-substituted compounds were accessed via directed lithiation of 4-methyl resorcinol **3.32** and addition of the desired alkyl bromide. Methyl ether deprotection followed by Kolbe-Schmidtt carboxylation and esterification afforded the desired products, although in low yield due to challenging chromatography of the acids. Halides could be installed at the C3 position via EAS of acids such as **3.33**. Alkylation of the C5 position was achieved through Friedel-Crafts acylation with the desired acyl chloride, Clemmensen reduction[27] of the corresponding ketone, and deprotection. These alkylated products then underwent Kolbe-Schmidtt carboxylation and esterification to afford crotyl esters **3.37-3.39**.

Chapter 3.3: Reactivity Profile

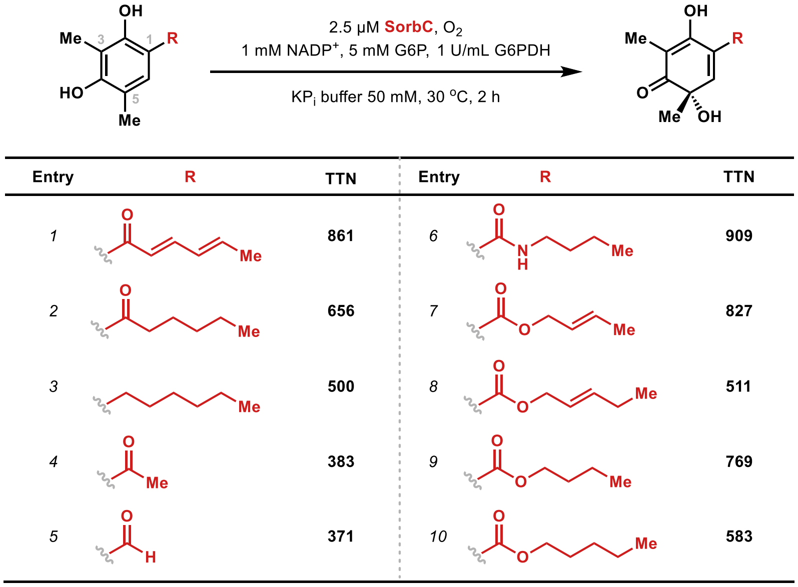
OH
Me
3
1
R
HO
5
Me
2.5 μM SorbC, O2
1 mM NADP+, 5 mM G6P, 1 U/mL G6PDH
KPi buffer 50 mM, 30 °C, 2 h
OH
Me
R
O
Me
OH
Entry
R
TTN
Entry
R
TTN
1
O
Me
861
6
O
N
H
Me
909
2
O
Me
656
7
O
O
Me
827
3
Me
500
8
O
O
Me
511
4
O
Me
383
9
O
O
Me
769
5
O
H
371
10
O
O
Me
583

Several analogs of the native substrate were evaluated in reactions containing 0.1 mol % SorbC.[28] First, the role of the double bonds and carbonyl group in the native substrate C1 substituent was gauged by comparing the total turnover number (TTN) of SorbC with (1) the native

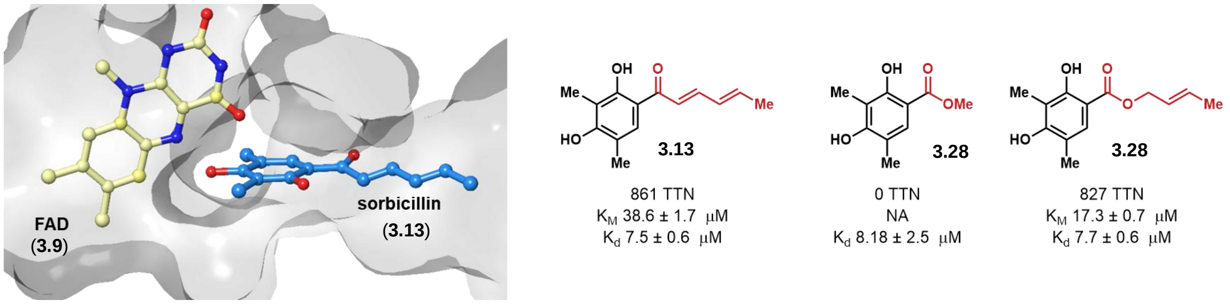

substrate, (2) a substrate bearing a saturated C1 substituent and (3) a compound in which the carbonyl group was reduced to a methylene group (Figure 3.5, entries 1-3). Each of these substrates was dearomatized by SorbC with the native substrate (**3.13**) having the highest TTN, 861, and the further reduced compounds exhibiting decreased TTNs (656 and 500, respectively). In reactions with substrates possessing a truncated C1 substituent, such as a methyl ketone or aldehyde, a further decrease in TTN was observed (383 and 371, entries 4 and 5). With evidence supporting the importance of a lipophilic linear chain for achieving a productive reaction, the ketone of the native substrate (**3.13**) was replaced with groups that meet the length requirement but are synthetically more tractable for further elaboration toward target molecules (see Figure 3.4, entries 6-10). This panel of amide and ester substrates were productively dearomatized by SorbC with TTNs ranging from 500 to 909. The amide substrate was converted to product most efficiently with a slightly higher TTN (909) than that observed for the native substrate, sorbicillin (**3.13**). This could be due to the increased nucleophilicity of the phenol due to the replacement of the electron-withdrawing ketone with the less electron-withdrawing amide. Of the ester substrates tested (Figure 3.5, entries 7-10), crotyl ester **3.26** exhibited the greatest TTN in reactions with SorbC, nearly matching the reactivity observed with SorbC's native substrate. In contrast, reactions with SorbC and methyl ester **3.28** afforded no detectable product. Concurrently with this work the

Gulder group also found that a number of esters could be converted to the dearomatized products by SorbC.[29]

To further probe the role of the lipophilic linear chain in substrate binding and reactivity, Attabey Rodríguez Benítez performed binding assays, and I carried out Michaelis-Menten kinetic analysis of SorbC with three test substrates: the native substrate (sorbicillin, **3.13**), methyl ester **3.28** and the crotyl ester **3.26**. Methyl ester **3.28** was chosen as a substrate mimic which lacked the long carbon chain at C1 present in **3.13** and **3.26**, but with similar electronics to **3.26** in order to probe the role of the long chain in binding and turnover. Interestingly, despite the differences in reactivity, the dissociation constants for SorbC with each substrate indicated similar binding affinity across the three substrates (Figure 3.7). This suggested that reactivity does not correlate with substrate binding, and that this group does not act as an anchoring group. Additionally, steady-state kinetic analysis of SorbC with this set of substrates revealed the K_M for sorbicillin (**3.13**) with SorbC was determined to be 38.6 ± 1.7 μM and crotyl ester **3.26** has a lower K_M than the native substrate, 17.3 ± 0.7 μM (Figure 3.7). For methyl ester **3.28** no reaction was observed.

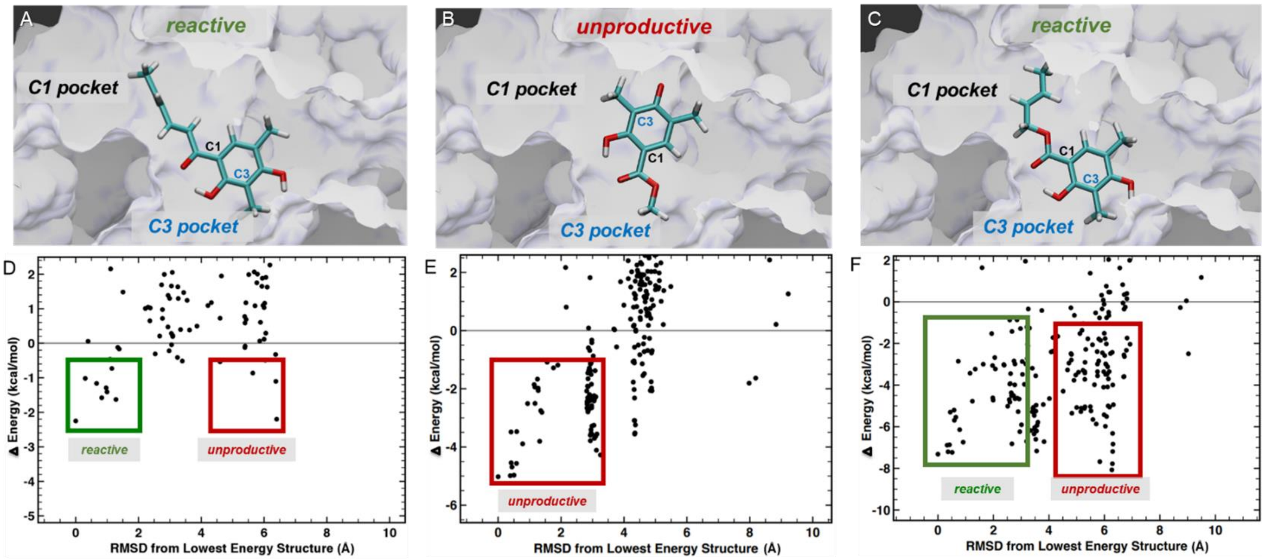

As binding experiments suggested that the role of the C1 substituent is not important for increasing the concentration of substrate in the active site, we explored the influence of this group on substrate orientation computationally. Docking studies performed by Troy Wymore revealed that substrates **3.13**, **3.26** and **3.28** can each achieve favorable binding interactions; however, only substrates with a C1 substituent of sufficient length are poised to undergo a productive reaction with the C4a-hydroperoxyflavin. The lowest energy poses identified through docking each of these three substrates (**3.13**, **3.26** and **3.28**) with SorbC are illustrated in Figure 3.8A-C. Notably, while the lipophilic group of **3.13** and crotyl ester moiety of **3.26** occupy the hydrophobic substrate entryway (C1 pocket, Figure 3.8A and 3.8C), the unreactive substrate **3.28** adopts a flipped orientation (Figure 3.6B), positioning the C1 methyl ester moiety of **3.28** in the binding pocket occupied by the C3 substituent of the native substrate **3.13** (C3 pocket). The RMSD values from the lowest energy structures of each of these three substrates were then plotted against the change in energy from the lowest energy structures (Figure 3.8D-F). This allowed us to rapidly identify clusters of favorable binding poses for the three substrates. The majority of the energetically favorable docking solutions for the native substrate place the C1 substituent in the hydrophobic entryway (boxed in green) and a smaller set of energetically favorable docking solutions place the C3 substituent in the hydrophobic entryway (boxed in red), which correspond with unreactive poses (FAD-C4a−C5 distances above 5 Å). For methyl ester substrate **3.28**, most energetically favorable docking poses position the substrate in a flipped orientation compared to the dominant binding mode for SorbC's native substrate **3.13**. This flipped orientation is anticipated to be unproductive (Figure 3.8E). Finally, crotyl ester **3.26** had numerous favorable docking solutions with SorbC in which the crotyl ester group occupied the hydrophobic entryway in the same fashion as the native substrate **3.13** (boxed in green, Figure 3.8F), and like **3.13** a number of favorable poses were also obtained with the C1 substituent in the C3 binding site in an unreactive pose (boxed in red, Figure 3.8F).

Taken together, these computational and experimental results indicate the necessity of the C1 substituent as a critical structural feature, not for lowering the K_d of a substrate, but for appropriately positioning the substrate within the active site for turnover. We envisioned exploiting this structural requirement for productive catalysis to expand the substrate scope of SorbC through a novel substrate engineering strategy. To execute a synthetically useful substrate engineering approach, the directing group must be both easily introduced prior to the biocatalytic step and readily removed or converted into a range of versatile handles following the targeted transformation. In addition to facilitating a high conversion to product, we recognized the synthetic advantages of the crotyl ester directing group, which could easily be installed from a carboxylic acid precursor and removed following the biocatalytic reaction. A number of substrates bearing a crotyl ester directing group were synthesized and evaluated for reactivity with SorbC. This substrate engineering strategy proved successful for resorcinol scaffolds with differing steric and electronic properties (Figure 3.9). Phenolic substrates **3.74** and **3.77** were not converted due perhaps to the reduced nucleophilicity of the arene. For example, hexasubstituted substrate **3.47** was efficiently converted to dearomatized product with a TTN close to that of the native scaffold. Additionally, halogen substituents were tolerated at the C3 position (see **3.36** and **3.37**), although substrate **3.76** which features only a proton at this position was not turned over. Docking studies indicated that the C3 pocket would have sufficient space to accommodate up to an *n*-propyl group. Substrates with increasing steric bulk at the C3 position, from a methyl group to an ethyl substituent and further to an *n*-propyl group, were efficiently turned over with only minor decrease in activity (see **3.28**, **3.73** and **3.52**), as predicted in Troy Wymore's computational studies.

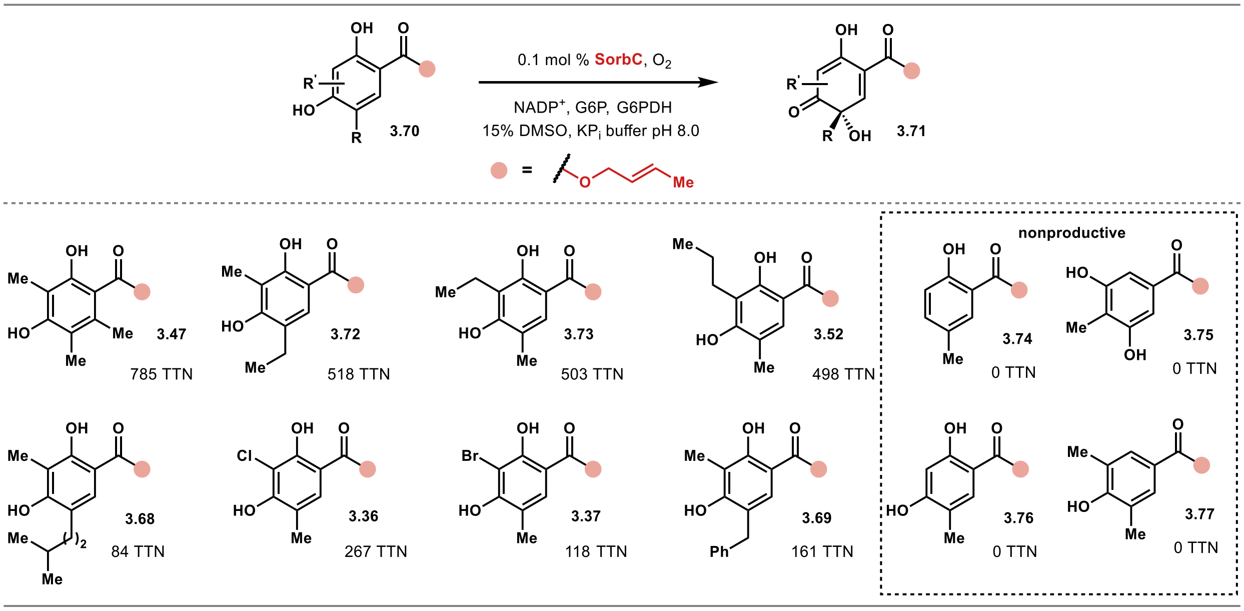
3.70
0.1 mol % SorbC, O2
NADP+, G6P, G6PDH
15% DMSO, KPi buffer pH 8.0
3.71
3.47
785 TTN
3.72
518 TTN
3.73
503 TTN
3.52
498 TTN
nonproductive
3.74
0 TTN
3.75
0 TTN
3.68
84 TTN
3.36
267 TTN
3.37
118 TTN
3.69
161 TTN
3.76
0 TTN
3.77
0 TTN

Figure 3.8: Values given are total turnover numbers (TTNs) of each enzyme/substrate pair. Reaction conditions: 2.5 mM substrate, 2.5 µM SorbC, 1 mM NADP$^+$, 5 mM glucose-6-phosphate (G6P), 1 U ml^{-1} glucose-6-phosphate dehydrogenase (G6PDH), 50 mM potassium phosphate buffer, pH 8.0, 30 °C, 15% v/v DMSO 1 h.

Substrates with additional steric bulk including a benzyl substituent at the C5 position (see **3.69**) or an isopentyl group (see **3.68**) were also tolerated. Phenolic crotyl esters and 3,5-dihydroxy crotyl esters were also prepared although these compounds were not found to be productive substrates in the enzymatic transformation (Figure 3.9).

Chapter 3.4: Preparative-scale Reactions

To evaluate the stereoselectivity achieved using this substrate engineering approach, the enantioenrichment of dearomatized products was measured. Preparative scale reactions were performed on 10 mg scale, employing the conditions outlined in Chapter 2.3. C5-hydroxylated racemic standards were synthesized using lead tetraacetate (LTA, yields shown in gray, Figure 3.10) and resolved using chiral SFC also as described in Chapter 2.3. Gratifyingly, all enzymatic products examined were obtained in good enantiopurity, supporting our hypothesis that the lipophilic substituent at C1 is critical for proper substrate positioning. The crotyl ester with the native substitution pattern was obtained in a 72% isolated yield and 98% ee. The C3 and C5 ethyl products were obtained in 98% and 96% ee, respectively. Notably, the *n*-propyl product **3.83** was also obtained in 98% ee, indicating that the crotyl group is recognized in preference to the C3 alkyl chain which, if recognized in the same manner as the C1 substituent, would result in diminished facial selectivity and ultimately eroded enantiopurity of the product. This is in contrast to the diminished enantiopurity observed in the ketone substrate class wherein the C3 ethyl product was obtained in 94% ee.

This substrate engineering strategy allowed us to expand the range of highly enantioenriched quinol products accessible through SorbC catalysis. To assess the utility of quinol products containing the crotyl ester positioning group, we explored conditions for removing the crotyl group as well as the innate reactivity of the ester-containing products. Removal of the crotyl group proved to be facile under Pd-catalyzed decrotylation conditions. By employing 7 mol % $Pd(PPh_3)_4$ and morpholine, the crotyl group of **3.79** was removed to unveil the carboxylic acid present in **3.84** (Figure 10B).[30] To further explore the innate reactivity of ester-containing products, we sought to transform these directly into analogs of the natural product urea sorbicillinoid (**4.6**, Figure 4.3).[31] Although previous reports have described ester derivatives of sorbicillinol as unreactive in the dimerization to afford the bisorbicillinol core,[32] we have demonstrated that esters undergo facile *in situ* [4+2] cycloaddition with maleimide to afford the [2,2,2] tricycle **3.87** in 23% yield over two steps (Figure 3.10C). Although the dimer of the dearomatized product was observed by MS, attempts at isolation proved unsuccessful, due in part to low reactivity and other decomposition pathways available to this compound. Based on these results, we anticipate this positioning group-based substrate engineering strategy will expand the utility of SorbC from a biocatalyst that is restricted to sorbicillinol derived natural products to a breadth of natural and unnatural compounds accessible through the dearomatization of structurally diverse resorcinol derivatives such as **3.87**.

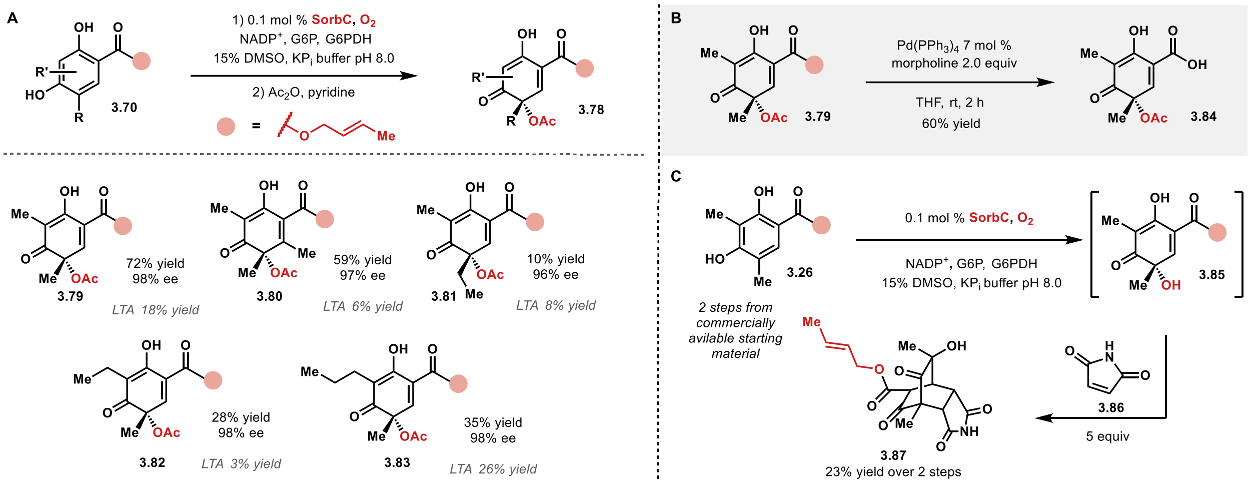
A
1) 0.1 mol % SorbC, O_2
NADP$^+$, G6P, G6PDH
15% DMSO, KP$_i$ buffer pH 8.0
2) Ac_2O, pyridine
3.70
3.78
72% yield
98% ee
LTA 18% yield
3.79
59% yield
97% ee
LTA 6% yield
3.80
10% yield
96% ee
LTA 8% yield
3.81
28% yield
98% ee
LTA 3% yield
3.82
35% yield
98% ee
LTA 26% yield
3.83
B
$Pd(PPh_3)_4$ 7 mol %
morpholine 2.0 equiv
THF, rt, 2 h
60% yield
3.79
3.84
C
0.1 mol % SorbC, O_2
NADP$^+$, G6P, G6PDH
15% DMSO, KP$_i$ buffer pH 8.0
3.26
3.85
2 steps from commercially avilable starting material
3.86
5 equiv
3.87
23% yield over 2 steps

Figure 3.9: Application of directing group strategy for preparative-scale oxidative dearomatization. (A) Evaluation of substrate scope and reaction enantioselectivities. Yields for racemic standard synthesis in grey. LTA = lead tetraacetate. (B) Removal of directing group through palladium-catalyzed decrotylation. (C) Elaboration of dearomatized product through [4+2] cycloaddition.

Chapter 3.5: Conclusions

Due to the high synthetic value of products obtained from the biocatalytic oxidative dearomatization catalyzed by SorbC, we endeavored to employ a substrate engineering strategy to overcome the limited product profile of this transformation. Initial investigations into the substrate scope of SorbC led us to hypothesize that the lipophilic carbon chain was critical for productive substrate binding in the active site. Further analysis of substrate binding experimentally and computationally revealed that the role of the C1 substituent is not in enhancing the binding affinity of the substrate for the protein, but rather the C1 substituent is critical for positioning the substrate in a reactive pose. Optimization of the positioning group led us to identify the crotyl ester as an ideal group to attain high TTNs on scaffolds which are otherwise not competent substrates in the enzymatic reaction. This ester group required for productive biocatalysis can be transformed into the corresponding carboxylic acid, a versatile handle for further chemical functionalization, or the ester-containing dearomatized products can be used directly in subsequent complexity-generating transformations. Ongoing work includes exploring the generality of this positioning group approach to other flavin-dependent monooxygenases. By profiling the substrate scope of wild-type FDMOs clear trends in reactivity can allow for the identification of key functionalities that govern productive substrate turnover. If this functionality lends itself to a directing group strategy this approach can significantly broaden the types of molecular scaffolds a wild-type protein can operate on.

Chapter 3.6 Experimental

Chapter 3.6.1: Substrate Synthesis

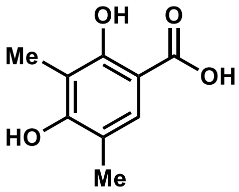

2,4-Dihydroxy-3,5-dimethylbenzoic acid (3.23)

Adapted from a report by Larrosa and coworkers.[26] In the glove box, NaH (60% dispersion in mineral oil, 1.43 g, 37.4 mmol, 4.0 equiv) was added to a vial containing 2,4-dimethylbenzene-1,3-diol (1.29 g, 9.34 mmol, 1.0 equiv) and 2,4,6-trimethylphenol (1.27 g, 9.34 mmol, 1.0 equiv). The resulting mixture was heated at 100 °C for 5 min, then cooled to room temperature and ground into powder with a spatula. The vial containing the mixture was taken out of the glove box, purged with CO_2, equipped with a balloon filled with CO_2, and heated at 185 °C for 2 h. After this time, the reaction mixture was cooled to room temperature, carefully quenched with water (5 mL), acidified to pH 4 with aq. HCl (1 M), and extracted with EtOAc (3 x 20 mL). The organic layers were dried over anhydrous Na_2SO_4, evaporated to dryness, and purified by column chromatography (10-50% EtOAc/hexanes) to yield 732 mg (43%) of salicylic acid **3.23** as a tan solid. **^{1}H NMR** (400 MHz, CD_3OD) δ 7.44 (s, 1 H), 2.07 (s, 3 H), 2.13 (s, 3 H). All spectra obtained were consistent with literature values.[32]

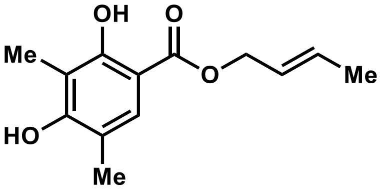

(*E*)-But-2-en-1-yl 2,4-dihydroxy-3,5-dimethylbenzoate (3.26)

0.50 mL DCM was added to an oven-dried vial equipped with a stir bar containing 2,4-dihydroxy-3,5-dimethylbenzoic acid (**3.23,** 50.0 mg, 0.270 mmol, 1.0 equiv). Oxalyl chloride (35 μL, 0.412 mmol, 1.5 equiv) was slowly added followed by DMF (1 drop, approx 10 μL). The mixture was stirred for 2 h before crotyl alcohol (36 μL, 0.450 mmol, 1.5 equiv mixture of *cis* and *trans* 1:19) was added dropwise. After 2 h, the reaction was quenched by addition of water (5 mL) and extracted with EtOAc (3 x 20 mL). The organic layers were dried over anhydrous Na_2SO_4, evaporated to dryness, and purified by column chromatography (0-15% EtOAc/hexanes) to yield 41 mg (65%) of the crotyl ester as a colorless solid. None of the undesired *cis* isomer was observed by UPLC-PDA. **^{1}H NMR** (400 MHz, CD_3OD) δ 7.42 (s, 1H), 5.89 (m, 1H), 5.70 (m, 1H), 4.70 (d, *J* = 6.4 Hz, 2H), 2.12 (s, 3H), 2.07 (s, 3H), 1.74 (d, *J* = 6.4 Hz, 3H); **^{13}C NMR** (100 MHz, $CDCl_3$) δ 170.3, 159.6, 159.6, 131.1, 127.9, 124.9, 115.8, 110.4, 103.6, 64.9, 16.5, 14.8, 6.8; **HRMS** (ESI) *m/z* calculated for $C_{13}H_{18}O_4$ $[M+H]^+$: 237.1121, found: 237.1121; **IR** (thin film): 3440, 2919, 1644, 1609, 1402, 1295 cm^{-1}; **MP**: 91-92 °C.

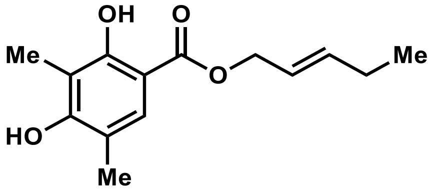

(*E*)-Pent-2-en-1-yl 2,4-dihydroxy-3,5-dimethylbenzoate (3.27)

0.50 mL DCM was added to an oven-dried vial equipped with a stir bar containing 2,4-dihydroxy-3,5-dimethylbenzoic acid (**3.23**, 50.0 mg, 0.270 mmol, 1.0 equiv). Oxalyl chloride (35 μL, 0.412 mmol, 1.5 equiv) was slowly added followed by DMF (1 drop, approx 10 μL). The mixture was stirred for 2 h before (*E*)-pent-2-en-1-ol (28 μL, 0.270 mmol, 1.0 equiv) was added dropwise. After 2 h, the reaction was quenched by addition of water (5 mL) and extracted with EtOAc (3 x 20 mL). The organic layers were dried over anhydrous Na_2SO_4, evaporated to dryness and purified by column chromatography (0-15% EtOAc/hexanes) to yield 17 mg (25%) of the pentenyl ester as a colorless solid. **^{1}H NMR** (400 MHz, $CDCl_3$) δ 11.11 (s, 1H), 7.51 (s, 1H), 5.90 (m, 1H), 5.66 (m, 1H), 5.16 (s, 1H), 4.75 (dt, *J* = 6.5, 1.2 Hz, 2H), 2.18 (s, 3H), 2.12 (s, 3 H), 2.09 (m, 2H), 1.03 (t, *J* = 7.5 Hz, 3H); **^{13}C NMR** (100 MHz, $CDCl_3$) δ 170.2, 159.8, 158.0, 138.4, 128.6, 122.6, 114.5, 110.0, 104.9, 65.6, 25.3, 15.3, 13.1, 7.7; **HRMS** (ESI) *m/z* calculated for $C_{14}H_{19}O_4$ $[M+H]^+$: 251.1278, found: 251.1262; **IR** (thin film): 3460, 2925, 1645, 1611, 1401, 1292 cm^{-1}; **MP**: 60-61 °C.

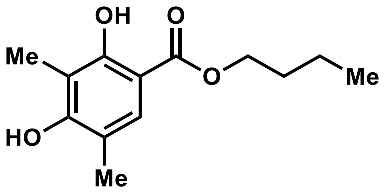

Butyl 2,4-dihydroxy-3,5-dimethylbenzoate (3.29)

0.50 mL DCM was added to an oven-dried vial equipped with a stir bar containing 2,4-dihydroxy-3,5-dimethylbenzoic acid (**3.23**, 50.0 mg, 0.270 mmol, 1.0 equiv). Oxalyl chloride (35 μL, 0.412 mmol, 1.5 equiv) was slowly added followed by DMF (1 drop, approx 10 μL). The mixture was stirred for 2 h before butanol (29 μL, 0.270 mmol, 1.0 equiv) was added dropwise. After 2 h, the reaction was quenched by addition of water (5 mL) and extracted with EtOAc (3 x 20 mL). The organic layers were dried over anhydrous Na_2SO_4, evaporated to dryness, and purified by column chromatography (0-15% EtOAc/hexanes) to yield 10 mg (16%) of the butyl ester as a colorless solid. **^{1}H NMR** (400 MHz, CD_3OD) δ 7.42 (s, 1H), 4.29 (t, *J* = 6.6 Hz, 2H), 2.13 (s, 3H), 2.07 (s, 3H), 1.74 (m, 2H), 1.48 (h, *J* = 7.4 Hz, 2H), 0.99 (t, *J* = 7.4 Hz, 3H); **^{13}C NMR** (100 MHz, CD_3OD) δ 170.5, 159.7, 159.6, 127.8, 115.7, 110.4, 103.6, 64.2, 30.5, 18.9, 14.8, 12.6, 6.8; **HRMS** (ESI) *m/z* calculated for $C_{13}H_{19}O_4$ $[M+H]^+$: 239.1278, found: 239.1275; **IR** (thin film): 3442, 2925, 1642, 1610, 1403, 1288 cm^{-1}; **MP**: 93-94 °C.

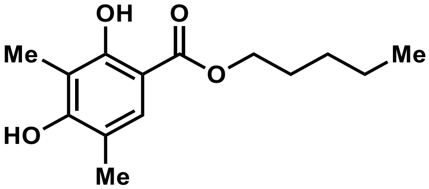

Pentyl 2,4-dihydroxy-3,5-dimethylbenzoate (3.30)

0.50 mL DCM was added to an oven-dried vial equipped with a stir bar containing 2,4-dihydroxy-3,5-dimethylbenzoic acid (**3.23,** 50.0 mg, 0.270 mmol, 1.0 equiv). Oxalyl chloride (35 μL, 0.412 mmol, 1.5 equiv) was slowly added followed by DMF (1 drop, approx 10 μL). The mixture was stirred for 2 h before pentanol (29 μL, 0.270 mmol, 1.0 equiv) was added dropwise. After 2 h, the reaction was quenched by addition of water (5 mL) and extracted with EtOAc (3 x 20 mL). The organic layers were dried over anhydrous Na_2SO_4, evaporated to dryness and purified by column chromatography (0-15% EtOAc/hexanes) to yield 50 mg (74%) of the pentyl ester as a colorless solid. **^{1}H NMR** (400 MHz, $CDCl_3$) δ 11.17 (s, 1H), 7.48 (s, 1H), 5.27 (s, 1H), 4.30 (t, *J* = 6.7 Hz, 2H), 2.19 (s, 3H), 2.14 (s, 3H), 1.77 (p, *J* = 6.9 Hz, 2H), 1.42 (m, 4H), 0.94 (m, 3H); **^{13}C NMR** (100 MHz, $CDCl_3$) δ 170.6, 159.8, 158.0, 128.4, 114.6, 110.0, 104.9, 65.1, 28.4, 28.1, 22.3, 15.4, 13.9, 7.7; **HRMS** (ESI) *m/z* calculated for $C_{14}H_{21}O_4$ $[M+H]^+$: 253.1434, found: 253.1438; **IR** (thin film): 3514, 2922, 1652, 1611, 1468, 1193 cm^{-1}; **MP**: 67-68 °C.

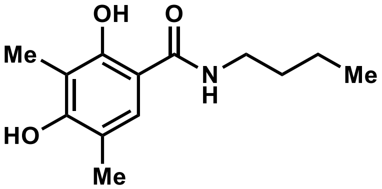

***N*-Butyl-2,4-dihydroxy-3,5-dimethylbenzamide (3.25)**

0.50 mL DCM was added to an oven-dried vial equipped with a stir bar containing 2,4-dihydroxy-3,5-dimethylbenzoic acid (**3.23,** 50.0 mg, 0.270 mmol, 1.0 equiv). Oxalyl chloride (35 μL, 0.412 mmol, 1.5 equiv) was slowly added followed by DMF (1 drop, approx 10 μL). The mixture was stirred for 2 h before butyl amine (29 μL, 0.270 mmol, 1.0 equiv) was added dropwise. After 2 h, the reaction was quenched by addition of water (5 mL) and extracted with EtOAc (3 x 20 mL). The organic layers were dried over anhydrous Na_2SO_4, evaporated to dryness and purified by column chromatography (0-15% EtOAc/hexanes) to yield 23 mg (34%) of the amide as a colorless oil. **^{1}H NMR** (400 MHz, $CDCl_3$) δ 12.77 (s, 1H), 6.95 (s, 1H), 6.07 (s, 1H), 5.02 (s, 1H), 3.43 (q, *J* = 6.6 Hz, 2H), 2.19 (s, 3H), 2.14 (s, 3H), 1.60 (m, 2H), 1.41 (q, *J* = 7.5 Hz, 2H), 0.96 (t, *J* = 7.3 Hz, 3H); **^{13}C NMR** (100 MHz, $CDCl_3$) δ 170.2, 159.7, 156.5, 123.9, 113.8, 110.8, 106.7, 39.3, 31.6, 20.1, 15.6, 13.7, 7.6; **HRMS** (ESI) *m/z* calculated for $C_{13}H_{20}NO_3$ $[M+H]^+$: 238.1438, found: 238.1432; **IR** (thin film): 3390, 2924, 1735, 1635, 1590, 1370 cm^{-1}.

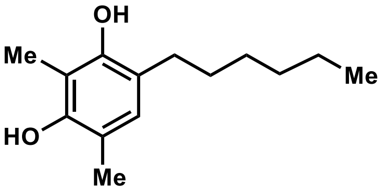

4-Hexyl-2,6-dimethylbenzene-1,3-diol (Figure 3.5, Entry 3)

A solution of 1-(2,4-dihydroxy-3,5-dimethylphenyl)hexan-1-one (115 mg, 0.692 mmol, 1.0 equiv) and Zn dust (452 mg, 6.92 mmol, 10 equiv) in EtOH (2.1 mL) was added to a round-bottom flask equipped with a stirbar and cooled to 0 °C. HCl conc. aq. (2.1 mL) was added dropwise over 15 min. The mixture slurry was then stirred at 0 °C for 20 min before filtration. The filtrate was quenched by the slow addition of saturated sodium bicarbonate (1 mL) and extracted with EtOAc (3 x 50 mL). The combined organic layers were dried over anhydrous Na_2SO_4, evaporated to dryness and purified by column chromatography silica gel (0-20% EtOAc/hexanes) to afford 103 mg (98% yield) of the title compound as a white solid. **^{1}H NMR** (600 MHz, $CDCl_3$) δ 6.72 (s, 1H), 4.55 (s, 1H), 4.53 (s, 1H), 2.49 (t, *J* = 8.1 Hz, 2H), 2.17 (overlapping s, 6H), 1.56 (m, 2H), 1.38 (m, 2H), 1.32 (m, 4H), 0.89 (t, *J* = 6.5, 3H); **^{13}C NMR** (150 MHz, $CDCl_3$) δ 150.6, 150.3, 128.2, 119.6, 114.4, 109.6, 31.8, 30.2, 29.8, 29.3, 22.6, 15.4, 14.1, 8.5; **HRMS** (ESI) *m/z* calculated for $C_{14}H_{23}O_2$ $[M+H]^+$: 223.1693, found: 223.1694; **IR** (thin film): 3512, 2923, 1611, 1468, 1377, 1191 cm^{-1}; **MP**: 84-86 °C.

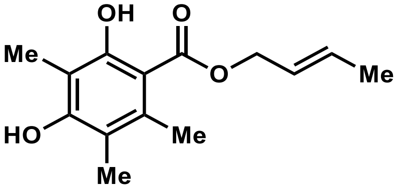

(*E*)-But-2-en-1-yl 2,4-dihydroxy-3,5,6-trimethylbenzoate (3.47)

Adapted from a protocol developed by Giannis.[34] Methyl 2,4-dihydroxy-3,5,6-trimethylbenzoate (180 mg, 1.20 mmol, 1.0 equiv) was dissolved in crotyl alcohol (2.4 mL) in a flame-dried vial. After the addition of dibutyltin oxide (71.0 mg, 0.120 mmol, 10 mol %) the mixture was heated at reflux for 12 h. The reaction was quenched by addition of water (5 mL) and extracted with EtOAc (3 x 20 mL). The combined organic layers were washed with brine (10 mL), dried over anhydrous Na_2SO_4, evaporated to dryness and purified by column chromatography (0-15% EtOAc/hexanes) to yield 140 mg (47%) of the crotyl ester as a colorless solid. **^{1}H NMR** (600 MHz, $CDCl_3$) δ 11.42 (s, 1H), 5.86 (m, 1H), 5.7 (m, 1H), 5.11 (s, 1H), 4.76 (d, *J* = 6.5 Hz, 2H), 2.43 (s, 3H), 2.12 (overlapping s, 6H), 1.74 (d, *J* = 6.5 Hz, 3H); **^{13}C NMR** (150 MHz, $CDCl_3$) δ 172.0, 159.5, 156.5, 137.6, 131.8, 124.7, 114.7, 107.2, 106.3, 65.9, 18.9, 17.8, 11.8, 8.0; **HRMS** (ESI) *m/z* calculated for $C_{14}H_{19}O_4$ $[M+H]^+$: 251.1278, found: 251.1277; **IR** (thin film): 3464, 3176, 2949, 2930, 1641, 1611, 1188 cm^{-1}; **MP**: 77-78 °C.

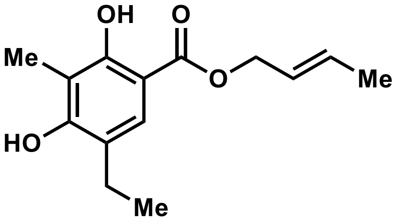

(*E*)-But-2-en-1-yl 5-ethyl-2,4-dihydroxy-3-methylbenzoate (3.72)

Adapted from a report by Larrosa and coworkers.[26] In the glove box, NaH (60% wt/wt dispersion in mineral oil, 1.43 g, 37.4 mmol, 4.0 equiv) was added to a vial containing 4-ethyl-2-methylbenzene-1,3-diol (1.29 g, 9.34 mmol, 1.0 equiv) and 4-ethyl-2-methyl resorcinol (**3.40**, 1.27 g, 9.34 mmol, 1.0 equiv). The resulting mixture was heated at 100 °C for 5 min, cooled to room temperature and ground into powder with a spatula. The vial containing the mixture was taken out of the glove box, purged with CO_2 and equipped with a balloon filled with CO_2 at 185 °C for 2 h. After this time, the reaction mixture was cooled to room temperature, carefully quenched with water (5 mL), acidified to pH 4 with aq. HCl (1 M), and extracted with EtOAc (3 x 20 mL). The organic layers were dried over anhydrous Na_2SO_4, evaporated to dryness and purified by column chromatography (30-50% EtOAc/hexanes) to yield 732 mg (43%) of salicylic acid **3.42** as a tan solid. DCM (10 mL) was added to an oven-dried vial equipped with a stir bar containing 5-ethyl-2,4-dihydroxy-3-methylbenzoic acid (**3.42**, 400 mg, 2.04 mmol, 1.0 equiv). Oxalyl chloride (192 μL, 2.24 mmol, 1.1 equiv) was slowly added followed by DMF (1 drop, approx 10 μL). The mixture was stirred for 2 h before crotyl alcohol (348 μL, 4.08 mmol, 2.0 equiv) was added dropwise. After 2 h, the reaction was quenched by addition of water (5 mL) and extracted with EtOAc (3 x 20 mL). The organic layers were dried over anhydrous Na_2SO_4, evaporated to dryness and purified by column chromatography (0-15% EtOAc/hexanes) to yield 23 mg (34%) of the crotyl ester as a colorless solid. **^{1}H NMR** (600 MHz, $CDCl_3$) δ 11.14 (s, 1H), 7.49 (s, 1H), 5.86 (m, 1H), 5.70 (m, 1H), 5.29 (s, 1H), 4.73 (d, *J* = 6.5 Hz, 2H), 2.55 (q, *J* = 7.5 Hz, 2H), 2.13 (s, 3H), 1.74 (m, 3H), 1.20 (t, *J* = 7.5 Hz, 3H); **^{13}C NMR** (150 MHz, $CDCl_3$) δ 170.3, 159.7, 157.7, 131.7, 127.1, 124.9, 121.0, 110.0, 104.9, 65.6, 22.7, 17.8, 14.1, 7.7; **HRMS** (ESI) *m/z* calculated for $C_{14}H_{19}O_4$ $[M+H]^+$: 251.1278, found: 251.1276; **IR** (thin film): 3439, 2820, 1643, 1609, 1400, 1194 cm $^{-1}$; **MP**: 75-76 °C.

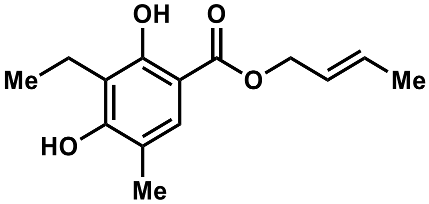

(*E*)-But-2-en-1-yl 3-ethyl-2,4-dihydroxy-5-methylbenzoate (3.73)

Adapted from a report by Larrosa and coworkers.[26] In the glove box, NaH (60% dispersion in mineral oil, 268 mg, 11.2 mmol, 4.0 equiv) was added to a vial containing 2-ethyl-4-methylbenzene-1,3-diol (380 mg, 2.79 mmol, 1.0 equiv) and 2-ehtyl-4-methylresorcinol (**3.39,** 425 mg, 2.79 mmol, 1.0 equiv). The resulting mixture was heated at 100 °C for 5 min, cooled to room temperature and ground into powder with a spatula. The vial containing the mixture was taken out of the glove box, purged with CO_2 and equipped with a balloon filled with CO_2 at 185 °C for 2 h. The reaction mixture was cooled to room temperature, carefully quenched with water (5 mL), acidified to pH 4 with aq. HCl (1 M), and extracted with EtOAc (3 x 20 mL). The organic layers were dried over anhydrous Na_2SO_4, evaporated to dryness and purified by column chromatography (30-50% EtOAc/hexanes) to yield 305 mg (56%) of salicylic acid **3.41** as a tan solid.

3-ethyl-2,4-dihydroxy-5-methylbenzoic acid (**3.41**, 305 mg, 1.55 mmol, 1.0 equiv) was stirred in DCM (9 mL) in a flame-dried round-bottom flask. Oxalyl chloride (147 μL, 1.71 mmol, 1.1 equiv) was slowly added followed by DMF (1 drop, approx 10 μL). The mixture was stirred for 2 h before crotyl alcohol (264 μL, 3.10 mmol, 2.0 equiv) was added dropwise. After 2 h, the reaction was quenched by addition of water (5 mL) and extracted with EtOAc (3 x 20 mL). The organic layers were dried over anhydrous Na_2SO_4, evaporated to dryness, and purified by column chromatography (0-15% EtOAc/hexanes) to yield 94 mg (24%) of the crotyl ester as a colorless solid. **^{1}H NMR** (600 MHz, $CDCl_3$) δ 11.07 (s, 1H), 7.49 (s, 1H), 5.86 (m, 1H), 5.68 (m, 1H), 5.23 (s, 1H), 4.72 (d, J = 6.5 Hz, 1H), 2.67 (q, J = 7.5 Hz, 2H), 2.17 (s, 3H), 1.75 (d, J = 6.5 Hz, 3H), 1.14 (t, J = 7.5 Hz, 3H); **^{13}C NMR** (150 MHz, $CDCl_3$) δ 170.3, 159.7, 157.6, 131.8, 128.7, 124.8, 116.4, 114.6, 104.9, 65.5, 17.8, 16.2, 15.3, 13.2; **HRMS** (ESI) *m/z* calculated for $C_{14}H_{19}O_4$ $[M+H]^+$: 251.1278, found: 251.1276; **IR** (thin film): 3570, 2952, 1746, 1641, 1196 $^{cm-1}$; **MP**: 89-90 °C.

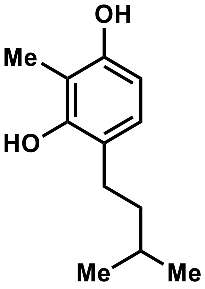

4-isopentyl-2-methylbenzene-1,3-diol (5.59)

1-Iodo-2,4-dimethoxy-3-methylbenzene (1.00 g, 3.60 mmol, 1.0 equiv) was added to a flame-dried round-bottom flask and dissolved in THF (25 mL). The mixture was cooled to 0 °C and *n*BuLi (1.73 mL, 4.32 mmol, 1.2 equiv, 2.5 M in hexanes) was slowly added. The mixture was stirred at 0 °C for 30 min, before 1-bromo-3-methylbutane (1.29 mL, 10.8 mmol, 3.0 equiv) was added. The mixture was then warmed to rt and stirred for 30 min at which time the reaction mixture was quenched by the slow addition of water and diluted with EtOAc (10 mL). The resulting layers were separated, and the aqueous layer was extracted with EtOAc (3 x 10 mL). The combined organic layers were washed with brine, dried over anhydrous Na_2SO_4 and concentrated under reduced pressure to afford a brown oil. The crude material was transferred to a flame-dried vial, dissolved in DCM (45 mL) and cooled to -78 °C. BBr_3 (7.20 mL, 7.20 mmol, 1 M in DCM, 2.0 equiv) was added dropwise. The mixture was warmed to rt and stirred for 16 h at which time the reaction mixture was quenched by the slow addition of water. The resulting solution was extracted with EtOAc (3 x 10 mL). The combined organic layers were washed with brine, dried over anhydrous Na_2SO_4 and concentrated under reduced pressure to afford a dark brown solid. Purification on silica gel (100% hexanes to 15% EtOAc in hexanes) afforded 650 mg (93% yield over two steps) of **5.59** as a tan crystalline solid. **^{1}H NMR** (400 MHz, $CDCl_3$) δ 6.81 (d, *J* = 8.1 Hz, 1H), 6.34 (d, *J* = 8.1 Hz, 1H), 4.76 (s, 1H), 4.72 (s, 1H), 2.51 (m, 2H), 2.14 (s, 3H), 1.58 (m, 1H), 1.46 (m, 2H), 0.94 (d, *J* = 6.6 Hz, 6H); **^{13}C NMR** (150 MHz, $CDCl_3$) δ 152.5, 152.4, 126.9, 126.7, 120.4, 109.9, 107.1, 39.2, 27.7, 27.6, 22.5, 8.2; **HRMS** (ESI) *m/z* calculated for $C_{12}H_{19}O_2$ $[M+H]^+$: 195.1385, found: 195.1384; **IR** (thin film): 3345, 2955, 1600, 1455, 1188 cm^{-1}; **MP**: 56-58 °C.

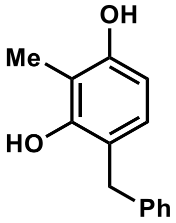

4-benzyl-2-methylbenzene-1,3-diol (5.60)

1-Iodo-2,4-dimethoxy-3-methylbenzene (1.00 g, 3.60 mmol, 1.0 equiv) was added to a flame-dried round-bottom flask and dissolved in THF (25 mL). The mixture was cooled to 0 °C and *n*BuLi (1.73 mL, 4.32 mmol, 1.2 equiv, 2.5 M in hexanes) was slowly added. The mixture was stirred at 0 °C for 30 min, before benzylbromide (1.28 mL, 10.8 mmol, 3.0 equiv) was added. The mixture was then warmed to rt and stirred for 30 min at which time the reaction mixture was quenched by the slow addition of water and diluted with EtOAc (10 mL). The resulting layers were separated, and the aqueous layer was extracted with EtOAc (3 x 10 mL). The combined organic layers were washed with brine, dried over anhydrous Na_2SO_4 and concentrated under reduced pressure to afford a brown oil. The crude material was transferred to a flame-dried vial, dissolved in DCM (45 mL) and cooled to -78 °C. BBr_3 (7.20 mL, 7.20 mmol, 1 M in DCM, 2.0 equiv) was added slowly. The mixture was warmed to rt and stirred for 16 h at which time the reaction mixture was quenched by the slow addition of water. The resulting solution was extracted with EtOAc (3 x 10 mL). The combined organic layers were washed with brine, dried over anhydrous Na_2SO_4 and concentrated under reduced pressure to afford a dark brown solid. Purification on silica gel (100% hexanes to 30% EtOAc in hexanes) afforded 563 mg (73% yield over two steps) of **5.60** as a tan crystalline solid. **^{1}H NMR** (400 MHz, $CDCl_3$) δ 7.25 (m, 5H), 6.85 (d, *J* = 8.2 Hz, 1H), 6.38 (d, *J* = 8.2 Hz, 1H), 3.93 (s, 2H), 2.12 (s, 3H). All values obtained were consistent with literature values.[33]

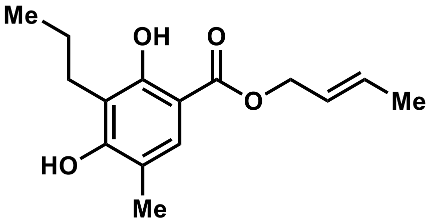

(*E*)-but-2-en-1-yl 2,4-dihydroxy-5-methyl-3-propylbenzoate (3.52)

Adapted from a report by Larrosa and coworkers.[26] In the glove box, NaH (60% dispersion in mineral oil, 1.43 g, 37.4 mmol, 4.0 equiv) was added to a vial containing 4-methyl-2-propylbenzene-1,3-diol (1.29 g, 9.34 mmol, 1.0 equiv) and 2,4,6-trimethylphenol (1.27 g, 9.34 mmol, 1.0 equiv). The resulting mixture was heated at 100 °C for 5 min, cooled to room temperature and ground into powder with a spatula. The vial containing the mixture was taken out of the glove box, purged with CO_2 and equipped with a balloon filled with CO_2 at 185 °C for 2 h. After this time, the reaction mixture was cooled to room temperature, carefully quenched with water (5 mL), acidified to pH 4 with aq. HCl (1 M), and extracted with EtOAc (3 x 20 mL). DCM (2.5 mL) was added to an oven-dried vial equipped with a stir bar containing 2,4-dihydroxy-5-methyl-3-propylbenzoic acid (**3.51,** 92.0 mg, 0.438 mmol, 1.0 equiv). Oxalyl chloride (45.0 μL, 0.525 mmol, 1.2 equiv) was slowly added followed by DMF (1 drop, approx 10 μL). The mixture was stirred for 2 h before crotyl alcohol (75.0 μL, 0.876 mmol, 2.0 equiv) was added dropwise. After 2 h, the reaction was quenched by addition of water (5 mL) and extracted with EtOAc (3 x 20 mL). The organic layers were dried over anhydrous Na_2SO_4, evaporated to dryness and purified by column chromatography (0-15% EtOAc/hexanes) to yield 78 mg (67%) of the crotyl ester as a colorless solid. **^{1}H NMR** (400 MHz, $CDCl_3$) δ 11.07 (s, 1H), 7.50 (s, 1H), 5.86 (dd, *J* = 10.7, 4.9

Hz, 1H), 5.70 (m, 1H), 5.26 (s, 1H), 4.73 (d, *J* = 5.4 Hz, 2H), 2.63 (t, *J* = 6.2 Hz, 3H), 2.17 (s, 3H), 1.76 (d, *J* = 6.5 Hz, 2H), 1.58 (m, 2H), 0.98 (t, *J* = 6.0 Hz, 3H); **^{13}C NMR** (100 MHz, $CDCl_3$) δ 170.3, 159.9, 157.9, 131.8, 128.8, 124.9, 114.9, 114.6, 104.9, 65.5, 24.9, 21.9, 17.8, 15.4, 14.1; **HRMS** (ESI) *m/z* calculated for $C_{15}H_{21}O_4$ $[M+H]^+$: 265.1434, found: 265.1433; **IR** (thin film): 3404, 2952, 1744, 1637, 1196, 1397, 1194 cm^{-1}; **MP**: 93-95 °C.

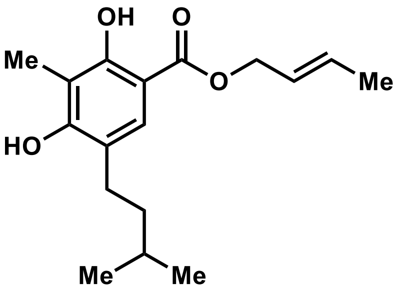

(*E*)-but-2-en-1-yl 2,4-dihydroxy-5-isopentyl-3-methylbenzoate (3.68)

Adapted from a report by Larrosa and coworkers.[26] In the glove box, NaH (60% wt/wt dispersion in mineral oil, 381 mg, 9.92 mmol, 4.0 equiv) was added to a vial containing 4-isopentyl-2-methylbenzene-1,3-diol (482 mg, 2.48 mmol, 1.0 equiv) and 2,4,6-trimethylphenol (338 mg, 2,48 mmol, 1.0 equiv). The resulting mixture was heated at 100 °C for 5 min, cooled to room temperature and ground into powder with a spatula. The vial containing the mixture was taken out of the glove box, purged with CO_2 and equipped with a balloon filled with CO_2 at 185 °C for 2 h. After this time, the reaction mixture was cooled to room temperature, carefully quenched with water (5 mL), acidified to pH 4 with aq. HCl (1 M), and extracted with EtOAc (3 x 20 mL). The organic layers were dried over anhydrous Na_2SO_4, evaporated to dryness and purified by column chromatography (10-50% EtOAc/hexanes) to yield 228 mg (45%) of salicylic acid **5.64** as a tan solid. 5 mL DCM was added to an oven-dried vial equipped with a stir bar containing 2,4-dihydroxy-5-isopentyl-3-methylbenzoic acid (**5.64,** 228 mg, 1.11 mmol, 1.0 equiv). Oxalyl chloride (105 μL, 1.22 mmol, 1.1 equiv) was slowly added followed by DMF (1 drop, approx 10 μL). The mixture was stirred for 2 h before crotyl alcohol (190 μL, 2.22 mmol, 2.0 equiv) was added dropwise. After 2 h, the reaction was quenched by addition of water (5 mL) and extracted with EtOAc (3 x 20 mL). The organic layers were dried over anhydrous Na_2SO_4, evaporated to dryness and purified by column chromatography (0-15% EtOAc/hexanes) to yield 201 mg (62%) of the crotyl ester as a colorless solid. **^{1}H NMR** (600 MHz, $CDCl_3$) δ 11.13 (s, 1H), 7.48 (s, 1H), 5.87 (m, 1H), 5.70 (m, 1H), 5.24 (s, 1H), 4.73 (d, 2H), 2.53 (m, 2H), 2.13 (s, 3H), 1.75 (d, *J* = 6.6, Hz, 3H), 1.60 (m, 1H), 1.55 (m, 2H), 0.94 (d, *J* = 6.5 Hz, 6H); **^{13}C NMR** (150 MHz, $CDCl_3$) δ 170.3, 159.6, 157.7, 131.7, 127.8, 124.9, 119.9, 110.0, 104.9, 65.6, 39.0, 28.0, 27.6, 22.52, 17.8, 7.7; **HRMS** (ESI) *m/z* calculated for $C_{17}H_{25}O_4$ $[M+H]^+$: 293.1747, found: 293.1721; **IR** (thin film): 3464, 3178, 2963, 1639, 1610, 1449, 1187 cm^{-1}; **MP**: 52-53 °C.

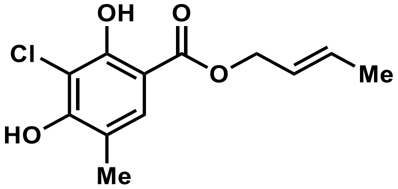

(*E*)-but-2-en-1-yl 3-chloro-2,4-dihydroxy-5-methylbenzoate (3.36)

2 mL MeCN was added to a flame-dried vial containing 2,4-dihydroxy-5-methylbenzoic acid (45.0 mg, 0.268 mmol, 1.0 equiv) and NCS (35.8 mg, 0.268 mmol, 1.0 equiv). The reaction was stirred at 40 °C for 3 h. After this time, the reaction mixture was cooled to room temperature, quenched with water (3 mL), and extracted with EtOAc (3 x 10 mL). The combined organic layers were washed with brine (5 mL), dried over anhydrous Na_2SO_4 and concentrated to dryness. 1.00 mL DCM was added to an oven-dried vial equipped with a stir bar containing 3-chloro-2,4-dihydroxy-5-methylbenzoic acid (**3.34,** 65.0 mg, 0.253 mmol, 1.0 equiv). Oxalyl chloride (24 μL, 0.28 mmol, 1.1 equiv) was slowly added followed by DMF (1 drop, approx 10 μL). The mixture was stirred

for 2 h before crotyl alcohol (43 μL, 0.51 mmol, 2.0 equiv) was added dropwise. After 2 h, the reaction was quenched by addition of water (5 mL) and extracted with EtOAc (3 x 10 mL). The organic layers were dried over anhydrous Na_2SO_4, evaporated to dryness and purified by column chromatography (0- 10% EtOAc/hexanes) to yield 30 mg (46%) of the crotyl ester as a colorless solid. **^{1}H NMR** (400 MHz, $CDCl_3$) δ 11.41 (s, 1H), 7.55 (s, 1H), 6.14 (s, 1H), 5.88 (dq, *J* = 13.4, 6.6 Hz, 1H), 5.68 (dt, *J* = 14.7, 6.6 Hz, 1H), 4.74 (d, *J* = 6.5 Hz, 2H), 2.20 (s, 3H), 1.76 (d, *J* = 6.6 Hz, 3H); **^{13}C NMR** (150 MHz, $CDCl_3$) δ 169.6, 156.7, 155.4, 132.4, 129.4, 124.4, 116.3, 107.1, 105.6, 66.1, 17.8, 15.5; **HRMS** (ESI) *m/z* calculated for $C_{12}H_{14}ClO_4$ $[M+H]^+$: 257.0575, found: 257.0575; **IR** (thin film): 3464, 3176, 2949, 2930, 1641, 1611, 1188 cm^{-1}.

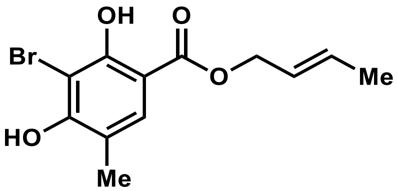

(*E*)-but-2-en-1-yl 3-bromo-2,4-dihydroxy-5-methylbenzoate (3.37)

2 mL MeCN was added to a flame-dried vial containing 2,4-dihydroxy-5-methylbenzoic acid (45.0 mg, 0.268 mmol, 1.0 equiv) and NBS (35.8 mg, 0.268 mmol, 1.0 equiv). The reaction was stirred at 40 °C for 3 h. After this time, the reaction mixture was cooled to room temperature, quenched with water (3 mL) then extracted with EtOAc (3 x 10 mL). The combined organic layers were washed with brine (5 mL), dried over anhydrous Na_2SO_4 and concentrated to dryness. 0.50 mL DCM was added to an oven-dried vial equipped with a stir bar containing 3-bromo-2,4-dihydroxy-5-methylbenzoic acid (**3.35,** 31.3 mg, 0.155 mmol, 1.0 equiv). Oxalyl chloride (15 μL, 0.17 mmol, 1.1 equiv) was slowly added followed by DMF (1 drop, approx 10 μL). The mixture was stirred for 2 h before crotyl alcohol (26 μL, 0.31 mmol, 2.0 equiv) was added dropwise. After 2 h, the reaction was quenched by addition of water (5 mL) and extracted with EtOAc (3 x 10 mL). The

organic layers were dried over anhydrous Na_2SO_4, evaporated to dryness and purified by column chromatography (0-15% EtOAc/hexanes) to yield 9.9 mg (21%) of the crotyl ester as a colorless oil. **^{1}H NMR** (400 MHz, $CDCl_3$) δ 11.56 (s, 1H), 7.60 (s, 1H), 6.14 (s, 1H), 5.90 (m, 1H), 5.65 (m, 1H), 4.76 (d, *J* = 6.6 2H), 2.23 (s, 3H), 1.77 (d, *J* = 6.5 Hz, 3H); **^{13}C NMR** (150 MHz, $CDCl_3$) δ 169.6, 157.8, 156.4, 132.4, 130.3, 124.4, 116.8, 105.8, 98.5, 66.1, 17.8, 15.8; **HRMS** (ESI) *m/z* calculated for $C_{12}H_{14}BrO_4$ $[M+H]^+$: 301.0070, found: 301.0072; **IR** (thin film): 3464, 2957, 2923, 2854, 1739, 1663, 1455 cm^{-1}.

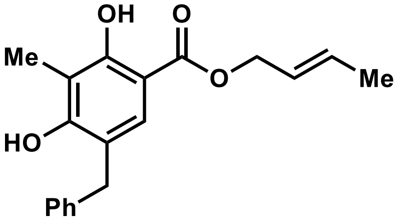

(*E*)-but-2-en-1-yl 5-benzyl-2,4-dihydroxy-3-methylbenzoate (3.69)

Adapted from a report by Larrosa and coworkers.[26] In the glove box, NaH (60% wt/wt dispersion in mineral oil, 1.43 g, 37.4 mmol, 4.0 equiv) was added to a vial containing 4-benzyl-2-methylbenzene-1,3-diol (1.29 g, 9.34 mmol, 1.0 equiv) and 2,4,6-trimethylphenol (1.27 g, 9.34 mmol, 1.0 equiv). The resulting mixture was heated at 100 °C for 5 min, cooled to room temperature and ground into powder with a spatula. The vial containing the mixture was taken out of the glove box, purged with CO_2 and equipped with a balloon filled with CO_2 at 185 °C for 2 h. After this time, the reaction mixture was cooled to room temperature, carefully quenched with water (5 mL), acidified to pH 4 with aq. HCl (1 M), and extracted with EtOAc (3 x 20 mL). The organic layers were dried over anhydrous $MgSO_4$, evaporated to dryness to afford a tan crystalline solid. 0.50 mL DCM was added to an oven-dried vial equipped with a stir bar containing 4-benzyl-2-methylbenzene-1,3-diol (**5.66,** 50.0 mg, 0.270 mmol, 1.0 equiv). Oxalyl chloride (35 μL, 0.412 mmol, 1.5 equiv) was slowly added followed by DMF (1 drop, approx 10 μL). The mixture was stirred for 2 h before crotyl alcohol (29 μL, 0.270 mmol, 1.0 equiv) was added dropwise. After 2 h, the reaction was quenched by addition of water (5 mL) and extracted with EtOAc (3 x 20 mL). The organic layers were dried over anhydrous Na_2SO_4, evaporated to dryness, and purified by column chromatography (0-15% EtOAc/hexanes) to yield 23 mg (34%) of the crotyl ester as a colorless oil. **^{1}H NMR** (400 MHz, $CDCl_3$) δ 11.18 (s, 1H), 7.58 (s, 1H), 7.20 (m, 5H), 5.86 (m, 1H), 5.70 (m, 1H), 5.12 (d, *J* = 1.2 Hz, 2H), 4.74 (m, 2H), 3.94 (s, 1H), 2.11 (s, 3H), 1.76 (d, *J* = 6.2 Hz, 2H); **^{13}C NMR** (150 MHz, $CDCl_3$) 170.2, 160.4, 158.1, 139.4, 131.8, 129.1, 128.8, 128.4, 126.6, 124.8, 117.8, 111.0, 105.1, 65.6, 36.4, 17.8, 7.8; **HRMS** (ESI) *m/z* calculated for $C_{19}H_{21}O_4$ $[M+H]^+$: 313.1434, found: 313.1438; **IR** (thin film): 3509, 3028, 2920, 1738, 1656, 1616, 1183 cm^{-1}.

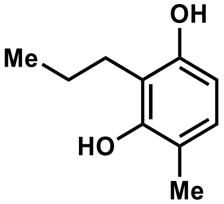

4-methyl-2-propylbenzene-1,3-diol (3.52)

2,4-dimethoxy-1-methylbenzene (874 mg, 5.74 mmol, 1.0 equiv) was added to a flame-dried round-bottom flask and dissolved in THF (12 mL). The mixture was cooled to 0 °C and *n*BuLi (3.44 mL, 8.61 mmol, 1.5 equiv, 2.5 M in hexanes) was slowly added. The mixture was stirred at 0 °C for 30 min, before 1-bromopropane (1.60 mL, 17.2 mmol, 3.0 equiv) was added. The mixture was then warmed to rt and stirred for 30 min at which time the reaction mixture was quenched by the slow addition of water (10 mL) and diluted with EtOAc (10 mL). The resulting layers were separated, and the aqueous layer was extracted with EtOAc (3 x 20 mL). The combined organic layers were washed with brine, dried over anhydrous Na_2SO_4 and concentrated under reduced pressure to afford a brown oil. The crude material was transferred to a flame-dried vial, dissolved in DCM (70 mL) and cooled to -78 °C. BBr_3 (11.5 mL, 11.5 mmol, 1 M in DCM, 2.0 equiv) was added slowly. The mixture was then warmed to rt and stirred for 16 h at which time the reaction mixture was quenched by the slow addition of water. The resulting solution was extracted with EtOAc (3 x 100 mL). The combined organic layers were washed with brine, dried over anhydrous Na_2SO_4 and concentrated under reduced pressure to afford a dark brown solid. Purification on silica gel (100% hexanes to 30% EtOAc in hexanes) afforded 897 mg (94% yield over two steps) of **3.52** as a tan crystalline solid. **^{1}H NMR** (400 MHz, $CDCl_3$) δ 6.81 (d, *J* = 8.0 Hz, 1H), 6.32 (d, *J* = 8.0 Hz, 1H), 4.67 (s, 1H), 4.63 (s, 1H), 2.62 (t, *J* = 8.4, 2H), 2.17 (s, 3H), 1.59 (h, *J* = 7.4 Hz, 2H), 0.99 (t, *J* = 7.4 Hz, 3H); **^{13}C NMR** (150 MHz, $CDCl_3$) δ 152.7, 152.6, 127.8, 115.1, 114.7, 107.1, 25.4, 22.3, 15.5, 14.2; **HRMS** (ESI) *m/z* calculated for $C_{10}H_{15}O_2$ $[M+H]^+$: 167.1067, found: 167.1066; **IR** (thin film): 3345, 2955, 1600, 1455, 1188 cm^{-1}; **MP**: 95-97 °C.

General procedure for lead tetraacetate (LTA)-mediated oxidative dearomatization: Adapted from a protocol developed by Nicolau.[32] Substrate (50 mg, 1 equiv) was dissolved in AcOH and DCM (5:1, 0.04 M). LTA (1.2 equiv) was added and the reaction was allowed to stir at rt for 1 h. The reaction was quenched by addition of water (10 mL) and the mixture was extracted with EtOAc (3 x 15 mL). The combined organic layers were washed with water (1 x 20 mL), brine (1 x 20 mL), dried over sodium sulfate, and concentrated under reduced pressure to afford a yellow oil. Purification on silica gel afforded the O-acylated *o*-quinol product. Full characterization given for enzymatically generated material.

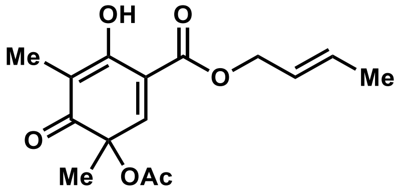

(*E*)-but-2-en-1-yl 3-acetoxy-6-hydroxy-3,5-dimethyl-4-oxocyclohexa-1,5-diene-1-carboxylate (±3.39)

The title compound was prepared according to the general procedure for LTA-mediated oxidative dearomatization. Purification on silica gel (20- 40% EtOAc in hexanes) afforded 10 mg (16% yield) of the *o*-quinol as a yellow oil. ^{1}**H NMR** (400 MHz, CDCl$_3$) δ 10.82 (s, 1H), 7.38 (s, 1H), 5.90 (dd, *J* = 15.0, 7.0 Hz, 1H), 5.66 (m, 1H), 4.71 (d, *J* = 6.8 Hz, 2H), 2.12 (s, 3H), 1.87 (s, 3H), 1.77 (d, *J* = 6.4 Hz, 3H), 1.46 (s, 3H).

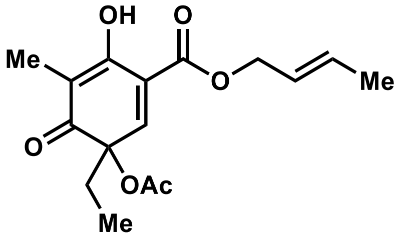

(*E*)-but-2-en-1-yl 3-acetoxy-3-ethyl-6-hydroxy-5-methyl-4-oxocyclohexa-1,5-diene-1-carboxylate (±3.81)

The title compound was prepared according to the general procedure for LTA-mediated oxidative dearomatization. Purification on silica gel (20-40% EtOAc in hexanes) afforded 4.9 mg (8.0% yield) of the *o*-quinol as a yellow oil. ^{1}**H NMR** (400 MHz, CDCl$_3$) δ 10.78 (s, 1H), 7.37 (s, 1H), 5.88 (dd, *J* = 14.9, 6.9 Hz, 1H), 5.63 (m, 1H), 4.71 (d, *J* = 6.9 Hz, 2H), 2.12 (s, 3H), 1.85 (s, 3H), 1.84 (m, 2H), 1.76 (d, *J* = 6.7 Hz, 3H), 0.91 (t, *J* = 7.5 Hz, 3H).

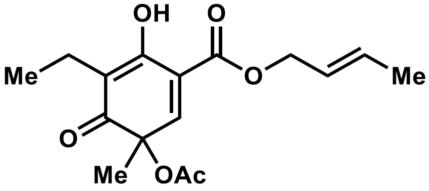

(*E*)-but-2-en-1-yl 3-acetoxy-5-ethyl-6-hydroxy-3-methyl-4-oxocyclohexa-1,5-diene-1-carboxylate (±3.82)

The title compound was prepared according to the general procedure for LTA-mediated oxidative dearomatization. Purification on silica gel (20-40% EtOAc in hexanes) afforded 1.8 mg (3.0% yield) of the *o*-quinol as a yellow oil. **^{1}H NMR** (400 MHz, $CDCl_3$) δ 10.77 (s, 1H), 7.37 (s, 1H), 5.89 (m, 1H), 5.64 (m, 1H), 4.71 (d, *J* = 3.5 Hz, 2H), 2.41 (q, *J* = 6.7 Hz, 2H), 2.12 (s, 3H), 1.77 (d, *J* = 6.5 Hz, 3H), 1.45 (s, 3H), 1.00 (t, *J* = 7.4 Hz, 3H).

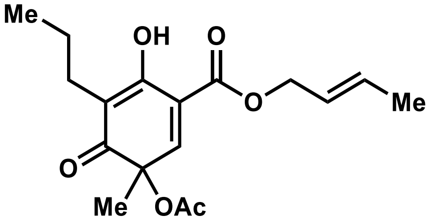

(*E*)-but-2-en-1-yl 3-acetoxy-6-hydroxy-3-methyl-4-oxo-5-propylcyclohexa-1,5-diene-1-carboxylate (±3.83)

The title compound was prepared according to the general procedure for LTA-mediated oxidative dearomatization. Purification on silica gel (20-40% EtOAc in hexanes) afforded 10 mg (16% yield) of the *o*-quinol as a yellow oil. **^{1}H NMR** (400 MHz, $CDCl_3$) δ 10.75 (s, 1H), 7.36 (s, 1H), 5.88 (m, 1H), 5.60 (m, 1H), 4.70 (t, *J* = 7.4 Hz, 2H), 2.36 (m, 2H), 2.10 (s, 3H), 1.75 (d, *J* = 6.7 Hz, 3H), 1.43 (m, 5H), 0.88 (t, *J* = 7.1 Hz, 3H).

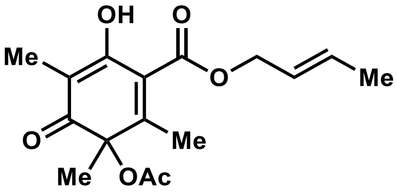

(*E*)-but-2-en-1-yl 3-acetoxy-6-hydroxy-2,3,5-trimethyl-4-oxocyclohexa-1,5-diene-1-carboxylate (±3.80)

The title compound was prepared according to the general procedure for LTA-mediated oxidative dearomatization. Purification on silica gel (20-40% EtOAc in hexanes) afforded 3.3 mg (6% yield) of the *o*-quinol as a yellow oil. **^{1}H NMR** (400 MHz, $CDCl_3$) δ 10.96 (s, 1H), 5.87 (m, 1H), 5.64 (dt, *J* = 15.1, 7.0 Hz, 1H), 4.74 (t, *J* = 6.7 Hz, 2H), 2.20 (s, 3H), 2.14 (s, 3H), 1.85 (s, 3H), 1.75 (d, *J* = 6.5 Hz, 3H), 1.44 (s, 3H).

Chapter 3.6.2: Biocatalytic Reactions

Stock solutions: Stock solutions of each substrate (50 mM) were prepared by dissolving the substrate in DMSO (analytical grade). Stock solutions of $NADP^+$ (100 mM) and glucose-6-phosphate (G6P, 500mM) were stored at –20 °C. Aliquots of SorbC (62 μM) and glucose-6-phosphate dehydrogenase (G6PDH, 100 U/mL) were stored at –80 °C. **Analytical-scale reactions**: Each reaction contained 25 μL 100 mM potassium phosphate buffer, pH 8.0, 2.5 mM substrate (2.5 μL of a 50 mM stock solution in DMSO), 2.5 μM SobC, 5 mM G6P (0.5 μL, 500 mM), 1 mM $NADP^+$ (0.5 μL, 100 mM), 1 U/mL G6P-DH (0.5 μL, 100 U/mL), and Milli-Q water to a final volume of 50 μL. The reaction was carried out at 30 °C for 1 h and quenched by addition of 75 μL acetonitrile with 25 mM pentamethylbenzene as an internal standard. Precipitated biomolecules were pelleted by centrifugation (16,000 x *g*, 12 min). The supernatant was analyzed by UPLC-DAD and conversion obtained by comparison to calibration curves of each substrate. **Determination of total turnover number (TTN):** Total turnover number was determined by analyzing (# of moles of starting material consumed)/(# of moles of enzyme) under the following conditions: 2.5 µM SorbC, 2.5 mM substrate, 1 mM NADP$^+$, 0.05 U G6PDH, and 5 mM G6P for NADPH regeneration in 50 µL of reaction buffer (50 mM potassium phosphate, pH 8.0). The reaction was carried out at 30 °C for 1 h and quenched by addition of 75 µL acetonitrile with 2.5 mM pentamethylbenzene as an internal standard. Precipitated biomolecules were pelleted by centrifugation (16,000 x g, 12 min). The subsequent liquid chromatography PDA spectrometry (UPLC) analysis was performed on a Waters Aquity H-Class UPLC-PDA using a Phenomenex Kinetex 1.7 µm C18, 2.1x150 mm column under the following conditions: Method A: mobile phase (A = deionized water + 0.1% formic acid, B = acetonitrile + 0.1% formic acid), 5% to 100% B over 1.5 min, 100% B for 1.0 min; flow rate, 0.5 mL/min; Method B: mobile phase (A = deionized water + 0.1% formic acid, B = acetonitrile + 0.1% formic acid), 5% to 100% B over 2 min, 100% B for 1 min; flow rate, 0.5 mL/min. Based on calibration curves of the starting materials, the percent conversion of the substrate to dearomatized product was calculated with $AUC_{substrate}/AUC_{internal\ standard}$ at 270 nm. All reactions were performed and analyzed in triplicate.

General procedure for in vitro milligram-scale reactions: Preparative-scale enzymatic reactions were conducted on 10 mg of each substrate under the following conditions: 2.5 µM SorbC, 2.5 mM substrate, 1 mM NADP$^+$, 1 U/mL G6PDH, and 5 mM G6P for NADPH generation in reaction buffer (50 mM potassium phosphate buffer, pH 8.0). The reaction mixture was added to a crystallizing dish and incubated at 30 °C for 2 h. The increased surface area afforded by the crystalizing dish as reaction vessel allowed for higher conversions with some substrates due to increased oxygen concentration. After 2 h, a 50 µL aliquot was removed and processed in an identical manner to the analytical-scale reactions described above to determine substrate conversion. The remaining reaction mixture was diluted with acetonitrile (2 x total reaction volume). Precipitated biomolecules were pelleted by centrifugation (4,000 x *g*, 12 min). The reaction mixture was cooled to 0 °C and pyridine (14.0 µL, 0.173 mmol) was added followed by Ac_2O (10.4 µL, 0.110 mmol). The resulting mixture was stirred at rt for 2 h. The reaction was then acidified to pH 2 and the mixture was extracted with EtOAc (3 x 70 mL). The combined organic layers were washed with brine (1 x 50 mL), dried over sodium sulfate and concentrated under reduced pressure. Purification on silica gel (30% hexanes to 50% EtOAc in hexanes) afforded the acylated *o*-quinol products.

Steady-state kinetics of SorbC with 3.13 and 3.26. To determine the time at which initial rates could be recorded, duplicate 50 µL reactions with 10 µM **3.13** or **3.27** were performed and analyzed compared to an internal standard (300 µM) by UPLC. The resulting time course demonstrated that 1 min is the optimal time to capture the initial reaction rates for a variety of concentrations of **3.13** or **3.26.**

To determine the steady-state kinetic parameters of the SorbC with sorbicillin (**3.13**) reactions were conducted on 50 µL scale with substrate ranging 10 µM–200 µM in duplicate with 12.5 nM SorbC and 50 mM KP_i pH 8.0 buffer in a 96-well plate. Reactions were initiated by addition of 500 µM NADH (10 µL distributed by multichannel pipette). Reactions were quenched after 30 s by addition of 100 µL acetonitrile. 96-well plates were centrifuged at 2000 x *g* for 2 min, then 100 µL of the centrifuged mixture was added to 100 µL of a dilution mix containing 450 µM in acetonitrile in a clean 96-well 0.22 µm filter plate. The plate was centrifuged over a clean 96-well plate at 2000 x *g* for 2 min. 2 µL each sample was injected on the TOF LC-MS. The resulting Michaelis-Menten curves for each substrate and standard curves used to quantify substrate are shown in Figure 3.10.

Steady-state kinetics of SorbC with sorbicillin (3.13) and crotyl ester 3.26. SorbC was prepared to a final concentration of 120 nM. To determine the steady-state kinetic parameters of SorbC with sorbicillin (**3.13**), reactions were conducted on 50 µL scale, in duplicate, under the following conditions: 10–250 µM substrate, 120 nM SorbC, 50 mM KP_i pH 8.0 buffer in a 96-well plate. For crotyl ester **3.26**, the substrate range was 10 µM–150 µM with all other reaction components the same as the sorbcillin (**3.13**) reactions. Reactions were initiated by the addition of 500 µM NADH (10 µL total volume added by multichannel pipette). Reactions were quenched after 1 min by addition of 150 µL acetonitrile containing 300 µM trimethoxy benzene as internal standard. 96-well plates were centrifuged at 2000 x *g* for 2 min, then 100 µL of the centrifuged mixture was added to a 96-well 0.22 µm filter plate. The plate was centrifuged over a 96-well plate at 2000 x *g* for 2 min. Product standards were prepared in the same manner. Samples were analyzed by TOF LC-MS. The resulting Michaelis-Menten curves for each substrate are shown in Figures 10 and 11.

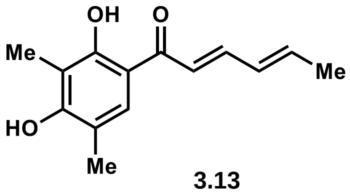

3.13

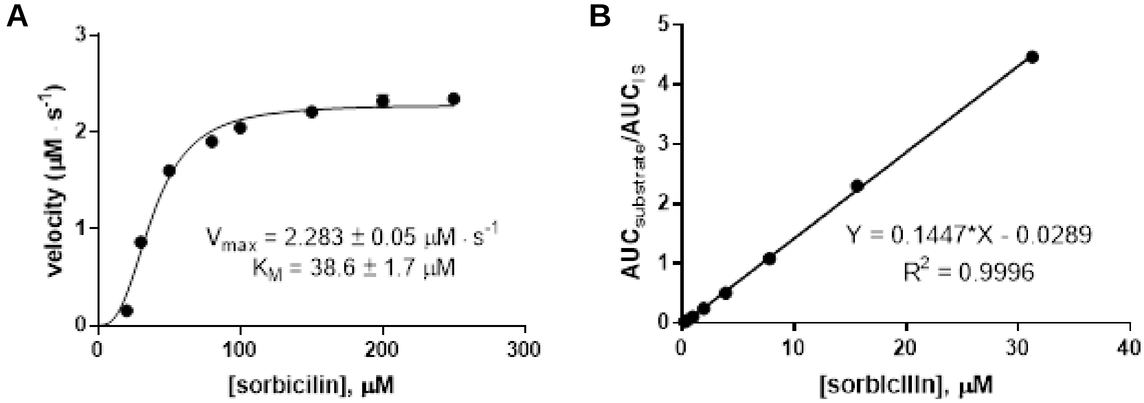

Figure 3.10: A) Michaelis-Menten plot of SorbC reactions with native substrate sorbicillin (**3.13**). B) Standard curve of sorbicillin (**3.13**).

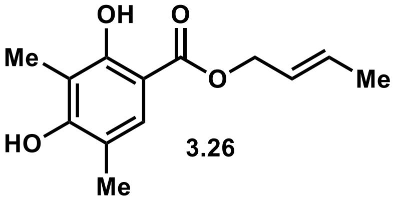

3.26

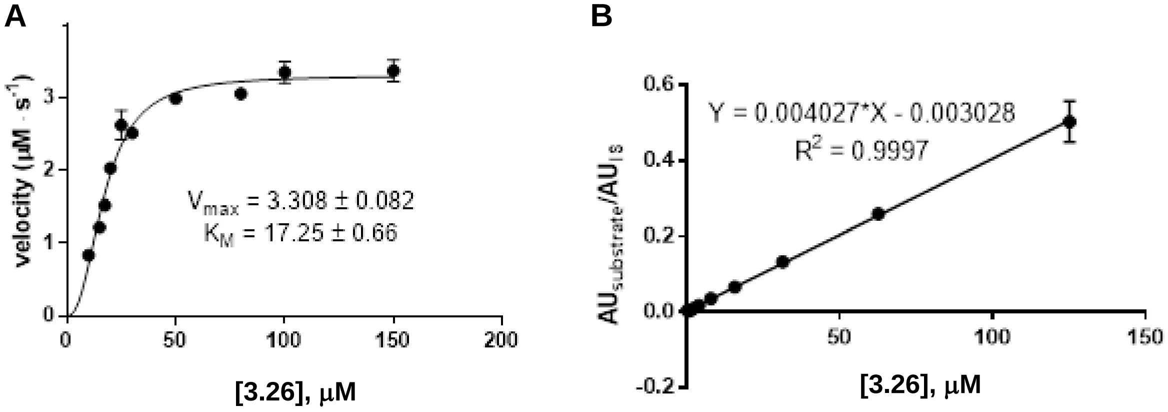

Figure 3.11: A) Michaelis-Menten plots of SorbC reactions with substrate **3.26**. B) Standard curve substrate **3.26**.

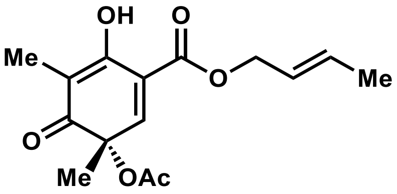

(*E*)-but-2-en-1-yl (*S*)-3-acetoxy-6-hydroxy-3,5-dimethyl-4-oxocyclohexa-1,5-diene-1-carboxylate (3.79)

The title compound was prepared according to the general procedure for milligram-scale in vitro enzymatic oxidative dearomatization. Purification on silica gel (20-40% EtOAc in hexanes) afforded 1.0 mg (8.0% yield) of the *o*-quinol as a yellow oil. **^{1}H NMR** (400 MHz, $CDCl_3$) δ 10.82 (s, 1H), 7.38 (s, 1H), 5.90 (dd, *J* = 15.0, 7.0 Hz, 1H), 5.66 (m, 1H), 4.71 (d, *J* = 6.8 Hz, 2H), 2.12 (s, 3H), 1.87 (s, 3H), 1.77 (d, *J* = 6.4 Hz, 3H), 1.46 (s, 3H); **^{13}C NMR** (150 MHz, $CDCl_3$) δ 195.4, 169.8, 167.4, 160.3, 151.9, 133.9, 123.5, 118.7, 111.7, 78.0, 67.3, 23.9, 20.4, 17.8, 7.3; **HRMS**

(ESI) *m/z* calculated for $C_{15}H_{19}O_6$ $[M+H]^+$: 295.1176, found: 295.1180; **IR** (thin film): 3426, 2923, 1736, 1699, 1659, 1396, 1194 cm^{-1}; $[\alpha]_D^{25}$ +65 (*c* 0.12, MeCN).

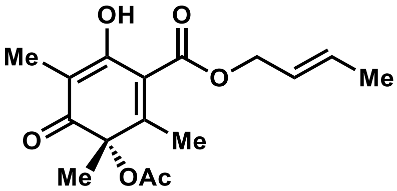

(*E*)-but-2-en-1-yl (*S*)-3-acetoxy-6-hydroxy-2,3,5-trimethyl-4-oxocyclohexa-1,5-diene-1-carboxylate (3.80)

The title compound was prepared according to the general procedure for milligram-scale in vitro enzymatic oxidative dearomatization. Purification on silica gel (20-40% EtOAc in hexanes) afforded 8.0 mg (59% yield) of the *o*-quinol as a yellow oil. **^{1}H NMR** (400 MHz, $CDCl_3$) δ 10.96 (s, 1H), 5.87 (m, 1H), 5.64 (dt, *J* = 15.1, 7.0 Hz, 1H), 4.74 (t, *J* = 6.7 Hz, 2H), 2.20 (s, 3H), 2.14 (s, 3H), 1.85 (s, 3H), 1.75 (d, *J* = 6.5 Hz, 3H), 1.44 (s, 3H); **^{13}C NMR** (150 MHz, $CDCl_3$) δ 195.2, 169.7, 169.1, 164.4, 161.4, 133.9, 123.5, 116.3, 109.7, 81.9, 67.4, 24.9, 20.5, 17.8, 17.1, 7.4; **HRMS** (ESI) *m/z* calculated for $C_{16}H_{21}O_6$ $[M+H]^+$: 309.1333, found: 309.1332; **IR** (thin film): 3165, 2963, 1737, 1698, 1654, 1396, 1235 cm^{-1}; $[\alpha]_D^{25}$ +27 (*c* 0.06, MeCN).

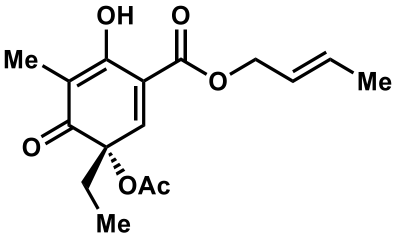

(*E*)-but-2-en-1-yl 3-acetoxy-3-ethyl-6-hydroxy-5-methyl-4-oxocyclohexa-1,5-diene-1-carboxylate (3.81)

The title compound was prepared according to the general procedure for milligram-scale in vitro enzymatic oxidative dearomatization. Purification on silica gel (20-40% EtOAc in hexanes) afforded 1.0 mg (8.0% yield) of the *o*-quinol as a yellow oil. **^{1}H NMR** (400 MHz, CDCl$_3$) δ 10.78 (s, 1H), 7.37 (s, 1H), 5.88 (dd, *J* = 14.9, 6.9 Hz, 1H), 5.63 (m, 1H), 4.71 (d, *J* = 6.9 Hz, 2H), 2.12 (s, 3H), 1.85 (s, 3H), 1.84 (m, 2H), 1.76 (d, *J* = 6.7 Hz, 3H), 0.91 (t, *J* = 7.5 Hz, 3H); **^{13}C NMR** (150 MHz, CDCl$_3$) δ 195.4, 169.9, 167.3, 160.3, 151.3, 133.8, 123.5, 119.6, 112.4, 80.9, 67.3, 32.0, 20.5, 17.8, 7.5, 7.1; **HRMS** (ESI) *m/z* calculated for $C_{16}H_{21}O_6$ $[M+H]^+$: 309.1333, found: 309.1335; **IR** (thin film): 3165, 2963, 1736, 1659, 1654, 1396, 1233 cm^{-1}; $[\alpha]_D^{25}$ +57 (*c* 0.08, MeCN).

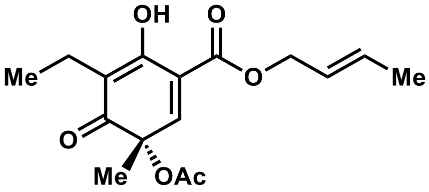

(*E*)-but-2-en-1-yl 3-acetoxy-5-ethyl-6-hydroxy-3-methyl-4-oxocyclohexa-1,5-diene-1-carboxylate (3.82)

The title compound was prepared according to the general procedure for milligram-scale in vitro enzymatic oxidative dearomatization. Purification on silica gel (20-40% EtOAc in hexanes) afforded 3.8 mg (28% yield) of the *o*-quinol as a yellow oil. **^{1}H NMR** (400 MHz, CDCl$_3$) δ 10.77

(s, 1H), 7.37 (s, 1H), 5.89 (m, 1H), 5.64 (m, 1H), 4.71 (d, *J* = 3.5 Hz, 2H), 2.41 (q, *J* = 6.7 Hz, 2H), 2.12 (s, 3H), 1.77 (d, *J* = 6.5 Hz, 3H), 1.45 (s, 3H), 1.00 (t, *J* = 7.4 Hz, 3H); **^{13}C NMR** (150 MHz, $CDCl_3$) δ 194.8, 169.8, 167.5, 159.9, 152.0, 133.8, 123.5, 118.8, 117.7, 78.0, 67.3, 23.8, 20.5, 17.8, 15.5, 12.6; **HRMS** (ESI) *m/z* calculated for $C_{16}H_{21}O_6$ $[M+H]^+$: 309.1333, found: 309.1337; **IR** (thin film): 3162, 2928, 1738, 1697, 1652, 1369, 1235 cm^{-1}; $[\alpha]_D^{25}$ +41 (*c* 0.06, MeCN).

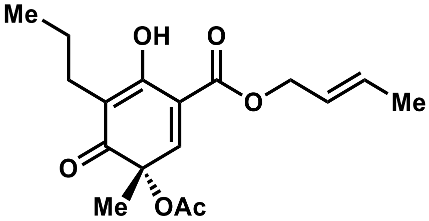

(*E*)-but-2-en-1-yl (S)-3-acetoxy-6-hydroxy-3-methyl-4-oxo-5-propylcyclohexa-1,5-diene-1-carboxylate (3.83)

The title compound was prepared according to the general procedure for milligram-scale in vitro enzymatic oxidative dearomatization. Purification on silica gel (20-40% EtOAc in hexanes) afforded 4.1 mg (35% yield) of the *o*-quinol as a yellow oil. **^{1}H NMR** (400 MHz, $CDCl_3$) δ 10.75 (s, 1H), 7.36 (s, 1H), 5.88 (m, 1H), 5.60 (m, 1H), 4.70 (t, *J* = 7.4 Hz, 2H), 2.36 (m, 2H), 2.10 (s, 3H), 1.75 (d, *J* = 6.7 Hz, 3H), 1.43 (m, 5H), 0.88 (t, *J* = 7.1 Hz, 3H); **^{13}C NMR** (150 MHz, $CDCl_3$) δ 195.0, 169.8, 167.5, 160.2, 152.0, 133.8, 123.5, 118.7, 116.2, 78.0, 67.3, 24.0, 23.9, 21.3, 20.4, 17.8, 13.9; **HRMS** (ESI) *m/z* calculated for $C_{17}H_{23}O_6$ $[M+H]^+$: 323.1489, found: 323.1494; **IR** (thin film): 3167, 2960, 2925, 1738, 1697, 1654, 1369, 1236 cm^{-1}; $[\alpha]_D^{25}$ +45 (*c* 0.06, MeCN).

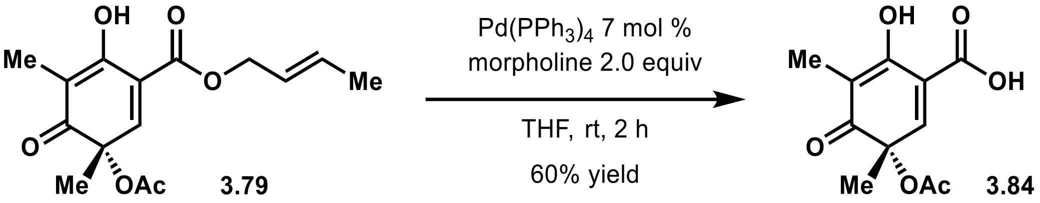

(*S*)-3-acetoxy-6-hydroxy-3,5-dimethyl-4-oxocyclohexa-1,5-diene-1-carboxylic acid (3.84)

o-quinol **3.79** (37.3 mg, 0.127 mmol, 1.0 equiv) and Pd(PPh$_3$)$_4$ (10.3 mg, 0.07 equiv, 0.0088 mmol) were added to a flame-dried vial equipped with a stir bar and dissolved in anhydrous THF (2.5 mL). Morpholine (33.0 μL, 0.381 mmol, 3.0 equiv) is then added and the reaction is stirred at rt. After 2 h, the reaction was quenched by addition of 1 M HCl, aq (1 mL) and extracted with EtOAc (3 x 5 mL). The organic layers were dried over anhydrous Na$_2$SO$_4$, evaporated to dryness and purified by column chromatography (30-100% EtOAc/hexanes) to yield 18 mg (60%) of the acid as a colorless solid. **^{1}H NMR** (600 MHz, CD$_3$OD) δ 7.55 (s, 1H), 2.07 (s, 3H), 1.78 (s, 3H), 1.44 (s, 3H); **^{13}C NMR** (300 MHz, CD$_3$OD) 169.3, 169.3,152.5, 119.3, 110.0, 110.0, 77.4, 56.03, 22.9, 18.8, 5.77; **HRMS** (ESI) *m/z* calculated for C$_{11}$H$_{13}$O$_6$ [M+H]$^+$: 241.0707, found: 241.0706; **IR** (thin film): 3263, 2945, 1710, 1650, 1614, 1347 cm^{-1}; **MP**: 87 – 90 °C.

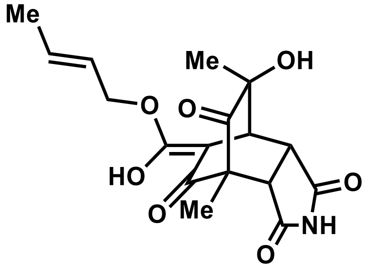

(*E*)-but-2-en-1-yl (,4*S*,5*S*,7*R*,9*S*)-9-hydroxy-7,9-dimethyl-1,3,6,8-tetraoxooctahydro-1*H*-4,7-ethanoisoindole-5-carboxylate (3.87)

The title compound was prepared according to the general procedure for milligram-scale in vitro enzymatic oxidative dearomatization, followed by addition of maleimde (25 mM in DMSO, 5 equiv). Purification on silica gel (20-100% EtOAc in hexanes) afforded 10.3 mg (23% yield) of the cycloadduct as a yellow oil. **^{1}H NMR** (600 MHz, $CDCl_3$) δ 11.60 (s, 1H), 8.20 (s, 1H), 5.83 (dq, *J* = 13.4, 6.5 Hz, 1H), 5.59 (dd, *J* = 14.7, 7.4 Hz, 1H), 4.67 (dd, *J* = 12.6, 6.4 Hz, 1H), 4.60 (m, 1H), 3.87 (d, *J* = 3.3 Hz, 1H), 3.76 (dd, *J* = 8.5, 3.2 Hz, 1H), 2.94 (d, *J* = 8.4 Hz, 1H), 1.74 (d, *J* = 6.6 Hz, 3H), 1.58 (s, 3H), 1.31 (s, 3H); **^{13}C NMR** (300 MHz, $CDCl_3$) δ 207.8, 176.6, 173.7, 168.6, 168.5, 132.0, 124.2, 100.0, 71.9, 65.9, 54.2, 47.0, 42.1, 41.3, 24.5, 17.8, 9.5. **HRMS** (ESI) *m/z* calculated for $[M+Na]^+$ $C_{17}H_{19}NO_7Na$ $[M+Na]^+$: 372.1054, found: 372.1048; **IR** (thin film): 2928, 1737, 1705, 1622, 1412, 1378 cm^{-1}; $[\alpha]_D^{25}$ +62 (*c* 0.1, MeCN)

Chapter 3.6.3: Substrate Calibration Curves

Entry 3

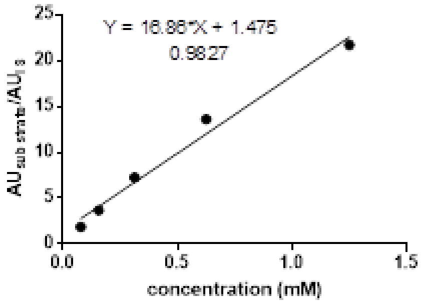

3.25

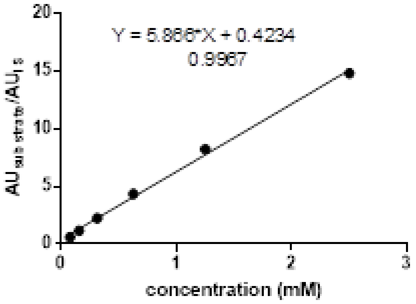

3.26

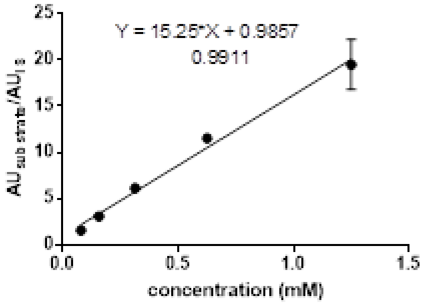

3.27

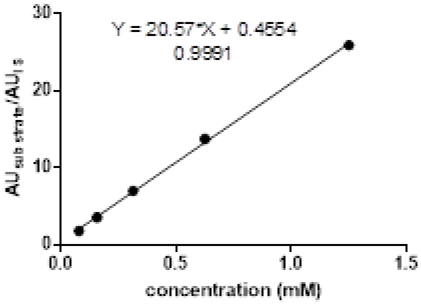

3.29

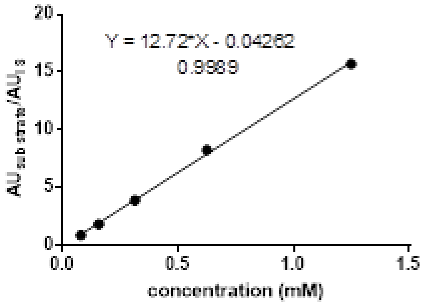

3.27

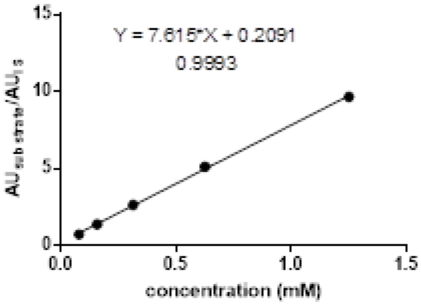

3.47

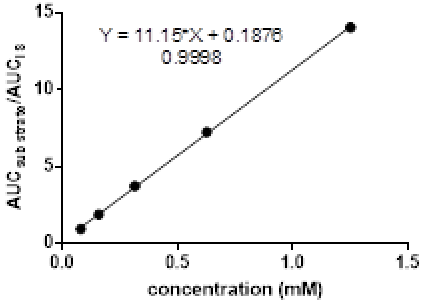

3.72

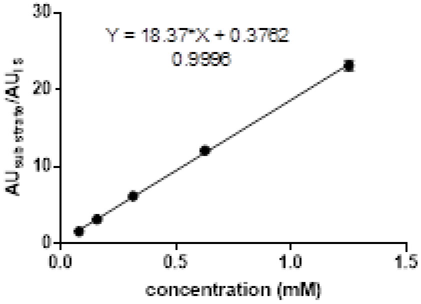

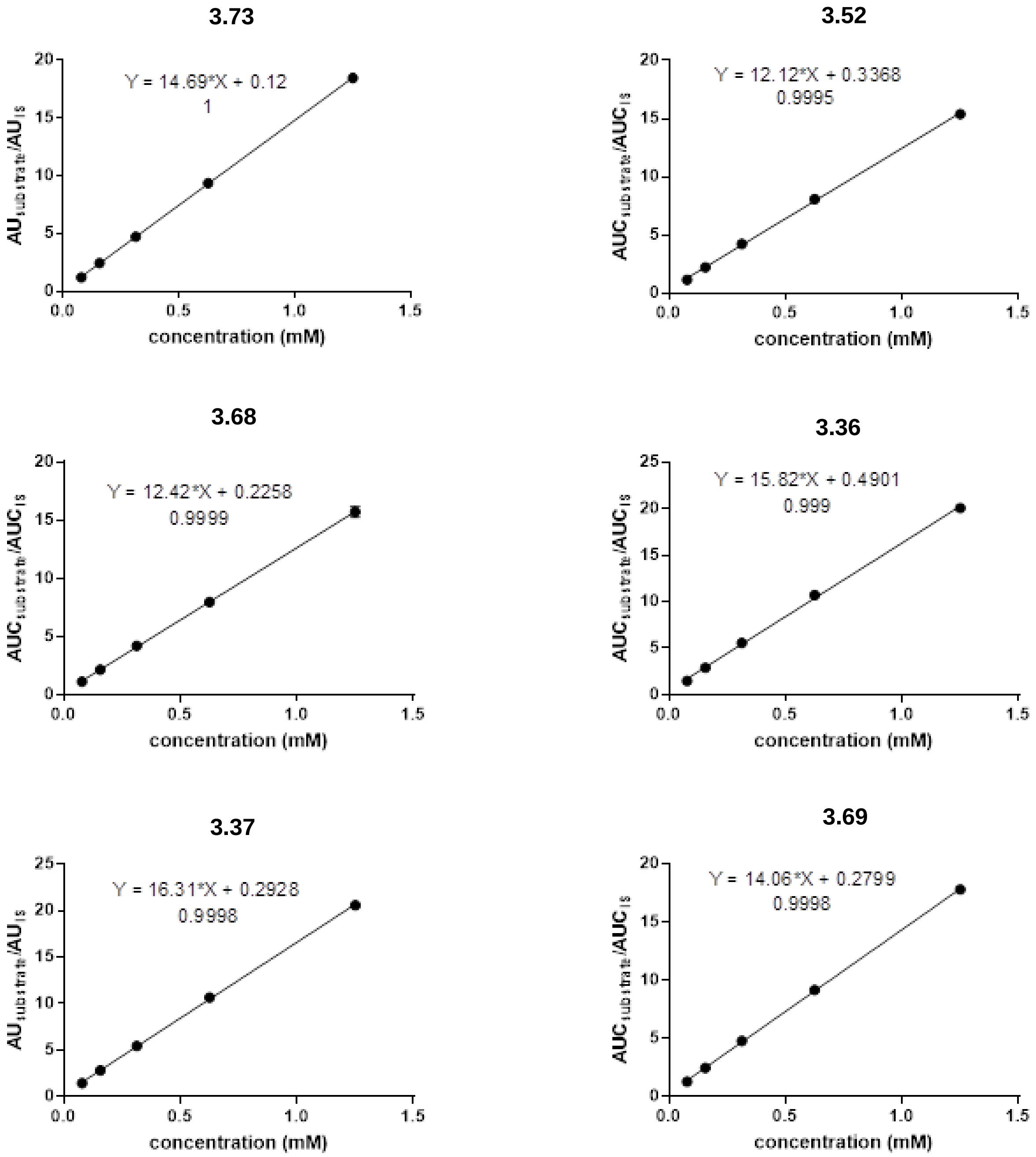

Figure 3.12: Substrate calibration curves.

Chapter 3.6.4: UPLC Traces of Biocatalytic Reactions

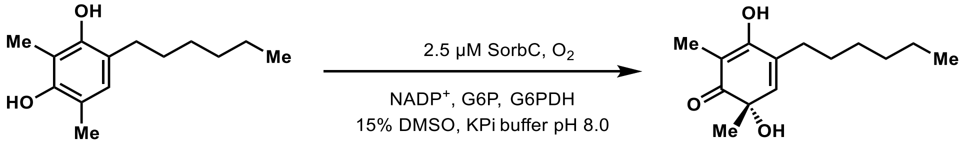
OH
Me
HO
Me
Me
2.5 µM SorbC, O₂
NADP⁺, G6P, G6PDH
15% DMSO, KPi buffer pH 8.0
OH
Me
O
Me
OH
Me

at 270 nm

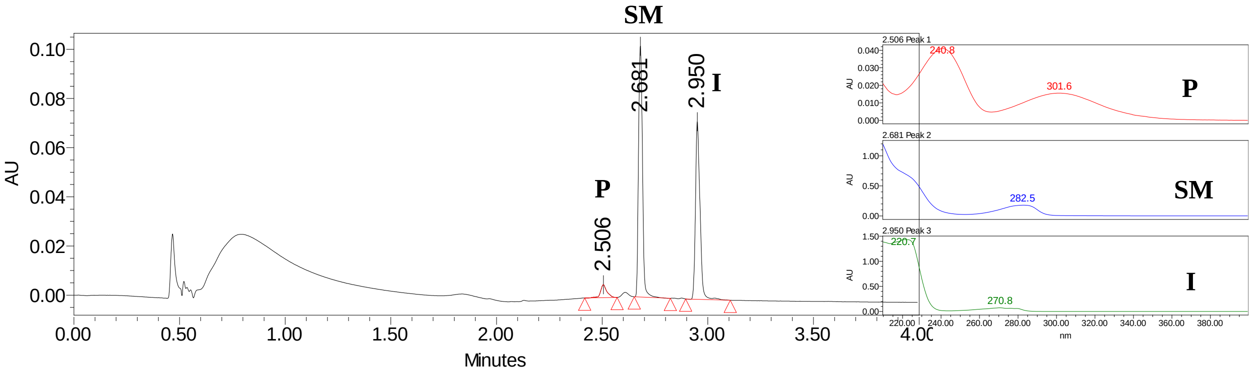

	Retention Time	Area	% Area	Height
1	2.506	11046	4.40	5286
2	2.681	132681	52.79	102077
3	2.950	107590	42.81	72312

NEC Table 1 Entry 3 at 270 nm

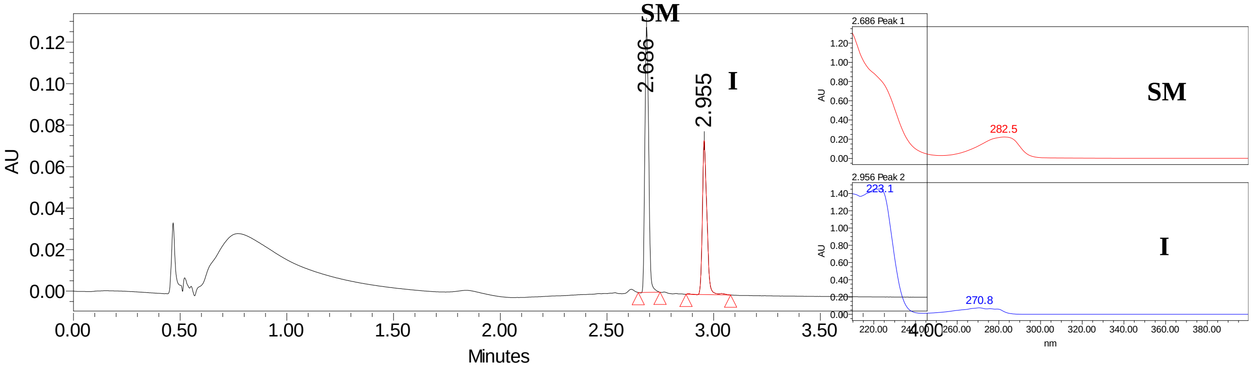

	Retention Time	Area	% Area	Height
1	2.686	159130	59.40	127839
2	2.955	108773	40.60	74266

Figure 3.13: UPLC-PDA trace of SorbC reactions with **Entry 3** and NEC.

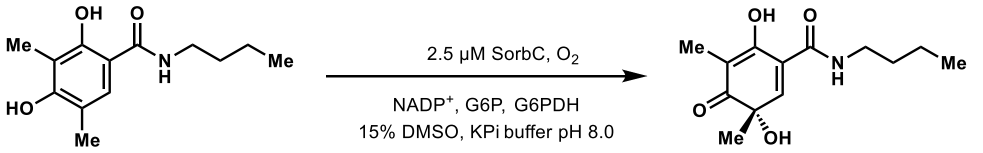
OH
O
Me
N
H
Me
HO
Me
2.5 μM SorbC, O_2
NADP$^+$, G6P, G6PDH
15% DMSO, KPi buffer pH 8.0
OH
O
Me
N
H
Me
O
Me
OH

SorbC 3.25 at 270 nm

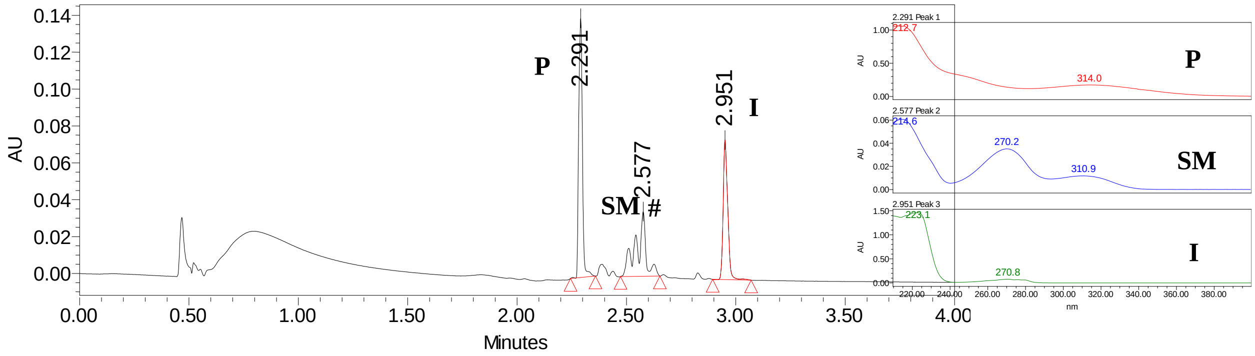

	Retention Time	Area	% Area	Height
1	2.291	164448	42.80	140660
2	2.577	109187	28.42	35115
3	2.951	110552	28.78	75766

NEC 3.25 at 270 nm

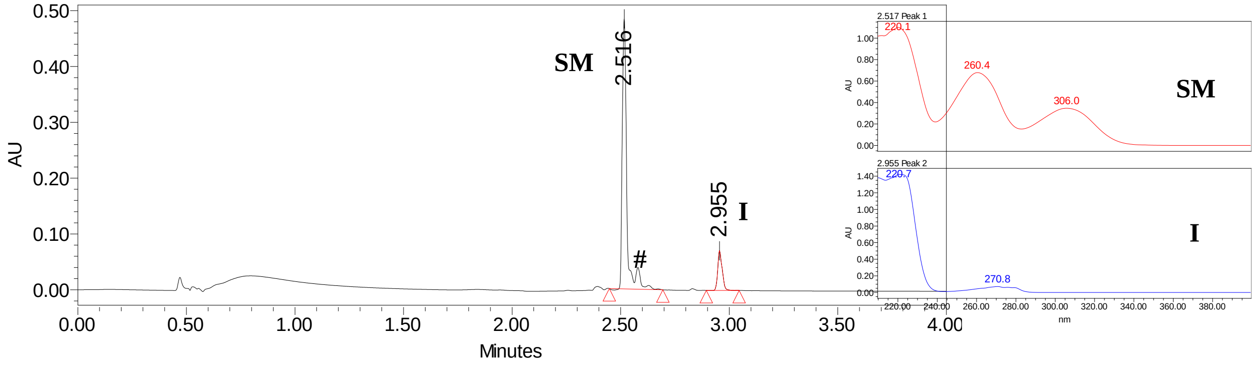

	Retention Time	Area	% Area	Height
1	2.516	707887	87.49	484263
2	2.955	101262	12.51	71033

Figure 3.14: UPLC-PDA trace of SorbC reactions with **3.25** and NEC.

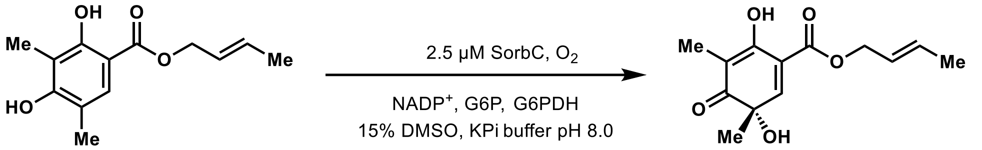

OH
O
Me
O
Me
HO
Me
2.5 μM SorbC, O$_2$
NADP$^+$, G6P, G6PDH
15% DMSO, KPi buffer pH 8.0
OH
O
Me
O
Me
O
Me
OH

SorbC and **3.26 at 240 nm**

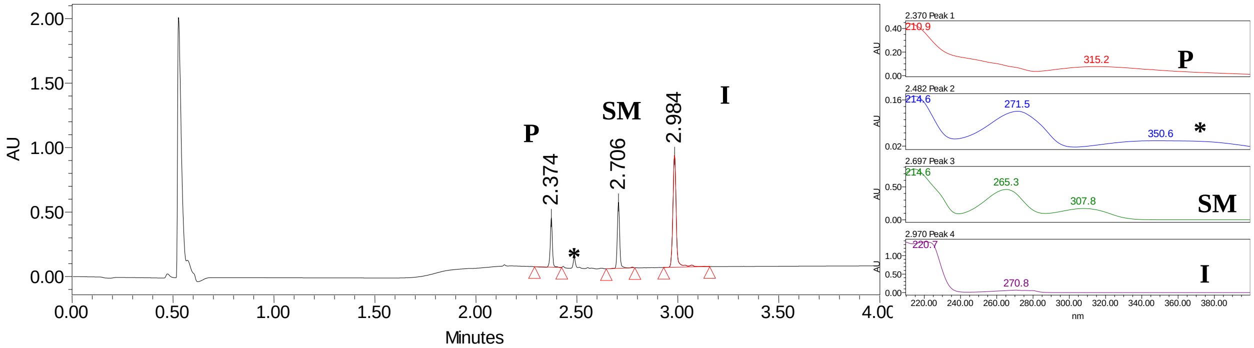

	Retention Time	Area	% Area	Height
1	2.374	284975	16.57	383174
2	2.706	423835	24.64	513156
3	2.984	1011156	58.79	868048

SorbC and **3.26 at 270 nm**

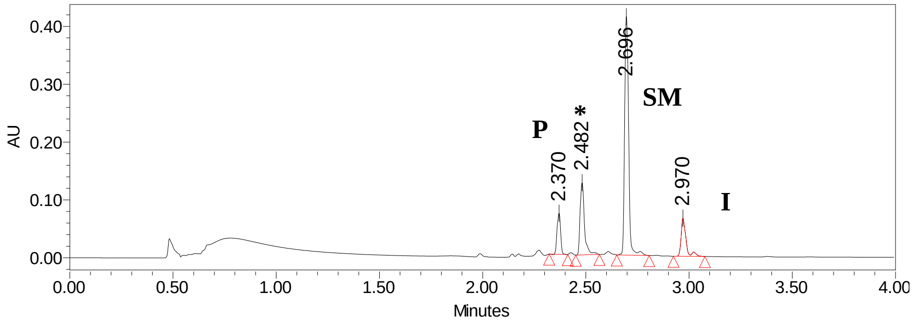

NEC 3.26 at 270 nm

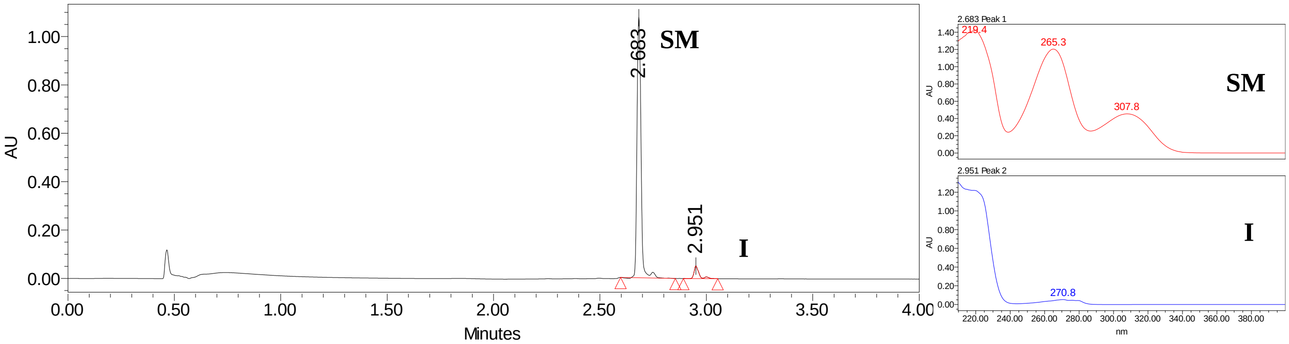

	Retention Time	Area	% Area	Height
1	2.683	1423901	94.40	1076742
2	2.951	84541	5.60	52324

Figure 3.15: UPLC-PDA trace of SorbC reactions with **Entry 3** and NEC.

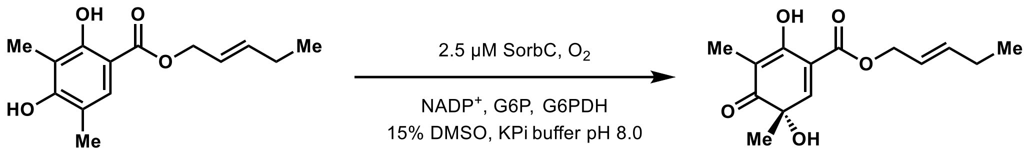

OH
O
Me
Me
HO
Me
O
2.5 µM SorbC, O_2
NADP$^+$, G6P, G6PDH
15% DMSO, KPi buffer pH 8.0
OH
O
Me
Me
O
O
Me
OH

SorbC 3.27 at 270 nm

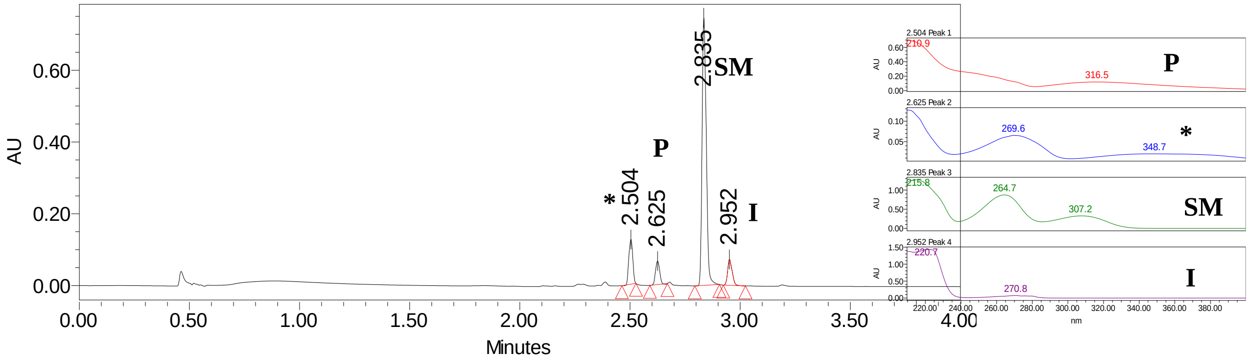

	Retention Time	Area	% Area	Height
1	2.440	205923	12.80	151877
2	2.765	326172	20.27	272984
3	2.954	1076817	66.93	743229

NEC 3.27

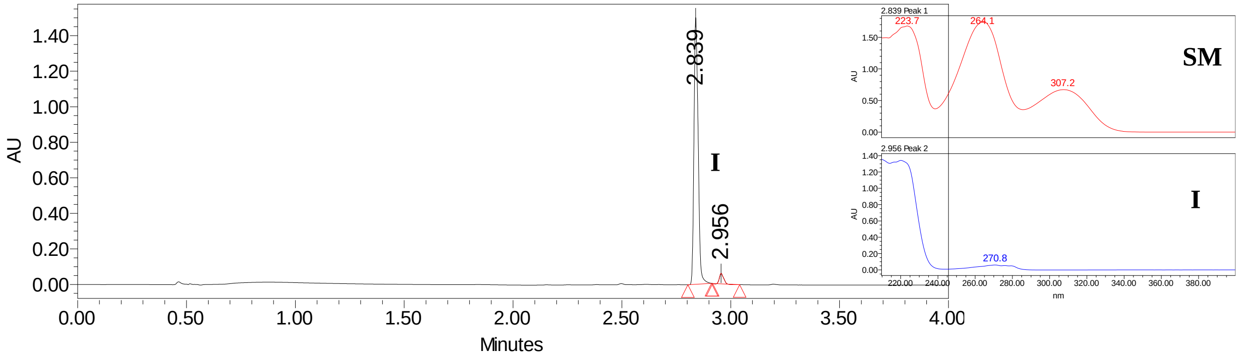

	Retention Time	Area	% Area	Height
1	2.839	1986512	94.81	1497370
2	2.956	108837	5.19	55981

Figure 3.16: UPLC-PDA trace of SorbC reactions with **3.27** and NEC.

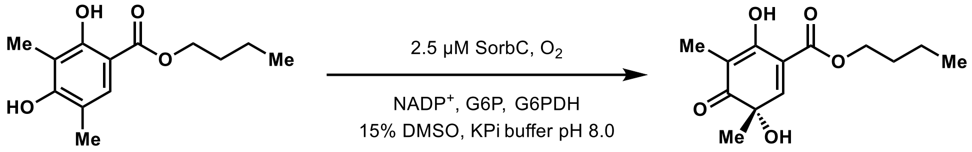
OH
O
Me
HO
Me
O
Me
2.5 µM SorbC, O_2
NADP$^+$, G6P, G6PDH
15% DMSO, KPi buffer pH 8.0
OH
O
Me
O
O
Me
Me
OH

SorbC 3.29 at 270 nm

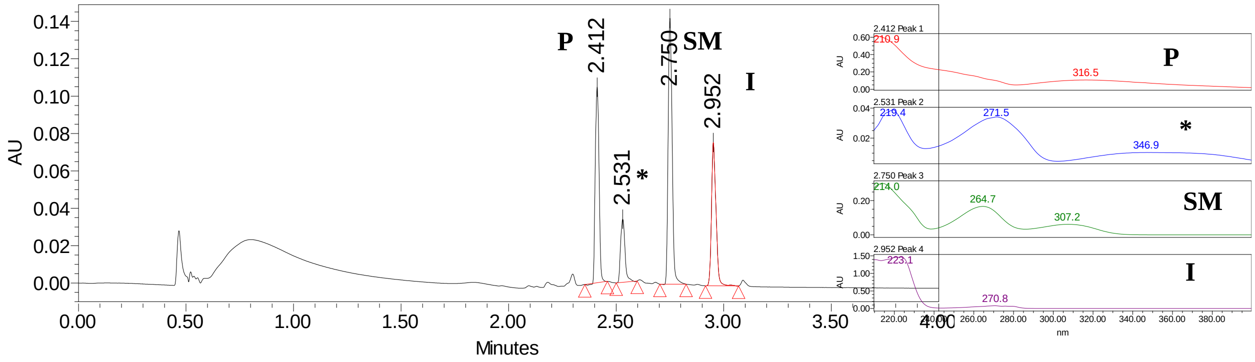

	Retention Time	Area	% Area	Height
1	2.413	301350	19.65	261174
2	2.752	220513	14.38	182022
3	2.954	1011612	65.97	713268

NEC 3.29

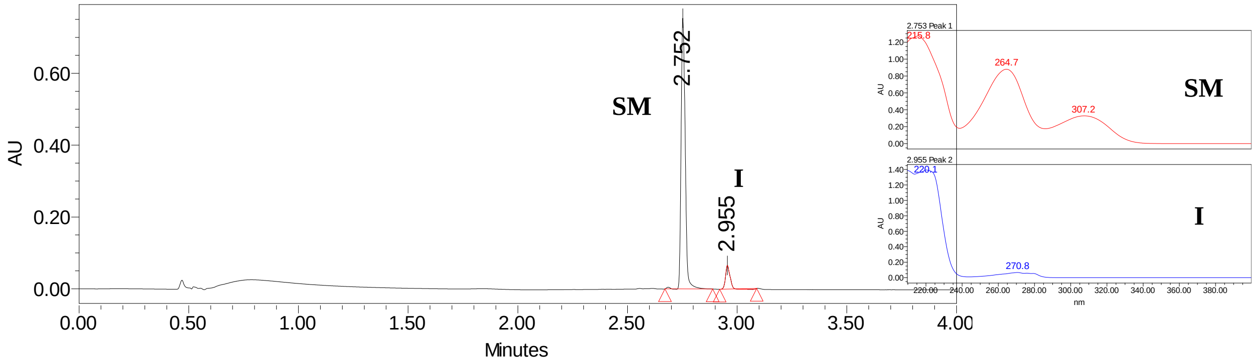

	Retention Time	Area	% Area	Height
1	2.752	988494	90.71	753607
2	2.955	101253	9.29	66180

Figure 3.17: UPLC-PDA trace of SorbC reactions with **3.29** and NEC. Byproduct annotated with an asterisk.

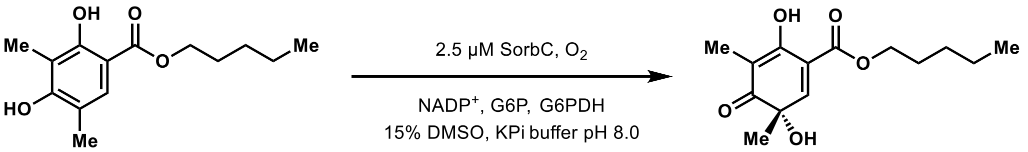
OH
O
Me
O
Me
HO
Me
2.5 μM SorbC, O$_2$
NADP$^+$, G6P, G6PDH
15% DMSO, KPi buffer pH 8.0
OH
O
Me
O
Me
O
Me
OH

SorbC and 3.30 at 270 nm

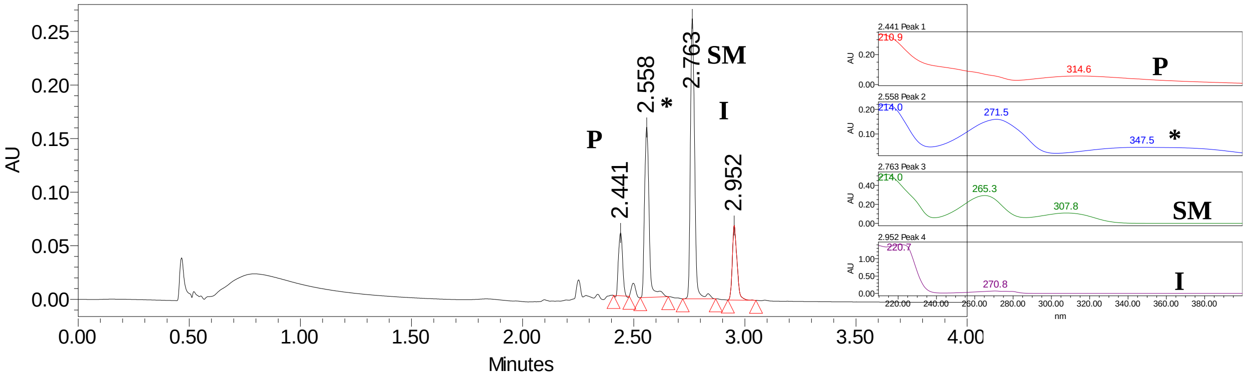

	Retention Time	Area	% Area	Height
1	2.441	77178	10.25	58829
2	2.558	230373	30.59	158864
3	2.763	344260	45.71	261422
4	2.952	101360	13.46	69715

NEC 3.30 at 270 nm

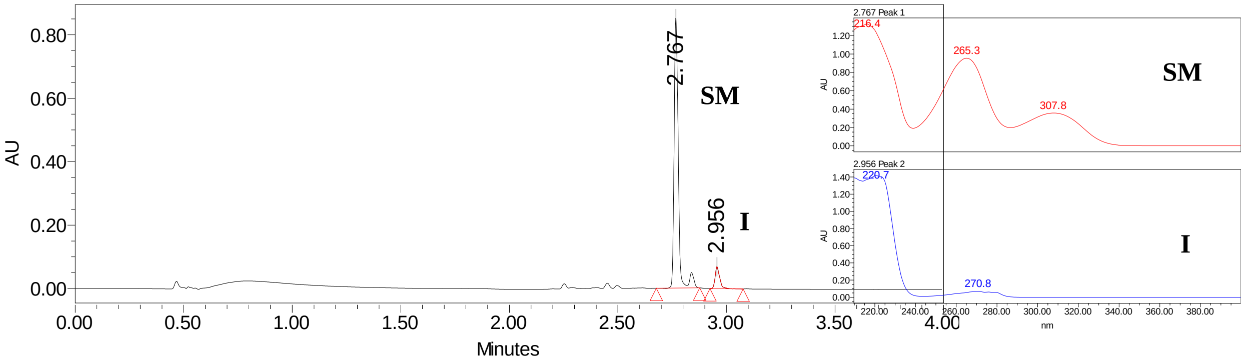

	Retention Time	Area	% Area	Height
1	2.767	1150031	91.91	850716
2	2.956	101217	8.09	69189

Figure 3.18: UPLC-PDA trace of SorbC reactions with **3.30** and NEC. Byproduct annotated by an asterisk

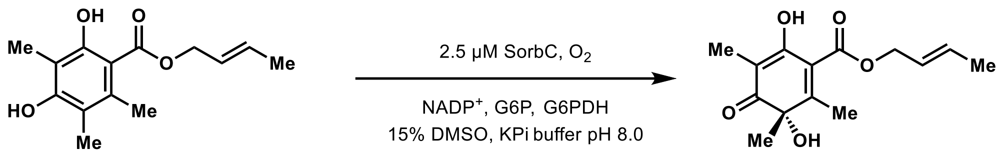
2.5 μM SorbC, O₂
NADP⁺, G6P, G6PDH
15% DMSO, KPi buffer pH 8.0

SorbC and 3.47 at 240 nm

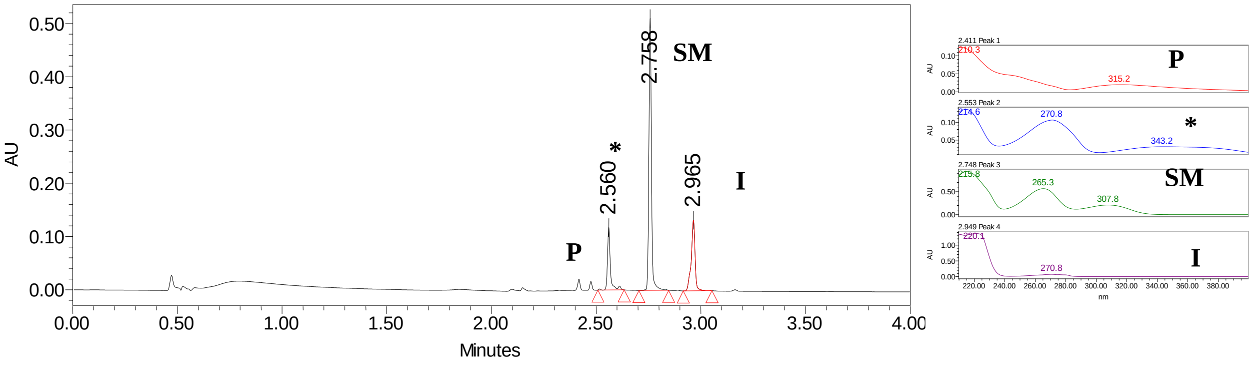

	Retention Time	Area	% Area	Height
1	2.560	113288	15.76	117345
2	2.758	437320	60.85	511516
3	2.965	168037	23.38	132927

NEC 3.47 at 270 nm

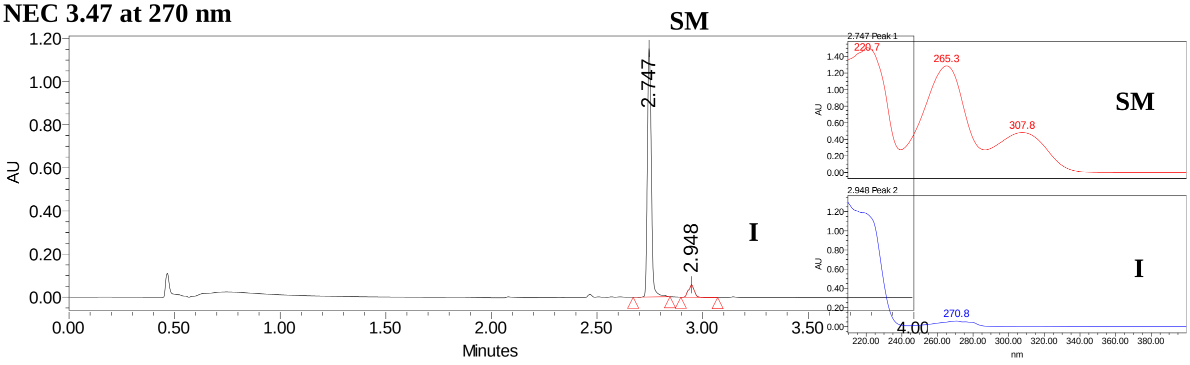

	Retention Time	Area	% Area	Height
1	2.747	1490565	93.12	1152913
2	2.948	110155	6.88	58135

Figure 3.19: UPLC-PDA trace of SorbC reactions with **3.47** and NEC. Byproduct annotated with an asterisk

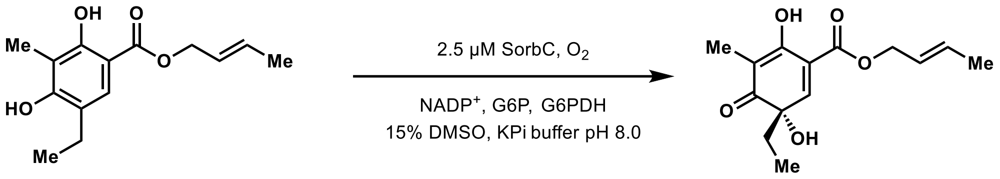
OH
O
Me
O
Me
HO
Me
2.5 µM SorbC, O_2
NADP⁺, G6P, G6PDH
15% DMSO, KPi buffer pH 8.0
OH
O
Me
O
Me
O
OH
Me

SorbC and **3.72 at 270 nm**

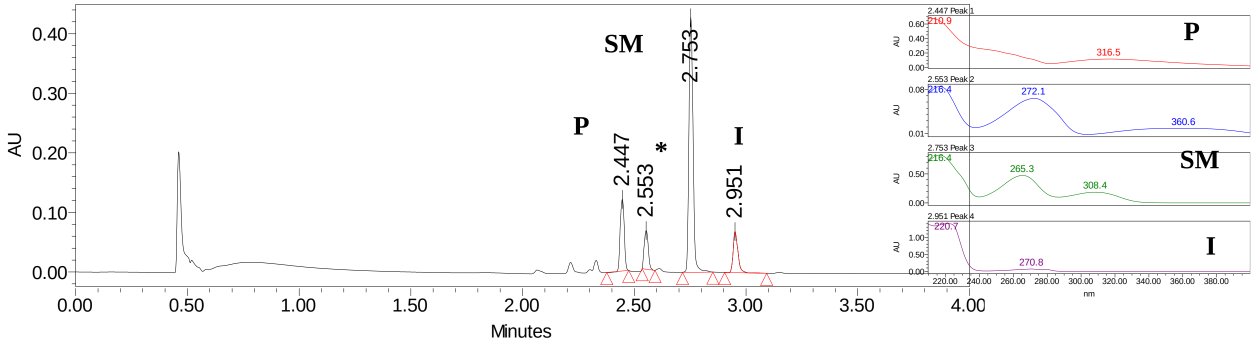

	Retention Time	Area	% Area	Height
1	2.447	153081	17.24	120344
2	2.553	83030	9.35	65133
3	2.753	549538	61.90	428628
4	2.951	102195	11.51	69156

NEC of 3.27 at 270 nm

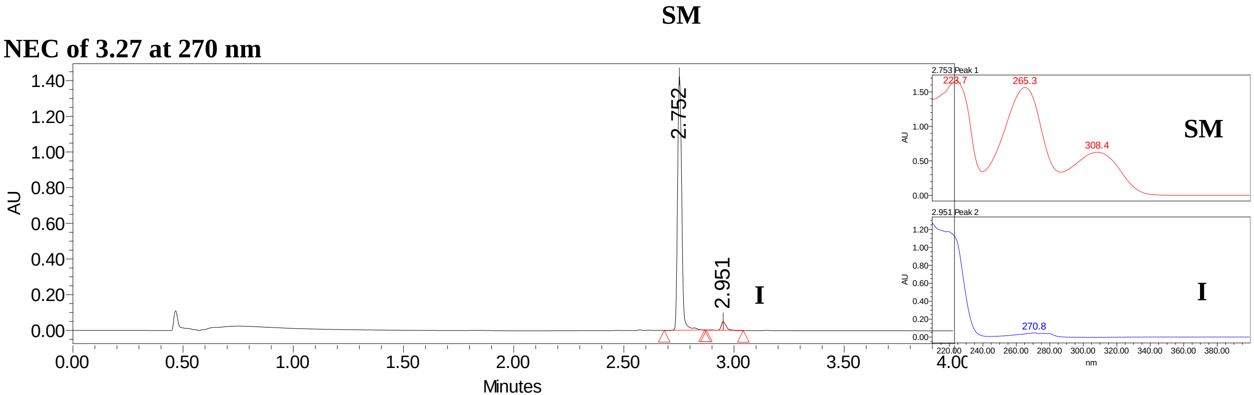

	Retention Time	Area	% Area	Height
1	2.752	1794595	94.76	1416054
2	2.951	99228	5.24	45478

Figure 3.20: UPLC-PDA trace of SorbC reactions with **3.72** and NEC. Byproduct annotated with an asterisk.

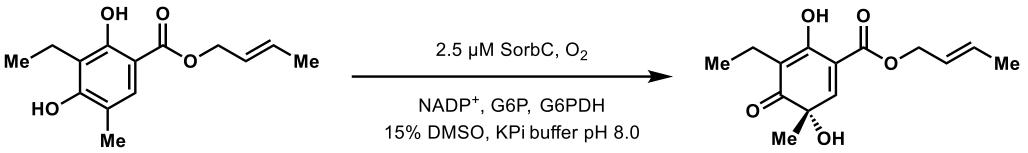
OH
O
Me
HO
Me
O
Me
2.5 μM SorbC, O$_2$
NADP$^+$, G6P, G6PDH
15% DMSO, KPi buffer pH 8.0
OH
O
Me
O
Me
OH
O
Me

SorbC and **3.73 at 270 nm**

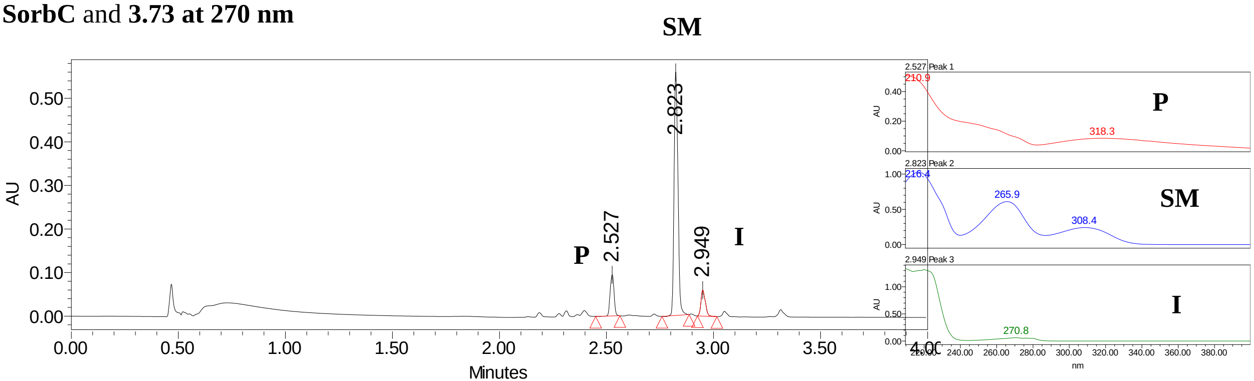

	Retention Time	Area	% Area	Height
1	2.527	120391	12.95	94531
2	2.823	708205	76.19	558891
3	2.949	100905	10.86	59824

NEC 3.73 at 270 nm

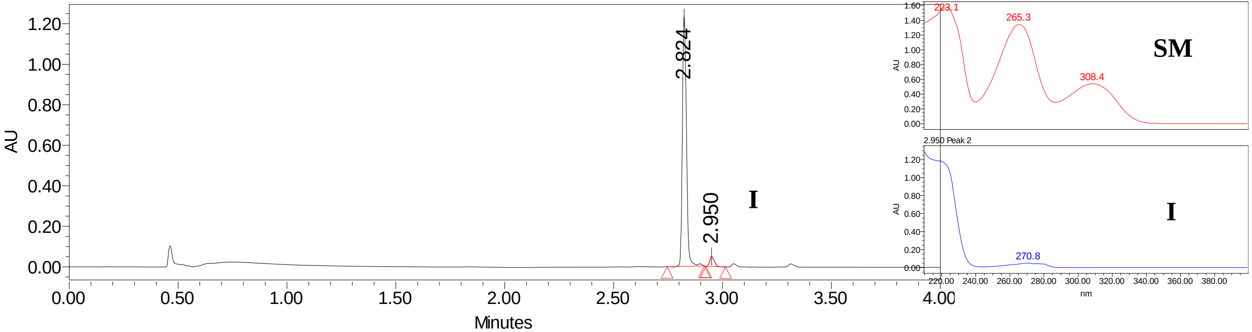

	Retention Time	Area	% Area	Height
1	2.824	1609098	94.60	1231662
2	2.950	91833	5.40	49450

Figure 3.21: UPLC-PDA trace of SorbC reactions with **3.73** and NEC.

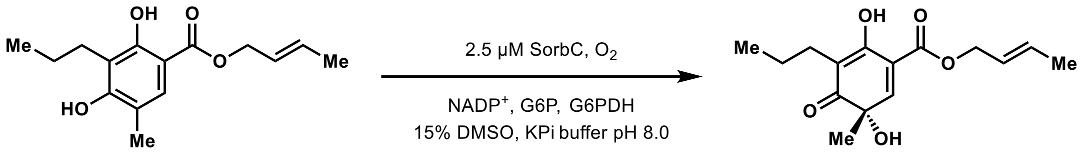
OH
O
Me
O
Me
HO
Me
2.5 μM SorbC, O_2
NADP$^+$, G6P, G6PDH
15% DMSO, KPi buffer pH 8.0
OH
O
Me
O
Me
O
Me
OH

SorbC and **3.52 at 270 nm**

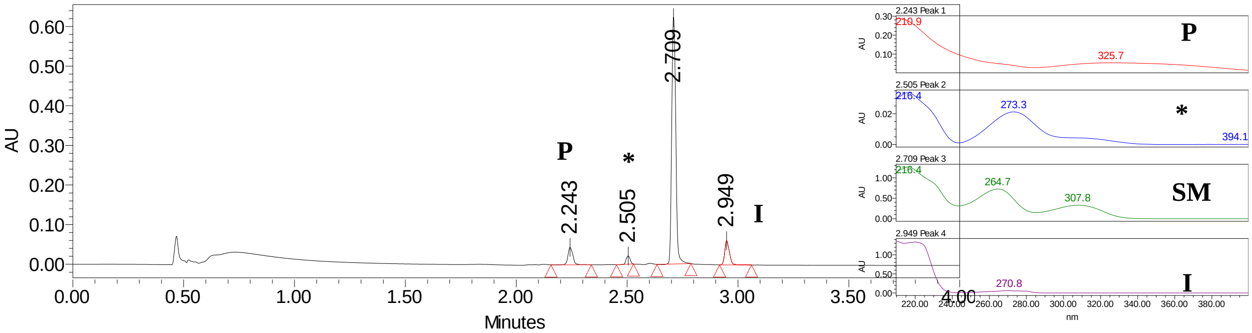

	Retention Time	Area	% Area	Height
1	2.249	60565	10.20	47548
2	2.719	509107	85.75	565565
3	2.962	24021	4.05	20471

NEC 3.52 at 270 nm

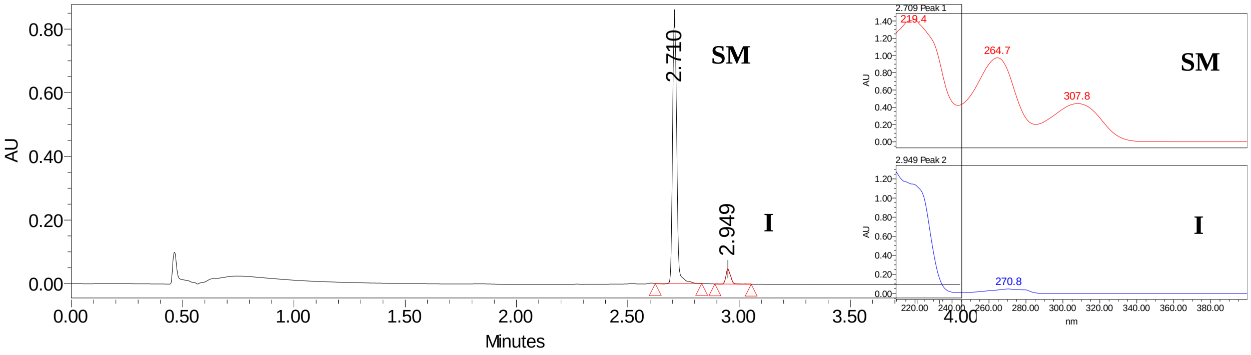

Figure 3.22: UPLC-PDA trace of SorbC reactions with **31** and NEC. Byproduct annotated with an asterisk.

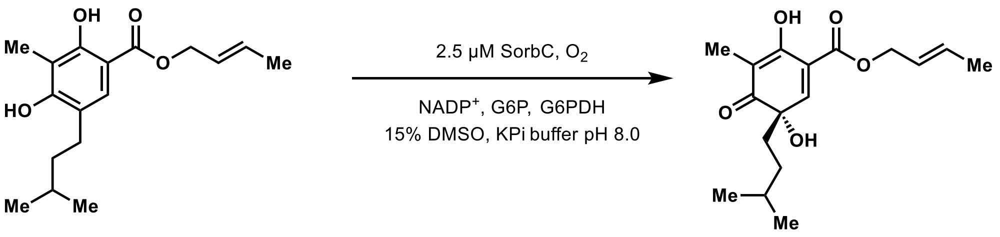
2.5 µM SorbC, O$_2$
NADP$^+$, G6P, G6PDH
15% DMSO, KPi buffer pH 8.0

SorbC and **3.84 at 270 nm**

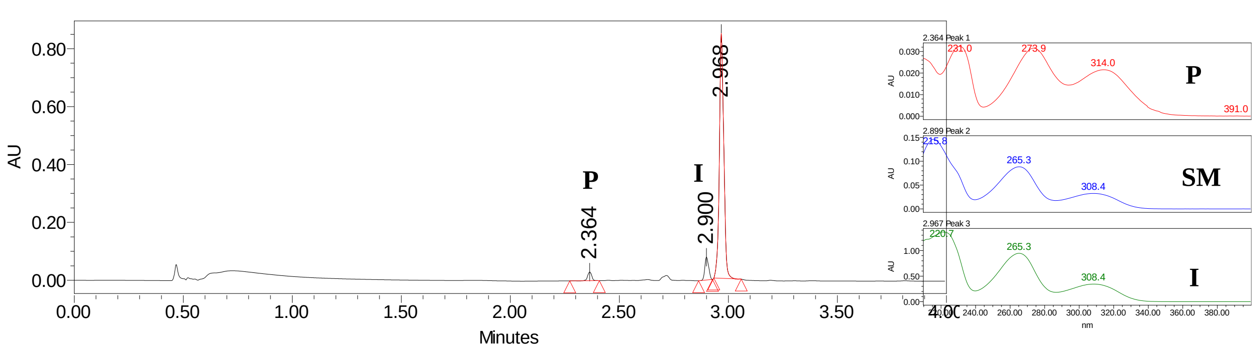

	Retention Time	Area	% Area	Height
1	2.364	39944	2.99	29879
2	2.900	97083	7.28	78987
3	2.968	1196964	89.73	846065

NEC 3.84 at 270 nm

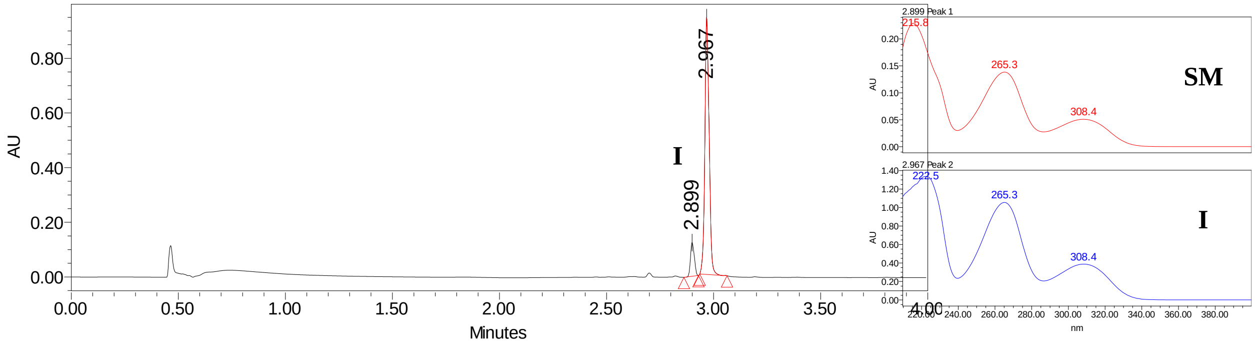

	Retention Time	Area	% Area	Height
1	2.899	153450	10.44	123568
2	2.967	1315706	89.56	941069

Figure 3.23: UPLC-PDA trace of SorbC reactions with **3.84** and NEC.

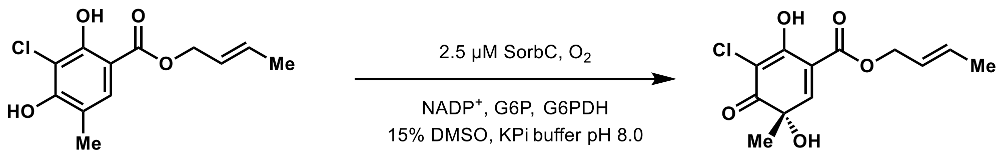
OH
O
Cl
HO
Me
O
Me
2.5 μM SorbC, O2
NADP+, G6P, G6PDH
15% DMSO, KPi buffer pH 8.0
OH
O
Cl
O
Me
OH
O
Me

SorbC and **3.36 at 270 nm**

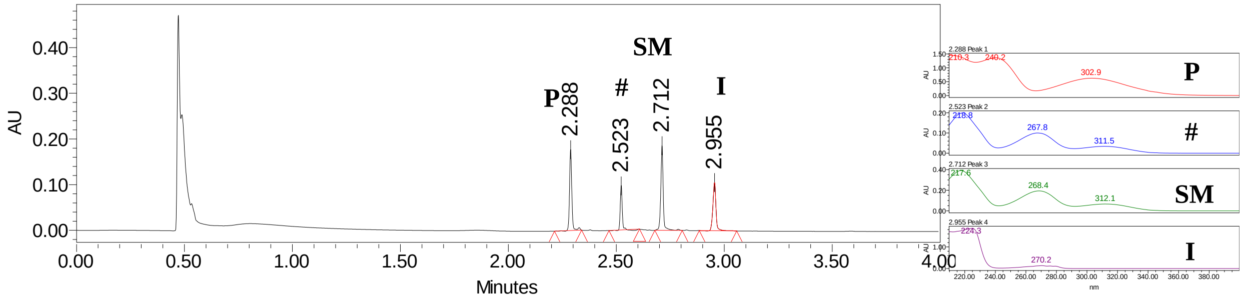

	Retention Time	Area	% Area	Height
1	2.286	666717	32.64	816017
2	2.713	269327	13.18	314630
3	2.959	1106633	54.18	956640

NEC of **3.36 at 270 nm**

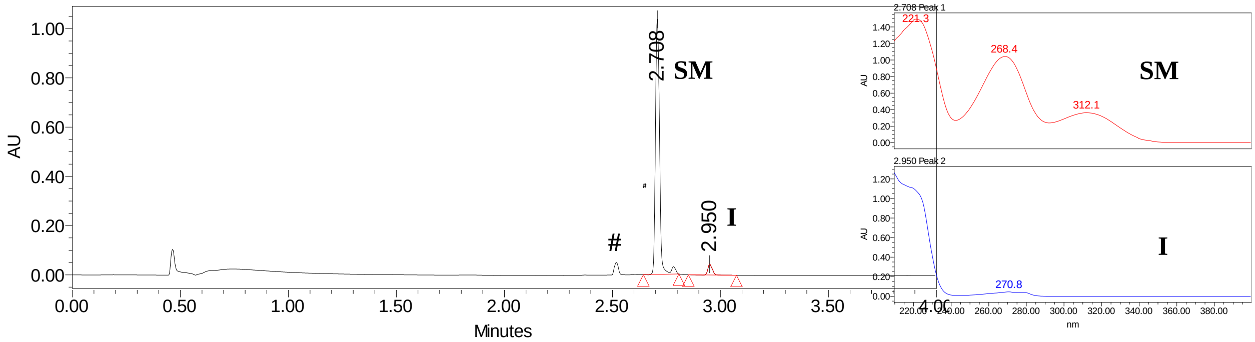

	Retention Time	Area	% Area	Height
1	2.708	1388407	95.55	1036838
2	2.950	64677	4.45	44282

Figure 3.24: UPLC-PDA trace of SorbC reactions with **3.36** and NEC. Impurity from SM denoted with #.

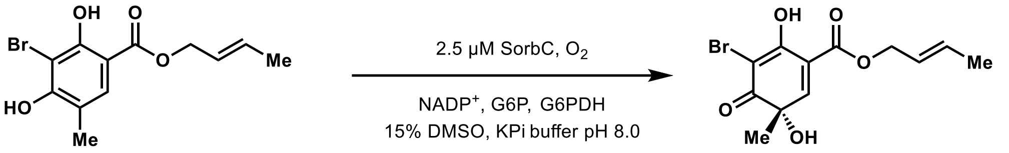
OH
O
Br
O
Me
HO
Me
2.5 μM SorbC, O_2
NADP$^+$, G6P, G6PDH
15% DMSO, KPi buffer pH 8.0
OH
O
Br
O
Me
O
Me
OH

SorbC and **3.37 at 270 nm**

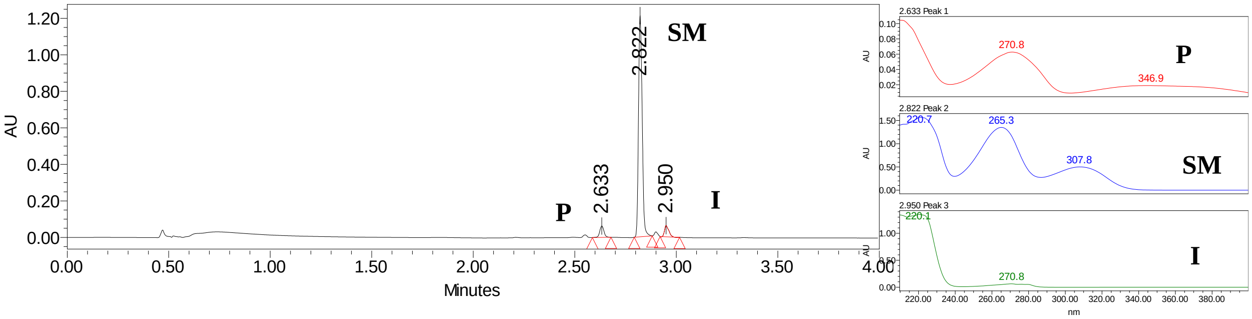

	Retention Time	Area	% Area	Height
1	2.633	90558	5.29	62617
2	2.822	1530254	89.33	1211491
3	2.950	92228	5.38	61719

NEC of 3.37 at 270 nm

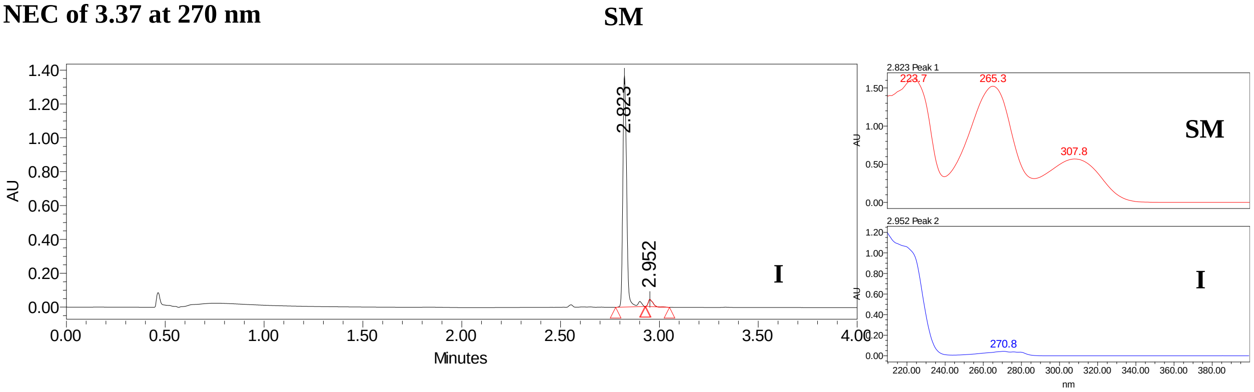

	Retention Time	Area	% Area	Height
1	2.823	1690490	94.21	1347865
2	2.952	103864	5.79	30952

Figure 3.25: UPLC-PDA trace of SorbC reactions with **3.37** and NEC.

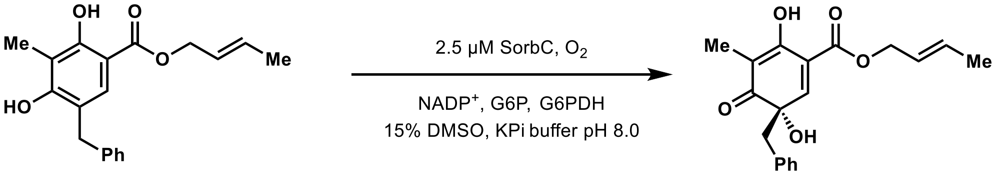
OH
O
Me
HO
Ph
O
Me
2.5 μM SorbC, O$_2$
NADP$^+$, G6P, G6PDH
15% DMSO, KPi buffer pH 8.0
OH
O
Me
O
OH
Ph
O
Me

SorbC and **3.69 at 270 nm**

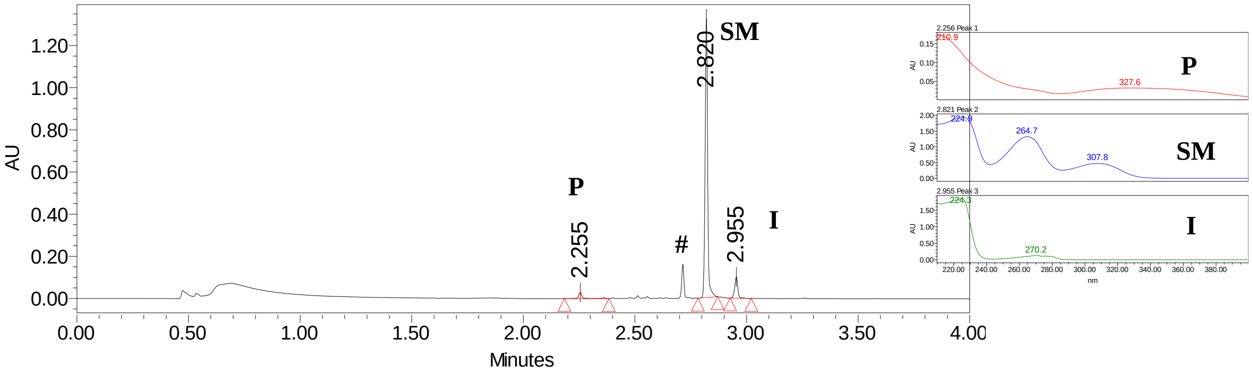

	Retention Time	Area	% Area	Height
1	2.255	34471	2.93	29745
2	2.820	1041179	88.62	1327825
3	2.955	99200	8.44	101574

NEC of **3.69 at 270 nm**

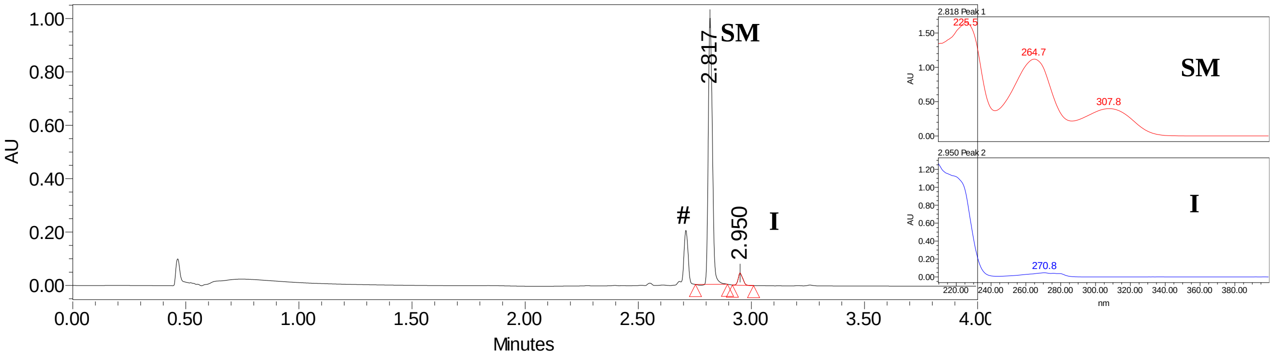

	Retention Time	Area	% Area	Height
1	2.817	1265846	95.17	997950
2	2.950	64266	4.83	45787

Figure 3.26: UPLC-PDA trace of SorbC reactions with **3.69** and NEC. Impurity from starting material denoted with a #.

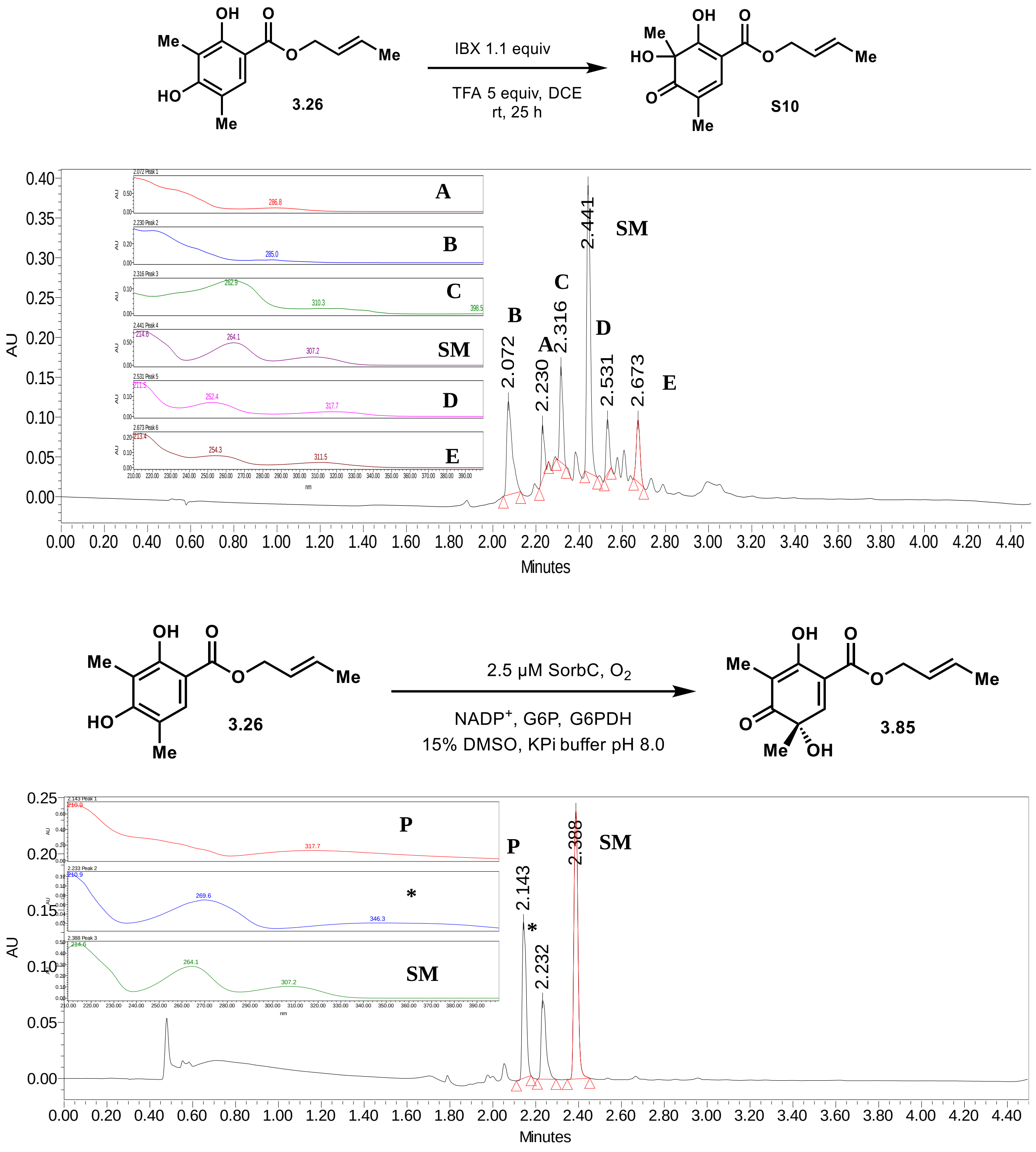

Figure 3.27. With a subset of substrates, in addition to the expected product a second peak with the same *m/z* was observed (See Figure 3.29). This byproduct, formed in SorbC reactions, was not found in reactions with IBX or LTA. Attempts to isolate and characterize the material corresponding to the peak marked with an asterisk either directly from enzymatic reactions or following acylation did not produce meaningful quantities of material. Preparative HPLC of the crude reaction mixture did allow for isolation of the material, as judged by UPLC-PDA analysis of the resulting fractions; however, this material accounted for little of the mass balance of the reaction mixture (<0.1 mg isolated from 10 mg-scale reactions) insufficient material was obtained for NMR analysis.

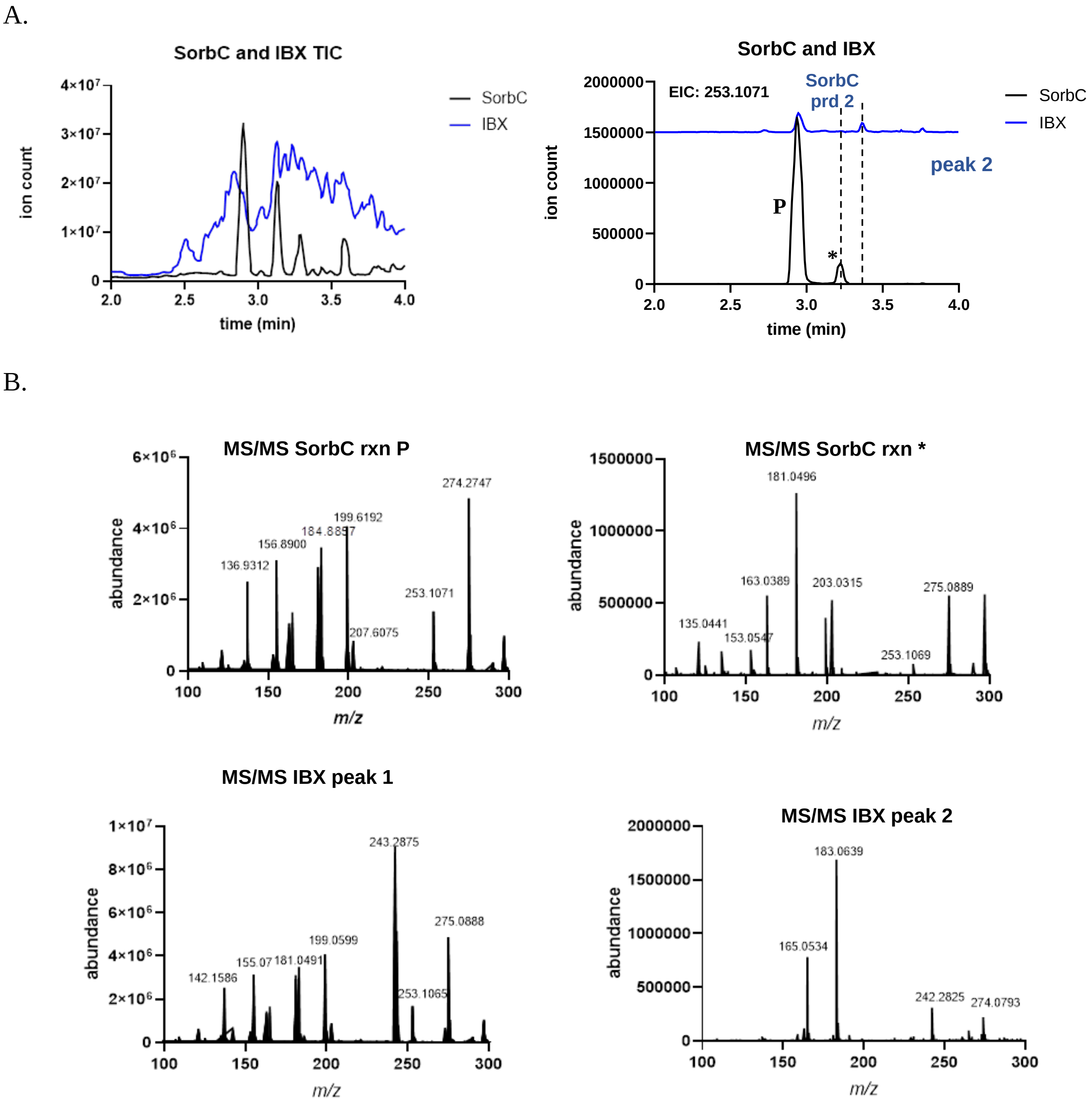

Figure 3.28: (A) LC-MS trace comparing reaction of **3.26** with SorbC and IBX. (B) MS/MS spectra comparing the products of the SorbC reaction and the IBX reaction. Note the second IBX product does not correspond to the more nonpolar SorbC product.

Chapter 3.6.5: Determination of Enantiomeric Excess

SFC-UV-Vis trace of Pb(OAc)$_4$ generated **3.77**.

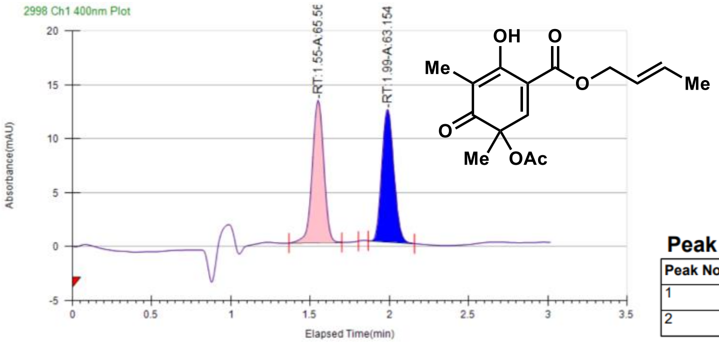

Peak Information

Peak No	% Area	Area	Ret. Time	Height
1	50.9375	65.5675	1.55 min	13.2068
2	49.0625	63.1541	1.99 min	12.255

Run Information

Instrument Method	Inj. Vol.	Solvent	Column	Sample	Well Location	Temp.	Flow	% Modifier	Pressure
AD-H_10%	5	iPrOH	AD-H Chiral Analytical	sbdVII-064_rac_#1	11C	40	3.5	10	120

SFC-UV-Vis trace of SorbC generated **3.77**.

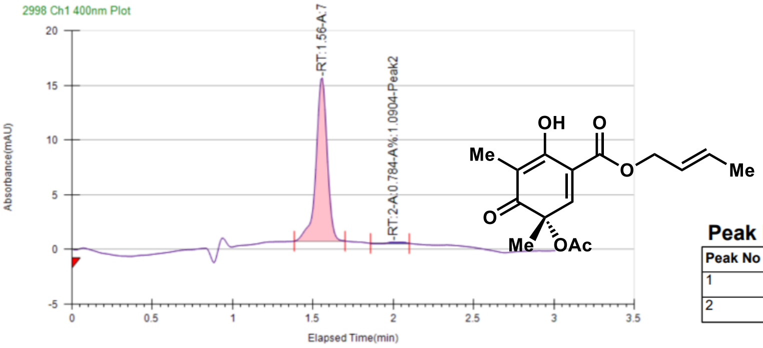

Peak Information

Peak No	% Area	Area	Ret. Time	Height
1	98.9096	71.1139	1.56 min	14.9031
2	1.0904	0.784	2 min	0.1165

Run Information

Instrument Method	Inj. Vol.	Solvent	Column	Sample	Well Location	Temp.	Flow	% Modifier	Pressure
AD-H_10%_320-400	10	iPrOH	AD-H Chiral Analytical	sbdVII-093_trimethyl rac 10%	11A	40	3.5	10	120

Pb(OAc)$_4$ generated **3.80**

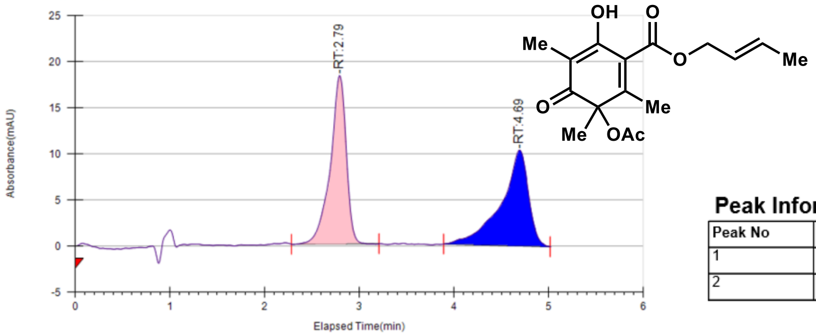

Peak Information

Peak No	% Area	Area	Ret. Time	Height
1	50.4209	211.1048	2.79 min	18.259
2	49.5791	207.5802	4.69 min	10.4048

SorbC generated **3.80**

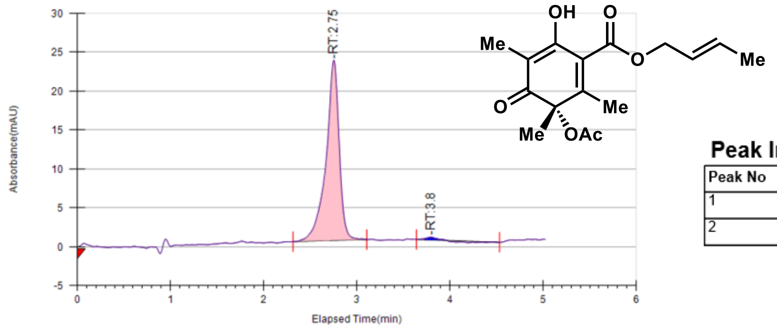

Peak Information

Peak No	% Area	Area	Ret. Time	Height
1	98.6029	226.0896	2.75 min	23.156
2	1.3971	3.2034	3.8 min	0.3673

Run Information

Instrument Method	Inj. Vol.	Solvent	Column	Sample	Well Location	Temp.	Flow	% Modifier	Pressure
AD-H_10%_320-400	2	iPrOH	AD-H Chiral Analytical	sbdVII-110_trimethyl SorbC_10%	12A	40	3.5	10	120

Pb(OAc)$_4$ generated ±**3.81**

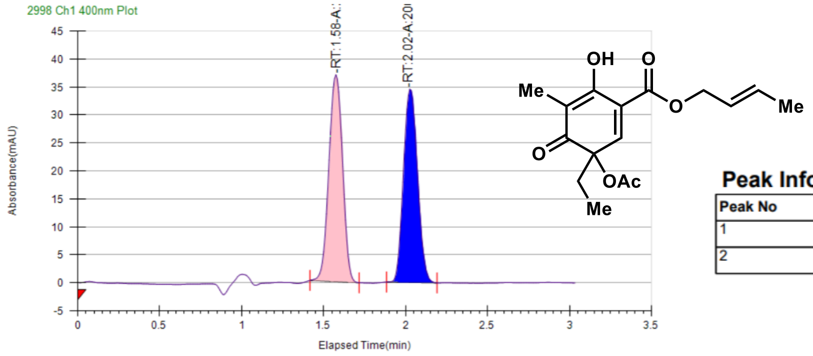

Peak Information

Peak No	% Area	Area	Ret. Time	Height
1	50.9847	208.7008	1.58 min	36.9957
2	49.0153	200.6391	2.02 min	34.5465

Run Information

Instrument Method	Inj. Vol.	Solvent	Column	Sample	Well Location	Temp.	Flow	% Modifier	Pressure
AD-H_10%_360-400	10	iPrOH	AD-H Chiral Analytical	sbdVII-090_5et_rac_10%	11A	40	3.5	10	120

SorbC generated **3.81**.

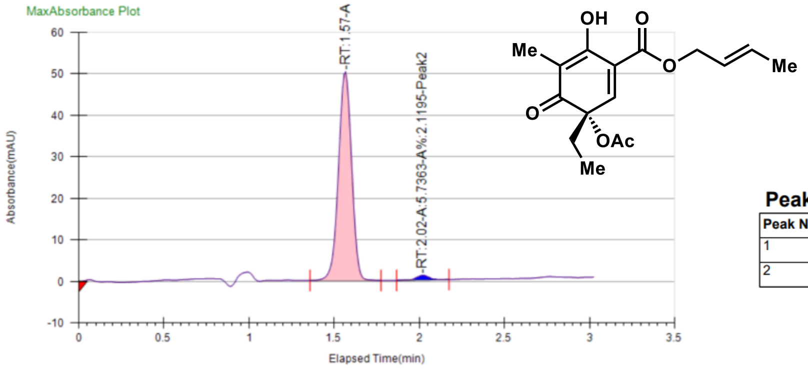

Peak Information

Peak No	% Area	Area	Ret. Time	Height
1	97.8805	264.9133	1.57 min	50.2939
2	2.1195	5.7363	2.02 min	1.106

Run Information

Instrument Method	Inj. Vol.	Solvent	Column	Sample	Well Location	Temp.	Flow	% Modifier	Pressure
AD-H_10%_360-400	5	iPrOH	AD-H Chiral Analytical	sbdVII-095_5et_SorbC_10%	12A	40	3.5	10	120

Pb(OAc)$_4$ generated ±**3.82**.

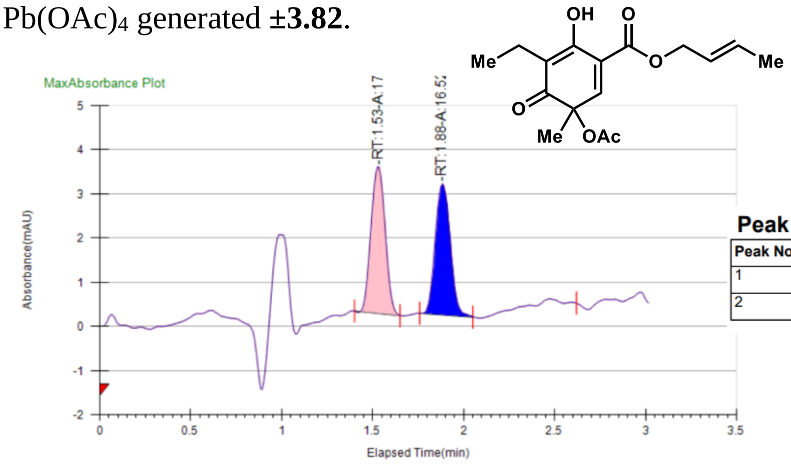

Peak Information

Peak No	% Area	Area	Ret. Time	Height
1	51.3911	17.4694	1.53 min	3.3158
2	48.6089	16.5237	1.88 min	2.9691

Run Information

Instrument Method	Inj. Vol.	Solvent	Column	Sample	Well Location	Temp.	Flow	% Modifier	Pressure
AD-H_10%_360-400	10	iPrOH	AD-H Chiral Analytical	sbdVII-091_3et_rac_10%	13A	40	3.5	10	120

SorbC generated **3.82**.

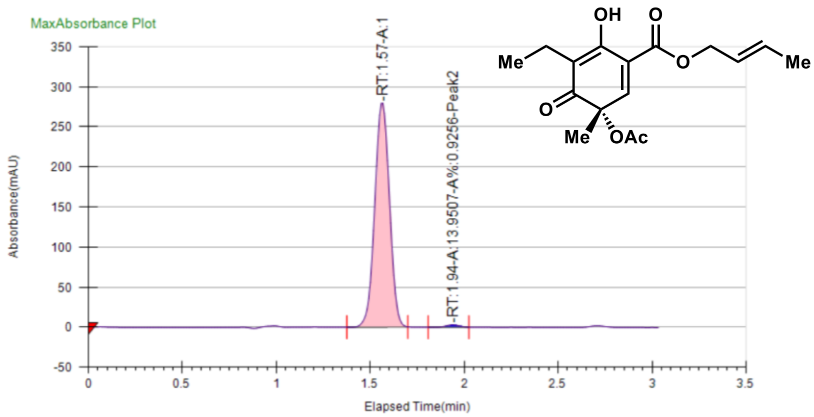

Peak Information

Peak No	% Area	Area	Ret. Time	Height
1	99.0744	1493.1926	1.57 min	279.9072
2	0.9256	13.9507	1.94 min	2.8653

Run Information

Instrument Method	Inj. Vol.	Solvent	Column	Sample	Well Location	Temp.	Flow	% Modifier	Pressure
AD-H_10%_360-400	5	iPrOH	AD-H Chiral Analytical	sbdVII-092_5et_SorbC_10%	14A	40	3.5	10	120

Pb(OAc)$_4$ generated ±**3.83**.

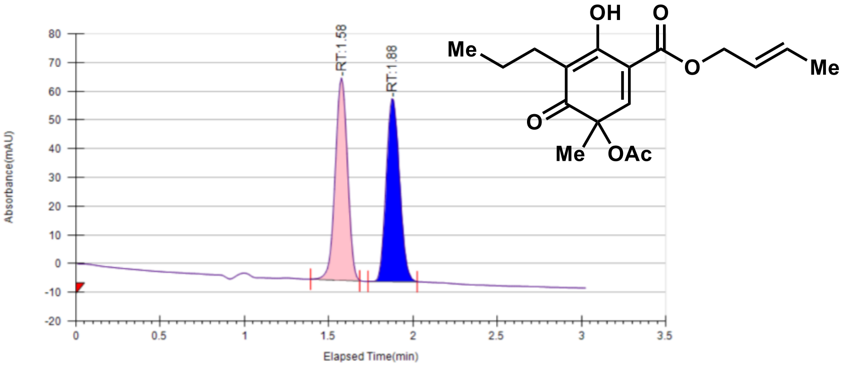

Run Information

Instrument Method	Inj. Vol.	Solvent	Column	Sample	Well Location	Temp.	Flow	% Modifier	Pressure
AD-H_10%	5	iPrOH	AD-H Chiral Analytical	sbdVII-078_3pr_rac_10%	11A	40	3.5	10	120

Peak Information

Peak No	% Area	Area	Ret. Time	Height	Cap. Factor
1	50.4443	348.0163	1.58 min	70.3778	0
2	49.5557	341.886	1.88 min	63.6737	0

SorbC generated **3.83**.

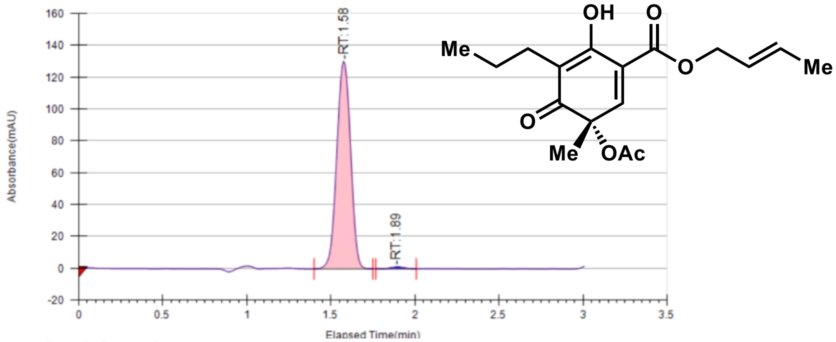

Run Information

Instrument Method	Inj. Vol.	Solvent	Column	Sample	Well Location	Temp.	Flow	% Modifier	Pressure
AD-H_10%	10	iPrOH	AD-H Chiral Analytical	sbdVII-112_3pr_SorbC_10%	12A	40	3.5	10	120

Peak Information

Peak No	% Area	Area	Ret. Time	Height	Cap. Factor
1	99.0969	728.2407	1.58 min	130.3905	0
2	0.9031	6.6364	1.89 min	1.1574	0

Chapter 3.6.6: NMR Spectra of Compounds

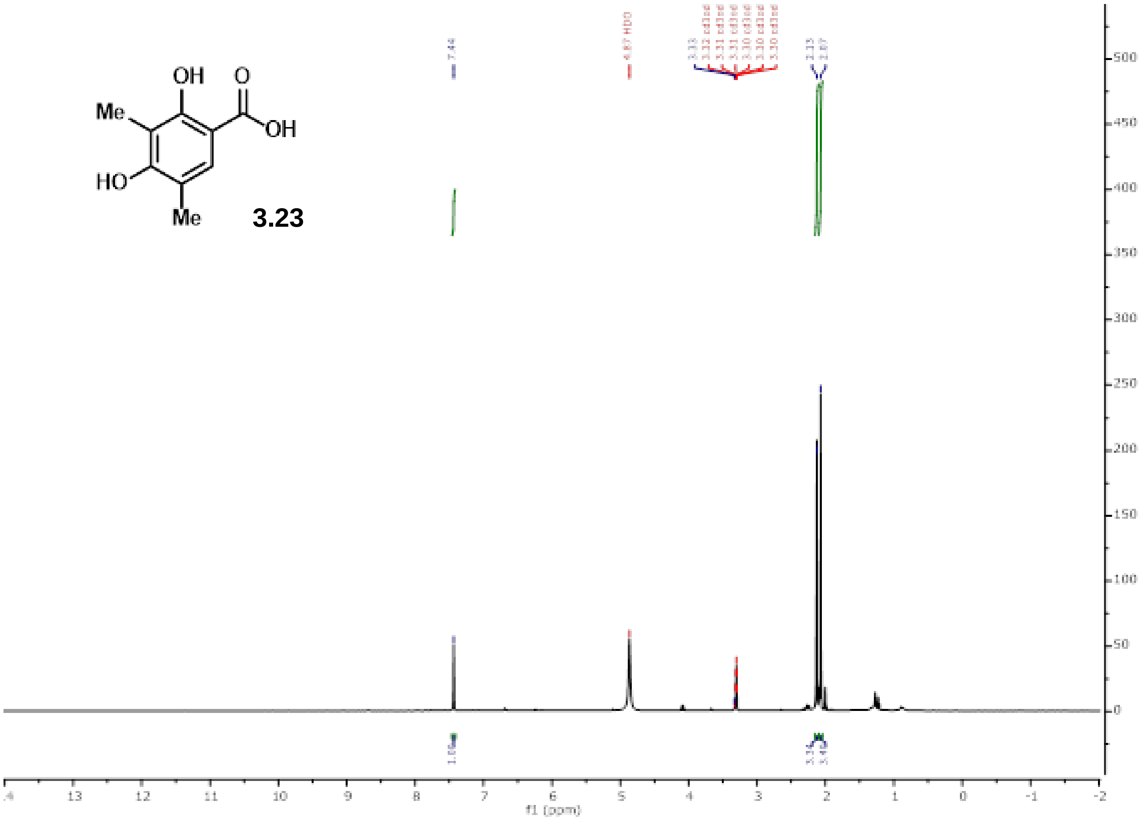

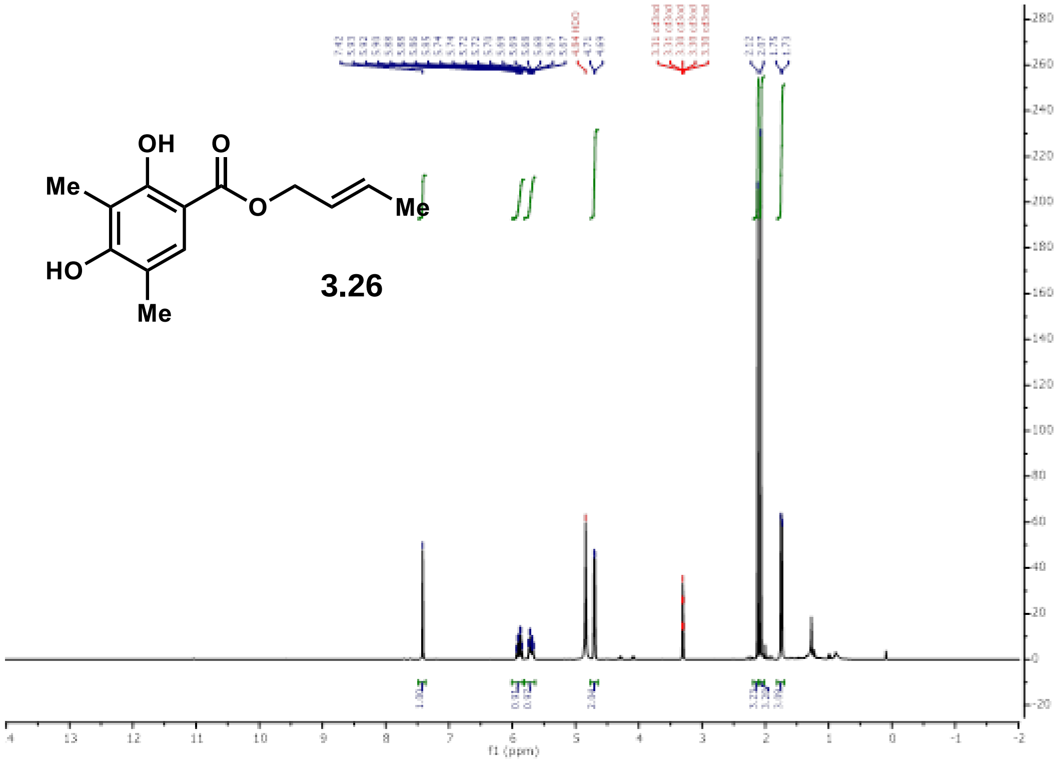

OH
O
Me
O
Me
HO
Me
7.42
4.84 H2O
4.71
4.69
2.12
2.07
1.75
1.73
1.00
0.91
0.92
2.04
f1 (ppm)

3.26

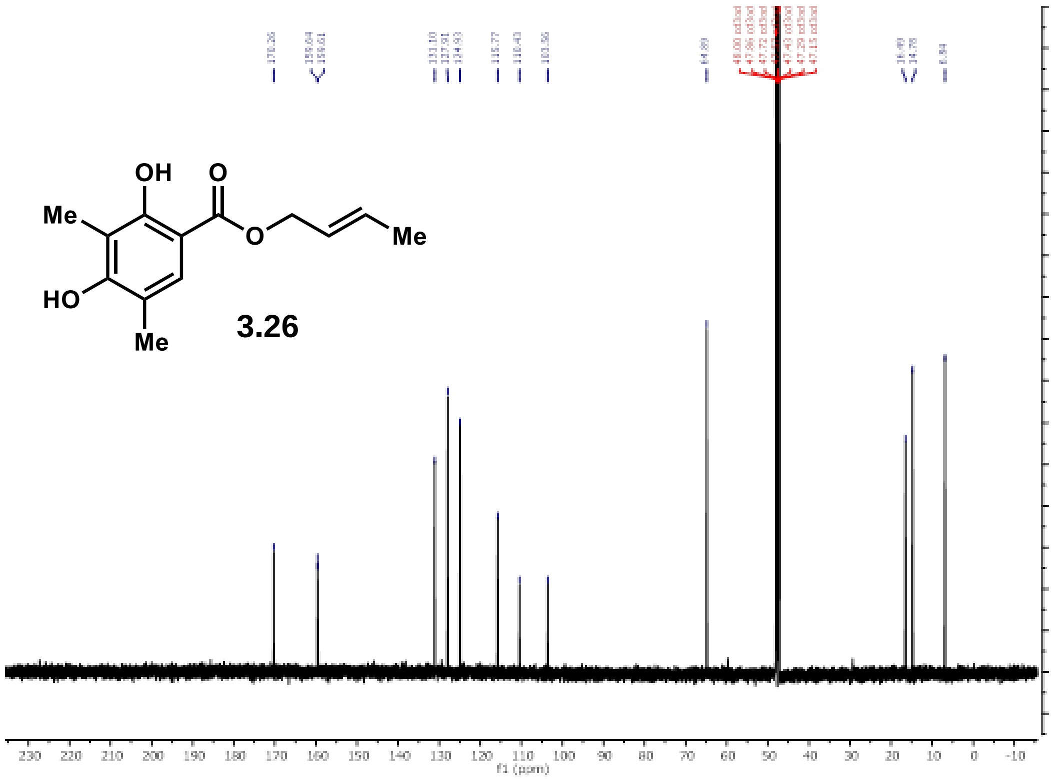

OH
O
Me
O
Me
HO
Me
170.26
131.10
127.91
124.93
115.77
110.43
103.56
64.89
16.49
14.78
6.84
f1 (ppm)

3.26

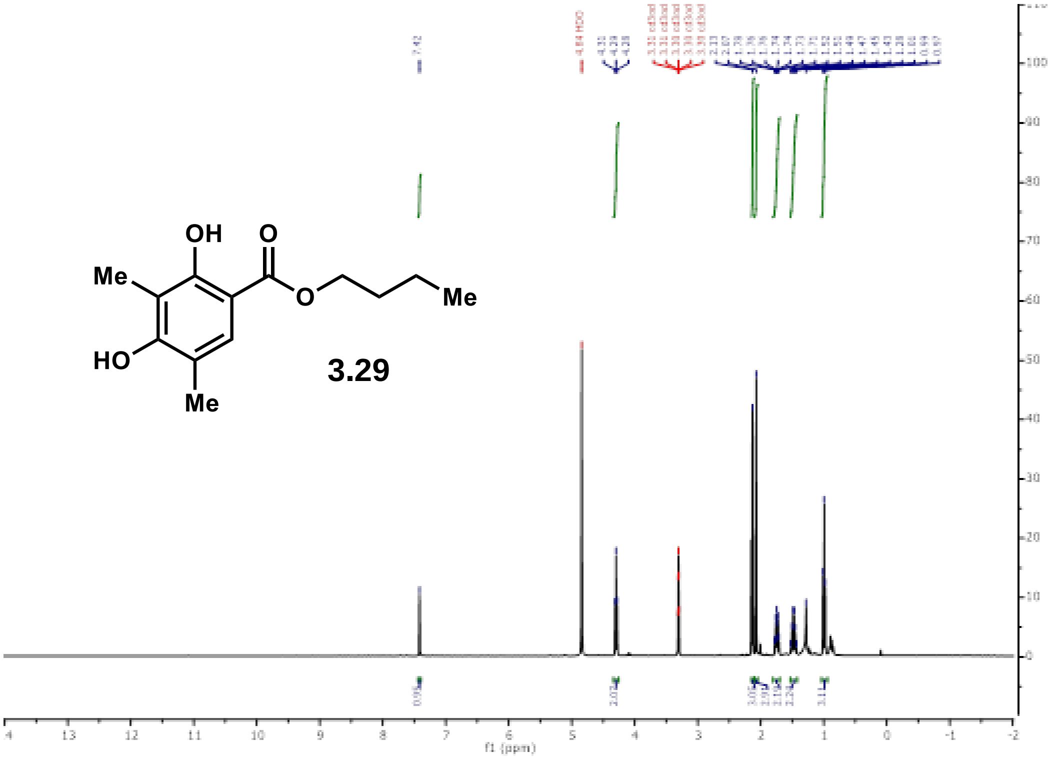
OH
O
Me
O
Me
HO
Me
7.42
4.84 HDO
4.31
4.29
4.28
3.31 cd3od
3.31 cd3od
3.30 cd3od
3.30 cd3od
3.30 cd3od
0.95
2.02
3.03
2.97
2.19
2.24
3.11
f1 (ppm)

3.29

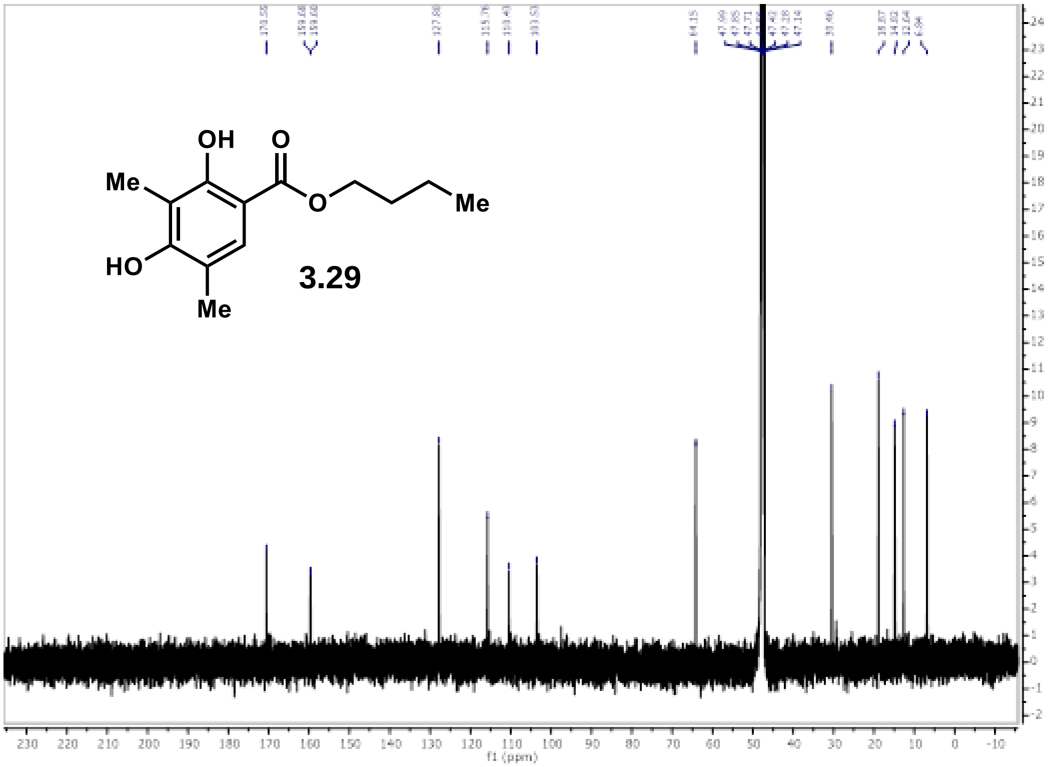
OH
O
Me
O
Me
HO
Me
170.55
159.68
159.60
127.88
115.76
110.43
103.53
64.15
30.46
18.87
14.02
12.64
6.84
f1 (ppm)

3.29

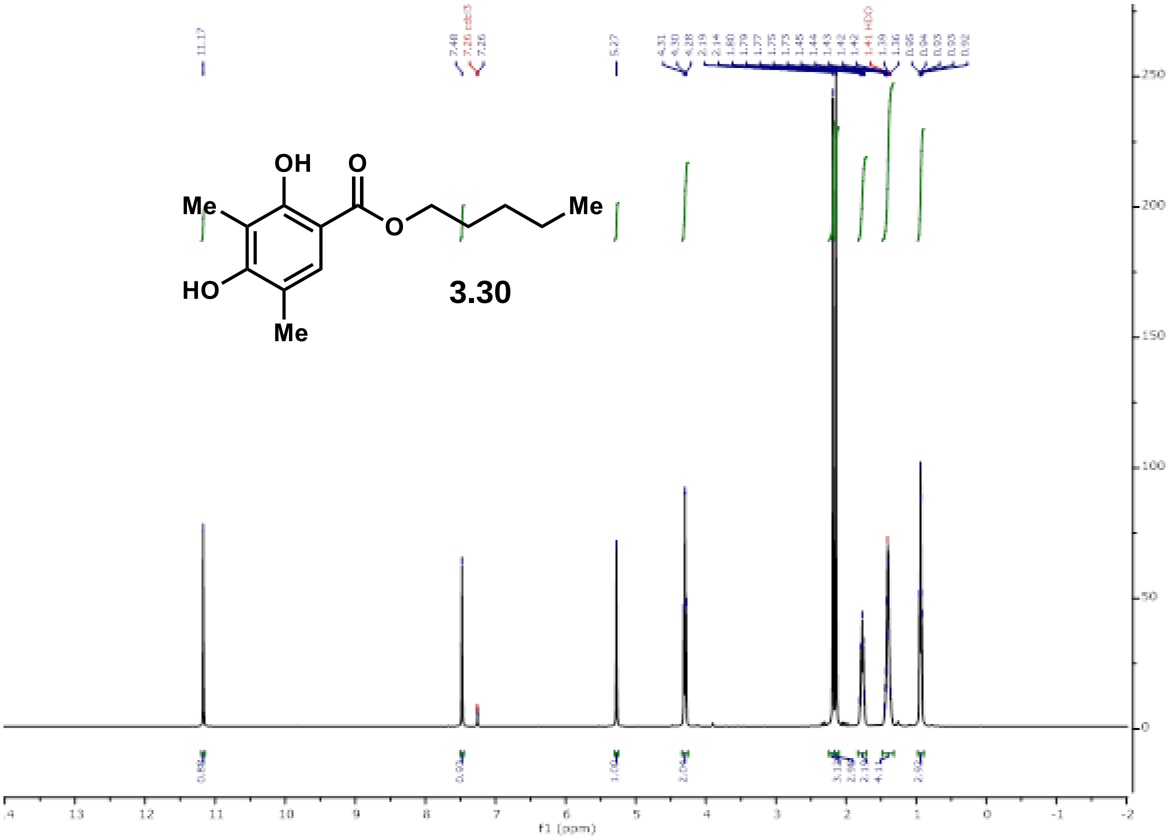

11.17
7.48
7.26 cdcl3
7.26
5.27
4.31
4.30
4.28
2.19
2.14
1.80
1.79
1.77
1.75
1.73
1.45
1.44
1.43
1.42
1.42
1.41 HDO
1.39
1.36
0.96
0.94
0.93
0.93
0.92
OH
O
Me
O
Me
HO
Me
Me
3.30
0.88
0.92
1.00
2.04
2.19
2.92
250
200
150
100
50
0
14
13
12
11
10
9
8
7
6
5
4
3
2
1
0
-1
-2
f1 (ppm)

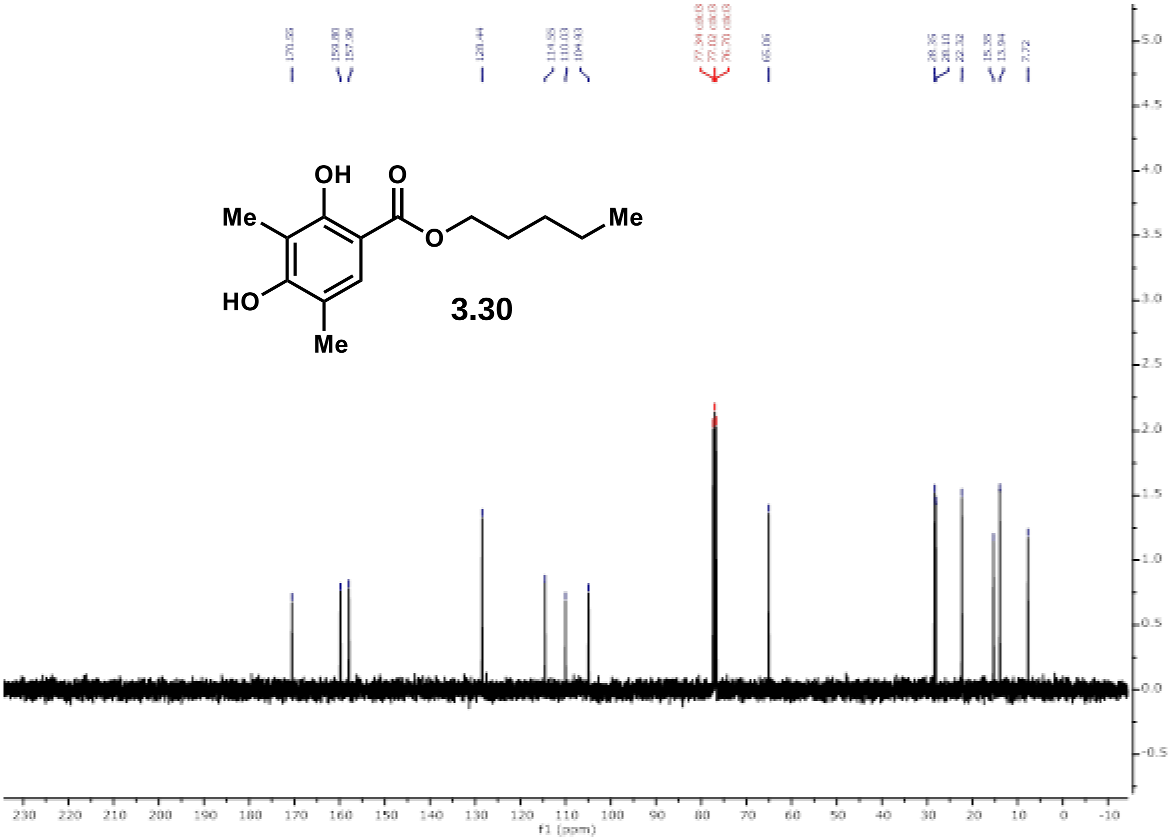

170.55
159.80
157.96
128.44
114.55
110.03
104.93
77.34 cdcl3
77.02 cdcl3
76.70 cdcl3
65.06
28.35
28.10
22.32
15.38
13.94
7.72
OH
O
Me
O
Me
HO
Me
Me
3.30
5.0
4.5
4.0
3.5
3.0
2.5
2.0
1.5
1.0
0.5
0.0
-0.5
230
220
210
200
190
180
170
160
150
140
130
120
110
100
90
80
70
60
50
40
30
20
10
0
-10
f1 (ppm)

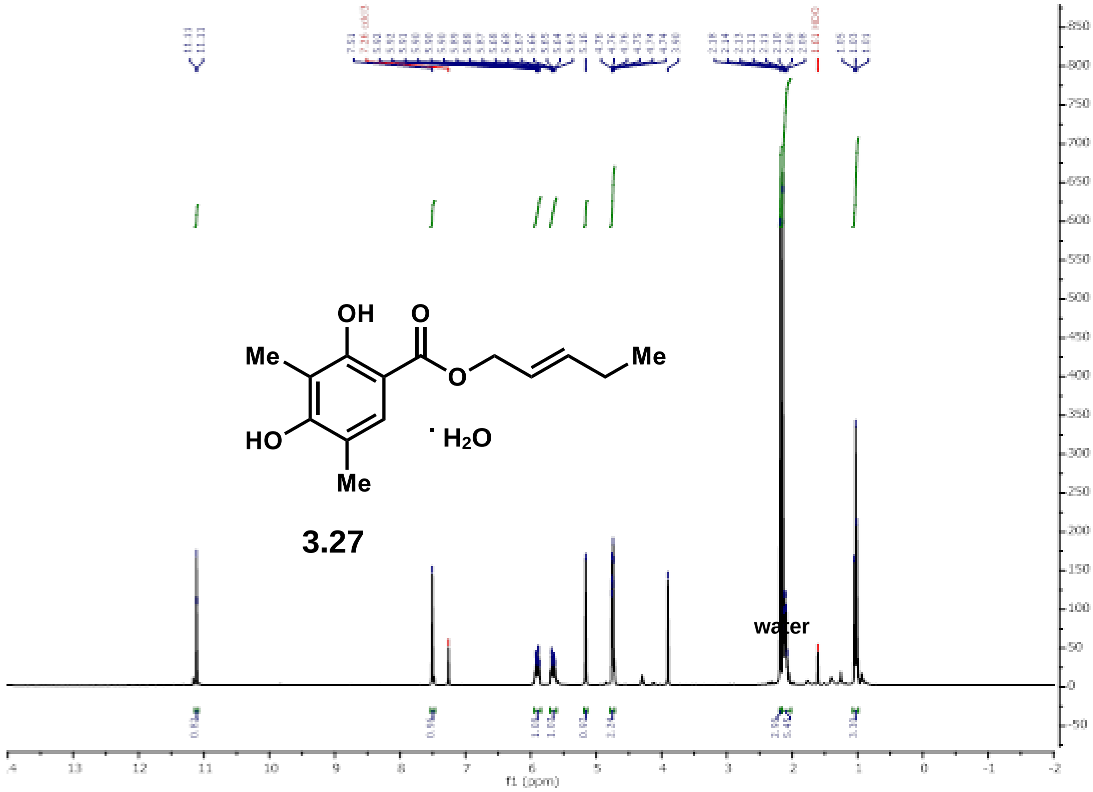

11.11
11.11
7.51
7.26 cdcl3
5.16
3.90
1.61 HDO
1.05
1.03
1.01
OH
O
Me
O
Me
HO
· H₂O
Me
3.27
water
0.84
0.94
1.00
1.03
0.92
1.24
2.95
5.42
3.10
f1 (ppm)

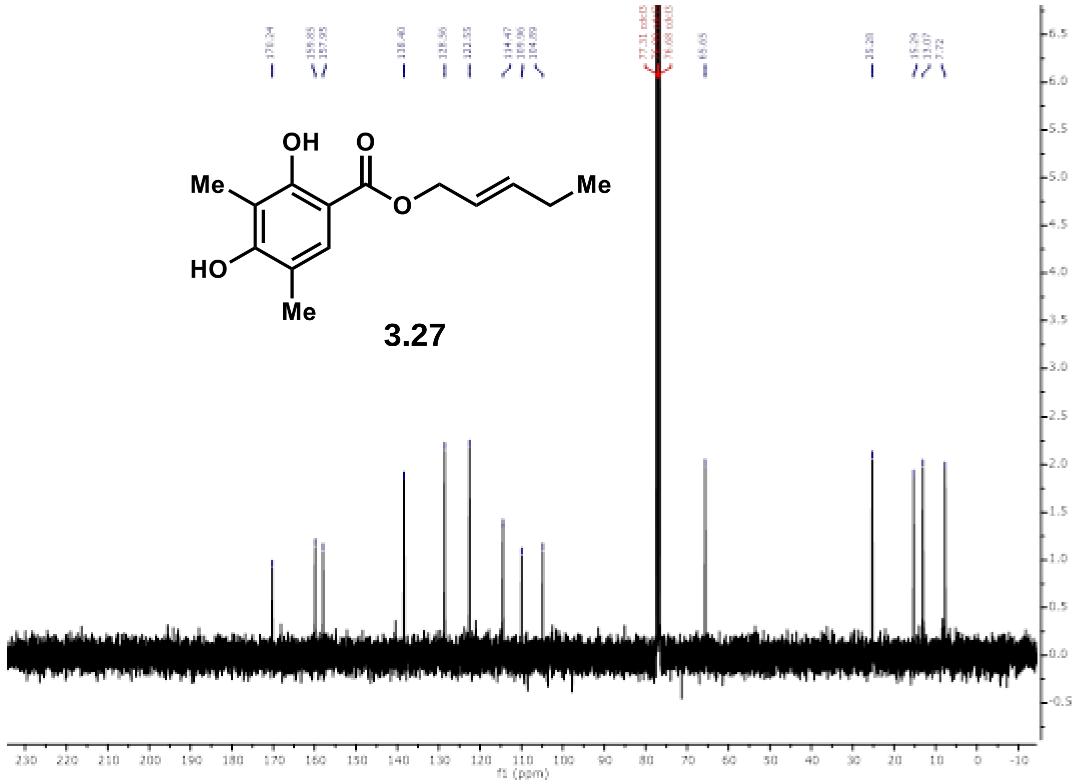

170.24
159.85
157.95
138.40
128.56
122.55
114.47
109.96
104.89
77.31 cdcl3
76.68 cdcl3
65.65
25.28
15.29
13.07
7.72
OH
O
Me
O
Me
HO
Me
3.27
f1 (ppm)

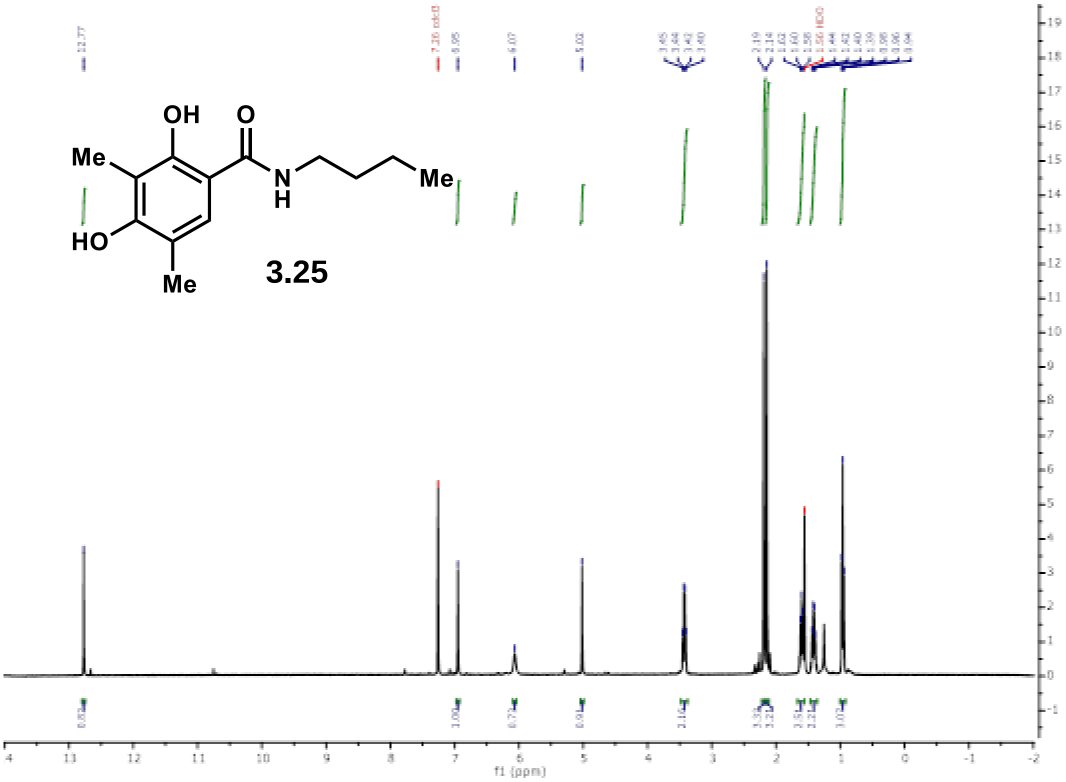
OH
O
Me
N
H
Me
HO
Me
12.77
7.26 cdcl3
6.95
6.07
5.02
3.45
3.44
3.42
3.40
2.19
2.14
1.62
1.60
1.58
1.56 HDO
1.44
1.42
1.40
1.39
0.96
0.96
0.94
0.92
1.00
0.72
0.91
2.16
3.35
3.28
2.54
2.28
3.03
f1 (ppm)

3.25

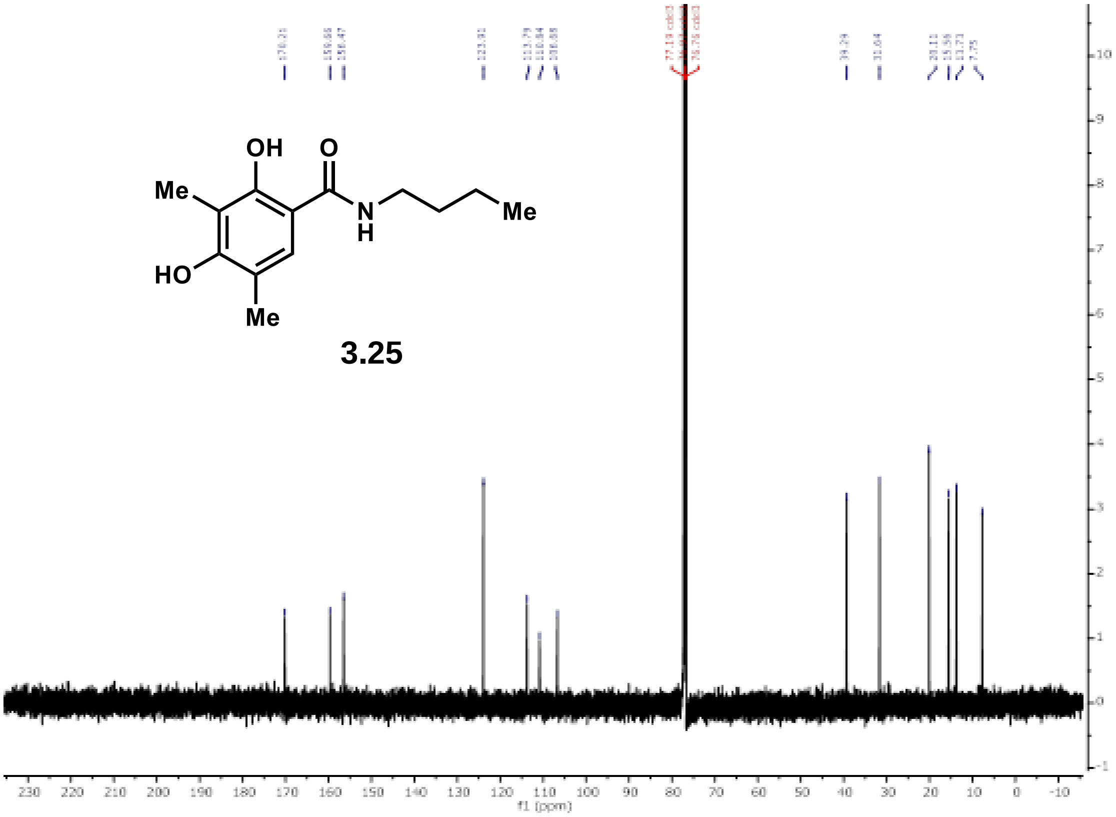
170.21
159.66
156.47
123.91
113.79
110.84
106.88
77.18 cdcl3
76.93 cdcl3
76.76 cdcl3
39.29
31.64
20.11
15.56
13.71
7.75
OH
O
Me
N
H
Me
HO
Me
f1 (ppm)

3.25

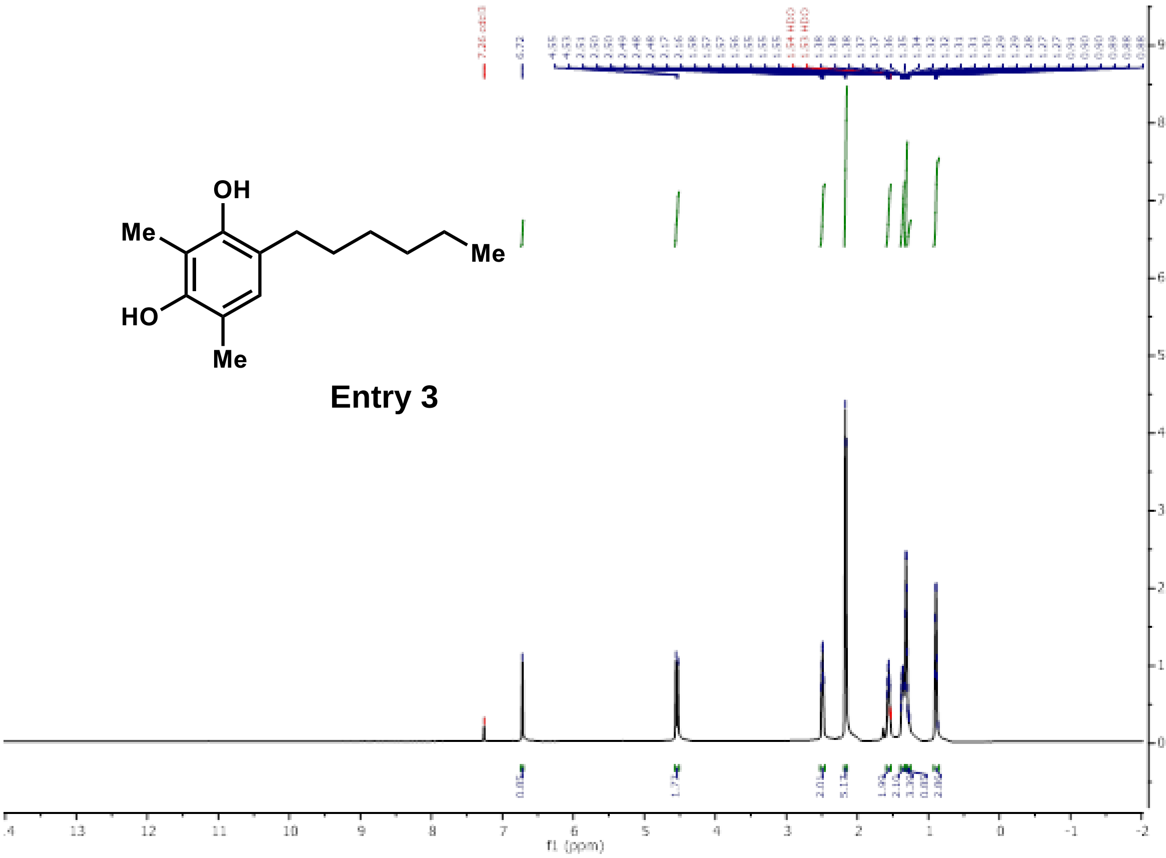

Entry 3

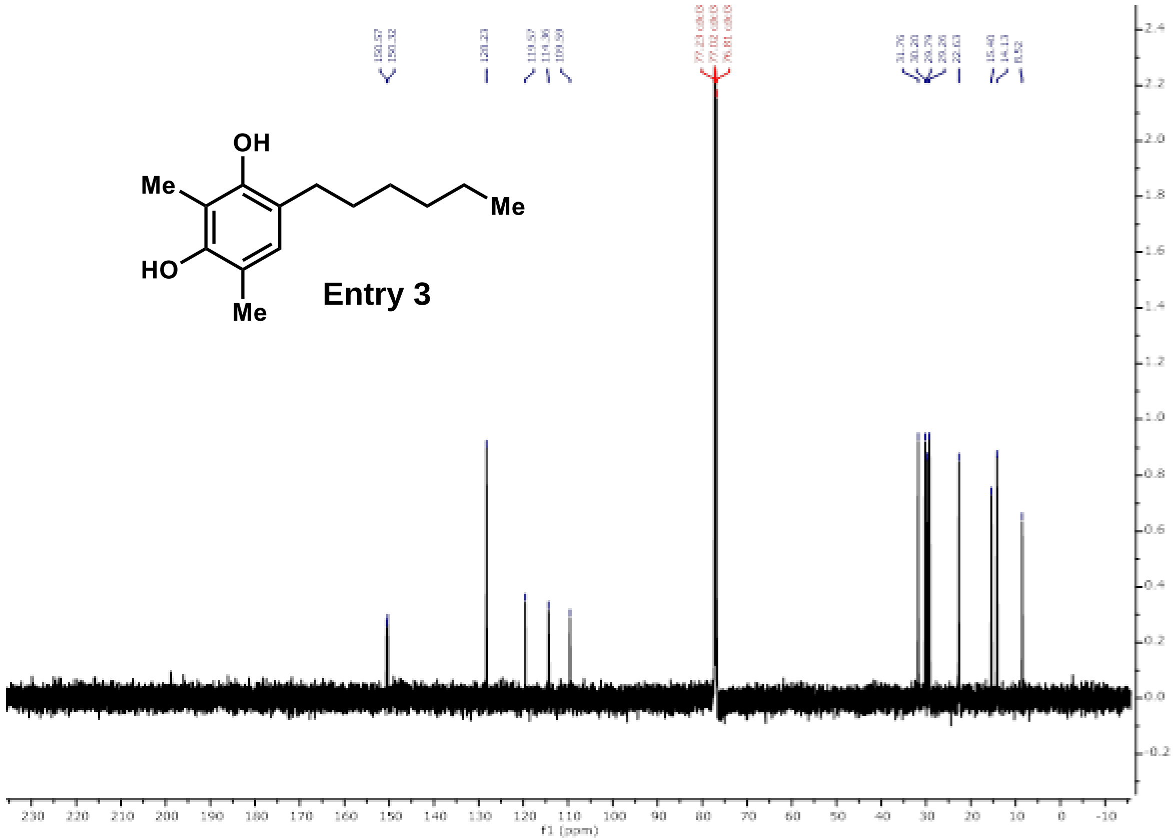

Entry 3

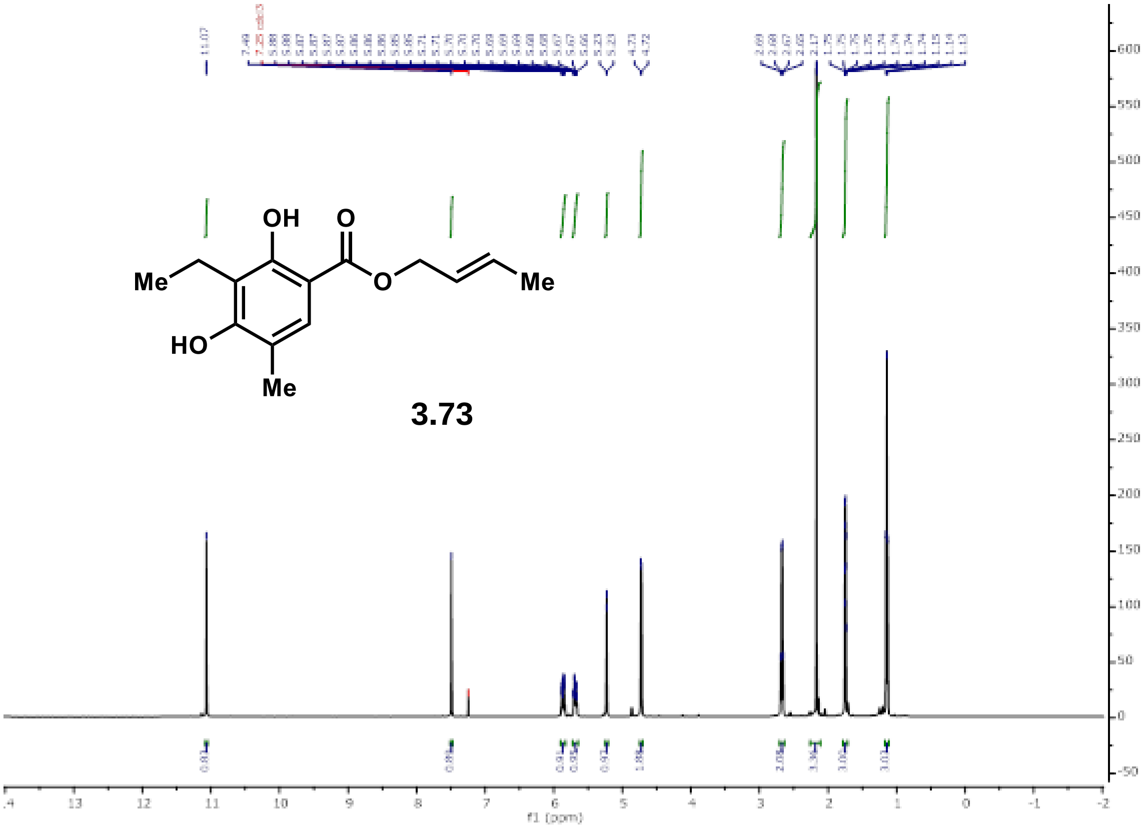
OH
O
Me
O
Me
HO
Me
11.07
7.49
7.26 cdcl3
5.23
4.73
4.72
2.69
2.68
2.67
2.65
2.17
1.75
1.14
1.13
0.81
0.88
0.91
0.94
0.97
1.88
2.05
3.36
3.01
3.01
f1 (ppm)

3.73

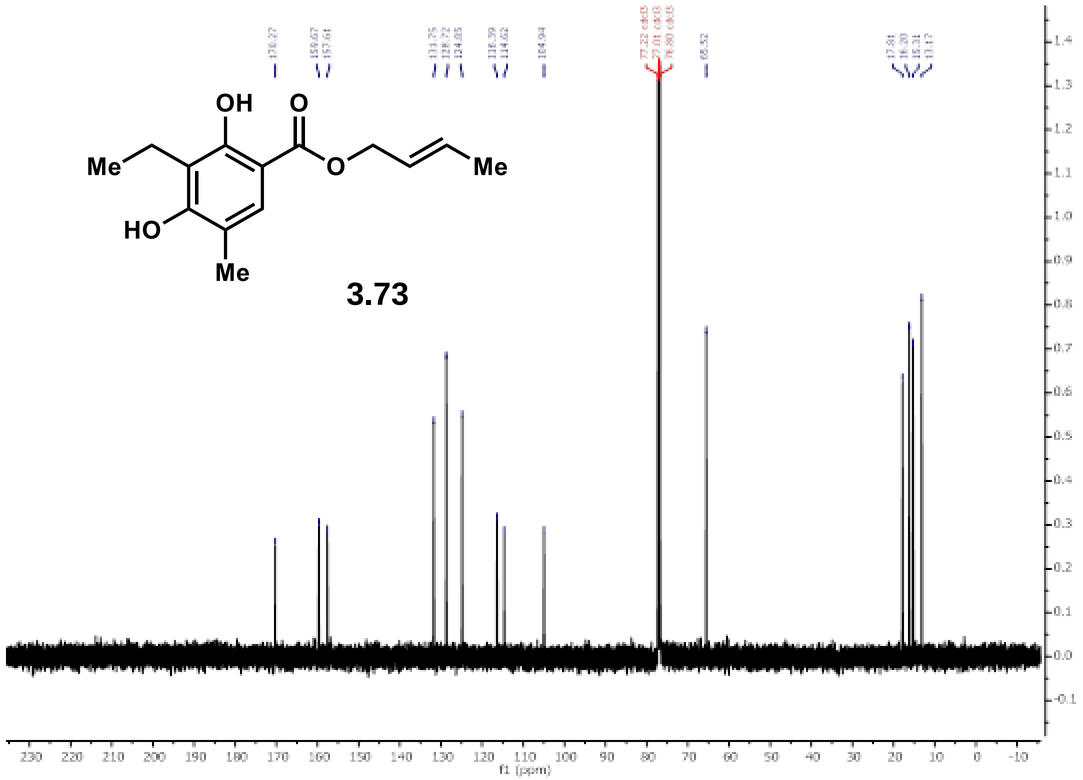
OH
O
Me
O
Me
HO
Me
170.27
159.67
157.61
131.75
128.72
124.85
115.59
114.62
104.94
77.22 cdcl3
77.01 cdcl3
76.80 cdcl3
65.52
17.81
16.20
15.31
13.17
f1 (ppm)

3.73

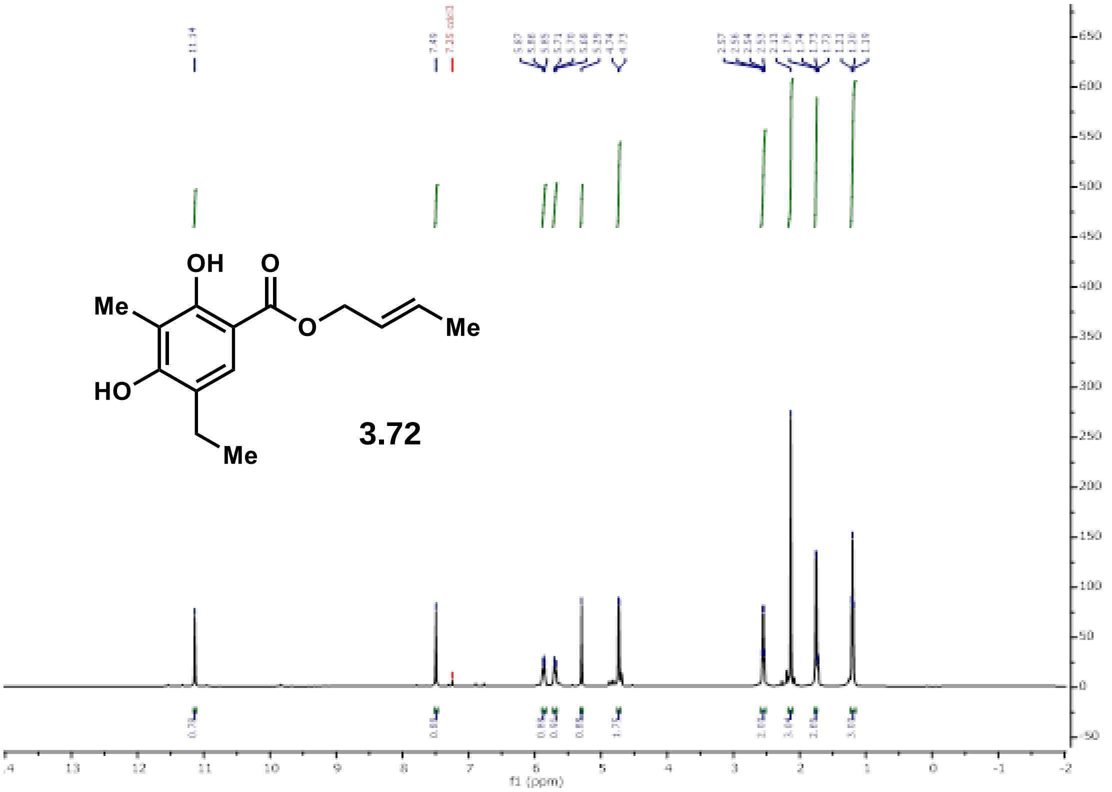
3.72

11.14
7.49
7.25 cdcl3
5.87
5.86
5.85
5.71
5.70
5.68
5.29
4.74
4.73
2.57
2.56
2.54
2.53
2.13
1.76
1.74
1.73
1.21
1.20
1.19
0.78
0.85
0.86
0.94
0.85
1.76
2.04
3.04
2.65
3.03
OH
O
Me
O
Me
HO
Me
650
600
550
500
450
400
350
300
250
200
150
100
50
0
-50
14
13
12
11
10
9
8
7
6
5
4
3
2
1
0
-1
-2
f1 (ppm)

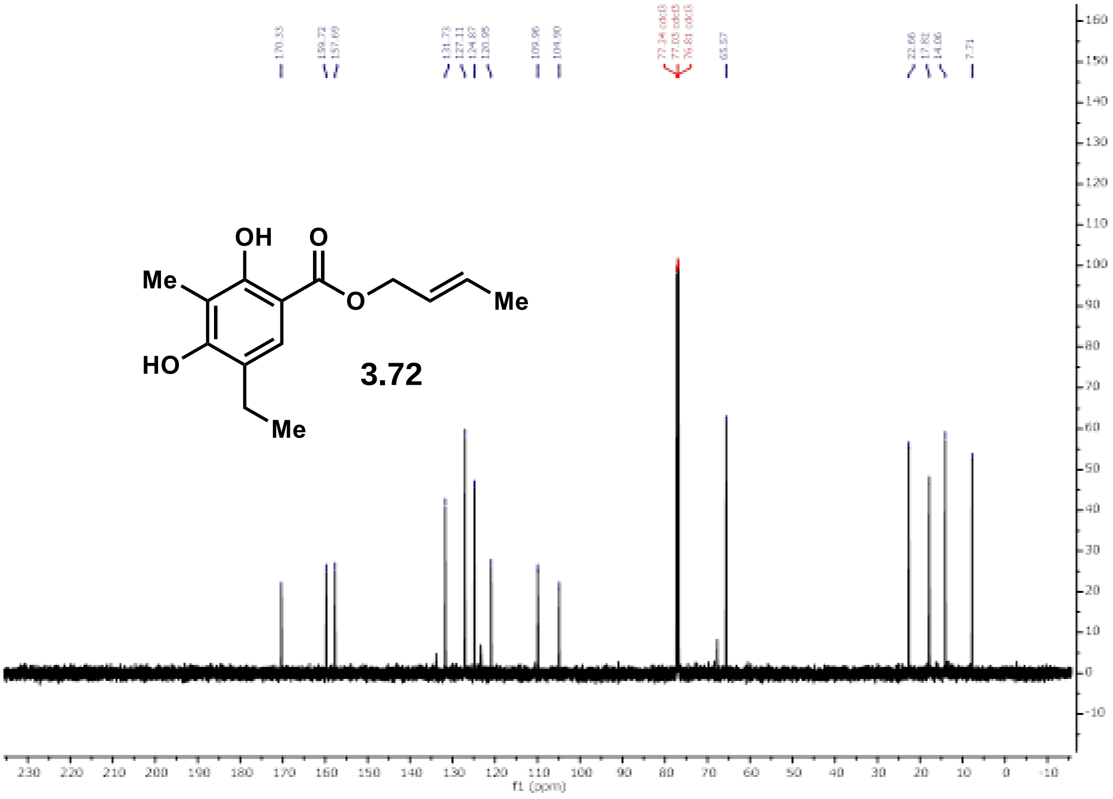
3.72

170.53
159.72
157.69
131.73
127.11
124.87
120.95
109.96
104.90
77.34 cdcl3
77.03 cdcl3
76.81 cdcl3
65.57
22.66
17.82
14.06
7.71
OH
O
Me
O
Me
HO
Me
160
150
140
130
120
110
100
90
80
70
60
50
40
30
20
10
0
-10
230
220
210
200
190
180
170
160
150
140
130
120
110
100
90
80
70
60
50
40
30
20
10
0
-10
f1 (ppm)

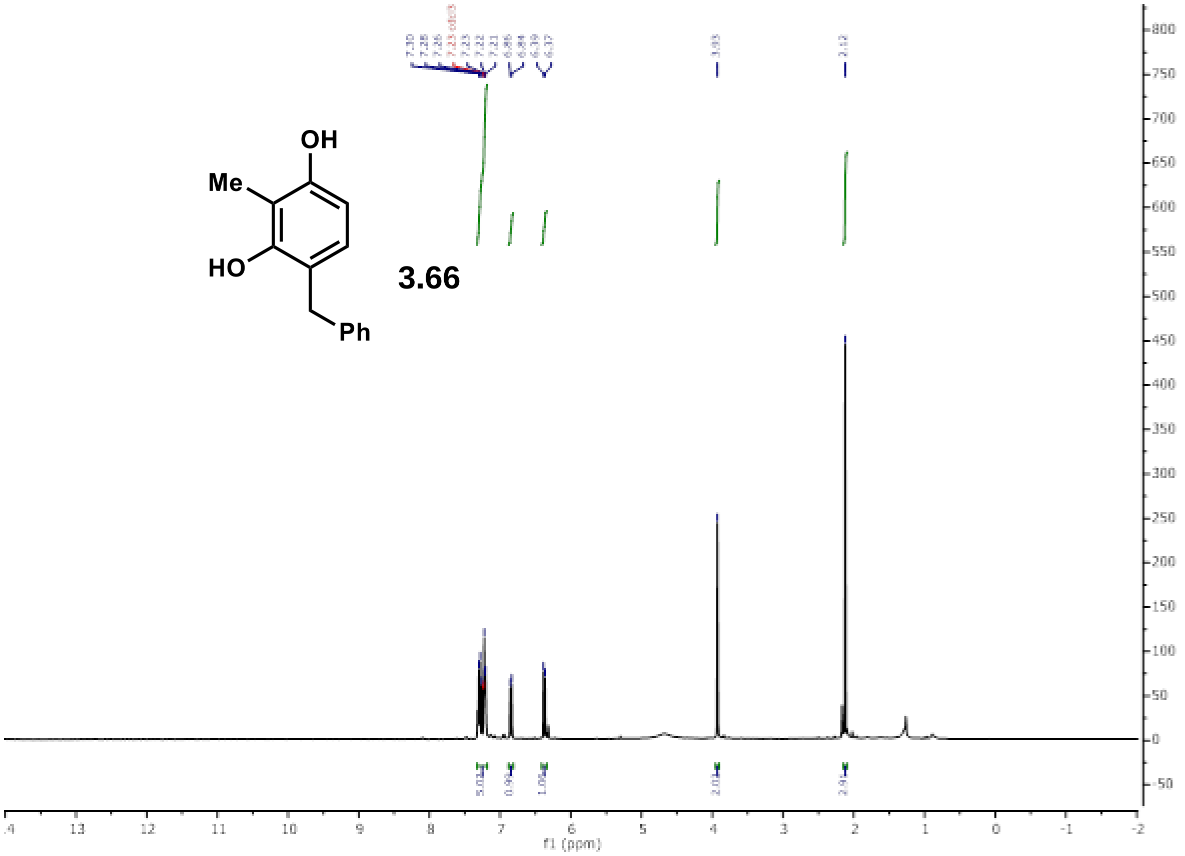
OH
Me
HO
Ph
3.66
7.30
7.28
7.26
7.23 cdcl3
7.23
7.22
7.21
6.86
6.84
6.39
6.37
3.93
2.12
5.02
0.96
1.05
2.01
2.94
14
13
12
11
10
9
8
7
6
5
4
3
2
1
0
-1
-2
f1 (ppm)
800
750
700
650
600
550
500
450
400
350
300
250
200
150
100
50
0
-50

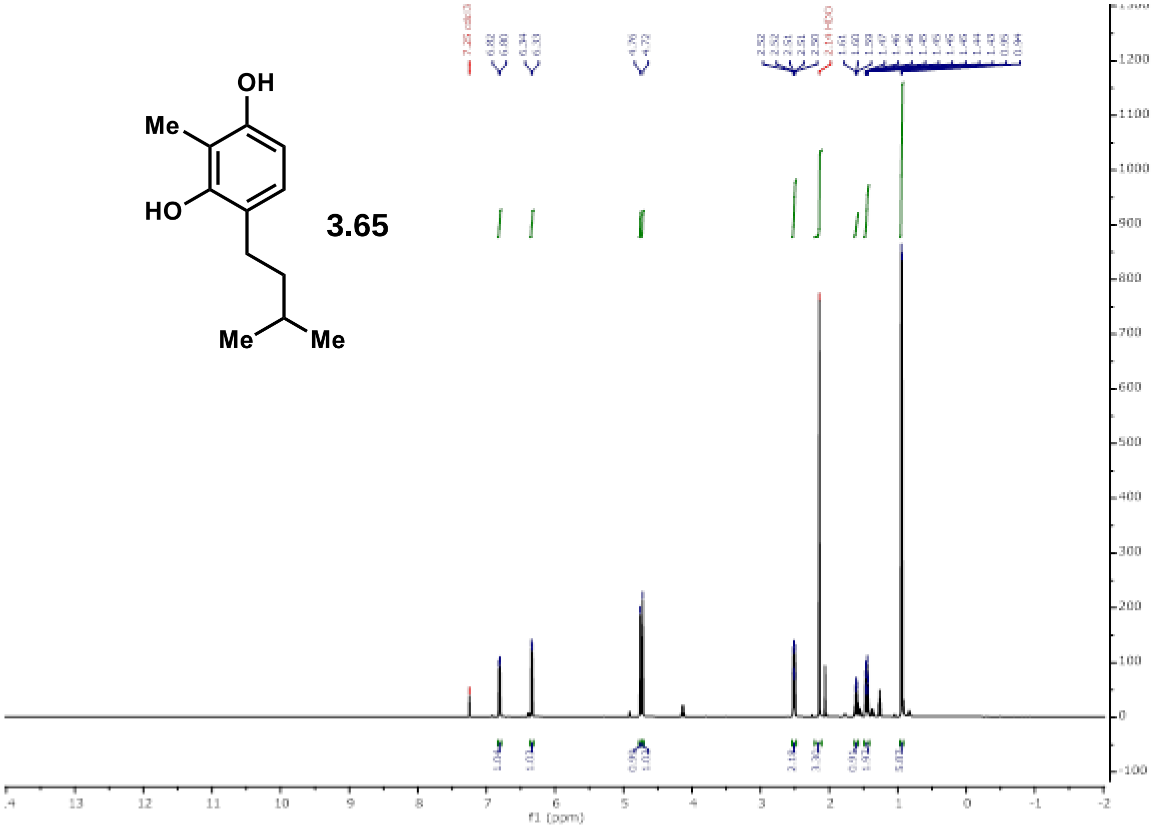
3.65
OH
Me
HO
Me
Me
7.26 cdcl3
6.82
6.80
6.34
6.33
4.76
4.72
2.52
2.52
2.51
2.51
2.50
2.14 HDO
1.61
1.60
1.59
1.47
1.46
1.46
1.45
1.45
1.45
1.45
1.44
1.43
0.95
0.94
1.04
1.01
0.99
1.03
2.18
3.30
0.91
1.94
5.87
14
13
12
11
10
9
8
7
6
5
4
3
2
1
0
-1
-2
f1 (ppm)
1300
1200
1100
1000
900
800
700
600
500
400
300
200
100
0
-100

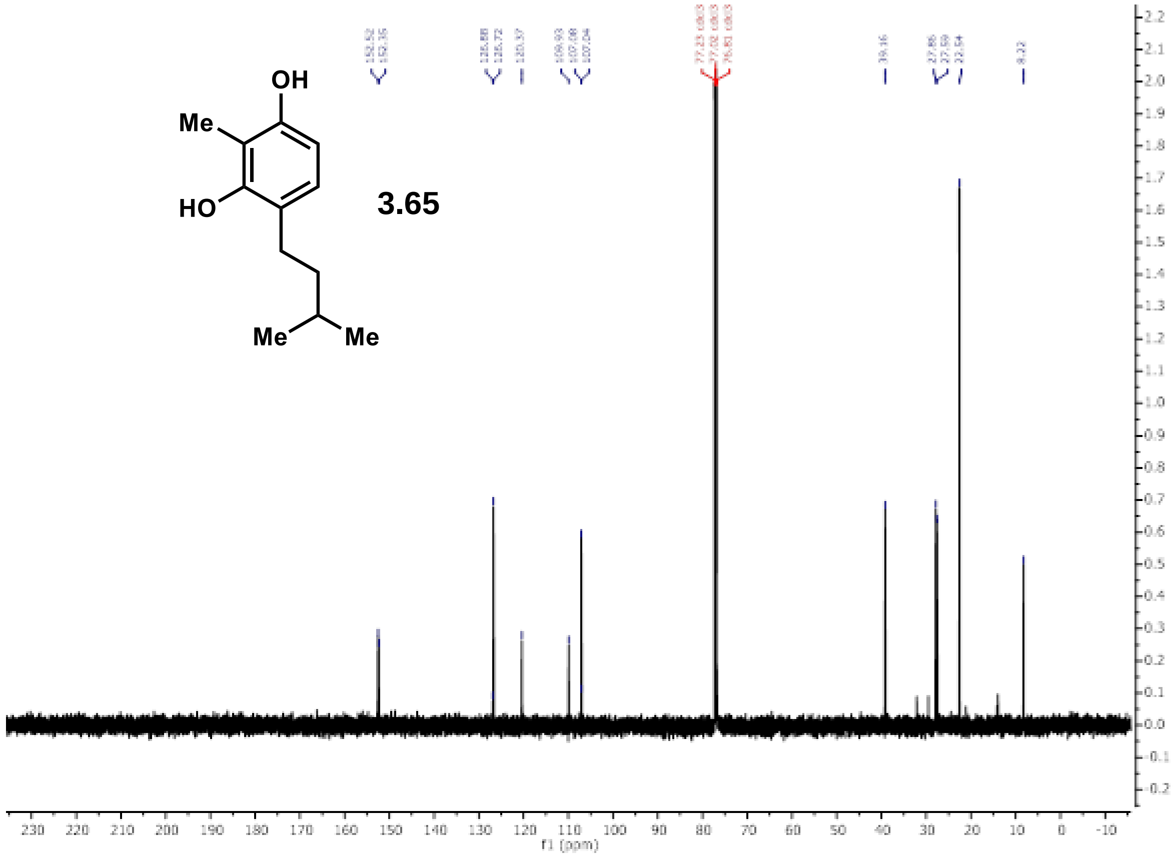
3.65
OH
Me
HO
Me
Me
152.52
152.35
126.88
126.72
120.37
109.93
107.08
107.04
77.23 cdcl3
77.02 cdcl3
76.81 cdcl3
39.16
27.86
27.69
22.54
8.22
230
220
210
200
190
180
170
160
150
140
130
120
110
100
90
80
70
60
50
40
30
20
10
0
-10
f1 (ppm)
2.2
2.1
2.0
1.9
1.8
1.7
1.6
1.5
1.4
1.3
1.2
1.1
1.0
0.9
0.8
0.7
0.6
0.5
0.4
0.3
0.2
0.1
0.0
-0.1
-0.2

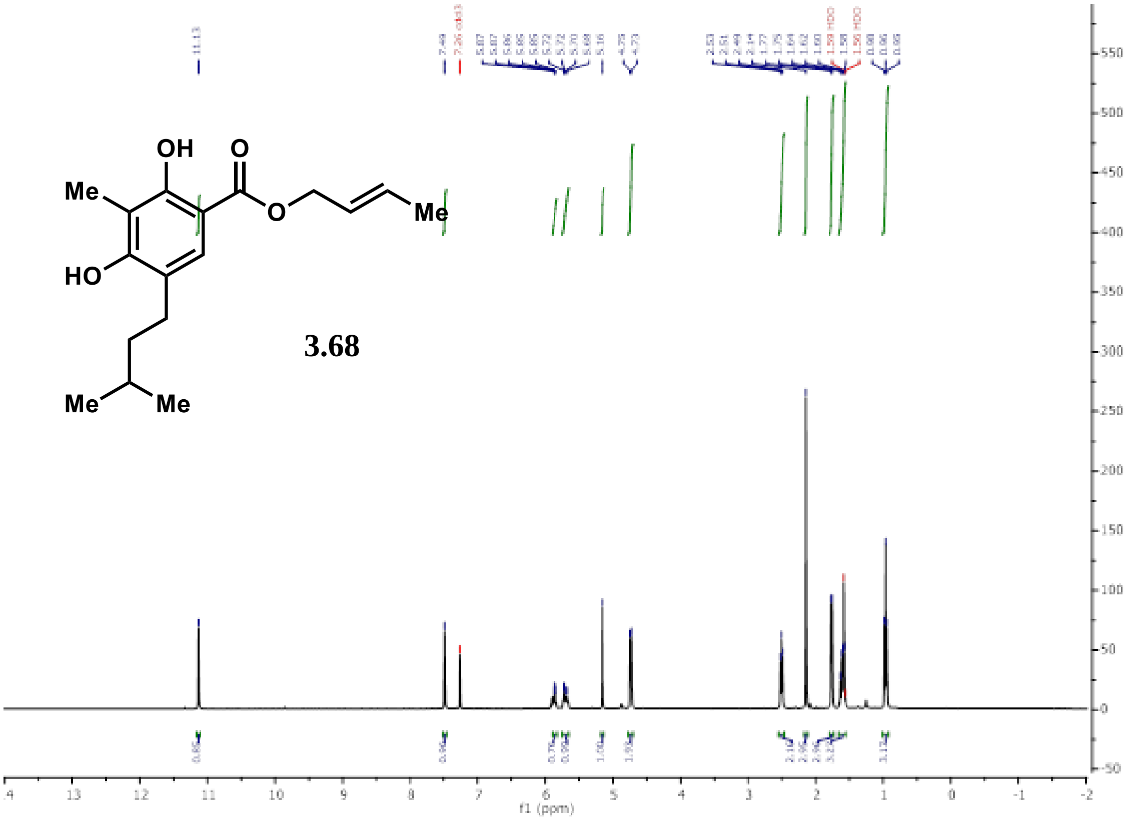
11.13
7.49
7.26 cdcl3
5.87
5.87
5.86
5.85
5.85
5.72
5.72
5.70
5.68
5.16
4.75
4.73
2.53
2.51
2.49
2.14
1.77
1.75
1.64
1.62
1.60
1.59 HDO
1.58
1.56 HDO
0.98
0.96
0.95
OH
O
Me
O
Me
HO
Me
Me
0.85
0.96
0.75
0.94
1.04
1.93
2.10
2.96
2.94
3.27
3.11
14
13
12
11
10
9
8
7
6
5
4
3
2
1
0
-1
-2
f1 (ppm)
550
500
450
400
350
300
250
200
150
100
50
0
-50

3.68

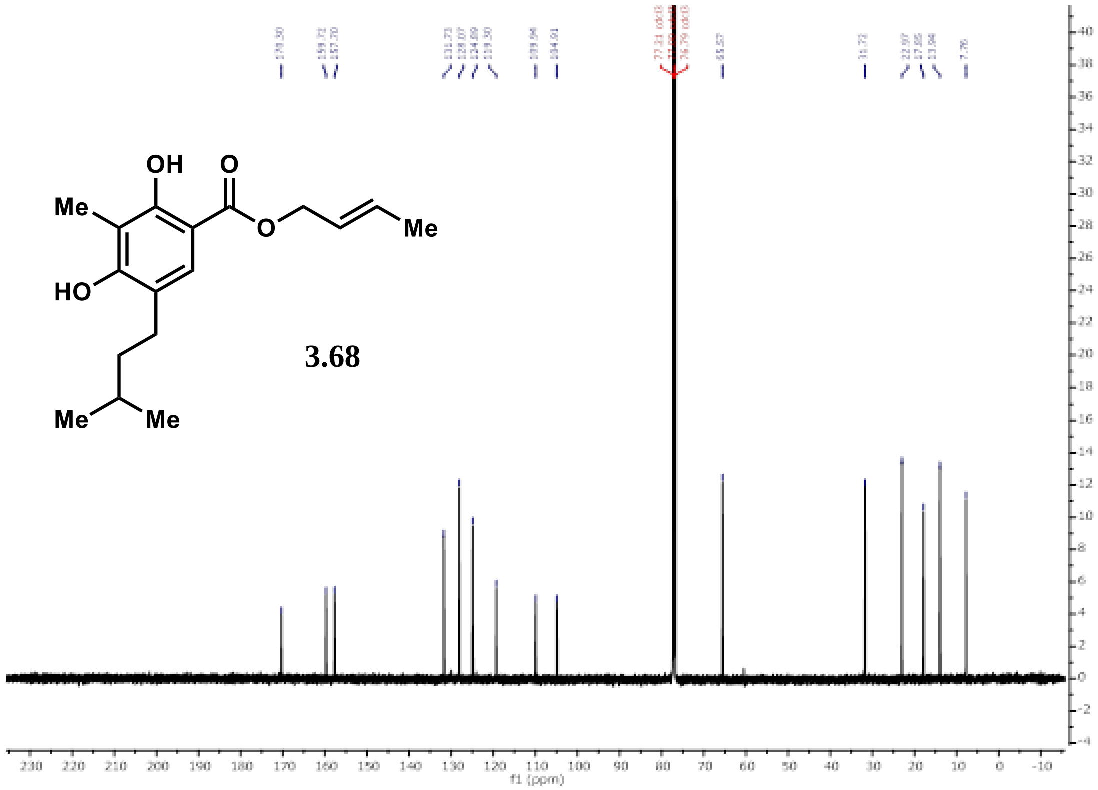
170.50
159.72
157.70
131.73
128.07
124.89
119.50
109.94
104.91
77.21 cdcl3
77.00 cdcl3
76.79 cdcl3
65.57
31.72
22.97
17.65
13.94
7.76
OH
O
Me
O
Me
HO
Me
Me
230
220
210
200
190
180
170
160
150
140
130
120
110
100
90
80
70
60
50
40
30
20
10
0
-10
f1 (ppm)
40
38
36
34
32
30
28
26
24
22
20
18
16
14
12
10
8
6
4
2
0
-2
-4

3.68

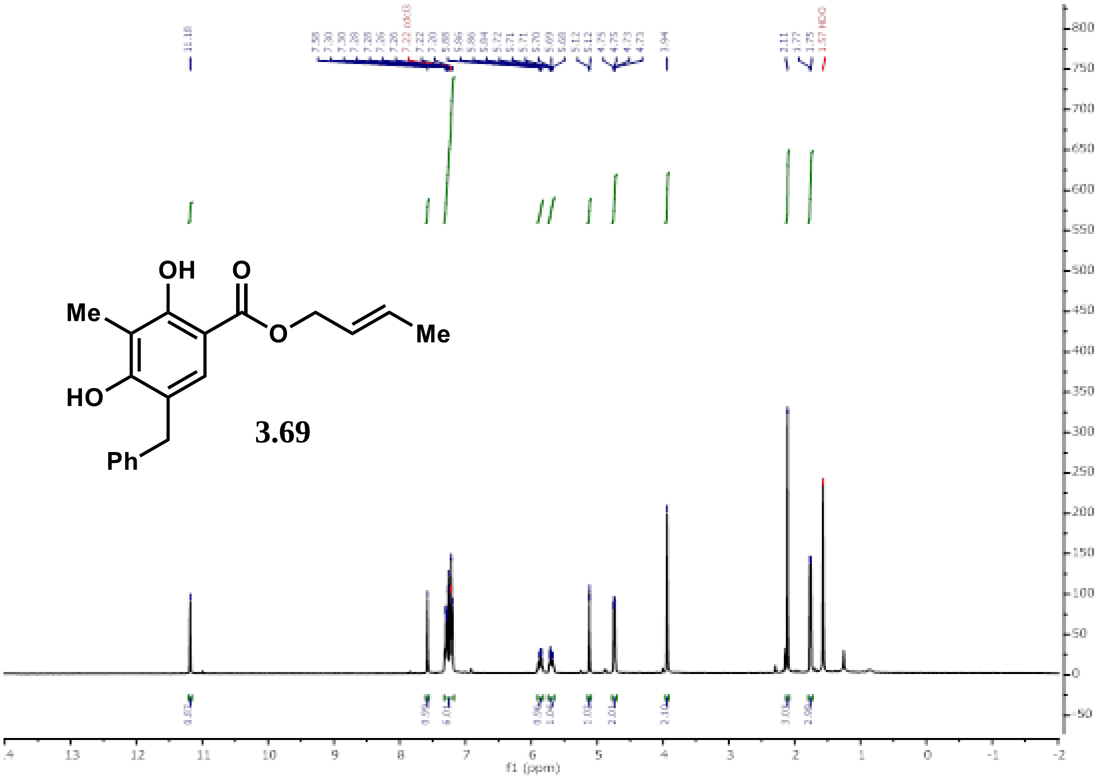

3.69

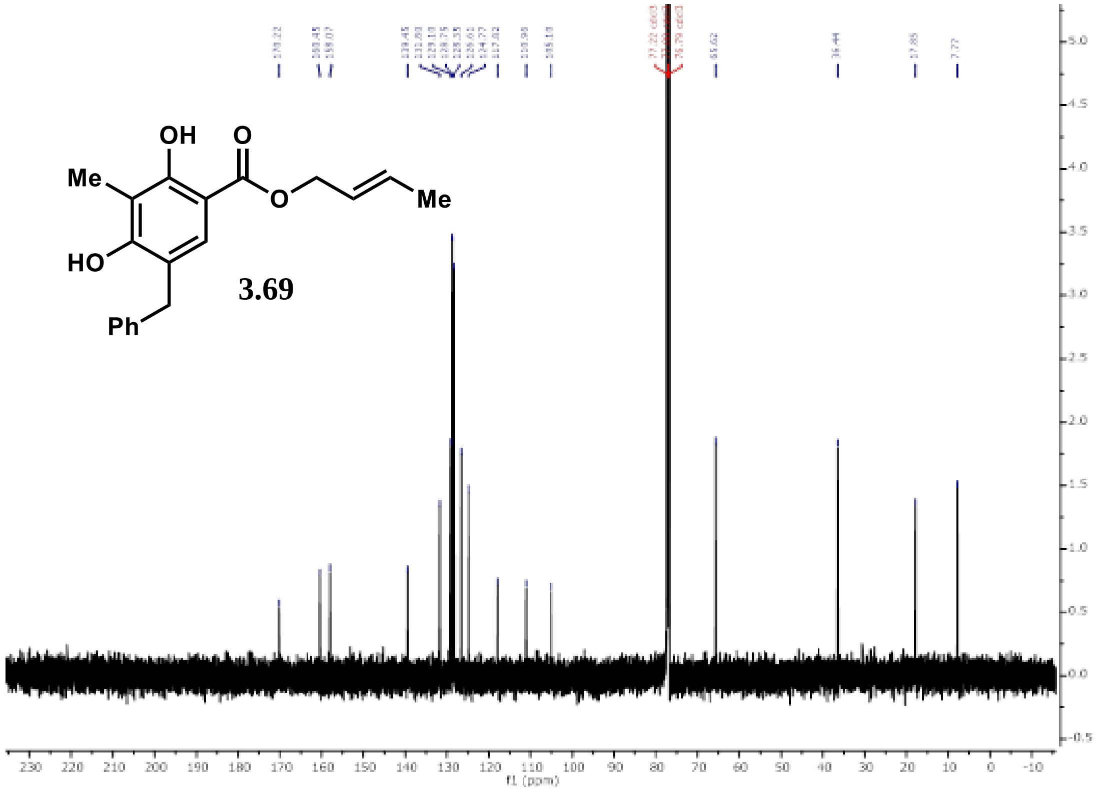

3.69

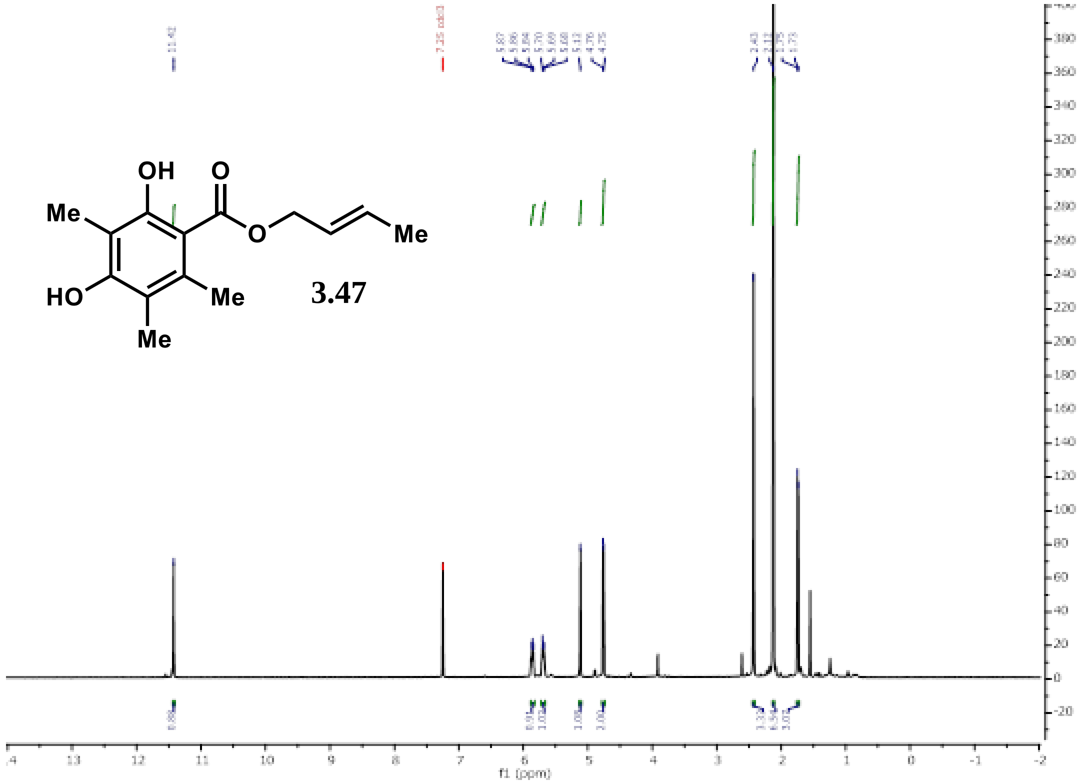
OH
O
Me
O
Me
HO
Me
Me
3.47
11.42
7.26 cdcl3
5.87
5.86
5.84
5.70
5.69
5.68
5.13
4.76
4.75
2.43
2.13
1.75
1.73
0.88
0.91
1.02
1.08
2.00
3.32
6.54
3.01
f1 (ppm)

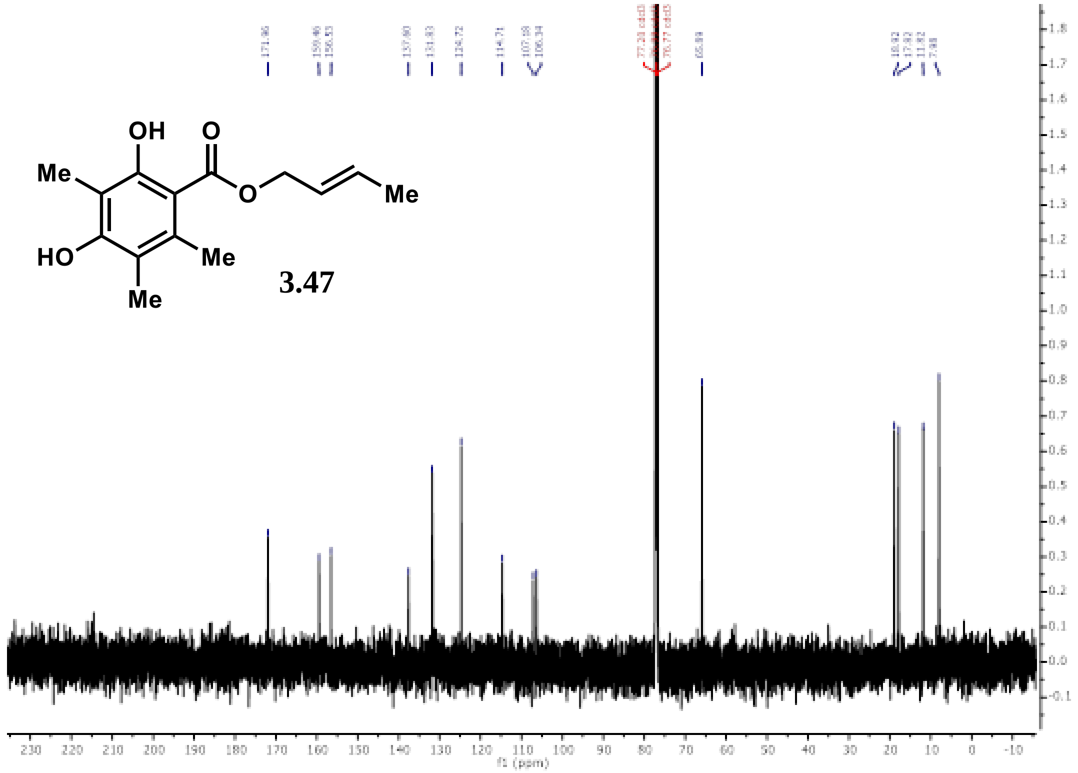
OH
O
Me
O
Me
HO
Me
Me
3.47
171.96
159.46
156.53
137.90
131.83
124.72
114.71
107.18
106.34
77.20 cdcl3
76.77 cdcl3
65.89
18.32
17.82
11.82
7.88
f1 (ppm)

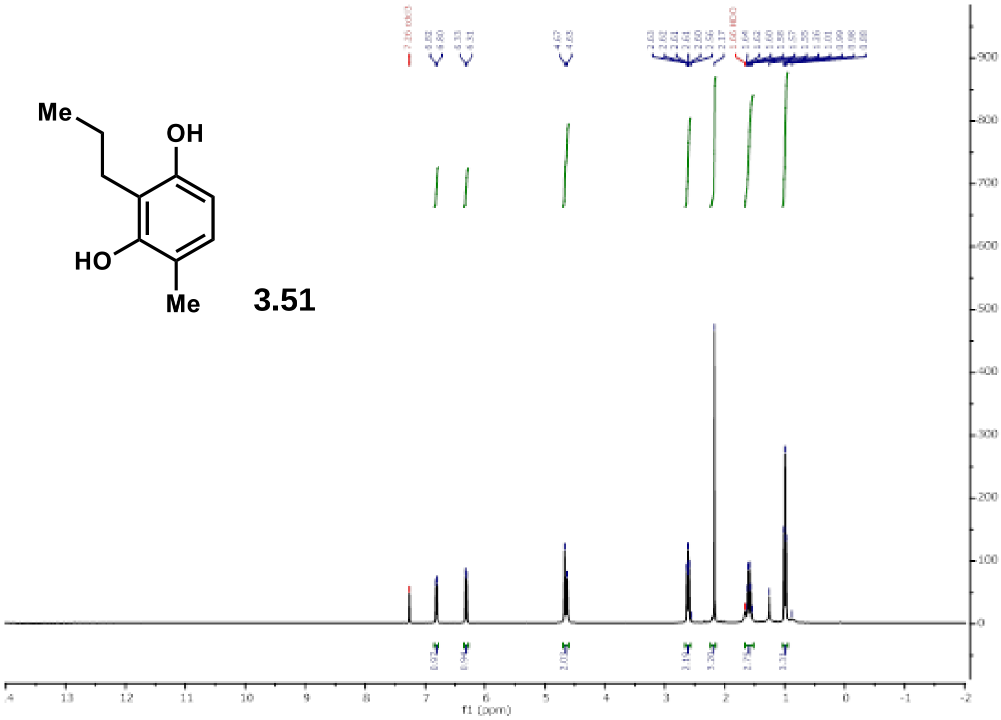
Me
OH
HO
Me
7.26 cdcl3
6.82
6.80
6.33
6.31
4.67
4.63
2.63
2.62
2.61
2.61
2.60
2.56
2.17
1.66 HDO
1.64
1.62
1.60
1.58
1.57
1.55
1.36
1.01
0.99
0.98
0.88
0.97
0.94
2.03
3.14
3.20
2.76
3.11
900
800
700
600
500
400
300
200
100
0
14
13
12
11
10
9
8
7
6
5
4
3
2
1
0
-1
-2
f1 (ppm)

3.51

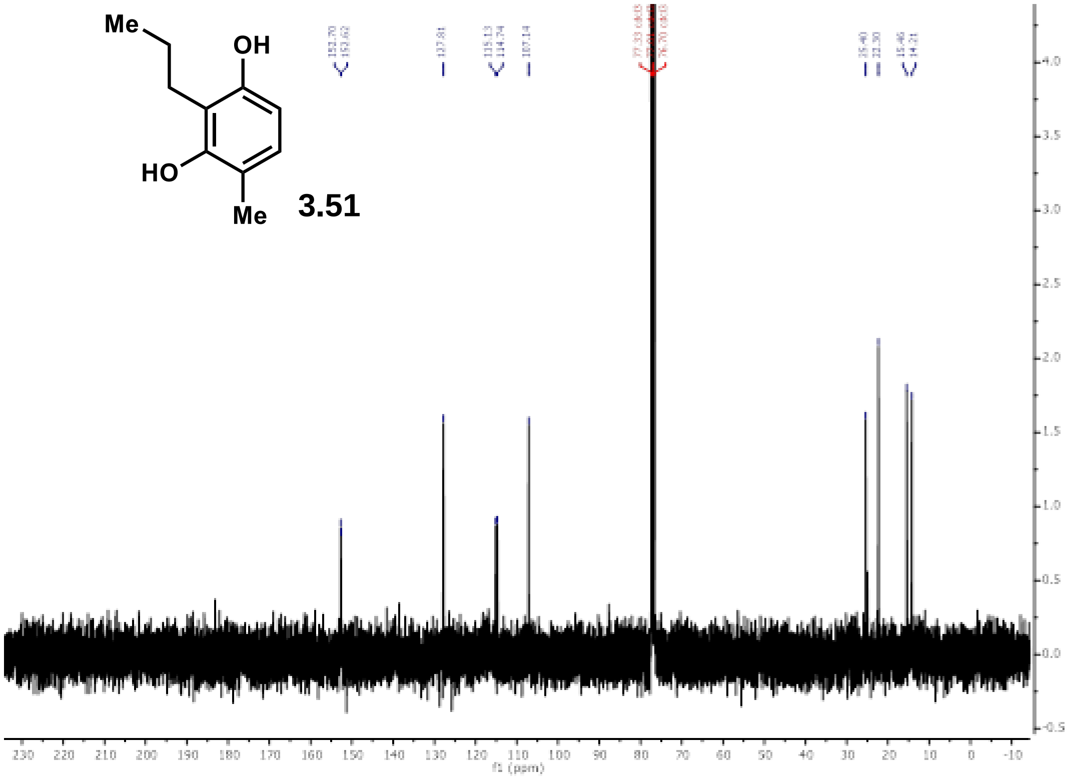
Me
OH
HO
Me
153.70
153.62
127.81
115.13
114.74
107.14
77.33 cdcl3
77.01 cdcl3
76.70 cdcl3
25.40
22.30
15.46
14.21
4.0
3.5
3.0
2.5
2.0
1.5
1.0
0.5
0.0
-0.5
230
220
210
200
190
180
170
160
150
140
130
120
110
100
90
80
70
60
50
40
30
20
10
0
-10
f1 (ppm)

3.51

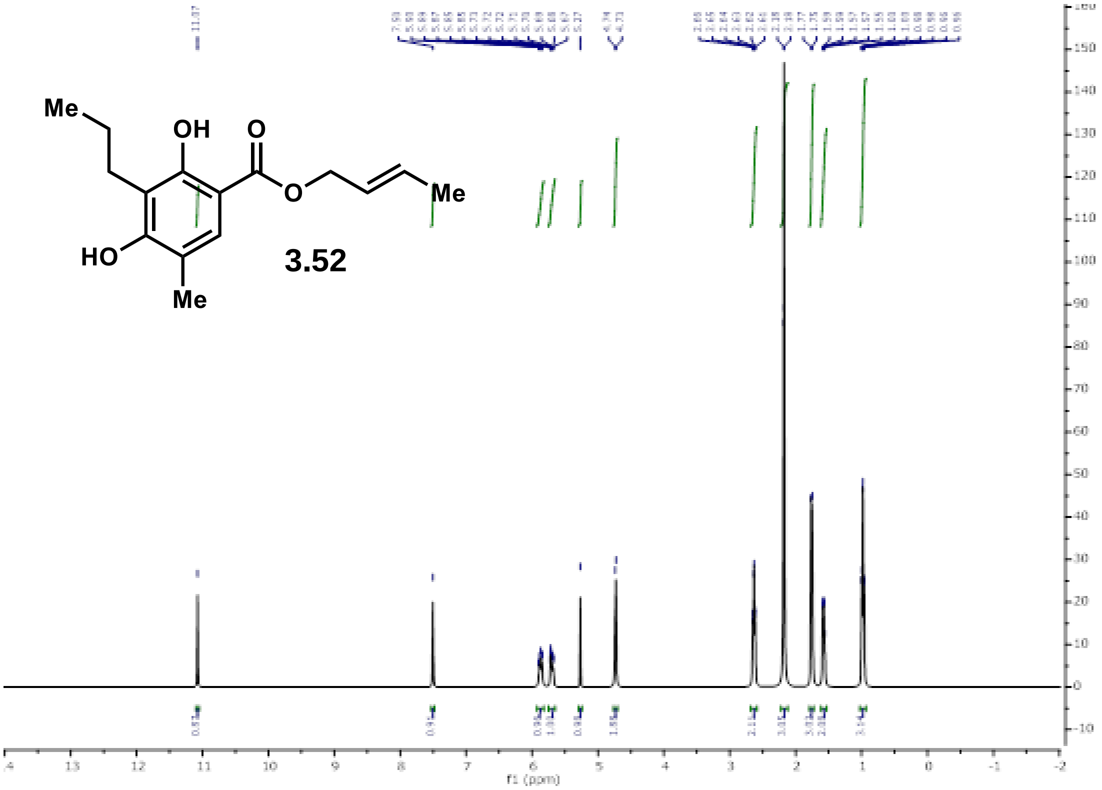

3.52

Me
OH
O
O
Me
HO
Me
11.07
4.74
4.73
f1 (ppm)

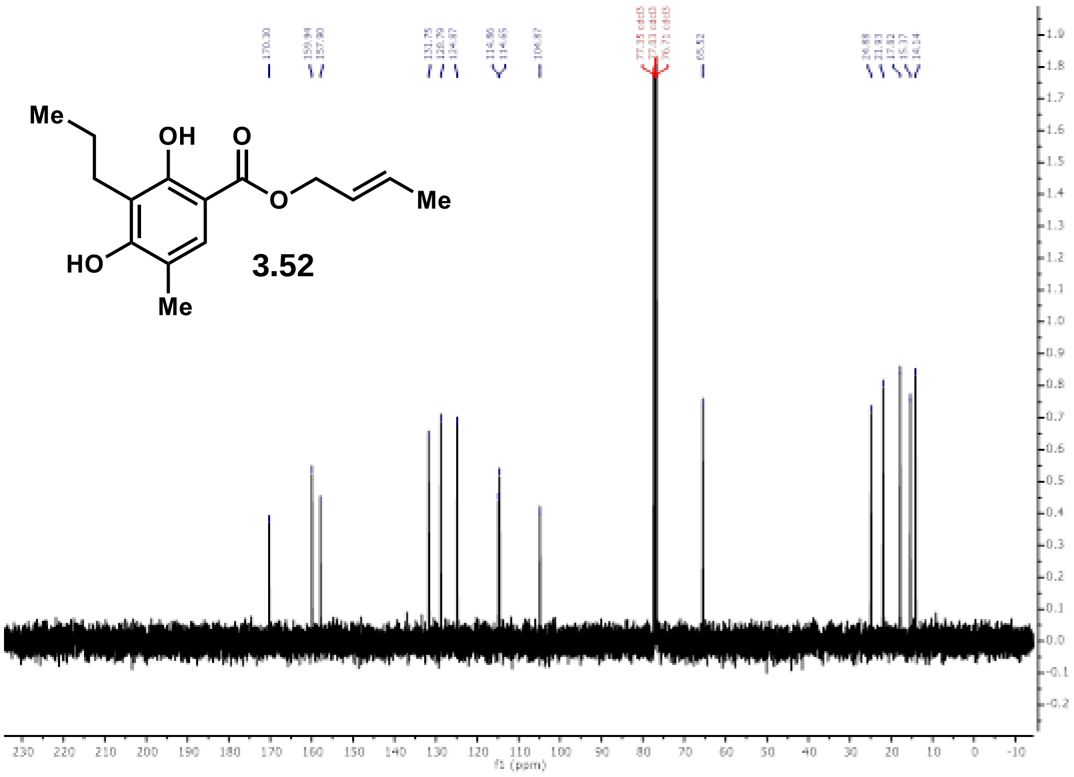

3.52

Me
OH
O
O
Me
HO
Me
170.30
159.94
157.80
131.75
128.79
124.87
114.86
114.65
104.87
77.35 cdcl3
77.03 cdcl3
76.71 cdcl3
65.52
24.88
21.83
17.82
15.37
14.54
f1 (ppm)

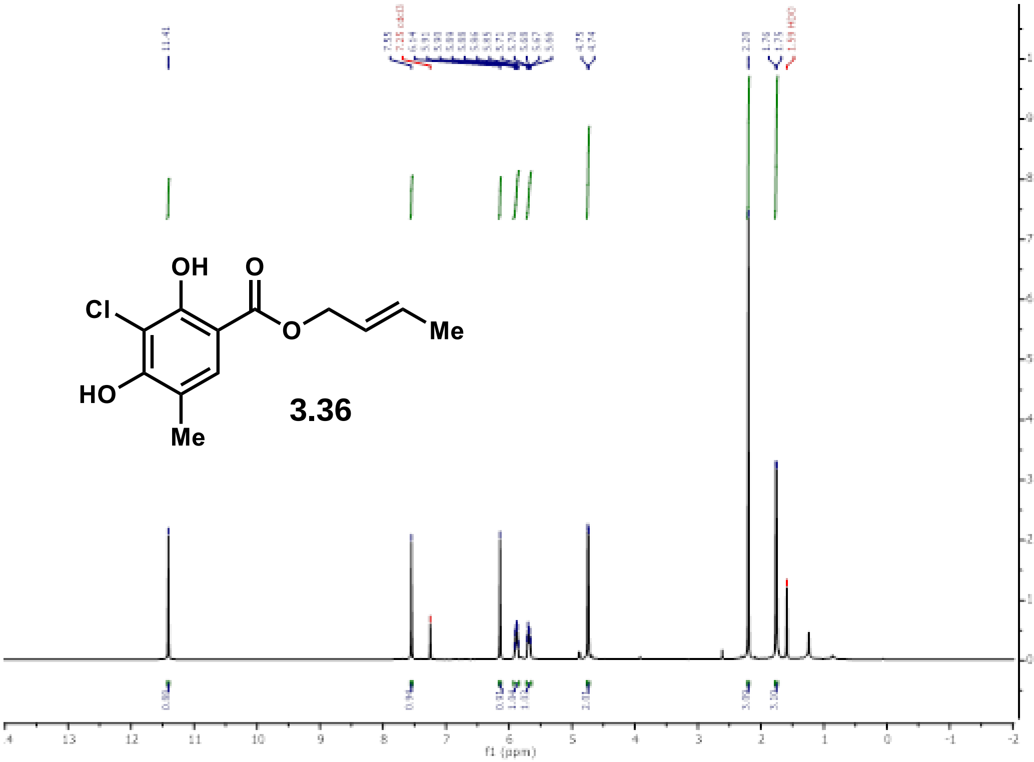

3.36

OH
O
Cl
O
Me
HO
Me
11.41
7.55
7.26 cdcl3
6.14
5.91
5.90
5.89
5.88
5.86
5.85
5.71
5.70
5.68
5.67
5.66
4.75
4.74
2.20
1.76
1.75
1.59 HDO
0.80
0.94
0.91
1.04
1.02
2.01
3.00
3.00
14
13
12
11
10
9
8
7
6
5
4
3
2
1
0
-1
-2
f1 (ppm)
1000
900
800
700
600
500
400
300
200
100
0

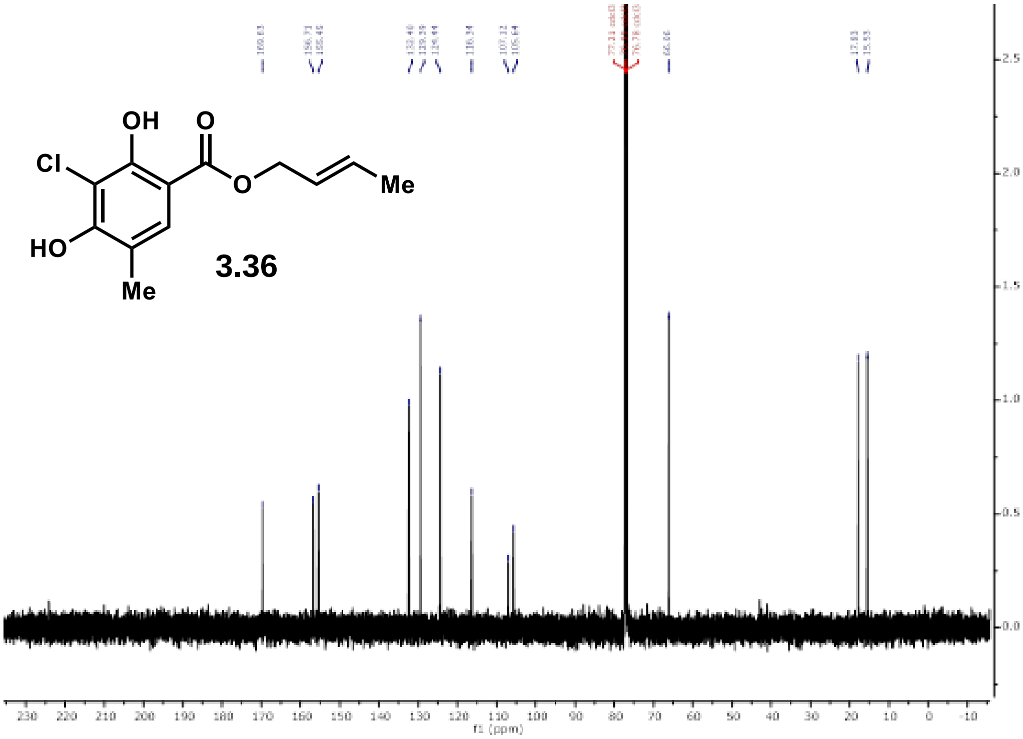

3.36

OH
O
Cl
O
Me
HO
Me
169.63
156.71
155.46
132.46
129.35
124.44
116.34
107.12
105.64
77.21 cdcl3
77.00 cdcl3
76.78 cdcl3
66.66
17.83
15.53
230
220
210
200
190
180
170
160
150
140
130
120
110
100
90
80
70
60
50
40
30
20
10
0
-10
f1 (ppm)
2.5
2.0
1.5
1.0
0.5
0.0

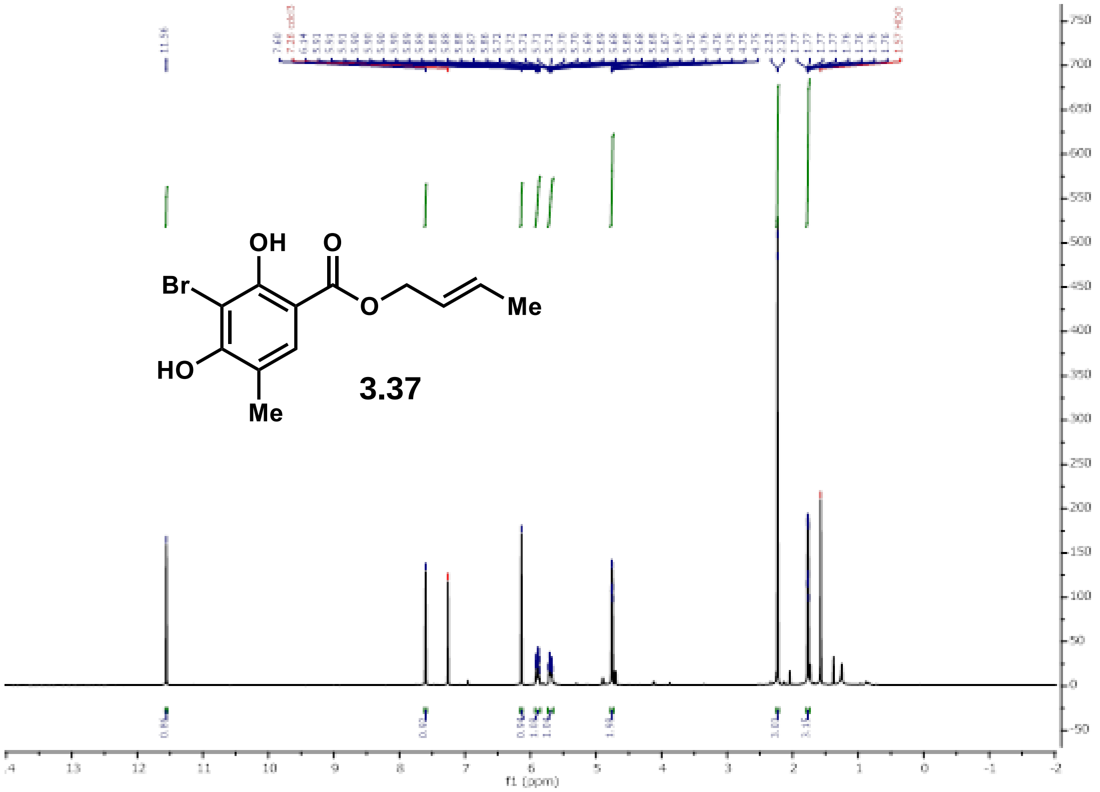

11.56
7.60
7.26 cdcl3
6.14
2.23
1.77
1.57 HDO
OH
O
Br
O
Me
HO
Me
3.37
f1 (ppm)

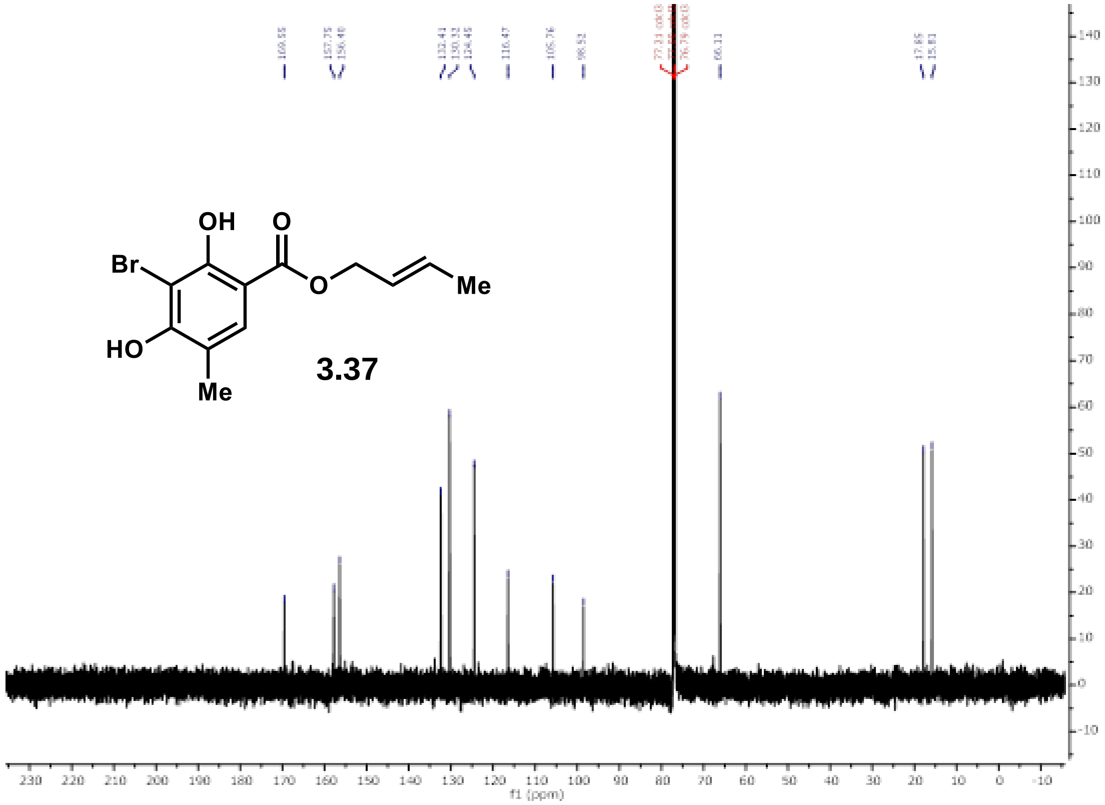

169.55
157.75
156.40
132.41
130.32
124.45
116.47
105.76
98.52
77.31 cdcl3
76.79 cdcl3
66.11
17.86
15.81
OH
O
Br
O
Me
HO
Me
3.37
f1 (ppm)

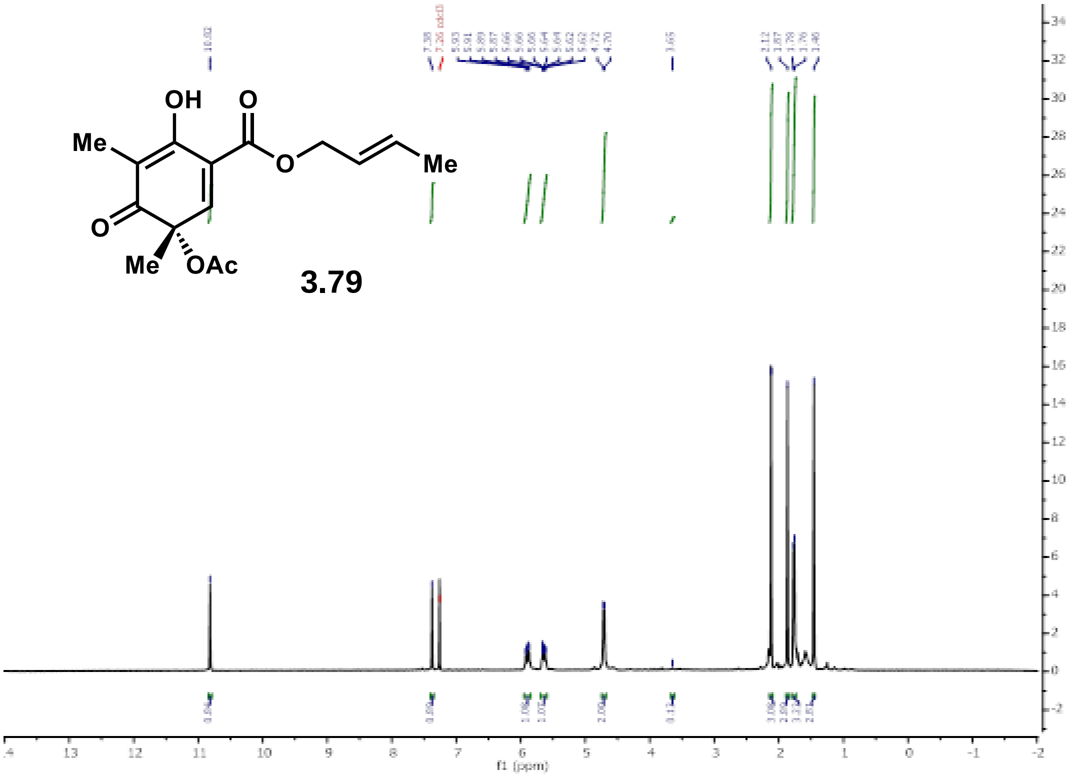
3.79

10.82
7.38
7.26 cdcl3
5.93
5.91
5.89
5.87
5.66
5.66
5.64
5.64
5.62
5.62
4.72
4.70
3.65
2.12
1.87
1.78
1.76
1.46
0.84
0.89
1.06
1.02
2.00
0.11
3.06
2.85
3.12
2.81
f1 (ppm)
OH
O
Me
O
Me
O
Me
OAc

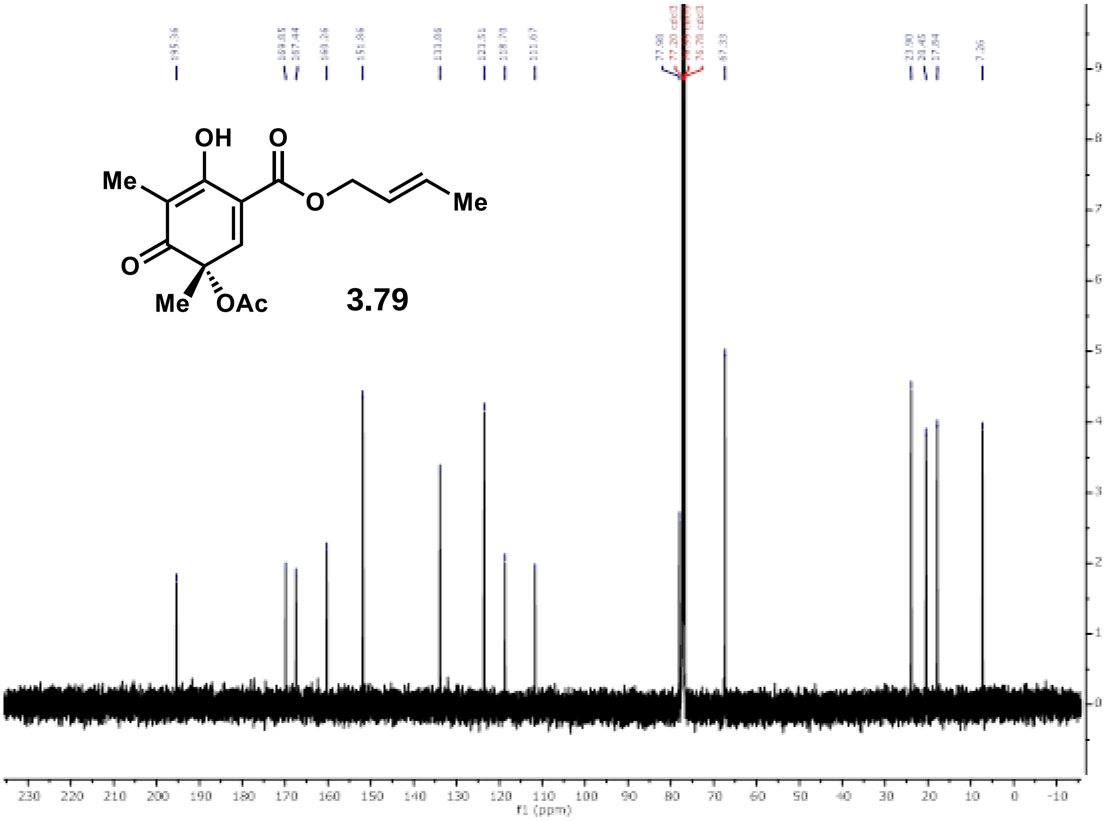
3.79

195.36
169.85
167.44
160.26
151.86
133.86
123.51
118.78
111.67
77.98
77.20 cdcl3
76.99 cdcl3
76.78 cdcl3
67.33
23.90
20.45
17.84
7.26
f1 (ppm)
OH
O
Me
O
Me
O
Me
OAc

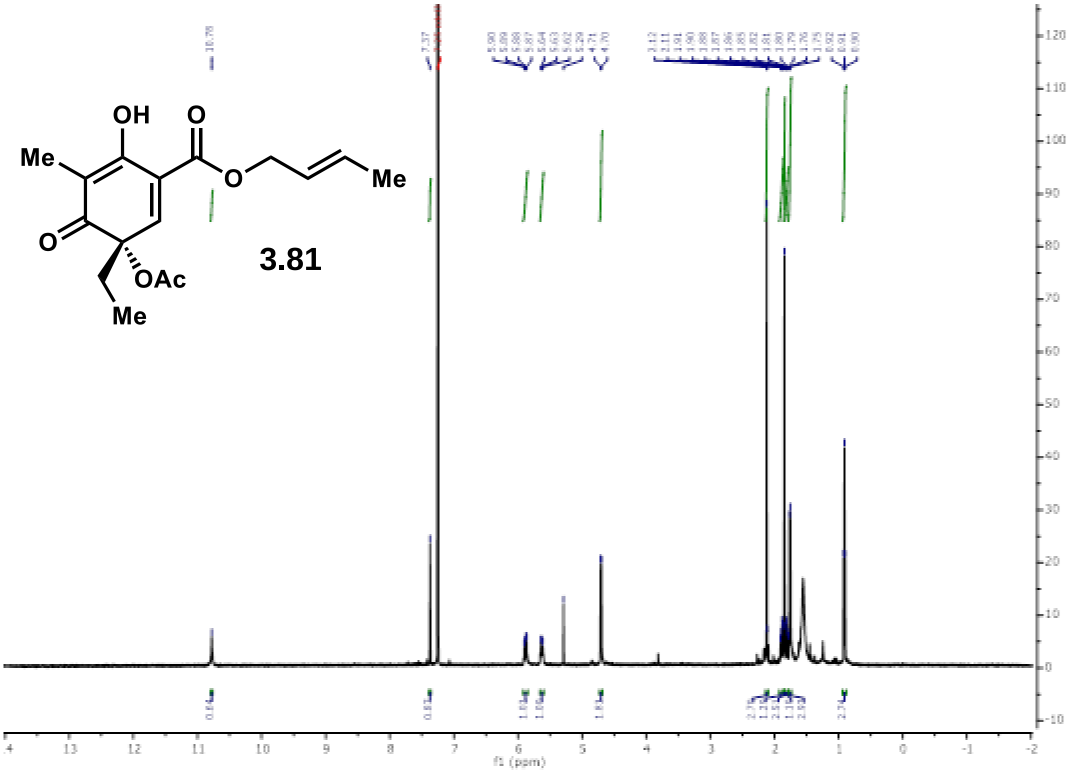
3.81
OH
O
Me
O
Me
O
OAc
Me
10.78
7.37
5.90
5.89
5.88
5.87
5.64
5.63
5.62
5.29
4.71
4.70
2.12
2.11
1.91
1.90
1.88
1.87
1.86
1.85
1.82
1.81
1.80
1.79
1.76
1.75
0.92
0.91
0.90
0.84
0.87
1.84
1.86
1.83
2.75
1.23
2.51
1.16
2.83
2.74
f1 (ppm)
14 13 12 11 10 9 8 7 6 5 4 3 2 1 0 -1 -2
120 110 100 90 80 70 60 50 40 30 20 10 0 -10

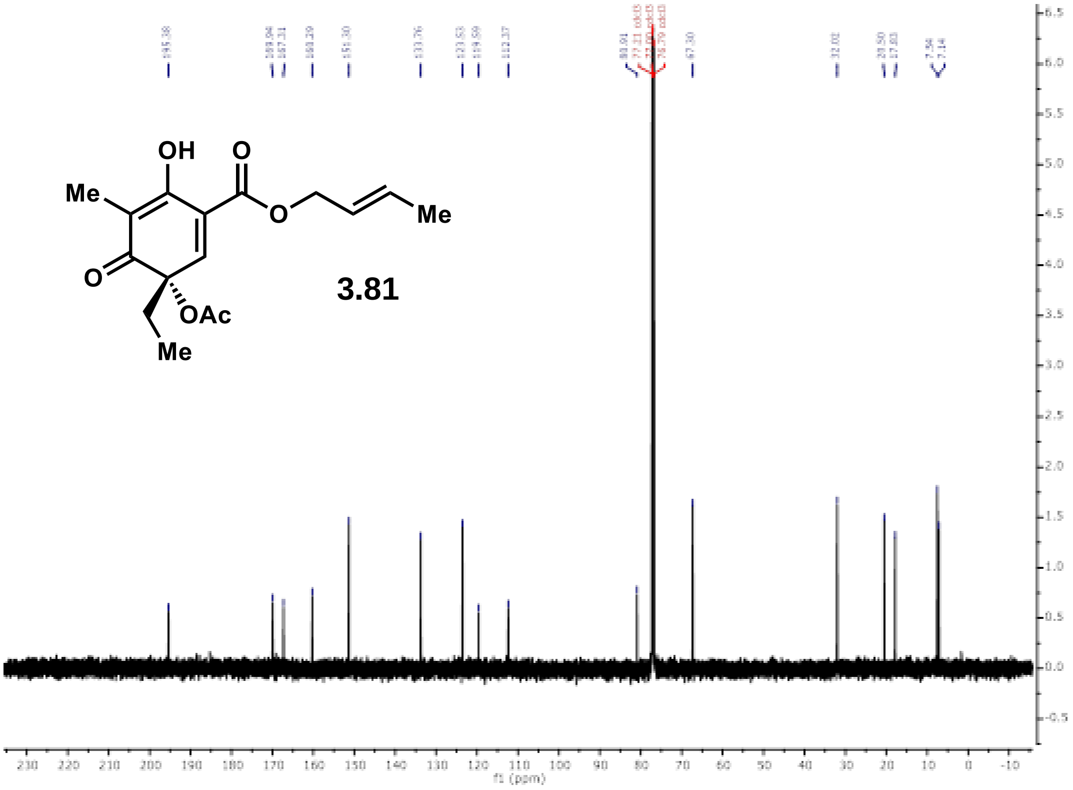
3.81
OH
O
Me
O
Me
O
OAc
Me
195.38
169.94
167.31
160.29
151.30
133.76
123.53
119.59
112.37
80.91
77.31 cdcl3
77.00 cdcl3
76.79 cdcl3
67.30
32.02
20.50
17.83
7.54
7.14
f1 (ppm)
230 220 210 200 190 180 170 160 150 140 130 120 110 100 90 80 70 60 50 40 30 20 10 0 -10
6.5 6.0 5.5 5.0 4.5 4.0 3.5 3.0 2.5 2.0 1.5 1.0 0.5 0.0 -0.5

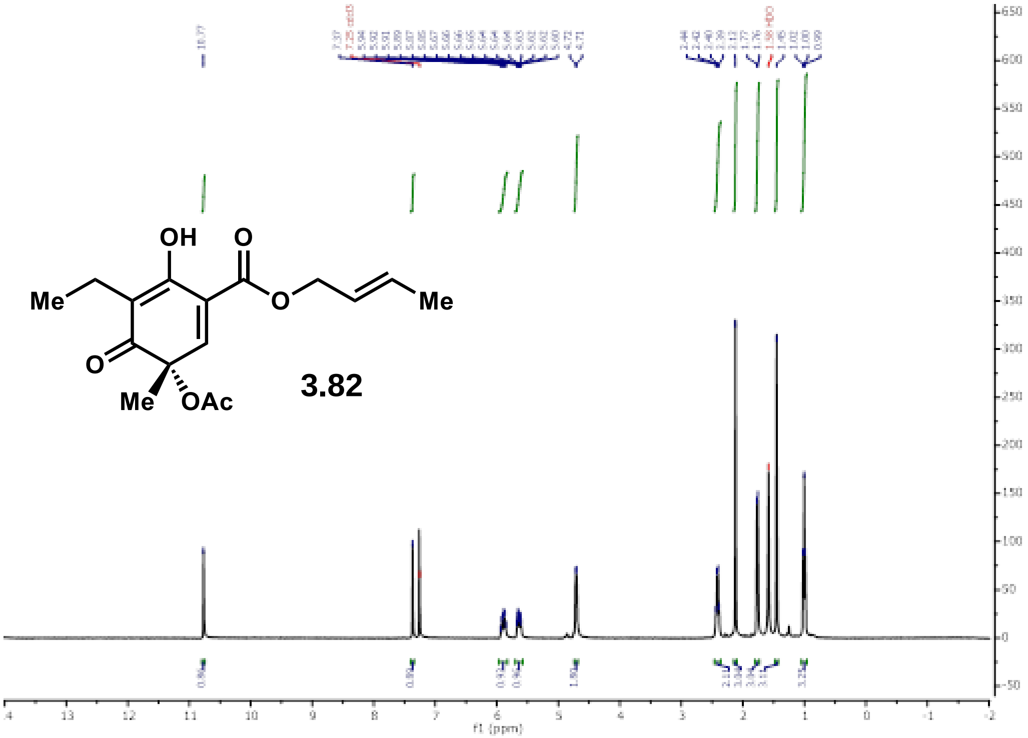

3.82

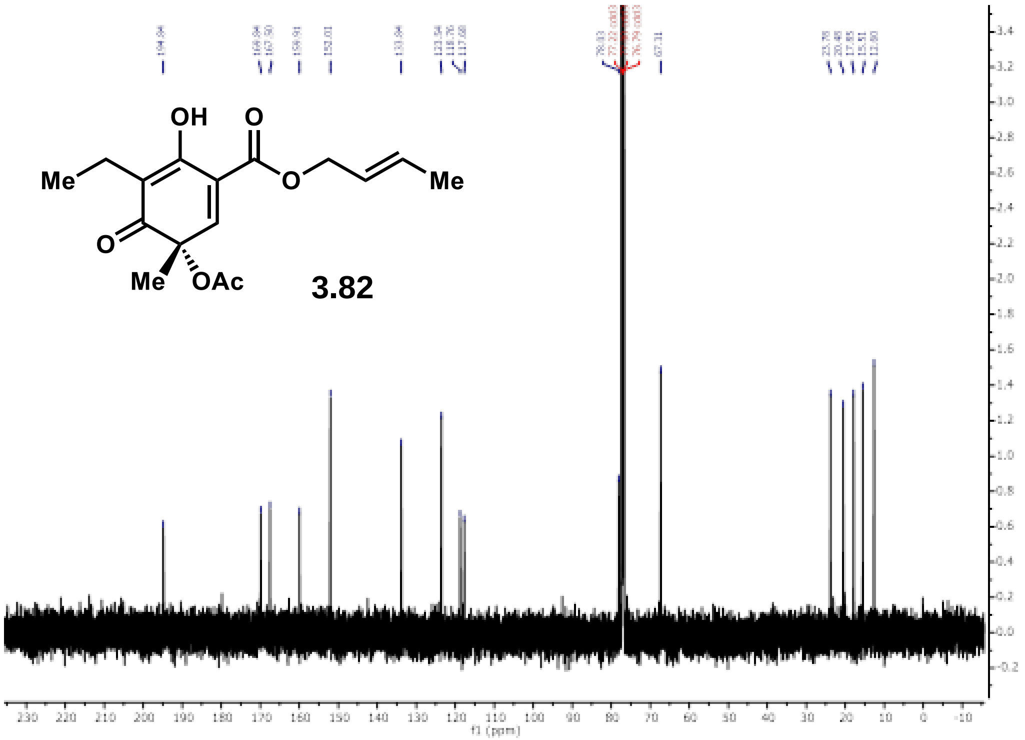

3.82

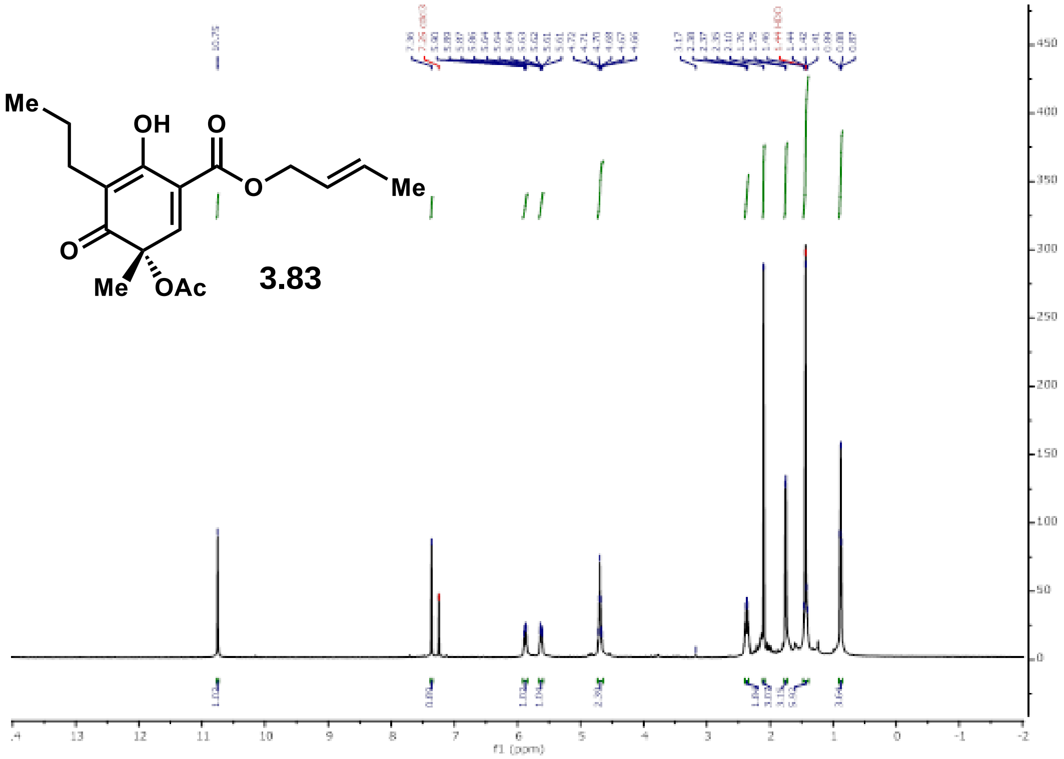

3.83

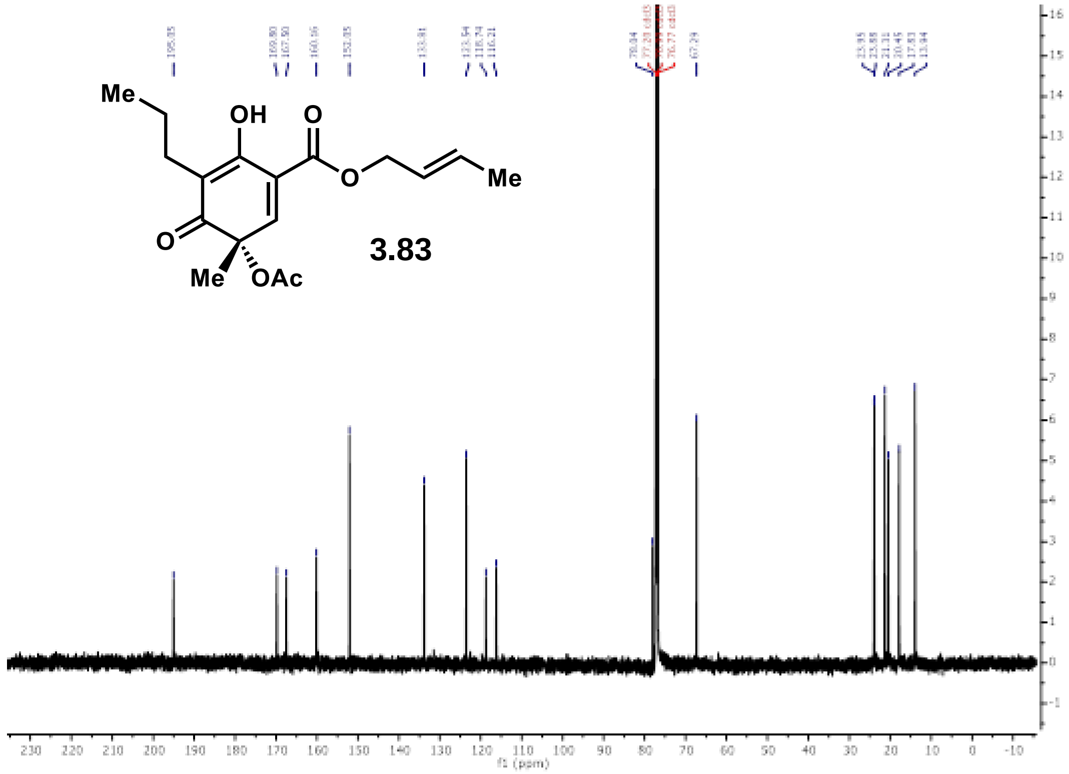

3.83

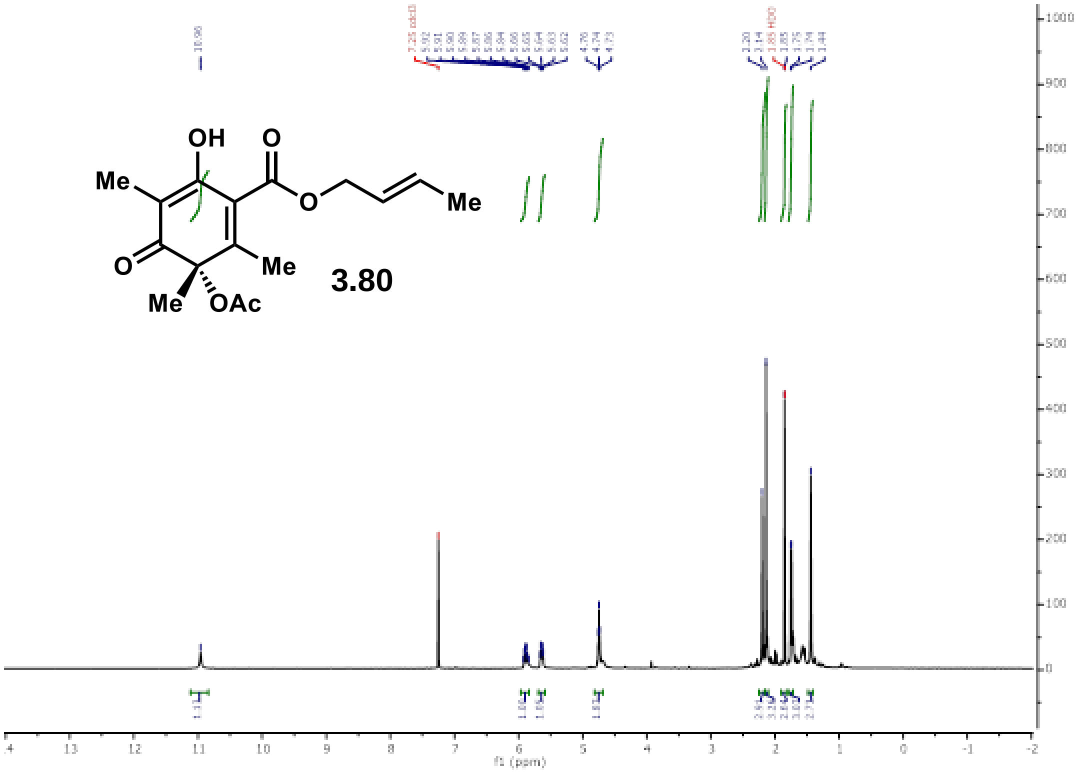

10.96
7.25 cdcl3
5.92
5.91
5.90
5.89
5.87
5.86
5.84
5.66
5.65
5.64
5.63
5.62
4.76
4.74
4.73
2.20
2.14
1.85 H2O
1.85
1.75
1.74
1.44
OH
O
Me
O
Me
O
Me
Me
OAc
3.80
1.11
1.00
1.05
1.87
2.91
3.20
2.85
3.02
2.74
f1 (ppm)

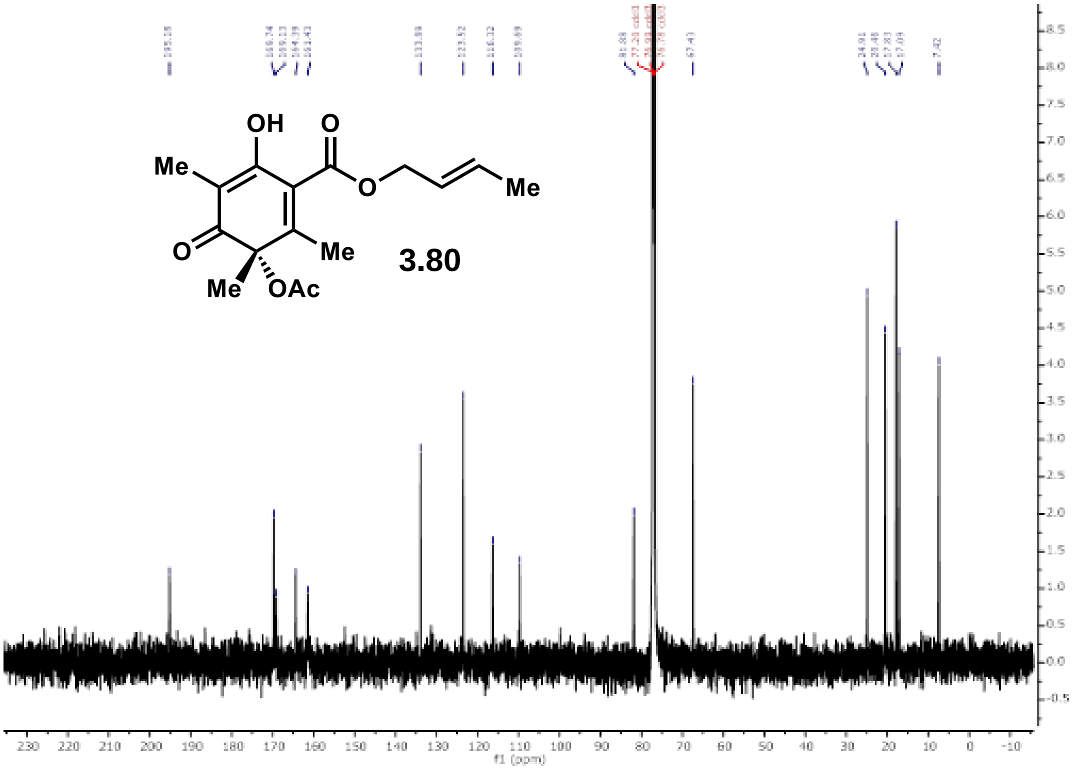

195.18
169.74
169.13
164.09
161.43
133.89
123.52
116.32
109.69
81.88
77.25 cdcl3
77.00 cdcl3
76.79 cdcl3
67.43
24.91
20.48
17.83
17.09
7.42
OH
O
Me
O
Me
O
Me
Me
OAc
3.80
f1 (ppm)

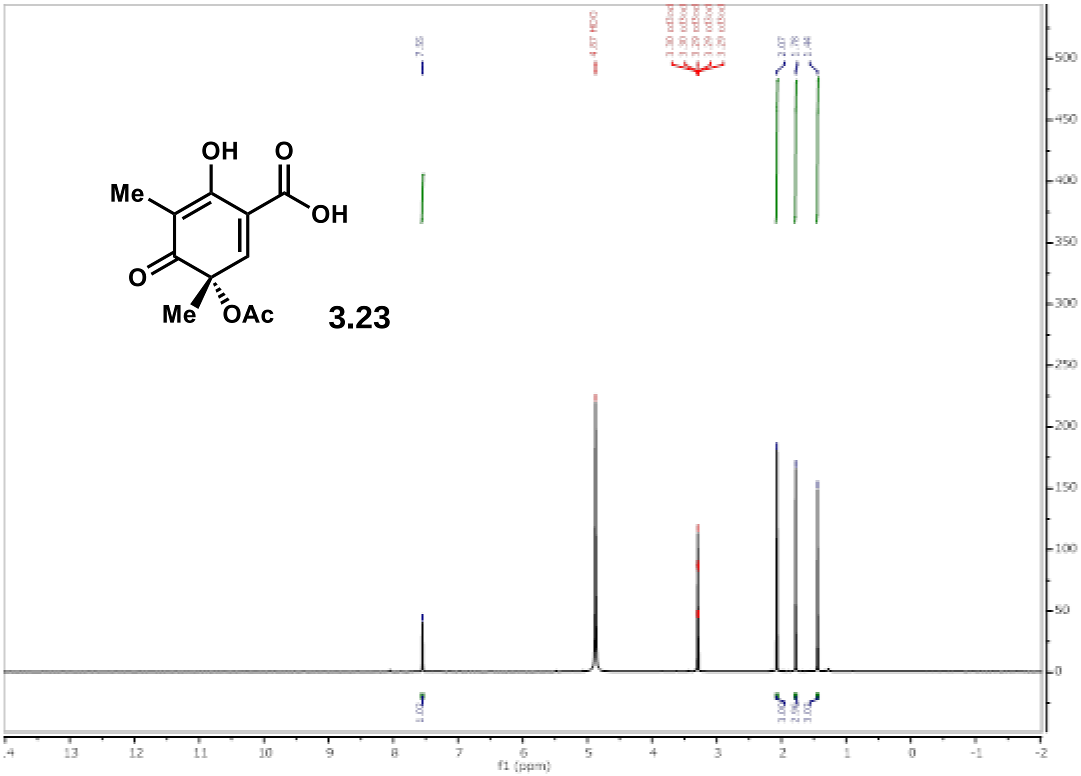
7.55
4.87 HDO
3.30 cd3od
3.30 cd3od
3.29 cd3od
3.29 cd3od
3.29 cd3od
2.07
1.78
1.44
OH
O
Me
OH
O
Me
OAc
1.02
3.00
2.96
3.01
14
13
12
11
10
9
8
7
6
5
4
3
2
1
0
-1
-2
f1 (ppm)
500
450
400
350
300
250
200
150
100
50
0

3.23

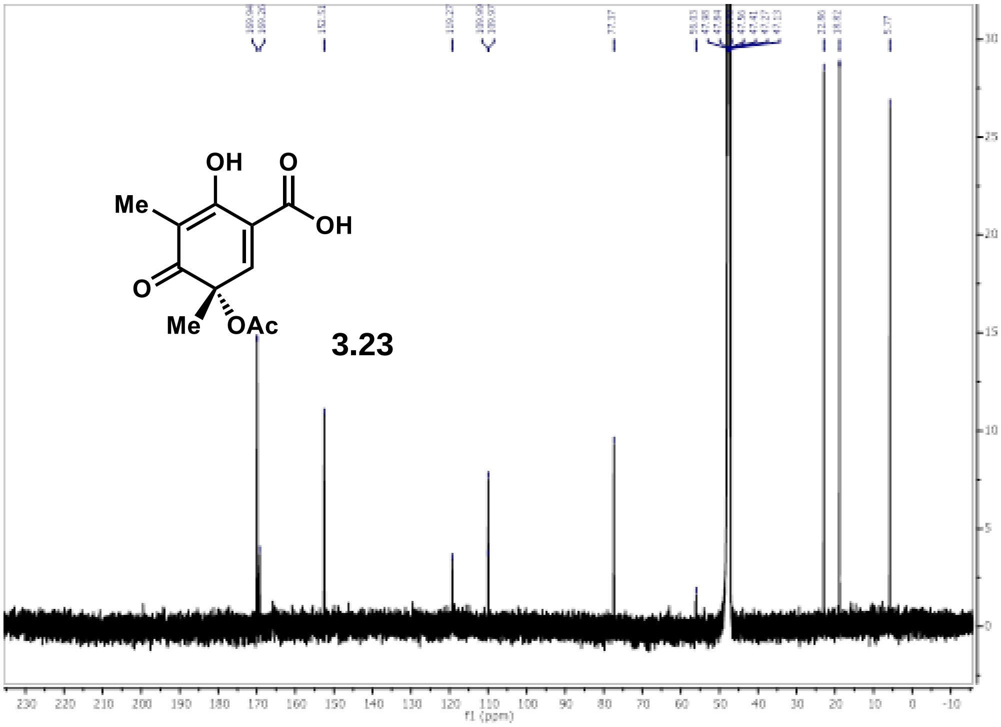
169.94
169.26
152.51
119.27
109.99
109.97
77.37
55.03
47.98
47.84
47.56
47.41
47.27
47.13
22.86
18.82
5.77
OH
O
Me
OH
O
Me
OAc
230
220
210
200
190
180
170
160
150
140
130
120
110
100
90
80
70
60
50
40
30
20
10
0
-10
f1 (ppm)
30
25
20
15
10
5
0

3.23

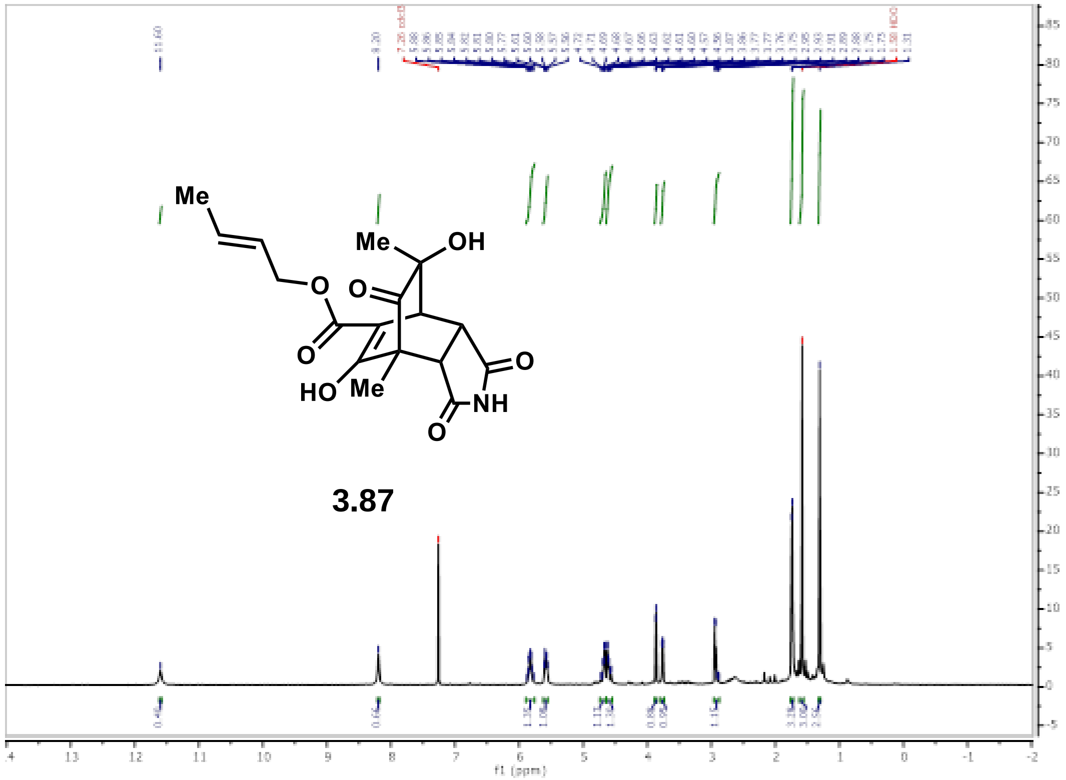

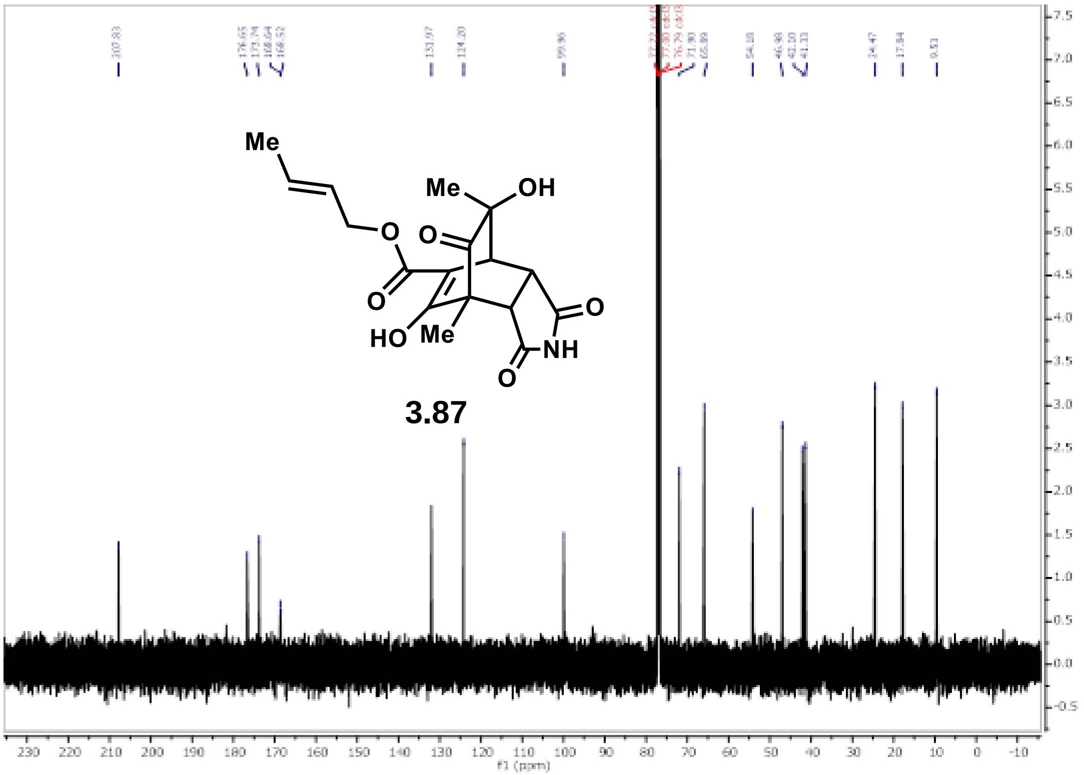

Figure 3.34: NMR spectra of synthetic compounds.

Chapter 3.7: References

1) Arnold, F. H. Design by directed evolution. *Acc. Chem. Res.* **1998**, *31*, 125–131.
2) Savile, C. K.; Janey, J. M.; Mundorff, E. C.; Moore, J. C.; Tam, S.; Jarvis, W. R.; Colbeck, J. C.; Krebber, A.; Fleitz, F. J.; Brands, J.; Devine, P. N.; Huisman, G. W.; Hughes, G. J. *Science* **2010**, 329, 305–310.
3) Rousseau, G.; Breit, B. *Angew. Chem., Int. Ed.* **2011**, *50*, 2450–2494.
4) Huang, Z.; Lumb, J.-P. Phenol-directed C-H functionalization. *ACS Catal.* **2018**, *9*, 521–555.
5) Polic, V.; Auclair, K. *Bioorganic Med. Chem.* **2014**, *22*, 5547–5554.
6) Polic, V.; Cheong, K. J.; Hammerer, F.; Auclair, K. *Adv. Synth. Catal.* **2017**, *359*, 3983–3989.
7) Lewis, J. C.; Bastian, S.; Bennett, C. S.; Fu, Y.; Mitsuda, Y.; Chen, M. M.; Greenberg, W. A.; Wong, C.-H.; Arnold, F. H. *Proc. Natl. Acad. Sci. U. S. A.* **2009**, *106*, 16550–16555.
8) Du, L.; Dong, S.; Zhang, X.; Jiang, C.; Chen, J.; Yao, L.; Wang, X.; Wan, X.; Liu, X.; Wang, X.; Huang, S.; Cui, Q.; Feng, Y.; Liu, S.-J.; Li, S. *Proc. Natl. Acad. Sci. U. S. A.* **2017**, 5129-5137.
9) Li, S.; Chaulagain, M. R.; Knauff, A. R.; Podust, L. M.; Montgomery, J.; Sherman, D. H. *Proc. Nat. Acad. Sci. U. S. A.* **2009**, *106*, 18463–18468.
10) Larsen, A. T.; May, E. M.; Auclair, K. *J. Am. Chem. Soc.* **2011**, *133*, 7853–7858.
11) Ma, C.; Chen, Z.; Chen, J.; Chen, J.; Wang, C.; Zhou, H.; Yao, L.; Shoji, O.; Watanabe, Y.; Cong, Z. *Angew. Chem., Int. Ed.* **2018**, *57*, 7628–7633.
12) Xu, J.; Wang, C.; Cong, Z. Stratagies for substrate-regulated P450 catalysis: From substrate engineering to co-catalysis. *Chem. Eur. J.* **2019**, *25*, 6853–6863.
13) Vickers, C.; Backfish, G.; Oellien, F.; Piel, I.; Lange, U. E. W. *Chem. Eur. J.* **2018**, *24*, 17936–17947.
14) Mansoorabadi, S. O.; Thibodeaux, C. J.; Liu, H. W. *J. Org. Chem.* **2007**, *72*, 6329–6342.
15) Badieyan, S.; Bach, R. D.; Sobrado, P. *J. Org. Chem.* **2015**, *80*, 2139–2147.
16) Colonna, S.; Gaggero, N.; Carrea, G.; Ottolina, G.; Pasta, P.; Zambianchi, F. *Tett. Lett.* **2002**, *43*, 1797–1799.
17) Senn, H. M.; Cisneros, G. A. *Front. Chem.* **2014**, *2*, 1–15.
18) Bučko, M.; Gemeiner, P.; Schenkmayerová, A.; Krajčovič, T.; Rudroff, F.; Mihovilovič, M. D. *Appl. Microbiol. Biotechnol.* **2016**, *100*, 6585–6599.
19) Hilker, I.; Gutiérrez, M. C.; Furstoss, R.; Ward, J.; Wohlgemuth, R.; Alphand, V. *Nat. Protoc.* **2008**, *3*, 546–554.
20) Baker Dockrey, S. A.; Lukowski, A. L.; Becker, M. R.; Narayan, A. R. H. *Nat. Chem.* **2018**, *10*, 119–125.
21) Volp, K. A.; Harned, A. M. *Chem. Commun.* **2013**, *49*, 3001-3003.
22) Hashimoto, T.; Shimazaki, Y.; Omatsu, Y.; Maruoka, K. *Angew. Chem., Int. Ed.* **2018**, *57*, 7200–7204.
23) Huijbers, M. M. E.; Montersino, S.; Westphal, A. H.; Tischler, D.; Van Berkel, W. J. H. *Arch. Biochem. Biophys.* **2014**, *544*, 2–17.
24) Sib, A.; Gulder, T. A. M. *Angew. Chem., Int. Ed.* **2017**, *56*, 12888–12891.
25) Sib, A.; Gulder, T. A. M. *Angew. Chem., Int. Ed.* **2018**, *57*, 14650–14653.
26) Luo, J.; Preciado, S.; Xie, P.; Larrosa, I. *Chem. Eur. J.* **2016**, *22*, 6798–6802.
27) Peng, L.; Xing, X.; Lili, C.; Lei, M.; Xu, S.; Lihong, L. *Bioorg. Med. Chem.* **2014**, *22*, 1596–1607.
28) Baker Dockrey, S. A.; Suh, C. S.; Benítez Rodríguez, A.; Wymore, W. Troy; Brooks, C. L. III; Narayan, A. R. H. *ACS Central Sci.* **2019,** *5*, 1010.
29) Milzarek, T. M.; Einsiedler, M.; Aldemir, H.; D'Agostino, P. M.; Evers, J. K.; Hertrampf, G.; Lamm, K.; Malay, M.; Matura, A.; Müller, J. I.; Gulder, T. A. M. *Org. Lett.* **2019**, *21*, 4520.
30) Wu, Y.; Esser, L.; De Brabander, J. K. *Angew. Chem., Int. Ed.* **2000**, *39*, 4308–4310.
31) Cabrera, G. M.; Butler, M.; Rodriguez, M. A.; Godeas, A.; Haddad, R.; Ederlin, M. N. *J. Nat. Prod.* **2006**, *69*, 1806.

32) Nicolaou, K. C.; Vassilikogiannakis, G.; Simonsen, K. B.; Baran, P. S.; Zhong, Y.-L.; Vidali, V. P.; Pitsinos, E. N.; Couladouros, E. A. *J. Am. Chem. Soc.* **2000**, *122*, 3071.
33) Kumar, J. A.; Tiwari, A. K.; Saidachary, G.; Kumar, D. A.; Ali, Z.; Sridhar, B.; Raju, B. C. *Med. Chem.* **2013**, *9*, 806.
34) Baumhof, P.; Mazitschek, R.; Giannis, A. *Angew. Chem., Int. Ed***.** **2001**, *40*, 3672.

CHAPTER 4: Large-scale Reaction and One-pot Platform Development

Portions adapted with permission from "Whole-cell biocatalysis platform for gram-scale oxidative dearomatization of phenols" *Chem Biol Drug Des.* **2018**, *93*, 1207 – 1213 and "Biocatalytic site- and enantioselective oxidative dearomatization" *Nat. Chem.* **2018,** *10*, 119–125.

Chapter 4.1: Introduction

The selectivity advantages of biocatalytic transformations are well established and generally appreciated by the synthetic community.[1] However, in order for biocatalytic methods to become routine in traditional synthetic laboratories, more transformations with robust scalabitliy and well-understood substrate scopes must be made available.[2] Our exploration of FDMO-mediated oxidative dearomatization aimed to fill that gap in biocatalytic methods.[3] A second challenge inherit to the wide-spread adoption of biocatalysis is catalyst availability.[1] Protein expression in genetically tractable and fast-growing hosts, such as *E. coli* or *Saccharomyces cerevisiae*, requires only inexpensive media and an incubator for protein production; however, purification of the desired protein from this matrix involves several time-intensive steps, specialized equipment and expensive reagents and materials.[4] In order to overcome this limitation and to enable multi-gram scale biocatalytic oxidative dearomatization, we envisioned a reaction platform employing whole *E. coli* cells expressing FDMOs as the catalyst source.

Chapter 4.2: Whole-cell Platform

Substrate **4.1**, which was fully converted in vitro by TropB in our initial assays was chosen as the model substrate for reaction development using whole *E. coli* cells. Two methods were used to prepare the cell pellet for use in whole cell (WC) reactions: flash- freezing or

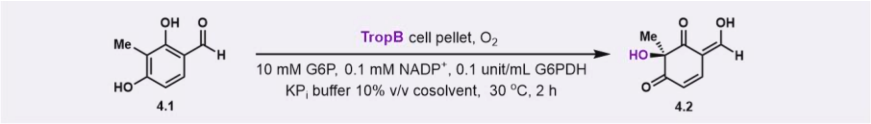

Me
OH
O
H
HO
4.1
TropB cell pellet, O_2
10 mM G6P, 0.1 mM NADP$^+$, 0.1 unit/mL G6PDH
KP$_i$ buffer 10% v/v cosolvent, 30 °C, 2 h
Me
HO
O
OH
H
O
4.2

1.0 g scale whole cell reaction

Lyophilized *E. coli* cells expressing TropB

wet cell (mg)	cosolvent	% conversion
500	none	23
500	THF	<5
500	methanol	62
500	acetonitrile	<5
500	toluene	>99
100	toluene	>99
50	toluene	86

excipient	% conversion
none	98
10 wt % skim milk	83
10 wt % sucrose	>99
PEG 4000	>99

lyophilization. For the former, the crude cell pellet was flash frozen in liquid nitrogen in small aliquots. This method greatly alleviated difficulties in weighing out wet cell pellet for accurate quantification of our WC reactions. For the preparation of lyophilized cells, the crude cell pellet was aliquoted into 1 g portions and re-suspended in an excipient solution (0.5 L, 10% w/v excipient in Milli- Q water) and pelleted in several 50 mL Falcon tubes. The tubes were then covered with a KimWipe® and lyophilized for 48–72 h. To identify the ideal preparation method for lyophilized cell pellet for use in our WC reactions, we added various excipients to cells prior to lyophilization based upon a survey of common excipients used in the literature.[5,6,7] We then compared the activity of each preparation in 1 g scale reactions with the non-native substrate **4.1** (Figure 4.1). The results of these experiments indicated that enzyme activity was maintained in lyophilized cells, and only improved nominally by the addition of 10 wt % sucrose or PEG 4000 (Figure 4.1, entries 3 and 4, respectively). Omission of co-solvent in whole-cell reactions with TropB resulted in low conversions of starting material, which we hypothesized was due to poor substrate solubility in the aqueous reaction environment, and issues in transporting the charged compound across the cell membrane. To resolve this issue, we tested the effect of both water- miscible and immiscible cosolvents on the WC reaction (Table 4.1). The addition of 10% v/v toluene drastically improved conversion to *o*-quinol **4.2**, with full conversion in 2 h under the described conditions. Additionally, we screened reactions with a reduced amount of wet cell pellet and noted complete conversion with cell loading as low as 20 weight equivalents. These optimized conditions were applied to gram-scale reactions, further demonstrating the appeal of this method for synthetic applications.

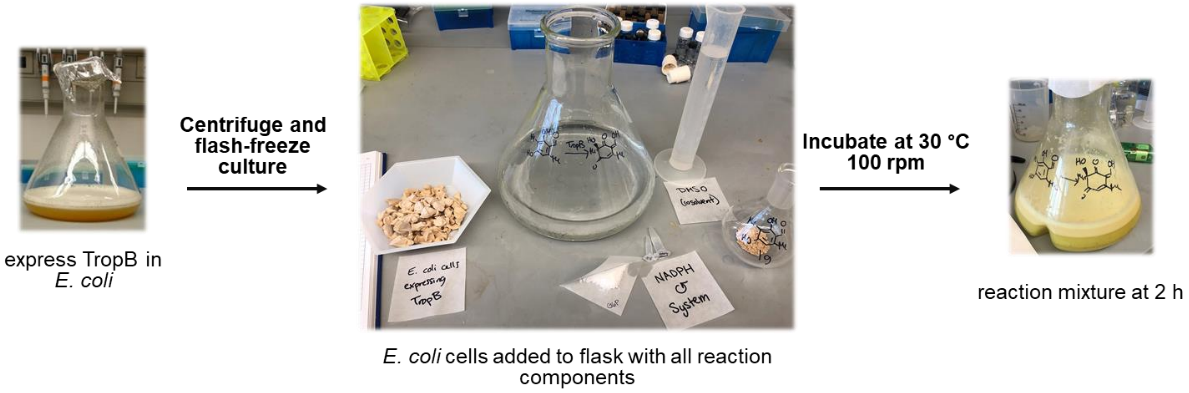
express TropB in *E. coli*
Centrifuge and flash-freeze culture
E. coli cells expressing TropB
DMSO (cosolvent)
NADPH ↺ System
E. coli cells added to flask with all reaction components
Incubate at 30 °C 100 rpm
reaction mixture at 2 h

Figure 4.2: Set-up for gram-scale whole-cell oxidative dearomatization. After the reaction is complete, the mixture is filtered and the filtrate is extracted with (3:1) EtOAc and *i*PrOH.

Using our optimized WC biocatalysis platform, the overall yield of usable biocatalyst from each protein expression was significantly higher than what was obtained following protein purification for in vitro reactions. In this case, more than 20 WC preparative-scale (100 mg) reactions could be carried out for every liter of TropB expression cell culture. In comparison, from 1 L of expression culture, the quantity of purified protein was sufficient for 2–3 reactions on the same scale. We suspect this was due to a loss of protein and activity over the course of the purification procedure. Reactions carried out with crude cell lysate gave diminished conversions relative to both in vitro and WC reactions, indicating that some enzyme stabilization may have been provided by the cellular environment. The WC biocatalyst also required significantly less time to prepare, saving 5–6 h for each batch of catalyst. Therefore, our WC platform demonstrated superior efficiency over in vitro reactions in both preparation time and scalability of the reaction.

Chapter 4.3: Complex Molecule Synthesis

To rapidly build molecular complexity from enzymatically generated *o*-quinols, we sought to leverage the reactivity of these compounds in cascade reactions by performing subsequent *in situ* enzymatic or chemical transformations. We anticipated that various natural product scaffolds could be accessed in one pot using biocatalytic dearomatization-initiated cascades.[8] Toward this goal, we explored the synthesis of the tropolone (**4.6**), azaphilone (**4.13**) and sorbicillinoid (**4.10**) cores (Figure 4.3).

Tropolones, seven-membered aromatic α-hydroxy ketones, are synthesized by a wide variety of organisms and are found in a number of biologically active natural products.[9,10] The biosynthesis of this motif remained a long-standing puzzle in the community until 2012 when Cox and coworkers elucidated the fungal two-enzyme cascade which affords the tropolone stipitaldehyde (**4.6**).[11,12] *O*-quinol **4.4** produced by TropB was found to undergo ring-expansion by the α-ketoglutarate-dependent non-heme iron (NHI) TropC.[11] NHI dioxygenases perform a wide variety of transformations, employing an Fe(IV)oxo intermediate to extract H-atoms from C-H bonds of substrates.[13,14] The resulting radical can undergo rebound hydroxylation, halogenation, or rearrangement and dehydration to form the final product. The mechanism for ring-expansion by TropC is the subject of ongoing study in our group by Tyler Doyon and Kevin Skinner.

The interesting biological activity of tropolone-containing natural products has sparked the development of numerous synthetic approaches, including Buchner reaction and subsequent rearrangement,[15] [5+2][16] and [4+3][17] cycloadditions, as well as construction of saturated 7-membered rings followed by iterative elimination.[18] These methods require specific arrangement of functionalization to enable the required ring-expansion or elimination, limiting the number of substituted tropolones which can be readily accessed. To address this limitation, we envisioned developing a biocatalytic cascade employing TropB and TropC, or homologs thereof, to enable access to highly elaborated tropolones from resorcinol starting materials. As a proof of concept for this reaction platform we sought to complete the chemoenzymatic synthesis of stipitaldehyde (**4.6**).

The one-pot cascade of TropB dearomatization of aldehyde **4.3** to *o*-quinol **4.4** and ring expansion by TropC proceeded in 53% conversion to afford stipitatic aldehyde (**4.6**). Isolation of the tropolone from the proteinaceous reaction mixture proved challenging, due to the apparent propensity of this compound to co-precipitate with protein.

As Tyler Doyon continued to explore the general synthetic utility of the TropB/TropC cascade, we tuned our attention to the development of other chemoenzymatic cascades featuring FDMO-mediated oxidative dearomatization. As SorbC allowed access to enantioenriched sorbicillinol (**4.8**) we were intrigued by the potential to access members of the sorbicillinoid family of natural products (see Figure 1.6).[20] These compounds, which include a variety of structurally distinct sorbicillinol dimers, have been the focus of synthetic efforts by several groups due to their promising biological activity including α-TNF inhibition and antifungal properties.[20,21,22,23] The most direct route to these compounds is biomimetic: oxidation of sorbicilin to bisorbicillinol followed by base-promoted dimerization and various rearrangements.[21,22] However, the chemical syntheses using this route reported to date employ an achiral oxidant, $Pb(OAc)_4$, in the dearomatization step, resulting in racemic products. [21,22] Having established SorbC as a highly enantioselective catalyst for the dearomatization of sorbicillin,[3] we envisioned completing the asymmetric synthesis of sorbicillin natural products by employing SorbC in the key oxidative step. We chose urea sorbicillin (**4.10**), a recently isolated sorbicillin from an interstitial *Nigrospora* fungus as our first target.[24]

Malaeimide was a competent dienophile for reaction with sorbicillinol, affording a single product when heated to 50 °C. Based on this result we hypothesized the natural product urea sorbicillinoid (**4.10**) could be accessed in a similar sequence of steps. Sorbicillin (**4.7)** could be elaborated to the natural product in a one pot cascade that commenced with SorbC oxidation to deliver sorbicillinol **4.8**. The addition of bisacylated urea **4.9** led to facile [4+2] cycloaddition. Addition of LiOH to remove the acyl protecting groups from the urea moiety completed the first synthesis of urea sorbicillinoid natural product **4.10** in 21% yield over three steps. Subsequent reaction showed protection of the urea moiety was unnecessary for high conversion to the cycloadduct under the given reaction conditions. Concurrent to these studies, the Gulder group employed SorbC to access a number of bisorbicillinoid natural products (see Figure 1.6).[25]

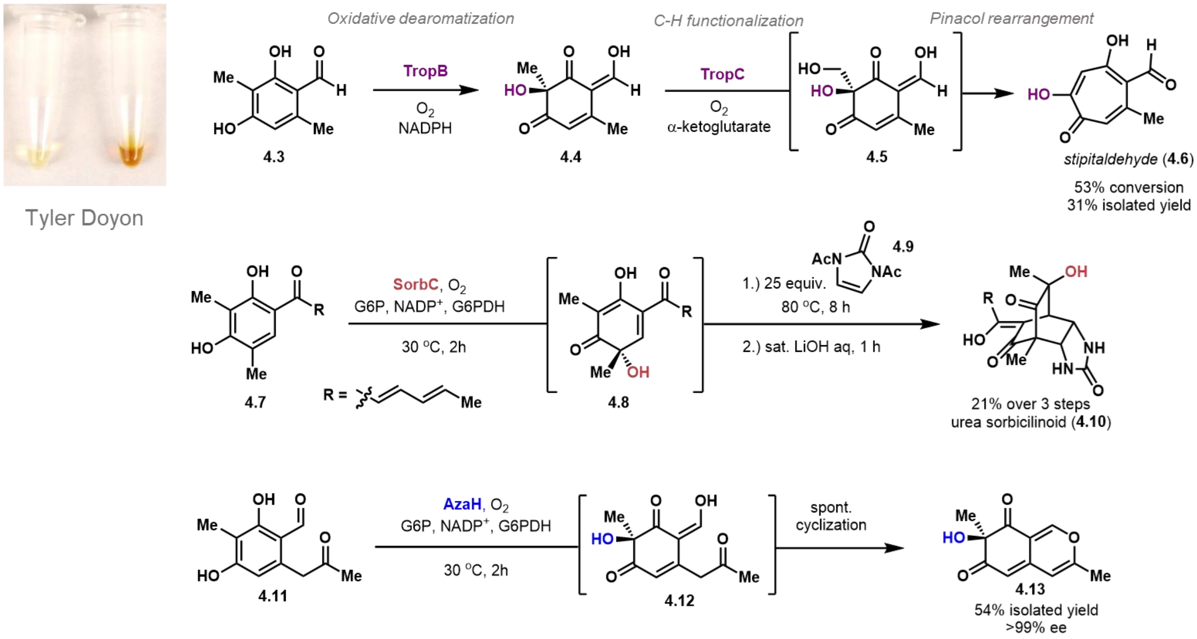
Tyler Doyon

Oxidative dearomatization
C-H functionalization
Pinacol rearrangement
4.3
TropB
O_2
NADPH
4.4
TropC
O_2
α-ketoglutarate
4.5
stipitaldehyde (4.6)
53% conversion
31% isolated yield
4.7
R =
SorbC, O_2
G6P, NADP$^+$, G6PDH
30 °C, 2h
4.8
4.9
1.) 25 equiv.
80 °C, 8 h
2.) sat. LiOH aq, 1 h
21% over 3 steps
urea sorbicilinoid (4.10)
4.11
AzaH, O_2
G6P, NADP$^+$, G6PDH
30 °C, 2h
4.12
spont.
cyclization
4.13
54% isolated yield
>99% ee

Figure 4.3: One-pot syntheses of secondary metabolites featuring biocatalytic oxidative dearomatization as a key synthetic step stipitaldehyde, urea sorbicillinoid and azaphilone from *Nigrospora* sp. YE3003.

The first asymmetric synthesis of azaphilone natural product **4.13**[26] was achieved from methyl ketone **4.11**, which was synthesized in two steps from aryl bromide **2.55** (see Chapter 5.3). The azaphilone family of natural products contains over two hundred members, a number of which have been shown to have interesting biological activities ranging from anticancer to antifugal.[27] Initial AzaH-mediated dearomatization delivered enol **4.12**, which spontaneously cyclized in buffer to azaphilone **4.13**, isolated in 54% yield and >99% ee. This reaction served as a blueprint for the chemoenzymatic synthesis of more complex azaphilone natural products and natural product analogs (see Chapter 5).

Chapter 4.4 Conclusions

In summary, we have developed a scalable and economical WC biocatalytic method for oxidative dearomatization of phenols. This biocatalytic method improves upon previously developed chemical methods in terms of environmental sustainability, as it uses water as a solvent and a biological catalyst as the oxidant. Compared to with in vitro reactions, WC biocatalytic methods can pro-vide distinct and significant advantages. With no requirement for enzyme purification, WC procedures reduce the overall time, cost, and specialized equipment associated with catalyst production. After the simple optimization of several parameters, such as cell preparation method and reaction cosolvent, our WC platform allowed us to perform tenfold more reactions per liter of cell culture when compared to purified enzyme. This improvement was achieved without loss of catalytic function or selectivity. Moreover, this highly scalable method provides a simple and accessible reaction platform, promoting use of biocatalysts in traditional synthetic chemistry.

We encountered substrate limitations in our WC reactions that were distinct from in vitro conditions. We hypothesized that this was due to sequestration of the substrate by the cellular membrane. Crude lysate could afford a potential solution to this limitation, by removal of the problematic cellular material but still offering an abbreviated purification procedure relative to purified lysate.

The modularity of the above described (chemo)enzymatic cascades could allow for the rapid generation of a library of complex molecules. The previously demonstrated substrate promiscuity of the three enzymes TropB, SorbC and AzaH enables access to a variety of enantioenriched *o*-quinol intermediates which can undergo cycloadditions with a number of electron poor olefins, intramolecular cyclizations or subsequent enzymatic steps. The substrate scope of the non-heme iron-dependent enzyme TropC has been explored by Tyler Doyon, allowing for the generation of a number of tropolone products.

Chapter 4.5: Experimental

Chapter 4.5.1: Whole Cell Reactions

Whole cell preparative-scale reactions: Whole-cell enzymatic reactions were conducted on 1 g of substrate under the following conditions: 20 weight equivalents of wet cell pellet, 5 mM substrate, 10% (v/v) toluene, 0.1 mM NADP$^+$, 0.1 U/mL G6PDH, and 10 mM G6P for NADPH generation in reaction buffer (50 mM potassium phosphate buffer, pH 8.0). The reaction mixture was added to a 1 L Erlenmeyer flask and incubated at 30 °C for 2 h at 100 rpm. After 2 h, a 50 µL aliquot was removed and processed in an identical manner to the analytical-scale reactions described above to determine substrate conversion. The remaining reaction mixture was filtered through Celite, acidified to pH 2.0 and extracted with EtOAc (3 x 500 mL). The combined organic layers were dried over sodium sulfate, filtered and concentrated under reduced pressure. The resulting mixture was purified on silica gel (MeOH/AcOH/DCM, 1:1:10) to afford the *o*-quinol product.

Preparation of freeze-dried cells: Expression of TropB was carried out as described above. The resulting crude cell pellet was aliquoted into 10 mg portions and resuspended in the appropriate excipient solution (40 mL, 10% w/v excipient in Milli-Q water) and pelleted in an Eppendorf tube. The tube was then covered with a KimWipe© and lyophilized for 10 h. The resulting powder was then used as in typical whole-cell reactions described below.

Chapter 4.5.2: Synthesis of Compounds

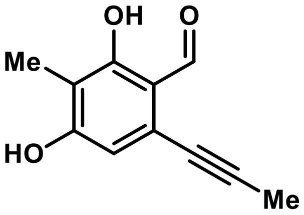

2,4-dihydroxy-3-methyl-6-(prop-1-yn-1-yl)benzaldehyde (4.14)

6-Bromo-2,4-dihydroxy-3-methylbenzaldehyde (100 mg, 0.433 mmol, 1.0 equiv), $PdCl_2(PPh_3)_2$ (30.4 mg, 0.043 mmol, 0.1 equiv) and CuI (8.2 mg, 0.043 mmol, 0.1 equiv) in 3.1 mL anhydrous DMF. Trimethyl(propargyl)silane (77.4 μL, 0.520 mmol, 1.2 equiv) and Et_3N (197 μL, 1.43 mmol, 3.3 equiv). The resulting mixture was heated at 60 °C for 14 h. The reaction mixture was cooled to rt, diluted with water (5 mL), and neutralized with 1.0 N aqueous HCl (2 mL). The mixture was extracted with EtOAc (3 x 15 mL). The combined organic layers were washed with water (10 mL) and brine (10 mL), dried over anhydrous sodium sulfate, filtered, and concentrated under reduced pressure. Purification on silica gel (20% EtOAc in hexanes) provided 54.0 mg (67% yield) of 2-alkynylbenzaldehyde **4.14** as a yellow solid; **^{1}H NMR** (600 MHz, CD_3OD) δ 10.13 (3, 1H), 6.47 (s, 1H), 2.08 (s, 3H), 2.02 (s, 3H); **^{13}C NMR** (150 MHz, CD_3OD) δ 194.5, 162.8, 162.6, 127.1, 113.4, 111.7, 111.4, 91.7, 74.5, 5.9, 2.4; **HR-ESI-MS** *m/z* calculated for $C_{11}H_9O_3$ $[M-H]^-$ 189.0557, found 189.0556; **IR** (thin film) 2942, 2851, 1753, 1700, 1673 cm^{-1}; **MP**: 94.7-95.3 °C.

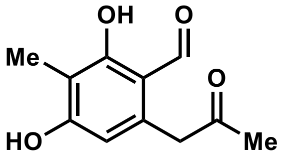

2,4-dihydroxy-3-methyl-6-(2-oxopropyl)benzaldehyde (4.11)

2,4-dihydroxy-3-methyl-6-(prop-1-yn-1-yl)benzaldehyde (50.0 mg, 0.263 mmol, 1.0 equiv) and $AgNO_3$ (4.4 mg, 0.026 mmol, 0.1 equiv) were added to a flame-dried round-bottom flask followed by DCE (2.5 mL) and TFA (99.0 μL, 0.148 mmol, 5.0 equiv). The resulting mixture was stirred at rt for 45 min. MeCN and water (5 mL, 10:1) were added and the mixture was stirred for 1 h. The mixture was then concentrated under reduced pressure. The residue was diluted with EtOAc (5 mL), washed with water (2 mL) and brine (2 mL). The organic layer was then dried over sodium sulfate, filtered, and concentrated under reduced pressure. Purification on silica gel (30% EtOAc in hexanes) provided 19.2 mg (35% yield) of the aldehyde **56** as a tan solid. **^{1}H NMR** (400 MHz, $CDCl_3$): 12.61 (s, 1H), 9.84 (s, 1H), 6.17 (s, 1H), 3.91 (s, 2H), 2.25 (s, 3H), 2.06 (s, 3H). All spectra obtained were consistent with literature values.[28]

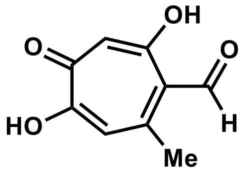

4,7-dihydroxy-2-methyl-5-oxocyclohepta-1,3,6-triene-1-carbaldehyde (4.6)

2,4-Dihydroxy-3,6-dimethylbenzaldehyde (**4.3**) (10 mg, 2.5 mM, 50 mM im DMSO) was added to a crystalizing dish containing 5 μM TropB, 16 μM TropC, 5 mM G6P, 0.2 units/mL GDPDH, 1 mM $NADP^+$, 0.2 μM $FeSO_4$, 5 mM α-ketoglutarate, 8 mM sodium ascorbate in 100 mM TES buffer pH 7.0. The mixture was heated to 30 °C for 17 h at which time the reaction was diluted with water (20 mL) and acidified to a pH of 2. Amberlite resin XAD 16N 20-60 mesh (2.5 g) was then added to the solution and allowed to stir at rt for 2 h. The mixture was filtered through a sintered glass funnel and the resin was washed with water (6 mL). The product was eluted with MeOH (12 mL) and the eluent concentrated. The crude residue was then purified by preparative HPLC using a Phenomenex Kinetex 5 µm C18, 150 x 21.2 mm column under the following conditions: mobile phase A = deionized water + 0.1% formic acid and B = acetonitrile + 0.1% formic acid; method = 5% to 100% B over 13 min, 100% B for 4 min; flow rate, 15 mL/min to afford 3.4 mg (31% yield) of the tropolone as an orange oil.**^{1}H NMR** (600 MHz, DMSO-d$_6$) δ 9.99 (s, 1H), 6.72 (s, 1H), 6.67 (s, 1H), 2.55 (s, 3H), 1.22 (s, 2H). All spectra obtained were consistent with literature values.[11]

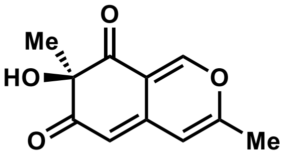

(*R*)-7-hydroxy-3,7-dimethyl-6H-isochromene-6,8(7H)-dione (4.13)

The title compound was synthesized according to the general procedure for 10 mg-scale in vitro enzymatic oxidative dearomatization. Purification by preparative HPLC afforded 5.3 mg (54% yield) of the title compound as a dark orange oil. **^{1}H NMR** (400 MHz, CDCl$_3$) δ 7.87 (s, 1H), 6.12 (s, 1H), 5.51 (s, 1H), 2.19 (s, 3H), 1.55 (s, 3H). All spectra obtained were consistent with literature values.[26] $[\alpha]_D^{25}$ -126 (*c* 0.1, MeOH); reported[22] $[\alpha]_D^{20}$ +54.7 (*c* 0.08, MeOH). As predicted, the *R* stereoselectivity of AzaH afforded the C7 epimer of the reported natural product.

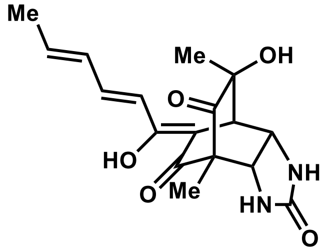

Urea sorbicillinoid (4.10)

Sorbicillin (**4.7**) (5 mg, 2.5 mM, 50 mM in DMSO) was added to a crystalizing dish containing 5 μM SorbC, 5 mM G6P, 0.2 units/mL GDPDH and 1 mM $NADP^+$ in 50 mM potassium phosphate buffer pH 8.0. The mixture was heated to 30 °C for 2 h at which time 1,3-diacetyl-2,3-dihydro-1H-imidazol-2-on (25 equiv, 0.538 mmol, 500 mM in DMSO) was added and the reaction was heated to 80 °C for 8 h. The reaction was acidified to pH of 4 and extracted with EtOAc (3 x 20 mL). The combined organic layers were dried over sodium sulfate, filtered and concentrated under reduced pressure. The crude residue was then dissolved in THF (53 μL) and LiOH (sat. aq. 25 μL) was added. After 1 h the reaction was halted by the addition of 1 M HCl (30 μL) and the mixture was extracted with EtOAc (3 x 2 mL). The combined organic layers were dried over sodium sulfate, filtered and concentrated under reduced pressure. The crude residue was then purified by preparative HPLC using a Phenomenex Kinetex 5 µm C18, 150 x 21.2 mm column under the following conditions: mobile phase A = deionized water + 0.1% formic acid and B = acetonitrile + 0.1% formic acid; method = 5% to 100% B over 20 min, 100% B for 5 min, flow rate, 15 mL/min to afford 1.5 mg (21%) of urea sorbicillinoid as a yellow oil. **^{1}H NMR** (600 MHz, DMSO) δ 14.16 (s, 1H), 7.20 (dd, J = 14.8, 10.8 Hz, 1H), 6.77 (s, 1H), 6.53 (s, 1H), 6.48 (J = 14.8 Hz, 1H), 6.35 (m, 1H), 6.04 (s, 1H), 4.48 (m, 1H), 3.85 (m, 1H), 3.26 (s, 5H), 3.20 (d, J = 3.0 Hz, 1H), 3.14 (d, J = 5.1 Hz, 1H), 1.83 (d, J = 6.7 Hz, 3H), 1.05 (s, 3H), 1.04 (s, 3H); $[\alpha]_D^{25}$ +99 (*c* 0.1, MeOH); reported[23] $[\alpha]_D^{25}$ +50 (*c* 0.1, MeOH). All spectra obtained were consistent with literature values.[24]

Chapter 4.5.3: SFC Traces of Chiral Compounds

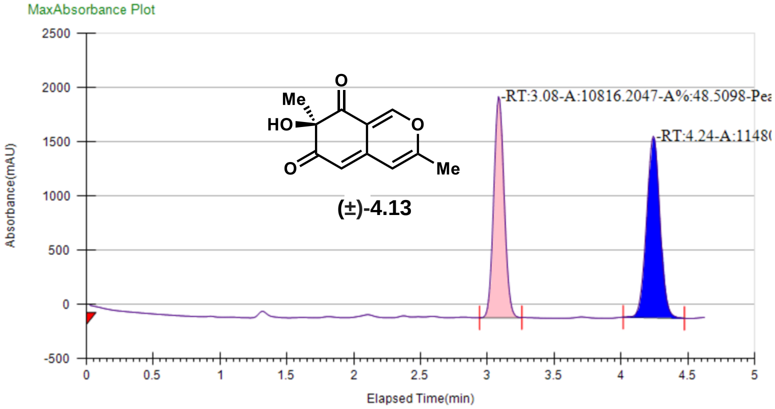

Run Information

Instrument Method	Inj. Vol.	Solvent	Column	Sample	Well Location	Temp.	Flow	% Modifier	Pressure
AD-H_30%_300-330	5	iPrOH	AD-H Chiral Analytical	sbdIV-174_30%	12A	40	3.5	30	120

Peak Information

Peak No	% Area	Area	Ret. Time	Height	Cap. Factor
1	48.5098	10816.2047	3.08 min	2038.3863	3082.3
2	51.4902	11480.7275	4.24 min	1675.0946	4240.6167

4.13 from AzaH reaction

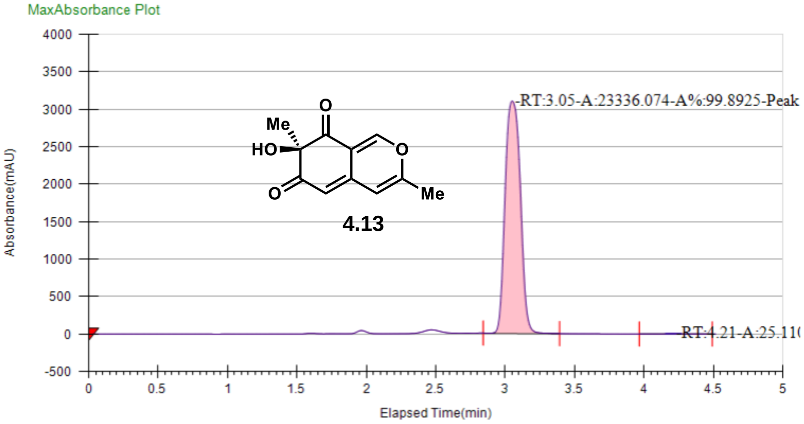

Run Information

Instrument Method	Inj. Vol.	Solvent	Column	Sample	Well Location	Temp.	Flow	% Modifier	Pressure
AD-H_30%_300-330	10	iPrOH	AD-H Chiral Analytical	sbdIV-108_30iPrOH	12A	40	3.5	30	120

Peak Information

Peak No	% Area	Area	Ret. Time	Height	Cap. Factor
1	99.8925	23336.074	3.05 min	3103.1264	3049.0167
2	0.1075	25.1102	4.21 min	2.823	4207.35

Chapter 4.5.4: NMR Spectra of Synthetic Compounds

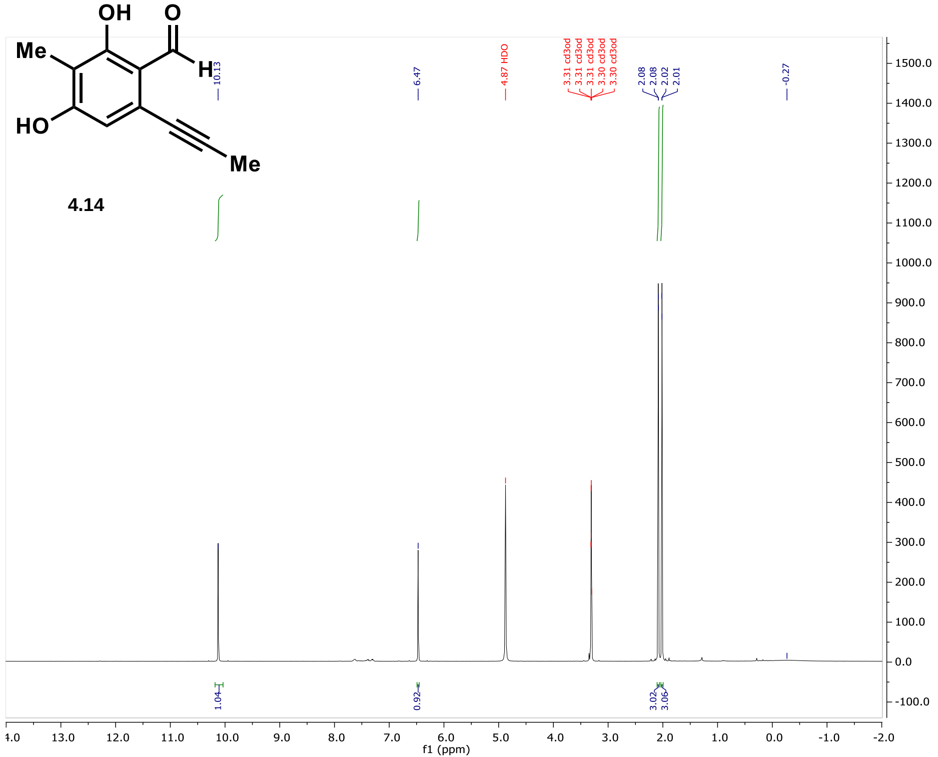

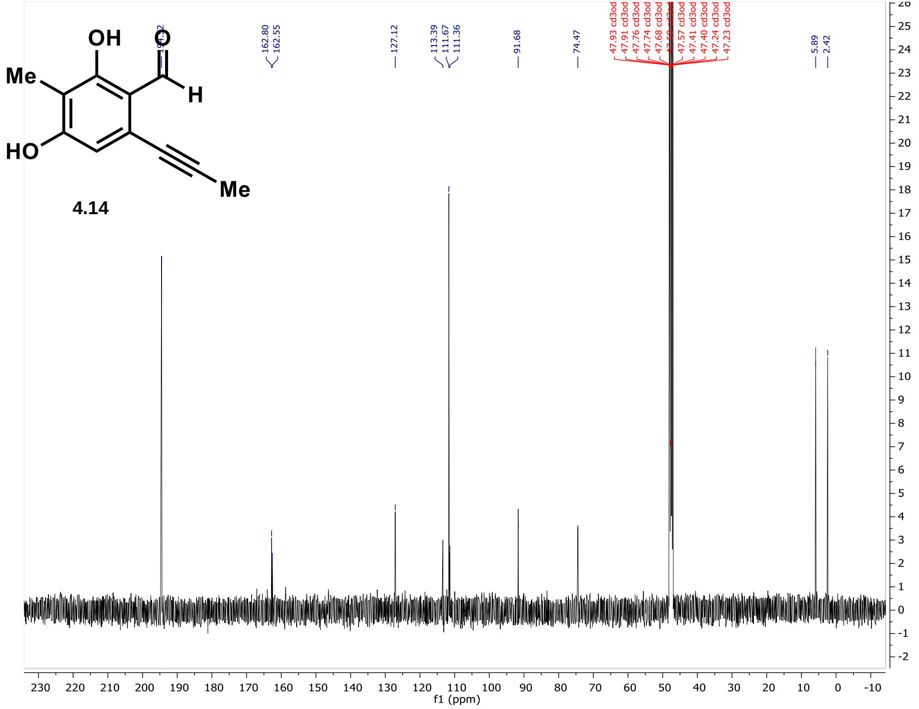

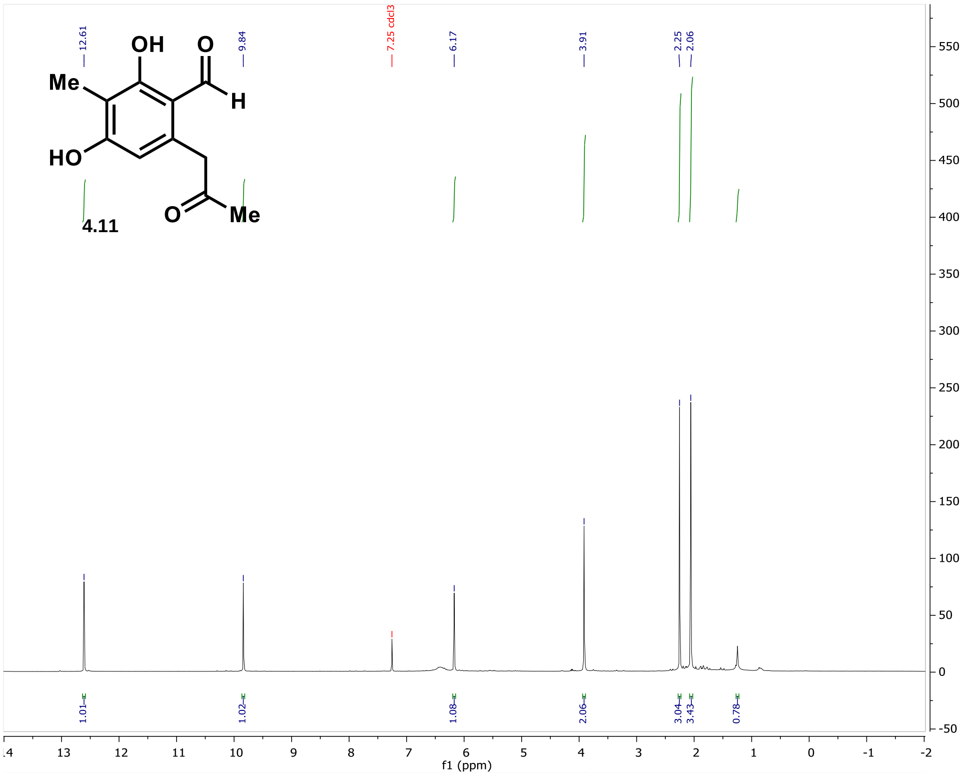

4.11
OH
O
Me
H
HO
O
Me
12.61
9.84
7.25 cdcl3
6.17
3.91
2.25
2.06
1.01
1.02
1.08
2.06
3.04
3.43
0.78
f1 (ppm)

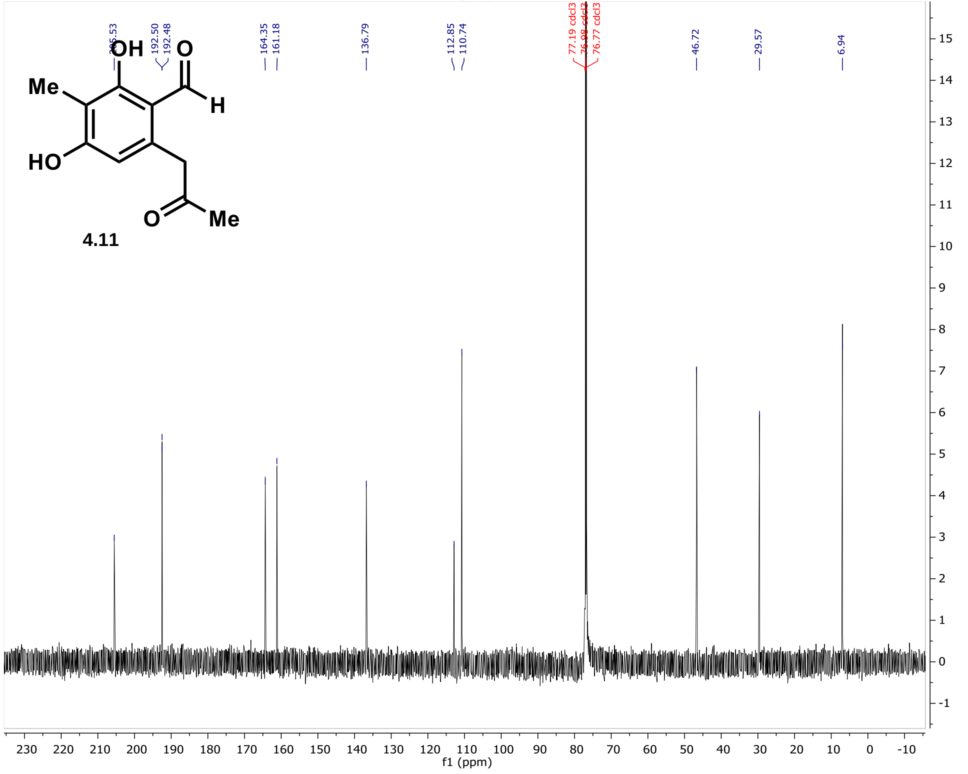

4.11
OH
O
Me
H
HO
O
Me
205.53
192.50
192.48
164.35
161.18
136.79
112.85
110.74
77.19 cdcl3
76.98 cdcl3
76.77 cdcl3
46.72
29.57
6.94
f1 (ppm)

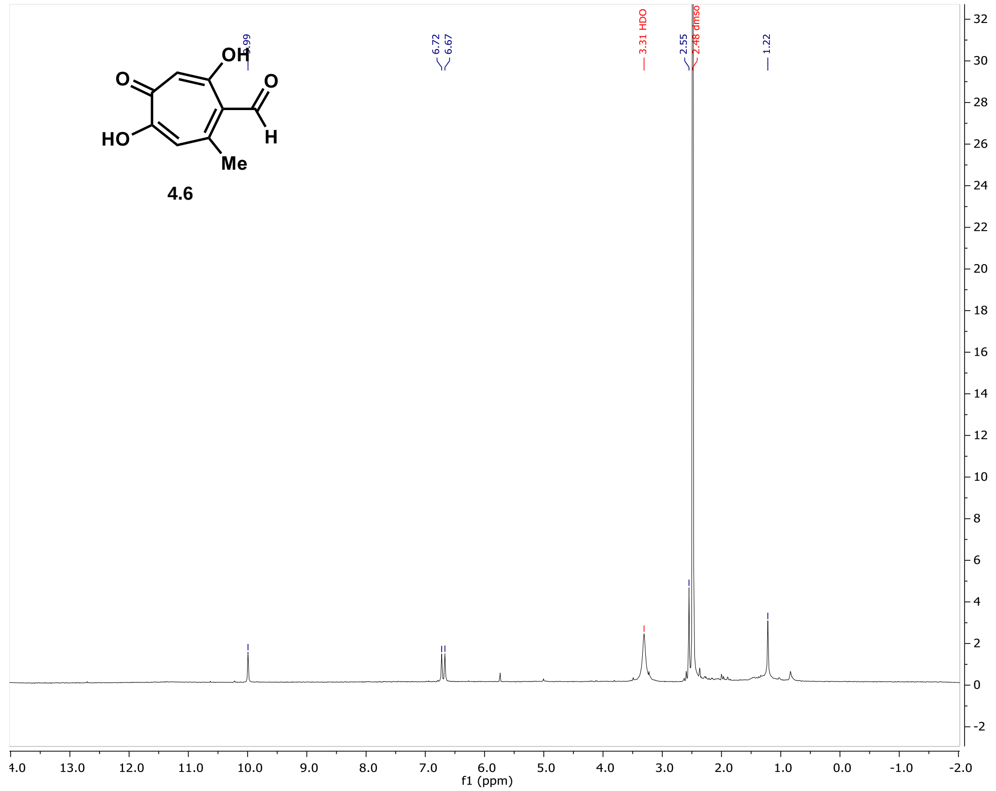
4.6
9.99
6.72
6.67
3.31 HDO
2.55
2.48 dmso
1.22
OH
O
HO
Me
H
f1 (ppm)

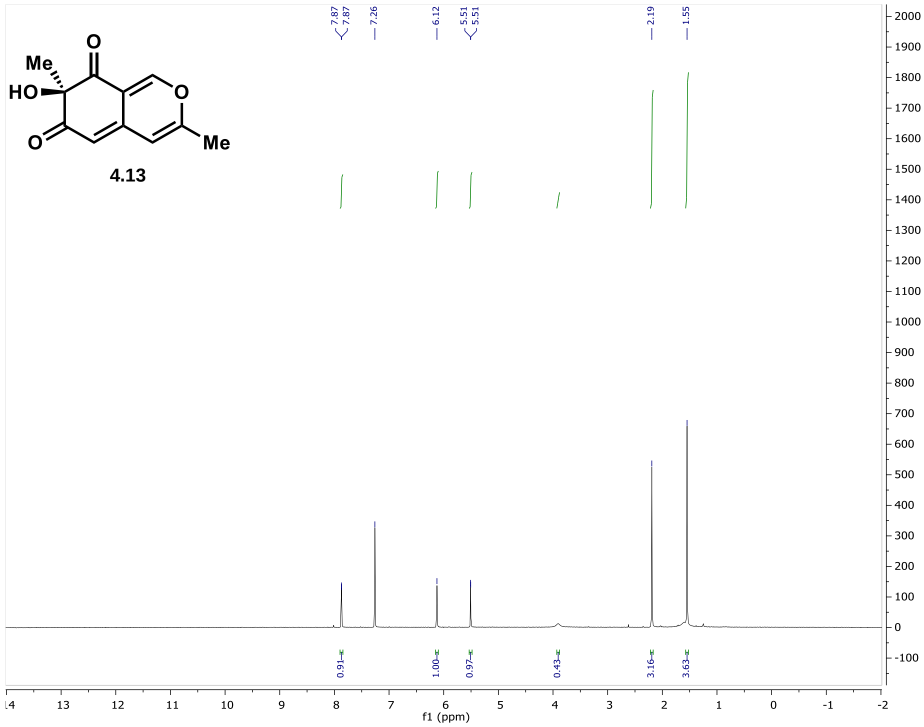
4.13
7.87
7.87
7.26
6.12
5.51
5.51
2.19
1.55
Me
HO
O
Me
0.91
1.00
0.97
0.43
3.16
3.63
f1 (ppm)

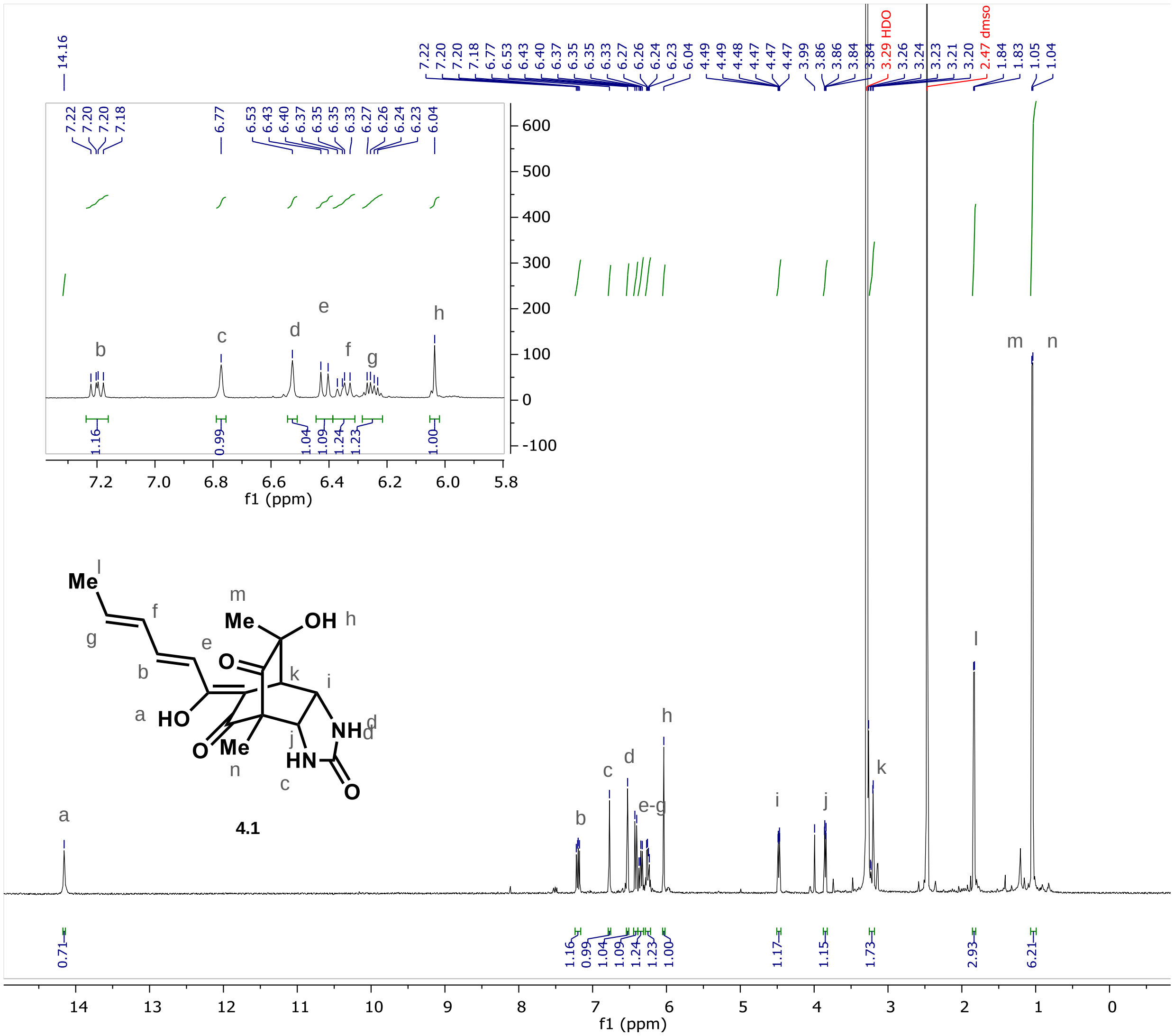

Figure 4.5: NMR spectra of synthetic compounds.

Chapter 4.6: References

1) Devine, P. N.; Howard, R. M.; Kumar, R.; Thompson, M. P.; Truppo, M. D.; Turner, N. J. *Nat. Rev. Chem.* **2018**, *2*, 409-421.
2) Campos, K. R.; Coleman, P. J.; Alvarez, J. C.; Dreher, S. D.; Garbaccio, R. M.; Terrett, N. K.; Tillyer, R. D.; Truppo, M. D.; Parmee, E. R. **2019**, *363*, eaat0805.
3) Baker Dockrey, S. A.; Lukowski, A. L.; Becker, M. R., Narayan, A. R. H. *Nat. Chem.* **2018**, *10*, 119.
4) Sheldon, R. A.; Woodley, J. M. *Chem. Rev*. **2018**, *118*, 801-838.
5) Bedu-Addu, F. K. *Pharmaceutical Technology (Lyophilization)* **2004**, *2*, 10–18.
6) Baheti, A.; Kumar, L.; Bansal, A. K. *J.Excip. Food Chem.* **2010**, *41*, 41–54.
7) Randolph, T. W. *J. Pharm. Sci.* **1997**, *86*, 1198–1203.
8) Schrittwieser, J. H.; Velikogne, S.; Hall, M.; Kroutil, W. *Chem. Rev.* **2018**, *118*, 270.
9) Mority, Y.; Matsumera, E.; Okabe, T.; Fukui, T.; Ohe, T.; Ishida, N.; Inamori, Y. *Biol. Pharm. Bull*. **2004**, *27*, 1666-1669.
10) Meck, C.; D'Erasmo, M. P.; Hirsch, D. R.; Murelli, R. P. *Med. Chem. Commun.* **2014**, *5*, 842-852.
11) Davison, J.; al Fahad, A.; Cai, M.; Song, Z.; Yehia, S.Y.; Lazarus, C.M.; Bailey, A.M.; Simpson, T.J.; Cox, R.J. *Proc. Nat'l. Acad. Sci.* **2012**, *109*, 7642-7647.
12) He, Y.; Cox, R.J. *Chem. Sci.* **2016**, *7*, 2119.
13) Solomon, E.L.; Decker, A.; Lehnert, N. *Proc. Nat'l. Acad. Sci.* **2003**, *100*, 3589-3594.
14) Hausinger, R.P. *Crit. Rev. Biochem. Mol. Biol.* **2004**, *39*, 21-68.
15) a) Bartels-Keith, J. R.; Johnson, A. W.; Taylor, W. I. *J. Chem. Soc.* **1951**, 2352. b) Reisman, S. E.; Nani, R. R.; Levin S. *Synlett.* **2011**, 2437.
16) a) Boger, D. L.; Brotherton, C. E. *Tetrahedron.* **1986**, *42*, 2777. b) Boger, D. L.; Zhu, Y. *Tetrahedron Lett.* **1991**, *32*, 764.
17) Burns, N. Z.; Witten, M. R.; Jacobsen, E. N. *J. Am. Chem. Soc.* **2011**, *133*,14578. b) Meck, C.; Mohd, N.; Murelli, R. P. *Org Lett.* **2012**,*14*, 5988.
18) a) Cook, J. W. *Chem. Ind.* **1950**, 427. b) Knight, J. D.; Cram, D. J. *J. Am. Chem. Soc.* **1951**, *73*, 4136.
19) Sticher, O. *Nat. Prod. Rep.* **2008**, *25*, 517.
20) Harned, A. M.; Volp, K. A. *Nat. Prod. Rep.* **2011**, *28*, 1790.
21) Nicolaou, K. C.; Vassilikogiannakis, G.; Simonsen, K. B.; Baran, P. S.; Zhong, Y.-L.; Vidali, V. P.; Pitsinos, E. N.; Couladouros, E. A. *J. Am. Chem. Soc.* **2000**, *122*, 3071.
22) Barnes-Seeman, D., Corey, E. J. *Org. Lett.* **1999**, *1*, 1503-1504.
23) Wood, J. L.; Thompson, B. D.; Yusuff, N.; Pflum, D. A.; Matthaus, M. S. P. *J. Am. Chem. Soc.* **2001**, *123*, 2097.
24) Zhang, S.-P.; Huang, R.; Li, F.-F.; Fange, X.-W.; Lin, D.-G.; He, J. *Fitoterapia*, **2016**, *112*, 85.
25) a) Sib, A.; Gulder, T. A. M. *Angew. Chem., Int. Ed.* **2017**, *56*, 12888–12891. b) Sib, A.; Gulder, T. A. M. *Angew. Chem., Int. Ed.* **2018**, *57*, 14650–14653.
26) Cabrera, G. M.; Butler, M.; Rodriguez, M. A.; Godeas, A.; Haddad, R.; Ederlin, M. N. *J. Nat. Prod.* **2006**, *69*, 1806.
27) For a review see: Gao, J.-M.; Yang, S.-X.; Qin, J.-C. *Chem. Rev.* **2013**, *113*, 4755.
28) Suzuki, T. Tanemura, K.; Okada C.; Arai, K.; Awaji, A.; Shimizu, T.; Horaguchi, T. *J. Heterocyclic Chem.* **2001**, *38*, 1409-1418.

CHAPTER 5: Chemoenzymatic, Stereodivergent Synthesis of Azaphilone Natural Products

Portions adapted with permission from “"Stereodivergent, Chemoenzymatic Synthesis of Azaphilone Natural Products." J. Am. Chem. Soc. **2019**, *141*, 18551-18559.

Chapter 5.1: Introduction

Azaphilone natural products are characterized by an oxygenated pyranoquinone bicyclic core bearing a single tetrasubstituted carbon (Figure 5.1A).[1] Isolated from fungal sources, this

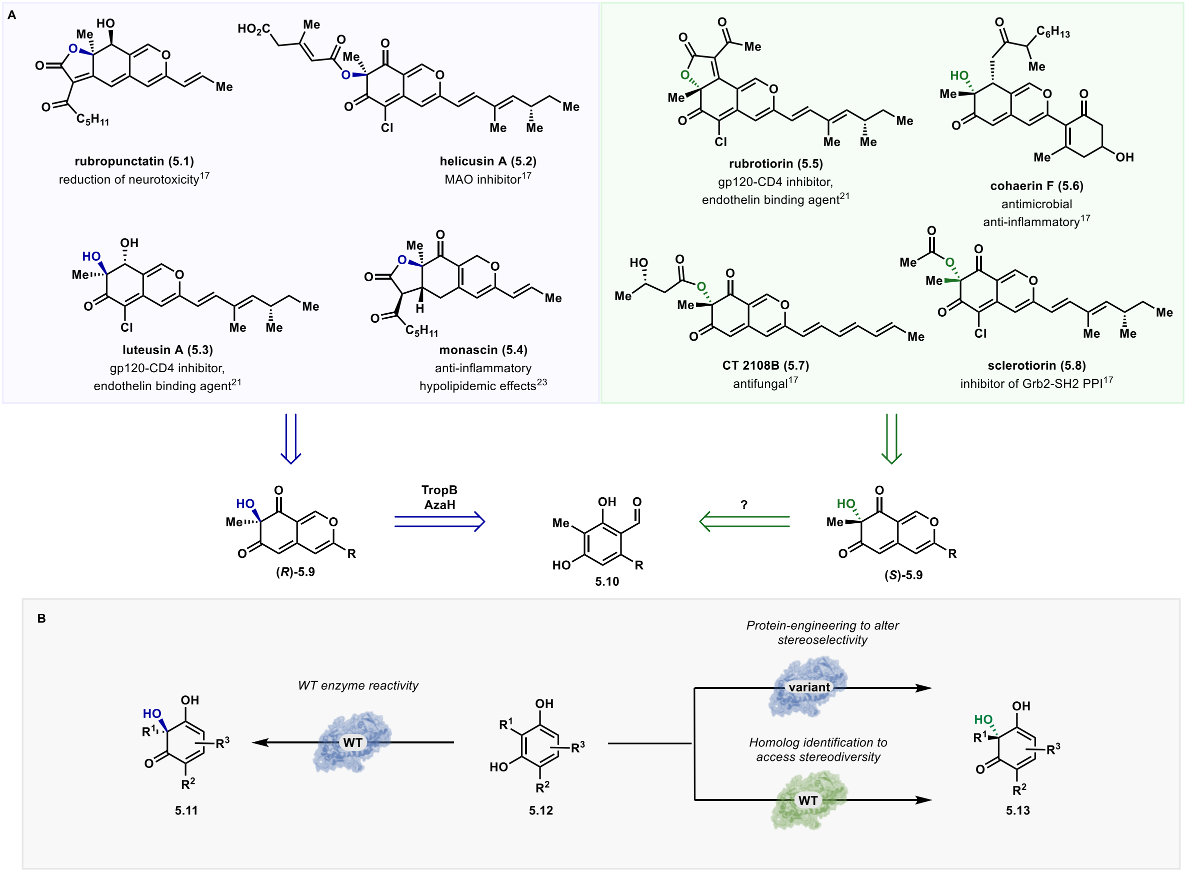
A
rubropunctatin (5.1)
reduction of neurotoxicity17
helicusin A (5.2)
MAO inhibitor17
luteusin A (5.3)
gp120-CD4 inhibitor,
endothelin binding agent21
monascin (5.4)
anti-inflammatory
hypolipidemic effects23
rubrotiorin (5.5)
gp120-CD4 inhibitor,
endothelin binding agent21
cohaerin F (5.6)
antimicrobial
anti-inflammatory17
CT 2108B (5.7)
antifungal17
sclerotiorin (5.8)
inhibitor of Grb2-SH2 PPI17
(R)-5.9
TropB
AzaH
5.10
?
(S)-5.9
B
WT enzyme reactivity
WT
5.11
5.12
Protein-engineering to alter stereoselectivity
variant
Homolog identification to access stereodiversity
WT
5.13

Figure 5.1: (A) Biologically active azaphilone natural products feature both the *R*- and *S*-configuration at the C7 stereocenter.[1,4,6] Biocatalytic oxidative dearomatization gives access to either enantiomer via AzaH or AfoD mediated oxidation. (A) Approaches to enabling biocatalytic stereodiversity.

large family of natural products is known to contain a diverse array of structural features that impart a wide range of biological properties including anticancer,[2,3,4] antiviral,[5] and anti-inflammatory activities.[4,6] For example, luteusin A (**5.3**) and rubrorotiorin (**5.5**) were found to inhibit the binding of the HIV surface glycoprotein gp120 to the human CD4 protein, making these natural products potential starting points for the development of therapeutic agents against the virus.[4] In addition, monascin (**5.4**), a tricyclic azaphilone natural product, has been shown to down-regulate steatohepatitis in a mouse model, indicating that these secondary metabolites have potential as therapeutics for non-alcoholic fatty liver disease.[6] As illustrated in Figure 5.1A, azaphilone natural products can contain either the *R*- or *S*-configuration at the C7-position. Several cases of epimeric azaphilones are known, in which each C7-epimer is produced by a distinct fungal source.[7, 8] The pharmaceutical potential of these molecules has been demonstrated through initial in vitro and cell-based assays of isolated natural products;[9,10,11] however, to gain a more comprehensive understanding of the therapeutic potential of these molecules, the challenge of constructing the densely functionalized core and C7-configuration for exploration of this stereocenter's impact on biological activity must be addressed.[7,8,12]

The first total syntheses of azaphilones were reported nearly half a century ago by Whalley and coworkers.[11] Their 11-step synthesis of (±)-mitorubrin features a $Pb(OAc)_4$ oxidative dearomatization of pyranoquinone as a key step.[11] This strategy of constructing densely functionalized aromatic precursors which undergo metal-catalyzed cyclization followed by dearomatization has been widely employed to access a number of azaphilones including citrinin,[13] the epicocconone core,[14] a number of chitoviridinins,[15] and chlorofusin.[16] Each of these syntheses employed either $Pb(OAc)_4$ or IBX in the dearomatizative step, resulting in racemic syntheses of the targets. The limitations during this period for enantioselective oxidative dearomatizations inspired a seminal contribution from the Porco group.[16] They reported a copper-oxo-sparteine oxidant which was capable of delivering dearomatized products from benzaldehyde or pyranoquinone substrates in good yields and excellent enantioselectivites (see Chapter 2, Figure 2.1).[16] The asymmetric total synthesis of a number of azaphilone natural products were synthesized using this oxidant. This methodology requires super-stoichiometric quantities of the chiral oxidant and cryogenic temperatures, making this a challenging method to employ in a high-throughput manner to access libraries of azaphilones to screen for biological activity.

Our interest in exploring the biologically activity of the azaphilone family has inspired us to develop a general platform for the generation of enantioenriched azaphilones from densely functionalized arene precursors. By employing our FDMOs in the critical dearomatization step, we are able to generate libraries of azaphilones in a relatively high-throughput manner. We had established AzaH as a promiscuous catalyst for oxidative dearomatization to afford the *R* enantiomer of the azaphilone core; however, we desired a stereocomplementary catalyst to enable access to either C7 configuration (Figure 5.1B). This would allow us to then rank and the stereoisomers' efficacy in our biological assays.

Chapter 5.2: Characterization of AzaH Homologs

To survey the selectivity of flavin-dependent monooxygenases related by sequence, Attabey Rodrìguez Benìtez constructed a sequence similarity network (SSN) of flavin-dependent monooxygenases (Figure 5.2A).[17,18,19] SSNs are visual representations of the relatedness of protein sequences, which cluster based on similarity thresholds. This approach can enable the rapid and logical investigation of proteins likely to demonstrate similar reactivity and/or selectivity, dramatically reducing the time and search space required during screening, considerations critical to improving the compatibility of biocatalytic approaches and traditional synthetic strategies. The protein family (Pfam01494) of flavin-dependent monooxygenases includes over 45,000 enzymes. This data set was truncated by limiting the search to edges possessing an alignment score greater than 110, which returned 1,211 sequences (Figure 5.2A). We noted that the enzymes we had previously investigated, AzaH, TropB, and SorbC, were each located in distinct groups or "clusters" within the network, and that a fourth tight clustering of sequences formed between the TropB and SorbC clusters containing an enzyme associated with asperfuranone biosynthesis, AfoD.[20,21,22] Previous in vivo studies[23] and bioinformatic analysis[24] indicated that AfoD is responsible for oxidative dearomatization of an asperfuranone precursor with the same site-selectivity as TropB and AzaH;[22] however, the absolute configuration of asperfuranone suggests that AfoD carries out this transformation with the opposite facial selectivity.[21]

We hypothesized that sequences with high similarity to *tropB*, *azaH*, *afoD* and *sorbC* would encode for enzymes that possess the ability to carry out oxidative dearomatization reactions, and further questioned if trends in site- and stereoselectivity could be predicted based on sequence. To test this hypothesis, seven sequences were selected based on proximity to either TropB, AzaH, AfoD or SorbC in the SSN (labeled FDMO1-7 in Figure 5.2A). Attabey Rodrìguez Benìtez and Sarah Ackenhusen transformed and expressed FDMO1-7. Under standard expression conditions, nine proteins were successfully obtained, whereas FDMO1 and FDMO3 proved insoluble under these conditions (Figure 5.2B). The reactivity of the nine soluble enzymes was evaluated with two substrates, **5.14** and **5.15**. Gratifyingly, all nine enzymes showed activity with one of the two model substrates, eight of which displayed sufficiently high activity for product isolation from preparative-scale reactions (Figure 5.2B). A single product was obtained from each biocatalytic reaction and a strong trend in site-selectivity was clear from this data: FDMO7, the enzyme most similar to SorbC, afforded C5-hydroxylated product (see **5.15**), whereas the remaining enzymes

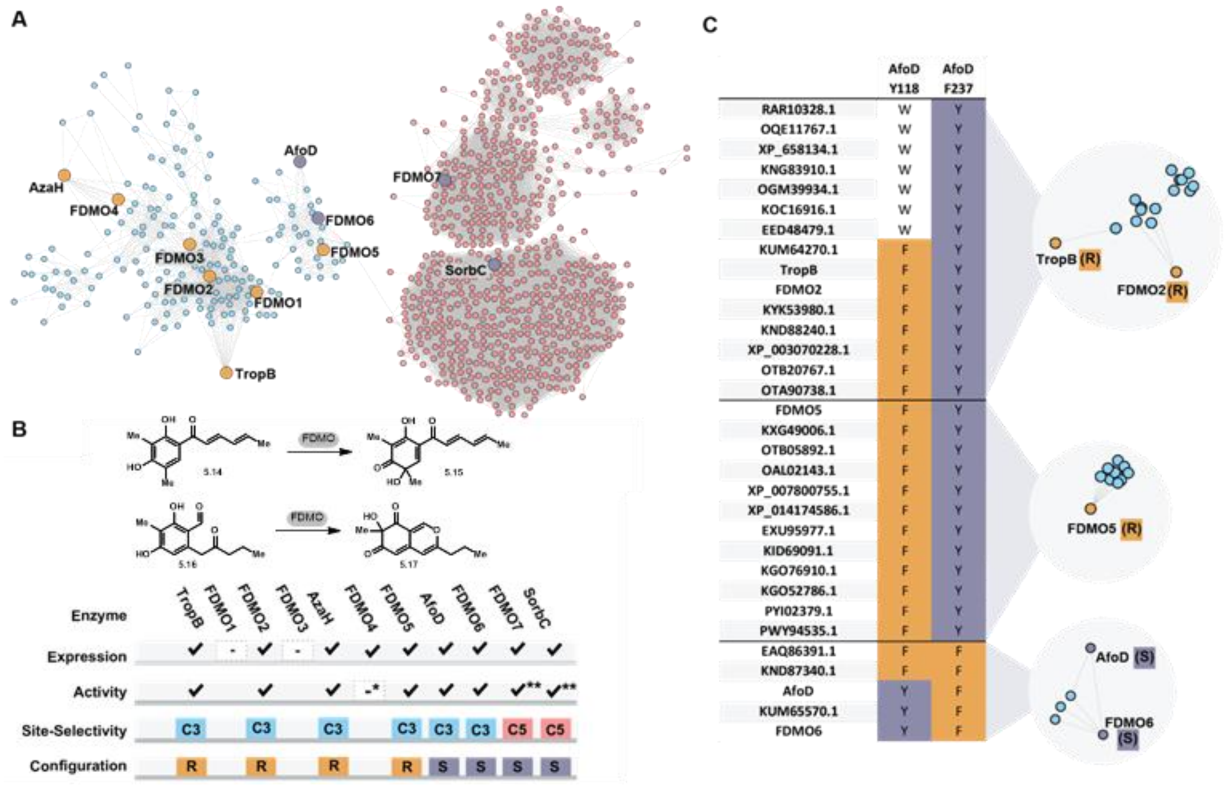
A
AzaH
FDMO4
FDMO3
FDMO2
FDMO1
TropB
AfoD
FDMO6
FDMO5
FDMO7
SorbC
B
FDMO
5.14
5.15
5.16
5.17
Enzyme
TropB
FDMO1
FDMO2
FDMO3
AzaH
FDMO4
FDMO5
AfoD
FDMO6
FDMO7
SorbC
Expression
Activity
Site-Selectivity
Configuration
C3
C5
R
S
C
AfoD Y118
AfoD F237
RAR10328.1
OQE11767.1
XP_658134.1
KNG83910.1
OGM39934.1
KOC16916.1
EED48479.1
KUM64270.1
TropB
FDMO2
KYK53980.1
KND88240.1
XP_003070228.1
OTB20767.1
OTA90738.1
FDMO5
KXG49006.1
OTB05892.1
OAL02143.1
XP_007800755.1
XP_014174586.1
EXU95977.1
KID69091.1
KGO76910.1
KGO52786.1
PYI02379.1
PWY94535.1
EAQ86391.1
KND87340.1
AfoD
KUM65570.1
FDMO6
W
F
Y
TropB (R)
FDMO2 (R)
FDMO5 (R)
AfoD (S)
FDMO6 (S)

Figure 5.2: A) Sequence similarity network (SSN) of FAD-dependent monooxygenases (Pfam01494) using a sequence alignment score of 110. B) Results of expression, activity with model substrate **5.14** or **5.16****, site- and stereoselectivity of enzymes chosen from the SSN in panel A. *FDMO4 demonstrated <10% conversion by UPLC with substrate **5.16**. C) Selected clusters from a more stringent SSN generated with an alignment score of 150 and corresponding analysis of the multisequence alignment of each cluster. Figure by Attabey Rodrìguez Benìtez.

more similar to TropB, AzaH and AfoD delivered C3-hydroxylated products (see **5.17**). However, the trend between location on the SSN (Figure 5.2A) and stereoselectivity was not apparent. Increasing the alignment score from 110 to 150 produced an SSN that provided greater insight to the relationships between sequences in this family. Notably, previously clustered sequences associated with divergent selectivity, such as AfoD and FDMO5, now clearly separated into distinct clusters (see Figure 5.2C). Analysis of sequence alignments between each of these clusters revealed conserved residues at positions 118 and 237 (AfoD numbering). In general, catalysts that generate products with the *R*-configuration possess a tyrosine at position 237 and an aromatic residue such as phenyalanine or tryptophan at position 118. In contrast, these conserved residues switch positions in biocatalysts that afford products with the *S*-configuration. We previously demonstrated that a two point coordination of the phenolate substrate by Tyr237 and an arginine residue is critical for positioning the substrate within the active site in the *R*-selective enzyme, TropB.[23] Obtaining further structural information on these proteins will aid in demystifying the elements that contribute to the precise stereocontrol exhibited by these catalysts. Beyond the importance of Tyr position in the active site, it is clear that other mechanisms for stereocontrol have evolved in this class of enzymes. For example, catalysts AzaH and SorbC break from this Tyr control mechanism, and in the case of SorbC, we have proposed an alternative mechanism for control of substrate position in the active site (see Chapter 3).[24]

Ultimately, this survey of sequence space surrounding known enzymes provides a greater understanding of the sequence features that can predict site- and stereoselectivity and has increased the number of biocatalysts vetted for this transformation. With catalysts capable of delivering enantiomeric products in hand, we chose to pursue an enantiodivergent synthetic strategy with AzaH and AfoD based on the robust expression and reactivity of these enzymes, in addition to the excellent stereoselectivity of each catalyst. Under reaction conditions to dearomatize model substrate **5.16** using AzaH and AfoD, enantiomeric bicycles (*R*)- and (*S*)-**5.17** were accessed in >99% ee and 98% ee, respectively.

Chapter 5.3: Design and Synthesis of a Common Intermediate

With access to either enantiomer of azaphilone **5.17**, we sought to complete the stereodivergent syntheses of two biologically active azaphilone natural products. To identify a common intermediate that would provide versatility in accessing an array of azaphilone natural products (Figure 5.1B), a number of aromatic substrates were synthesized and subjected to oxidative dearomatization with stereo-complementary biocatalysts. We hypothesized that the orcinaldehyde motif and homobenzylic ketone group would be critical for substrate recognition. In addition, we desired a functional handle to enable late-stage functionalization of the eastern portion of the azaphilone scaffold. Interestingly, the AzaH native substrate was not converted by AfoD (Figure 4, **5.18**). We hypothesize that the β-hydroxy group prevents the substrate from engaging in productive binding interactions and leads to the lack of activity of AfoD as the native substrate of AfoD features a hydrophobic group at this position.[20] This is supported by the activity of the saturated substrate **5.17** with AfoD, which does not contain this polar functional group.

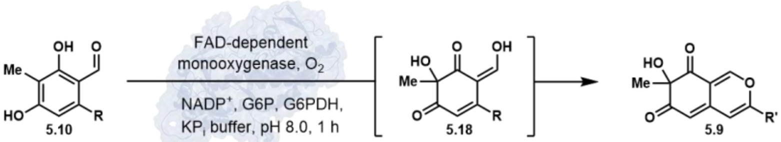
OH
O
Me
HO
R
5.10
FAD-dependent monooxygenase, O$_2$
NADP$^+$, G6P, G6PDH, KP$_i$ buffer, pH 8.0, 1 h
HO
Me
O
OH
O
R
5.18
HO
Me
O
O
R'
O
5.9

substrate	% conversion AzaH	% conversion AfoD	substrate	% conversion AzaH	% conversion AfoD
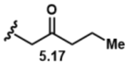 5.17	64	24	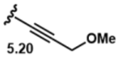 5.20	>99	0
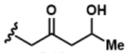 5.18	73	0	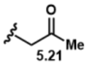 5.21	94	19
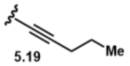 5.19	48	0	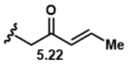 5.22	95	83

Promisingly, two alkynyl substrates that are intermediates in the synthesis of the ketone substrates were accepted by AzaH (**5.19** and **5.20**); however, neither alkyne substrate was converted by AfoD. A simple methyl ketone derivative (**5.21**) demonstrated activity with both enzymes as well; however, its low activity with AfoD ultimately disqualified it as the common substrate. The enone substrate depicted in entry 7 was efficiently dearomatized by both AfoD and AzaH in 83% and 95% conversion, respectively. The high conversions observed for this compound with both enzymes and the synthetic handle afforded by the double bond made it an ideal candidate for the common intermediate in our envisioned divergent synthesis of azaphilone natural products.

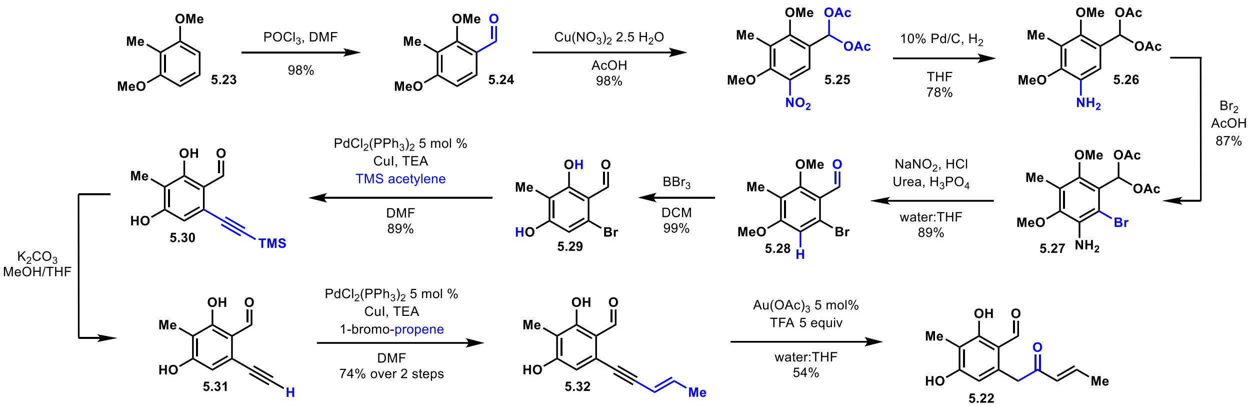

5.23
POCl$_3$, DMF
98%
5.24
Cu(NO$_3$)$_2$ 2.5 H$_2$O
AcOH
98%
5.25
10% Pd/C, H$_2$
THF
78%
5.26
Br$_2$
AcOH
87%
5.27
NaNO$_2$, HCl
Urea, H$_3$PO$_4$
water:THF
89%
5.28
BBr$_3$
DCM
99%
5.29
PdCl$_2$(PPh$_3$)$_2$ 5 mol %
CuI, TEA
TMS acetylene
DMF
89%
5.30
K$_2$CO$_3$
MeOH/THF
5.31
PdCl$_2$(PPh$_3$)$_2$ 5 mol %
CuI, TEA
1-bromo-propene
DMF
74% over 2 steps
5.32
Au(OAc)$_3$ 5 mol%
TFA 5 equiv
water:THF
54%
5.22

Figure 5.4: First-generation synthetic route[25] to common intermediate **5.22** through bromination and iterative Shonogashira couplings.

A drawback to employing this substrate was the added synthetic complication of the double-bond present in **5.22**. A robust and concise route to **5.22** was desired to afford sufficient material for exploration of the late-stage chemistry. Our first-generation route employed aryl bromide **5.29**, accessed as described by Porco[25] as the key synthetic intermediate. Subsequent iterative Sonogashira coupling and Au-catalyzed cyclization and hydration afforded **5.22**. The length of this sequence coupled with the low yielding final step motivated our search for an alternative route.

Inspired by the work of Franck[12] and others[26] we designed a second-generation route which featured a 1,2-addition of densely functionalized arene **5.36** to Weinreb amide **5.37**. Although this was a much more concise route, requiring only five rather than nine steps, several transformations proved to be low yielding, particularly upon scale-up, and required optimization. The first challenge we sought to address was the large amount of competing conjugate addition during Weinreb amide addition. We attributed formation of this byproduct to the stability of lithiate **5.36**. Addition of HMPA as the cosolvent afforded exclusively the 1,4-product.[27] We hypothesized that elevating the temperature of the addition could afford improved selectivity for the desired product,

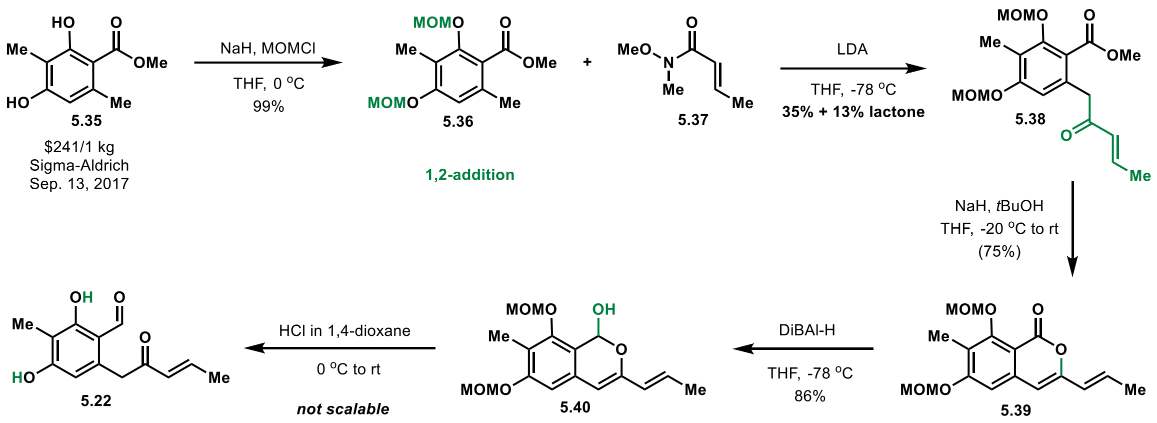
5.35
$241/1 kg
Sigma-Aldrich
Sep. 13, 2017
NaH, MOMCl
THF, 0 °C
99%
5.36
1,2-addition
5.37
LDA
THF, -78 °C
35% + 13% lactone
5.38
NaH, tBuOH
THF, -20 °C to rt
(75%)
5.39
DiBAl-H
THF, -78 °C
86%
5.40
HCl in 1,4-dioxane
0 °C to rt
not scalable
5.22

Figure 5.5: Second-generation synthetic route to common intermediate **5.22** through 1,2-addition and reduction.

however the same ratio of 1,2 to 1,4-addition was observed. However, overall conversion increased, affording a 35% yield of the enone **5.38** and a small amount of the lactone which had undergone base-mediated cyclization during the reaction. This initial trial conducted on 500 mg, was promising however multigram scale reactions typically afforded 20-25%.

Concurrently, we worked to optimize the final step of the sequence towards **5.22**. The deprotection of both MOM groups proved remarkably challenging due to the presence of several acid-sensitive moieties in lactol **5.40**. The masked aldehyde, electron-rich resorcinol and enone fragments were all structural liabilities during this final stage, resulting in decomposition to NMR and UV-Vis silent byproducts when **5.40** was subjected to protic acids under aqueous and anhydrous conditions. A survey of the total synthesis literature featuring late-stage MOM-deprotections afforded several alternatives to protic acids for this deprotection.[28] The strong Lewis acids $LiBF_4$[28d] and $NbCl_5$[28e] were both competent acids to afford the free resorcinol product when

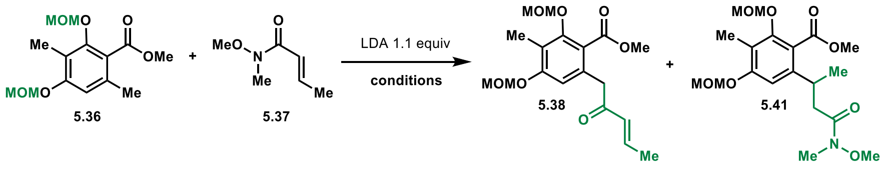
5.36
5.37
LDA 1.1 equiv
conditions
5.38
5.41

Lewis acid	equiv	% conversion	% yield
HCl	2.0 M	75%	38%
TsOH	0.4	>99%	0%
BF_3•OEt_2 PhSH	4.0	58%	0%
$LiBF_4$	14	83%	24%
$LiBF_4$	7.0	99%	62%
$NbCl_5$	7.0	99%	75%

Figure 5.6. Reaction conditions surveyed to improve yield and chemoselectivity of 1,2-addtion.

used in superstoichiomeric amounts with apparently clean reaction profiles as observed by UPLC-PDA. Upon scale-up, however, we encountered reproducibility issues with $LiBF_4$ conditions, with yields between 98 – 20%. Happily, $NbCl_5$ afforded reproducible yields, however, when this material was subjected to our enzymatic oxidative dearomatization conditions, none of the desired activity was observed.

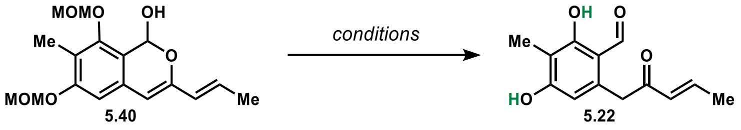

Lewis acid	equiv	% conversion	% yield
HCl	2.0 M	75%	38%
TsOH	0.4	>99%	0%
BF_3•OEt_2 PhSH	4.0	58%	0%
$LiBF_4$	14	83%	24%
$LiBF_4$	7.0	99%	62%
$NbCl_5$	7.0	99%	75%

Figure 5.7: Conditions assayed for MOM-deprotection of **5.40**.

We attributed the lack of reactivity to inorganic impurities in our material. Recrystallization of the crude enone afforded light red crystals which were turned over with the expected efficiency by both FDMOs, although typically 40 to 50% of the mass was lost in this manipulation. Having encountered so many challenges with this second-generation route we reconsidered our strategy towards **5.22**. Porco had reported an abbreviated route to **5.44**, which Katie Rykaczewski, a rotation student at the time, was able to reproduce.[29] This directed lithiation allowed us to eliminate three steps in the synthesis of the meta-functionalized resorcinol core. This improved route allowed for the delivery of the hundreds of milligrams required for downstream chemistry towards the azaphilone natural products.

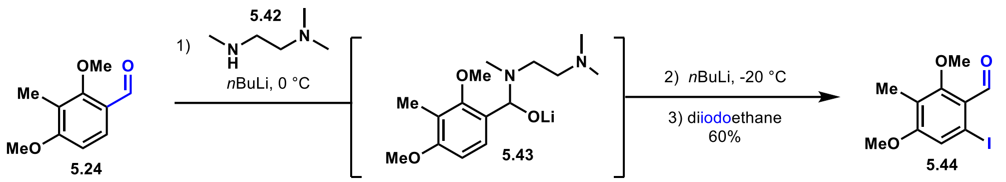
5.24
1)
5.42
nBuLi, 0 °C
5.43
2) nBuLi, -20 °C
3) diiodoethane
60%
5.44

Figure 5.8: 3-step one-pot synthetic of aryl iodide **5.44**.

Chapter 5.4: Total Synthesis of Trichoflectin and Lunatoic Acid A

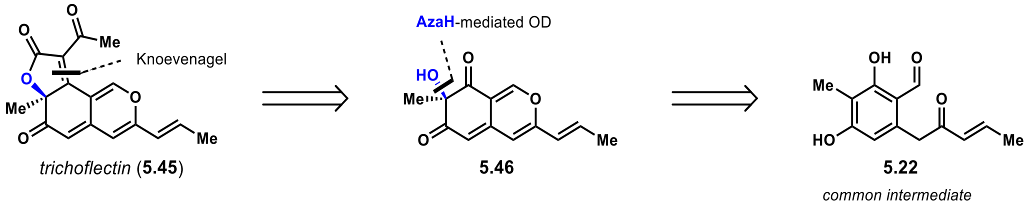
Knoevenagel
trichoflectin (5.45)
AzaH-mediated OD
5.46
5.22
common intermediate

Figure 5.9: Retrosynthetic analysis for trichofectin.

Angular azaphilone, trichoflectin (**5.45**), was the first natural product target chosen as a model for route development that would enable the synthesis of more complex tricyclic azaphilones. First isolated by Sterner in 1998, trichoflectin exhibits moderate antimicrobial activity as well as the ability to inhibit DHN-melanin biosynthesis in certain fungal species.[30] Despite interest in the biological activity of this compound, no total synthesis of trichoflectin has been reported to date. Our proposed retrosynthesis is described in Figure 5.10. We envisioned constructing the butenolide ring of trichoflectin through an intramolecular Knoevenagel condensation following acylation of bicycle **5.46**.[12,14] To obtain the reported (-)-trichoflectin, the C7-stereocenter would be set by stereoselective oxidative dearomatization of enone **5.22** with AzaH.

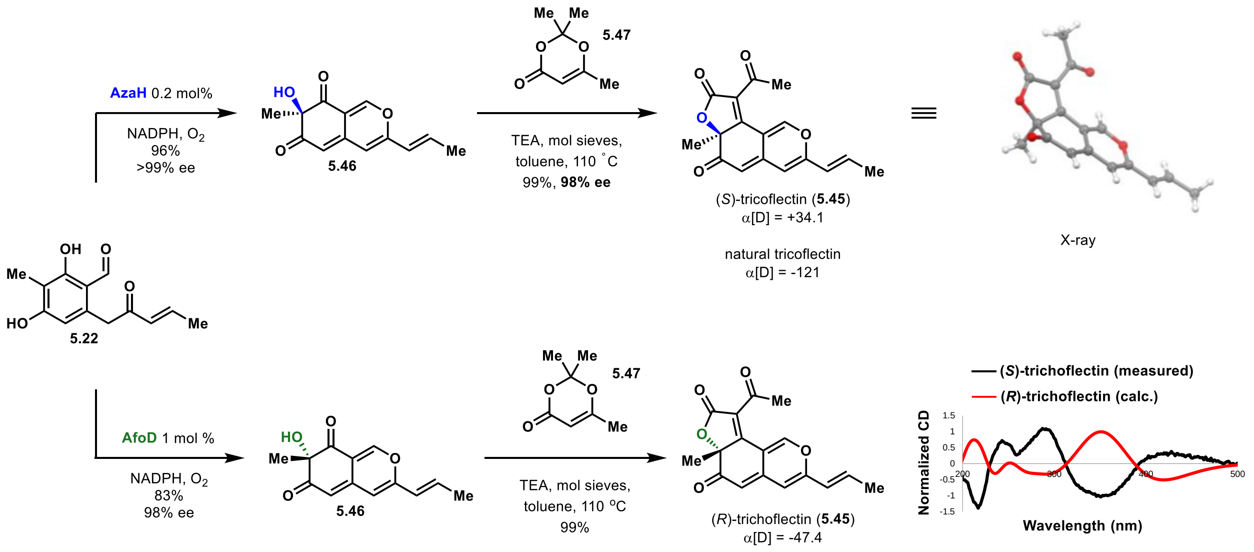
AzaH 0.2 mol%
NADPH, O2
96%
>99% ee
HO
Me
O
5.46
Me
Me Me
5.47
TEA, mol sieves,
toluene, 110 °C
99%, 98% ee
(S)-tricoflectin (5.45)
α[D] = +34.1
natural tricoflectin
α[D] = -121
≡
X-ray
OH
Me
HO
5.22
AfoD 1 mol %
NADPH, O2
83%
98% ee
TEA, mol sieves,
toluene, 110 °C
99%
(R)-trichoflectin (5.45)
α[D] = -47.4
(S)-trichoflectin (measured)
(R)-trichoflectin (calc.)
Normalized CD
1.5
1
0.5
0
-0.5
-1
-1.5
200
300
400
500
Wavelength (nm)

Figure 5.10: Total synthesis of (*S*)- and (*R*)-trichoflectin. Inset: Calculated and measured CD data for (*S*)- and (*R*)-trichoflectin. *NADPH recycling system: G6P (2 equiv), NADP$^+$ (0.4 equiv), G6PDH (1 U/mL).

The synthesis of trichoflectin was initiated with dearomatization of **5.22** with 0.2 mol % AzaH which afforded azaphilone scaffold (*R*)-**5.46** in 96% yield and >99% ee (Figure 5.24). Next, acylation of (*R*)-**5.46** with the acylketene generated *in situ* from precursor **5.47** followed by Knoevenagel condensation provided (*S*)-trichoflectin ((*S*)-**5.45**) in 99% yield. This level of selectivity was unexpected as Franck and coworkers reported the isolation of both angular and linear tricycles when constructing the butenolide ring of a similar azaphilone scaffold, proposing the distribution of these products is controlled by the steric properties of the acyl group.[14] However, in our system, the desired angular tricycle was produced exclusively. We attribute this to a difference in electronic properties of the extended π-system and have observed through attempts to reduce the C8-ketone that this position is more electrophilic than the C6-ketone.

Unexpectedly, the sign of the optical rotation of our synthetic (*S*)-**5.45** was opposite to that which is reported for the natural product (measured +34.1, reported -121).[29] To rule out the possibility of stereocenter inversion during the construction of the butenolide ring or that the enzyme performed the dearomatization on this particular substrate with unanticipated facial selectivity, a CD spectrum was calculated by our collaborator Dr. Leo Joyce, currently of Arrowhead Pharmaceuticals, and compared to the measured spectrum of synthetic (*S*)-**5.45**. As depicted in Figure 5.10, the calculated CD spectrum for (*R*)-trichoflectin is equal and opposite to the measured spectrum from (*S*)-trichoflectin, initially suggesting that the C7-stereocenter had been installed as anticipated. Ultimately, with the aid and expertise of Dr. Ren Wiscons, an X-ray crystal structure was obtained of the AzaH-produced tricycle, unambiguously confirming the C7-configuration of (+)-trichoflectin as *S* (Figure 5.10). Based on these data, we suspected that the natural product was misassigned. A 1976 report, which has been the basis for assignment of absolute configuration in the case of trichoflectin and many other azaphilone natural products, suggests that the optical rotation of these compounds is controlled solely by the C7-stereocenter.[30] However, we have found that the electronic properties of the azaphilone core, as well as the presence of other stereocenters in the compound, can have a significant impact on the optical rotation based on computational modeling performed by Dr. Leo Joyce. To confirm the configuration of the natural product as *R* rather than *S* as assigned upon isolation, Joshua Pyser synthesized the enantiomeric tricycle from the AfoD generated product (*S*)-**5.45** (Figure 5.10). The optical rotation of (*R*)-**5.45** was measured as -47.4, agreeing in sign with the characterization of the isolated natural product. Therefore, it is proposed that the structure of the natural product be revised to the *R*-configuration.

This revision prompted a careful inspection of the absolute configuration of structurally related angular tricycles. An azaphilone series called the deflectins, which are reported to possess inhibitory activity of bacteria and erythrocytes as well as cytotoxicity towards carcinoma cells, share the same tricyclic core as trichoflectin (Figure 5.12).[31] Upon isolation, the absolute C7-configuration was assigned solely by optical rotation, as was done in the case of **5.50**.[29]

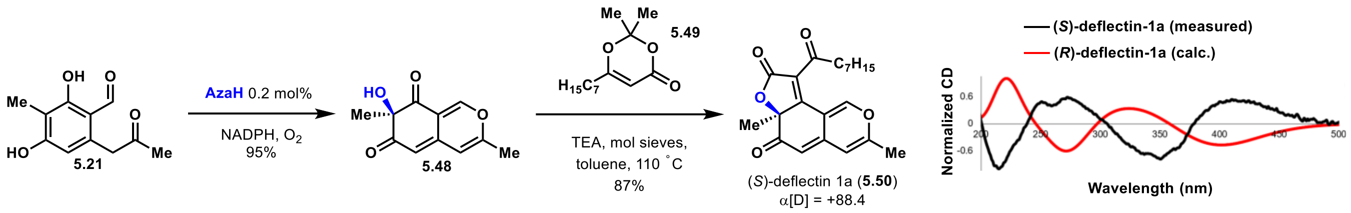
5.21
AzaH 0.2 mol%
NADPH, O_2
95%
5.48
5.49
TEA, mol sieves,
toluene, 110 °C
87%
(S)-deflectin 1a (5.50)
α[D] = +88.4
(S)-deflectin-1a (measured)
(R)-deflectin-1a (calc.)
Normalized CD
0.6
0
-0.6
200
250
300
350
400
450
500
Wavelength (nm)

Figure 5.11: Total synthesis of deflectin and calculated (red) and measured (black) CD-spectra.

To answer the question surrounding the absolute configuration of these molecules, Joshua Pyser completed the total synthesis of (*S*)-deflectin-1a (**5.50**, Figure 5.11). Methyl ketone **5.21** was dearomatized with AzaH to produce bicycle **5.48** in 95% yield and >99% ee. Acylation and subsequent Knoevenagel condensation with the acylketene derived from precursor **5.49** furnished the desired butenolide to deliver (*S*)-deflectin-1a in 87% yield. The spectral data for **5.50** matched all available reported values. A measured optical rotation of +88.4 for this *S*-enantiomer confirms the need for structural revision of the natural product from the *R*-configuration to *S* at C7.

With both trichoflectin and deflectin-1a in hand, we set out to construct the natural product lunatoic acid A (**5.51**), which was reported to possess the opposite configuration at C7 to the newly established configuration of natural trichoflectin and deflectin-1a. Isolated by Marumo, this natural product exhibited interesting antibacterial properties, as well as the ability to act as an antifungal agent by inducing chlamydospore-like cells in certain fungi.[32,33] As depicted by the retrosynthesis in Figure 5.12, we envisioned accessing the carboxylic acid moiety of **5.51** through a cross metathesis with the C9,10 double bond of intermediate **5.52**.[27c] We anticipated that the chiral aliphatic ester of **5.53** could be constructed through an acylation of the C7-hydroxyl group of (*R*)-**5.46**, which would be accessed through dearomatization of common intermediate **5.22** with AzaH.

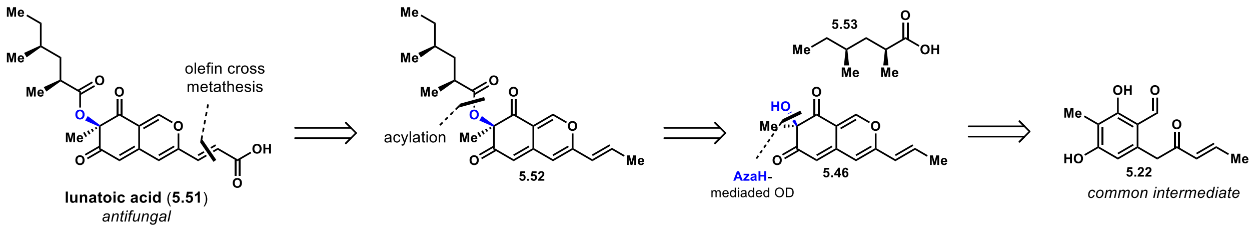

Figure 5.12: Retrosynthetic analysis for lunatoic acid.

Having established a robust method for biocatalytic dearomatization of enone **5.22**, the first challenge we encountered en route to lunatoic acid A was the acylation of tertiary alcohol **5.46**. While the acylation had proceeded smoothly with the ketene en route to trichoflectin and deflectin-1a, our attempts at acylation of **5.46** using acyl chlorides or symmetric anhydrides consistently failed to produce chiral ester **5.52**, affording only starting material or under more forcing conditions, complete decomposition of **5.46**. Ultimately, Joshua Pyser discovered that Yamaguchi esterification with **5.54** (Figure 5.13) did afford the desired product, although after optimization of reaction conditions, a maximum 50% yield was obtained.[34] Mixed anhydride **5.54** was generated *in situ* from the corresponding carboxylic acid, prepared as previously reported.[35] The carboxylic acid moiety present in lunatoic acid A was appended as the masked methyl ester through olefin metathesis with methyl acrylate and Grubbs 2nd generation catalyst in 48% yield.[36] Our attempts to perform the metathesis prior to esterification resulted in decomposition of the starting material, indicating that protection of the C7-hydroxyl group increases the stability of the compound to the reaction conditions. The expected mass of lunatoic acid A was observed by TOF-MS upon saponification of methyl ester **5.55** using LiOH; however, sufficient quantities of the pure compound for NMR studies could not be obtained. This observed instability parallels the nature of the free acid from culture extracts. These extracts were methylated to obtain lunatoic acid A methyl ester (**5.55**), which was fully characterized in lieu of the free acid.[32] All spectral data from the fully synthetic **5.55** match with reported literature values, including an agreement in the sign of the optical rotation and Cotton effects from the reported CD, indicating in this case that the original assignment of *R* at C7 is accurate.[32]

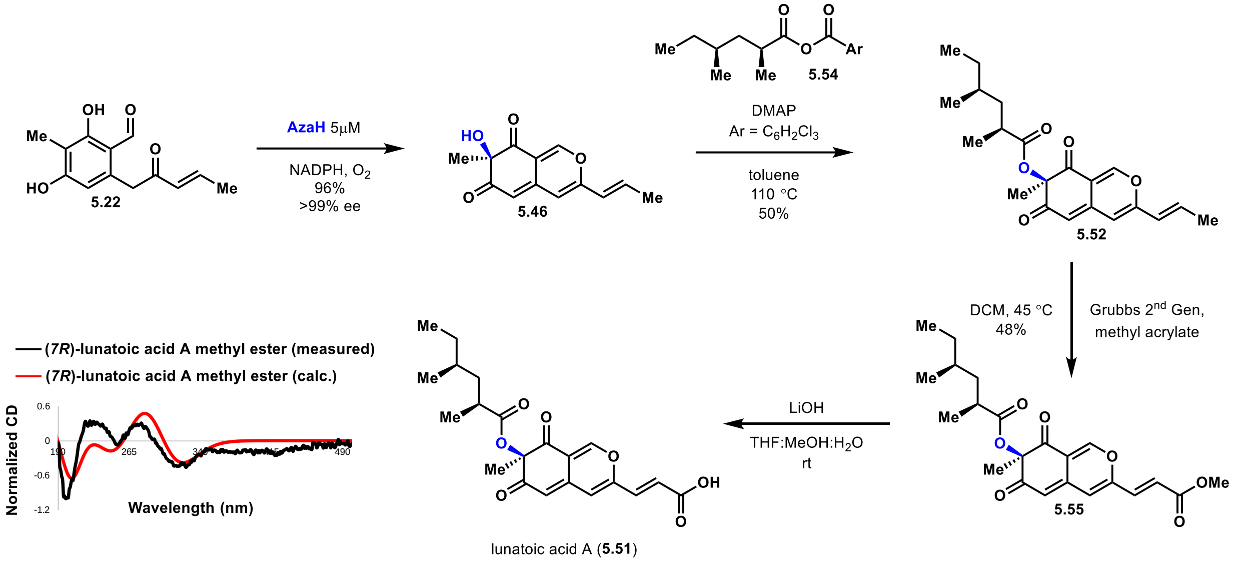

5.22
AzaH 5μM
NADPH, O2
96%
>99% ee
5.46
5.54
Ar
DMAP
Ar = C6H2Cl3
toluene
110 °C
50%
5.52
DCM, 45 °C
48%
Grubbs 2nd Gen,
methyl acrylate
5.55
OMe
LiOH
THF:MeOH:H2O
rt
lunatoic acid A (5.51)
(7R)-lunatoic acid A methyl ester (measured)
(7R)-lunatoic acid A methyl ester (calc.)
Normalized CD
Wavelength (nm)
0.6
0
-0.6
-1.2
190
265
340
490

Figure 5.13: Total synthesis of lunatoic acid A. Inset: calculated (red) and measured CD spectra of lunatoic acid A methyl ester (**5.55**).

Chapter 5.5: Conclusion

A set of complementary biocatalysts for oxidative dearomatization have been identified and applied to the enantiodivergent, chemoenzymatic synthesis of azaphilone natural products. Comparison of sequences related to characterized enzymes involved in natural product biosynthesis, has provided an expanded set of biocatalysts for this transformation and insight on the sequence features that govern site- and stereoselectivity. A focused substrate library was created to identify a suitable common intermediate for dearomatization by both AzaH and AfoD. These enzymes were then used to construct both enantiomers of scaffold **5.46** to access the desired natural products containing either the *R*-or *S*-configuration at C7. The AzaH-produced scaffold (*R*)-**5.46** was initially used to access the natural product trichoflectin ((*S*)-**5.45**); however, it was discovered that this tricycle contained the opposite stereocenter from the natural product based on its optical rotation, CD spectral data, and X-ray crystal structure. Synthesis of the opposite enantiomer of trichoflectin ((*R*)-**5.45**) was achieved using the dearomatized scaffold accessed through AfoD, with an optical rotation that led to the reassignment of the C7-stereocenter of trichoflectin to *S* from the original literature report of *R*. This prompted the construction of related tricycle deflectin-1a (**5.49**) using analogous substrates, which allowed for the reassignment of its C7-stereocenter. Lunatoic acid A (**5.51**) was then constructed from (*R*)-**5.46** and its structure confirmed through CD spectra and optical rotation. We anticipate these methods will enable the rapid construction of libraries of natural and unnatural azaphilones. By utilizing modern tools in bioinformatics, we have rapidly identified homologs with desired properties, an orthogonal approach to protein engineering.

A challenge in accessing large pools of complex azaphilones from arene starting materials is the development of conditions for functionalizing the core which can be run in a high-throughput manner and, ideally, in a one-pot cascade with the oxidative dearomatization step. Toward this aim, new enzymatic cascades could be developed to allow for the derivatization of resorcinols into complex azaphilone derivatives.

Chapter 5.6: Experimental

Chapter 5.6.1: Synthesis of Compounds

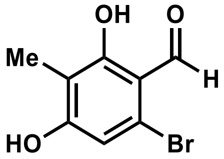

6-Bromo-2,4-dihydroxy-3-methylbenzaldehyde (5.29)

See Chapter 2.6.1.

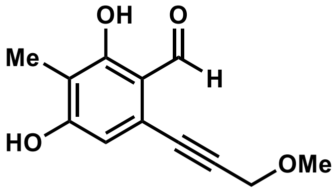

2,4-Dihydroxy-6-(3-methoxyprop-1-yn-1-yl)-3-methylbenzaldehyde (5.20)

Aryl bromide **5.29** (150 mg, 0.65 mmol), $PdCl_2(PPh_3)_2$ (23 mg, 0.033 mmol, 0.050 equiv), CuI (12 mg, 0.065 mmol, 0.10 equiv) was stirred in 4.8 mL of anhydrous DMF in a flame-dried round bottom flask equipped with a stir bar. Et_3N (0.30 mL, 2.2 mmol, 3.3 equiv) was added and the mixture was sparged with N_2 for 15 min before methyl propargyl ether (0.11 mL, 1.3 mmol, 2.0 equiv) was added. The resulting mixture was heated to 60 °C for 14 h. The reaction mixture was cooled to rt, diluted with water (2.0 mL), and acidified with 1 M HCl (4.0 mL). The mixture was extracted with EtOAc (3 x 10 mL) and the combined organic layers were washed with water and brine, dried over anhydrous Na_2SO_4, filtered, and concentrated under reduced pressure to afford a dark brown solid. Purification on silica gel (10-20% EtOAc in hexanes) afforded 135 mg (94% yield) of **5.20** as a tan solid. **^{1}H NMR** (400 MHz, CD_3OD) δ 10.13 (s, 1H), 6.54 (s, 1H), 4.36 (s, 2H), 3.43 (s, 3H), 2.03 (s, 3H). All spectra obtained were consistent with literature values.[37]

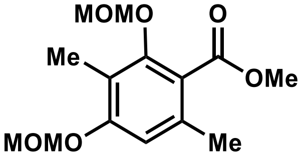

Methyl 2,4-bis(methoxymethoxy)-3,6-dimethylbenzoate (5.35)

Methyl atratate (13 g, 66 mmol, 1.0 equiv) in THF (650 mL) was cooled to 0 °C and NaH (60%, 7.9 g, 200 mmol, 3.0 equiv) was added portionwise. MOMCl[38] (15 mL, 200 mmol, 3.0 equiv) was slowly added to the resulting mixture. The solution was warmed to rt and stirred for 5 h before it was cooled to 0 °C and quenched with NH_4Cl (500 mL, saturated aq.). The layers were separated, and the aqueous layer was extracted with EtOAc (3 x 500 mL). The combined organic layers were washed with $NaHCO_3$, dried over Na_2SO_4 and concentrated under reduced pressure to afford a yellow oil. Purification on silica gel (0-20% EtOAc in hexanes) afforded 15 g of the ester as a colorless oil (90% yield). **^{1}H NMR** (300 MHz, $CDCl_3$): δ 6.72 (s, 1H), 5.19 (s, 2H), 4.96 (s, 2H), 3.89 (s, 3H), 3.54 (s, 3H), 3.47 (s, 3H), 2.28 (s, 3H), 2.15 (s, 3H). All spectra obtained were consistent with literature values.[39]

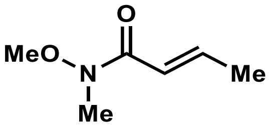

(*E*)-N-methoxy-N-methylbut-2-enamide (5.37)

Crotonic acid (10 g, 120 mmol, 1.0 equiv) was dissolved in oxalyl chloride (12 mL, 140 mmol, 1.2 equiv) and stirred at 70 °C for 1 h. The resulting acyl chloride was distilled at 124 °C, then added to a solution of N,O-dimethylhydroxylamine hydrochloride (10 g, 100 mmol, 0.90 equiv) in DCM (190 mL). The mixture was cooled to 0 °C before pyridine (21 mL, 260 mmol, 2.2 equiv) was added slowly. The mixture was stirred at 0 °C for 30 min, then allowed to warm to rt for 30 min before it was diluted with 1 M HCl (150 mL) and extracted Et_2O (3 x 150 mL). The combined organic layers were washed with brine (300 mL), dried over $MgSO_4$, and concentrated to afford a red oil. Purification on silica gel (60-80% Et_2O in hexanes) afforded 12 g (82% yield) of the title compound as a pale yellow oil. **^{1}H NMR** (400 MHz, $CDCl_3$) δ 6.98 (m, 1H), 6.41 (d, J = 15.4 Hz, 1H), 3.69 (s, 3H), 3.23 (s, 3H), 1.90 (d, J = 8.6 Hz, 3H). All spectra obtained were consistent with literature values.[40]

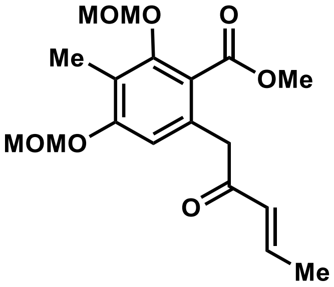

Methyl (*E*)-2,4-bis(methoxymethoxy)-3-methyl-6-(2-oxopent-3-en-1-yl)benzoate (5.38)

Diisopropylamine (9.1 mL, 65 mmol, 1.1 equiv) in THF (300 mL) was stirred at -78 °C. *n*-BuLi (2.5 M in hexane, 26 mL, 65 mmol, 1.1 equiv) was slowly added. The resulting mixture was warmed to 0 °C and stirred for 15 min before it was cooled to -78 °C and a solution of ester **5.36** (15 g, 20 mmol, 1.0 equiv) in THF (50 mL) was added. The resulting mixture was stirred at -78 °C for 15 min before a solution cooled to -78 °C of amide **5.37** (9.2 g, 71 mmol, 1.2 equiv) in THF (25 mL) was added by cannula. The mixture was stirred for 1 h at -78 °C and was then acidified with 1 M HCl (aq. 100 mL). The layers were separated, and the aqueous layer was extracted with EtOAc (3 x 400 mL). The combined organic layers were washed with brine (400 mL), dried over Na_2SO_4, and concentrated under reduced pressure to afford a yellow oil. Purification on silica gel (5-15% EtOAc in hexanes) afforded 4.5 g of an inseparable mixture of the title compound and remaining amide **5.37**. This mixture was carried forward without further purification.

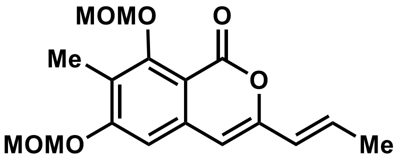

(*E*)-6,8-Bis(methoxymethoxy)-7-methyl-3-(prop-1-en-1-yl)-1H-isochromen-1-one (5.39)

NaH (170 mg, 4.50 mmol, 1.05 equiv, 60%, dispersion in mineral oil) was stirred in THF (290 mL) at -20 °C. Enone **S7** (1.5 g, 4.3 mmol, 1.0 equiv) in THF (50 mL) was slowly added to the suspension. *t*-BuOH (10 μL) was added and the solution was stirred for 1 h at 20 °C. The reaction was cooled to 0 °C and quenched with EtOAc (30 mL), followed by addition of a saturated aqueous solution of NH_4Cl (40 mL). The mixture was then allowed to warm to rt. The layers were separated, and the aqueous layer extracted with EtOAc (3 x 200 mL). The combined organic layers were washed with brine (400 mL), dried over Na_2SO_4, and concentrated under reduced pressure to afford a white solid. Purification on silica gel (0-20% EtOAc in hexanes) afforded 1.3 g of the lactone **5.39** as a white crystalline solid (22% yield over 2 steps). **^{1}H NMR** (400 MHz, $CDCl_3$): δ 6.78 (s, 1H), 6.59 (m, 1H), 6.12 (s, 1H), 5.99 (dt, J = 15.7, 1.7 Hz, 1H), 5.28 (s, 2H), 5.16 (s, 2H), 3.64 (s, 3H), 3.49 (s, 3H), 2.27 (s, 3H), 1.89 (d, J = 6.9 Hz, 3H); **^{13}C NMR** (150 MHz, $CDCl_3$) δ 161.0, 159.2, 158.9, 152.2, 139.1, 131.6, 122.9, 122.3, 107.4, 105.1, 103.7, 101.6, 94.2, 57.7, 56.4, 18.3, 9.9; **HR-ESI-MS**: *m/z* calculated for $C_{17}H_{21}O_6$ $[M+H]^+$: 321.1333, found: 321.1335; **IR** (thin film): 2934, 2832, 1715, 1658, 1598 cm^{-1}**;** **MP**: 124-126 °C.

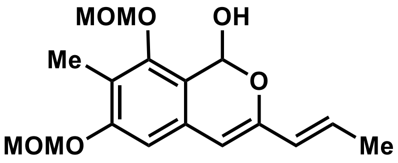

(*E*)-6,8-bis(methoxymethoxy)-7-methyl-3-(prop-1-en-1-yl)-1H-isochromen-1-ol (5.40)

Lactone **S8** (1.0 g, 2.6 mmol, 1.0 equiv) in THF (13 mL) was stirred at -78 °C. DIBALH (0.48 mL, 2.7 mmol, 1.1 equiv) was added dropwise via syringe. The resulting solution was allowed to stir at -78 °C for 30 min, and then the reaction was quenched by the addition of EtOAc (1.0 mL) and Rochelle's salt (saturated, 4.0 mL). The resulting mixture was stirred for 1 h at rt. The crude mixture was extracted with EtOAc (3 x 50 mL), and the combined organic layers were washed brine (20 mL), dried over Na_2SO_4, and concentrated under reduced pressure. Purification on silica gel (0-20% EtOAc in hexanes) afforded 730 mg of the lactol **5.40** as a colorless oil (89% yield).

^{1}H NMR (400 MHz, $CDCl_3$): δ 6.63 (s, 1H), 6.56 (d, J = 5.8 Hz, 1H), 6.33 (m, 1H), 5.97 (dd, J = 15.3, 2.1 Hz, 1H), 5.78 (s, 1H), 5.16 (s, 2H), 5.01 (s, 2H), 3.60 (s, 2H), 3.45 (s, 3H), 2.15 (s, 2H), 1.84 (m, 3H); **^{13}C NMR** (100 MHz, $CDCl_3$) δ 156.7, 153.0, 148.7, 129.1, 128.3, 126.0, 119.0, 116.4, 105.8, 102.0, 99.9, 94.4, 89.0, 57.5, 56.0, 18.2, 9.9; **HR-ESI-MS**: *m/z* calculated for $C_{17}H_{23}O_6$ $[M+H]^+$: 323.1489, found: 323.1489**; IR** (thin film): 3357, 2930, 2823, 1604, 1447 cm^{-1}; **MP**: 62-65 °C.

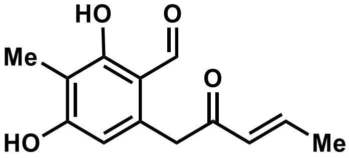

(*E*)-2,4-Dihydroxy-3-methyl-6-(2-oxopent-3-en-1-yl)benzaldehyde (5.22)

Lactol **S9** (300 mg, 0.933 mmol) in MeCN and water (7:1, 0.04 M) was stirred at rt. $LiBF_4$ (630 mg, 6.7 mmol, 7.2 equiv) was added and the resulting mixture was stirred at 70 °C for 3 h. The reaction mixture was cooled to rt and quenched by the addition of water (15 mL). The mixture was diluted with EtOAc (30 mL) and the layers were separated. The aqueous layer was extracted with EtOAc (3 x 30 mL) and the combined organic layers were washed brine (40 mL), dried over Na_2SO_4, and concentrated under reduced pressure. Purification on silica gel (10-40% EtOAc in hexanes) afforded 200 mg (90% yield) of the title compound as a tan crystalline solid. **^{1}H NMR** (600 MHz, CD_3OD) δ 9.77 (s, 1H), 7.06 (m, 1H), 6.25 (d, J = 1.8 Hz, 1H), 6.22 (s, 1H), 4.12 (s, 2H), 2.00 (s, 3H), 1.92 (d, J = 5.2 Hz, 3H); **^{13}C NMR** (150 MHz, CD_3OD) δ 197.5, 193.4, 163.7, 163.0, 144.8, 138.0, 130.3, 112.3, 110.3, 109.9, 42.5, 17.0, 5.8; **HR-ESI-MS**: *m/z* calculated for $C_{13}H_{15}O_4$ $[M+H]^+$: 235.0965, found: 235.0947**; IR** (thin film): 3231, 2928, 2824, 2409, 1614 cm^{-1}; **MP**: 139-142 °C.

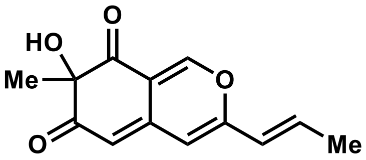

(*E*)-7-hydroxy-7-methyl-3-(prop-1-en-1-yl)-6*H*-isochromene-6,8(7*H*)-dione (5.46)

26 (20 mg, 0.085 mmol, 1.0 equiv) and $Au(OAc)_3$ (1.7 mg, 0.0043 mmol, 0.05 equiv) in DCE (0.94 mL) were added to a flame-dried vial. The mixture was stirred at rt for 30 min before IBX (28 mg, 0.10 mmol, 1.1 equiv), TBAI (19 mg, 0.051 mmol, 0.60 equiv), and TFA (0.094 mL, 10% total volume) were added. The mixture was stirred for an additional 40 min before the reaction was quenched with 5 drops of a saturated $Na_2S_2O_3$ solution. The mixture was filtered through a plug of ceilte, which washed with DCM, before the solution was concentrated under reduced pressure. Purification by preparative TLC with 2.5% MeOH in DCM yielded 4.7 mg **5.46** (22% yield) of the title compound as an orange oil. **^{1}H NMR** (400 MHz, CDl_3) δ 7.89 (s, 1H), 6.59 (m, 1H), 6.10 (s, 1H), 6.01 (d, J = 15.6 Hz, 1H), 5.57 (s, 1H), 2.62 (s, 2H), 1.94 (d, J = 7.0 Hz, 3H), 1.55 (s, 3H). All spectra obtained were consistent with reported values.[41]

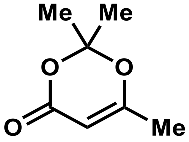

2,2,6-trimethyl-4H-1,3-dioxin-4-one (5.47)

Prepared as reported previously by Fuse *et al*.[42] 1.04 g (73% yield) of the title compound was obtained as a yellow oil. **^{1}H NMR** (400 MHz, $CDCl_3$) δ 5.24 (s, 1H), 1.98 (s, 3H), 1.68 (s, 6H). All spectra obtained were consistent with literature values.[42]

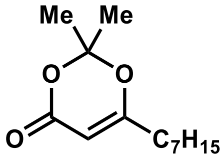

6-heptyl-2,2-dimethyl-4H-1,3-dioxin-4-one (5.49)

Prepared as reported previously by Franck and coworkers.[12] 356 mg (26% yield over 3 steps) of the title compound was obtained as a yellow oil and taken on crude without further purification.

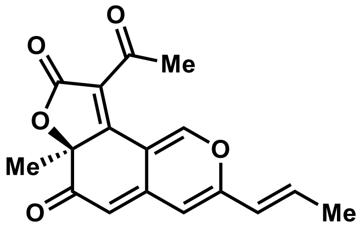

trichoflectin (5.45)

To a solution of **5.46** (5.5 mg, 0.023 mmol, 1.0 equiv) and dioxinone **5.47** (5 mg, 0.035 mmol, 1.5 equiv) in toluene (0.64 mL) in a flame dried vial under N_2 was added mol sieves. The mixture was stirred at rt for 10 min and then heated to 110 °C. After 1 h, Et_3N (0.0064 mL, 0.046 mmol, 2.0 equiv) was added. The mixture was stirred for an additional hour at 110 °C before it was cooled to room temperature and quenched with 1 M HCl (1.0 mL). The mixture was extracted with EtOAc (3 x 2.0 mL). The organic layers were combined, washed with brine, dried over Na_2SO_4, and concentrated under reduced pressure. Purification by preparative HPLC yielded 7.2 mg of **5.45** (>99% yield) as a yellow oil. **^{1}H NMR** (600 MHz, $CDCl_3$) δ 8.82 (s, 1H), 6.63 (m, 1H), 6.06 (s, 1H), 6.01 (d, J = 13.8 Hz, 1H), 5.35 (d, J = 1.2 Hz, 1H), 2.60 (s, 3H), 1.95 (d, J = 5.2 Hz, 3H), 1.69 (s, 3H); **^{13}C NMR** (150 MHz, $CDCl_3$) δ 194.5, 190.0, 168.2, 165.6, 155.2, 153.1, 144.0, 136.3, 123.3, 122.3, 110.9, 107.5, 105.8, 87.6, 30.1, 29.7, 26.3, 18.7; **HR-ESI-MS**: *m/z* calculated for

$C_{17}H_{15}O_5$ [M+H]$^+$: 299.0914, found: 299.0922; **IR** (thin film): 2921, 2827, 1721, 1614, 1503 cm^{-1}; [α]$_D$ +34 ° (*c* 0.1, $CHCl_3$). All spectra obtained were consistent with literature values.[29]

The following compounds were synthesized by Joshua Pyser:

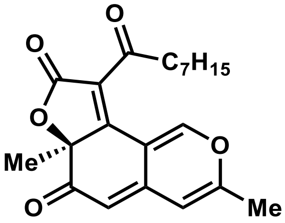

deflectin-1a (5.50)

To a solution of **5.48** (4.0 mg, 0.019 mmol, 1.0 equiv) and dioxinone **5.49** (6.6 mg, 0.029 mmol, 1.5 equiv) in toluene (0.55 mL) in a flame dried vial under N_2 was added mol sieves. The mixture was stirred at rt for 10 min and then was heated to 110 °C. After 1 h, Et_3N (53 µL, 0.038 mmol, 2.0 equiv) was added. The mixture was stirred for an additional hour at 110 °C before it was cooled to room temperature and quenched with 1 M HCl (1.0 mL). The mixture was extracted with EtOAc (3 x 2.0 mL) and the combined organic layers were washed with (5.0 mL), dried over Na_2SO_4, and concentrated under reduced pressure. Purification on silica gel (20% EtOAc in hexanes) yielded 5.9 mg of **5.39** (87% yield) as a yellow oil. **^{1}H NMR** (599 MHz, $CDCl_3$) δ 8.77 (s, 1H), 6.08 (s, 1H), 5.28 (s, 1H), 3.16 (m, 1H), 2.83 (m, 1H), 2.20 (s, 3H), 1.68 (s, 3H), 1.62 (m, 2H), 1.55 (s, 3H), 1.27 (m, 8H), 0.87 (m, 3H); **^{13}C NMR** (151 MHz, $CDCl_3$) δ 197.3, 190.3, 168.1, 165.2, 158.7, 153.3, 144.1, 123.6, 111.1, 108.4, 104.9, 87.6, 42.1, 31.6, 29.0, 29.0, 26.2, 23.4, 22.6, 19.4, 14.1; **HR-ESI-MS**: *m/z* calculated for $C_{21}H_{25}O_5$ [M+H]$^+$: 357.1697**,** found: 357.1754; **IR** (thin film): 2924, 1763, 1684, 1642 1540 cm^{-1}; [α]$_{\mathbf{D}}$ +88 ° (*c* 0.1, EtOAc). All spectra obtained were consistent with literature values.[31]

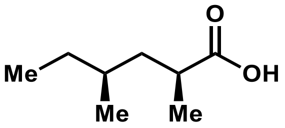

(2S,4S)-2,4-dimethylhexanoic acid (5.56)

Prepared as reported previously by Myers *et al.*[43] 278 mg (32% yield over 3 steps) of the title compound was obtained as a white crystalline solid. **^{1}H NMR** (599 MHz, $CDCl_3$) δ 2.56 (m, 1H), 1.72 (m, 1H), 1.39 (m, 1H), 1.32 (m, 1H), 1.17 (d, J = 7.0 Hz, 3H), 1.13 (m, 2H), 0.88 (d, J = 6.6 Hz, 3H), 0.86 (t, J = 7.4 Hz, 3H). All spectra obtained were consistent with literature values.[43]

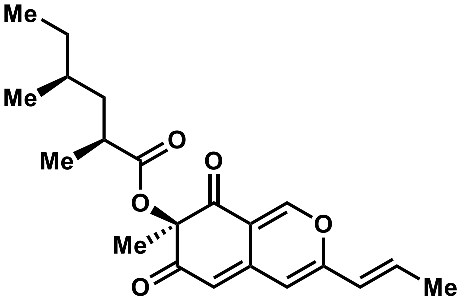

(R)-7-methyl-6,8-dioxo-3-((E)-prop-1-en-1-yl)-7,8-dihydro-6H-isochromen-7-yl (2S,4S)-2,4-dimethylhexanoate (5.52)

To a solution of carboxylic acid **5.56** (4.5 mg, 0.031 mmol, 1.1 equiv) in THF (0.2 mL) was added 2,4,6-trichlorobenzoyl chloride (0.0048mL, 0.031 mmol, 1.1 equiv) and Et_3N (0.0043 mL, 0.031 mmol, 1.1 equiv). The mixture was stirred at rt for 30 min before it was filtered through celite and concentrated. The resulting clear oil was dissolved in toluene (0.8 mL) and added to **5.46** (6.5 mg, 0.028 mmol, 1 equiv) and DMAP (10.3 mg, 0.084 mmol, 3 equiv). This mixture was stirred at 110 °C for 1 h before it was cooled to rt, acidified with a saturated solution of NH_4Cl (1 mL), and extracted with EtOAc. The organic layers were washed with brine, dried over Na_2SO_4, and concentrated under reduced pressure. Purification on silica gel (10-30% EtOAc in hexanes) provided 5 mg (50% yield) of the title compound as an orange oil. **^{1}H NMR** (400 MHz, $CDCl_3$) δ

7.88 (s, 1H), 6.55 (m, 1H), 6.07 (s, 1H), 6.00 (d, J = 15.0 Hz, 1H), 5.57 (s, 1H), 2.70 (m, 1H), 1.93 (d, J = 6.9 Hz, 3H), 1.77 (m, 1H), 1.53 (s, 3H), 1.34 (m, 2H), 1.19 (d, J = 6.9 Hz, 3H), 1.13 (m, 2H), 0.89 (m, 6H). **^{13}C NMR** (151 MHz, $CDCl_3$) δ 193.20, 192.70, 176.30, 155.27, 153.38, 142.59, 135.27, 122.37, 114.89, 108.50, 107.75, 83.76, 40.81, 36.16, 31.76, 29.44, 22.14, 19.08, 18.61, 17.60, 11.10; **HR-ESI-MS**: *m/z* calculated for $C_{21}H_{27}O_5$ $[M+H]^+$: 359.1853, found: 359.1858; **IR** (thin film): 2925, 2853, 1717, 1634, 1453 cm^{-1}.

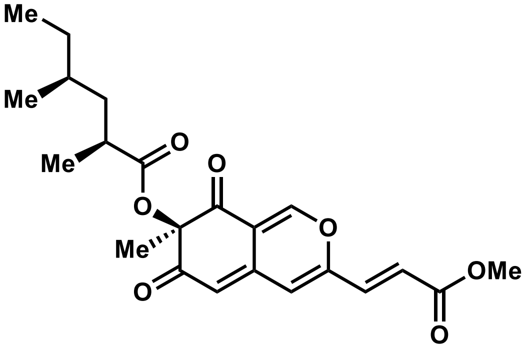

(*R*)-3-((E)-3-methoxy-3-oxoprop-1-en-1-yl)-7-methyl-6,8-dioxo-7,8-dihydro-6H-isochromen-7-yl (2S,4S)-2,4-dimethylhexanoate (5.55)

To a solution of **5.52** (5.5 mg, 0.015 mmol, 1 equiv) and methyl acrylate (5.4 µL, 0.060 mmol, 4.0 equiv) in degassed DCM (0.6 mL) was added a solution of Grubbs Catalyst 2nd generation (2.5 mg, 0.0030 mmol, 0.20 equiv) in degassed DCM (0.5 mL). The mixture was stirred at 45 °C for 4 h before it was cooled to rt and concentrated. Purification on silica gel (10-35% EtOAc in hexanes) afforded 2.6 mg (48% yield) of the title compound as a yellow glass. **^{1}H NMR** (400 MHz, $CDCl_3$) δ 7.88 (s, 1H), 7.13 (d, J = 15.6 Hz, 1H), 6.52 (d, J = 15.6 Hz, 1H), 6.45 (s, 1H), 5.69 (s, 1H), 3.82 (s, 3H), 2.69 (m, 1H), 1.75 (m, 1H), 1.53 (s, 3H), 1.29 (m, 2H), 1.19 (d, J = 6.8 3H), 1.13 (m, 2H), 0.89 (m, 6H). **^{13}C NMR** (201 MHz, $CDCl_3$) δ 192.8, 192.5, 165.8, 153.2, 153.1, 152.7, 140.7, 133.5, 124.0, 115.8, 114.9, 110.5, 83.8, 77.2, 77.0, 76.8, 76.7, 52.3, 40.8, 36.2, 31.8, 29.5, 21.9, 19.1, 17.6, 11.1; **HR-ESI-MS**: *m/z* calculated for $C_{22}H_{27}O_6$: 403.1751, found: 403.1728; **IR** (thin film): 2926, 2853, 1718, 1630, 1454 cm^{-1}. $[\alpha]_{\mathbf{D}}$ -12.2 ° (*c* 0.1, $CHCl_3$). All spectra obtained were consistent with literature values.[32]

Chapter 5.6.2: Plasmids and Proteins

Plasmids: The plasmid encoding *afoD* was synthesized by GeneArt and cloned into a pET21a vector by Attabey Rodrìguez Benìtez.

Codon-Optimized *afoD* Sequence

```
ATGAGTACAGACTCGATCGAAGTTGCCATTATAGGCGCCGGGATCACGGAATCACCCTGGCCC
TGGGCCTCCTGTCTCGCGGCATTCCCGTCCGCGTCTACGAGCGAGCCCGCGACTTTCACGAAAT
TGGAGCCGGTATCGGTTTCACCCCCAACGCCGAATGGGCGATGAAAGTCGTCGACCCGCGCATT
CAAGCTGCTTTCAAACGCGTCGCTACCCCCAATGCCTCCGACTGGTTCCAGTGGGTGGACGGAT
TCAACGAGTCCGGTACCGACCCGCGCGAGACCGAGGAACAGCTACTCTTCAAGATCTACCTCGG
CGAGCGTGGATTTGAGGGCTGCCACCGTGCCGACTTCCTAGGTGAGCTGGCACGTCTACTACCG
GAAGGTGTGGTGACATTCCAGAAGGCGCTGGATACCGTGGAGCCTGCAGCAGATAATAGCCTCG
GCCAGCTTCTTCGATTCCAAGATGGCACGACAGCTACCGCCCACGCGGTGATCGGCTGCGATGG
CATTCGGTCGCGCGTTCGTCAGATCCTCCTAGGTGAAGACCATCCGACAGCATCAGCCCATTAC
AGTCATAAATATGCAGCACGCGGCCTTATTCCCATGGACCGCGCCCGGGAGGCGCTGGGCGAAG
ATAAAGTGGCGACACGCTTCATGCATCTCGGTCCGGATGCCCATGCCCTGACCTTCCCCGTTAG
CCATGGGTCCTTGTTGAACGTCGTCGCCTTCGTCACGGACCCTAACCCTTGGCCATATGCTGAT
CGCTGGACGGCGCAGGGGCCCAAGAAAGACGTGACGGCTGCCTTTTCCCGCTTTGGTCCGACCA
TGCGCACCATAATTGACCTCTTGCCTGATCCTATTGATCAATGGGCCGTTTTTGATACATACGA
CCATCCCCCAAATACGTATTCCCGGGGAGCTGTCTGTATAGCAGGGGATGCTGCTCATGCCGCG
GCTCCGCATCACGGTGCAGGTGCAGGTTGTGGTGTGGAAGACGCGGCTGTGCTGTGCGCTGTGC
TTCATATGGCTGCGAAAAAAGTTAACACCGCAAAAACTGGTTCTGAGGGGAAAGCCGCTCTTAT
CACGGCCGCATTCGAAACCTATGATTCGGTTTGTCGCGAGCGTGCGCAGTGGCTGGTGGAAAGT
AGTCGCGTTATCGGTAATCTGTATGAGTGGCAGGATAAGGAGGTAGGGTCGGATGCTTCCAGGT
GCCACGATGAGGTGTATTGGCGCTCTCATCGCATTTGGGACTATGATATTGATGCGATGATGAG
AGAGACAGCTGAGGTGTTTGAGGCGCAGGTAGCTGGGGTGGCGAGAAAT
```

AfoD Protein Sequence

```
MADHEQEQEPLSIAIIGGGIIGLMTALGLLHRNIGKVTIYERASAWPDIGAAFAFTGIARECMQ
RLDPAILSALSKVAQRNPHDKVRYWDGFHPKSKEEAQDPEKSVLFEIEEKNMAYWACLRGVFHA
EMARLLPERVVRFGKRLVAYEDGGDQKVVLRFEDGEVEEADIVIACDGVHSTARRVLLGAEHPA
ANARYSRKAVYRALVPMPAAIDALGTEKAHVQIAHCGPDAHIVSFPVNNAQIYNVFLFTHDSNE
WTHGHTMTVPSSKEEILSAVENWGPHIKELASLFPEQLSKYAIFDQADHPLPYYAAGRVALAGD
AAHASSPFHGAGACMGVEDALVLAELLEKVQNGSAFKEKKSNIELALKTYSDVRIERSQWLVKS
SREMGDLYEWRYEDIGGDGVKCKAEWERRSRVIWDFDVQGMVDQAREAYERAVVKV
```

Protein overexpression and purification: Plasmids containing *azaH* and *afoD* were transformed using standard heat-shock protocols into chemically competent *E. coli* into BL21(DE3) cells. Overexpression of AfoD was achieved in 500 mL 4% glycerol (v/v) Terrific Broth (TB) in 2.8 L flasks. 500 mL portions of media were inoculated with 5 mL overnight culture prepared from a single colony in Luria Broth (LB) and 100 μg/mL ampicillin (Gold Biotechnology). Cultures were grown at 37 °C and 250 rpm until the optical density at 600 nm reached 0.8. The cultures were then cooled to 18 °C for 1 h and protein expression was induced with 0.1 mM isopropyl-β-D-1-thiogalactopyranoside (IPTG, Gold Biotechnology). Expression continued at 20 °C overnight (approx. 18 h) at 200 rpm. The typical yield for one 500 mL culture was ~15 g cell pellet.

General purification procedure: 25-30 g of cell pellet was resuspended in 100 mL of lysis buffer containing 50 mM Tris HCl pH 7.4, 300 mM NaCl, 10 mM imidazole, and 10% glycerol. Protease inhibitors were added to lysis buffer of AzaH only and consisted of 1 mM phenylmethane sulfonyl fluoride (v), 0.1 mg/mL benzamidine HCl, 0.5 mg/mL leupeptin, and 0.5 mg/mL pepstatin. Approximatley 1 mg/mL lysozyme was added to resuspended cells that were then incubated on a rocker at 4 °C for 30 min. Cells were lysed by passing the total cell lysate through an Avestin pressure homogenizer at 15000 psi. The total lysate was centrifuged at 40,000 x g for 30 min and the supernatant was filtered through a 0.45 μm filter. The crude cell lysate was loaded onto a 5 mL HisTrap HP column (General Electric) on an ÄKTA Pure FPLC system (General Electric) at a flow rate of 2.5 mL/min. Buffer A = the lysis buffer listed above, and Buffer B = 50 mM Tris HCl pH 7.4, 300 mM NaCl, 10% glycerol, and 400 mM imidazole. The column was washed with 25 mM imidazole (6.3% Buffer B) for 6 CV and eluted in a gradient to 100% Buffer B over 8 CV. Fractions containing AfoD or AzaH were visibly yellow and pooled for desalting on a PD10 desalting column. Average yields: 100 mg from 1 L AfoD, 20 mg from 1 L AzaH. Molecular weights including 6xHis-tags for each protein were estimated by the ProtParam tool on the Expasy server to be 49.0 kDa for AfoD and 47.6 kDa for AzaH. These molecular weights are consistent with the mass of proteins bands observed by SDS-PAGE analysis (Figure 5.14). The purified proteins were aliquoted into 0.6 mL tubes and frozen in liquid nitrogen before long-term storage at -80 °C.

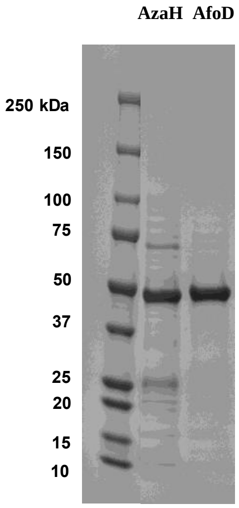

Determination of flavin incorporation and extinction coefficients: Experiments performed by Attabey Rodrìguez Benìtez: Samples of each protein were diluted to 10 µM in 1 mL using dialysis buffer for UV-vis analysis using a disposable poly(methyl 2-methylpropenoate) cuvette. The absorbance spectrum for each protein was taken from 300 nm to 700 nm in 2 nm increments (blue traces in Figure 5.15). A 20 µL aliquot of fresh 10% sodium dodecyl sulfate (w/v) was added to each 1 mL solution and mixed. Samples were incubated at room temperature for 10 min before reading the absorbance spectra again under the same conditions (red traces in Figure 5.15). The absorbance at 450 nm for the denatured enzymes and the extinction coefficient of free FAD (11300 M^{-1} cm^{-1}) was used to calculate the concentration of FAD in each protein sample using Beer’s law. The typical FAD incorporation was 82% for AzaH, 81% for AfoD. Extinction coefficients were calculated using the concentrations of free flavin obtained and the absorbance at 450 nm of the native enzymes. At 450 nm, the extinction coefficients of the proteins are 17490 M^{-1} cm^{-1} for AzaH, 6,870 M^{-1} cm^{-1} for AfoD.

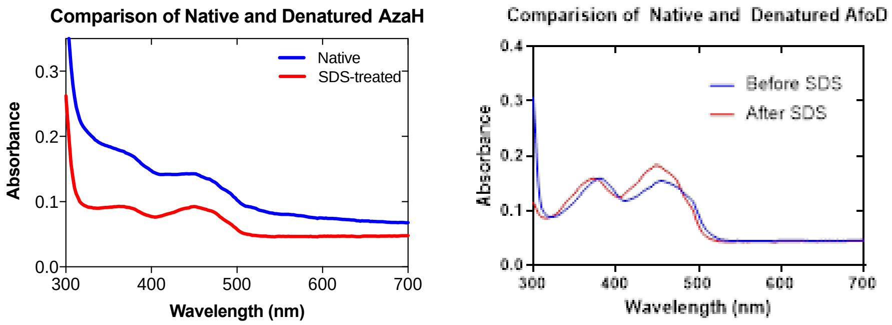

Figure 5.15: UV-vis spectra of native and denatured FDMOs AzaH and AfoD

Chapter 5.6.3: Biocatalytic Reactions

Stock solutions: Stock solutions of each substrate (50 mM) were prepared by dissolving the substrate in DMSO (analytical grade). Stock solutions of $NADP^+$ (100 mM) and glucose-6-phosphate (G6P, 500mM) were stored at -20 °C. Aliquots of AzaH (62 µM) and AfoD (95 µM) and glucose-6-phosphate dehydrogenase (G6PDH, 100 U/mL) were stored at -80 °C. Analytical-scale reactions: Each reaction contained 25 µL 100 mM potassium phosphate buffer, pH 8.0, 2.5 mM substrate (2.5 µL of a 50 mM stock solution in DMSO), 5 µM AzaH or 20 µM AfoD, 5 mM G6P (0.5 µL, 500 mM), 1 mM NADP+ (0.5 µL, 100 mM), 1 U/mL G6P-DH (0.5 µL, 100 U/mL), and Milli-Q water to a final volume of 50 µL. The reaction was carried out at 30 °C for 1 h and quenched by addition of 75 µL acetonitrile with 25 mM pentamethylbenzene as an internal standard. Precipitated biomolecules were pelleted by centrifugation (16,000 x g, 12 min). The supernatant was analyzed by UPLC-DAD and conversion obtained by comparison to calibration curves of each substrate. The subsequent liquid chromatography PDA spectrometry (UPLC) analysis was performed on a Waters Aquity H-Class UPLC-PDA using a Phenomenex Kinetex 1.7 µm C18, 2.1x150 mm column under the following conditions: Method A: mobile phase (A = deionized water + 0.1% formic acid, B = acetonitrile + 0.1% formic acid), 5% to 100% B over 1.5 min, 100% B for 1.0 min; flow rate, 0.5 mL/min; Method B: mobile phase (A = deionized water + 0.1% formic acid, B = acetonitrile + 0.1% formic acid), 5% to 100% B over 2 min, 100% B for 1 min; flow rate, 0.5 mL/min. Based on calibration curves of the starting materials, the percent conversion of the substrate to dearomatized product was calculated with AUCsubstrate/AUCinternal standard at 270 nm. All reactions were performed and analyzed in triplicate.

General procedure for in vitro preparative-scale reactions: Preparative–scale enzymatic reactions were conducted on 20 mg of each substrate under the following conditions: 5 µM AzaH or 20 µM AfoD, 2.5 mM substrate, 1 mM NADP+, 1 U/mL G6PDH, and 5 mM G6P for NADPH generation in reaction buffer (50 mM potassium phosphate buffer, pH 8.0). The reaction mixture was added to a 50 mL Erlenmeyer flask and incubated at 30 °C with 100 rpm shaking. After 2 h, a 50 µL aliquot was removed and processed in an identical manner to the analytical-scale reactions described above to determine substrate conversion. The remaining reaction mixture was diluted with acetone (2 x total reaction volume). Precipitated biomolecules were pelleted by centrifugation (4,000 x g, 12 min). Isolation procedure: The supernatant was concentrated under reduced pressure to a final volume of approximately 2 mL. The resulting mixture was filtered through a 0.22 µm filter and purified by preparative HPLC using a Phenomenex Kinetex 5 µm C18, 150 x 21.2 mm column under the following conditions: mobile phase A = deionized water + 0.1% formic acid and B = acetonitrile + 0.1% formic acid; method = 5% to 100% B over 13 min, 100% B for 4 min; flow rate, 15 mL/min.

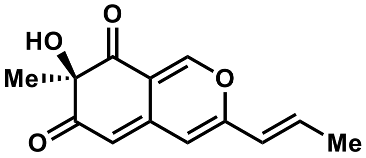

(*R*,*E*)-7-hydroxy-7-methyl-3-(prop-1-en-1-yl)-6H-isochromene-6,8(7H)-dione ((*R*)-5.46)

The title compound was synthesized using AzaH according to the general procedure for milligram-scale in vitro enzymatic oxidative dearomatization and isolated using the general isolation method. Purification by preparative HPLC afforded 9.6 mg (96% yield) of the title compound as a yellow oil. **^{1}H NMR** (400 MHz, $CDCl_3$) δ 7.89 (s, 1H), 6.59 (m, 1H), 6.10 (s, 1H), 6.01 (d, J = 15.6 Hz, 1H), 5.57 (s, 1H), 2.62 (s, 2H), 1.94 (d, J = 7.0 Hz, 3H), 1.55 (s, 3H). All spectra obtained were consistent with reported values.[41]

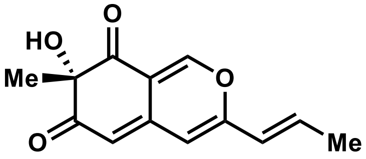

(*S,E*)-7-hydroxy-7-methyl-3-(prop-1-en-1-yl)-6H-isochromene-6,8(7H)-dione ((*S*)-5.46)

The title compound was synthesized using AfoD according to the general procedure for milligram-scale in vitro enzymatic oxidative dearomatization and isolated using the general isolation method. Purification by preparative HPLC afforded 4 mg (83% yield) of the title compound as a yellow oil. **^{1}H NMR** (400 MHz, CDl$_3$) δ 7.89 (s, 1H), 6.59 (m, 1H), 6.10 (s, 1H), 6.01 (d, J = 15.6 Hz, 1H), 5.57 (s, 1H), 2.62 (s, 2H), 1.94 (d, J = 7.0 Hz, 3H), 1.55 (s, 3H). All spectra obtained were consistent with reported values.[41]

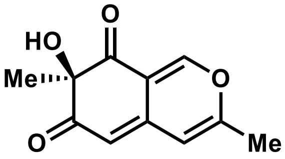

(*R*)-7-hydroxy-3,7-dimethyl-6H-isochromene-6,8(7H)-dione (5.48)

The title compound was synthesized using AzaH according to the general procedure for milligram-scale in vitro enzymatic oxidative dearomatization and isolated using the general isolation method. Purification by preparative HPLC afforded 9.5 mg (95% yield) of the title compound as a yellow oil. **^{1}H NMR** (400 MHz, CDCl$_3$) δ 7.88 (s, 1H), 7.26 (s, 2H), 6.13 (s, 1H), 5.51 (s, 1H), 2.20 (s, 3H), 1.55 (s, 3H).

Chapter 5.6.4: Substrate Calibration Curves

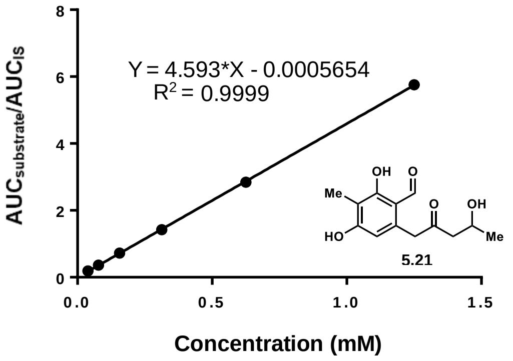

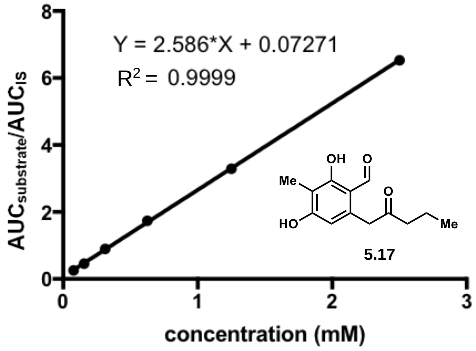

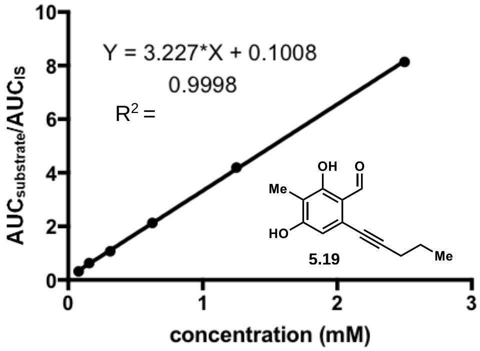

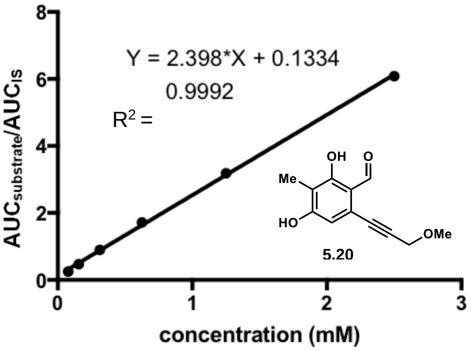

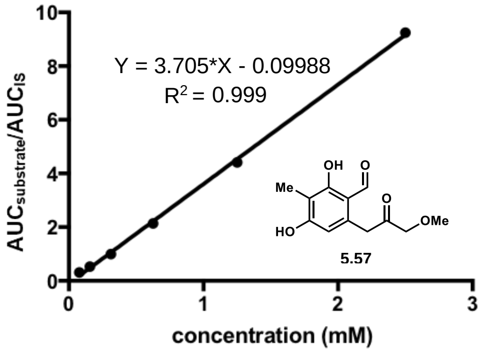

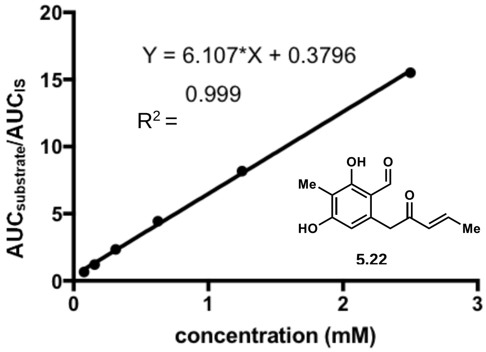

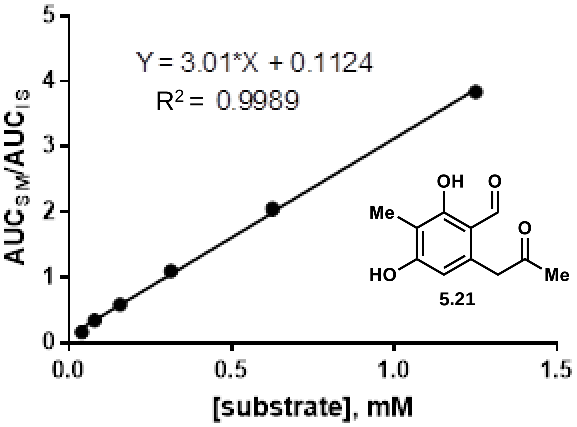

Figure 5.16: Calibration curves for substrates.

Chapter 5.6.5: UPLC Traces of Biotransformations

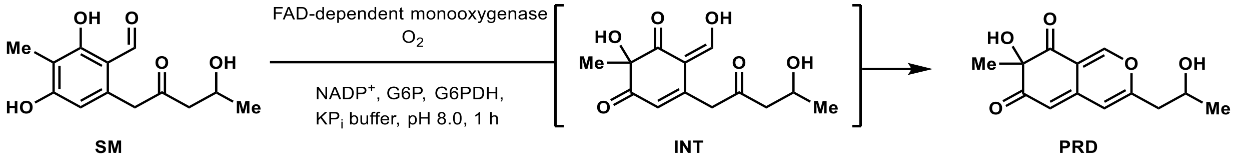
FAD-dependent monooxygenase
O_2
NADP$^+$, G6P, G6PDH,
KP$_i$ buffer, pH 8.0, 1 h
SM
INT
PRD
OH
O
Me
HO
OH
Me

With AzaH

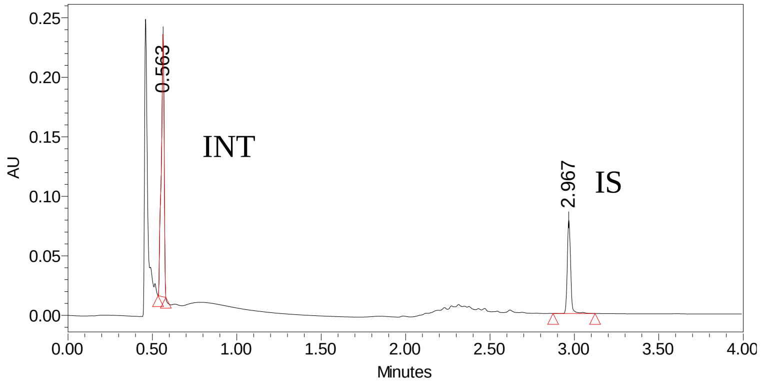

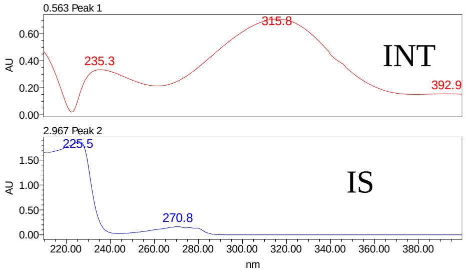

	Retention Time	Area	% Area	Height
1	0.563	258810	70.42	220721
2	2.967	108693	29.58	78693

With AfoD

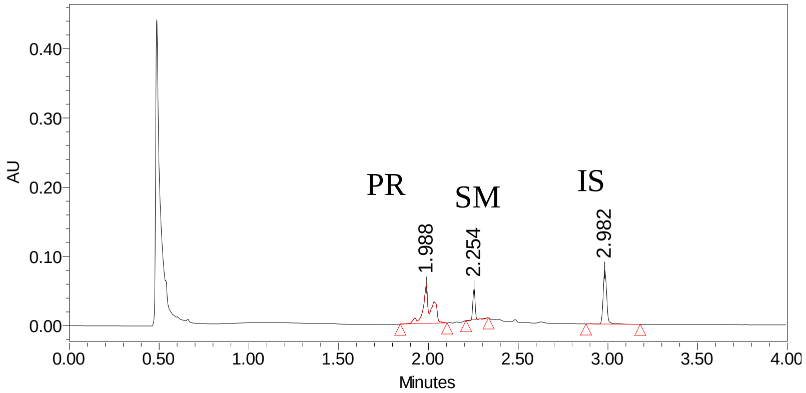

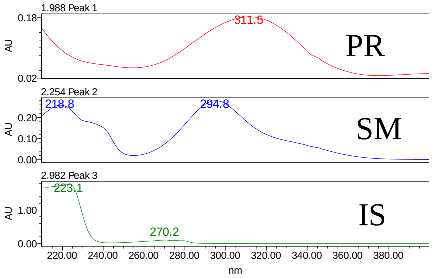

	Retention Time	Area	% Area	Height
1	1.988	174634	54.03	55311
2	2.254	41199	12.75	44106
3	2.982	107399	33.23	77715

NEC

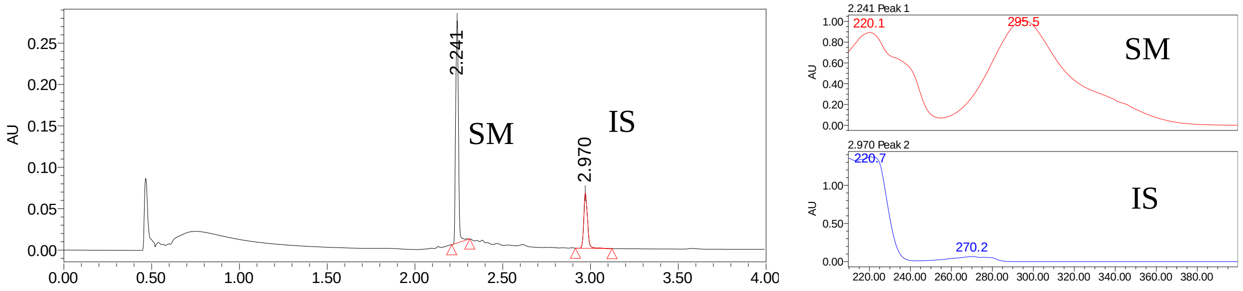

	Retention Time	Area	% Area	Height
1	2.241	292664	74.92	268642
2	2.970	97969	25.08	66721

Figure 5.17: Oxidative dearomatization of **5.18** by AfoD and AzaH. PDA traces of enzymatic reaction and control reaction. (Table 1, entry 2). SM = starting material, INT = intermediate, PRD = product, IS = internal standard. The anionic form of the intermediate elutes near the solvent front.

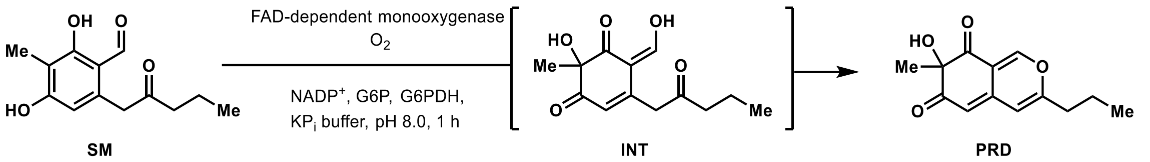

OH
O
Me
O
HO
Me
SM
FAD-dependent monooxygenase
O_2
$NADP^+$, G6P, G6PDH,
KP_i buffer, pH 8.0, 1 h
HO
O
OH
Me
O
O
Me
INT
HO
O
Me
O
O
Me
PRD

With AzaH

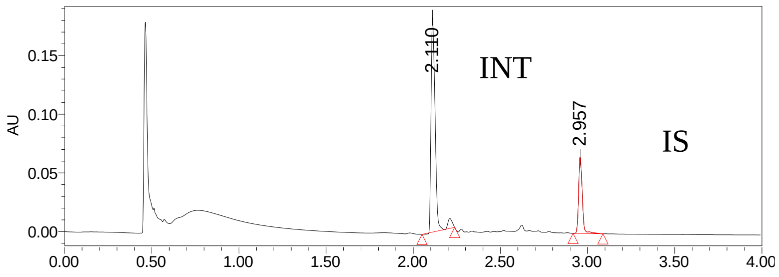

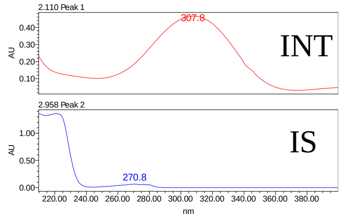

	Retention Time	Area	% Area	Height
1	2.110	305704	76.28	183131
2	2.957	95087	23.72	65154

With AfoD

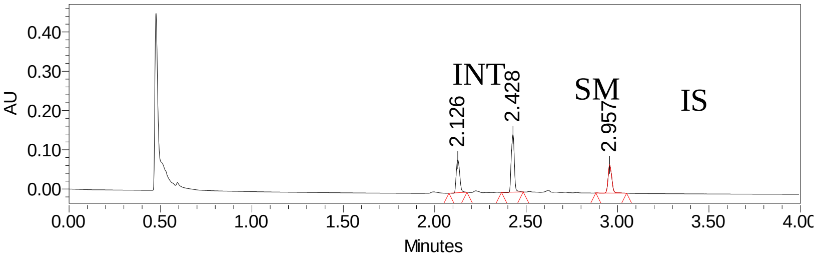

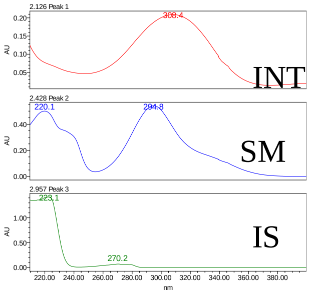

9	Retention Time	Area	% Area	Height
1	2.126	111917	29.11	83638
2	2.428	171664	44.65	146387
3	2.957	100880	26.24	72085

NEC

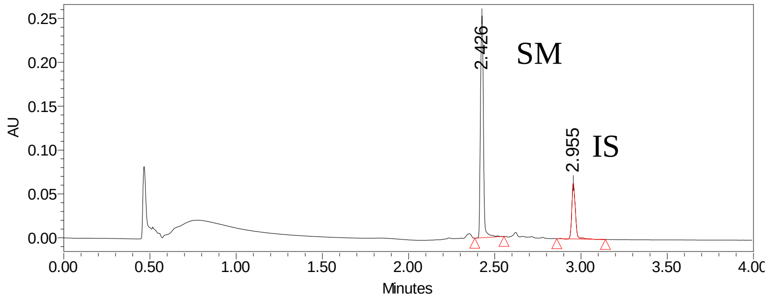

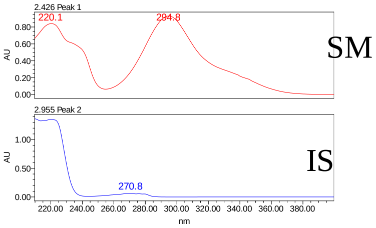

	Retention Time	Area	% Area	Height
1	2.426	301558	76.61	252996
2	2.955	92051	23.39	63755

Figure 5.18: Oxidative dearomatization of **5.17** by AfoD and AzaH. PDA traces of enzymatic reaction and control reaction.

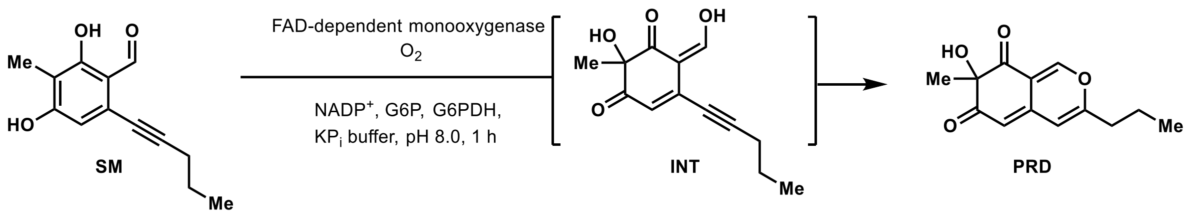
SM
FAD-dependent monooxygenase
O_2
$NADP^+$, G6P, G6PDH,
KP_i buffer, pH 8.0, 1 h
INT
PRD

With AzaH

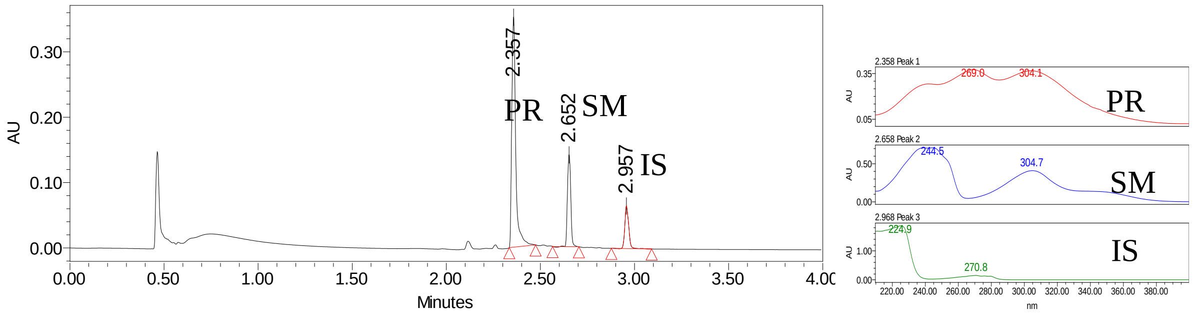

	Retention Time	Area	% Area	Height
1	2.357	517469	65.70	351986
2	2.652	176051	22.35	140720
3	2.957	94126	11.95	65187

With AfoD

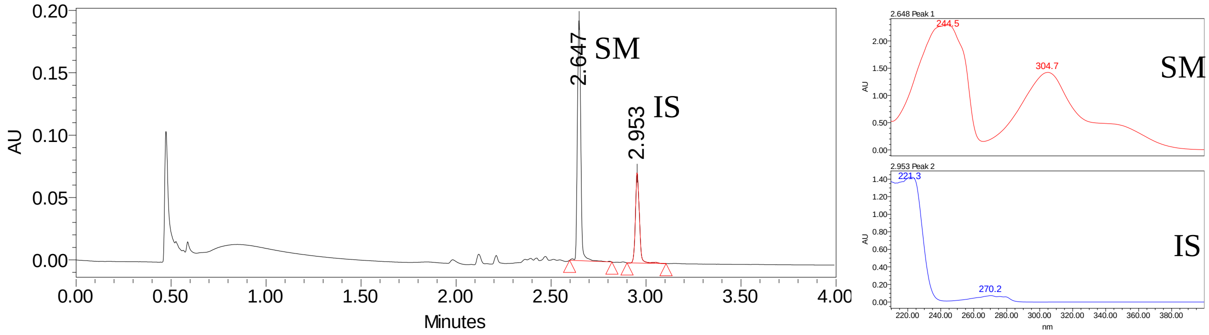

	Retention Time	Area	% Area	Height
1	2.647	240563	69.66	192549
2	2.953	104788	30.34	72317

NEC

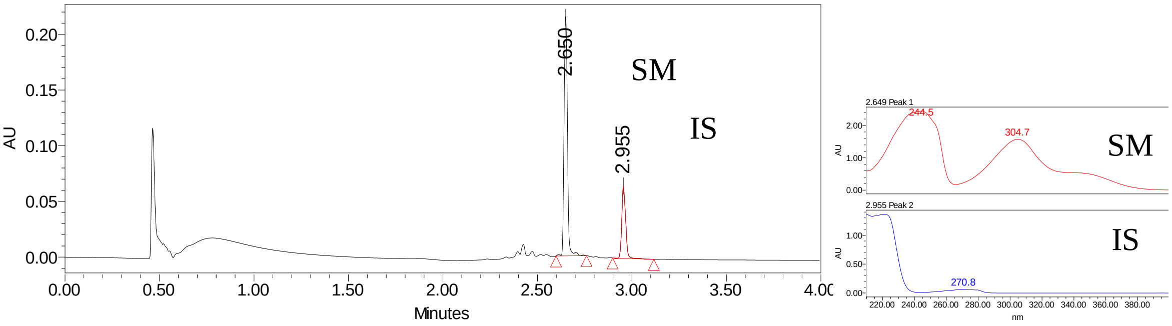

	Retention Time	Area	% Area	Height
1	2.650	266100	74.22	214826
2	2.955	92442	25.78	64989

Figure 5.19: Oxidative dearomatization of **5.19** by AfoD and AzaH. PDA traces of enzymatic reaction and control reaction.

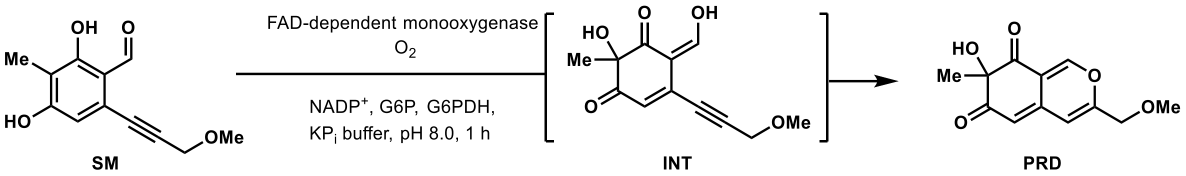
FAD-dependent monooxygenase
O_2
NADP$^+$, G6P, G6PDH,
KP$_i$ buffer, pH 8.0, 1 h
OH
O
Me
HO
OMe
HO
Me
O
OH
O
OMe
HO
Me
O
O
O
OMe

SM **INT** **PRD**

With AzaH

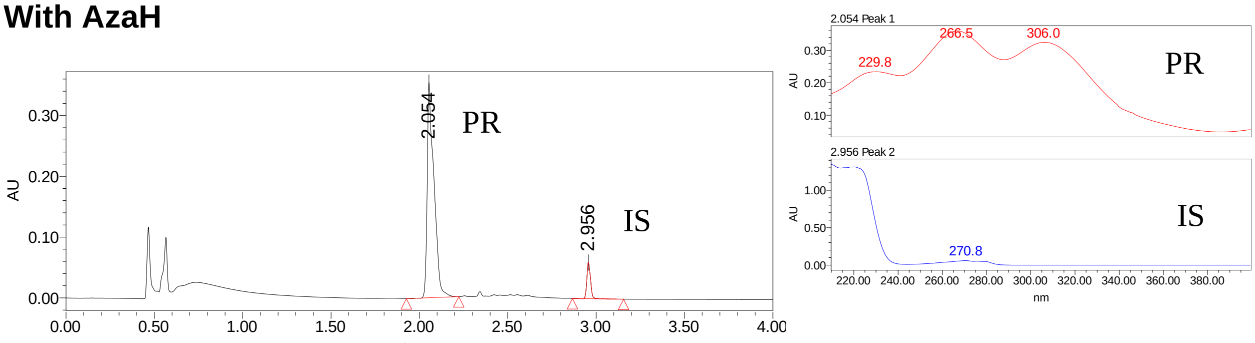

	Retention Time	Area	% Area	Height
1	2.054	944560	91.63	354150
2	2.956	86293	8.37	59688

With AfoD

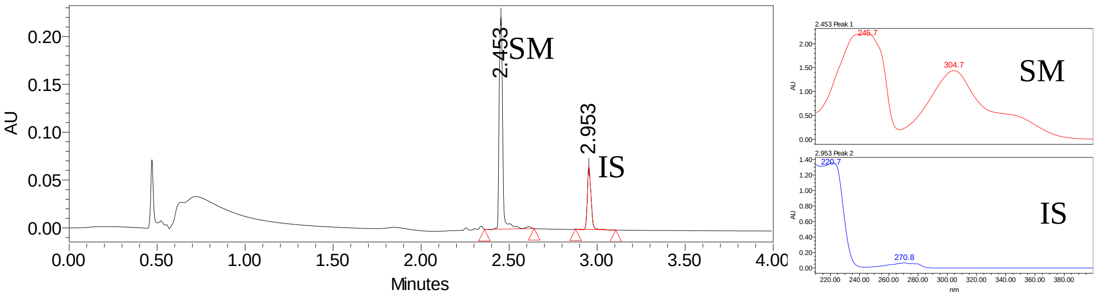

	Retention Time	Area	% Area	Height
1	2.453	309943	76.49	222375
2	2.953	95246	23.51	65655

NEC

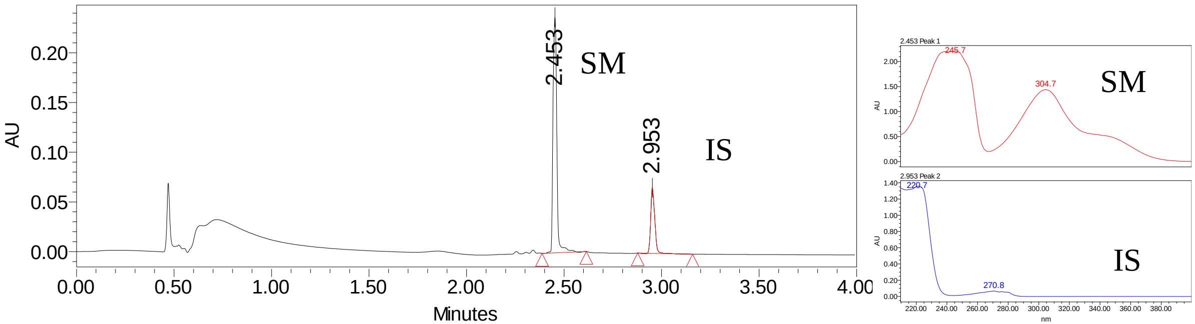

	Retention Time	Area	% Area	Height
1	2.453	321740	77.09	237334
2	2.953	95619	22.91	65898

Figure 5.20: Oxidative dearomatization of **5.20** by AfoD and AzaH. PDA traces of enzymatic reaction and control reaction.

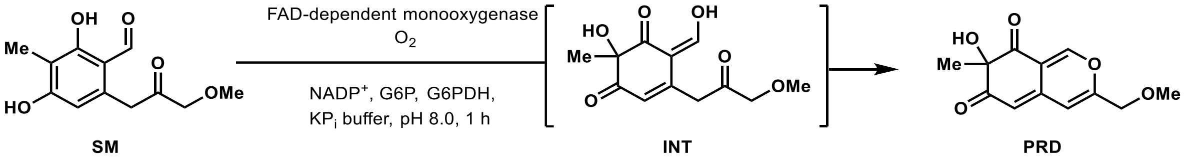
FAD-dependent monooxygenase
O_2
NADP$^+$, G6P, G6PDH,
KP$_i$ buffer, pH 8.0, 1 h
SM
INT
PRD
OH
O
Me
HO
OMe

With AzaH

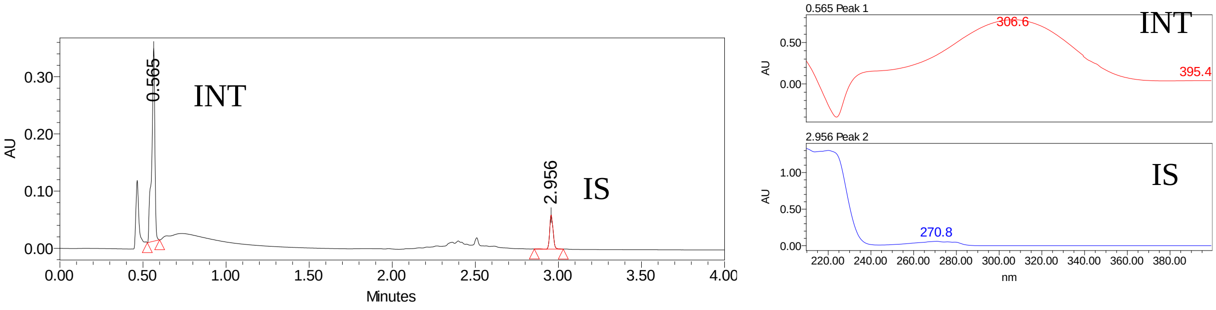

	Retention Time	Area	% Area	Height
1	0.565	434990	83.72	338239
2	2.956	84593	16.28	59668

With AfoD

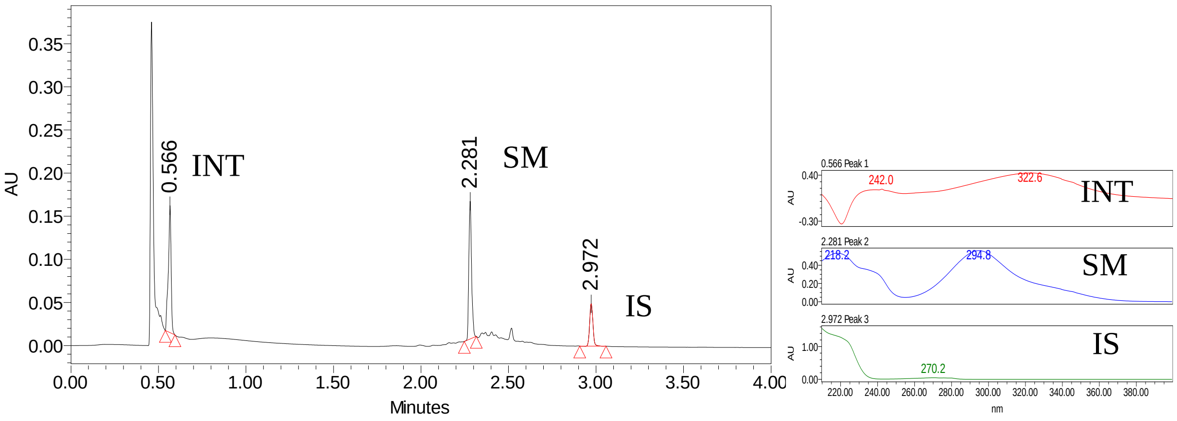

	Retention Time	Area	% Area	Height
1	0.572	113995	30.42	89263
2	2.271	157150	41.94	133701
3	2.953	103585	27.64	72398

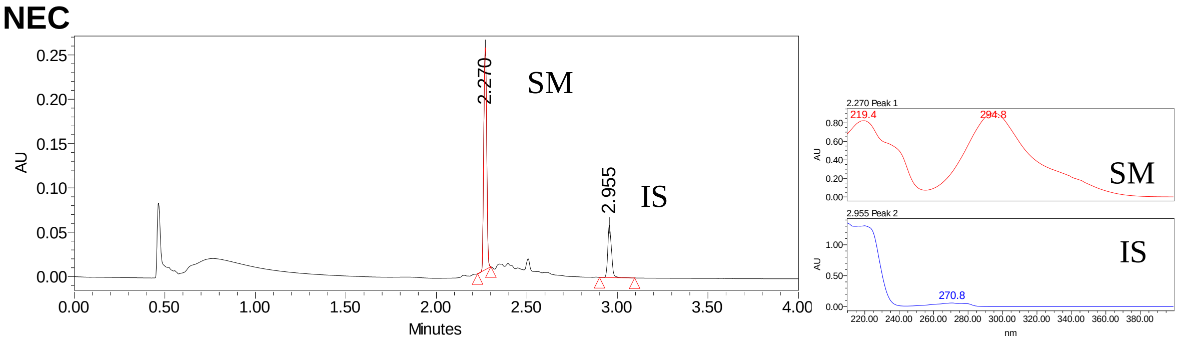

	Retention Time	Area	% Area	Height
1	2.270	284197	77.11	250475
2	2.955	84347	22.89	58999

Figure 5.21: Oxidative dearomatization of **5.57** by AfoD and AzaH. PDA traces of enzymatic reaction and control reaction.

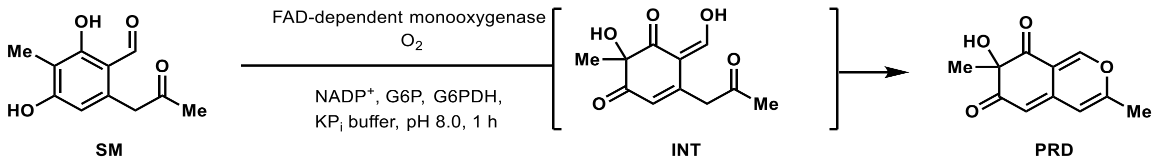
OH
O
Me
O
HO
Me
SM
FAD-dependent monooxygenase
O_2
NADP$^+$, G6P, G6PDH,
KP$_i$ buffer, pH 8.0, 1 h
HO
O
OH
Me
O
O
Me
INT
HO
O
Me
O
O
Me
PRD

With AzaH

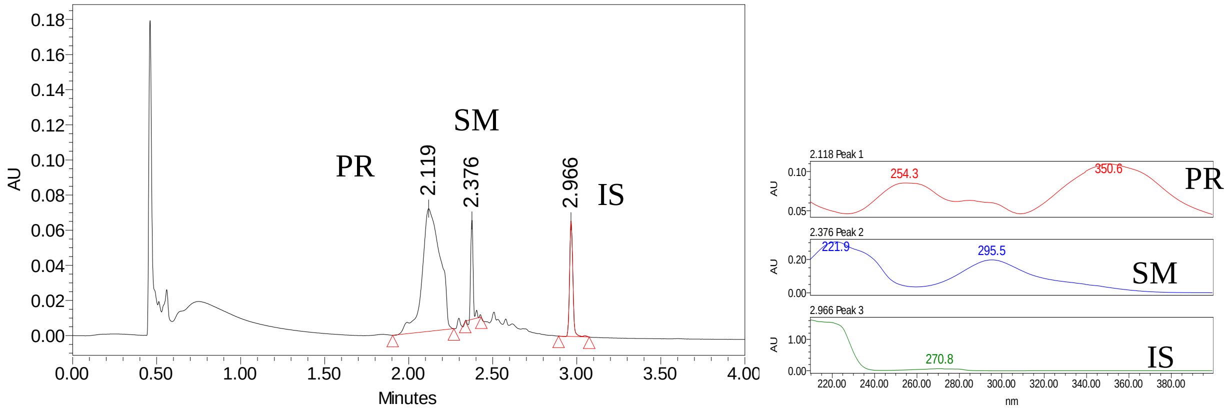

	Retention Time	Area	% Area	Height
1	2.119	519413	77.67	69861
2	2.376	60100	8.99	56370
3	2.966	89232	13.34	65670

With AfoD

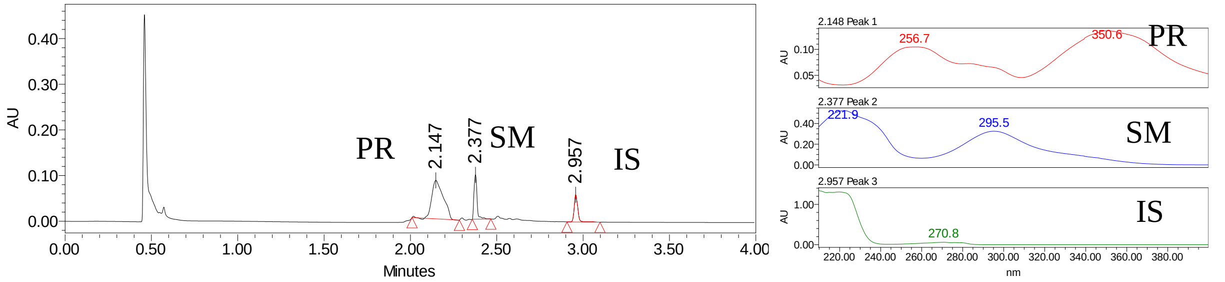

	Retention Time	Area	% Area	Height
1	2.147	398043	65.96	84339
2	2.377	119827	19.86	97170
3	2.957	85588	14.18	59788

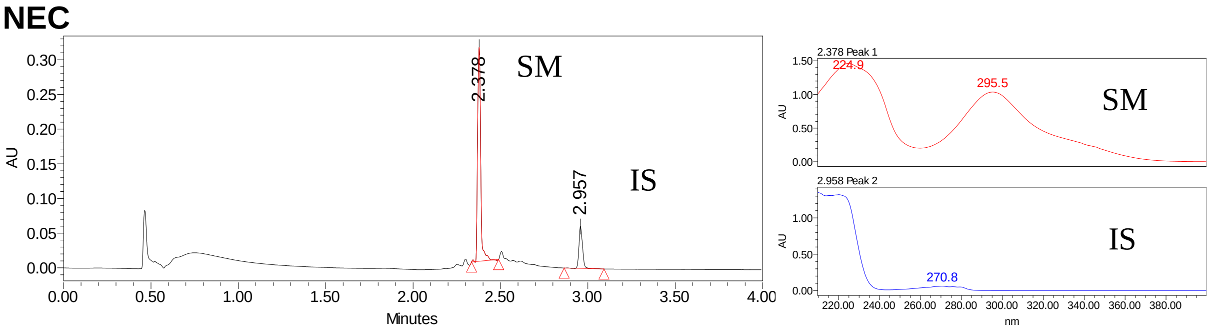

	Retention Time	Area	% Area	Height
1	2.378	383633	81.55	308926
2	2.957	86811	18.45	60584

Figure 5.22: Oxidative dearomatization of **5.21** by AfoD and AzaH. PDA traces of enzymatic reaction and control reaction.

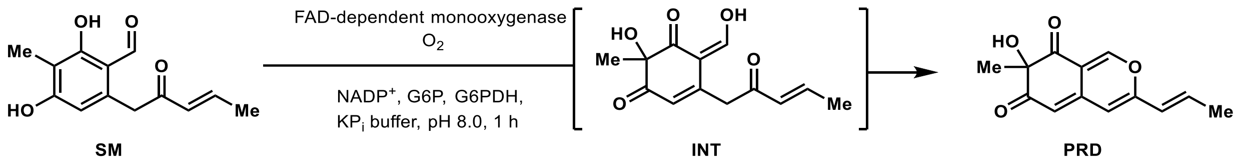

SM
FAD-dependent monooxygenase
O_2
NADP$^+$, G6P, G6PDH,
KP$_i$ buffer, pH 8.0, 1 h
INT
PRD
OH
O
Me
HO
Me

With AzaH

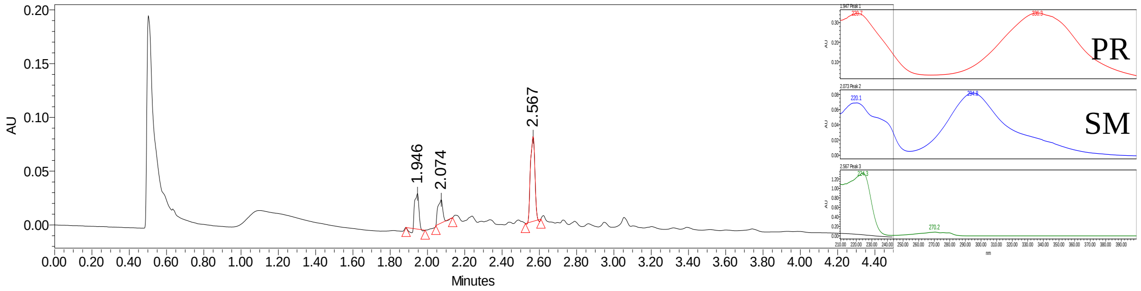

	Retention Time	Area	% Area	Height
1	1.946	59575	25.80	32920
2	2.074	40004	17.33	21701
3	2.567	131297	56.87	78806

With AfoD

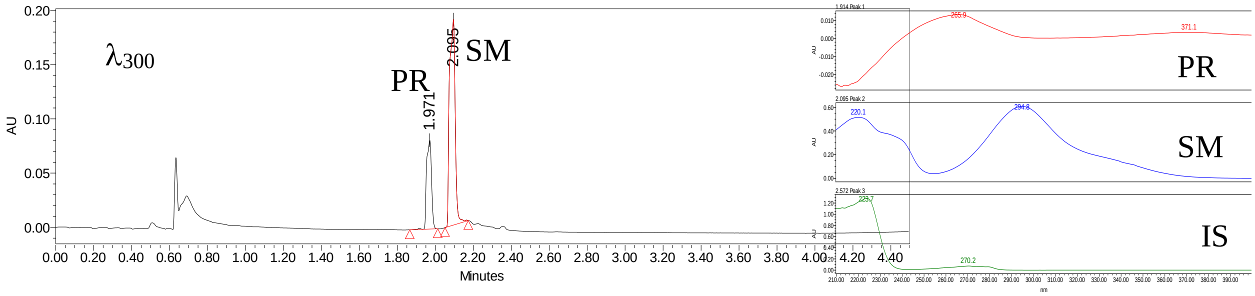

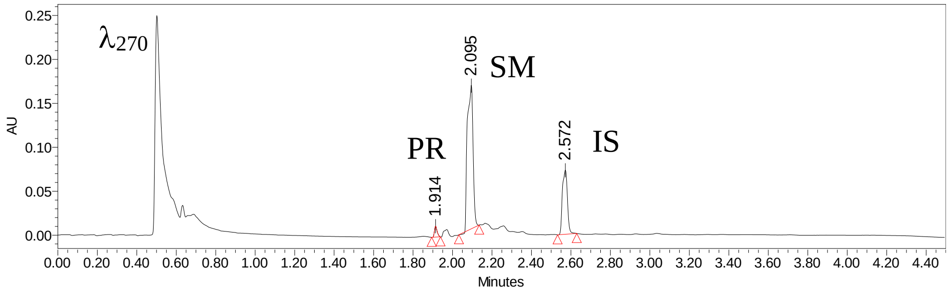

	Retention Time	Area	% Area	Height
1	1.946	59575	25.80	32920
2	2.074	40004	17.33	21701
3	2.567	131297	56.87	78806

NEC

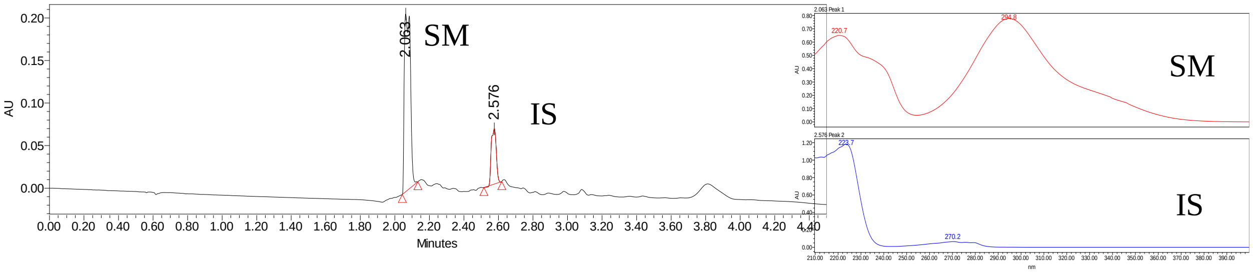

	Retention Time	Area	% Area	Height
1	2.063	507851	79.50	208715
2	2.576	130976	20.50	65081

Figure 5.23: Oxidative dearomatization of **5.22** by AfoD and AzaH. PDA traces of enzymatic reaction and control reaction. Two wavelengths are shown to visualize product.

Chapter 5.6.6: Determination of Enantiomeric Excess

Racemic standard

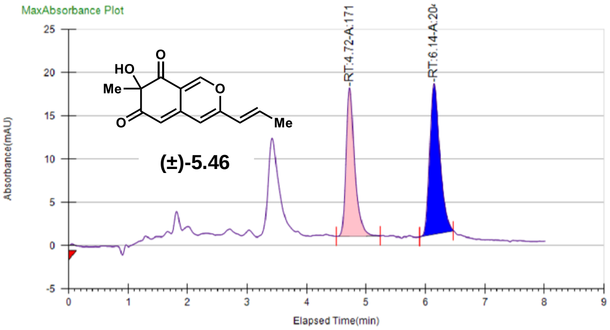

Run Information

Instrument Method	Inj. Vol.	Solvent	Column	Sample	Well Location	Temp.	Flow	% Modifier	Pressure
AD-H_30%_300-330	5	iPrOH	AD-H Chiral Analytical	Rac_bicycle	11A	40	3.5	30	120

Peak Information

Peak No	% Area	Area	Ret. Time	Height	Cap. Factor
1	45.5935	171.6805	4.72 min	17.1822	0
2	54.4065	204.8656	6.14 min	17.4111	0

XX from AfoD reaction

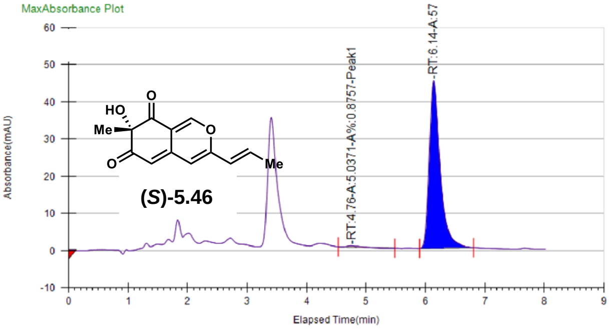

Run Information

Instrument Method	Inj. Vol.	Solvent	Column	Sample	Well Location	Temp.	Flow	% Modifier	Pressure
AD-H_30%_300-330	5	iPrOH	AD-H Chiral Analytical	AfpD_bicycle	13A	40	3.5	30	120

Peak Information

Peak No	% Area	Area	Ret. Time	Height	Cap. Factor
1	0.8757	5.0371	4.76 min	0.3701	0
2	99.1243	570.1434	6.14 min	45.0677	0

XX from AzaH reaction

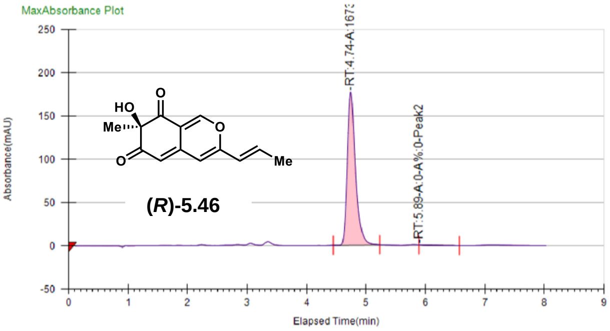

Run Information

Instrument Method	Inj. Vol.	Solvent	Column	Sample	Well Location	Temp.	Flow	% Modifier	Pressure
AD-H_30%_300-330	5	iPrOH	AD-H Chiral Analytical	AzaH_bicycle	12A	40	3.5	30	120

Peak Information

Peak No	% Area	Area	Ret. Time	Height	Cap. Factor
1	100	1673.5999	4.74 min	176.9264	0
2	0	0	5.89 min	0	0

Figure 5.24: PDA traces of racemic **5.46** obtained from a 1:1 mixture of the compound generated using AzaH and AfoD, (*S*)-**25** obtained from AfoD-mediated oxidative dearomatization, (*R*)-**5.46** obtained from AzaH-mediated oxidative dearomatization (CHIRALPAK® AD-H, 30%, CO_2, 3.5 mL/min).

Racemic standard

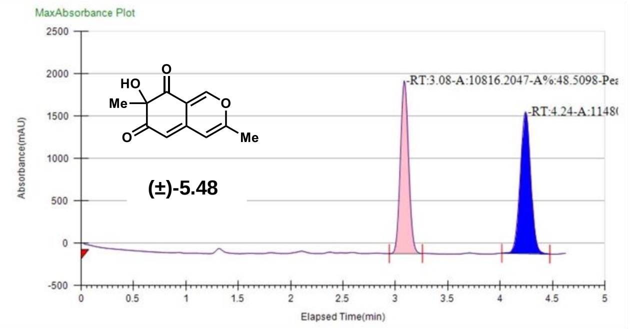

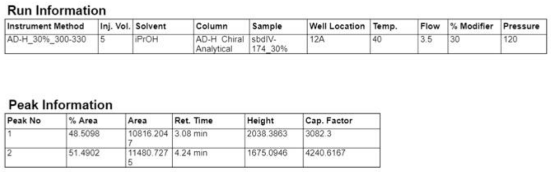

Run Information

Instrument Method	Inj. Vol.	Solvent	Column	Sample	Well Location	Temp.	Flow	% Modifier	Pressure
AD-H_30%_300-330	5	iPrOH	AD-H Chiral Analytical	sbdIV-174_30%	12A	40	3.5	30	120

Peak Information

Peak No	% Area	Area	Ret. Time	Height	Cap. Factor
1	48.5098	10816.2047	3.08 min	2038.3863	3082.3
2	51.4902	11480.7275	4.24 min	1675.0946	4240.6167

XX from AfoD reaction

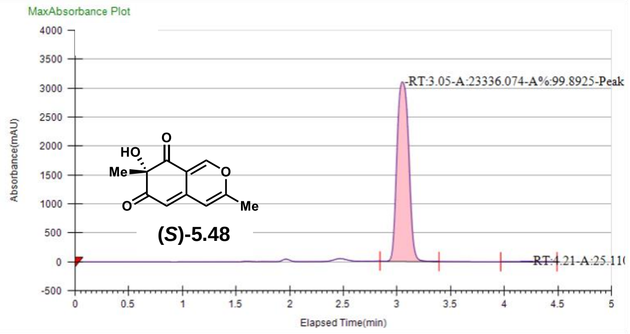

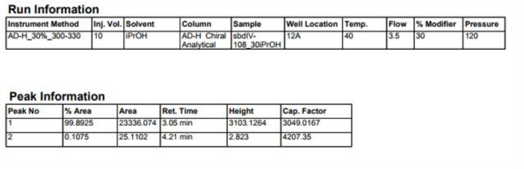

Run Information

Instrument Method	Inj. Vol.	Solvent	Column	Sample	Well Location	Temp.	Flow	% Modifier	Pressure
AD-H_30%_300-330	10	iPrOH	AD-H Chiral Analytical	sbdIV-108_30iPrOH	12A	40	3.5	30	120

Peak Information

Peak No	% Area	Area	Ret. Time	Height	Cap. Factor
1	99.8925	23336.074	3.05 min	3103.1264	3049.0167
2	0.1075	25.1102	4.21 min	2.823	4207.35

XX from AzaH reaction

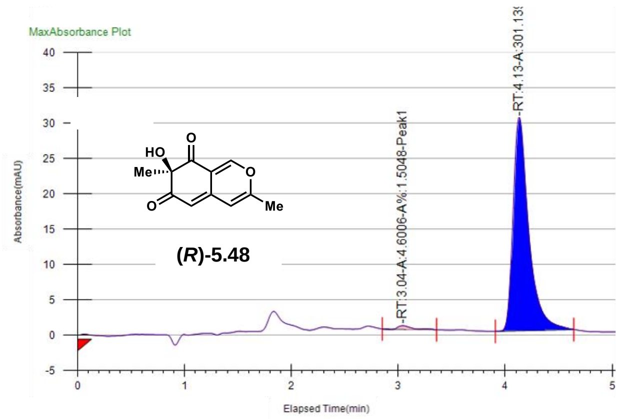

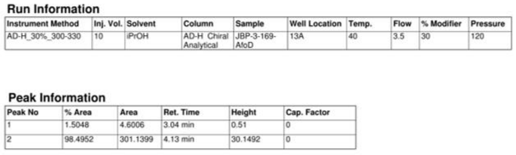

Run Information

Instrument Method	Inj. Vol.	Solvent	Column	Sample	Well Location	Temp.	Flow	% Modifier	Pressure
AD-H_30%_300-330	10	iPrOH	AD-H Chiral Analytical	JBP-3-169-AfoD	13A	40	3.5	30	120

Peak Information

Peak No	% Area	Area	Ret. Time	Height	Cap. Factor
1	1.5048	4.6006	3.04 min	0.51	0
2	98.4952	301.1399	4.13 min	30.1492	0

Figure 5.25: PDA traces of racemic **5.48** obtained IBX-mediated oxidative dearomatization, (*S*)-**5.48** obtained from AfoD-mediated oxidative dearomatization, (*R*)-**5.48** obtained from AzaH-mediated oxidative dearomatization (CHIRALPAK® AD-H, 30%, CO_2, 3.5 mL/min).

Chapter 5.6.7: NMR Spectra of Compounds

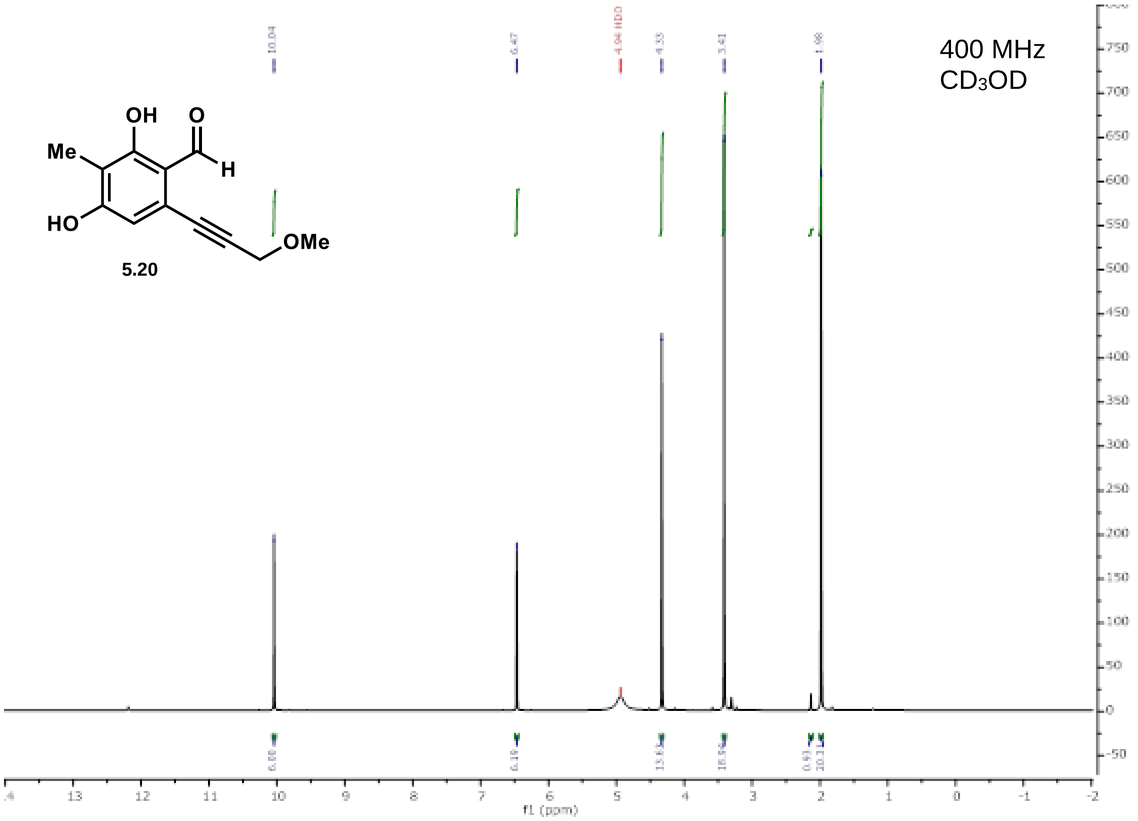

5.20

400 MHz
CD_3OD

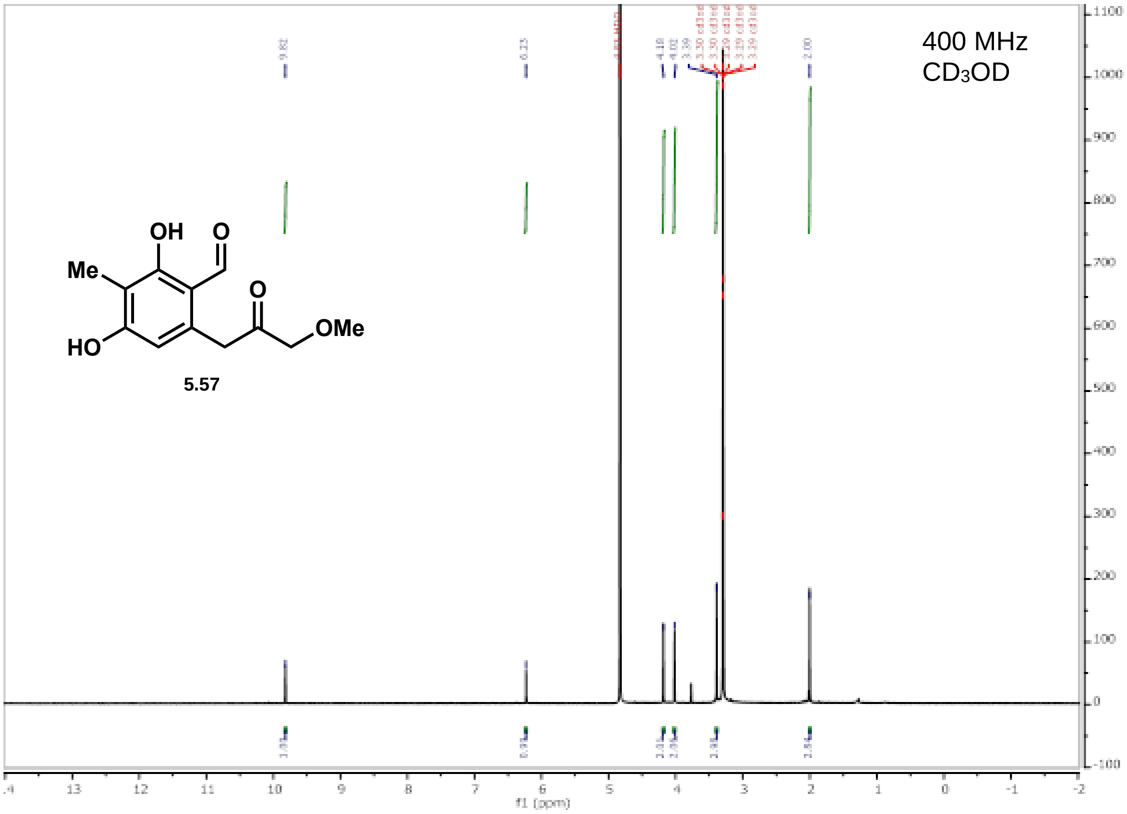
400 MHz
CD3OD
OH
O
Me
O
OMe
HO
5.57
9.82
6.23
4.18
4.02
3.39
2.00
f1 (ppm)

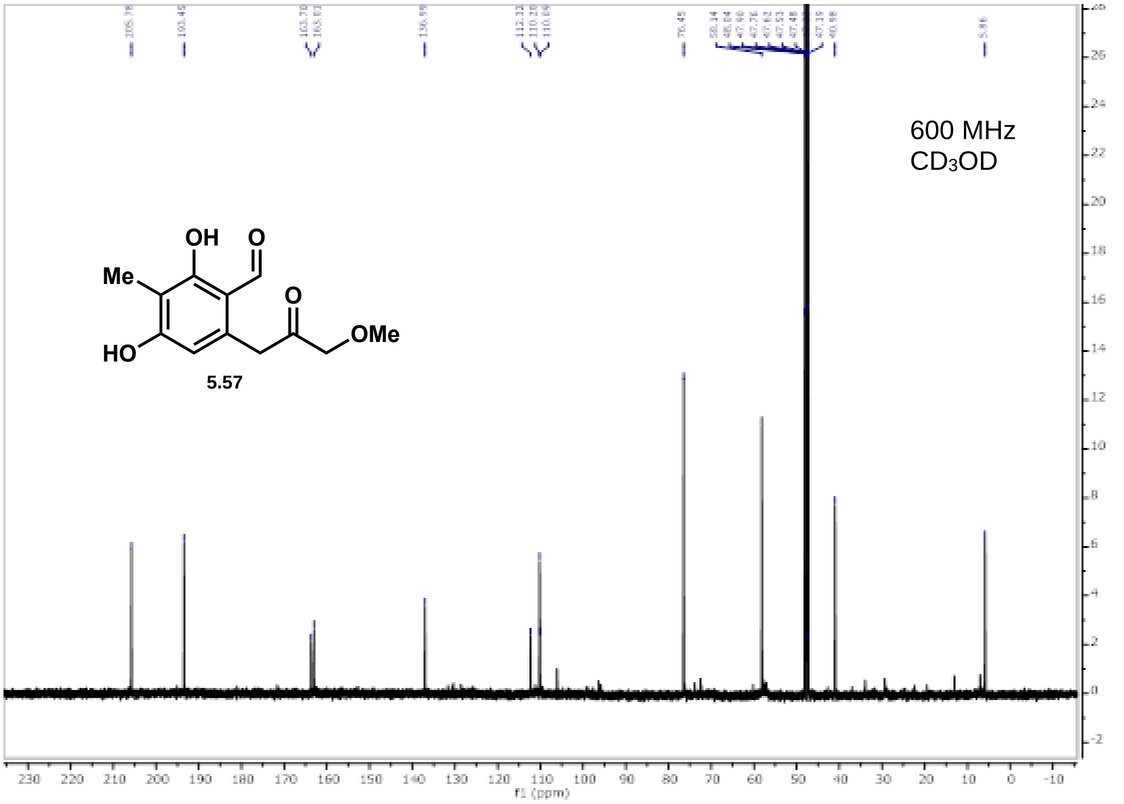
600 MHz
CD3OD
OH
O
Me
O
OMe
HO
5.57
205.78
193.45
163.70
163.63
136.99
112.12
110.18
110.09
76.45
58.14
47.19
40.98
5.86
f1 (ppm)

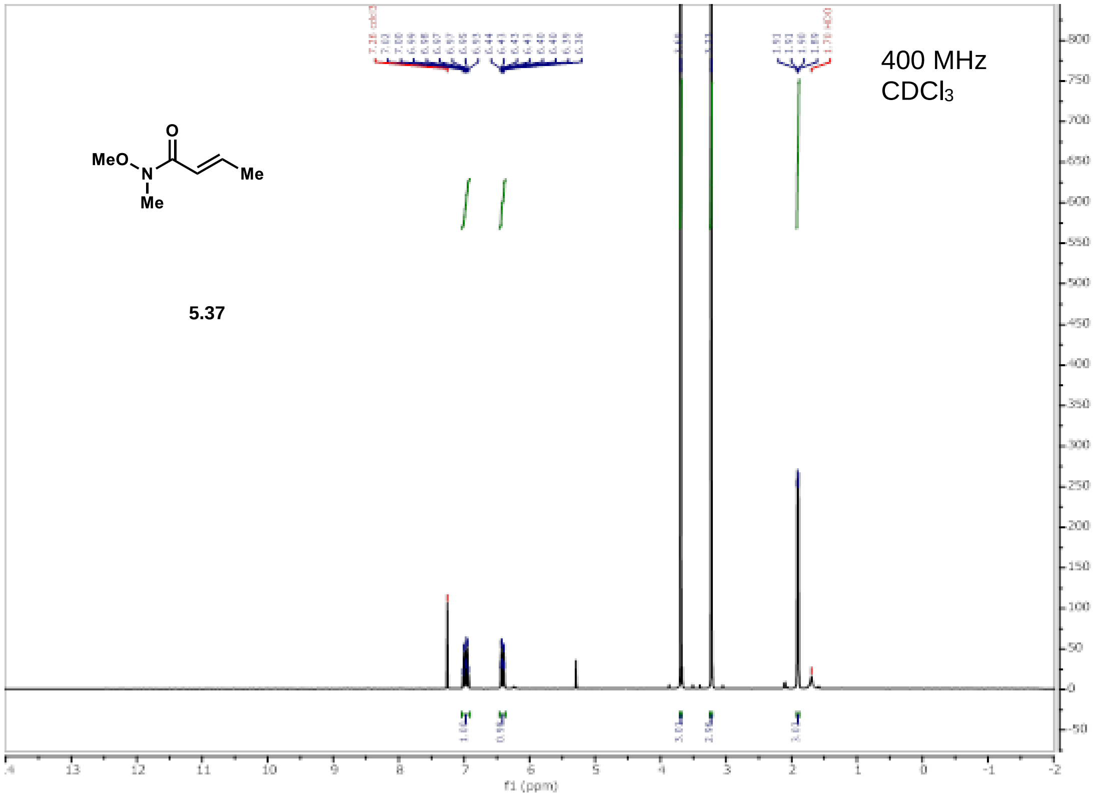
MeO
N
Me
O
Me
5.37
400 MHz
CDCl3
7.26 cdcl3
7.03
7.00
6.99
6.98
6.97
6.95
6.95
6.93
6.44
6.43
6.43
6.42
6.40
6.39
6.39
1.93
1.93
1.90
1.89
1.70 HDO
1.00
0.98
3.01
2.96
3.02
800
750
700
650
600
550
500
450
400
350
300
250
200
150
100
50
0
-50
14
13
12
11
10
9
8
7
6
5
4
3
2
1
0
-1
-2
f1 (ppm)

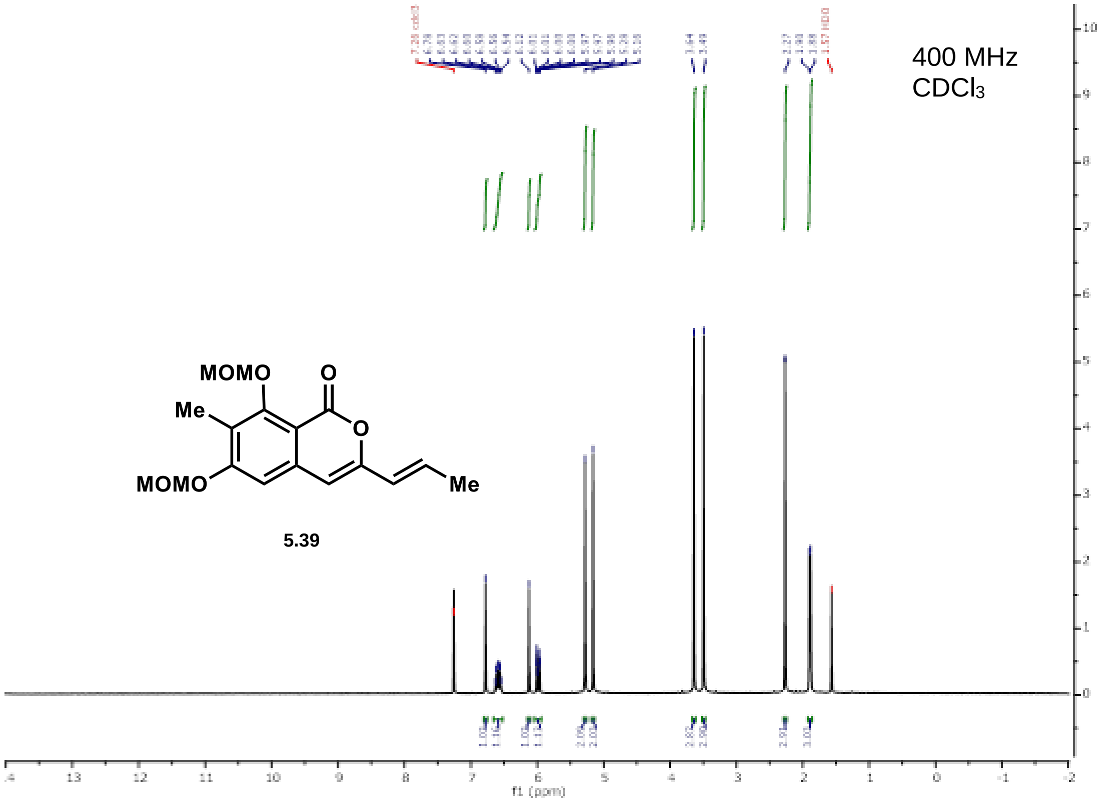
400 MHz
CDCl3
MOMO
O
Me
O
MOMO
Me
f1 (ppm)

5.39

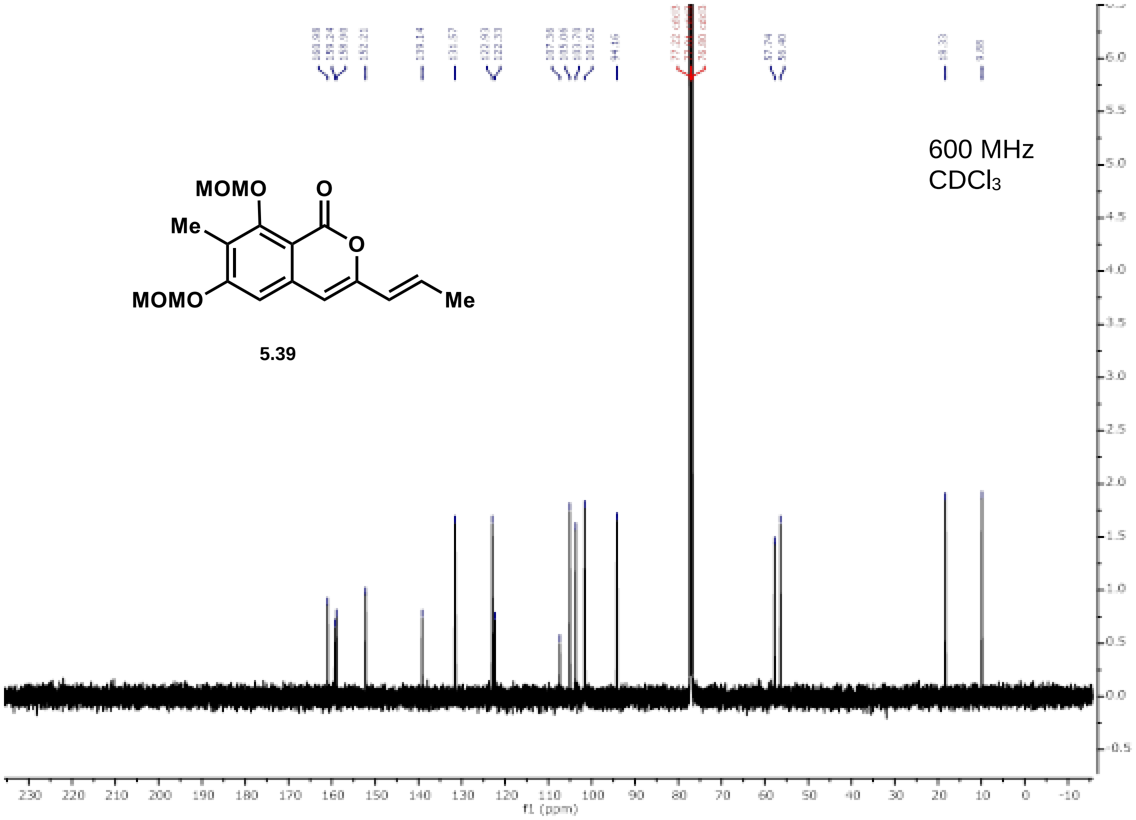
600 MHz
CDCl3
MOMO
O
Me
O
MOMO
Me
f1 (ppm)

5.39

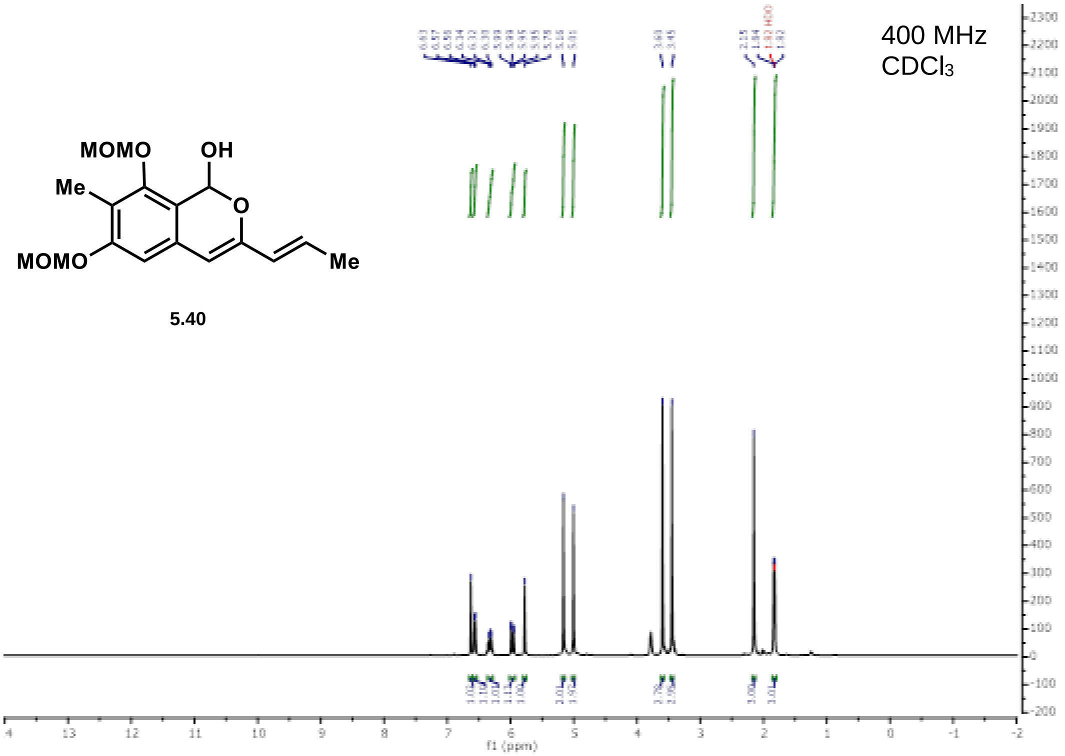
400 MHz
CDCl3
MOMO
OH
Me
O
MOMO
Me
6.63 6.57 6.58 6.34 6.32 6.30 5.99 5.99 5.95 5.95 5.78 5.16 5.01
3.60 3.45
2.15 1.84 1.82 H2O 1.82
1.00 1.10 1.01 1.11 1.04 2.01 1.97 2.75 2.96 3.00 3.01
14 13 12 11 10 9 8 7 6 5 4 3 2 1 0 -1 -2
f1 (ppm)
2300 2200 2100 2000 1900 1800 1700 1600 1500 1400 1300 1200 1100 1000 900 800 700 600 500 400 300 200 100 0 -100 -200

5.40

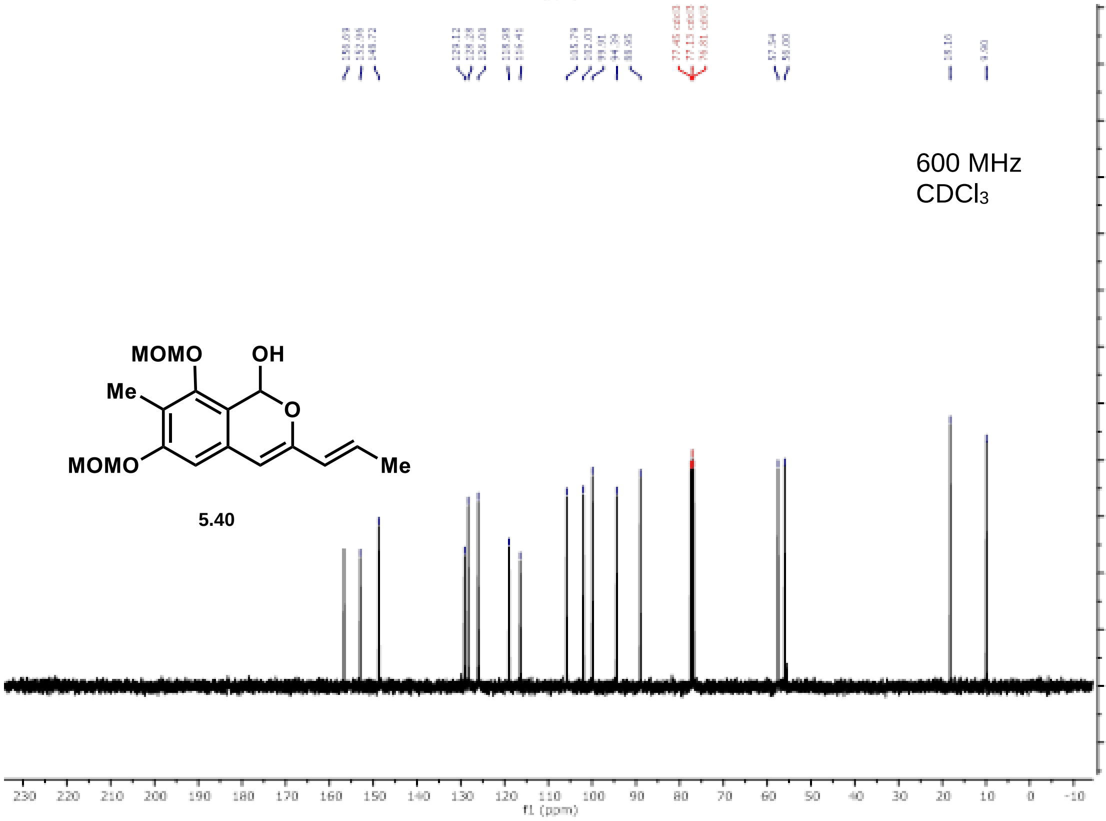
600 MHz
CDCl3
MOMO
OH
Me
O
MOMO
Me
156.69 152.96 148.72
129.12 128.28 126.03
118.98 116.41
105.79 102.03 99.91 94.39 88.95
77.45 cdcl3 77.13 cdcl3 76.81 cdcl3
57.54 56.00
18.10
9.90
230 220 210 200 190 180 170 160 150 140 130 120 110 100 90 80 70 60 50 40 30 20 10 0 -10
f1 (ppm)
12 11 10 9 8 7 6 5 4 3 2 1 0 -1

5.40

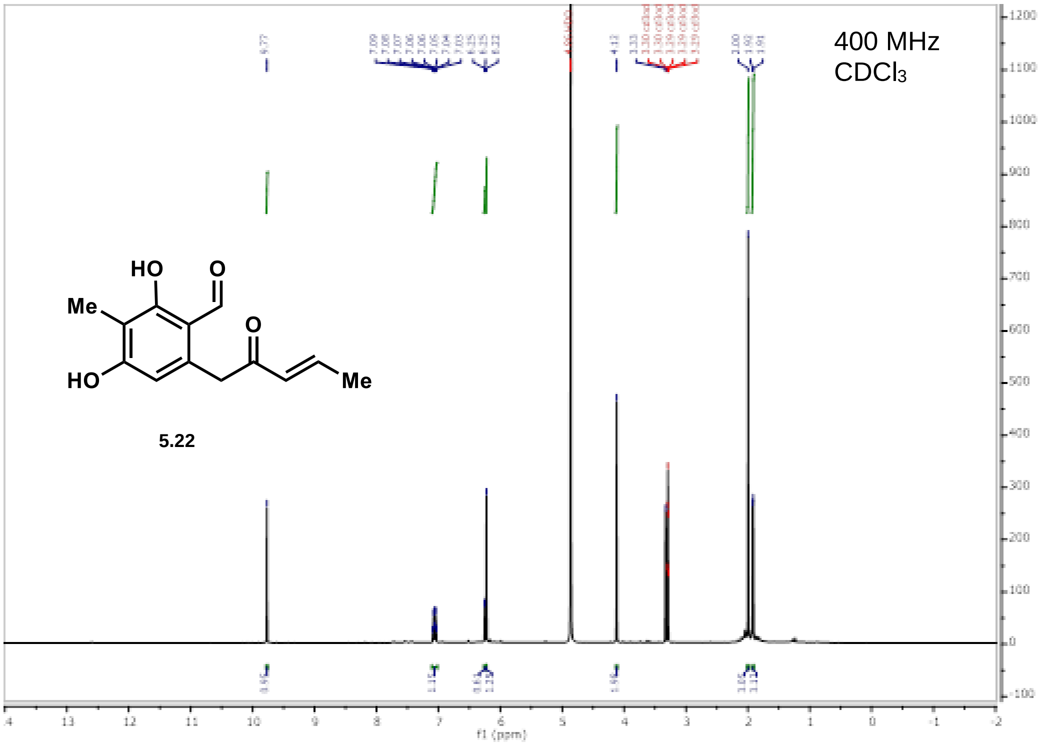
400 MHz
CDCl3
HO
O
Me
O
HO
Me
9.77
7.09
7.08
7.07
7.06
7.06
7.05
7.04
7.03
6.25
6.25
6.22
4.12
3.33
2.00
1.92
1.91
0.95
1.15
0.83
1.15
1.96
1200
1100
1000
900
800
700
600
500
400
300
200
100
0
-100
14
13
12
11
10
9
8
7
6
5
4
3
2
1
0
-1
-2
f1 (ppm)

5.22

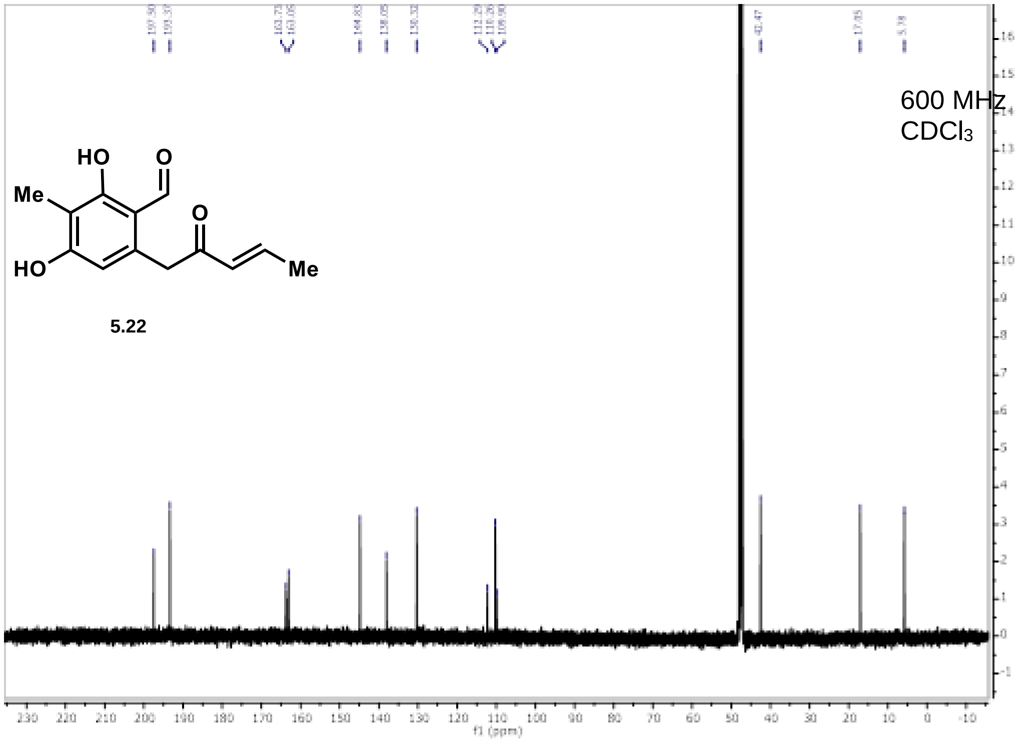
600 MHz
CDCl3
HO
O
Me
O
HO
Me
197.90
193.37
163.73
163.05
144.83
138.05
130.32
112.29
110.26
109.90
42.47
17.85
5.78
16
15
14
13
12
11
10
9
8
7
6
5
4
3
2
1
0
-1
230
220
210
200
190
180
170
160
150
140
130
120
110
100
90
80
70
60
50
40
30
20
10
0
-10
f1 (ppm)

5.22

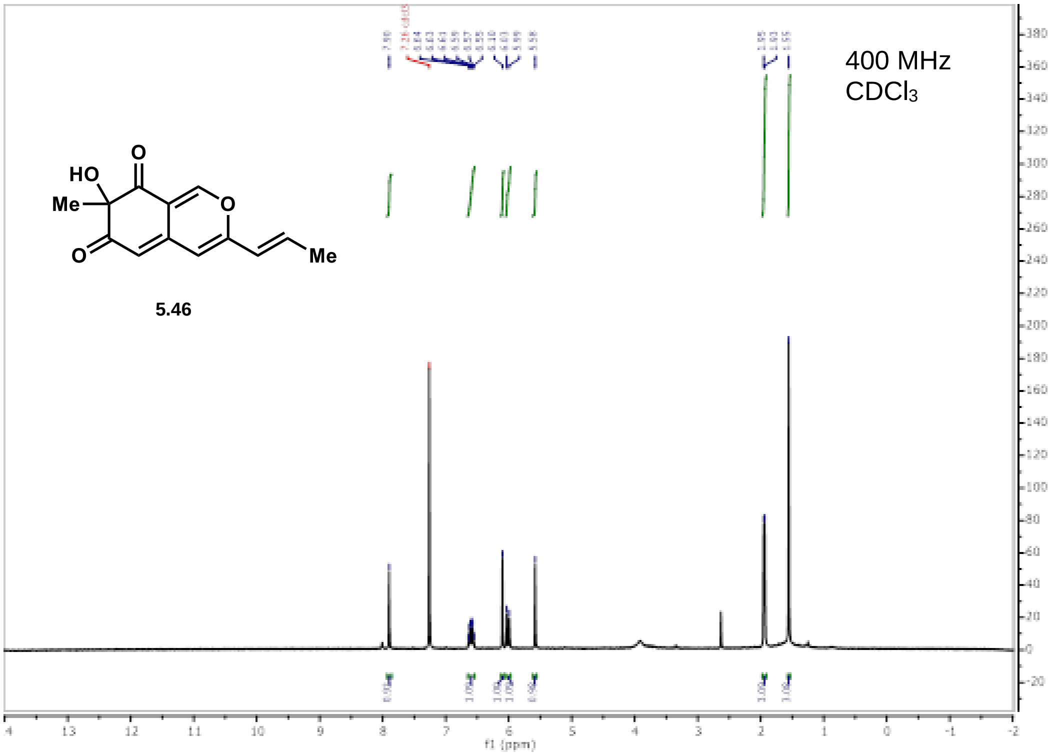
HO
Me
O
O
O
Me
5.46
400 MHz
CDCl3
7.90
7.26 cdcl3
6.64
6.63
6.61
6.59
6.57
6.55
6.10
6.03
5.99
5.58
1.95
1.61
1.59
f1 (ppm)

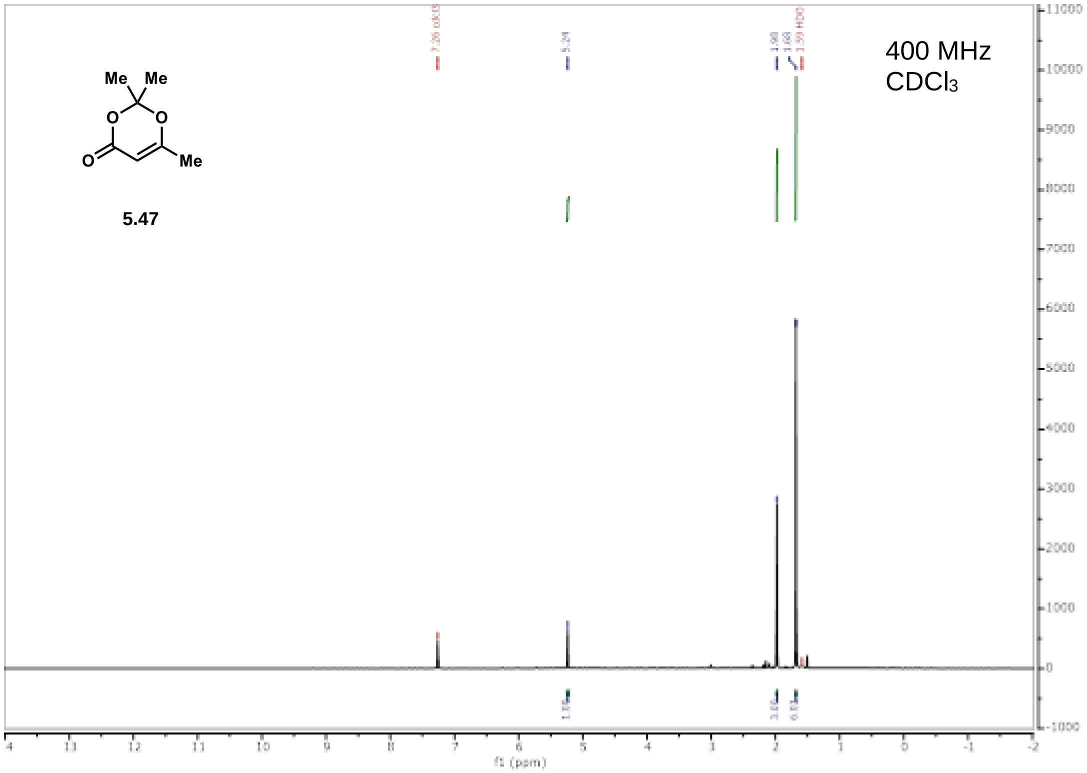
Me
Me
O
O
O
Me
5.47
400 MHz
CDCl3
7.26 cdcl3
5.24
1.98
1.68
1.59 HDO
f1 (ppm)

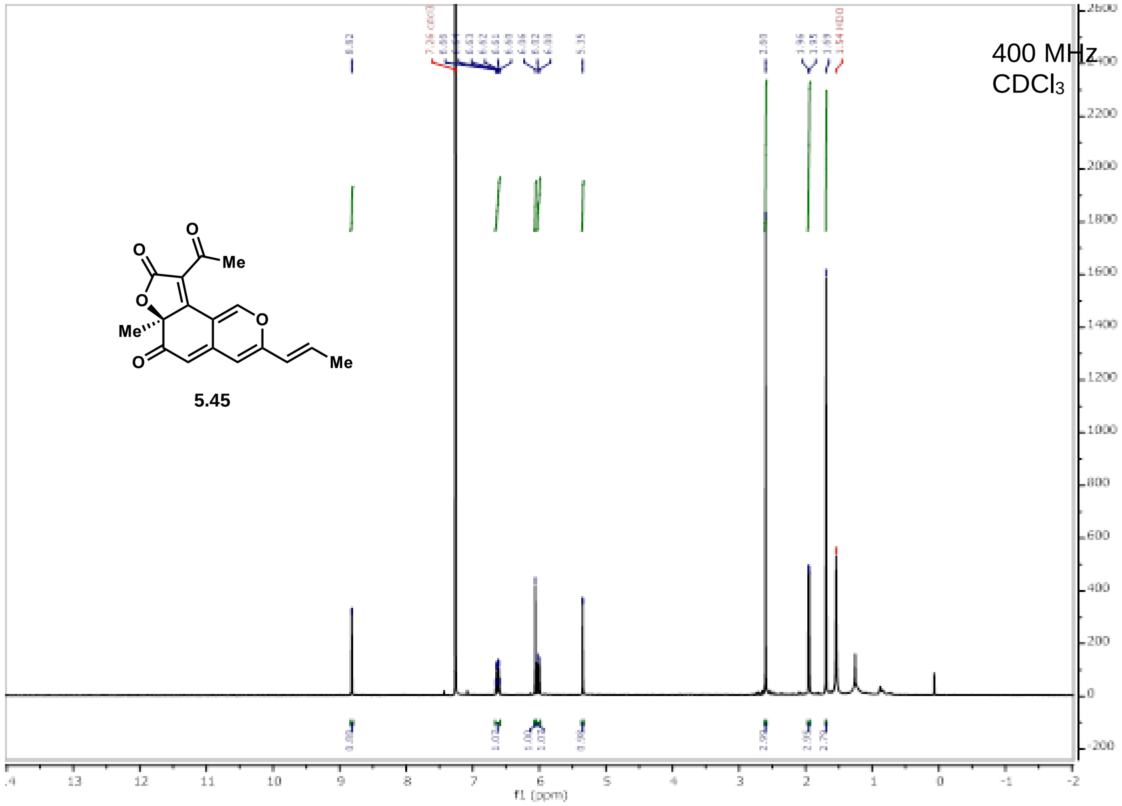
5.45

400 MHz
CDCl3
8.82
7.26 cdcl3
6.68
6.64
6.63
6.62
6.61
6.60
6.06
6.02
6.00
5.35
2.63
1.96
1.95
1.69
1.54 HDO
0.88
1.03
1.00
1.03
0.98
2.99
2.95
2.79
O
O
Me
O
Me
O
O
Me
f1 (ppm)
14
13
12
11
10
9
8
7
6
5
4
3
2
1
0
-1
-2
2600
2400
2200
2000
1800
1600
1400
1200
1000
800
600
400
200
0
-200

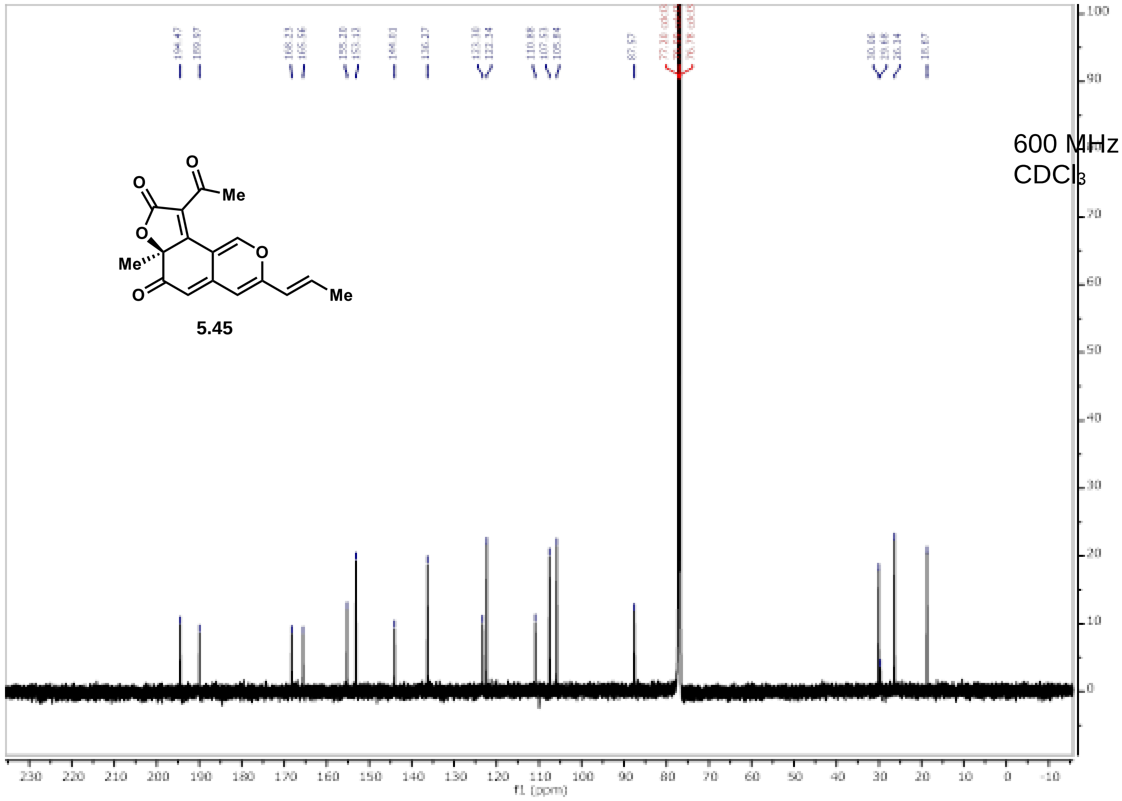
5.45

600 MHz
CDCl3
194.47
189.97
168.23
165.56
155.20
153.13
144.03
136.27
123.10
122.34
110.88
107.53
105.84
87.57
77.16 cdcl3
76.78 cdcl3
30.66
29.68
26.34
18.67
O
O
Me
O
Me
O
O
Me
f1 (ppm)
230
220
210
200
190
180
170
160
150
140
130
120
110
100
90
80
70
60
50
40
30
20
10
0
-10
100
90
70
60
50
40
30
20
10
0

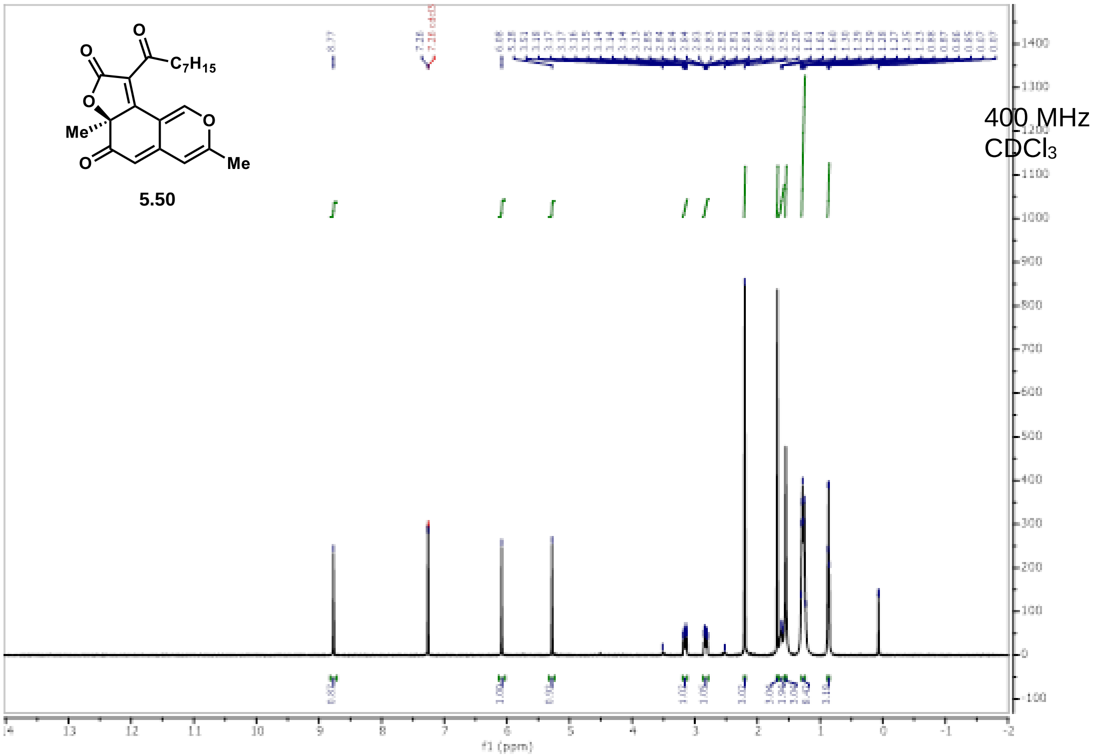
O
O
C7H15
O
O
Me
O
Me
5.50
400 MHz
CDCl3
f1 (ppm)
14
13
12
11
10
9
8
7
6
5
4
3
2
1
0
-1
-2
1400
1300
1200
1100
1000
900
800
700
600
500
400
300
200
100
0
-100

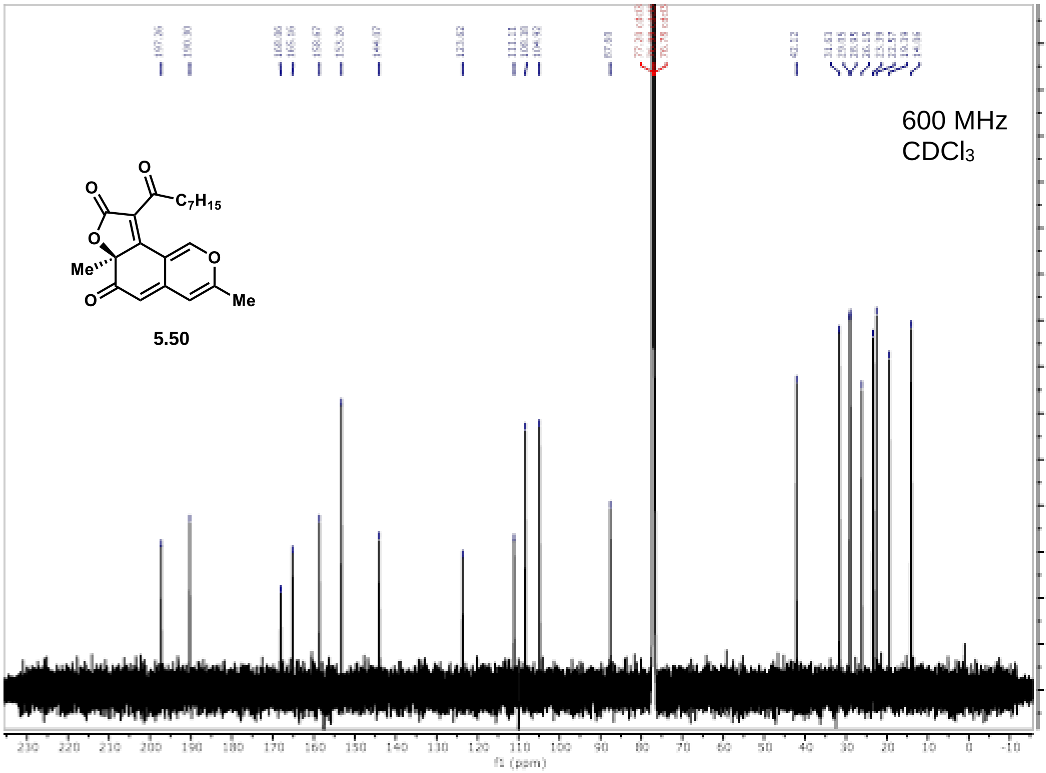
197.26
190.30
165.16
158.47
144.07
123.62
111.11
104.92
87.88
42.12
600 MHz
CDCl3
O
O
C7H15
O
O
Me
O
Me
5.50
f1 (ppm)
230
220
210
200
190
180
170
160
150
140
130
120
110
100
90
80
70
60
50
40
30
20
10
0
-10
28
26
24
22
20
18
16
14
12
10
8
6
4
2
0

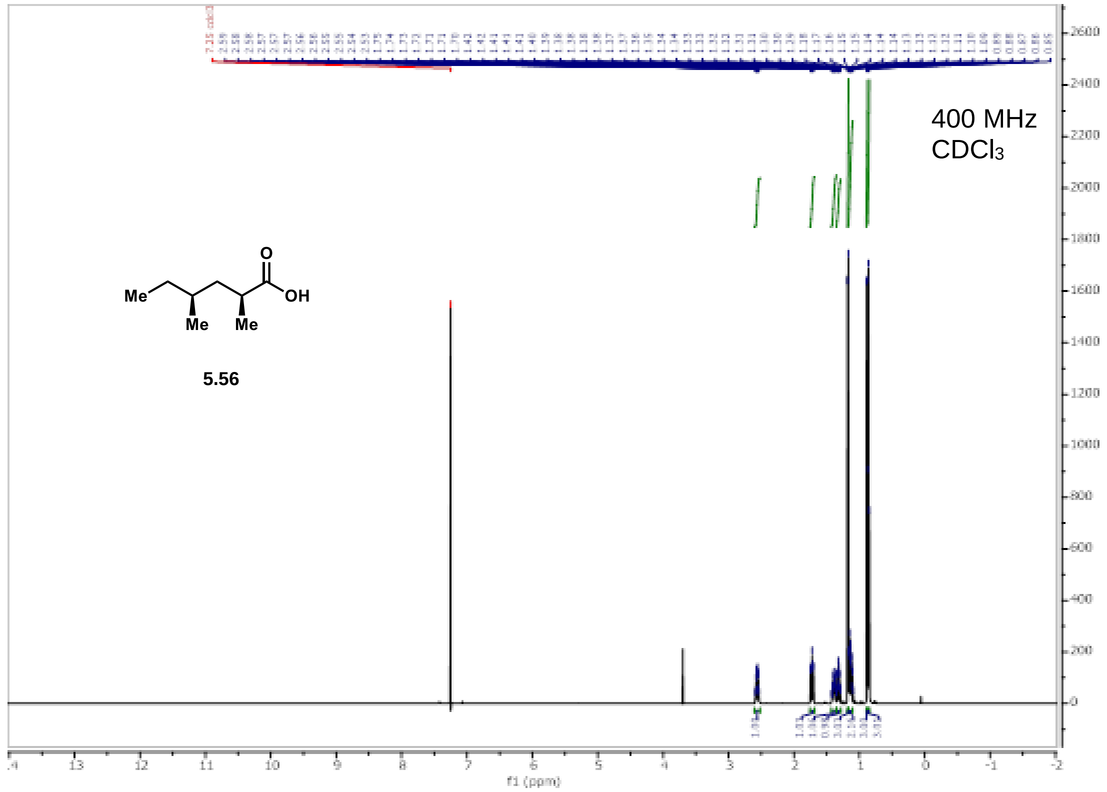
400 MHz
CDCl3
Me
Me
Me
O
OH
5.56
f1 (ppm)
14
13
12
11
10
9
8
7
6
5
4
3
2
1
0
-1
-2
2600
2400
2200
2000
1800
1600
1400
1200
1000
800
600
400
200
0

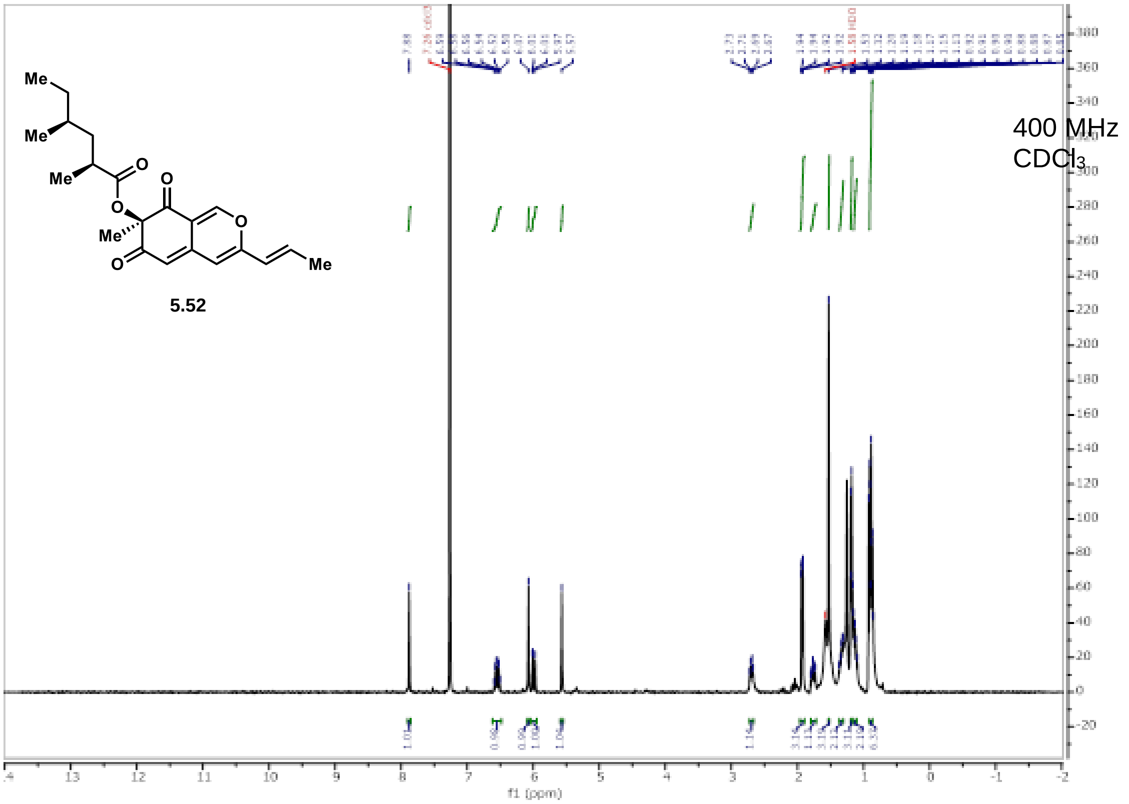
Me
Me
Me
O
O
O
Me
O
O
Me
5.52
400 MHz
CDCl3
7.26 cdcl3
1.58 H2O
1.07
0.98
0.99
1.00
1.04
1.14
f1 (ppm)

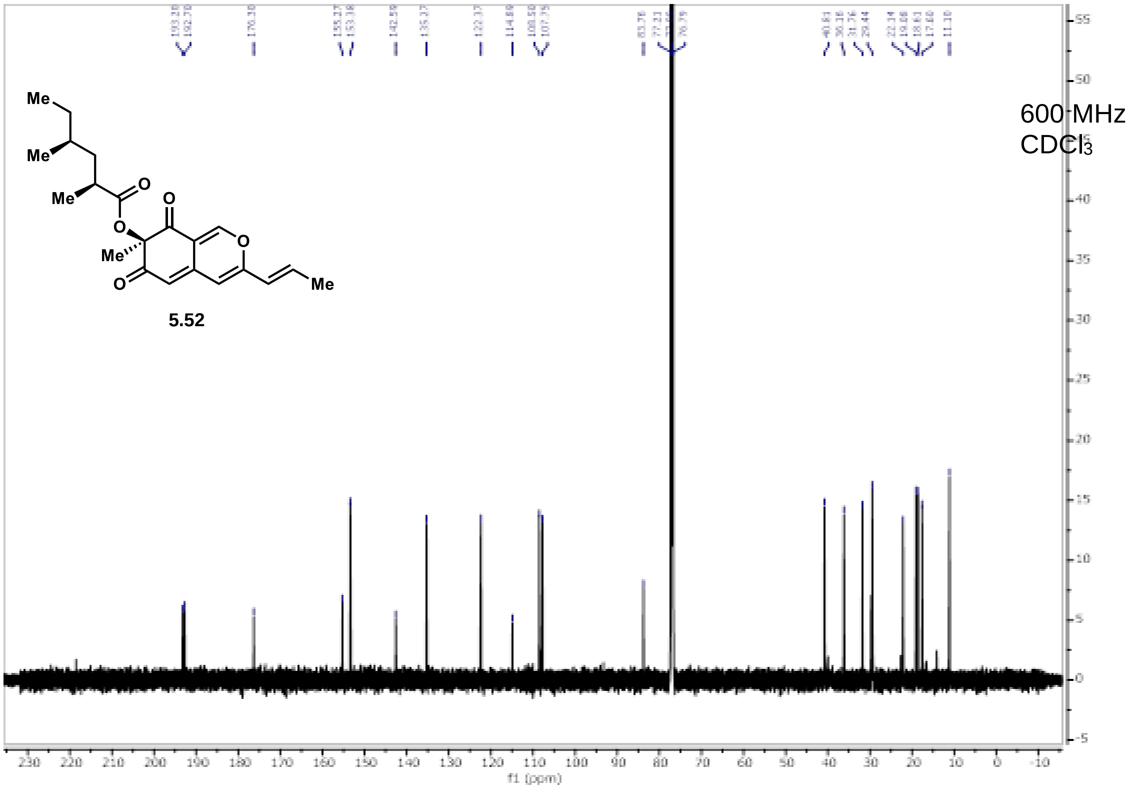
Me
Me
Me
O
O
O
Me
O
O
Me
5.52
600 MHz
CDCl3
193.28
192.78
176.30
155.27
153.18
142.59
135.27
122.17
114.89
108.50
107.75
83.78
77.21
76.79
40.81
36.16
31.76
29.44
22.14
19.08
18.61
17.60
11.10
f1 (ppm)

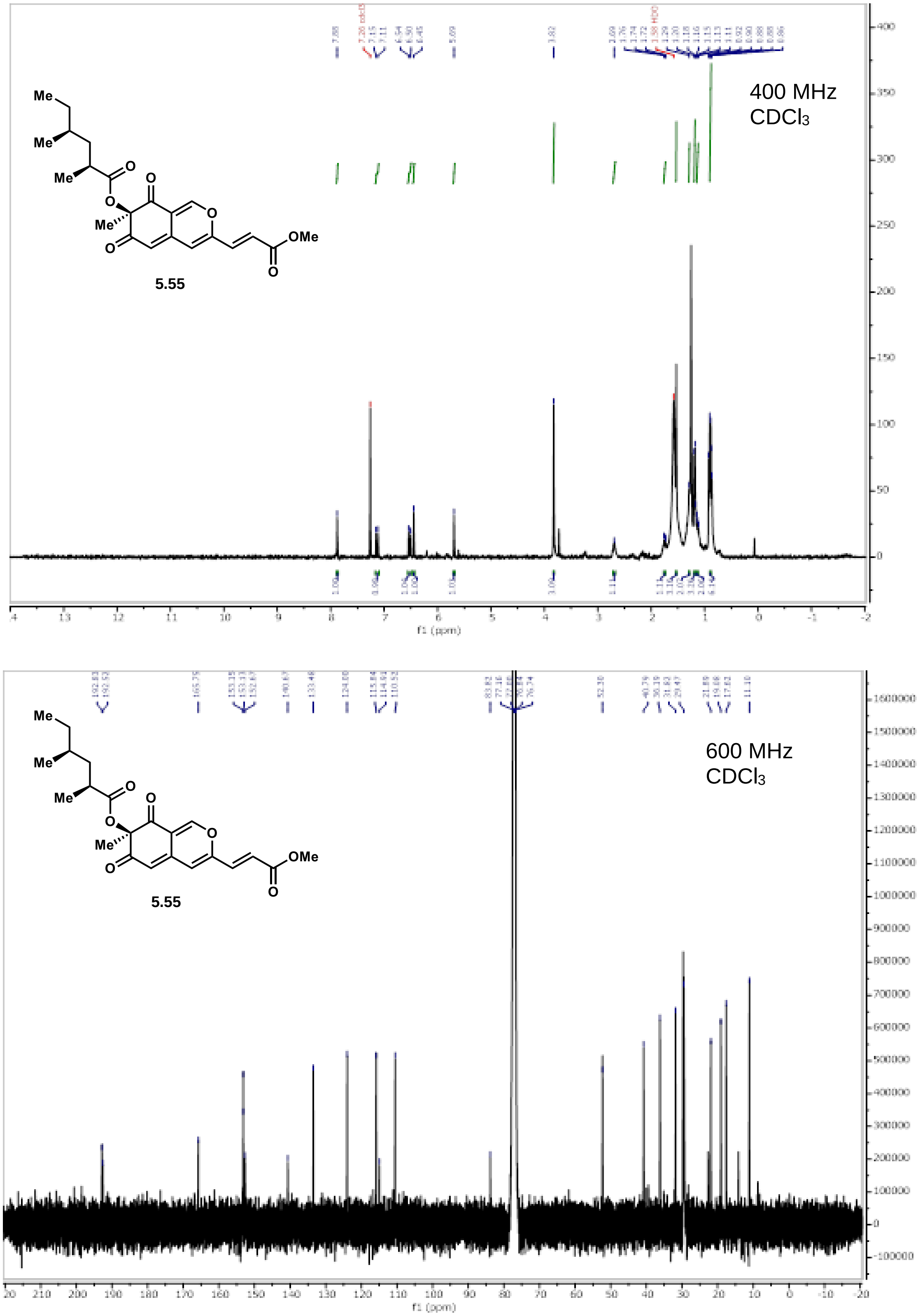

Figure 5.26: NMR spectra of synthetic compounds.

Chapter 5.6: References

1) For a review see: Gao, J.-M.; Yang, S.-X.; Qin, J.-C. *Chem. Rev.* **2013**, *113*, 4755.
2) Suzuki, T. Tanemura, K.; Okada C.; Arai, K.; Awaji, A.; Shimizu, T.; Horaguchi, T. *J. Heterocyclic Chem.* **2001**, *38*, 1409-1418.
3) a) Stierle, A. A.; Stierle, D. B.; Bugni, T. *J. Org. Chem.* **1999**, *64*, 5479. b) Yoshida, E.; Fujimoto, H.: Baba, M.; Yamazaki, M. *Chem. Pharm. Bull.* **1995**, *43*, 1307. c) Quang, D. N.; Stadler, M.; Fournier, J.; Tomita, A.; Hashimoto, T. *Tetrahedron* **2006**, *62*, 6349. d) Laakso, J. A.; Raulli, R.; McElhaney-Feser, G. E.; Actor, P.; Underiner, T. L.; Hotovec, B. J.; Mocek, U.; Cihlar, R. L.; Broedel, S. E., Jr. *J. Nat. Prod.* **2003**, *66*, 1041 e) Nam, J. Y.; Son, K. H.; Kim, H. K.; Han, M. Y.; Kim, S. U.; Choi, J. D.; Kwon, B. M. *J. Microbiol. Biotechnol.* **2000**, *10*, 544.
4) Kaur, K.; Wu, X.; Fields, J. K.; Johnson, D. K.; Lan, L.; Pratt, M.; Somoza, A. D.; Wang, C. C. C.; Karanicolas, J.; Oakley, B. R.; Xu, L.; De Guzman, R. N.. *PLOS ONE* **2017**, *12*, e0175471.
5) Wang, W.; Liao, Y.; Chen, R.; Hou, Y.; Ke, W.; Zhang, B.; Gao, M.; Shao, Z.; Chen, J.; Li, F., *Mar. Drugs* **2018**, *16*.
6) Yasukawa, K.; Takahashi, M.; Natori, S.; Kawai, K. I.; Yamazaki, M.; Takeuchi, M.; Takido, M., *Oncology* **1994**, *51*, 108-112.
7) Matsuzaki, K.; Inokoshi, J.; Tanaka, H.; Masuma, R. *J. Antibiot.* **1998**, *51*, 1004-1011.
8) Tang, J.-L.; Zhou, Z.-Y.; Yang, T.; Yao, C.; Wu, L.-W.; Li, G.-Y. **2019**, *67*, 2175-2182.
9) Hsu, W.-H.; Chen, T.-H.; Lee, B.-H.; Hsu, Y.-W.; Pan, T.-M. *Food Chem. Toxicol.* **2014**, *64*, 94-103.
10) Udagawa, S. *Chem. Pharm. Bull.* **1963,** *11*, 366-367.
11) Whalley, W. B.; Ferguson, G.; Marsh, W. C.; Restivo, R. J. *J. Chem. Soc., Perkin Trans. 1* **1976**, *13*, 1366-1369.
12) Makrerougras, M.; Coffinier, R.; Oger, S.; Chevalier, A.; Sabot, C.; Franck, X. *Org. Lett.* **2017**, *19*, 4146-4149.
13) Mehta, P. P.; Whalley, W. B. *J. Chem. Soc.* **1963**, 3777.
14) Lee, S. Y.; Clark, R. C.; Boger, D. L. *J. Am. Chem. Soc.* **2007**, *129*, 9860.
15) Zhu, J.; Grigoriadis, N. P.; Lee, J. P.; Porco, J. A. *J. Am. Chem. Soc.* **2005**, *127*, 9342-9343.
16) Zallot, R.; Oberg, N. O.; Gerlt, J. A. *Curr. Opin. Chem. Biol.* **2018**, *47*, 77-85.
17) 40. Gerlt, J. A. *Biochemistry* **2017,** *56*, 4293-4308.
18) 41. Gerlt, J. A.; Bouvier, J. T.; Davidson, D. B.; Imker, H. J.; Sadkhin, B.; Slater, D. R.; Whalen, K. L. *Biochim. Biophys. Acta. Proteins Proteom.* **2015**, *1854*, 1019-1037.
19) Chiang, Y.-M.; Szewczyk, E.; Davidson, A. D.; Keller, N.; Oakley, B. R.; Wang, C. C. C. *J. Am. Chem. Soc.* **2009**, *131*, 2965-2970.
20) Davison, J.; al Fahad, A.; Cai, M.; Song, Z.; Yehia, S. Y.; Lazarus, C. M.; Bailey, A. M.; Simpson, T. J.; Cox, R. J. *Proc. Natl. Acad. Sci.* **2012**, *109*, 7642-7647.
21) Somoza, A. D.; Lee, K.-H.; Chiang, Y.-M.; Oakley, B. R.; Wang, C. C. C. *Org. Lett.* **2012**, *14*, 972-975.
22) Rodríguez Benítez, A.; Tweedy, S. E.; Baker Dockrey, S. A.; Lukowski, A. L.; Wymore, T.; Khare, D.; Brooks, C. L.; Palfey, B. A.; Smith, J. L.; Narayan, A. R. H. *ACS Catal.* **2019**, *9*, 3633-3640.
23) Dockrey, S. A. B.; Suh, C. E.; Benítez, A. R.; Wymore, T.; Brooks, C. L.; Narayan, A. R. H. *ACS Cent. Sci.* **2019**, *5*, 1010-1016.
24) Zhu, J.; Porco, J. A., Asymmetric Syntheses of (−)-Mitorubrin and Related Azaphilone Natural Products. *Org. Lett.* **2006**, *8*, 5169-5171.
25) a) Barluenga, S.; Moulin, E.; Lopez, P.; Winssinger, N. *Chem. Eur. J.* **2005**, *11*, 4935. b) Katoh, T.; Kirihara, M.; Nagata, Y.; Kobayachi, Y.; Arai, K.; Minami, J.; Terashima, S. *Tetrahedron* **1994**, *50*, 6239.
26) Reich, H. J.; Sikorski, W. H. *J. Org. Chem.* **1999**, *64*, 14.
27) a) Park, S.; Kim, S.-H.; Jeong, J.-H.; Shin, D. *Org. Chem. Front*. **2019**, *6*, 704. b) Little, A.; Porco, J. A. *Org. Lett.* **2012,** *14*, 2862. c) Ireland, R. E.; Varney, M. D. *J. Org. Chem.* **1986,** 51, 635. d)

Yadav, J.S.; Ganganna, B.; Bhunia, D.C.; Srihari, P. *Tetrahedron Lett.* **2009,** *50*, 4318. e) Azevedo, C. M. G.; Alfonso, C. M. M.; Pinto, M. M. M. *Eur. J. Med. Chem.* **2013**, *69*, 798.

28) Germain, A. R.; Bruggemeyer, D. M.; Zhu, J.; Genet, C.; O'Brien, P.; Porco, J. A. Jr *J. Org. Chem.* **2011**, *76*, 2577.
29) Thines, E.; Anke, H.; Sterner, O. *J. Nat. Prod.* **1998**, *61*, 306-308.
30) Steyn, P. S.; Vleggaar, R. *J. Chem. Soc., Perkin Trans. 1* **1976**, *2*, 204-206.
31) Anke, H.; Kemmer, T.; Höfle, G. *J. Antiobiot.* **1981**, *34*, 923-928.
32) Nukina, M.; Marumo, S. *Tetrahedron Lett.* **1977**, *18*, 2603-2606.
33) Marumo, S.; Nukina, M.; Kondo, S.; Tomiyama, K. *Agric. Biol. Chem.*, **1982**, *46*, 2399-2401.
34) Kawanami, Y.; Ito, Y.; Kitagawa, T.; Taniguchi, Y.; Katsuki, T.; Yamaguchi, M. *Tetrahedron Lett.* **1984**, *25*, 857-860.
35) Myers, A. G.; Yang, B. H.; Chen, H.; McKinstry, L.; Kopecky, D. J.; Gleason, J. L. *J. Am. Chem. Soc.* **1997**, *119*, 6496-6511.
36) Blackwell, H. E.; O'Leary, D. J.; Chatterjee, A. K.; Washenfelder, R. A.; Bussmann, D. A.; Grubbs, R. H. *J. Am. Chem. Soc.* **2000**, *122*, 58-71.
37) Zhu, J.; Germain, A. R.; Porco Jr., J. A. *Angew. Chem. Int. Ed.* **2004**, *43*, 1239-1243.
38) Chong, M. J.; Shen, L. *Synth. Commun.* **1998**, *28*, 2801-2806.
39) Bosset, C.; Coffinier, R.; Peixoto, P. A.; El Assal, M.; Miqueu, K.; Sotiropoulos, J.-M.; Pouységu, L.; Quideau, S. *Angew. Chem. Int. Ed.* **2014**, *53*, 9860-9864.
40) Evans, D. A.; Fandrick, K. R.; Song, H.-J. *J. Am. Chem. Soc.* **2005**, *127*, 8942- 8943.
41) Zhu, J.; Porco, J. A. *Org. Lett.* **2006**, *8*, 5169-5171.
42) Fuse, S.; Yoshida, H.; Oosumi, K.; Takahashi, T. *Eur. J. Org. Chem.* **2014**, *22*, 4854-4860.
43) Myers, A. G.; Yang, B. H.; Chen, H.; McKinstry, L.; Kopecky, D. J.; Gleason, J. L. *J. Am. Chem. Soc*. **1997**, *119*, 6496-6511.

CHAPTER 6: Photocatalytic Oxidative Dearomatization of Resorcinol Compounds

Chapter 6.1 Introduction

The use of lead(IV) tetraacetate for oxidative dearomatization was first reported over half a century ago and is still in use to this day, despite the instability of the oxidant and the stoichiometric quantities of lead waste that are generated.[1,2] More recently, hypervalent iodide reagents have been employed to perform this transformation, most notably IBX,[3] PIDA,[4] and PIFA.[4,5] These reagents each result in stoichiometric iodide byproducts which can be challenging to separate from the quinol products (Figure 6.1A).[6] Recent advances in catalytic oxidative dearomatization have demonstrated that iodide reagents can be employed in catalytic amounts in conjunction with stoichiometric quantities of inexpensive oxidants, such as *m*-CPBA, to afford dearomatized products.[7] This renders the method catalytic in iodide, but can limit the functional group tolerance of these methods, as well as producing byproducts.[8]

Nature employs flavin-dependent monooxygenases (FDMOs) to perform this challenging oxidation with perfect site- and stereoselectivity.[9] These enzymes use the noncovalent cofactor $FADH_2$ (see **6.7**) which reacts with molecular oxygen to form hydroperoxyflavin (**6.8**), an electrophilic source of oxygen that can react with electron-rich arenes posed in the enzyme active site (Figure 6.1B).[10] This environmentally benign system employs molecular oxygen as the stoichiometric oxidant and water as the solvent, ultimately affording a single isomer of the *o*-quinol product.[9] Recently we have disclosed our computational findings which support a radical reaction pathway between hydroperoxy flavin (see **6.8**) and resorcinol **6.13**.[11] Homolysis of the peroxyl O−O bond followed by a single electron transfer from the electron-rich arene to the flavin radical was found to be more energetically favorable pathway than the two-electron mechanism that is commonly proposed.[9] These findings inspired us to develop a small molecule-catalyzed method for oxidative dearomatization that mimics Nature's approach, however alleviates the requirement for a biological stoichiometric reductant. We envisioned developing a catalytic method which employs molecular oxygen as the stoichiometric oxidant, to produce water as the sole byproduct; thus, improving the overall atom economy and sustainability of the transformation.

Upon photoexcitation, riboflavin and derivatives thereof (see Table 1) have been employed as oxidants in the aerobic oxidation of benzylic C-H bonds,[12] cinnamic acids,[13] benzylic alcohols[14] amines[15], and sulfides.[16] This work combined with our computational results supporting single-electron oxidation of **6.13** by flavin through a low-barrier single electron transfer (SET) from the

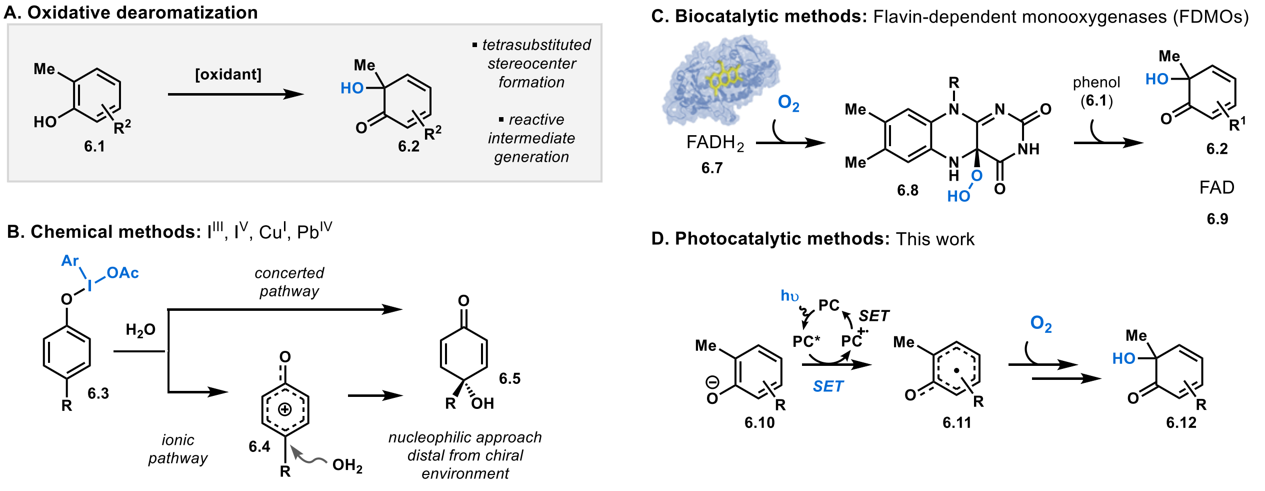
A. Oxidative dearomatization
Me
HO
R²
6.1
[oxidant]
Me
HO
O
R²
6.2
▪ tetrasubstituted stereocenter formation
▪ reactive intermediate generation
B. Chemical methods: I^III, I^V, Cu^I, Pb^IV
Ar
OAc
I
O
R
6.3
H₂O
concerted pathway
ionic pathway
O
⊕
R
6.4
OH₂
O
R OH
6.5
nucleophilic approach distal from chiral environment
C. Biocatalytic methods: Flavin-dependent monooxygenases (FDMOs)
O₂
FADH₂
6.7
R
N
N
O
Me
Me
NH
N
H
O
HO
O
6.8
phenol (6.1)
Me
HO
O
R¹
6.2
FAD
6.9
D. Photocatalytic methods: This work
hυ
PC
SET
PC*
PC⁺
Me
⊖O
R
6.10
SET
Me
O
R
6.11
O₂
Me
HO
O
R
6.12

Figure 6.1. (A) General scheme for oxidative dearomatization (OD). (B) Mechanism for I(III)-mediated OD. (C) Abbreviated mechanism for FMDO-mediated OD. (D) Proposed single-electron OD.

substrate,[11] encouraged us to investigate oxidation of **6.13** by photoexcited flavin. We envisioned the resulting radical could then be trapped by molecular oxygen to form the desired C-O bond.

Table 6.1: Optimization of photocatalytic oxidative dearomatization.

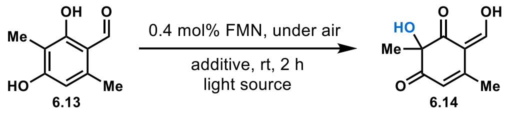

entry	base	buffer	light source	% conversion^a
1^{b,c}	NaH	--	blue LEDs	0.5
2^{b,c}	KO*t*Bu	--	blue LEDs	1
3	--	water pH 8.0	blue LEDs	0.5
4	--	HEPES pH 8.0	blue LEDs	60
5	--	HEPES pH 6.0	blue LEDs	3
6	--	Kp$_i$ pH 8.0	blue LEDs	53
7	**--**	**Tris pH 8.0**	**blue LEDs**	**95**
8	--	Tris pH 6.0	blue LEDs	2
9^c	--	Tris pH 8.0	ambient light	10
10	--	Tris pH 8.0	dark	0
11	--	Tris pH 8.0	blue LEDs	21

a) determined by UPLC-PDA b) in MeCN c) with riboflavin

Chapter 6.2 Reaction Development

Irradiation of **6.13** in MeCN with 0.4 mol% riboflavin, conditions commonly employed in benzylic oxidation of arenes,[12] returned only starting material. We hypothesized **6.13** was too electron poor to undergo the single electron oxidation or alternatively, the resulting radical was not sufficiently stable to allow for radical-cage escape.[17] Porco and coworkers have shown that less electron-rich arenes are oxidized by a copper-oxo-sparteine catalyst when the substrate is deprotonated prior to introduction of the oxidant.[18] Inspired by this solution to low reactivity, we next explored the addition of a number of organic and inorganic bases to our oxidation conditions; however, this strategy afforded only trace amounts of product **6.14** (Table 1, entries 1 and 2).

Taking advantage of the solvent effect offered by moving to aqueous reaction conditions, wherein the pKa of resorcinol **6.13** was measured to be 7.2,[10] the phenolate could be generated cleanly under mild conditions. We were gratified to find that in a variety of buffers at a pH of 8.0, with 0.1 mol % FMN, **6.13** was converted to a single, dearomatized product (Table 1, entries 4, 6, 7). Tris buffer afforded superior results, providing 95% conversion of starting material to a single product, compared to 60% with HEPES and 53% with potassium phosphate (KPi) buffered solutions. We also noted a precipitous drop in reactivity with decreasing pH (Table 1, entries 5 and 8), supporting our hypothesis that the phenolate is the competent species for SET. However, increasing the pH did not afford improved reaction outcomes. Interestingly, we found FMN to be the superior photocatalyst to riboflavin, perhaps due to the increased solubility in our aqueous reaction media. Exclusion of light resulted in no conversion of the starting material and reactions conducted in ambient light afforded diminished yields relative to blue LED irradiation (entries 9-11).

The clean reaction profiles afforded by these mild, photocatalytic conditions were in sharp contrast to the results we obtained with model substrate **6.13** using traditional methods for oxidative dearomatization. $Pb(OAc)_4$, PIDA and IBX afforded a number of byproducts including structural isomers, overoxidation to quinone products due to decomposition upon exposure to strong oxidants and challenges in separating the stoichiometric oxidant byproduct.

Chapter 6.3 Mechanistic Studies

The quenching rates for each of the reaction components were measured using Stern−Volmer analyses.[19] Under both aerobic and anaerobic conditions, tris was found to quench the FMN excited state, with quenching rates (k_q) of 2 × 108 M^{-1} s^{-1} (see Figures 6.10 and 6.12 and Figure 6.16). However, when the phenolate was employed as the photo quencher in pH 7.0 water the

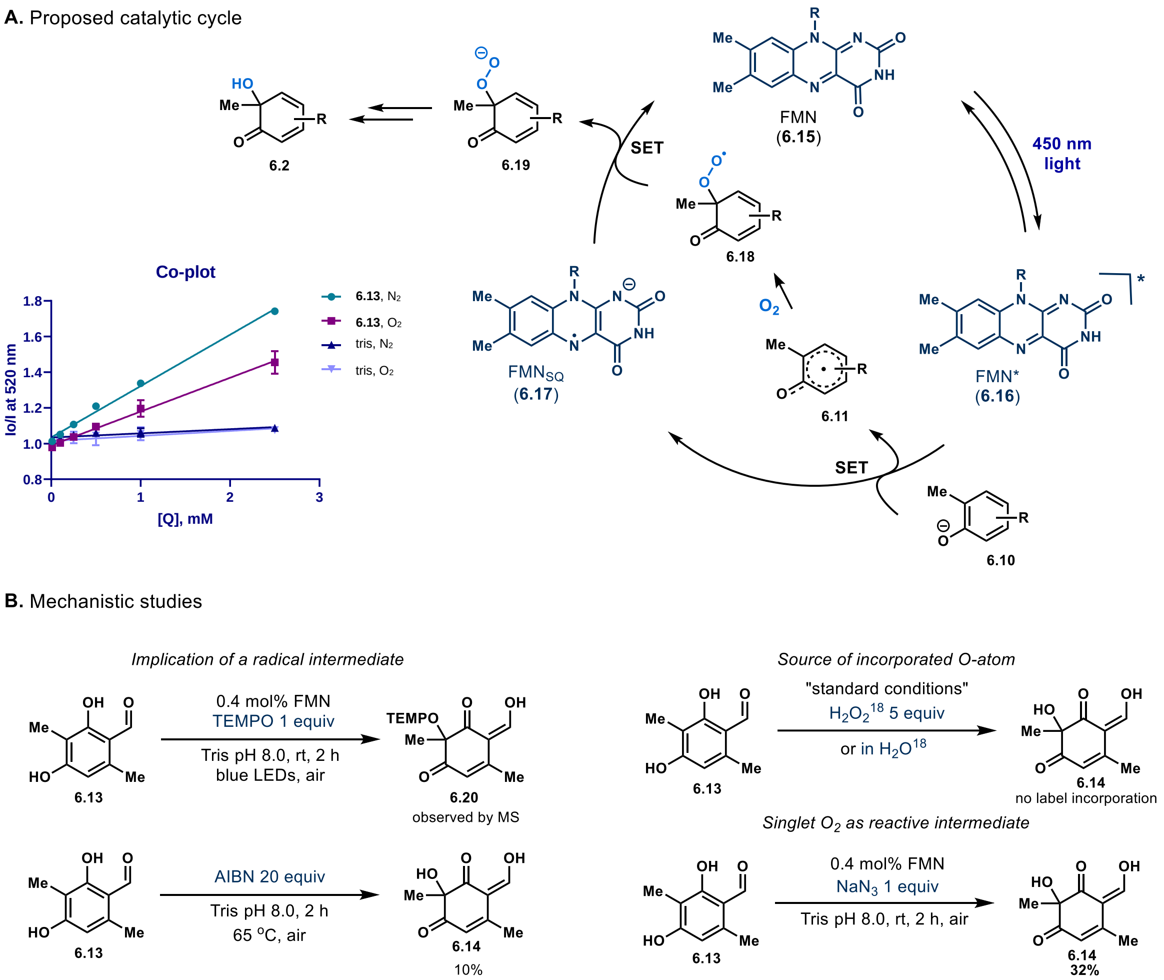
A. Proposed catalytic cycle
HO
Me
O
R
6.2
6.19
SET
FMN
(6.15)
450 nm
light
6.18
O2
FMNSQ
(6.17)
6.11
FMN*
(6.16)
SET
6.10
Co-plot
6.13, N2
6.13, O2
tris, N2
tris, O2
Io/I at 520 nm
1.8
1.6
1.4
1.2
1.0
0.8
0
1
2
3
[Q], mM
B. Mechanistic studies
Implication of a radical intermediate
0.4 mol% FMN
TEMPO 1 equiv
Tris pH 8.0, rt, 2 h
blue LEDs, air
6.13
TEMPO
6.20
observed by MS
AIBN 20 equiv
Tris pH 8.0, 2 h
65 °C, air
6.14
10%
Source of incorporated O-atom
"standard conditions"
H2O2^18 5 equiv
or in H2O^18
6.14
no label incorporation
Singlet O2 as reactive intermediate
0.4 mol% FMN
NaN3 1 equiv
Tris pH 8.0, rt, 2 h, air
6.14
32%

Figure 6.2: A) Proposed catalytic cycle for PCOD. B) Mechanistic studies. Inset: Stern-Vollmer plots. Standard conditions: 0.4 mol% FMN, 50 mM tris pH 8.0 buffer, rt, blue LEDs 2h.

quenching rate was found to be two orders of magnitude faster than the rate of tris quenching (see Figures 6.6 and 6.8 and Table 6.14). Under aerobic conditions, the phenolate gave a decreased rate due to the formation of product as evidenced in the UV-Vis spectrum (see Figure 6.15).

To gain experimental support for the formation of radical **6.11** under the reaction conditions, we attempted to trap the phenoxy radical with several radical trapping reagents and found that in the presence of TEMPO the appropriate adduct mass was observed by MS (Figure 6.2B). With preliminary support for the intermediacy of a radical such as **6.11** we next sought support for this phenoxy radical being on a productive pathway to dearomatized product. To generate radical **6.11** by alternative means, **6.13** was subjected to AIBN under aerobic conditions.

These conditions produced 10% of the dearomatized product along with a number of additional oxidation products, including the Baeyer-Villiger oxidation product. With evidence for the intermediacy of the substrate radical our attention turned to the source of hydroxyl group incorporated into the final product.

Our observation of the peroxy product by mass spectrometry and UV-Vis was support for the role of O_2 as the oxygen atom donor. To probe the operation of a second mechanism which could proceed through a carbocation arising from a second PSET, we performed the reaction in isotopically labeled water (Figure 6.2B). As predicted, we observed no incorporation of the labelled water in the hydroxylated product, providing support against the intermediacy of a carbocation species en route to dearomatized product **6.14.** It has been reported that in the presence of amine reductants and light, flavin containing species are capable of forming hydrogen peroxide.[21] In order to determine if this oxidant might play a role in the photocatalytic oxidative dearomatization, model substrate **6.13** was subjected to the optimized reaction conditions with five equivalents of ^{18}O-labeled hydrogen peroxide (Figure 6.2B). Again, no incorporation of ^{18}O was observed in the dearomatized product.

Finally, we hypothesized that photoexcited flavin might be responsible for generating singlet oxygen which then could undergo nucleophilic attack by our phenolate **6.10**.[22] The addition of the strong singlet oxygen quencher sodium azide did result in a diminished yield of the product; however, the reaction was not sufficiently suppressed to implicate singlet oxygen as the terminal oxidant.

Based on these data and previous reports of flavin mediated oxidation of arenes[12-16] and experimental observations, we propose the following mechanism for the photocatalytic oxidative dearomatization (Figure 6.2A). First, photoexcitation of the flavin photocatalyst could afford **6.16**, which subsequently performs a single electron oxidation of phenolate **6.10**. The resulting neutral substrate radical **6.11** could then undergo a recombination event with triplet oxygen to form peroxyl radical **6.18**. SET from flavin semiquinone **6.17** to **6.18** would afford peroxy intermediate **6.19**, which has been observed by MS and disproportionates over time to the desired product and water.

We envisioned employing this photocatalytic oxidation to access the phenoxy radical which could then undergo C-C or C-X bond formation by reacting with a radicalphile. However, the addition of electron-deficient and electron-rich olefins, metal catalysts, fluorine atom and trifluoromethyl radical donors each resulted in attenuation of reactivity and no new adduct masses by MS. We hypothesized that the inherit stability of the neutral substrate radical precluded reaction with low-energy species and that the addition of Lewis acids results in coordination of the phenolate substrate which is then unreactive in the single-electron oxidation.

Chapter 6.4: Substrate Scope

Having obtained support for the proposed catalytic cycle, we next investigated the substrate scope of this photocatalytic oxidative dearomatization. We were gratified to find several structural perturbations from the model substrate **6.13** were tolerated, including alternative electron-withdrawing moieties at C1 were dearomatized cleanly (Figure 6.3), however these reactions had to be conducted under an oxygen atmosphere to obtain high conversions. Interestingly, we found that the presence of an electron-withdrawing group at C1 was critical to obtain a dearomatized product rather than the known C–H oxidation product.[12] We hypothesize that the added resonance stabilization of the extended π-system in these compounds is critical to allow for sufficient radical character at the tertiary carbon, rather than on the primary benzylic carbon to afford an aromatic species.

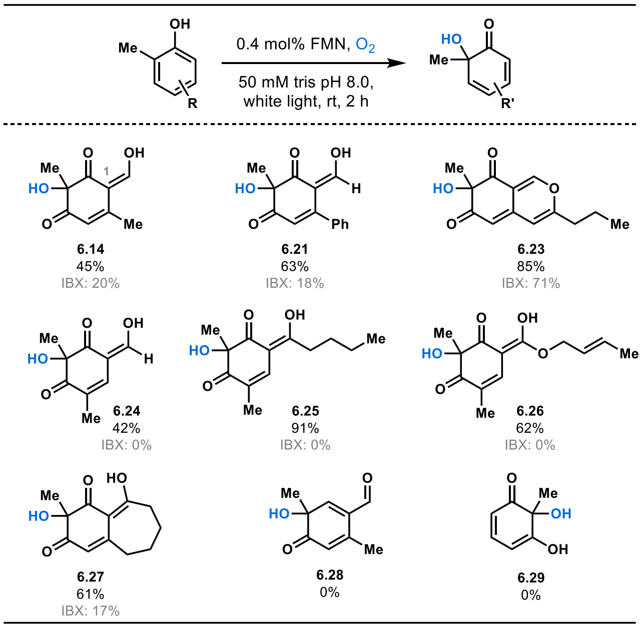

Figure 6.3: Substrate table for photocatalytic oxidative dearomatization.

Chapter 6.5 Conclusions

In conclusion, we have developed a photocatalytic method for oxidative dearomatization of densely functionalized arenes using molecular oxygen as the stoichiometric oxidant. The clean reaction profile of this photocatalytic transformation makes it an attractive alternative to traditional small molecule-mediated methods. The mechanism of this transformation has been investigated using a number of techniques, including luminescence quenching, radical trapping reagents, and isotopic labeling studies. Current limitations of this method include the requirement for a carbonyl group *ortho* to the hydroxyl group. This method allows for the generation of highly substituted *o*-quinols including azaphilones under mild, photocatalytic conditions. Work to expand this methodology to include less-electron rich arenes by tuning the redox properties of the photocatalyst is currently underway. A new exciting frontier for this reaction manifold could be to utilize this methodology to enable alternative disconnects allowing access to C–C and C–X bond formation products through reaction of alternative radicalphiles with the phenoxy radical.

Chapter 6.6: Experimental

Chapter 6.6.1: Protocol for PCOD

General Procedure: Stock solutions of each substrate (50 mM) were prepared by dissolving the substrate in DMSO (analytical grade). Stock solutions of FMN (1.0 mM) and riboflavin (1.0 mM) were prepared in MilliQue water and stored at -20 °C. Substrates (20 mg, 2.5 mM final concentration) were added to a round-bottom flask containing 50 mM tris buffer pH 8.0. The desired photocatalyst was then added as a solution in water (final concentration 0.1 μM, 0.4 mol%). Reactions were stirred at rt for 2 h under an O_2 atmsphere, with white light illumination from hood lights. After 2 h, the reaction was quenched by addition of 1 M HCl (5 mL). The reaction was concentrated under reduced pressure to a final volume of approximately 2 mL. The resulting mixture was filtered through a 0.22 µm filter and purified by preparative HPLC using a Phenomenex Kinetex 5 µm C18, 150 x 21.2 mm column under the following conditions: mobile phase A = deionized water + 0.1% formic acid and B = acetonitrile + 0.1% formic acid; method = 5% to 100% B over 13 min, 100% B for 4 min; flow rate, 15 mL/min.

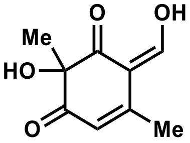

(Z)-2-hydroxy-6-(hydroxymethylene)-2,5-dimethylcyclohex-4-ene-1,3-dione (6.14)

Prepared according to general procedure A. 9.4 mg (45%) of the title compound isolated as a yellow glass. All recorded spectra agreed with previously reported values.[3] **^{1}H NMR** (400 MHz, CD_3CN) δ 8.08 (s, 1H), 5.81 (s, 1H), 2.1 (s, 3H), 1.47 (s, 3H).

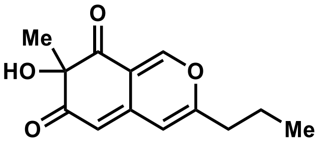

7-hydroxy-7-methyl-3-propyl-6H-isochromene-6,8(7H)-dione (**6.23**)

Prepared according to general procedure A. 16.9 mg (85%) of the title compound isolated as a yellow glass. All recorded spectra were in agreement with previously reported values.[3] **^{1}H NMR** (600 MHz, CD_3CN): δ 7.91 (s, 1H), 6.27 (s, 1H), 5.46 (s, 1H), 2.43 (t, *J* = 7.5 Hz, 2H), 2.15 (s, 2H), 1.65 (m, 2H), 1.20 (s, 3H), 1.00 (t, *J* = 7.5 Hz, 3H).

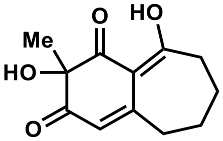

2,9-dihydroxy-2-methyl-5,6,7,8-tetrahydro-1H-benzo[7]annulene-1,3(2H)-dione (**6.27**)

Prepared according to general procedure A. 13.1 mg (61%) of the title compound isolated as a yellow glass. All recorded spectra agreed with previously reported values.[3] **^{1}H NMR** (600 MHz, CDCl3): δ 5.71 (s, 1H), 2.72 (m, 2H), 2.70 (m, 2H), 1.89 (m, 4H), 1.48 (s, 3H).

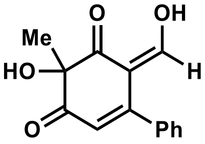

(Z)-4-hydroxy-2-(hydroxymethylene)-4-methyl-[1,1'-biphenyl]-3,5(2H,4H)-dione (**6.21**)

Prepared according to general procedure A. 13.4 mg (63%) of the title compound isolated as a yellow glass. All recorded spectra agreed with previously reported values.[3] **^{1}H NMR** (600 MHz, CD_3CN): δ 7.73 (s, 1H), 7.51 (m, 3H), 7.45 (m, 2H), 5.84 (s, 1H), 1.60 (s, 3H).

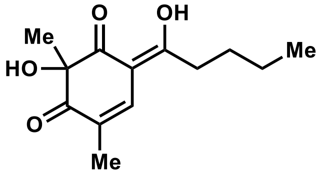

(*Z*)-2-hydroxy-6-(1-hydroxypentylidene)-2,4-dimethylcyclohex-4-ene-1,3-dione (**6.25**)

Prepared according to general procedure A. 16.4 mg (91%) of the title compound isolated as a yellow glass. **^{1}H NMR** (400 MHz, CD_3CN) δ 7.41 (s, 1H), 2.63 (m, 2H), 1.91 (s, 3H), 1.65 (m, 2H), 1.44 (s, 3H), 1.43 (m, 2H), 0.96 (t, *J* = 7.3 Hz, 3H); **^{13}C NMR** (150 MHz, $CDCl_3$) δ; 201.3, 199.2, 188.6, 137.1, 123.7, 117.4, 80.5, 32.5, 28.9, 28.4, 22.1, 14.6, 13.1; **HRMS** (ESI) *m/z* calculated for $C_{13}H_{19}O_4$ $[M+H]^+$: 239.1278, found: 239.1279.

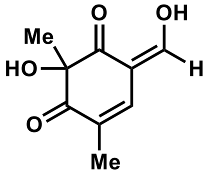

(*Z*)-2-hydroxy-6-(hydroxymethylene)-2,4-dimethylcyclohex-4-ene-1,3-dione (**6.24**)

Prepared according to general procedure A. 9.2 mg (42%) of the title compound isolated as a yellow glass. **^{1}H NMR** (400 MHz, CD_3CN) δ 7.81 (s, 1H), 7.18 (s, 1H), 1.91 (s, 1H), 1.44 (s, 1H). **^{13}C NMR** (150 MHz, $CDCl_3$) δ 210.2, 206.7, 198.8, 161.6, 144.7, 125.9, 110.0, 28.3, 14.6; **HRMS** (ESI) *m/z* calculated for $C_9H_{11}O_4$ $[M+H]^+$: 183.0652, found: 183.0650.

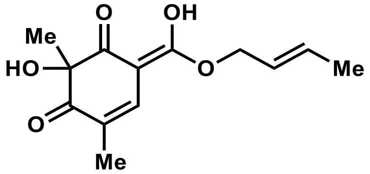

(E)-6-((((E)-but-2-en-1-yl)oxy)(hydroxy)methylene)-2-hydroxy-2,4-dimethylcyclohex-4-ene-1,3-dione (**6.26**)

Prepared according to general procedure A. 13.1 mg (62%) of the title compound isolated as a yellow glass. **^{1}H NMR** (600 MHz, CD_3CN) δ 7.39 (s, 1H), 5.52 (dt, J = 12.8, 6.2 Hz, 2H), 2.68 (t, J = 7.7 Hz, 2H), 1.91 (s, 3H), 1.64 (d, *J* = 6.0 Hz, 3H), 1.44 (s, 3H). **^{13}C NMR** (150 MHz, CD_3CN) δ 201.2, 199.1, 187.7, 137.2, 129.0, 126.6, 123.8, 105.9, 80.5, 32.8, 29.0, 17.1, 14.6. **HRMS** (ESI) *m/z* calculated for $C_{13}H_{17}O_5$ $[M+H]^+$: 253.1071, found: 253.1069.

Chapter 6.6.2: Stern-Volmer Plots

The Stern-Volmer luminescence quenching studies were performed in duplicate using freshly prepared solutions of FMN (10 μM) in MilliQue water at room temperature. Samples were prepared in a 1.0 cm cuvette by adding 1.0 mL of the photocatalyst solution and the appropriate amount of the quencher solution, and diluted with MilliQue water to 1.5 mL. The solutions were irradiated at λ= 450 nm and luminescence was detected at λ = 530 nm.

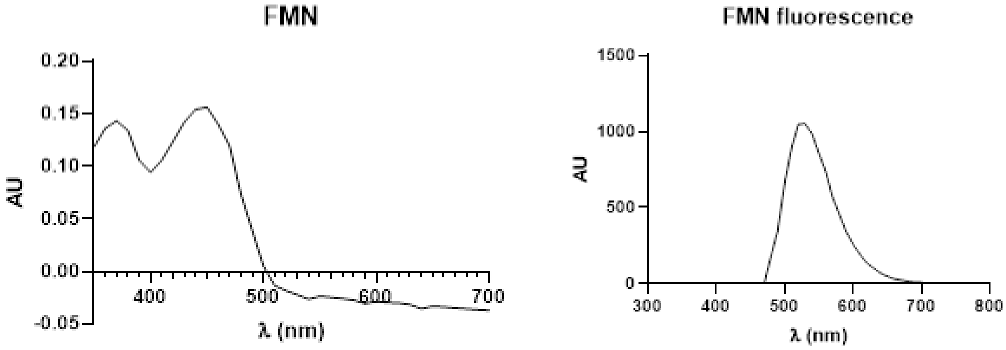

Figure 6.4: Absorbance and emission spectra of FMN.

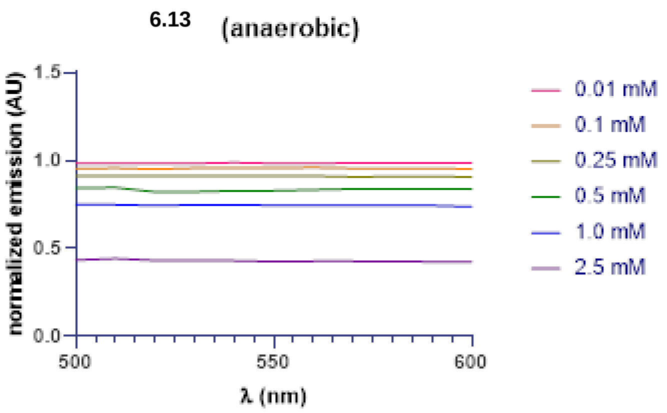

Figure 6.5: Emission quenching of FMN in water in the presence of 0 to 2.5 mM substrate **6.13** under N_2

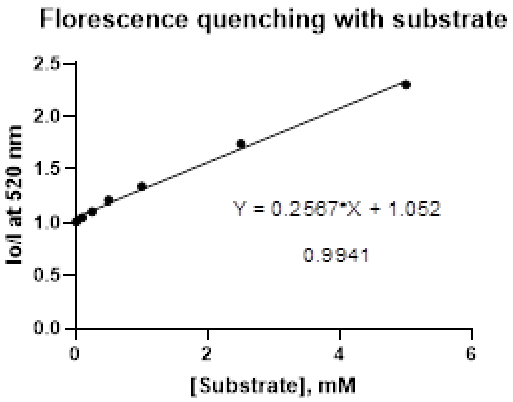

Figure 6.6: Stern-Volmer quenching experiments of FMN with **6.13** under N_2.

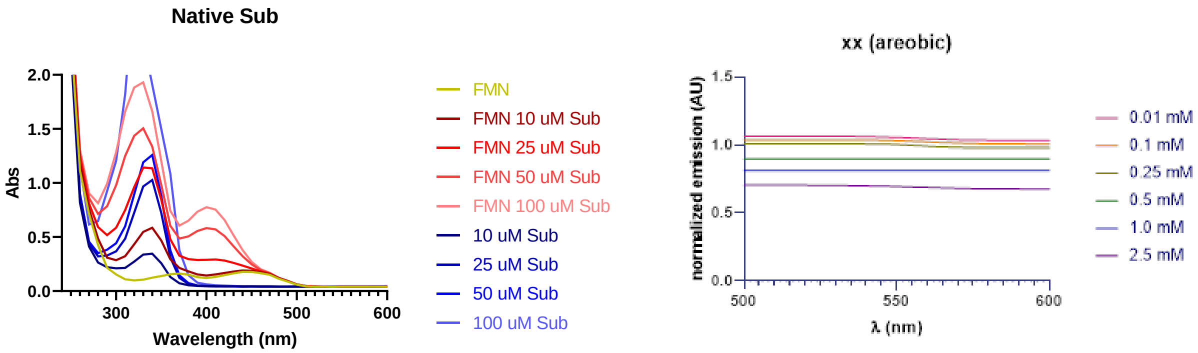

6.13

Figure 6.7: Emission quenching of FMN in water in the presence of 0 to 2.5 mM substrate **6.13** under air.

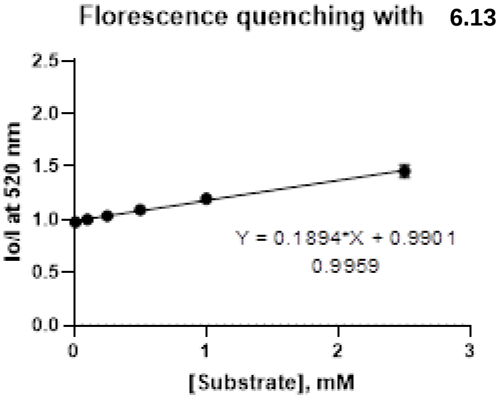

Figure 6.8: Stern-Volmer quenching experiments of FMN with **6.13** under air

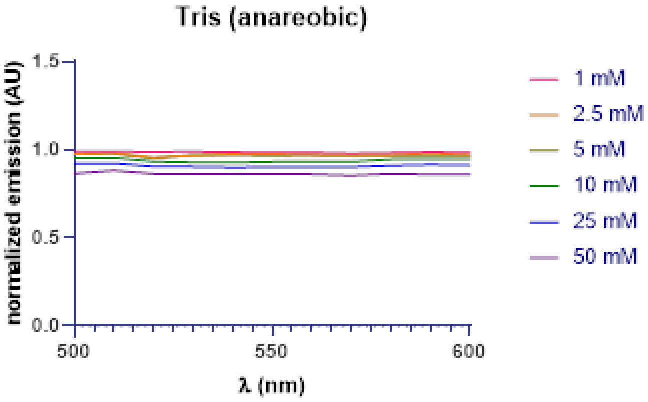

Figure 6.9: Emission quenching of FMN in water in the presence of 0 to 25 mM tris buffer, pH 8.0 under N_2.

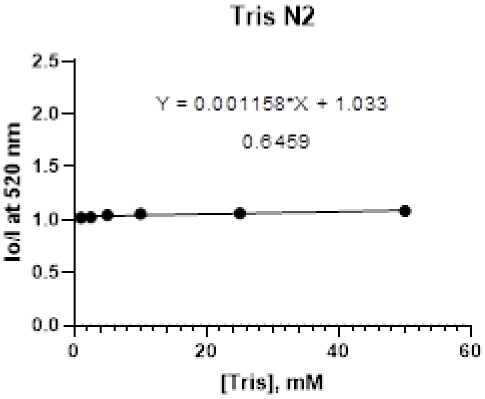

Figure 6.10: Stern-Volmer quenching experiments of FMN with tris under N_2

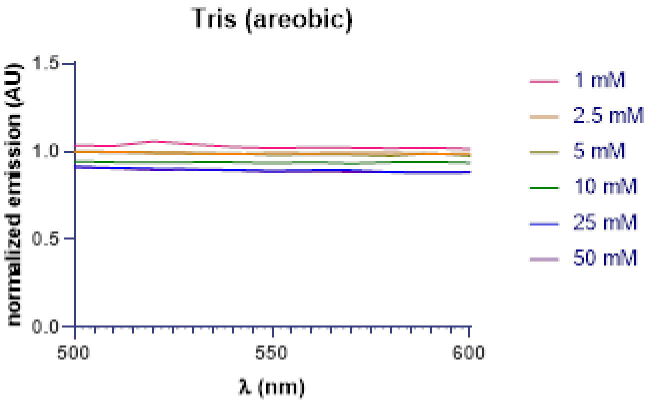

Figure 6.11: Emission quenching of FMN in water in the presence of 0 to 25 mM tris buffer, pH 8.0 under air.

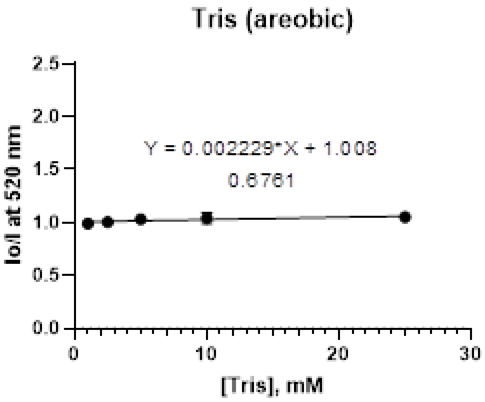

Figure 6.12: Stern-Volmer quenching experiments of FMN with **t**ris under air.

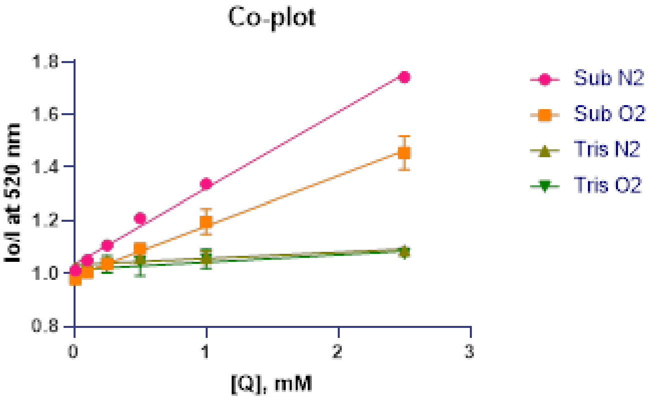

Figure 6.13: Co-plot of Stern-Volmer quenching experiments of FMN with quenchers **6.13** and Tris buffer under aerobic or anaerobic conditions.

$$\frac{I_0}{I} = 1 + k_q\tau_0[Q] \qquad \text{Equation (1)}$$

entry	quencher	$k_q \cdot \tau_0$ (K_{SV}; M^{-1})	k_q (M^{-1}s^{-1})
1	phenolate	258	5.26×10^{10}
2	phenolate, air	206	4.20×10^{10}
3	Tris	1.23	2.51×10^{8}
4	Tris, air	1.13	2.31×10^{8}

Figure 6.14: Summary of the luminescence quenching data for the evaluated quenchers. Rates were calculated according to Equation 1, where I_0/I is the emission intensity ratio, τ_0 is the lifetime of the photosensitizer excited state, k_q is the rate of quenching by quencher Q, The lifetime of the emissive excited state of the FMN in the absence of a quencher (τ_0) was estimated to be 4.4 ns.[24]

Part IV. Labeling studies

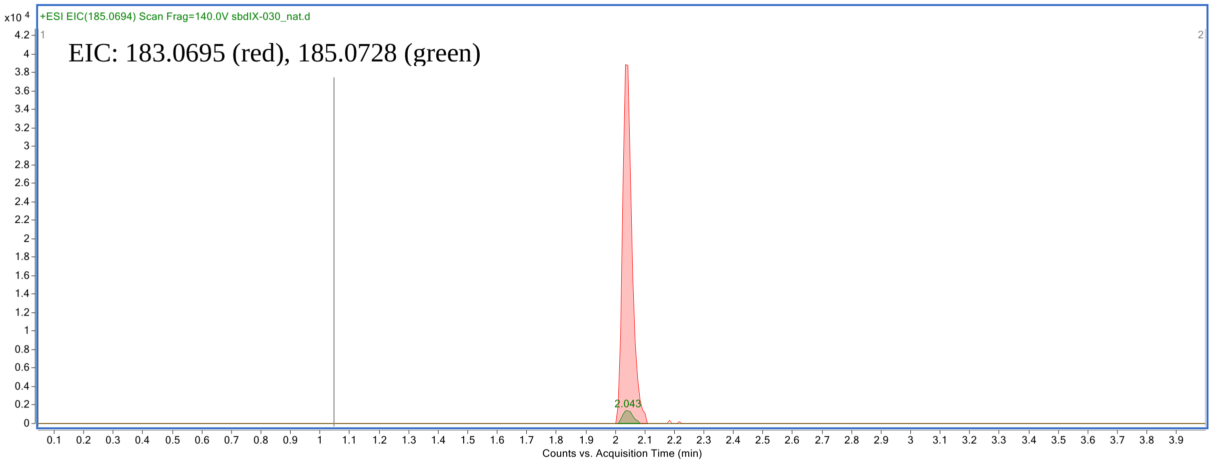

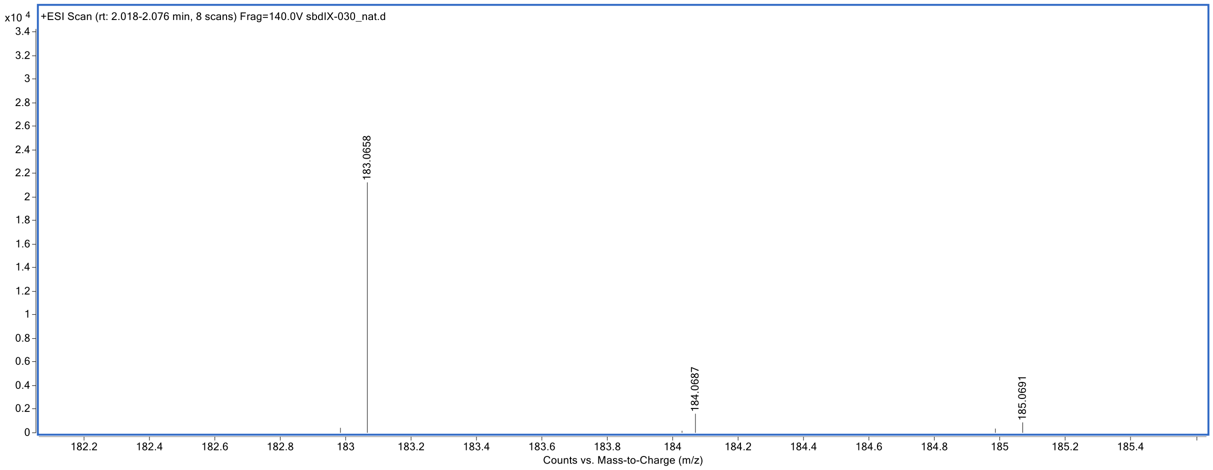

Peak	**RT**	**Area**	**Height**
1	2.034	87993.54	38868.54
Peak	**RT**	**Area**	**Height**
1	2.043	3504.48	135.89
	% ^{18}O	**3.8%**	

Figure 6.15: LC-MS trace of photocatalytic reaction in unlabeled water.

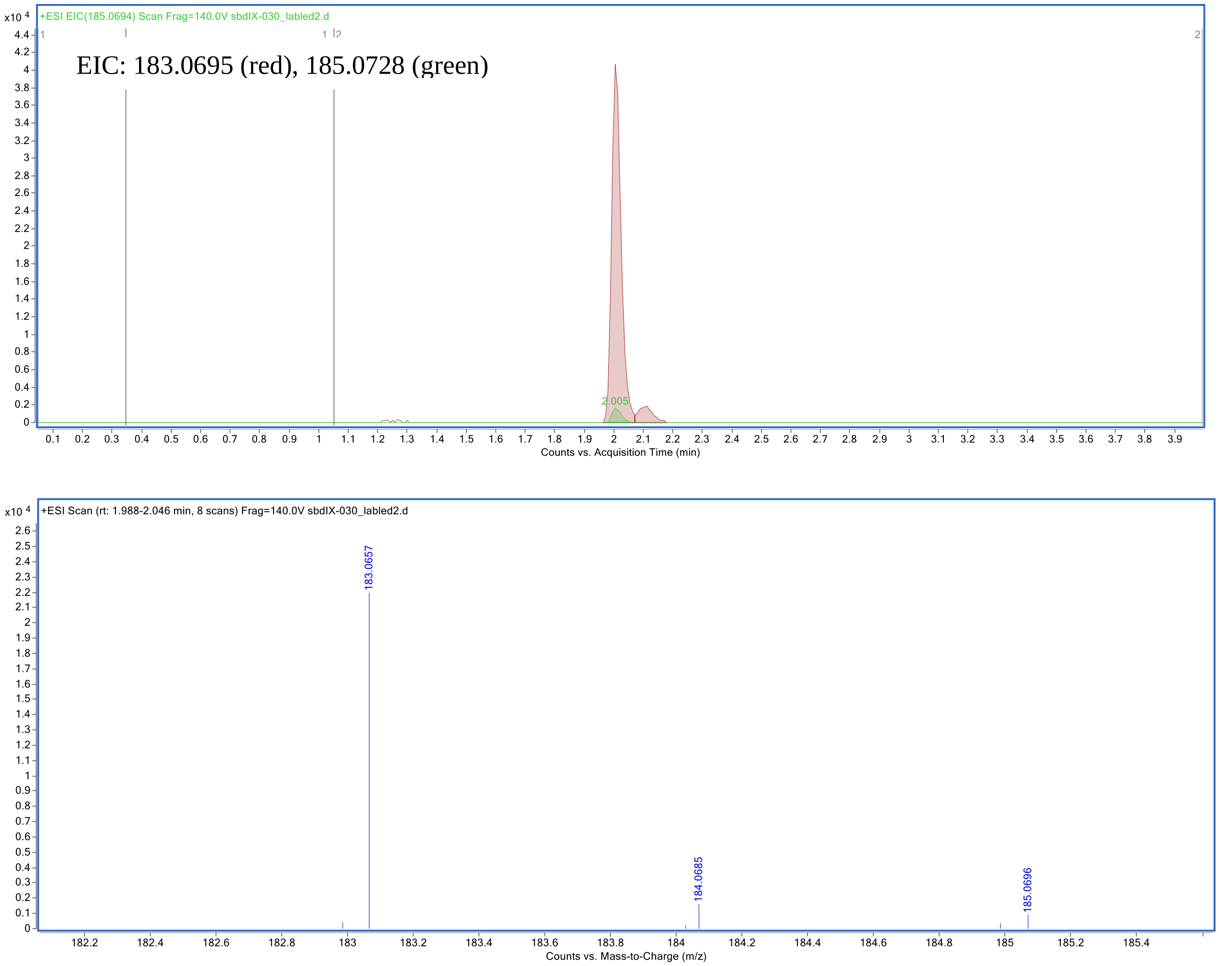

Peak	RT	Area	Height
1	2.005	91509.52	40643.73

Peak	RT	Area	Height
1	2.005	3623.51	1642.42

	% ^{18}O	**3.8%**	

Figure 6.16: LC-MS trace of photocatalytic reaction in H_2O^{18}.

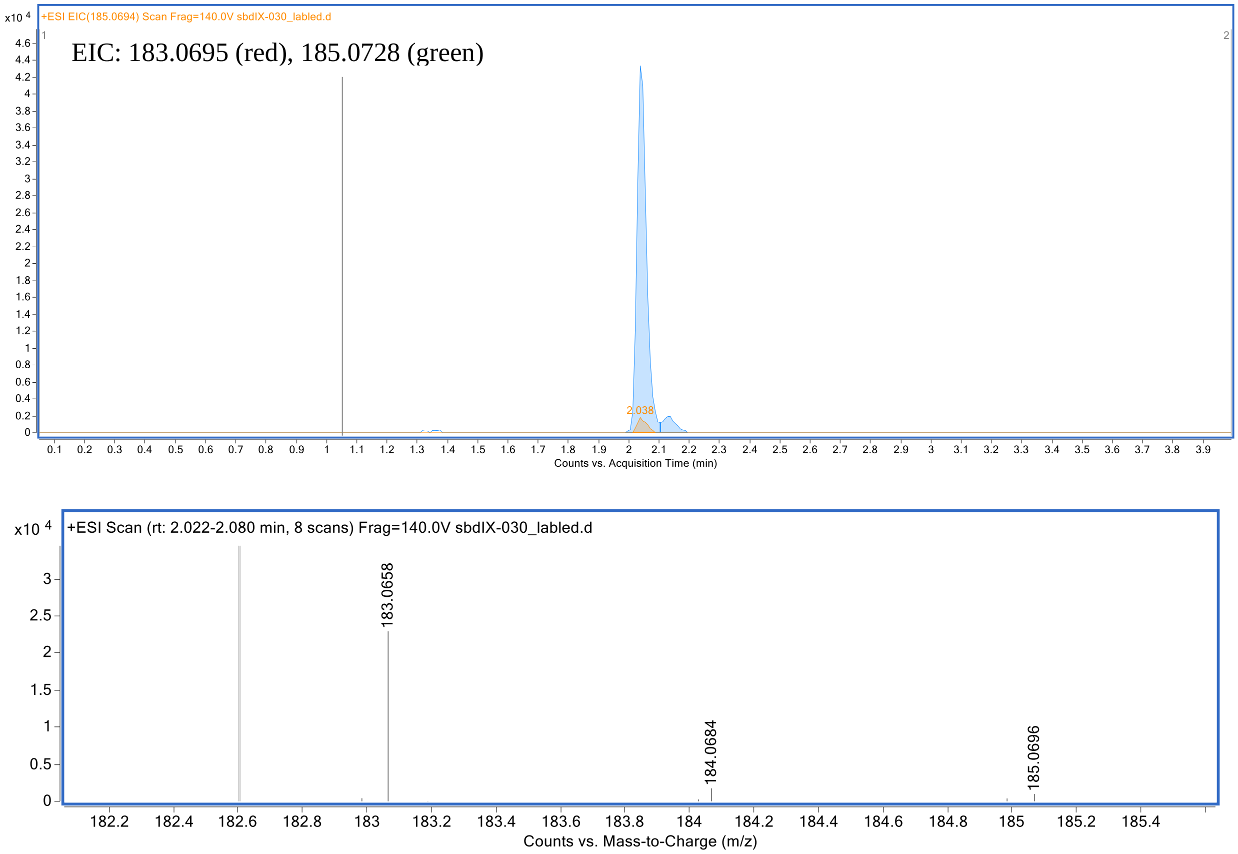

Peak	RT	Area	Height
1	2.038	95035.51	43367.36
Peak	**RT**	**Area**	**Height**
1	2.138	3850.18	1924.77
	% ^{18}O	**3.9%**	

Figure 6.17: LC-MS trace of photocatalytic reaction with 1 equiv H_2O^{18}.

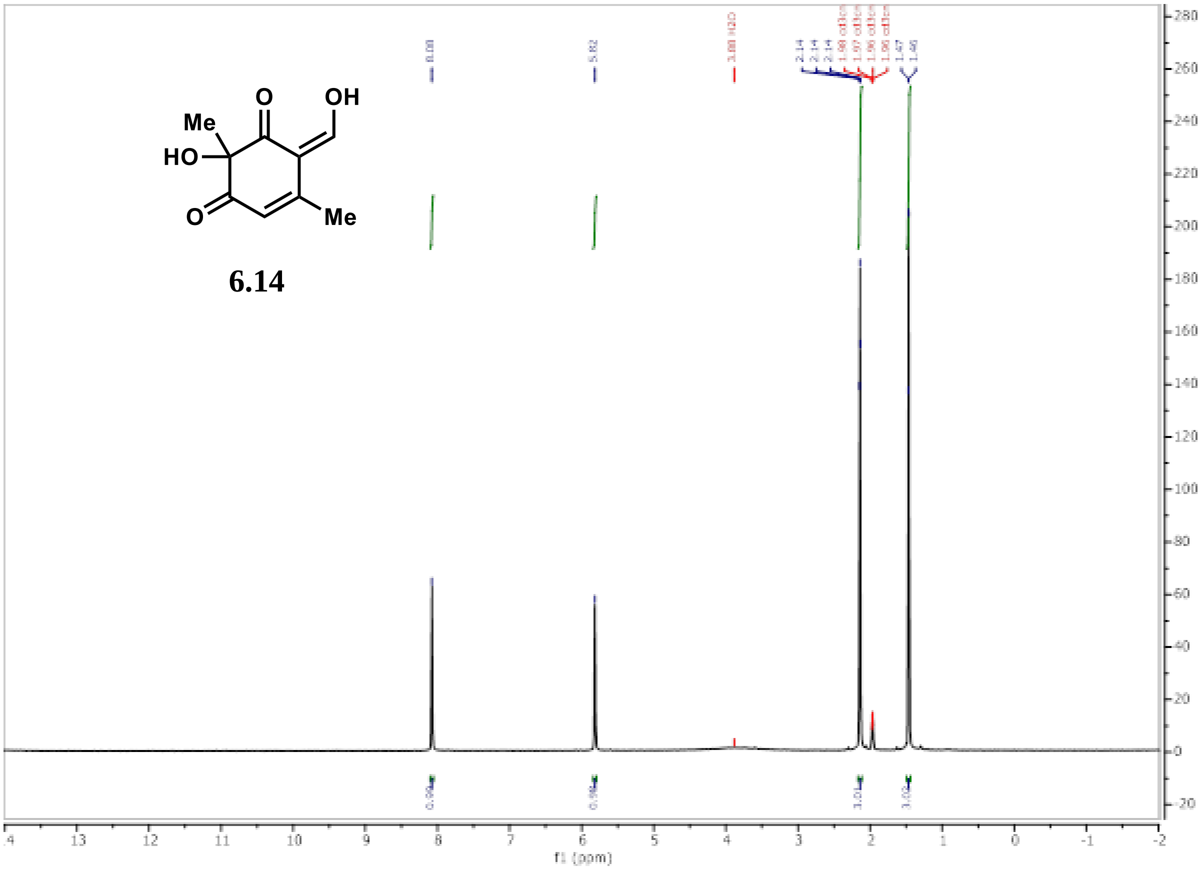
Me
HO
O
O
OH
Me
8.08
5.82
3.88 H2O
2.14
2.14
2.14
1.98 cd3cn
1.97 cd3cn
1.96 cd3cn
1.96 cd3cn
1.47
1.46
0.99
0.98
3.04
3.02
280
260
240
220
200
180
160
140
120
100
80
60
40
20
0
-20
14
13
12
11
10
9
8
7
6
5
4
3
2
1
0
-1
-2
f1 (ppm)

6.14

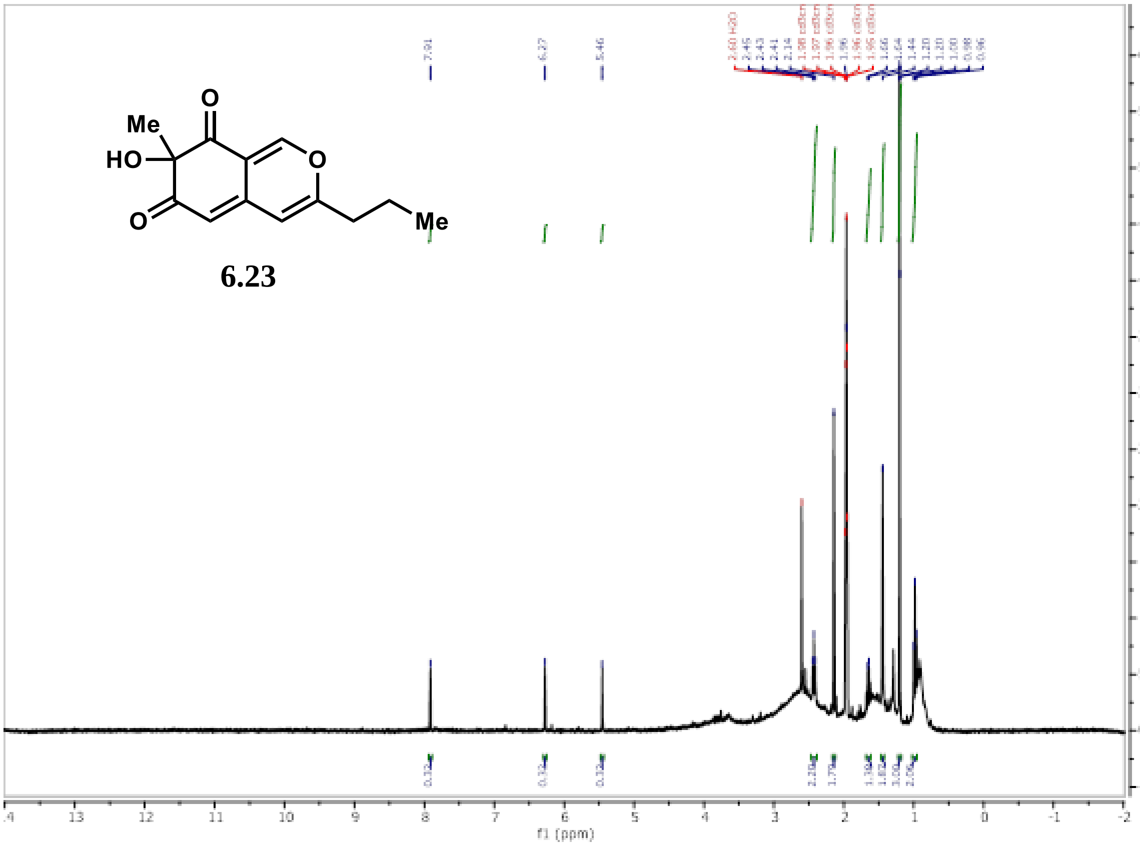
Me
HO
O
O
O
Me
7.91
6.27
5.46
2.60 H2O
2.45
2.43
2.41
2.14
1.98 cd3cn
1.97 cd3cn
1.96 cd3cn
1.96
1.96 cd3cn
1.96 cd3cn
1.66
1.64
1.44
1.20
1.20
1.20
1.00
0.98
0.96
0.32
0.32
0.32
2.20
1.79
1.38
1.82
3.00
2.06
60
55
50
45
40
35
30
25
20
15
10
5
0
-5
14
13
12
11
10
9
8
7
6
5
4
3
2
1
0
-1
-2
f1 (ppm)

6.23

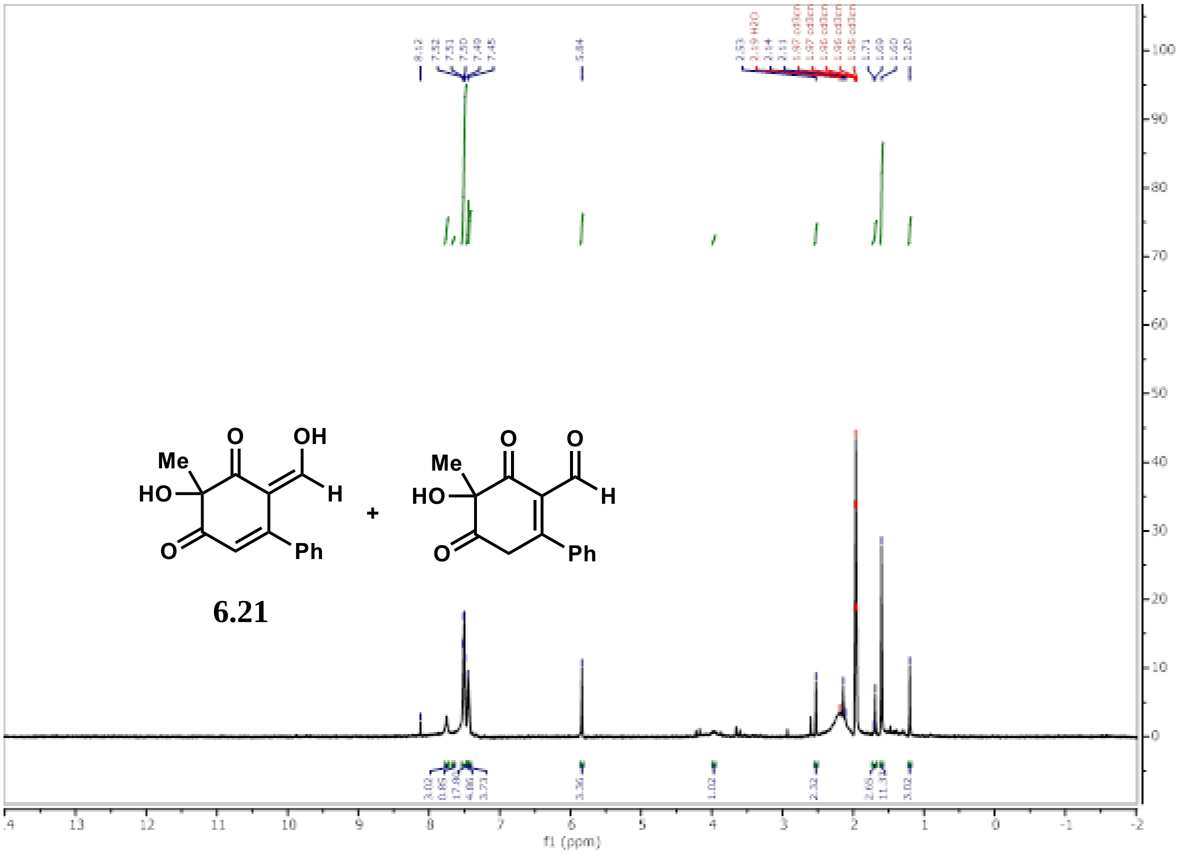
8.12
7.52
7.51
7.50
7.49
7.45
5.84
2.53
2.19 H2O
2.14
2.11
1.97 cd3cn
1.97 cd3cn
1.96 cd3cn
1.96 cd3cn
1.95 cd3cn
1.71
1.69
1.60
1.20
Me
HO
O
O
OH
H
Ph
+
Me
HO
O
O
O
H
Ph
3.02
0.86
17.86
4.86
3.73
3.36
1.02
2.32
2.65
11.39
3.02
14
13
12
11
10
9
8
7
6
5
4
3
2
1
0
-1
-2
f1 (ppm)
100
90
80
70
60
50
40
30
20
10
0

6.21

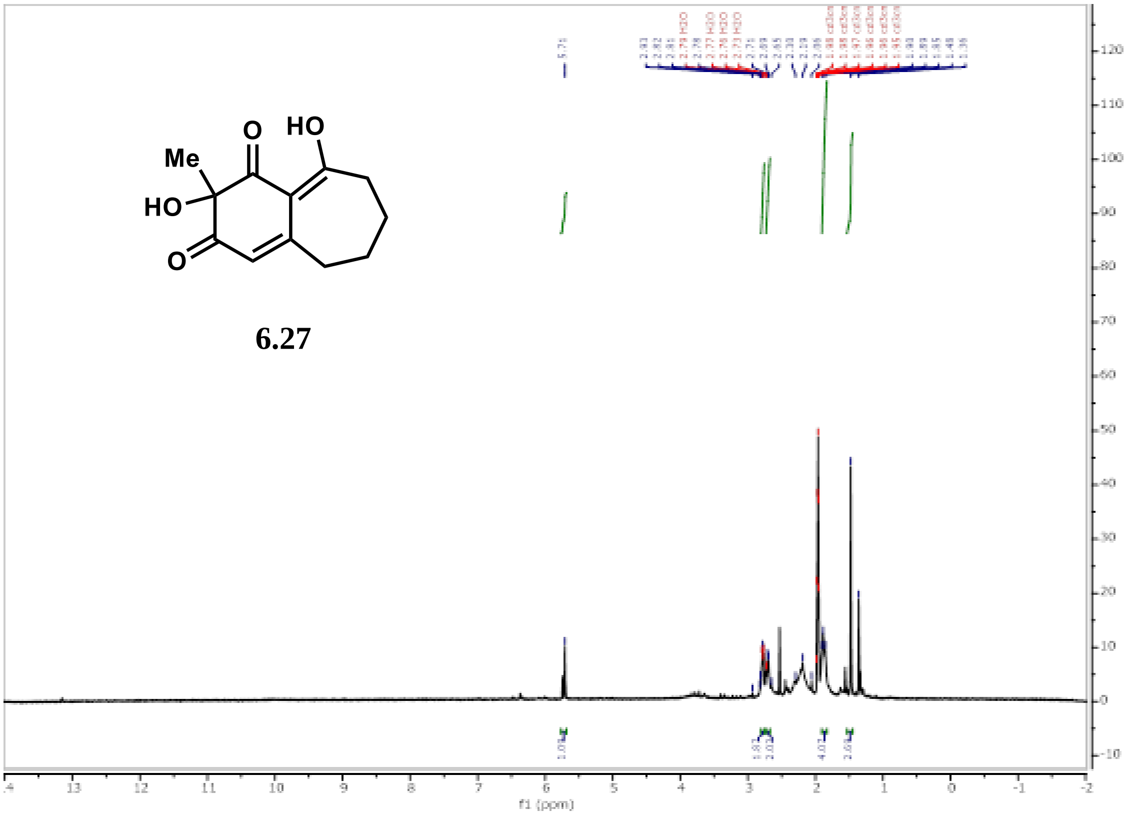
5.71
2.83
2.82
2.81
2.79 H2O
2.78
2.77 H2O
2.76 H2O
2.73 H2O
2.71
2.69
2.65
2.33
2.19
2.06
1.98 cd3cn
1.98 cd3cn
1.97 cd3cn
1.96 cd3cn
1.96 cd3cn
1.95 cd3cn
1.93
1.89
1.85
1.48
1.39
Me
HO
O
O
HO
1.04
1.87
2.02
4.07
2.64
14
13
12
11
10
9
8
7
6
5
4
3
2
1
0
-1
-2
f1 (ppm)
120
110
100
90
80
70
60
50
40
30
20
10
0
-10

6.27

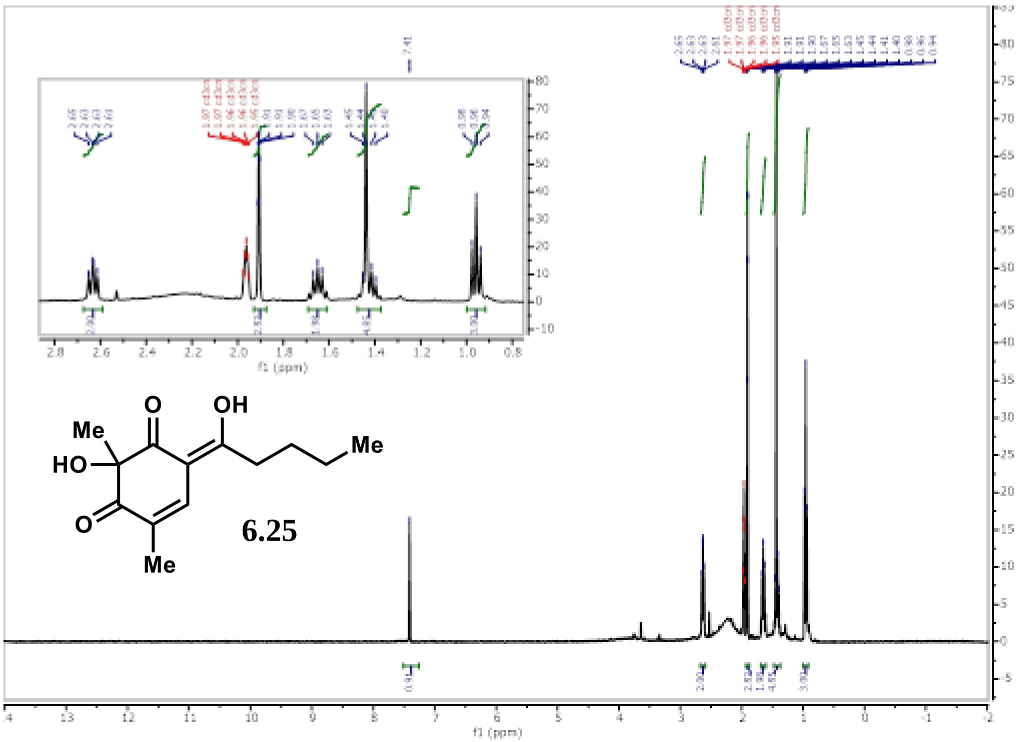
7.41
O
OH
Me
HO
Me
O
Me
6.25
f1 (ppm)

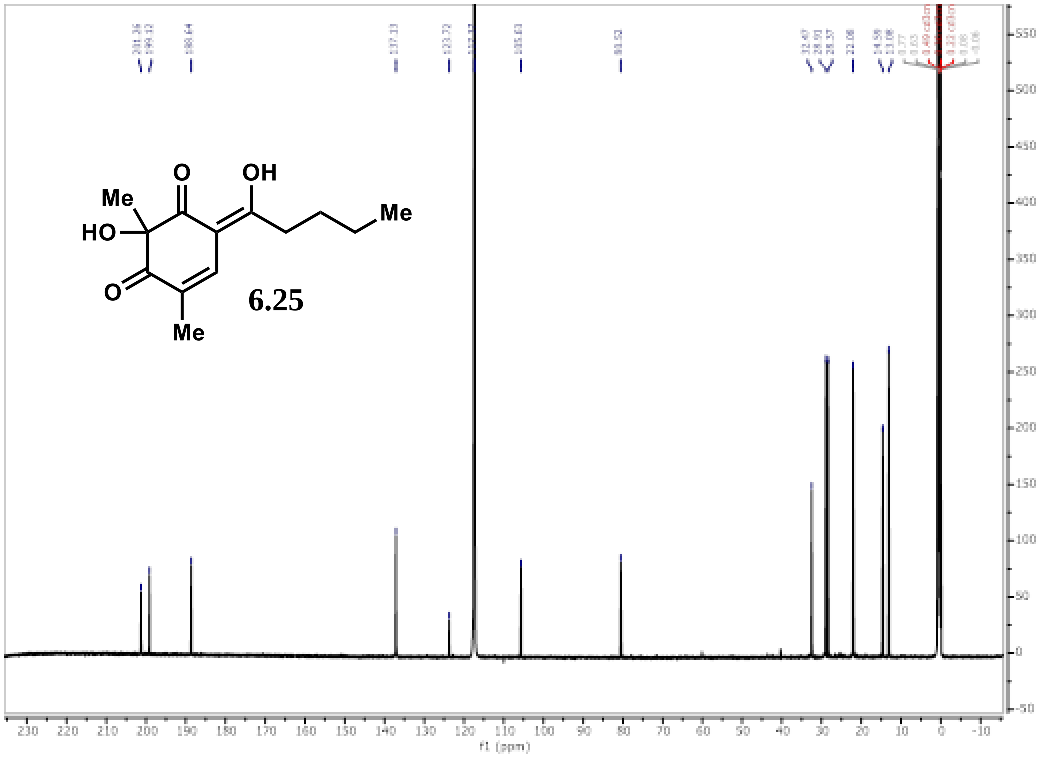
O
OH
Me
HO
Me
O
Me
6.25
f1 (ppm)

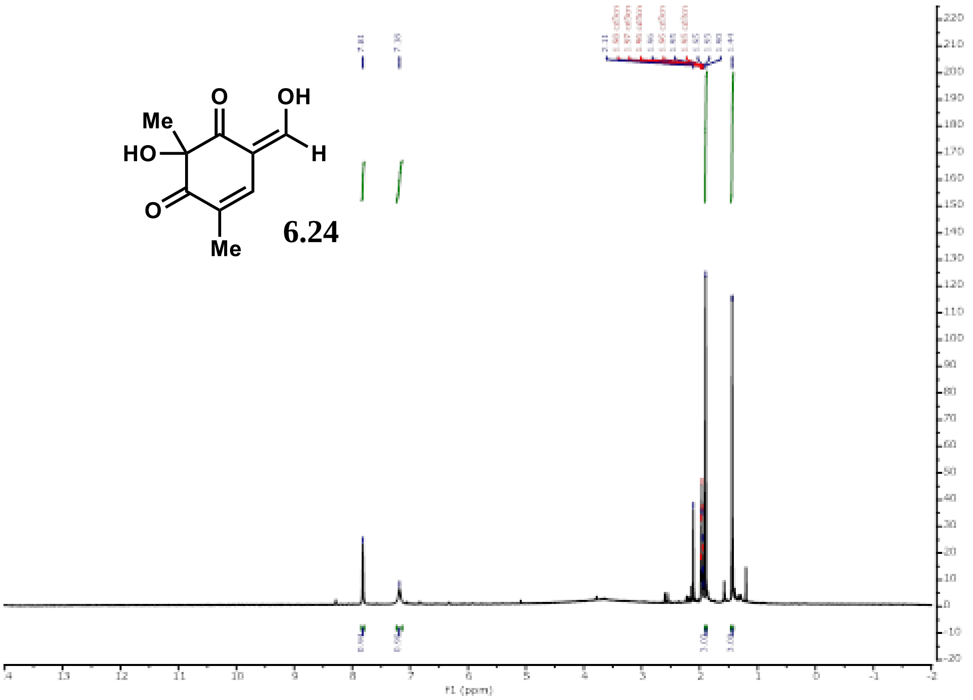

6.24

Me
HO
O
OH
H
O
Me
7.81
2.11
1.44
0.94
3.00
3.03
f1 (ppm)

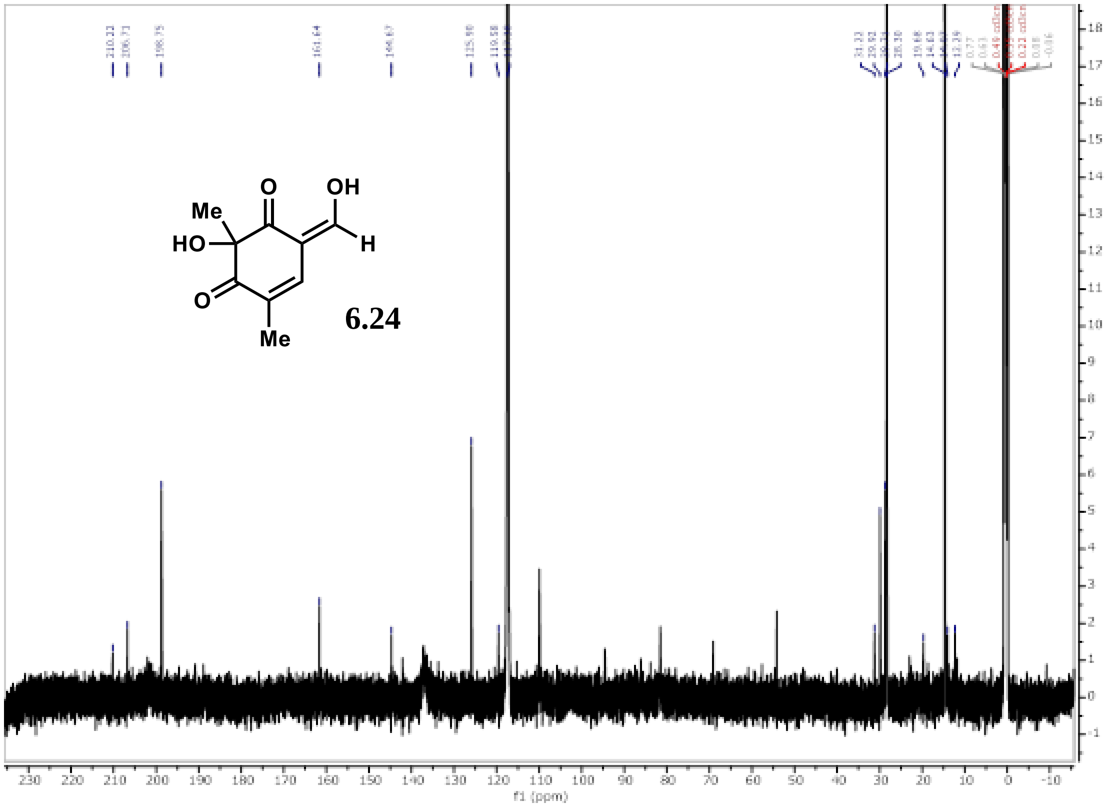

6.24

Me
HO
O
OH
H
O
Me
210.23
206.71
198.75
161.64
144.67
125.90
119.58
f1 (ppm)

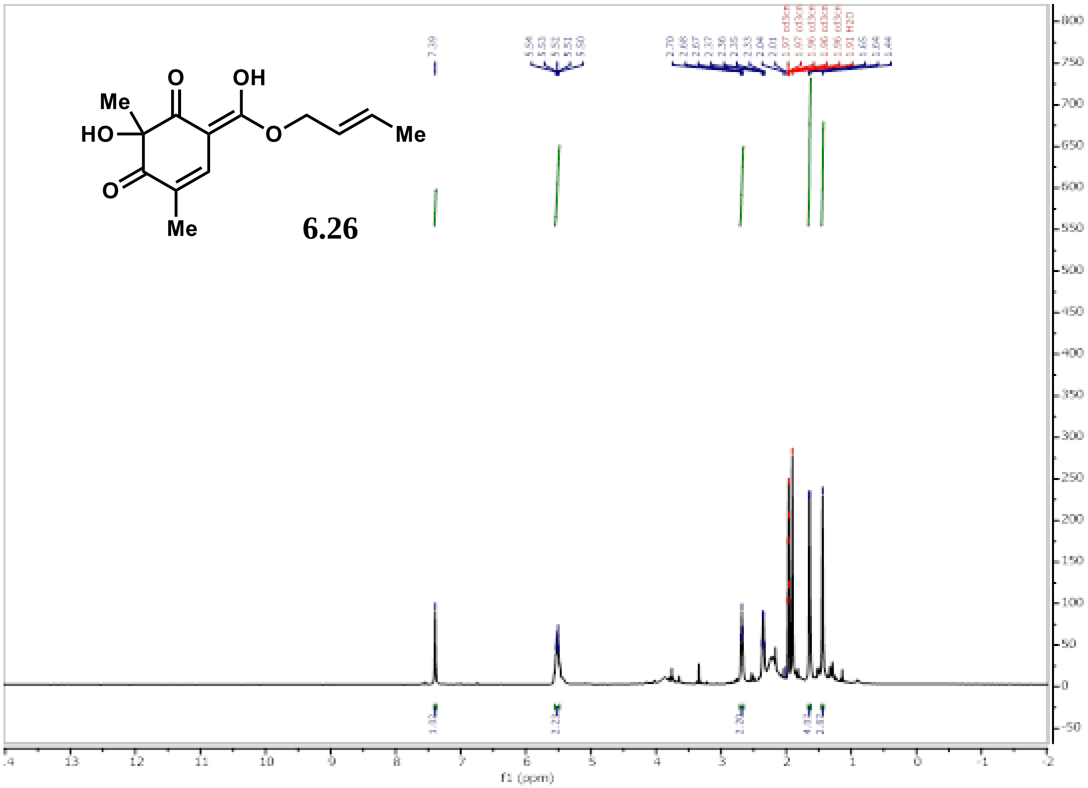

6.26

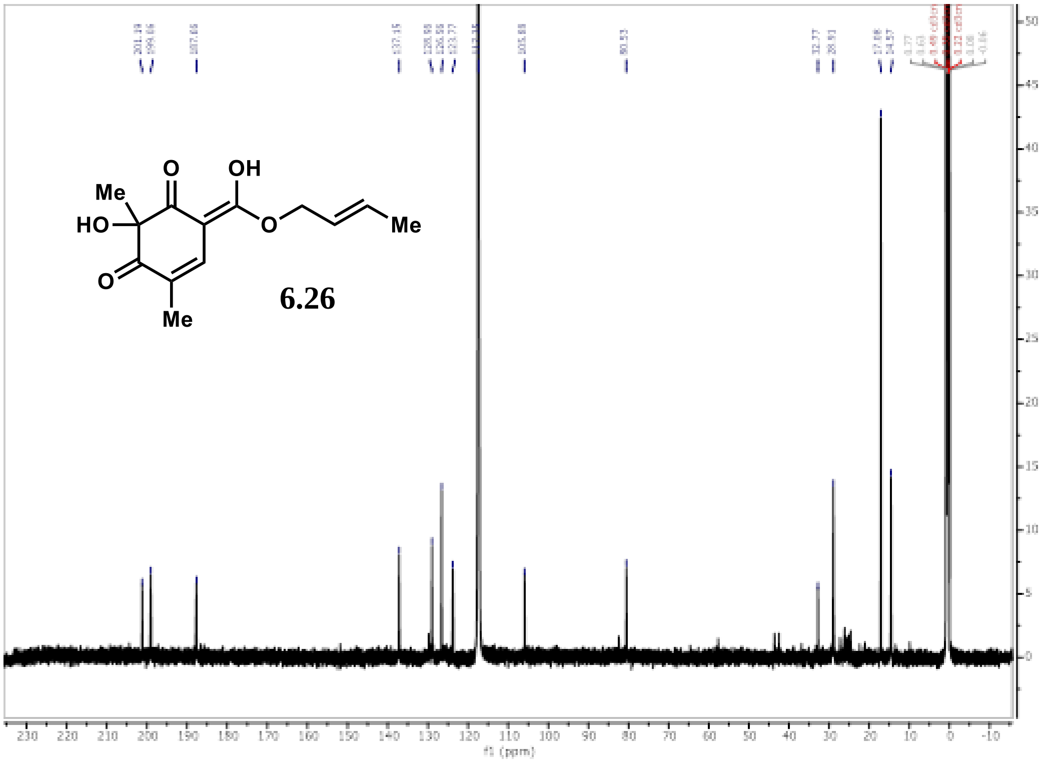

6.26

Figure 6.18: NMR spectra of synthetic compounds.

Chapter 6.7: References

1) a) Wessely, F.; Lauterbach-Keil, G.; Schmid, F. Monatsh. Chem. **1950**, *81*, 811. b) Wessely, F. and Sinwel, F. Monatsh. Chem. **1950**, *81*, 1055. c) Bichan, D. J.; Yates, P. *J. Am. Chem. Soc.* **1972**, *94*, 4773.
2) a) Green, J.; Pettus, T. R. R. *J. Am. Chem. Soc.* **2011**, *133*, 1603. b) Baker Dockrey, S. A.; Suh, C. S.; Benítez Rodríguez, A.; Wymore, W. T.; Brooks, C. L. III; Narayan, A. R. H. *ACS Central Sci.* **2019,** *5*, 1010. c) Nicolaou, K. C.; Vassilikogiannakis, G.; Simonsen, K. B.; Baran, P. S.; Zhong, Y.-L.; Vidali, V. P.; Pitsinos, E. N.; Couladouros, E. A. *J. Am. Chem. Soc.* **2000**, *122*, 3071.
3) a) Quideau, S.; Pouysegu, L.; Peixoto, P. A.;´ Deffieux, D. Phenol Dearomatization with Hypervalent Iodine Reagents. In Hypervalent Iodine Chemistry; Wirth, T., Ed.; Springer: Cham, Switzerland, 2016; pp 25−74. b) Zhu, J.; Germain, A. R.; Porco, J. A., Jr. *Angew. Chem. Int. Ed. Engl.* **2004**, *43*, 1239-1243. c) Lebrasseur, N.; Gagnepain, J.; Ozanne-Beaudenon, A.; Léger, J.-M.; Quideau, S. *J. Org. Chem.* **2007**, *72*, 6280-6283.
4) Wenderski, T. A.; Hoarau, C.; Mejorado, L.; Pettus, T. R. R. *Tetrahedron*, **2010**, *66*, 5873.
5) a) Volp, K. A.; Harned, A. M. *Chem. Commun*. **2013**, 3001. b) Sun, W.; Li, G.; Hong, L.; Wang, R. Org. Biomol. Chem. **2016**, *14*, 2164−2176.
6) a) Moschitto, M. J.; Anthony, D. R.; Lewis, C. A. *J. Org. Chem.* **2015**, *80*, 3339–3342. b) Dohi, T.; Uchiyama, T.; Yamashita, D.; Washimi, N.; Kita, Y. *Tetrahedron Lett.* **2011**, *52*, 2212–2215. c) Wardrop, D. J.; Burge, M. S.; Zhang, W.; Ortíz, J. A. *Tetrahedron Lett.* **2003**, *44*, 2587–2591. d) Wang, K.; Fu, X.; Liu, J.; Liang, Y.; Dong, D. *Org. Lett.* **2009**, *11*, 1015–1018.
7) a) Hashimoto, T.; Shimazaki, Y.; Omatsu, Y.; Maruoka, K. *Angew. Chem., Int. Ed.* **2018**, *57*, 7200–7204. b) Boppisetti, J. K; Birman, V. B. *Org. Lett.* **2009**, *11*, 1221.
8) Zhuo, C.-X.; Zhang, W.; You, S.-L. *Angew. Chem., Int. Ed.* **2012**, *51*, 12662−12686.
9) a) van Berkel, W. J. H.; Kamerbeek, N. M.; Fraajie, M. W. J. Biotechnol. **2006**, *124*, 670. b) Baker Dockrey, S. A.; Lukowski, A. L.; Becker, M. R., Narayan, A. R. H. *Nat. Chem.* **2018**, *10*, 119.
10) Rodríguez Benítez, A.; Tweedy, S.; Baker Dockrey, S.; Lukowski, A.; Wymore, T.; Khare, D.; Brooks, C. III.; Palfey, B. A.; Smith, J.; Narayan, A. *ACS Catal.* **2019**, *9*, 3633.
11) Tweedy, S. E.; Rodríguez Benítez, A.; Narayan, A. R. H.; Zimmerman, P. M.; Brooks, C. L., III; Wymore, T. *J. Phys. Chem. B.* **2019**, *123*, 38, 8065.
12) a) Muhldorf, B.; Wolf, R.; *Chem. Commun.* **2015**, *51*, 8425. b) Lechner, R.; Kummel, S.; Konig, B. *Photochem. Photobio.* **2010**, *9*, 1367. c) Dongare, P.; MacKenzie I.; Wang, D.; Nicewicz, D. A.; Meyer, T. J. *Proc. Natl. Acad. Sci. USA* **2017**, *114*, 9279.
13) Metternich, J. B.; Gilmour, R. *J. Am. Chem. Soc.* **2016**, *138*, 1040.
14) a) Fukuzumi, S.; Tanii, K.; Tanaka, T. J. *Chem. Soc. Chem. Commun.* **1989**, 816. b) Cibulka, R.; Vasold, R.; Konig, B. *Chem. Eur. J.* **2004**, *10*, 6223. c) Svoboda, J.; Schmaderer, H.; Konig, B. *Chem. Eur. J.* **2008**, *14*, 1854. d) Schmaderer, H.; Hilgers, P. Lechner, R. Konig, B. *Adv. Synth. Catal.* **2009**, 351,163. e) Feldmeier, C.; Bartling, H.; Magerl, K.; Gschwind, R. M. *Angew. Chem. Int. Ed.* **2015**, *54*, 1347.
15) a) Lechner, R.; Konig, B. *Synthesis* **2010**, 1712. b) Murray, A. T.; Dowley, M. J. H.; Pradaux-Caggiano, F.; Baldansuren, A.; Fielding, A. J.; Tuna, F. Hendon, C. H. Walch, A.; Lloyd-Jones, G. C. John, M. P.; Carbery, D. R. *Angew. Chem. Int. Ed.* **2015**, *54*, 8997.
16) Dang, C.; Zhu, L.; Gua, H.; Xia H.; Zhao, J.; Dick, B. *ACS Sustainable Chem. Eng.* **2018**, *6*, 15254.
17) Tan, S. L. J.; Novianti, M. L.; Webster, R. D. *J. Phys. Chem. B* **2015**, *119*, 14043.
18) Dong, S.; Zhu, J.; Porco, J. A., Jr. *J. Am. Chem. Soc.* **2008**, *130*, 2738.

19) a) Turro, N. J. *Modern Molecular Photochemistry*, University Science Books: Mill Valley, 1991. b) Stern, O.; Volmer, M. *Physik. Zeitschr*. **1919**, *20*, 183.
20) a) Ingold, K. U.; Pratt D. A. *Chem. Rev*. **2014**, *114*, 9022. b) Dvoranová, D.; Barbieriková, Z.; Brezová, V. *Molecules* **2014**, *19*, 17279.
21) a) Massey, V. *Biochem. Soc. Trans.* **2000**, *28*, 283. b) De laRosa, M.A., P.F. Heelis, K.K. Rao and D.O. Hall (1987) Flavin-mediated hydrogen peroxide production by biological and chemical photosystems. *In Flavins and Flavoproteins* (Edited by D.E. Edmonson and D.B. McCormick), pp. 597–600, Walter de Gruyter, Berlin.
22) Peault, L.; Nun, P.; Le Grognec, E.; Coeffard, V. *Chem. Commun*. **2019**, *55*, 7398.
23) Bancirova, M. *Luminescence* **2011**, *26*, 685.
24) Kao, Y.-T.; Saxena, C.; He, T.-F.; Guo, L.; Wang, L.; Sancar, A.; Zhong, D. *J. Am. Chem. Soc.* **2008**, *130*, 13132.